STOCHASTIC WAVE EQUATIONS

Stratonovich Waves Driven by Space-Time Gaussian Noise

Second Moment and Exact Asymptotics

An experiment in doing mathematics with AI

Le Chen

Department of Mathematics and Statistics

Auburn University

Construction, moment bounds
and the variational constant

Version 1.0.0

November 16, 2026

Stratonovich Waves Driven by Space-Time Gaussian Noise: Second Moment and Exact Asymptotics

Le Chen

Version 1.0.0, November 16, 2026

This work is licensed under the Creative Commons Attribution 4.0 International licence (CC BY 4.0):
https://creativecommons.org/licenses/by/4.0/

Source and development record:
https://github.com/chenle02/stratonovich-ham-second-moment

Preface

This book studies the second moment of the Stratonovich hyperbolic Anderson model driven by a Gaussian noise that is fractional in time. For this model, X. Chen [17] constructed the solution and showed that $\mathbb{E}u^2(t,x) \le e^{Ct^2}$ for large t. We ask two questions. What is the correct growth scale of $\log \mathbb{E}u^2(t,x)$, and what determines the constant in front of it? The scale is t^κ with $\kappa = (4-\alpha-\alpha_0)/(3-\alpha)$, and the limit is given by an explicit variational formula. The first moment is better understood because its exact representation uses the time order of a single chain. The second moment is an integral over two chains whose points interleave, and most of this book is about what replaces that representation. The precise statements are in Chapter 1.

How this book was written

This book was drafted together with Amy, our AI research system. The name began as a typo. In an email to a coauthor in the summer of 2026, the author meant to write "my AI Army" but missed the letter r, so Army became Amy. The coauthor started calling the system Amy, and the name stayed. Amy is not a single language model. She is a research environment that we built: written rules for how the work is done (how each step is organized, how reviews are requested, what counts as evidence, when to stop), a research library (a bibliography, a collection of papers and their LaTeX sources, and a wiki on stochastic partial differential equations), and interfaces through which a language model can use all of these. For this book, Amy was run with models from four families: Anthropic Claude, OpenAI GPT (through Codex), DeepSeek and Kimi. Amy is model-agnostic by design: any of these can be replaced. We have used Qwen through its API in earlier projects, though not in this one. Running open-weight models on our own machines, such as the open-weight Qwen models, is the next thing to test.

One way to picture this is as a car. The author built the car and keeps it up: the written rules, a library of more than a thousand skills learned from earlier work, the research library, and the interfaces. The bibliography is SPDEs-Bib, and the wiki is built on Andrej Karpathy's LLM Wiki pattern [35]: a knowledge base that the language models write and maintain. The models are the fuel; they can be replaced, and this book used four. The author is the driver.

Of the parts of this car, the wiki is the one we expect to last. It is the author's second brain. One way to see it: the papers are the source code, a language model is the compiler, and the wiki is the compiled form, written by models for models to read. A person can read it too. Unlike a compiler, a model can misread, which is why a result is checked against its source before it is used. This is also how a general model becomes

a specialist. No model was trained for this book. What Amy knows about stochastic partial differential equations is in the wiki, not in the model, and it reflects what the author has read and how he connects it. Change the model, and the specialist is still there. The wiki is a graph: its pages are linked, and Amy finds what bears on a question by searching the text and by ranking pages along their links with PageRank, the method Google first used to rank web pages. The models will be replaced. So, in time, will the rules, skills and interfaces around them, which engineers now call the harness. What has been read and linked stays. The wiki grows with every project, and the more it is used, the more it knows. Connections that nobody planned may then appear between pages written far apart. Drawn as a graph, it looks like a starry night.

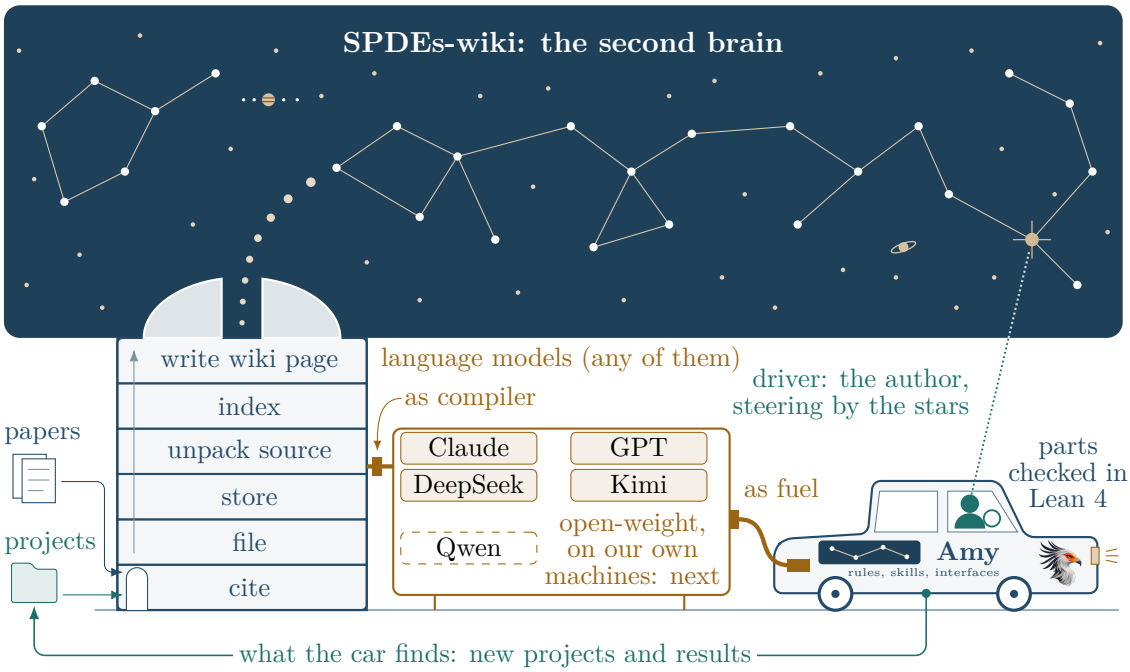

The wiki as a night sky. Language models compile papers and projects into it, one star for each page. The car steers by it, and what the car finds comes back as new projects.

The name Amy is used in two ways. In the narrow sense, Amy is the car: the rules, skills and interfaces, with a model in the tank, that the author drives on one project. In the broad sense, Amy is everything in the picture: the car, the tower that turns papers into wiki pages, and the sky they fill. When we say that Amy drafted a proof, we mean the car. When we speak of what Amy knows, we mean the whole.

References and results are looked up in the bibliography and the wiki instead of being recalled, which guards against invented citations and misremembered theorems, and it is what makes checking every cited result against its source practical. Beyond the mathematics, the choices were ours: what goes into the book and what stays out, how it is built, the standard of presentation, what is claimed, what is stated only as a conjecture, and what is left for future work. Terence Tao has said that mathematics is entering an era of proof abundance [42]; when proofs are plentiful, choices like these shape a book as much as any proof does.

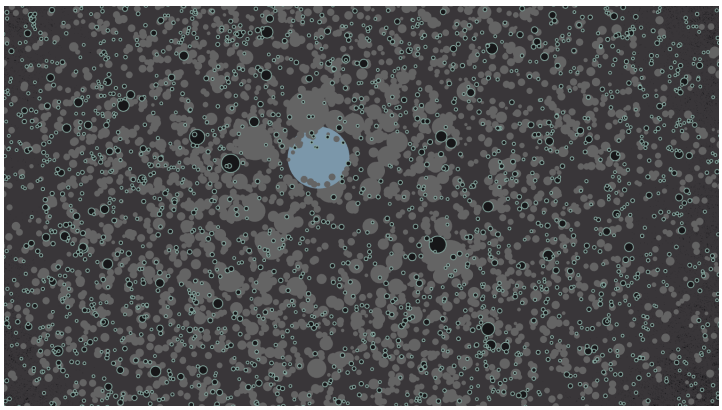

The SPDEs-wiki as a graph: each dot is one of its more than 4,000 pages, each a Markdown file the models wrote from a paper, a concept or a person they read about. With SPDEs-Bib, it is Amy's long-term memory, which helps her not to hallucinate. Both are parts of the infrastructure, with agent-agnostic skills and the command-line tools built around them.

The division of labour was as follows. Amy developed the mathematics: the models working within her drafted the proofs, the LaTeX source and the bookkeeping. Our role was to drive the work: we chose the problem, set and revised the goals, decided which approaches to pursue or abandon, chose the reviewers and decided which results to keep. Each new proof was sent to a reviewer from a different model family than its author, and every finding was answered in writing. We treat an argument produced by AI with more suspicion than one from a trusted colleague, and we ask where each of its ideas comes from: every cited result is checked against its source before it is used. Hairer recommends both practices in his advice on writing mathematics with AI [P1]. The proof assistant Lean was also used: it checks some results in full under the book's own hypotheses and the finite and algebraic steps of others; analytic inputs that enter Lean as hypotheses are not verified there, and two of the four main theorems, the full upper scale (Theorem 3.3.8) and the second-moment constant (Theorem 11.2.6), are outside Lean.

Mathematics is after what is true, and with AI the bottleneck has moved: it is no longer finding an argument but understanding it. Galileo's telescope showed Saturn's strange shape half a century before Huygens could say it was a ring; the new instruments, too, reach results faster than anyone can understand them. This book is such an observation, made with the checks described above and with its development record, failed attempts included, open to view. The present author, Le Chen, set up the instrument and ran it, and is responsible for what it reports; later versions may have more authors, as described below. We will look into every objection, and correct, qualify or withdraw any claim that does not hold up, recording each change in the public history. We have not read every line: the technical chapters have not yet been read in full by a human, and the public table records, result by result, what was checked and how. Understanding what we have seen is work for many eyes, and it is where we expect the next ideas to come from. The eyepiece is open to anyone, and every check, correction or explanation is recorded and credited by name. Amy will take part in this work too, as she did in writing the book:

under our guidance she can answer mathematical questions, check arguments and repair them. She is not an author, any more than Galileo's telescope was, because she cannot be held responsible for what she produces; that responsibility rests with a person. But she did far more than a telescope does, so we acknowledge her here by name, and the AI-use statement records in detail which models did what.

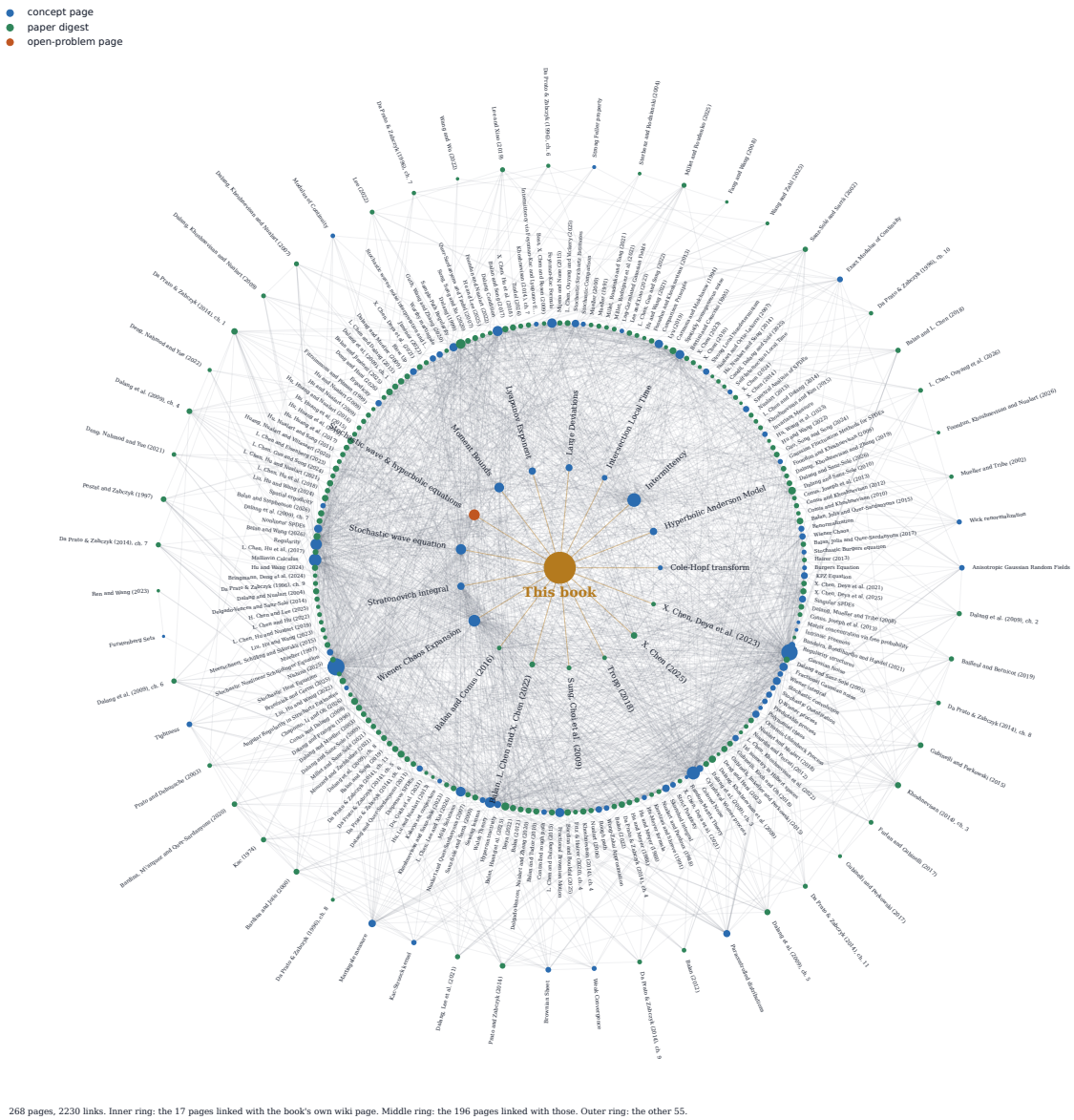

268 pages, 2230 links. Inner ring: the 17 pages linked with the book's own wiki page. Middle ring: the 196 pages linked with those. Outer ring: the other 55.

A close-up of the graph shown earlier in this preface: the wiki around the stochastic wave equation, with this book in the centre. Each dot is one page of the wiki, a Markdown file that the models write and maintain from what they have read: a digest of a paper, or a page on a concept or on open problems. Lines are links between pages. Shown are 268 pages and the 2,230 links among them, on three rings: the pages linked with this book's project page, the pages linked with those, and the rest of this selection. Drawn from the wiki's link index, November 16, 2026; see `media/spdes-wiki-graph/`.

An experiment in doing mathematics

In 1610 Galileo pointed a telescope that magnified about twenty times at the sky. Within about a week he saw four moons moving around Jupiter, which no one had seen before [31]. A few months later he looked at Saturn and reported a planet made of three bodies. Two years later the two side bodies disappeared, and he could not explain why. What he saw was real, but its meaning was harder to understand. Christiaan Huygens later explained these changing appearances by a ring around Saturn; he published the explanation in 1659 [46]. An AI system is a new instrument of this kind. It lets us see arguments that we could not see before, but people still have to check what it shows and decide what it means. A telescope finds things; the astronomer still has to check them, name them, put them in order and explain them. Mourrat [P5] suggests that mathematicians will become naturalists in this sense.

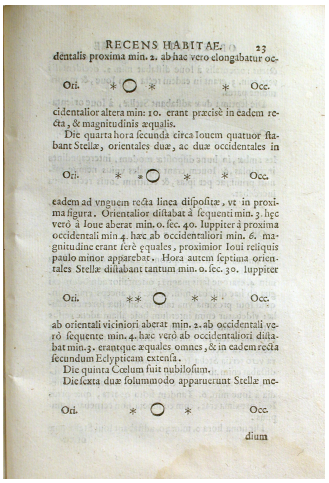
RECENS HABITAE. 23
dentalis proxima min. 2. ab hac vero elongabatur oc-
Ori. * ○ * * Occ.
cidentalior altera min. 10. erant præcisè in eadem re-
cta, & magnitudinis æqualis.
Die quarta hora secunda circa Iouem quatuor ſtabant Stellæ, orientales duæ, ac duæ occidentales in
Ori. * * ○ * * Occ.
eadem ad vnguem recta linea dispositæ, vt in proxima figura. Orientalior distabat à sequenti min. 3. hæc verò à Ioue aberat min. 0. sec. 40. Iuppiter à proxima occidentali min. 4. hæc ab occidentaliori min. 6. magnitudine erant ferè æquales, proximior Ioui reliquis paulo minor apparebat. Hora autem septima orientales Stellæ distabant tantum min. 0. sec. 30. Iuppiter
Ori. ** ○ * * Occ.
ab orientali viciniori aberat min. 2. ab occidentali verò sequente min. 4. hæc verò ab occidentaliori distabat min. 3. eranteque æquales omnes, & in eadem recta secundum Eclypticam extensa.
Die quinta Cœlum fuit nubilosum.
Die sexta duæ solummodo apparuerunt Stellæ me-
Ori. * ○ * Occ.
dium

Galileo, *Sidereus Nuncius* (1610): Jupiter (the circle) and its moons (the stars) on several nights.

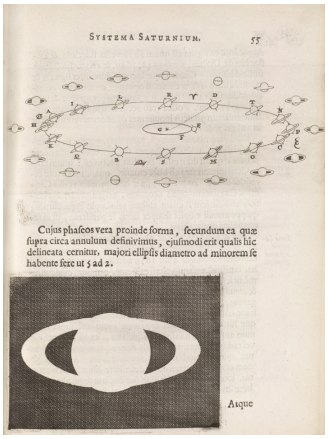
SYSTEMA SATURNIUM. 55
Cujus phaseos vera proinde forma, secundum ea quæ supra circa annulum definivimus, ejusmodi erit qualis hic delineata cernitur, majori ellipsis diametro ad minorem se habente fere ut 5 ad 2.
Atque

Huygens, *Systema Saturnium* (1659): Saturn's ring as seen from Earth around its orbit.

Scans: University of Oklahoma Libraries; Smithsonian Libraries. Public domain; see `media/historical-astronomy/`.

This book is also an experiment in how such mathematics can be checked, shared and understood. It has four parts: opening the arguments to community review, preserving the development and the failed attempts, distinguishing what has been checked, and asking what general ideas can be extracted from the work. The development, the writing and much of the checking were done with AI. We also use AI in the search for an explanation, as described below. Human understanding and public discussion remain aims of the experiment. The manuscript and its filtered development record are on GitHub. Each result has a row in a public table, and readers can check a proof, dispute it, repair it or explain it through a pull request, or extend the Lean verification and the tools behind the book. Every merged contribution is acknowledged by name, and a substantial contribution, to the mathematics, the Lean verification or the tools, leads to coauthorship of the next version. Help with de-slopping is especially welcome: turning AI-written arguments into ones a person can read and trust. And whether it is the mathematics or the methodology, we would be happy to see this work inspire your own. This is version 1.0.0 of the book. Later versions follow one rule, written in the repository: the last number changes for corrections of wording and form, the middle number for changes to the mathematics that leave the main theorems as stated, and the first number for a new version on arXiv, which comes with any change to a main theorem, a correction that affects one, or a substantially simpler proof. Similar proposals have appeared on the blog *Proofs and Prompts*: an open platform

where AI-generated results gradually acquire "collective mathematical confidence" on a "Git Hub" of proofs [P4], open work groups that explain important preprints in a Git repository [P11], a community-owned repository of AI proof reports [P12], teams of researchers who work to understand AI-generated proofs [P14], and credit for works at the level of a doctoral thesis, defended in public with open reviews [P10].

We also treat the development record as data for an experiment in doing mathematics with AI. The public repository preserves a filtered history: proof revisions, failed approaches with their reasons, Lean records, review summaries, selected original reports, and marked copies whose output format was repaired. It does not contain every reviewer input or response. Readers cannot reconstruct every earlier state from the public repository alone.

Withheld material includes other authors' texts and images, private model reasoning, system and account details, correspondence and planning notes, collaborators' unpublished work, assessments of other authors' manuscripts awaiting release review, and evidence archives. The redaction record gives the reasons. The original history and review records are retained privately. The released material lets readers trace the construction, criticism and repair it records, and study where the process failed. Several posts on *Proofs and Prompts* argue in the same direction: Kretschmer calls a detailed disclosure of AI use "a worthy scientific unit" [P7], Kaipel proposes that every interaction with AI that influenced a manuscript be recorded in full and made available [P8], Lewin [P12] compares AI proofs with experimental data released with documentation for others to analyze, and Gonen Cohen [P2] discusses releasing the full prompting history to improve reproducibility.

Review arguments themselves require checking: No-go 33 records three incorrect steps proposed in reviews and the calculations that exposed them.

We also treat an approach that does not work as a result. Chapter 12 gives numbered statements and proofs for the mathematical obstructions, explaining why each approach was attractive, where it fails and what it does not rule out. Readers can use these results without repeating the failed attempts. This echoes Morris's call for more accounts of failed attempts [P9], Duminil-Copin's account of how failed attempts on one conjecture brought him collaborators and ideas that he later used elsewhere [P3], and Tao's remark that negative results are rarely reported, so that what one hears about AI in mathematics is skewed towards success [43].

For the same reason, the book keeps its claims separate. Proved results, imported statements, conditional consequences and open questions are distinguished throughout. Lerario makes the same point about mathematics in general: it should always be clear how far a result has been checked, and an argument checked step by step by a proof assistant such as Lean should not have the same standing as a heuristic analogy [P13]. A review by a language model is a check, not a proof, and Lean checks only part of the book; two of the four main theorems are outside it. At the time of writing, the technical chapters have not yet been checked line by line by a human reader; the public table records how far each result has been checked.

What can we learn from the proof?

A long argument produced with AI leaves another task: to understand which ideas make it work and whether they can be used elsewhere. This book offers a small experiment in that direction. We ask Amy to return to the arguments she helped produce, including failed approaches, and to look for recurring constructions, indispensable assumptions and possible general principles. We use her proposals to guide further questions and checks. The aim is to involve AI in the search for an explanation as well as in the production of an argument. A proposed principle should explain why several steps belong together and help us treat a second problem with less repeated work; whether it does is for people to judge. Madore [P6] describes open problems as milestones toward understanding and new theories, and argues that understanding is a human activity that computers cannot perform for us. Lerario [P13], in "Qualitative growth" and "Continuity of research," discusses organizing separate results through common principles and allows that theories and research directions could originate in artificial systems.

Section 1.10 records the first candidates from this exercise. It separates the classical tools, the structure visible in this proof and the extensions that remain to be tested. The length of the computation does not establish that a new theory has emerged. The useful test is what the proposed principle explains, what hypotheses it needs and what it lets us do next.

A further aim is a much shorter proof. The argument in this book is long because it was built step by step: each obstruction was met by a new estimate, and each estimate was kept once it had been checked. Once the ideas that make the proof work are understood, many of these steps should merge or disappear. Several estimates may follow from one principle, some detours may turn out to be unnecessary, and the sharp constant may need only part of the present machinery. We expect this simplification to come after, and through, human understanding of the argument, with AI used to test each proposed shortcut against the full proof. No reduction in length is claimed in this version. Hairer makes a similar point: in digesting an argument produced by AI, one may well realize that it can be presented in a clearer and simpler way [P1].

How to read this book

The reader should have a background in graduate probability and analysis. Familiarity with Gaussian processes, Fourier analysis, Sobolev spaces and bounded operators will be useful, and the later chapters also use spectral theory and Young integration. A separate reading edition gives a short account of the model, the main statements and the proof strategy, with links to the detailed arguments here. Readers who want only the upper bound at the correct scale can read Chapters 1–2 and then Chapter 3. The proof of the sharp constant occupies Chapters 4–11. The guide to the proof after these front pages maps the dependencies, and each chapter opens with its purpose and the earlier results it needs. The appendices are not prerequisites for the main theorems. They keep low-order calculations, shorter estimates under additional assumptions, covariance comparisons

and an obstruction to a proposed clock representation, which show what a successful argument must retain. Chapter 12 gathers these and other obstructions by mathematical cause, with links back to the successful arguments. The final three appendices give the AI work in numbers (Appendix E), what Lean checks (Appendix F) and how far each result has been checked (Appendix G).

Where to find everything. The source and development record are in the book's repository at release 1.0.0. The verification ledger there records, for each numbered result, how far it has been checked and how a reader can check it. The Lean companion, at release 0.10.0 (DOI 10.5281/zenodo.24295453), is described in Appendix F.

`github.com/chenle02/stratonovich-ham-second-moment/tree/v1.0.0`
`github.com/chenle02/stratonovich-ham-second-moment/blob/v1.0.0/VERIFICATION.md`
`github.com/chenle02/stratonovich-ham-second-moment-lean/tree/v0.10.0`

Acknowledgements

We thank Robert Dalang, Aurélien Deya and Samy Tindel for their comments on an early unpublished version of this work, and Raluca Balan, Yaozhong Hu, Jian Song and Xiong Wang for their interest and correspondence.

The author was supported in part by the U.S. National Science Foundation under Grant DMS-2246850 and CAREER Grant DMS-2443823, and by Simons Foundation Collaboration Grant for Mathematicians 959981. We thank OpenAI for providing access to its AI tools through the ChatGPT for Academic Researchers program.

Le Chen, with Amy
Auburn, Alabama
November 2026

Posts from *Proofs and Prompts*

In the text these posts are marked [P1]–[P14]. They are listed here in order of date, not in the bibliography, and each title is a link to the post. They include proposals we try to put into practice and criticisms we seek to address; citing a post does not imply that its author endorses this experiment.

[P1] Martin Hairer, *Writing mathematics in the age of AI*, August 7, 2026.

[P2] Segev Gonen Cohen, *The question of reasoning traces*, August 11, 2026.

[P3] Hugo Duminil-Copin, *Care for a little more AI?*, August 30, 2026.

[P4] Marco Trombetti, *ProofForum: Keeping AI-generated mathematics human*, September 22, 2026.

[P5] Jean-Christophe Mourrat, *Why I chose to do math, and how I'm grappling with AI advances*, October 8, 2026.

[P6] David A. Madore, *Letter to a worried student*, October 20, 2026.

[P7] William Kretschmer, *On AI disclosures*, October 27, 2026.

[P8] Maximilian Kaipel, *Why and how to transparently disclose AI use in mathematics research*, October 28, 2026.

[P9] Patrick Morris, *Let's stop writing papers...*, October 30, 2026.

[P10] Andrew Ng, *A new system of accreditation*, November 1, 2026.

[P11] Alexander Van Werde, *Collaborative work groups on exposition problems*, November 1, 2026.

[P12] Mathieu Lewin, *Please STOP writing papers! (there is another way)*, November 2, 2026.

[P13] Antonio Lerario, *The shape of mathematical knowledge*, November 9, 2026.

[P14] Jonathan Noel, *I'm giving my theorems away*, November 10, 2026.

Abstract

Motivated by Xia Chen's moment conjecture [17, (1.22)], we determine the exact second-moment asymptotics through an intrinsic variational formula. We study the Stratonovich hyperbolic Anderson model with temporal covariance $|s-t|^{-\alpha_0}$ and an even, nonnegative, positive-definite tempered Radon spatial covariance Γ homogeneous of order $-\alpha$. We assume $d \in \{1,2,3\}$, $0 < \alpha_0 < 1$, $0 < \alpha < d$ or $\alpha = d = 1$, and $\alpha + \alpha_0 < 2$. For initial displacement one and velocity zero, our main result, Theorem 1.5.2, is the exact limit

$$\lim_{T\to\infty} T^{-\kappa} \log \mathbb{E}u^2(T,x) = C_2(\Gamma,\alpha_0), \qquad \kappa = \frac{4-\alpha-\alpha_0}{3-\alpha},$$

for every fixed $x \in \mathbb{R}^d$, with

$$C_2(\Gamma,\alpha_0) = \sup_{\substack{\Psi\in C_c^\infty((0,1)\times\mathbb{R}^d;\mathbb{R}) \\ \Psi\geq 0,\ \Psi\neq 0}} \left\{ 2\int_0^1 \sqrt{\mathcal{R}_\Psi(s)}\,\mathrm{d}s - \frac{v_\Psi}{2} \right\}.$$

Here the covariance mean, variance and Rayleigh value are

$$\begin{aligned} h_{\Psi,s}(x) &= \int_0^1 |s-r|^{-\alpha_0} (\Gamma * \Psi_r)(x)\,\mathrm{d}r, \\ v_\Psi &= \int_0^1 \int_{\mathbb{R}^d} \Psi(s,x) h_{\Psi,s}(x)\,\mathrm{d}x\,\mathrm{d}s, \\ \mathcal{R}_\Psi(s) &= \sup_{\substack{f\in H^1(\mathbb{R}^d;\mathbb{R}) \\ \|f\|_2=1}} \left\{ \int_{\mathbb{R}^d} h_{\Psi,s}(x) f(x)^2\,\mathrm{d}x - \|\nabla f\|_2^2 \right\}. \end{aligned}$$

The spatial norms are L^2 norms, and $\Psi_r = \Psi(r,\cdot)$. The variational class includes controls that do not separate in time and space. The formula retains the original covariance amplitude, kinetic coefficient one and Gaussian cost $v_\Psi/2$. Its value is positive and finite when $\Gamma \neq 0$; for $\Gamma = 0$, the solution is one and the constant is zero.

An independent upper bound establishes finiteness at the scale T^κ. The identification of the constant combines Gaussian phase operators, convergence from the regularized noise, estimates uniform in the spatial localization radius, and finite optimization with nonnegative Gram entries. We also obtain bounds for the same constant through spatial energies and occupation measures, including explicit bounds for spatial white noise in one dimension.

Contents

Preface **i**

Abstract **x**

Illustrations **xvii**

A guide to the proof **xix**

1 Introduction **1**
1.1 A guitar in a sandstorm: forty years since Walsh . . . 1
1.2 Model and standing assumptions . . . 3
1.3 Skorohod and Stratonovich wave equations . . . 7
1.3.1 The two products and their consequences . . . 7
1.3.2 White-in-time noise . . . 7
1.3.3 Time-independent noise . . . 9
1.3.4 Fractional temporal correlation . . . 10
1.3.5 Advantages, limitations and the present contribution . . . 10
1.4 What is known . . . 12
1.4.1 Stratonovich expansion and moments . . . 12
1.4.2 The universal two-chain bound . . . 13
1.4.3 Known moment bounds . . . 13
1.5 Main results . . . 14
1.6 Why the scale is t^{κ} . . . 16
1.7 Consistency checks . . . 17
1.8 Strategy of the proof . . . 18
1.9 Future work . . . 20
1.9.1 Higher moments and pointwise estimates . . . 20
1.9.2 Real orders and upper-tail deviations . . . 22
1.9.3 Compactness of optimizing controls . . . 23
1.9.4 Sharper bounds near the static case . . . 24
1.9.5 Logarithmic wavefields and possible scaling limits . . . 24
1.9.6 Rough noise beyond the present covariance class . . . 25
1.9.7 Exact first-moment asymptotics . . . 27
1.10 Toward a general variational method for random evolution equations . . . 28

2 Construction and two-chain estimates **30**
2.1 The complete two-chain expansion . . . 30
2.2 A small-order check and a source uniformity issue . . . 32
2.3 Recovering the quadratic-exponential bound . . . 33
2.4 A finite product bound for two ordered chains . . . 39
2.5 Spatial Wick measures and fixed-order construction . . . 44
2.6 The mild equation with the corrected bound . . . 50
2.7 What homogeneity recovers, and what the bound still loses . . . 55

3 An independent upper bound **57**
3.1 A static phase estimate at first variance order . . . 57
3.2 All static orders with arbitrary initial phase . . . 61
3.2.1 Finite Gaussian products and their degree cutoffs . . . 65
3.2.2 Uniform bounds for all orders . . . 65
3.3 Interval fields and the full upper bound . . . 70
3.3.1 Contractions and complex phase estimates . . . 70
3.3.2 Summing the coefficient bounds . . . 73
3.3.3 Finite Gaussian models and their terminal kernels . . . 85
3.3.4 Removing the regularization . . . 87
3.3.5 Temporal comparison and the full upper bound . . . 87

4 Covariance estimates and Gaussian approximation **93**
4.1 Covariance bounds for physically masked wave fields . . . 93
4.1.1 Translated spectral growth and physical masks . . . 94
4.1.2 Temporal completion and the original noise . . . 96
4.1.3 Temporal modulation and continuous wave factors . . . 99
4.2 Frequency estimates and both wave variance directions . . . 102
4.2.1 A scalar row estimate for a measure . . . 102
4.2.2 Forms on the full phase . . . 105
4.2.3 Bessel's inequality and the two variances . . . 108
4.2.4 Mean-square columns on the original probability space . . . 110
4.3 Finite Gaussian moments and whole-space Sobolev compactness . . . 111
4.3.1 Finite Gaussian matrices with both variance powers . . . 112
4.3.2 Whole-space cutoffs through an auxiliary periodic space . . . 115
4.3.3 Balanced adjoints and localized variance envelopes . . . 119
4.3.4 A nonzero witness and the need for a compact cutoff . . . 124

5 The original noise and operator paths **126**
5.1 The Gaussian operator path . . . 126
5.1.1 A test basis and explicit covariance coefficients . . . 127
5.1.2 Gain, adjoints and localization . . . 129
5.1.3 Finite variances and first Wiener chaos tails . . . 131
5.1.4 Interval limits on the given probability space . . . 134
5.1.5 Time-path convergence and Gaussian norm bounds . . . 136

5.2 Convergence of the regularized Gaussian operator paths 138
5.2.1 Gaussian transfer in the full path norm 139
5.2.2 The spatial covariance space and an extension preserving the given noise 141
5.2.3 Exact joint source law and convergence 143
5.2.4 Regularized random fields and the ordinary first response 145

6 Fixed masks and wave evolution **149**
6.1 Fixed masks and displacement moments 149
6.2 Young evolution with constant initial data 153
6.2.1 The distributional phase and its free evolution 153
6.2.2 The two columns for constant initial data 155
6.2.3 The exact linear Young equation 156
6.2.4 Ordinary source solutions and the original tested observable . . 160
6.3 Compact mean families and the spectral gap for wave evolution 164
6.3.1 The ground family and the global phase 164
6.3.2 The growing projection and its complementary wave evolution . 168
6.3.3 The original nonnegative control and a common trial 171

7 Scaling and the point lower bound **174**
7.1 Exact scaling of the canonical solution 174
7.2 Time blocks for the original noise and the pointwise lower bound 175
7.2.1 The common original noise and its exact Gaussian shift 176
7.2.2 Small noisy blocks and a cone in the displacement-velocity space 178
7.2.3 Source restart and comparison with the original point 182
7.3 The unmasked Rayleigh rate and nonnegative controls 188
7.3.1 Global bounds and the unmasked spectral bottom 189
7.3.2 Removing masks from the numerical lower rate 191
7.3.3 Full-class dilation and finite variational values for nonnegative controls 192

8 Spatial controls and Gaussian means **196**
8.1 The temporal equilibrium density 196
8.2 Physical spatial pairings and the full occupation class 198
8.2.1 The kernel row and full occupation energy 204
8.3 The compact mean and Cameron map on time blocks 206
8.3.1 Fractional products and the compact spatial map 206
8.3.2 The supported tensor and temporal mean 209
8.3.3 The noise residual and its Cameron operator 212
8.4 Young perturbations retaining the deterministic endpoint 215

9 Bounds as the spatial radius grows **217**
9.1 Mean and Cameron bounds uniform in the spatial radius 217
9.1.1 Uniform multiplier and spatial tails 218

9.1.2 Tensor products and mean approximation 220
9.1.3 The block Cameron embedding for the given noise 222
9.2 Bounds for the operator path with explicit radius dependence 224
9.2.1 Uniform outer factors and the exact whole-space envelope . . . 225
9.2.2 The operator path and covariance contractions 227
9.2.3 The growing-radius expected-norm anchor 229
9.3 Signed rough static potentials and the physical wave 230

10 Gaussian estimates for the point upper bound 235
10.1 The symplectic form and mean evolution on time blocks 235
10.2 Gaussian enlargement and the Rayleigh comparison 242
10.2.1 The Wiener-space realization 242
10.2.2 Closed Gaussian enlargements and the quadratic cost 244
10.2.3 The wave tuple and its globally defined endpoint 246
10.2.4 Uniform coarse envelope and the exact radial integral 248
10.3 Uniform spectral rates and phase products 250
10.3.1 The operator class on E and its spectral constants 251
10.3.2 Scalar-time averaging and mean bounds 254
10.3.3 Full blocks, the true last cell and polynomial control balls 256
10.3.4 Arbitrary small residual paths and the ordered product 258
10.4 The original point moment and the growing-cone phase 259
10.5 An upper bound from a signed variational expression 265

11 The constant and its consequences 270
11.1 Finite optimization with nonnegative Gram entries 270
11.2 A variational formula for the second-moment limit 275
11.3 Occupation bounds for the intrinsic constant 282
11.4 Spatial white noise: energy and explicit moment bounds 287
11.5 Established steps and open questions 290

12 Obstructions and failed approaches 291
12.1 How to read the negative results 291
12.2 Pairings, ordering, and comparison kernels 293
12.2.1 NG-01: one common estimate loses a factorial power 293
12.2.2 NG-02: a single adjacent diagram is too large 294
12.2.3 NG-03: a squared-mean comparison fails 295
12.2.4 NG-04: constants near the time boundary 296
12.2.5 NG-05: chronological merging breaks wave support 297
12.2.6 NG-06: erasing geometry before summation loses the scale . . . 299
12.2.7 NG-07: block labels are not chronological ranks 299
12.2.8 NG-10: crossing covariance survives merging 300
12.2.9 NG-17: direct copying of the first-moment clock undercounts . . 301
12.2.10 NG-18: an oversized middle-cross envelope 302
12.3 Covariance transformations and their limits 304

12.3.1 NG-08: the translated spatial maximum . . . 304
12.3.2 NG-09: radial lowering in three dimensions . . . 305
12.3.3 NG-11: additive variance interpolation . . . 306
12.3.4 NG-12: a heat–Mellin square need not be locally finite . . . 307
12.3.5 NG-13: angular smoothing and isotropic envelopes . . . 308
12.3.6 NG-19: discarding an independent Gaussian residual . . . 309
12.4 Phase propagation and Gaussian controls . . . 311
12.4.1 NG-14: scalar moments do not compose across blocks . . . 311
12.4.2 NG-15: the missing second-order mean term . . . 313
12.4.3 NG-16: replacing a tilted mean by a deterministic value . . . 314
12.4.4 NG-20: covariance profiles need not separate . . . 315
12.4.5 NG-31: initial phase and the backward cone . . . 316
12.5 Topology, localization and limits of variational arguments . . . 316
12.5.1 The first driver cannot always be Hilbert–Schmidt . . . 317
12.5.2 A physical mask may not act on the noise quotient . . . 320
12.5.3 Frequency decay does not give whole-space compactness . . . 320
12.5.4 Fixed projections do not control growing spatial masks . . . 321
12.5.5 Two distinct limitations of block costs . . . 322
12.5.6 Concentrating temporal controls restrict integrability . . . 323
12.5.7 Pointwise convergence does not pass through a supremum . . . 324
12.5.8 A cutoff point feature can lie outside the raw-noise image . . . 324
12.6 Finite optimization and checks on review arguments . . . 326
12.6.1 NG-23: both Gaussian variance directions . . . 327
12.6.2 NG-28: the normalization matters when bounds are compared . . . 327
12.6.3 NG-29: three safeguards in the Gram optimization . . . 329
12.6.4 NG-33: check the mathematics returned by a reviewer . . . 330

A Finite-order calculations **332**
A.1 Finite-order checks in one space dimension . . . 332
A.1.1 Spatial white noise: all order-four diagrams . . . 332
A.1.2 Riesz covariance: order two and an order-four integral . . . 336
A.1.3 Calibration table and limits of the finite-order test . . . 338

B Direct upper bounds and static interpolation **339**
B.1 Upper bounds for spatial exponents at most one . . . 339
B.1.1 A spatial bound retaining the ordered increments . . . 340
B.1.2 Summing temporal pairings before using time ordering . . . 341
B.1.3 Spectral bounds for $0 < \alpha \leq 1$ in all three dimensions . . . 343
B.1.4 Checks on the scale, constants and scope . . . 347
B.2 Higher spatial exponents under a convolution bound . . . 348
B.3 Riesz bounds by interpolation with static noise . . . 354

C Covariance comparisons in higher dimensions **359**
C.1 General homogeneous covariance in dimension two . . . 359
C.2 Three-dimensional bounds from covariance endpoints . . . 366
C.3 Physical and spectral energy for measure covariances . . . 379

D Static comparisons and the clock obstruction **382**
D.1 A static lower comparison and a near-static mean gap . . . 382
D.1.1 Temporal interpolation of the full moment . . . 388
D.2 A small-order test for direct Brownian clock copying . . . 391

E The AI work in numbers **397**

F What Lean checks **408**
F.1 How to read the entries . . . 408
F.2 How the match with the book was reviewed . . . 409
F.3 How the Lean package was checked . . . 411
F.4 The results . . . 411
F.4.1 Formalized with the paper's own hypotheses; nothing supplied . 411
F.4.2 With the paper's hypotheses; Lean proves a narrower conclusion 413
F.4.3 Every conclusion proved; named analytic inputs supplied as hypotheses . . . 415
F.4.4 Steps checked, not the result itself; analytic inputs either supplied as hypotheses or left outside Lean . . . 415
F.4.5 Not formalized . . . 425
F.5 Counts and growth . . . 426

G How far each result has been checked **428**
G.1 What the main theorems rest on . . . 429

Bibliography **438**

Working words and common misreadings **441**

List of notation **443**

Subject index **449**

Illustrations

1.1 A guitar in a sandstorm . . . 1
1.2 Chapter and appendix roadmap . . . 5
1.3 Two meanings of the noise product . . . 8
1.4 Source-qualified literature comparison . . . 11
1.5 The exponent κ against the temporal exponent . . . 16
1.6 Proof dependencies and destinations . . . 19
1.7 Regular, white and rough noise in one dimension . . . 26

2.1 Pairings of two ordered chains . . . 32
2.2 Endpoint elimination in two ordered chains . . . 43
2.3 The order of construction limits . . . 49

3.1 Exact cutoffs for selected Gaussian words . . . 66
3.2 The noise remembers across time blocks . . . 68
3.3 Degree splits and pair-count allocations . . . 75
3.4 One phase-norm charge at each interval end . . . 78
3.5 Cross-color subsets and chronological regions . . . 81
3.6 Three shifted interval grids . . . 92

4.1 A physical mask as a window on the potential . . . 94

5.1 The original and auxiliary Gaussian noises . . . 143

7.1 Correlated blocks and one Gaussian cost . . . 184
7.2 Controls that need not factor . . . 188

8.1 From a Gaussian control to the wave it drives . . . 196

10.1 Gaussian enlargement by an image of a Hilbert ball . . . 245
10.2 Finite propagation and spatial cutoffs . . . 265

11.1 Minimize within each subset, then maximize over subsets . . . 273
11.2 Positive combinations and singular Gram matrices . . . 273

12.1 What lies below the waterline . . . 292
12.2 Merging two chains can violate wave support . . . 298
12.3 Velocity survives a block boundary . . . 313
12.4 Escape from a fixed spatial projection . . . 322
12.5 The point feature and the closed noise image . . . 326

A.1 The rectangle and strip in the fourth-order calculation 334

E.1 The work day by day, with milestones 407

A guide to the proof

The reading edition states the main results and explains the route through this volume. The chapters below supply the proofs in their dependency order. The appendices retain the direct estimates, finite-order calculations and alternative approaches, together with their original hypotheses and limitations. They are useful comparisons; they are not all inputs to the main argument. Each chapter opens with its motivating question, the earlier definitions or results needed to enter it, and an outline of the argument. Readers may use these openings to choose a starting point and follow the linked prerequisites when needed.

How much to read depends on the time at hand.

Time	What to read
Ten minutes	The two main theorems in Section 1.5, the reason for the exponent in Section 1.6, and the map in Figure 1.2.
One evening	The reading edition, or Chapter 1 followed by the opening of each later chapter. The first two videos cover Chapter 1.
The full proof	Chapters 2–11 in order. Each opening says which results to keep and which proofs can wait on a first reading.

Lemma 2.2.1 gives concrete variance and mean calculations. No-go 05 shows geometrically why merging two chains can violate wave support.

Chapters	Purpose
1–2	Model, literature and construction of one solution.
3	A finite upper bound at the correct time scale.
4–6	Covariance estimates, operator paths and wave evolution.
7	Exact scaling and the lower bound for fixed controls.
8–9	Spatial means and estimates uniform in the localization radius.
10–11	The point upper bound and the variational constant.
12	Obstructions and failed approaches: every mathematical no-go, and what it does not rule out.
A–D	Other estimates, consistency checks and alternative approaches.
E	The AI work in numbers: who did the work, the reviews, and how many approaches failed.
F	What the Lean companion checks, result by result.
G	How far each result has been checked: by AI review, by Lean and by people.

Figure 1.2 gives a map of all twelve chapters and the four mathematical appendices. The reader links to the labelled statements in this companion. The numbering includes the chapter and section, so a statement can be located without searching the entire volume. The figures are explanatory schematics; their captions identify the precise results and the limits of the drawings.

Video introduction. An introduction to this book in eleven videos, each about twenty minutes and narrated by a synthetic voice, is on YouTube at `https://www.youtube.com/playlist?list=PLWiXjeUrQ62k`. We made the series with Amy: she drafted the scripts and animations from this book, every displayed formula is copied from the statement that carries its label, and each script was reviewed against the manuscript by a model family different from the one that drafted it. The table lists what each episode covers; each episode number is a link, and the red badges in Figure 1.2 lead to the same videos. Episodes 1–10 follow the draft at version `38d67ec` and episode 11 the draft at version `0f553e08`, so statement numbers quoted in them may differ from this version. The videos explain the argument; they are not part of it or of its review.

Ep.	Title	Covers
▶ 1	A guitar in a sandstorm	Chapter 1: the model, its history, the exponent κ.
▶ 2	The answer: a growth rate and a variational constant	Chapter 1: the two main theorems and the constant.
▶ 3	Two chains and their pairings	Chapter 2.
▶ 4	The correct time scale	Chapter 3.
▶ 5	A Gaussian toolkit for wave fields	Chapters 4–6.
▶ 6	The lower bound: steering the noise	Chapters 7–8.
▶ 7	The upper bound: no control does better	Chapters 9–10.
▶ 8	The constant and what it tells us	Chapter 11 and the open questions of Chapter 1.
▶ 9	Roads not taken	Appendices A–D.
▶ 10	How this book was written	The preface and Appendices E–G.
▶ 11	Approaches that do not work	Chapter 12.

Chapter 1

Introduction

A wave is driven by a random force that remembers its past. How fast can its second moment grow? The answer depends on the covariance and on what the stochastic product means. This chapter introduces the Stratonovich model and states the answer in two parts: the scale of the growth, and the constant at that scale. Both parts hold in space dimensions one, two and three.

We begin with a guitar in a sandstorm (Figure 1.1) and a short history. Section 1.2 states the model, the covariance and the initial data. Section 1.4 records what was known, including the difference between the author and arXiv versions of the source. Section 1.5 states the two main theorems, and Section 1.6 explains the scale. Figure 1.2 maps the rest of the book.

No earlier chapter is needed. On a first reading, the literature comparison in Section 1.3 and the outlook in Sections 1.9 and 1.10 can wait. A reader entering later should start with the model and initial data in Section 1.2, Hypothesis 1.2.1 and the exponent in (1.2.4). Episodes ▶ 1 and ▶ 2 of the video series follow this chapter. The series retells the book in eleven short episodes, and each chapter guide names its episode.

1.1 A guitar in a sandstorm: forty years since Walsh

Imagine leaving a guitar outside during a sandstorm. Each grain gives a string an unpredictable impulse. The string carries the disturbance away, while new grains strike elsewhere. How can we describe the motion when the individual impacts are too numerous to follow? Walsh used this picture to introduce a stochastic wave equation in his Saint-Flour lectures, delivered in 1984 and published in 1986 [47, p. 282, (1.14)]. Forty years after their publication, the picture still provides a useful way into the subject. We take these lectures as a starting point for this account. Earlier work on stochastic wave equations lies outside its scope.



Figure 1.1: AI illustration by Le Chen, SPDE-Visuals. CC0 (public domain). Not a simulation.

1986: from random impacts to a mathematical equation. A physical guitar has finite strings and endpoints, but Walsh makes a deliberate simplification in the worked example: the string is infinite and initially at rest, so boundary conditions do not obscure

the random forcing. Centering the impacts and replacing their fluctuations by space-time white noise gives an additively forced wave equation. The differential notation is suggestive, but the solution need not possess the derivatives appearing in it. The integral formulation gives the equation its meaning. We must first specify what we mean by a solution and the space in which it is defined. The guitar is a motivation for this model, not a derivation of every stochastic wave equation considered below.

1999: how far does the integration theory reach? The one-dimensional string is only the beginning. In higher dimensions the wave propagator may itself be a measure, and spatially correlated noise calls for a wider integration framework. Dalang's extension of the martingale-measure integral [24] made it possible to treat SPDEs with more singular Green kernels under spectral integrability conditions. The question now includes the interaction of propagation, spatial dimension and noise covariance. These conditions determine whether the equation admits a random-field solution.

The 2000s and 2010s: from existence to growth. Once a solution is available, we can ask how its fluctuations develop over long times. Multiplicative noise changes the problem: the forcing depends on the current solution, so the disturbance and its random environment interact. Moments measure the size of the fluctuations and the contribution of rare, large values. Dalang–Mueller–Tribe [26] developed probabilistic moment representations using Poisson processes and random flights. Dalang–Mueller [25] obtained intermittency estimates for a three-dimensional model under their spatial covariance assumptions. These results illustrate how the wave equation has its own probabilistic methods, while the form of the noise continues to matter.

For one-dimensional space-time white noise, Chen–Dalang [12] developed moment bounds and explicit second-moment formulas, including rough initial data. Temporally correlated forcing brings another change: random impacts at distinct times are no longer independent. Balan–Conus [4] studied the resulting Skorohod moment growth under their covariance assumptions. For white-in-time noise, Balan–Song [7] related hyperbolic and parabolic second-moment Laplace transforms and obtained an actual second Lyapunov limit in their Riesz case. Construction, bounds of the correct growth order and exact limits are successive questions, but a theorem answering one need not answer the others.

The 2020s: exact rates and the meaning of multiplication. The same formal multiplicative equation can describe different stochastic models. Skorohod integration uses Wick products; ordinary Stratonovich approximation retains the self-contractions generated by multiplication of smooth Gaussian fields. This distinction is central when the noise is static or correlated in time. For time-independent Skorohod noise, Balan–Le Chen–Xia Chen [3] obtained exact moment asymptotics. Chen–Eisenberg [13] treated a related fractional differential family, with time order below two and static noise. Chen–Guo–Song [14] obtained exact second moments for a white-noise fractional SPDE family and matching higher-moment growth orders in its wave specialization. The latter are growth orders, not sharp higher-moment constants.

On the Stratonovich side, Balan [2] constructed static-noise solutions and compared chaos expansions, while Xia Chen–Hu [20] established static homogeneous moment asymptotics. For fractional temporal correlation, Xia Chen's author version [17] gives two-sided first-moment bounds and a coarse second-moment upper bound. The source editions and all model, data and normalization restrictions are detailed in Section 1.3.

The present question. These works lead to three questions. How do we construct a solution? At what rate do its moments grow? Can we identify the leading constant? Our problem is the second moment of a multiplicative Stratonovich wave equation with fractional temporal correlation and homogeneous spatial covariance. We give an upper bound at the correct scale and a variational expression for the second-moment limit. We do not obtain a numerical closed form or a sharp formula for every moment order. The scientific review status is recorded separately. The following sections specify the model and explain why its self-pairings and correlated forcing require more than a transfer of the Skorohod results.

1.2 Model and standing assumptions

We study the hyperbolic Anderson model [17, (1.1)]

$$\frac{\partial^2 u}{\partial t^2}(t,x) = \Delta u(t,x) + \dot{W}(t,x)u(t,x), \qquad u(0,x) = 1, \quad \frac{\partial u}{\partial t}(0,x) = 0, \tag{1.2.1}$$

for $(t,x) \in \mathbb{R}_+ \times \mathbb{R}^d$, $d \in \{1,2,3\}$, interpreted in the Stratonovich sense (limit of classical wave equations driven by smoothed noises $\dot{W}_{\epsilon,\delta}$). The noise is centered Gaussian with

$$\operatorname{Cov}\left(\dot{W}(s,x), \dot{W}(t,y)\right) = |s-t|^{-\alpha_0}\gamma(x-y), \qquad 0 < \alpha_0 < 1, \tag{1.2.2}$$

where $\gamma \geq 0$ is nonnegative definite with spectral measure μ.

Hypothesis 1.2.1 (Homogeneous covariance)**.** Let $d \in \{1,2,3\}$ and $0 < \alpha_0 < 1$. The spatial covariance is a nonnegative, even, positive-definite tempered Radon measure Γ on $\mathbb{R}^d$, with positive even tempered Radon spectral measure μ in the convention

$$\Gamma = \int e^{i\xi\cdot x}\mu(\,\mathrm{d}\xi) \quad \text{in the sense of tempered distributions.}$$

The symbol γ in (1.2.2) denotes this covariance as a function when one exists, and as a distribution otherwise. For every Borel set A and $c > 0$, $\Gamma(cA) = c^{d-\alpha}\Gamma(A)$, and

$$\alpha_0 + \alpha < 2, \tag{1.2.3}$$

with $0 < \alpha < d$, or $\alpha = d = 1$. In particular, the last case includes spatial white noise $\Gamma = \delta_0$.

Zero covariance. Hypothesis 1.2.1 allows $\Gamma = 0$ by design. In this case the centered Gaussian noise is $\dot{W} = 0$, and the solution with initial data $(1, 0)$ is $u(t, x) = 1$. Thus $\mathbb{E}|u(t, x)|^p = 1$ for every $p > 0$, and all normalized logarithmic moment rates are zero. Results asserting strict positivity of covariance-dependent quantities impose $\Gamma \neq 0$ locally.

Throughout we write

Lean full

$$\kappa := \frac{4 - \alpha - \alpha_0}{3 - \alpha} \in (1, 2). \tag{1.2.4}$$

Contribution of the present work. We address the second moment of the original Stratonovich solution with fractional temporal covariance throughout Hypothesis 1.2.1. The independent upper bound reaches the scale t^κ, rather than only the coarse quadratic exponential scale in the source. The main identification gives an intrinsic variational expression for the limiting constant over all nonnegative smooth compact spacetime controls, without a separability restriction. It retains the covariance amplitude, kinetic coefficient one and a Gaussian cost equal to one half of the variance, and includes the zero covariance case. The upper and lower comparisons refer to the same canonical solution. The occupation and spatial-energy estimates then give bounds on this constant; evaluating the white spatial energy is not a numerical evaluation of the full moment supremum. The earlier results discussed below concern different stochastic interpretations or temporal covariances and do not supply this identification by substitution.

Figure 1.6 summarizes the main dependencies and identifies the results used at each step. Figure 1.2 places these steps within the chapters and distinguishes the auxiliary appendices.

Main result and dependencies. Theorem 11.2.6 identifies the original point-moment limit for every covariance in Hypothesis 1.2.1. Its full variational domain and normalization are displayed in (11.2.9). Theorem 11.3.4 and Corollary 11.3.5 give derived bounds; Section 11.4 evaluates the white spatial energy and its resulting moment bounds. These bounds need not be attained at the moment constant.

The independent earlier Theorem 3.3.8 establishes finite upper growth at scale t^κ and precedes its uses proving variational finiteness. It uses the fixed-order construction proved in Lemma 2.5.2, the Gaussian and complex phase estimates in Sections 3.1–3.2, and the interval coefficient and bounds for the finite family of time intervals in Section 3.3. It does not use the alternative covariance interpolation arguments in Sections B.2–C.3 as inputs. Its uniform geometric tail is proved here from scaled finite-model moments; the older mixed-series and crude estimates in Chapter 2 are not needed for that moment-limit passage. The separate verification of the mild equation is proved in Proposition 2.6.2, using the corrected vertexwise bound of Lemma 2.6.1. The alternative arguments are retained to record their separate hypotheses and limitations. Section B.1 also gives explicit constants for $\alpha \leq 1$; the full-class theorem asserts a finite uniform constant, without giving a numerically optimized value. The later proof constructs the operator and regularized noises preserving the original noise in Sections 5.1–6.2, then proves the same-solution lower bound and positive-control variational expressions in Sections 7.2–7.3. The Gaussian upper argument culminates in Sections 10.4–10.5. Finite Gram optimization

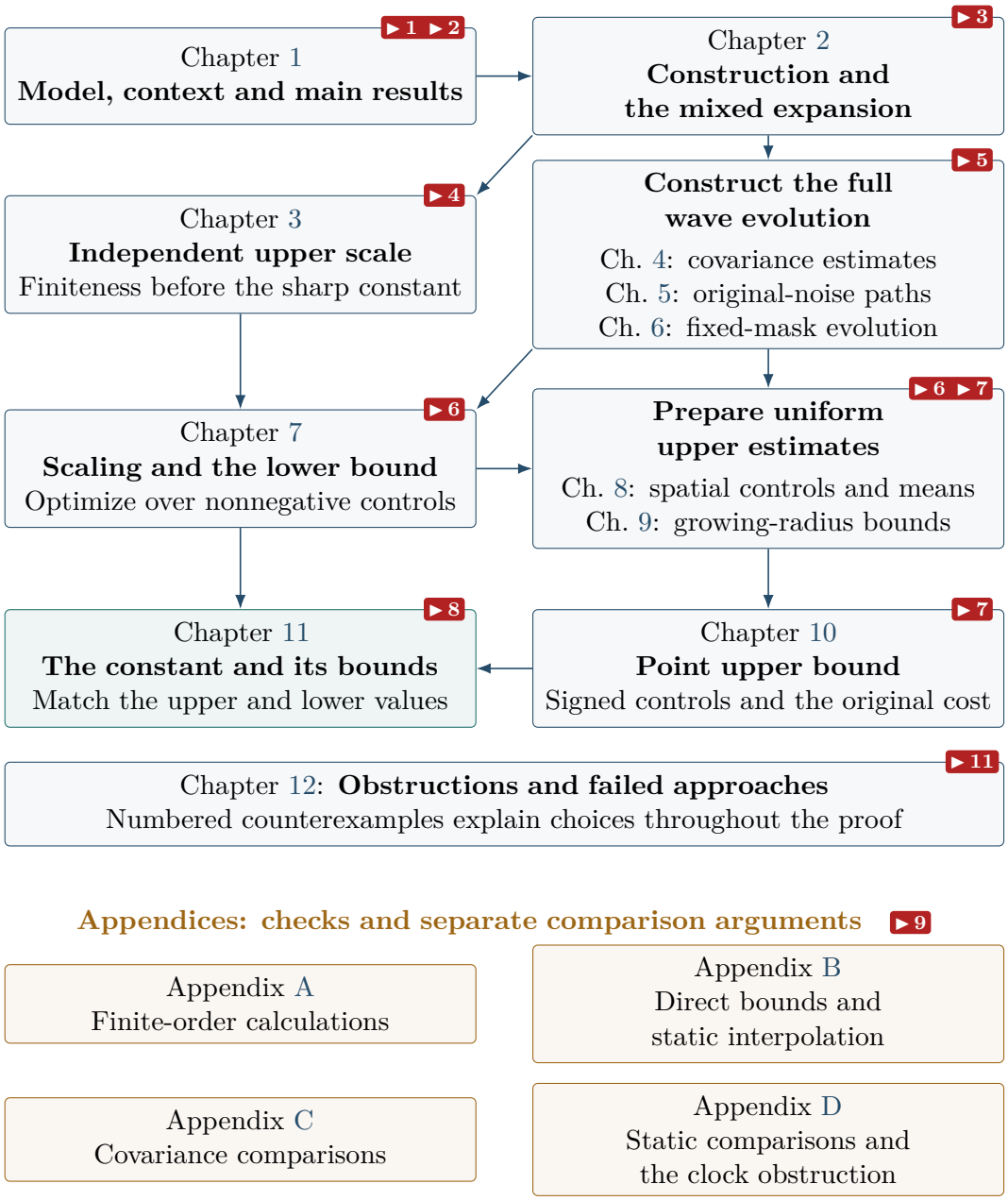

Figure 1.2: A reading map for the whole book. Blue arrows select principal inputs, not every dependency. In particular, the independent upper scale supplies finiteness for the variational lower value, which is also used in the spatial estimates. The upper argument retains the earlier wave construction and the radius estimates; it does not follow from the lower bound alone. The green box joins the two moment bounds. Chapter 12 explains failed alternatives to these steps. Gold boxes identify auxiliary checks and comparisons with their own hypotheses. No arrow from an appendix into the main proof is asserted. Every chapter and appendix label is a link to its opening guide. Red badges link to the episodes of the video introduction that cover each box; the table in the guide to the proof lists them.

and its physical application then match the upper and lower values in Section 11.2. This dependency order does not use that final identification to prove its own finiteness.

Notation and source-dependent statements. The target spatial degree is α, whereas χ denotes the degree of an auxiliary static covariance in Sections B.3–C.3. The coefficient power is $\beta = 4 - \alpha - \alpha_0$; the factorial power in Section 3.3 is $\nu = 3 - \alpha$. The local exponent $b = 2 - \alpha$ in Section B.1 is different from coordinate powers b_j in Section C.2. In Section B.2, $\delta = \alpha - 1$ is an exponent; when used for temporal noise smoothing, δ is a cutoff width. The covariance measure $\Gamma(\,\mathrm{d}x)$ and the Euler Gamma function $\Gamma(q)$ are distinguished by their arguments. The local $p = 2 - \alpha_0$ in Section 3.3 is an interval-length decay exponent; it is not the moment order p in Conjecture 1.4.3. The unconditional first-to-second moment comparison is Proposition 1.4.4. Any numerical consequence involving the source's L_* explicitly assumes a valid first-moment lower bound with that constant. No correction of its printed normalization is adopted. When a radius is given for topological support, the closed ball is meant unless a strict open inclusion is specified. In particular, the spatial cutoffs have support in $\overline{B}_{2R}$ and the wave Green measures have support in $\overline{B}_t$, including the sphere measure in dimension three. Plateau and causal-cone arguments retain their strict margins.

Which source statements are inputs. The moment estimate uses the bounded-operator Crouzeix–Palencia theorem in (3.2.1). The fixed-order construction is supplied here by Lemmas 2.5.1–2.5.2, using Lemma 2.4.1, which proves the finite product envelope used here, and the direct norm bounds in Lemma 2.3.1. The Case 2 covariance step is proved independently in Lemma 2.3.2; the precise source-display qualifications and regularized application are in Remark 2.3.3. Thus, neither Theorem 4.1 nor Lemma 4.4 nor Appendix A.1 of the source is an analytic construction input. The finite-width Gaussian field and multiple Stratonovich integral use its definitions and regularization conventions, with Green smoothing removed before noise smoothing.

Proposition 2.6.2 proves that the resulting series satisfies its onefold Stratonovich mild equation, using the corrected vertexwise bound. It does not import the author's Section 5(ii) argument or (5.3)–(5.4). No uniqueness assertion is made. The uniform tail passage for the target-scale moment estimate is proved in Lemma 3.3.7, independently of the crude bound and the source's series estimate. The mixed-width and order-limit passages for the mild equation are supplied here as well.

The first-moment formulas in Theorem 1.4.1 are quoted source statements, with the printed-normalization qualification there; they are not premises of the full upper theorem. Chen–Hu's static coefficient estimates and Chen's 2023 variational finiteness theorem are used only in the explicitly identified auxiliary sections. In particular, our uses of the latter cite Theorem 1.1, not Corollary 1.2. Thus, neither a disputed first-moment constant nor an auxiliary static coefficient theorem enters the interval-field upper bound.

1.3 Skorohod and Stratonovich wave equations

The meaning of the noise product is part of the model. The same formal wave operator and covariance do not specify the same equation under the Skorohod and Stratonovich interpretations. We review both interpretations below, separating existence results, moment-growth bounds and exact asymptotics. All comparisons retain the hypotheses of the cited papers.

1.3.1 The two products and their consequences

The Skorohod integral is the divergence operator of Malliavin calculus. For the linear equation with deterministic initial data, its iterated integrals form orthogonal homogeneous Wiener chaoses. In the convergent expansion, every positive-order term has mean zero, so the mean solution is the deterministic free wave. Orthogonality reduces its second moment to a sum of squared chaos norms. For adapted integrands and white-in-time noise, this interpretation agrees with the Itô integral in the corresponding integration framework; see Walsh [47] and Dalang [24]. Temporal correlation removes the martingale structure, even when the Skorohod integral remains available.

The Stratonovich construction considered here takes ordinary products of regularized Gaussian noise and then removes the regularization. Wick's formula retains contractions within an iterated term as well as contractions between different terms. These self-pairings change the mean; terms of unequal iteration orders can contribute to the second moment. This is why the Skorohod second-moment isometry does not directly solve the present problem. It does not mean that a Stratonovich solution has no orthogonal chaos expansion: trace terms can be regrouped into Wiener chaoses, as in Balan [2]. The iteration order and the final Wiener chaos order are different indices.

For regular noise, ordinary multiplication connects the equation to deterministic wave evolution in a random potential. Stratonovich models are therefore natural for specified smooth-noise approximations. For singular noise, convergence, the approximation scheme and any required counterterms must be proved. There is no universal conversion formula that identifies the two wave equations. In particular, an adapted white-in-time Skorohod solution being an Itô solution does not identify it with an unspecified smooth-noise limit. The three-dimensional approximation analysis of Delgado-Vences–Sanz-Solé [27] shows why regularization requires care.

1.3.2 White-in-time noise

White-in-time wave equations provide a useful starting point because adapted stochastic integration is available. Conus–Dalang [21] develop constructions in higher dimensions under their noise and initial-data assumptions. Dalang–Mueller–Tribe [26] obtain Feynman–Kac-type representations using Poisson processes and random flights. Thus, the absence of the usual Brownian heat-equation representation does not imply the absence of all probabilistic moment representations for wave equations.

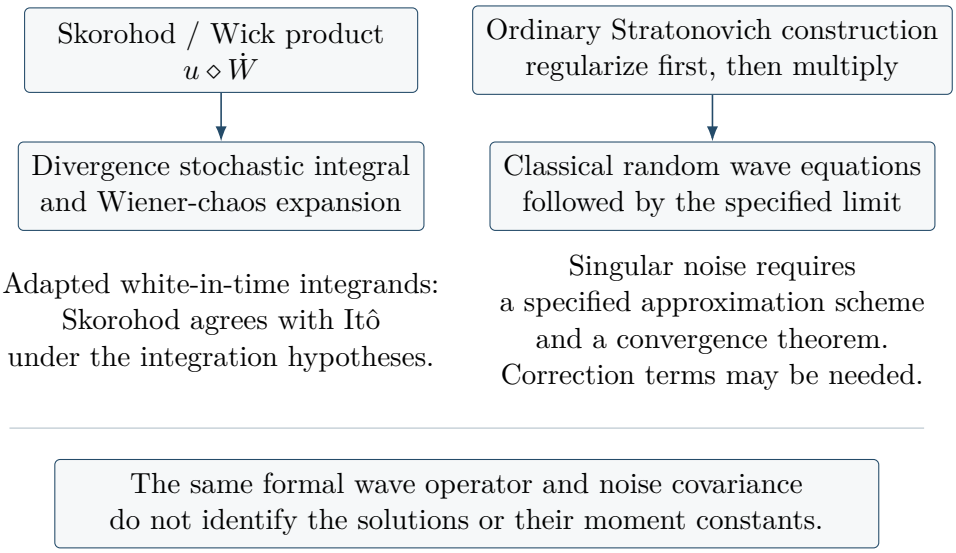

Figure 1.3: The stochastic product is part of the model. The arrows run only within each construction; there is no conversion arrow between the columns. For the linear Skorohod equation with deterministic data, iteration order agrees with orthogonal chaos order. Ordinary Stratonovich iteration retains self-contractions and unequal-order moment terms, although the final solution can still be regrouped into orthogonal Wiener chaoses. See Balan [2] for a comparison of the expansions. An adapted Itô identification does not identify an unspecified smooth-noise approximation.

Chen–Dalang [12, Theorem 2.3 and Corollary 1.1] derive moment bounds and explicit second-moment formulas for the one-dimensional space-time white-noise equation, including rough initial data. Chen–Guo–Song [14, Theorem 1.1] study a fractional SPDE family driven by space-time white noise. Their second moments and second Lyapunov exponents are explicit. Their wave specialization gives matching upper and lower $p^{3/2}$ moment-growth orders under the stated data conditions [14, Proposition 5.10; (1.10)–(1.11), pp. 4257–4258]. The higher-moment constants are not optimal, and these bounds do not assert an exact higher-moment leading constant or a general higher-moment limit.

Balan–Song [7, Theorems 1.1 and 1.3] relate the second-moment Laplace transforms of hyperbolic and parabolic Anderson models. Their general result identifies an upper second Lyapunov exponent; their Riesz specialization proves an actual limit. These conclusions should not be interchanged. In three dimensions with a different spatial covariance class, Dalang–Mueller [25] establish upper and lower moment-growth bounds of order $p^{4/3}$, with the lower bound at even orders and with separate hypotheses on the two bounds. The power of the moment order therefore depends on the spatial covariance, not only on the word "wave".

Rough spatial noise is another distinct direction. Balan–Jolis–Quer-Sardanyons [5] treat one-dimensional spatial fractional noise with Hurst index between $1/4$ and $1/2$; Liu–Hu–Wang [37] develop nonlinear well-posedness in this range under their coefficient assumptions. Such distributional spatial covariances are outside the nonnegative spatial-measure class of the present paper. Their results do not extend the scope of Hypothesis 1.2.1 by analogy.

1.3.3 Time-independent noise

For the static Skorohod equation with initial data $(1, 0)$, Balan–Le Chen–Xia Chen [3, Theorem 1.6] obtain exact large-time and high-moment asymptotics with a variational constant. Their homogeneous spatial covariances cover dimensions at most three; their global spatial white-noise case covers dimensions one and two. Three-dimensional white noise belongs to a separate finite-time discussion, not this global large-time assertion. Chen–Eisenberg [13, Theorems 1.6–1.7] study fractional differential operators with static Skorohod noise. Their time order lies strictly below two. Fractional time differentiation is distinct from temporal correlation of the noise and does not silently include the ordinary wave endpoint.

For ordinary static Stratonovich products, Balan [2] constructs solutions in dimensions one and two under a spectral condition stronger than Dalang's condition, and gives both a probabilistic representation and a comparison of chaos expansions. Xia Chen–Hu [20] treat dimensions at most three under Dalang's condition and establish homogeneous moment asymptotics at positive integer orders. Their published variational expressions require the normalization qualifications recorded in this manuscript; we do not import a numerical white-noise constant from them.

There is a concrete difference in admissible roughness for these unrenormalized static constructions. For the common flat data and homogeneous function covariances, the Skorohod range in the preceding exact-asymptotics result allows spatial homogeneity expo-

nent below three, subject to its dimension restriction, whereas the ordinary Stratonovich range requires exponent below two. This comparison concerns those solution classes. Renormalized Anderson-Hamiltonian wave equations, such as those in Gubinelli–Ugurcan–Zachhuber [32], are a related but different construction; their existence does not identify an ordinary Stratonovich product with a Skorohod product.

1.3.4 Fractional temporal correlation

On the Skorohod side, Balan–Song [6] develop the space-time homogeneous Gaussian-noise construction. Its higher-dimensional statements have additional spectral hypotheses, including absolute continuity of the spectral measure in the relevant results. Xia Chen–Deya–Song–Tindel [19] sharpen the spectral solvability analysis. For homogeneous spatial covariance and temporal singularity exponent α_0, the resulting noise threshold is $\alpha + \alpha_0 < 3$, under the paper's stated data conditions. The sufficiency statement in dimensions two and three imposes Fourier integrability on the initial displacement; the necessity statement uses a positive lower bound on the free wave. These are different hypotheses and directions, not an unconditional common-data equivalence with the present construction. The static endpoint also needs separate treatment.

Balan–Conus [4] give moment bounds for fractional-in-time noise under their spatial covariance conditions, including a second-moment lower bound in dimensions at most three at the same time-growth order as the upper bound for positive constant initial displacement and nonnegative constant initial velocity. Hu–Wang [33, Theorem 3.7] obtain matching higher-moment growth orders under their covariance and Green-kernel hypotheses. Neither conclusion by itself identifies a sharp leading constant. Space-time white noise is not an automatic specialization of their functional spatial lower-bound hypotheses.

On the Stratonovich side, Xia Chen–Deya–Song–Tindel [18] construct solutions in dimensions one and two using Strichartz estimates and weighted function spaces. Their sufficient regularity ranges and initial-data assumptions differ from the full homogeneous range considered here. Xia Chen's current author version [17] treats fractional temporal correlation in dimensions one through three, with homogeneous condition $\alpha + \alpha_0 < 2$. It proves two-sided first-moment asymptotic bounds and a coarse quadratic-exponential second-moment upper bound. The stronger exact first-moment statement of arXiv:2510.01412v1 is not the statement of this edition; the version convention is specified in Section 1.4.

1.3.5 Advantages, limitations and the present contribution

For second-moment analysis, the main advantage of the Skorohod formulation is orthogonality: it removes unequal-chaos-order cross terms and makes isometries and hypercontractivity directly available. In some static covariance classes it also permits rougher noise than ordinary Stratonovich multiplication. The price is that Wick-ordered multiplication specifies a different stochastic model; it cannot generally be substituted

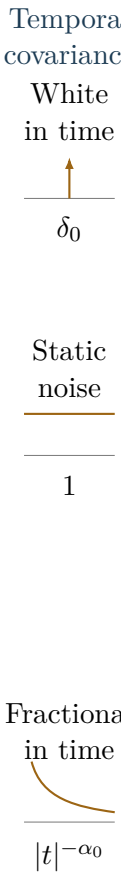

	Skorohod	Ordinary Stratonovich
White in time	**Exact second moments** Chen–Dalang [12] Space-time white noise, $d = 1$. Chen–Guo–Song [14] Exact $p = 2$; wave higher-p growth orders $p^{3/2}$.	**Approximation matters** No source claim is listed here. Specify smoothing and convergence. No Itô equality or openness is inferred.
Static noise	**Exact rates** Balan–Le Chen–Xia Chen [3]: $p \geq 2$. Homogeneous: $d \leq 3$; spatial white: $d \leq 2$. Chen–Eisenberg [13] Exact rates; static noise; fractional time order < 2.	**Construction / exact rates** Balan [2]: $d = 1, 2$ construction. Stronger spectral condition. Xia Chen–Hu [20] Exact rates, integer $p \geq 1$; Dalang and homogeneity hypotheses.
Fractional in time	**Bounds / construction** Balan–Conus; Hu–Wang [4, 33] Growth orders; no sharp constant. Chen–Deya–Song–Tindel [19]: construction; data hypotheses depend on d.	**First-moment bounds** Xia Chen, author version [17] $d = 1, 2, 3$, $\alpha + \alpha_0 < 2$. Two-sided first-moment bounds; the exact limit is predicted.

Present manuscript **Fractional-time Stratonovich, $p = 2$**
Intrinsic variational formula for the second-moment limit.
Written proof; independent review remains pending.

Figure 1.4: Selected results, organized by temporal covariance and stochastic product. The small profiles are schematic covariance sketches, not sample noise paths or limiting arrows. Construction, growth orders and exact rates are different conclusions. Every source retains its spatial covariance, dimension and data hypotheses; the Chen–Guo–Song higher-moment constants are nonoptimal, and the higher-dimensional Skorohod construction retains its data qualifications. Chen–Hu supplies no numerical constant here. Xia Chen's author version gives first-moment bounds, unlike the stronger arXiv-v1 wording. The highlighted manuscript claim has a separate review status. The columns assert neither inclusions nor a universal conversion between products.

for an ordinary smooth random potential. With temporally correlated noise, it does not restore adapted martingale methods.

The Stratonovich formulation retains the interactions generated by ordinary multiplication and can connect to deterministic wave and Gaussian variational methods. Its cost is control of traces, self-pairings and unequal iteration orders, together with potentially stronger conditions for an unrenormalized limit. Neither interpretation supplies a general wave maximum principle. Both admit chaos methods and, in suitable settings, probabilistic representations. The appropriate choice is determined by the model and the specified approximation, rather than by a universal preference for one calculus.

The present contribution concerns the temporally correlated Stratonovich problem. Theorem 3.3.8 gives the full homogeneous-class upper bound at the scale t^{κ}. Theorem 11.2.6 identifies the second-moment limit through nonnegative compact space-time controls, retaining the original covariance amplitude, unit kinetic coefficient and global half-variance cost. This intrinsic expression is not a numerical closed form, a sharp all-moment formula or an identification with the source's first-moment variational constants. These are the claims of the written proofs; the independent review status is recorded separately from this literature comparison.

Related work in progress with Raluca Balan and Jinxin Wang treats three Skorohod projects: noise colored in time and space in one dimension; colored noise in two dimensions; and white-in-time noise in dimensions one, two and three. We mention these scopes to locate the present work within the broader program. No unpublished result from them is used here, and no equality of their constants with the present Stratonovich constant is asserted.

1.4 What is known

Pinpoints to Xia Chen's time-dependent Stratonovich paper refer to his public author version [17]. Theorem 1.2 differs from the statement in arXiv:2510.01412v1 [16]; we therefore cite that theorem from the author version.

1.4.1 Stratonovich expansion and moments

The solution is the Stratonovich expansion [17, (2.13)–(2.16)]

$$\begin{aligned} u(t,x) &= \sum_{n=0}^{\infty} S_n\Big(g_n(\cdot,t,x)\Big), \\ g_n(s_1,\dots,s_n,x_1,\dots,x_n,t,x) &= \Big(\prod_{l=1}^{n} G(s_{l+1}-s_l, x_{l+1}-x_l)\Big)\mathbf{1}_{[0,t]^n_<}(s_1,\dots,s_n), \end{aligned} \tag{1.4.1}$$

with $s_{n+1} = t$, $x_{n+1} = x$, G the fundamental solution of the wave equation, and $[0,t]^n_< = \{0 < s_1 < \cdots < s_n < t\}$. Odd expected Stratonovich integrals vanish and even ones are given by Wick's formula [17, (2.19)–(2.21)], a sum over pair partitions $\mathcal{D} \in \Pi_n$ of $\{1,\dots,2n\}$ that includes self-pairings within one chain. The second moment of one

ordered term is the two-chain pairing integral, stated in [17, Theorem 4.1, (4.3)] and proved here under Hypothesis 1.2.1 in Proposition 2.1.1:

$$\mathbb{E}\Big[S_n(g_n(\cdot,t,x))^2\Big] = \sum_{\mathcal{D}\in\Pi_n} \int_{[0,t]^n_< \times [0,t]^n_<} \mathrm{d}s \int_{(\mathbb{R}^d)^n\times(\mathbb{R}^d)^n} \mathrm{d}x \Big(\prod_{\rho=1}^{2} \prod_{l\in I_\rho} G(s_l - s_{p(l)}, x_l - x_{p(l)}) \Big) \times \prod_{(j,k)\in\mathcal{D}} |s_j - s_k|^{-\alpha_0} \gamma(x_j - x_k), \tag{1.4.2}$$

with $I_1 = \{1,\dots,n\}$ and $I_2 = \{n+1,\dots,2n\}$. Here $p(l)$ is the preceding label in its own chain; at the first vertex of either chain use the common root $(s_{p(l)}, x_{p(l)}) = (0,0)$. Thus, the second chain does not continue the first one. This spells out the source's conventions in Theorem 4.1.

The full mixed-term expansion is justified in Proposition 2.1.1.

1.4.2 The universal two-chain bound

[17, Theorem 3.1, (3.6), p. 15] states an estimate for such two-chain pairing integrals with nonnegative kernels G_l by products of the norms $\|G_l\|^{(0)}$, $\|G_l\|^{(1)}_{j,k}$, $\|G_l\|^{(2)}_{j,k}$ of [17, (3.3)–(3.5)], over a partition $\{Q_0, Q_1, Q_2\}$ of $\{1,\dots,2n\}$ with $\#Q_0 = \#Q_1$ and $\#Q_2$ even. As stated, the theorem uses finite spatial spectral measures $\mu_{j,k}$ with nonnegative covariance functions and temporal kernels $\Gamma(\alpha_0)^{-1}\int_{A_{j,k}} e^{-\lambda|r|}\lambda^{\alpha_0-1}\,\mathrm{d}\lambda$ for measurable $A_{j,k}\subset\mathbb{R}_+$. The application to the full covariance therefore requires regularization; this is carried out in Lemma 2.5.3. The theorem includes cross-pairings between the two chains. Our finite maximum formulation is proved in Lemma 2.4.1; a maximizing assignment may depend on the kernels. Lemma 2.3.2 supplies its Case 2 estimate with the predecessor-time difference retained, as explained in Remark 2.3.3. In the source it is used only for Stratonovich integrability (Section 4) and, via Lemma A.1 with $G_l(t,x) = e^{-\theta t}G(t,x)$, in Laplace variables.

1.4.3 Known moment bounds

The following statement records the source as printed. Its variational constants require normalization clarification; see Remark C.2.8. We retain the printed formulas without adopting a correction. The upper-bound proofs below do not use the first-moment upper constant.

Theorem 1.4.1 ([17, Theorem 1.2, (1.10)–(1.13)])**.** Source statement as printed. *Under its covariance and homogeneity assumptions* [17, (1.2), (1.3), (1.8), (1.9)]*, the author version states*

$$L_* \le \liminf_{t\to\infty} t^{-\kappa}\log \mathbb{E}u(t,x) \le \limsup_{t\to\infty} t^{-\kappa}\log \mathbb{E}u(t,x) \le L^*,$$

where, for $\mathcal{E}^\sharp \in \{\mathcal{E}_*, \mathcal{E}\}$*,*

$$L(\mathcal{E}^\sharp) := (3-\alpha)\left(\frac{(4-\alpha-2\alpha_0)^{\frac{4-\alpha-2\alpha_0}{2}}}{2^3(4-\alpha-\alpha_0)^{4-\alpha-\alpha_0}}\left(\frac{2\mathcal{E}^\sharp}{2-\alpha}\right)^{\frac{2-\alpha}{2}}\right)^{\frac{1}{3-\alpha}}, \qquad L_* = L(\mathcal{E}_*), \quad L^* = L(\mathcal{E}),$$

and $\mathcal{E}_*, \mathcal{E}$ are the variational quantities [17, (1.11)–(1.13)]. *The strict source comparison $\mathcal{E}_* < \mathcal{E}$ is asserted only for $\Gamma \neq 0$; it is not asserted at $\Gamma = 0$, where both quantities vanish. These printed normalizations are quoted, not adopted as established inputs. Numerical calibrations using L_* below explicitly assume the intended first-moment lower bound.*

The source writes its spatial covariance as a function and explicitly includes one-dimensional spatial white noise. We do not claim an extension of this quoted result to every singular Radon covariance in Hypothesis 1.2.1.

The source predicts that the limit exists and equals L^* [17, p. 4]; this is not proved. The source also suggests that the constant in its lower estimate may not be sharp, relating the difficulty to the complex-valued intersection-local-time representation [17, Remark 8.1, (8.8)].

Theorem 1.4.2 ([17, Remark 5.1, (5.8)])**.** $\mathbb{E}u^2(t,x) \le e^{Ct^2}$ *for large t.*

Conjecture 1.4.3 ([17, (1.22)])**.** *For $p = 1, 2, \dots,$*

$$\lim_{t\to\infty} t^{-\kappa} \log \mathbb{E}|u(t,x)|^p = p^{\frac{4-\alpha}{3-\alpha}} L^*.$$

Since $p^{(4-\alpha)/(3-\alpha)}$ grows faster than p, the conjectured second-moment constant $2^{(4-\alpha)/(3-\alpha)}L^*$ exceeds $2L^*$. The source explains why its method stops at $p = 1$ [17, Remark 6.3]: the representation of Theorem 6.1 there uses the monotone order $s_1 \le \cdots \le s_{2n}$ of a single chain.

Proposition 1.4.4 (Jensen lower bound)**.** *Under Hypothesis 1.2.1,* $\mathbb{E}u(t,x) \ge 1$ *and* $\mathbb{E}u^2(t,x) \ge (\mathbb{E}u(t,x))^2$. *Consequently, for every real ℓ,*

$$\liminf_{t\to\infty} t^{-\kappa} \log \mathbb{E}u(t,x) \ge \ell \quad \Longrightarrow \quad \liminf_{t\to\infty} t^{-\kappa} \log \mathbb{E}u^2(t,x) \ge 2\ell.$$

The specialization $\ell = L_*$ is conditional on the intended first-moment lower bound with that constant. It is not an unconditional adoption of the printed normalization in Theorem 1.4.1.

Proof. For each fixed t, x, Lemma 2.6.1 below gives $\sum_n \|X_n(t,x)\|_2 < \infty$; its proof does not use the present proposition. Thus, $\sum_n \mathbb{E}|X_n(t,x)| < \infty$, and the mean of the canonical series is the sum of its means. By (1.4.1) and [17, (2.20)–(2.21)], $\mathbb{E}u(t,x) = \sum_{n\ge 0} \mathbb{E}S_{2n}(g_{2n}(\cdot,t,x)) \ge 1$, since every term is a pairing integral of a nonnegative integrand and $S_0 = 1$. By the Cauchy–Schwarz inequality, $\mathbb{E}u^2(t,x) \ge (\mathbb{E}u(t,x))^2$, so $t^{-\kappa}\log \mathbb{E}u^2(t,x) \ge 2\,t^{-\kappa}\log \mathbb{E}u(t,x)$. Taking lower limits proves the implication for every valid ℓ. Substituting L_* requires its stated first-moment premise. This proves Proposition 1.4.4. □

1.5 Main results

We state the two main results for the model in Section 1.2. Throughout this section, Hypothesis 1.2.1 holds, u is the canonical Stratonovich expansion (1.4.1) with initial data

$(1,0)$, and κ is the exponent in (1.2.4). The spectral measure μ has the normalization specified in Hypothesis 1.2.1. Write B_1 for the unit ball in $\mathbb{R}^d$, and put

$$R_\alpha = \frac{\alpha\pi\mu(B_1)}{2\sin(\pi\alpha/2)}. \tag{1.5.1}$$

Theorem 1.5.1 (Upper bound at the correct scale)**.** *For every admissible dimension $d \in \{1,2,3\}$, there is a finite constant $C = C(\alpha,\alpha_0)$ such that, for all $T \geq 1$ and $x \in \mathbb{R}^d$,*

$$\mathbb{E}u^2(T,x) \leq e(T+2)^d \exp\left\{CR_\alpha^{1/(3-\alpha)}T^\kappa\right\}. \tag{1.5.2}$$

In particular, for every fixed $x \in \mathbb{R}^d$,

$$\limsup_{T\to\infty} T^{-\kappa}\log \mathbb{E}u^2(T,x) < \infty.$$

The proof is given in Theorem 3.3.8. It establishes finiteness independently of the variational identification below. The more explicit bounds for $0 < \alpha \leq 1$ are retained in Section B.1.

To state the limiting constant, let $I = (0,1)$ and define

$$\mathcal{C}_{\mathrm{pos}} = \left\{\Psi \in C_c^\infty(I\times\mathbb{R}^d;\mathbb{R}) : \Psi \geq 0,\ \Psi \neq 0\right\}. \tag{1.5.3}$$

No-go 20 exhibits controls whose covariance profiles do not separate into a scalar time factor and one spatial function. This does not decide whether a smaller family suffices for optimization.

This class includes controls that do not separate into a function of time and a function of space. For $\Psi \in \mathcal{C}_{\mathrm{pos}}$, its covariance mean and variance are

$$h_{\Psi,s}(x) = \int_I |s-t|^{-\alpha_0}\int_{\mathbb{R}^d}\Psi(t,x-y)\Gamma(\,\mathrm{d}y)\,\mathrm{d}t, \tag{1.5.4}$$

$$v_\Psi = \int_{I\times\mathbb{R}^d}\Psi(s,x)h_{\Psi,s}(x)\,\mathrm{d}x\,\mathrm{d}s. \tag{1.5.5}$$

For $s \in I$, define the nonnegative Rayleigh value

$$\mathcal{R}_\Psi(s) = \sup_{\substack{f\in H^1(\mathbb{R}^d;\mathbb{R})\\ \|f\|_2=1}}\left\{\int_{\mathbb{R}^d} h_{\Psi,s}(x)f(x)^2\,\mathrm{d}x - \|\nabla f\|_2^2\right\}. \tag{1.5.6}$$

Here $H^1(\mathbb{R}^d;\mathbb{R})$ is the real Sobolev space of square-integrable functions with square-integrable first weak derivatives, and $\|\cdot\|_2$ denotes the spatial L^2 norm. The spatial covariance retains its original amplitude in these definitions.

Theorem 1.5.2 (Second-moment limit)**.** *For every fixed $x \in \mathbb{R}^d$,*

$$\lim_{T\to\infty} T^{-\kappa}\log \mathbb{E}u^2(T,x) = C_2(\Gamma,\alpha_0), \tag{1.5.7}$$

where

$$C_2(\Gamma,\alpha_0) = \sup_{\Psi\in\mathcal{C}_{\mathrm{pos}}}\left\{2\int_I\sqrt{\mathcal{R}_\Psi(s)}\,\mathrm{d}s - \frac{v_\Psi}{2}\right\}. \tag{1.5.8}$$

If $\Gamma \neq 0$, then $0 < C_2(\Gamma,\alpha_0) < \infty$. If $\Gamma = 0$, then $u(T,x) = 1$ and $C_2(0,\alpha_0) = 0$.

The proof is given in Theorem 11.2.6. The variational formula uses the full class of nonnegative smooth compact controls. Its kinetic coefficient is one, and its Gaussian cost is one half of the original variance. It does not identify an auxiliary variational value with the first-moment limit or with the constants in Chen's conjecture. Theorem 11.3.4, Corollary 11.3.5 and Theorem 11.4.3 give bounds for this same constant. In particular, the explicit spatial white-noise energy yields moment bounds, not a closed-form evaluation of the full supremum.

1.6 Why the scale is t^{κ}

This section explains, without proof, where the exponent κ and the form of $C_2(\Gamma, \alpha_0)$ in Theorem 1.5.2 come from.

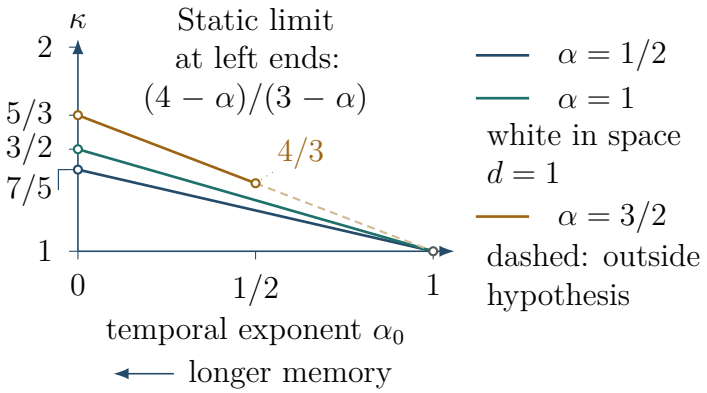

Figure 1.5: The exponent $\kappa = 1 + (1-\alpha_0)/(3-\alpha)$ of (1.2.4), drawn against the temporal exponent α_0 for three spatial exponents α. Longer memory in time (smaller α_0) and a more singular spatial covariance (larger α) both raise κ. As $\alpha_0 \downarrow 0$ each line tends to the static exponent $(4-\alpha)/(3-\alpha)$. The end points are excluded: Hypothesis 1.2.1 requires $0 < \alpha_0 < 1$ and $\alpha + \alpha_0 < 2$, so the line for $\alpha = 3/2$ stops at $\alpha_0 = 1/2$. The picture shows the exponent only; it says nothing about the constant $C_2(\Gamma, \alpha_0)$.

The first step is an exact scaling, proved in Lemma 7.1.1. Stretch time by a factor T and space by $r_T = T^{(\alpha_0-1)/(3-\alpha)}$. Because the temporal covariance $|s-t|^{-\alpha_0}$ and the spatial covariance Γ are homogeneous (Hypothesis 1.2.1), the stretched noise has the law of the original noise multiplied by a constant. With $\delta = T^{-\kappa}$, the stretched solution has the law of the solution V_δ of

$$\delta^2 \partial_t^2 V_\delta = \Delta V_\delta + \sqrt{\delta}\, \dot{W} V_\delta, \qquad V_\delta(0,\cdot) = 1, \quad \partial_t V_\delta(0,\cdot) = 0,$$

and

$$T^{-\kappa} \log \mathbb{E}|u(T,0)|^2 = \delta \log \mathbb{E}|V_\delta(1,0)|^2$$

(see (7.1.1) and (7.1.2)). With this choice of κ, the time derivative carries the factor δ^2 and the noise the factor $\sqrt{\delta}$. The growth of the second moment over long times thus becomes a question about small noise: does $\delta \log \mathbb{E}|V_\delta(1,0)|^2$ have a limit as $\delta \to 0$?

Heuristically it does, because a gain and a cost of the same order $1/\delta$ balance. Shift the noise toward a deterministic potential, chosen through a nonnegative control Ψ, so that the potential seen by the wave at time s is $h_{\Psi,s}$ of (1.5.4). In the scaled equation this needs a shift of order $1/\sqrt{\delta}$, and its Gaussian cost is $v_\Psi/(2\delta)$, one half of the variance (1.5.5) divided by δ. Freezing the potential at time s gives the equation $\delta^2 a'' = \mathcal{R}_\Psi(s)\, a$ for the amplitude of the leading mode, whose growing solution has exponential rate $\sqrt{\mathcal{R}_\Psi(s)}/\delta$. Heuristically, the square of the wave then grows like $\exp\bigl(2\int_I \sqrt{\mathcal{R}_\Psi(s)}\,\mathrm{d}s/\delta\bigr)$. Gain minus cost, multiplied by δ, is $2\int_I \sqrt{\mathcal{R}_\Psi(s)}\,\mathrm{d}s - v_\Psi/2$, and taking the supremum over $\Psi \in \mathcal{C}_{\mathrm{pos}}$ gives $C_2(\Gamma,\alpha_0)$. Returning to the original variables, $\log \mathbb{E}u^2(T,x)$ grows like $C_2(\Gamma,\alpha_0)\,T^\kappa$.

This argument only explains the answer. A proof needs a lower bound for each control, which computes the cost using the original covariance, retaining correlations between different time intervals (Chapter 7), and an upper bound showing that no other fluctuation of the noise does better (Chapters 8–10); Chapter 11 matches the two. Section 1.8 describes these steps.

1.7 Consistency checks

These comparisons place the second-moment theorem alongside known bounds and Chen's conjecture. They are not inputs to the proof of Theorem 1.5.2.

Time-independent noise. As $\alpha_0 \downarrow 0$, the exponent κ tends to $(4-\alpha)/(3-\alpha)$, the exponent of the time-independent Stratonovich model found by Chen and Hu [20, Theorem 1.2]. This is a formal boundary limit: the large-time limit and the limit $\alpha_0 \downarrow 0$ are not interchanged (Remark A.1.5).

The first moment. If $\liminf_{t\to\infty} t^{-\kappa}\log \mathbb{E}u(t,x) \geq \ell$, then Jensen's inequality $\mathbb{E}u^2(t,x) \geq (\mathbb{E}u(t,x))^2$ gives the corresponding second-moment lower limit at least 2ℓ (Proposition 1.4.4). Hence $C_2(\Gamma,\alpha_0) \geq 2\ell$ in Theorem 1.5.2. Taking $\ell = L_*$ of Theorem 1.4.1 is conditional on the intended first-moment lower bound with that constant; its printed normalization is not adopted unconditionally.

The Skorohod model. For Riesz covariances with $a = \alpha < d$ and $\alpha < 2$, set $H = 1-\alpha_0/2 > 1/2$. The Skorohod upper bound of Balan and Conus [4, Theorem 2.1(b)] has the time exponent $(2H+2-a)/(3-a) = \kappa$. The comparison concerns time exponents only: the solution concepts and covariance normalizations differ, and no constants are compared. The Stratonovich moment expansion also includes self-pairings, that is, pairs of noise factors from the same ordered integral, which are absent from the Skorohod expansion (Remark A.1.5).

Chen's conjecture. For $p = 1, 2, \ldots$, Chen conjectures that $t^{-\kappa}\log \mathbb{E}|u(t,x)|^p$ tends to $p^{(4-\alpha)/(3-\alpha)}L^*$ (Conjecture 1.4.3). For $p = 2$ the conjectured value is $2^{(4-\alpha)/(3-\alpha)}L^*$.

When $L^* > 0$, this exceeds $2L^*$, the lower bound that Jensen's inequality would give if the first-moment rate were L^*; at zero covariance both values vanish. Theorem 1.5.2 does not decide this conjecture: its constant $C_2(\Gamma, \alpha_0)$ is given by its own variational formula and is not identified with the conjectured constant or with the first-moment limit. The conjectured value is a point of comparison, not a target of the proof.

1.8 Strategy of the proof

The second moment is a convergent sum of two-chain pairing integrals, including empty chains and all relative time orders. Stratonovich integrals retain pairings within either chain as well as between the chains, so products of different orders can contribute (Proposition 2.1.1). Estimating every pairing by one common bound gives a finite moment but loses the target growth scale (Proposition 2.7.1). Chapter 12 discusses this and the other approaches that do not work. The proof proceeds in four steps, shown in Figure 1.6.

One solution and an upper bound at the right scale. Chapter 2 derives the complete pairing expansion and constructs the solution used throughout (Proposition 2.6.2). Chapter 3 then proves an upper bound at the scale t^κ for the full covariance class, before the limiting constant is known (Theorem 3.3.8). The wave equation forces this argument to carry both displacement and velocity across time intervals. The constant of this bound is not claimed to be optimal.

A lower bound for each control. A lower bound comes from shifting the Gaussian noise toward a deterministic potential that makes the wave grow, and comparing the gain with the cost of the shift. Because the noise is correlated in time, the cost of a control is charged in the original covariance space, not added over time intervals as if they were independent. Chapters 4–6 prepare the tools: covariance estimates for a potential multiplied by a smooth spatial cutoff of compact support, a random operator path driven by the noise of the original equation, and the evolution on the displacement–velocity phase space, identified with the physical wave. Chapter 7 converts long time into an equivalent small-noise problem by equality in law (Section 7.1), for nonzero covariance, proves a lower bound for each fixed control in the class defined in Section 1.5, with an eligible fixed spatial mask (Proposition 7.2.7), and then removes that mask and optimizes over controls to obtain a variational lower value (Section 7.3). For zero covariance, the solution is identically one and the rate is zero. Together with the upper bound of the first step, this value is finite (Proposition 7.3.6).

A matching upper bound. The upper bound must account for all Gaussian fluctuations, not only the favourable shifts, and it must control the moment at one point while the region reached by the wave grows with time. Chapter 8 relates limits of smooth controls in the norm determined by the noise covariance to the deterministic means they induce. Chapter 9 separates the estimates that are uniform in the radius of the

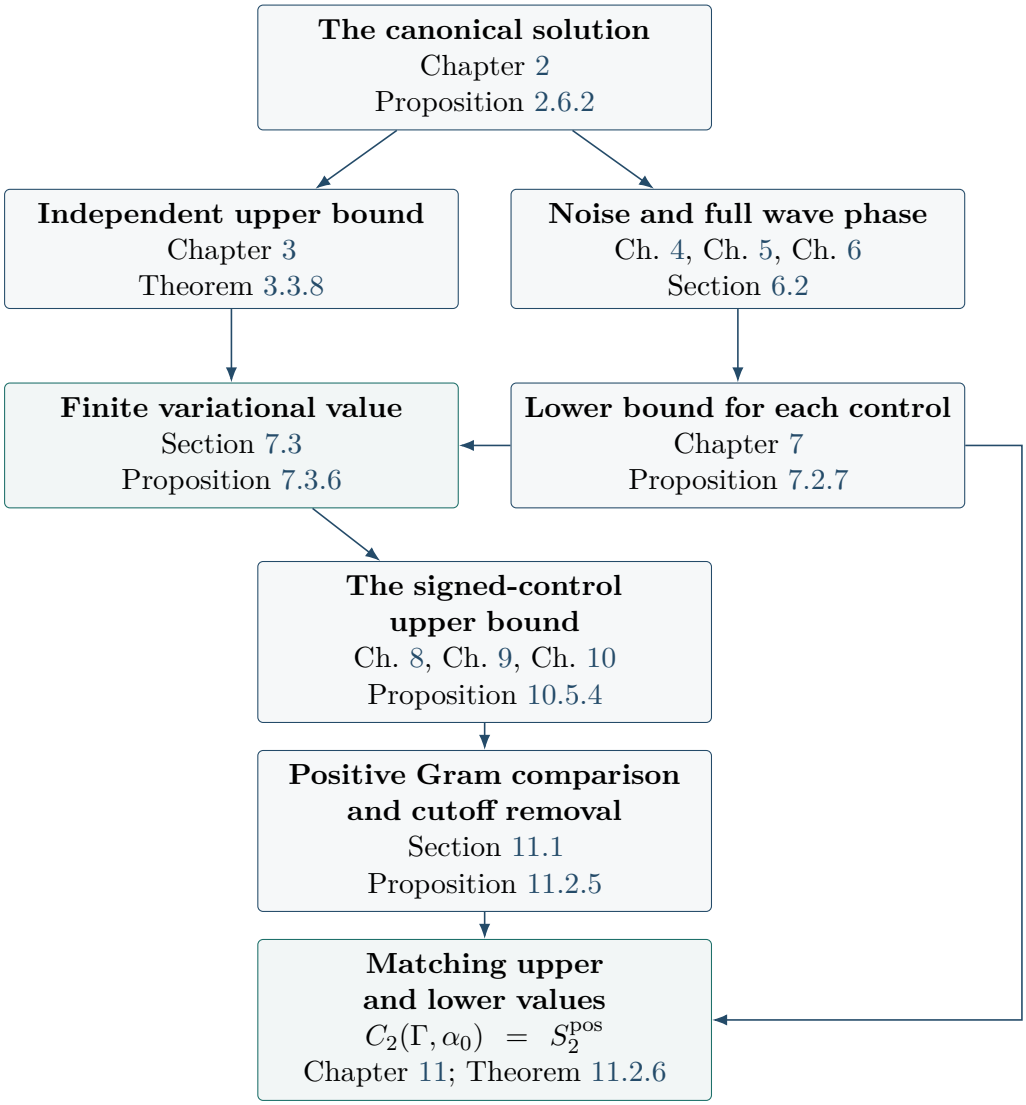

Figure 1.6: The principal proof dependencies, with links to chapters and results in the technical companion. The independent upper bound and the fixed-control lower bound first give a finite variational lower value. Further operator and Gaussian estimates give a signed-control upper bound for the same point moment. Positive Gram comparison and cutoff removal identify the two values. Arrows show principal uses; each box also has the hypotheses and earlier inputs stated at its linked destination. They do not assert independence of successive time blocks. The zero-covariance case is included in the final theorem.

spatial cutoff from those whose dependence on the radius must be shown, and constructs the wave for completed static mean potentials of either sign at a fixed spatial cutoff. Chapter 10 reduces the probabilistic estimate to growth under deterministic controls, returns to the original point moment through finite propagation and a spatial average of squared solutions, controls the Gaussian tail, and obtains an upper variational expression over signed controls (Proposition 10.5.4).

Identifying the constant. The two bounds now concern the same point moment, but over different controls: nonnegative smooth controls below, signed controls in the covariance-norm completion just described above. Chapter 11 shows that the two optimizations have the same value. It first solves a finite optimization problem whose matrix of pairwise covariance inner products has nonnegative entries (Section 11.1), then applies it to the physical means and removes the spatial cutoff (Proposition 11.2.5). Theorem 11.2.6 states the resulting limit. The remaining sections give bounds for its constant and, for spatial white noise in one dimension, explicit moment bounds; they do not evaluate the full supremum.

1.9 Future work

The second-moment argument suggests questions about higher moments, optimizing controls and scaling limits. The following subsections separate precise conjectures, conditional consequences and exploratory questions. The proposed extensions require further proof. We retain the initial data $(1, 0)$ throughout this section. Except in Subsection 1.9.6, we also retain Hypothesis 1.2.1 and the exponent κ from (1.2.4).

1.9.1 Higher moments and pointwise estimates

Conjecture 1.9.1 (Higher even-moment asymptotics)**.** *Under Hypothesis 1.2.1, let u be the canonical Stratonovich solution with initial data $(1, 0)$. For each fixed even integer $p \geq 4$ and each fixed $x \in \mathbb{R}^d$,*

$$\lim_{t\to\infty} t^{-\kappa} \log \mathbb{E}|u(t, x)|^p = \left(\frac{p}{2}\right)^{\frac{4-\alpha}{3-\alpha}} C_2(\Gamma, \alpha_0). \tag{1.9.1}$$

Here C_2 is the intrinsic constant in Theorem 1.5.2.

The case $p = 2$ is the theorem already stated. For zero covariance, the conjectured identity reduces to zero on both sides. The open assertion concerns higher even moments for nonzero covariance.

The candidate comes from the variational expression in Theorem 1.5.2. If a Gaussian shift produces an integrated deterministic growth rate I_Ψ, its contribution to the pth moment should be compared with the same Gaussian cost $v_\Psi/2$. This suggests optimizing $pI_\Psi - v_\Psi/2$ over the full positive-control class. The homogeneity of these variational values is already proved for every positive coefficient in Proposition 7.3.6. What remains

is their identification with the higher point-moment limits. Formula (1.9.1) uses the intrinsic second-moment constant; it does not require identifying that constant with the one predicted in the source.

Even orders allow us to use $|u|^p = u^p$ and Gaussian pairing expansions without assuming that the solution is nonnegative. A p-chain expansion must retain self-pairings, cross-pairings, unequal chain lengths and empty chains. The scaling identity and the Gaussian change of measure offer a different starting point that may avoid estimating all these pairings separately. The lower-bound construction and finite Gram optimization also suggest extensions with coefficient p. Higher-moment convergence, uniform integrability and the comparison with the original point observable must still be justified.

Point moments and spatial regularity. The main obstacle in the present upper-bound method occurs in Proposition 10.4.5. Stationarity and finite propagation identify the pointwise second moment with an expected spatial L^2 norm. The displacement component of the wave phase controls this norm. For a pth moment, the corresponding argument would require a spatial L^p bound. Taking a higher power of an L^2 bound does not supply it.

The existing displacement space is $H^{1/2}(\mathbb{R}^d)$. Its embeddings into L^p on a fixed ball give the ranges in Table 1.1; see [29, Section 6]. The table describes the present proof method. The conjecture covers every admissible dimension, including orders beyond these embedding ranges.

Table 1.1: Higher moments through the current wave phase. The Sobolev ranges are known; the proposed moment extensions still require proof.

d	Available L^p range	First target	Remaining step
1	$2 \le p < \infty$	$p = 4$, then fixed even p	Higher-moment source limits and point comparison; matching Gaussian upper and shifted lower bounds.
2	$2 \le p \le 4$	$p = 4$	The same probabilistic steps at the critical embedding exponent. Larger even orders need additional spatial control.
3	$2 \le p \le 3$	A point estimate for $p = 4$	A new comparison or stronger spatial estimates before applying the higher-moment Gaussian argument.

The failure of this embedding route at a higher order is not a nonexistence statement for the moment. Any stronger spatial estimate must be proved under the original covariance assumptions. Even within the displayed ranges, the embedding alone does not establish the conjectured limit.

A first test and further questions. The fourth moment in one spatial dimension is a useful first test. One would first establish the fourth-moment point comparison and

the required source limits. The Gaussian upper argument would then need to control the fourth power of the evolution norm, with bounds uniform in the growing spatial radius. Matching this bound with the shifted lower estimate would test the prediction $C_4 = 2^{(4-\alpha)/(3-\alpha)}C_2$. The validity of the Sobolev embedding alone does not complete these steps.

Even a proof for every fixed even p would leave two separate questions: absolute moments of other orders, and estimates uniform as $p \to \infty$. Interpolation between adjacent even moments need not identify the exact constant at an intermediate order. Uniform large-p estimates also require tracking the dependence on p throughout the construction, source limits and Gaussian tail bounds. These questions may clarify which parts of the present method apply to moment growth beyond the second moment.

1.9.2 Real orders and upper-tail deviations

A stronger question is whether (1.9.1) holds for every fixed real $p \geq 1$. The variational homogeneity allows real coefficients, and the Gaussian change of measure applies to absolute powers. However, the comparison between masked and original moments in Proposition 6.1.3 uses nonnegative Gaussian pairing terms. Such an expansion does not directly represent a noninteger absolute power. A replacement comparison and the required moment convergence are therefore needed. Interpolation between even orders gives bounds, but does not in general identify the exact constant at an intermediate order. At $p = 1$, the proposed quantity is $\mathbb{E}|u|$, which must be distinguished from the signed mean $\mathbb{E}u$ in the source. We do not assume positivity of the wave solution. Thus, the real-order extension is plausible from the control formula, but remains a separate open question.

For a nonzero covariance, suppose that the real-order extension has been established for every $p \geq 1$. For this discussion, set

$$m = \frac{4-\alpha}{3-\alpha} > 1, \qquad A = 2^{-m}C_2(\Gamma, \alpha_0) > 0, \qquad z_* = mA.$$

Then the limiting logarithmic moment function on this range is Ap^m. The corresponding sharp upper-tail consequence is

$$\lim_{t\to\infty} t^{-\kappa} \log \mathbb{P}\Big\{|u(t,x)| \geq e^{zt^\kappa}\Big\} = -\mathcal{I}(z), \qquad z \geq z_*, \tag{1.9.2}$$

for each fixed x, where

$$\mathcal{I}(z) = (m-1)m^{-m/(m-1)}A^{-1/(m-1)}z^{4-\alpha}. \tag{1.9.3}$$

The threshold comes from the maximizing moment order $p_z = (z/(mA))^{1/(m-1)}$. For $z > z_*$ this order lies in $(1, \infty)$, where the hypothesized moment limits are available on both sides of p_z. The exponential-tilting argument uses this local information for the lower bound and the moment inequality for the upper bound; the endpoint follows from thresholds above z_* by monotonicity. This is the moment-method application described in [28, Section 2.3]. We do not invoke a full Gärtner–Ellis theorem on an unverified

domain of moment orders. Formula (1.9.2) is conditional on the real-order extension, not a large-deviation result established here for the wave equation.

For $0 < z < z_*$, optimizing only over $p \geq 1$ gives the upper bound

$$\limsup_{t\to\infty} t^{-\kappa} \log \mathbb{P}\Big\{|u(t,x)| \geq e^{zt^\kappa}\Big\} \leq -\max\{0, z - A\}.$$

Those moment orders do not determine the sharp rate on this remaining range. If the same moment formula were proved for every real $p > 0$, the sharp upper-tail expression would extend to every $z > 0$. Neither version supplies a lower-tail principle for $\log|u|$, where small values and zeros require separate analysis. For spatial white noise in one dimension, $m = 3/2$ and the predicted upper-tail rate is $\mathcal{I}(z) = 32z^3/(27C_2^2)$; with real orders only above one, its stated range is $z \geq 3C_2/(4\sqrt{2})$. The time speed and C_2 still depend on the temporal covariance.

1.9.3 Compactness of optimizing controls

The variational formula raises a question about the controls responsible for large moment growth. Its admissible tests are smooth and compactly supported, so attainment in that class should not be presumed. We first ask for a weaker form of compactness in the one-dimensional spatial-white case.

Fix $\Gamma = c\delta_0$, with $c > 0$, and write $a = \alpha_0 \in (0,1)$. Let H_a be the completion of real smooth compactly supported tests on $I \times \mathbb{R}$, where $I = (0,1)$, modulo covariance-null tests, under the norm

$$\|\Phi\|_{H_a}^2 = c\int_{I^2} |s-t|^{-a} \int_{\mathbb{R}} \Phi(s,x)\Phi(t,x)\,\mathrm{d}x\,\mathrm{d}s\,\mathrm{d}t.$$

For $\Psi \in \mathcal{C}_{\mathrm{pos}}$ of (1.5.3), put

$$J_a(\Psi) = 2\int_I \sqrt{\mathcal{R}_\Psi(s)}\,\mathrm{d}s - \frac{1}{2}\|\Psi\|_{H_a}^2, \qquad (\tau_y\Psi)(s,x) = \Psi(s,x+y).$$

The Rayleigh value is defined in (1.5.6).

Conjecture 1.9.2 (Compactness of an optimizing sequence)**.** *For every $c > 0$ and $0 < a < 1$, there are $\Psi_j \in \mathcal{C}_{\mathrm{pos}}$, spatial translations $y_j \in \mathbb{R}$ and a nonzero $\Phi_* \in H_a$ such that*

$$J_a(\Psi_j) \longrightarrow C_2(c\delta_0, a), \qquad \|\tau_{y_j}\Psi_j - \Phi_*\|_{H_a} \longrightarrow 0.$$

The conjecture asks for one strongly convergent optimizing sequence after spatial translation. It asserts neither compactness of every optimizing sequence nor a smooth compactly supported maximizer. Identifying the Rayleigh functional at the limit would be a further step. Another question is whether controls that separate into a time factor and a space factor give the full supremum. Comparing such controls with sums of two products is a first test; we do not assume either equality or strict improvement.

1.9.4 Sharper bounds near the static case

The lower and upper formulas in Theorem 11.4.3 have the same limit as $a \downarrow 0$. A more precise question concerns the first correction to this limit.

Conjecture 1.9.3 (First correction in the spatial-white case)**.** *For each fixed $c > 0$,*

$$\lim_{a \downarrow 0} \frac{1}{a} \left(\frac{3C_2(c\delta_0, a)}{2\sqrt{c}} - 1 \right) = \frac{3}{4}.$$

The coefficient is suggested by formally expanding a temporally constant trial and the temporal covariance operator around the constant kernel. Justifying the trial approximation and a matching upper estimate remains part of the question. The common zeroth-order limit of the existing bounds does not establish this first-order correction.

For a fixed $0 < a < 1$, another question is whether both inequalities in Theorem 11.4.3 are strict. Varying the temporal equilibrium trial may improve the lower formula. On the upper side, the norm of the temporal covariance operator may improve the current row-integral estimate. A separate numerical objective is a certified enclosure of C_2 for a fixed a, with explicit errors from truncation and discretization. Optimizing a finite family of controls alone gives lower bounds and does not certify the continuum supremum from above.

1.9.5 Logarithmic wavefields and possible scaling limits

A logarithmic change of variables provides another way to view random wave propagation. This idea has classical precedents in the Rytov transformation, which represents a complex wavefield through its logarithmic amplitude and phase. For example, Sung et al. [40, Section 2] substitute $U = e^{\psi}$ into a Helmholtz equation before applying a weak-scattering approximation. The substitution and the subsequent approximation are distinct steps. That frequency-domain setting does not supply a scaling limit for the time-dependent model considered here.

For the smooth equation $u_{tt} = \Delta u + Vu$, set $h = \log |u|$ on a region where u is nonzero. The ordinary chain rule gives

$$h_{tt} + (h_t)^2 = \Delta h + |\nabla h|^2 + V. \tag{1.9.4}$$

Thus, the logarithmic wave equation retains both a second time derivative and a quadratic temporal derivative. In the stochastic model, this calculation applies first to smooth noise approximations. Passing through zeros or to the singular-noise limit requires a separate argument; we do not assert a global logarithmic equation for the canonical solution.

A possible mechanism for an effective first-order time evolution can be seen formally by writing $h = b(t) + \varphi$, where b is a smooth deterministic centering. Then

$$\varphi_{tt} + 2b'(t)\varphi_t + (\varphi_t)^2 = \Delta\varphi + |\nabla\varphi|^2 + V - b''(t) - (b'(t))^2. \tag{1.9.5}$$

If b' approached a positive constant and the other temporal terms on the left became negligible on a fluctuation scale, the term $2b'\varphi_t$ could produce an effective parabolic evolution. Neither condition follows from moment growth. In particular, logarithmic moments need not give the typical centering, and the long temporal memory of the noise must still be accounted for. This is a heuristic mechanism to investigate.

The ordinary one-dimensional KPZ comparison concerns the centered logarithm of the positive stochastic heat solution. Its height, space and time scaling exponents have ratio $1 : 2 : 3$; convergence to the KPZ fixed point is a statement about random fields and their evolution [48, Theorems 1.6 and 1.8]. The moment normalization in the present wave problem controls rare amplification. It does not identify the typical fluctuation size or spatial correlation length. The cubic upper-tail prediction in the spatial-white case also gives no evidence by itself for KPZ behavior: the usual KPZ upper-tail power is $3/2$, while a cubic power appears in a lower-tail regime [22]. Different rare-event scales do not, by themselves, exclude a common limit in another centered fluctuation regime.

The open question is whether a specified logarithmic amplitude observable H admits deterministic functions b, S and L for which

$$\frac{H(Tt, L(T)x) - b(Tt)}{S(T)}$$

converges to a nondegenerate random field as $T \to \infty$. A logarithm of a local spatial L^2 amplitude is one possible observable that reduces sensitivity to isolated pointwise zeros. It can itself vanish, so its domain must also be specified; it differs from $\log|u|$. The scales and topology must be specified, and a claim of universality would require stability under changes of regularization and microscopic covariance details. Temporal correlations and sensitivity to the initial velocity would help determine whether a scalar amplitude describes the limiting evolution or whether additional variables remain necessary. We leave this as an exploratory question, without prescribing exponents or a new universality class.

1.9.6 Rough noise beyond the present covariance class

We ask whether we can construct the Stratonovich wave equation with initial data $(1, 0)$, and determine its moment growth, beyond Hypothesis 1.2.1. We use $d = 1$ to illustrate these questions and consider Gaussian noises with product spectral measure $\mu_0 \otimes \mu$, where

$$\mu_0(\,\mathrm{d}\tau) = c_0|\tau|^{\alpha_0 - 1}\,\mathrm{d}\tau, \qquad \mu(\,\mathrm{d}\xi) = c_1|\xi|^{\alpha - 1}\,\mathrm{d}\xi, \qquad c_0, c_1 > 0,$$

with $\alpha_0, \alpha > 0$ and $\alpha_0 + \alpha < 2$. The corresponding Hurst parameters are $H_0 = 1 - \alpha_0/2$ and $H = 1 - \alpha/2$. Thus, the proposed condition is $H_0 + H > 1$. We propose this region for investigation, without asserting a solvability criterion. The physical covariance in the rough regions is understood as a distribution and need not be a nonnegative Radon measure.

After matching the covariance normalization, the current theorem covers $0 < \alpha_0 < 1$, $0 < \alpha < 1$, and the spatial white noise segment $\alpha = 1$, $0 < \alpha_0 < 1$. Figure 1.7 separates

this range from the two proposed regions: rough space with $\alpha > 1$, and rough time with $\alpha_0 > 1$. The temporal white noise segment $\alpha_0 = 1$, $0 < \alpha < 1$ is outside the current theorem. Its integration convention and its relation to the present variational formula require separate treatment. On either white noise line we mean a Dirac covariance with its specified normalization, not the literal function $|r|^{-1}$. The point $(\alpha, \alpha_0) = (1, 1)$ lies on the excluded boundary $\alpha_0 + \alpha = 2$; this exclusion is not a nonexistence statement.

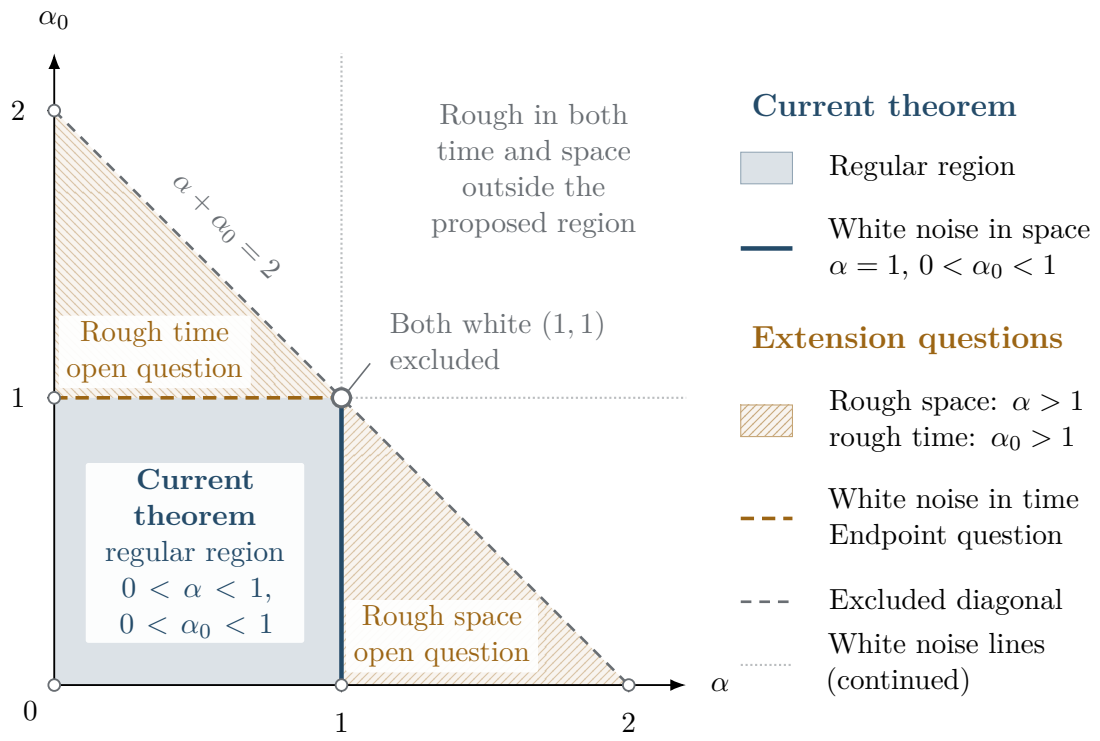

Figure 1.7: Parameter schematic for $d = 1$. The candidate range for investigation is $\alpha > 0$, $\alpha_0 > 0$, $\alpha + \alpha_0 < 2$. Blue marks the current theorem under its standing covariance assumptions: the open regular region, together with the segment white in space, $\alpha = 1$ and $0 < \alpha_0 < 1$. The hatched rough regions and the dashed segment white in time, $\alpha_0 = 1$ and $0 < \alpha < 1$, are questions about extending the present results. The axes and the diagonal are excluded, including $(1, 1)$. The region rough in both time and space does not meet the triangle. No solvability claim is made outside the triangle. White in space or time means that the corresponding covariance factor is a multiple of a Dirac mass. For $d \geq 2$, white noise in space lies on $\alpha = d$, outside the open positive candidate triangle.

Rough spatial covariance is already used in related equations. Balan, Chen and Ma [1, Theorem 1.1] construct the Skorohod solution of the parabolic Anderson model for their class of initial data, with $H_0 \in (1/2, 1)$, $0 < H < 1/2$ and $H_0 + H > 3/4$. In the notation above, this gives $0 < \alpha_0 < 1$, $1 < \alpha < 2$ and $\alpha_0 + \alpha < 5/2$. Their frequency estimates and bounds for ratios of Gamma functions suggest methods to investigate. Their estimates for the heat kernel and orthogonal chaos expansion do not directly treat

the oscillatory wave kernel or the self-pairings in an ordinary Stratonovich expansion. Related results for wave equations with rough spatial noise are given by Song, Song and Xu [38, Theorem 3.2] and Liu, Hu and Wang [37]; their parameter ranges and definitions of the stochastic integral must also be retained.

The present proof uses nonnegative physical covariance in its pairing bounds and comparisons of masked moments. It also uses Young integration to construct the wave evolution. These arguments require further work for the proposed spectral model. Their limitations do not by themselves imply that the model is ill posed. At each regularization, noise enters the velocity equation, while displacement is its time integral. This structure may permit a different construction. Even after a construction, the sharp moment asymptotics would remain a separate question. The rough temporal range requires particular care. The formal continuation of the expression in (1.2.4) gives

$$\frac{4-\alpha-\alpha_0}{3-\alpha} = 1 + \frac{1-\alpha_0}{3-\alpha}.$$

It equals one at $\alpha_0 = 1$ and falls below one when $\alpha_0 > 1$. For $\alpha_0 \geq 1$, the factor $\delta^{(1-\alpha_0)/2}$ used in the current block error estimate no longer tends to zero. This factor still vanishes in the proposed rough spatial range with $\alpha_0 < 1$. We leave both the appropriate moment scale and its limiting constant open in these extensions.

1.9.7 Exact first-moment asymptotics

For a nonzero spatial covariance and a fixed positive temporal exponent α_0, can we determine the exact large-time growth of the signed mean $\mathbb{E}u(t,x)$? This question is distinct from determining the growth of $\mathbb{E}|u(t,x)|$. The current author version of Xia Chen's paper gives two-sided bounds for the signed mean and predicts that the upper bound is sharp; see [17, Theorem 1.2, (1.10), the discussion following (1.14), and Remark 8.1]. The second-moment result of this book does not identify either first-moment constant.

The positive-control variational problem provides a quantity to investigate. Proposition 7.3.6 and Theorem 11.2.6 give

$$S_1^{\mathrm{pos}} = 2^{-m} C_2, \qquad m = \frac{4-\alpha}{3-\alpha}.$$

This identity concerns control suprema. It does not prove that either $t^{-\kappa}\log \mathbb{E}u(t,x)$ or $t^{-\kappa}\log \mathbb{E}|u(t,x)|$ converges to S_1^{pos}. Before proposing such an identification, we must check it against the actual mean bounds, the static limit and the source's covariance normalization. A variational characterization of the first mean may require a different functional.

The main missing lower-bound argument concerns cancellation. The second-moment proof restricts a nonnegative squared observable to a favorable event. For a signed observable, the contribution from the complementary event cannot be discarded. Positivity of the unconditional Wick coefficients does not supply this comparison. Absolute values

remove that particular obstruction, but a first absolute-moment argument still needs a comparison between the localized observable and the original solution, together with a matching upper bound. The completed quadratic comparisons do not provide these statements.

There is a useful boundary calibration. At $\alpha_0 = 0$, Chen–Hu's static first-mean asymptotic is an imported result; see (D.1.1). Corollary D.1.8 shows that the signed first-mean lower and upper growth rates approach that constant as $\alpha_0 \downarrow 0$, after the large-time liminf and limsup have been taken. It does not establish an exact time limit at a fixed positive α_0. A first step is to test a proposed first-moment formula on the small-order pairing coefficients and this static calibration, then isolate the needed cancellation or localization estimate. We leave the existence and variational identification of both first-moment limits open.

1.10 Toward a general variational method for random evolution equations

The preceding section asks how to extend the results. Here we ask what the proof itself teaches us. Several long arguments preserve the same three objects: the displacement–velocity evolution, the covariance of the original noise, and a variational reward for deterministic amplification. Their connection suggests a possible method for other random evolution equations. These questions arose by asking Amy to revisit the calculations and failed approaches, then checking her proposed abstractions against the arguments. The present book supplies a detailed case study; a general theorem would require assumptions that can be verified independently in a second model.

Compose the evolution and retain the joint Gaussian cost. For a wave equation, displacement at the end of a time block does not determine the next block: velocity is also needed. Lemma 7.2.5 composes the full phase-space propagators and identifies them through limits of the same regularized noise. The Gaussian change of law in Proposition 7.2.2 acts on that common noise. It does not replace correlated blocks by independent copies.

Even two Gaussian coordinates show why this distinction matters. If their covariance matrix is

$$C_\rho = \begin{pmatrix} 1 & \rho \\ \rho & 1 \end{pmatrix}, \qquad |\rho| < 1,$$

then a shift by $h = (q, q)$ has Cameron–Martin cost

$$\frac{1}{2} h^{\mathsf{T}} C_\rho^{-1} h = \frac{q^2}{1+\rho}.$$

Indeed, $C_\rho h = (1+\rho)h$ and $|h|^2 = 2q^2$. The cost is q^2 for independent coordinates and tends to $q^2/2$ as $\rho \uparrow 1$. Discarding correlation can therefore change the leading variational cost. The Gaussian shift formula is classical [34, Theorem 14.1]; the work here is to

connect it to the physical wave evolution and its terminal observable, with estimates uniform in the necessary limits.

This suggests a precise task: find sufficient conditions under which a phase-space evolution, controlled by one Gaussian field, has matching long-time upper and lower moment bounds with the same deterministic reward and the same covariance cost. The conditions must include convergence from the original regularized equation, control of products on growing intervals, and passage from phase-space estimates to the chosen observable. Proposition D.2.2 rules out one unweighted constant-correlation Brownian-clock substitution; it does not rule out every probabilistic representation. The pathwise composition used here supplies neither a conditional-expectation identity nor a general martingale calculus.

Separate the finite optimization from the wave estimates. Propositions 11.1.3 and 11.1.5 already apply in any real Hilbert space. For the square-root reward in (11.1.1), nonnegative Gram entries permit a positive conic maximizer and an entrywise comparison of optimized values. Singular matrices and inactive labels are included. This is the most explicit piece of the argument that can be stated without wave notation. Its physical application still needs the covariance and spectral estimates in Section 11.2.

A useful test would replace the square-root reward by the growth rate of a damped equation. For the scalar equation $u'' + 2\eta u' = vu$, with $\eta > 0$ and $v \geq 0$, substituting $u(t) = e^{rt}$ gives $r^2 + 2\eta r - v = 0$. Its larger root is

$$r_\eta(v) = \sqrt{\eta^2 + v} - \eta.$$

Unlike $\sqrt{v}$, this reward has a finite derivative at zero and is not homogeneous in v when η is fixed. The active-set analysis and dilation argument therefore need to be checked again. A damped-wave transfer would also require new bounds for the physical propagator and noise approximation; the scalar calculation alone supplies none of these bounds.

From an optimized value to the shape of large events. The constant C_2 identifies an optimized reward, but does not show that the noise or solution, conditioned on large amplification, is close to an optimizing profile. Conjecture 1.9.2 asks for compactness of one optimizing sequence after spatial translation. A further question is whether a suitable conditioned or moment-weighted law concentrates near such profiles. This needs a specified observable and scaling, tightness of the relevant laws, and upper bounds away from the optimizing set. Neither the moment limit nor the compactness conjecture alone provides these ingredients. This question concerns the shape of rare large events; its relation to typical fluctuations remains open, as discussed in Section 1.9.5.

The first test of a broader method should be a second model for which one abstract statement removes a substantial part of the proof. A damped wave with correlated Gaussian forcing is a candidate. The Gaussian geometry and finite optimization should be separated from the estimates specific to its propagator. If those estimates require rebuilding nearly every argument, then the current work offers an instructive organization of a proof, while the proposed general method remains to be found.

Chapter 2

Construction and two-chain estimates

Which solution do we mean, and which terms does its second moment contain? A Stratonovich integral keeps the pairings inside one ordered chain as well as the pairings between two chains (Figure 2.1). So products of different orders need not have zero expectation, and dropping them would change the moment under study.

We work with the model of Section 1.2. Proposition 2.1.1 gives the complete formula for the mixed moments. Lemma 2.5.2 constructs each fixed-order term. The summable bounds of Lemma 2.6.1 then construct their series, and Proposition 2.6.2 identifies it as a mild solution. These results give the construction and mixed-moment formula used later.

The last section asks how far one common bound for every pairing can go. It still loses the correct growth scale (Proposition 2.7.1). Chapters 3–11 do not use that proposition, so it can wait on a first reading. Episode ▶ 3 of the video series follows this chapter.

Put $X_n(t,x) = S_n(g_n(\cdot,t,x))$, with $X_0 = 1$, and

$$\beta = 4 - \alpha - \alpha_0 > 2, \qquad P_k = \#\Pi_k = \frac{(2k)!}{2^k k!}.$$

The count follows by pairing the smallest remaining label with one of $2k-1$ labels: $P_0 = 1$ and $P_k = (2k-1)P_{k-1}$, which gives the displayed formula by induction. All constants below may depend on the fixed covariance and its parameters, but not on the orders or on t.

2.1 The complete two-chain expansion

For $m+n = 2k$, label the two chains by $I_1 = \{1,\dots,m\}$ and $I_2 = \{m+1,\dots,m+n\}$. A self-pairing has both endpoints in one chain; a cross-pairing has one endpoint in each chain. Both are included in Π_k. Let $p(l)$ denote the preceding vertex in its own chain; at each first vertex set $(s_{p(l)}, y_{p(l)}) = (0,0)$. Thus, the second chain has its own root, rather than the last vertex of the first chain. For $D \in \Pi_k$, set

$$J_{m,n,D}(t) = \int_{[0,t]^m_< \times [0,t]^n_<} \mathrm{ds} \int_{(\mathbb{R}^d)^{m+n}} \mathrm{dy} \prod_{\rho=1}^{2} \prod_{l \in I_\rho} G(s_l - s_{p(l)}, y_l - y_{p(l)}) \times \prod_{(j,h)\in D} |s_j - s_h|^{-\alpha_0} \gamma(y_j - y_h). \tag{2.1.1}$$

An empty chain contributes the factor one. For $d = 3$, the spatial Green kernels are measures; for spatial white noise the covariance is a delta measure. Integrals in (2.1.1)

use the generalized-kernel and regularization conventions of the source, not pointwise values of these measures. Lemmas 2.5.1–2.5.2 construct them with the convention of [17, Remark 2.3, p. 11, and the Green regularization on pp. 13–14].

Proposition 2.1.1 (Mixed terms)**.** *Under Hypothesis 1.2.1,*

$$\mathbb{E}[X_m(t,x)X_n(t,x)] = \begin{cases} \displaystyle\sum_{D\in\Pi_k} J_{m,n,D}(t), & m+n=2k, \\ 0, & m+n \text{ odd}, \end{cases} \tag{2.1.2}$$

where the case $m=n=0$ equals one. In particular,

$$\mathbb{E}u^2(t,x) = \sum_{k=0}^{\infty}\sum_{m=0}^{2k}\sum_{D\in\Pi_k} J_{m,2k-m,D}(t). \tag{2.1.3}$$

This is a convergent series of nonnegative terms.

Proof. We first pass the finite Wick formula to the fixed-order limits. We then reverse the two terminal chains separately and identify their initial-chain diagrams. Finally, norm summability and nonnegativity justify the complete second-moment series.

Step 1. We identify the fixed-order limits without using the infinite series. Lemma 2.5.2 below constructs each X_n and each individual two-chain diagram at arbitrary vertexwise widths, including unequal and empty chains. Its proof uses the positive spatial-measure limit and Lemma 2.4.1; it uses neither the present proposition nor any infinite solution series.

Here Y_m, Y_n denote the positive-width terminal integrals $Y_m^{\boldsymbol{a}}, Y_n^{\boldsymbol{a}}$ with the respective vertexwise widths suppressed; their joint width limit is the L^2 limit in Lemma 2.5.2. At positive noise widths Wick's formula gives zero at odd total order and the finite pairing sum at even total order. The Green-width limit is taken first, as in the construction preceding Lemma 2.5.1. At fixed m, n, joint L^2 convergence of the two factors gives product convergence in L^1:

$$\|Y_mY_n - X_mX_n\|_1 \le \|Y_m - X_m\|_2\|Y_n\|_2 + \|X_m\|_2\|Y_n - X_n\|_2 \longrightarrow 0.$$

A zero-order factor stays equal to one. Each individual Wick diagram also has the finite nonnegative limit in Lemma 2.5.2.

Step 2. We reverse the two chains and relabel the pairings. To identify its initial-chain form, for terminal variables in the first chain set

$$s'_j = t - s_{m+1-j}, \qquad y'_j = x - y_{m+1-j}, \qquad 1 \le j \le m,$$

and use the corresponding length-n transformation on the second chain. Each transformed chain has initial root $(0,0)$. For example, $G(t-s_m, x-y_m)$ becomes $G(s'_1, y'_1)$; every other factor becomes the corresponding successive increment. The differences in each covariance change sign, absorbed by evenness. The vertex involution is

$$\rho(j) = m+1-j \ (1 \le j \le m), \qquad \rho(m+j) = m+n+1-j \ (1 \le j \le n).$$

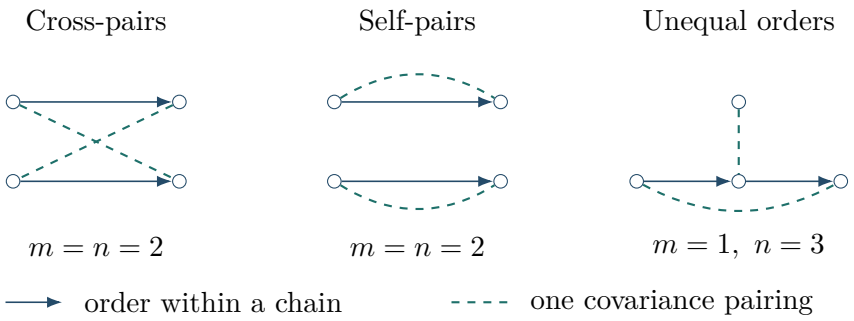

Figure 2.1: Three permitted pairing contributions. Each chain has its own time order; no common interleaving is imposed by the picture. Stratonovich products include self-pairs and unequal orders, as well as cross-pairs. These examples do not list every pairing. See Proposition 2.1.1.

It induces the pairing bijection $D \mapsto \{\{\rho(a), \rho(b)\} : \{a, b\} \in D\}$. The same transformation holds before removing noise smoothing. Passing to the finitely many diagram limits proves (2.1.2) with precisely (2.1.1).

Step 3. We sum the mixed expectations using absolute norm convergence. Lemmas 2.5.3 and 2.6.1 independently prove fixed-t norm summability of the X_n, using the fixed-order construction just cited and Lemma 2.4.1. Proposition 2.6.2 identifies their series as a Stratonovich mild solution. None of those proofs uses the present mixed-term identity. Hence, $U_N = \sum_{n=0}^{N} X_n \to u$ in L^2, and

$$|\mathbb{E}U_N^2 - \mathbb{E}u^2| \le \|U_N - u\|_2(\|U_N\|_2 + \|u\|_2) \longrightarrow 0.$$

Each finite square expands over the square of indices $0 \le m, n \le N$.

The finite expansions of $\mathbb{E}U_N^2$ increase, since every mixed expectation computed above is nonnegative. Their limit is the full double sum, independent of its enumeration. Regrouping by total order gives (2.1.3). This proves Proposition 2.1.1. □

The two chain orders must remain distinct: chronological concatenation can violate wave support, and a difference of block labels need not measure chronological separation. No-gos 05 and 07 give explicit positive-measure witnesses.

2.2 A small-order check and a source uniformity issue

Lean partial

Lemma 2.2.1 (White-space test)**.** *For $d = \alpha = 1$ and $\gamma = \delta_0$, put $c_0 = ((1-\alpha_0)(2-\alpha_0)(3-\alpha_0))^{-1}$. Then*

$$\mathbb{E}X_1(t,x)^2 = c_0 t^{3-\alpha_0}, \qquad \mathbb{E}X_2(t,x) = \tfrac{1}{2}c_0 t^{3-\alpha_0}. \tag{2.2.1}$$

In particular, the total-order-two contribution to (2.1.3) is $2c_0 t^{3-\alpha_0}$.

Proof. Here $G(s,y)=\frac{1}{2}\mathbf{1}_{\{|y|<s\}}$. Therefore, $\int_{\mathbb{R}} G(s,y)G(r,y)\,\mathrm{d}y=\min(s,r)/2$. The $(1,1)$ integral is

$$\int_0^t \mathrm{d}s\int_0^s r(s-r)^{-\alpha_0}\,\mathrm{d}r=\frac{t^{3-\alpha_0}}{(1-\alpha_0)(2-\alpha_0)(3-\alpha_0)}.$$

For the $(0,2)$ integral, the delta covariance sets the two spatial vertices equal. Write $0<r<s<t$ for their ordered time variables. The first factor G_r has spatial mass r, while $G_{s-r}(0)=1/2$. Its time integral is half the preceding display. The $(2,0)$ term is identical. This proves Lemma 2.2.1. □

Remark 2.2.2 (Source fidelity)**.** The author version's Remark 5.1 refers to (4.4), but (4.4), on p. 22, is a smoothing limit. The relevant bound is (5.4), on p. 35, $\mathbb{E}X_n(t,x)^2\le C^n t^{2n}/n!$, with the preceding sentence asserting that C is independent of n and t. Taken for all $t>0$, this uniformity contradicts (2.2.1) at $n=1$. The proof on pp. 34–35 sets $\theta=n/t$. Its first-norm estimate uses (A.1), which is finite for every positive θ but does not give a constant uniform as $\theta\downarrow 0$. Its second-norm estimate uses the large-θ bound (A.3) without retaining that restriction. Both losses of uniformity matter when n/t is small. This is a source-internal uniformity discrepancy; it does not refute Remark 5.1's final large-time conclusion. The next lemma repairs this particular deduction without importing the asserted uniformity of (5.4).

2.3 Recovering the quadratic-exponential bound

Write $G_\theta(s,y)=e^{-\theta s}G(s,y)$ and $\widehat{G}_s(\xi)=\sin(s|\xi|)/|\xi|$, with value s at $\xi=0$. We use the norms in the source's (3.3)–(3.5), with the full covariance, but give their bounds directly. Write Γ_{E} for Euler's Gamma function in the following definitions, to distinguish it from the covariance measure:

$$\begin{aligned}
N_0(\theta)&=\int_0^\infty e^{-\theta s}G_s(\mathbb{R}^d)\,\mathrm{d}s,\\
N_1(\theta)&=\frac{1}{\Gamma_{\mathrm{E}}(\alpha_0)}\int_0^\infty \lambda^{\alpha_0-1}\,\mathrm{d}\lambda\int\frac{\mu(\,\mathrm{d}\xi)}{(\theta+\lambda)^2+|\xi|^2},\\
N_2(\theta)^2&=\int_0^\infty\int_0^\infty e^{-\theta(s+t)}|s-t|^{-\alpha_0}\int\widehat{G}_s(\xi)\overline{\widehat{G}_t(\xi)}\mu(\,\mathrm{d}\xi)\,\mathrm{d}s\,\mathrm{d}t.
\end{aligned}\tag{2.3.1}$$

The second expression uses the elementary wave Laplace transform $\int_0^\infty e^{-as}\widehat{G}_s(\xi)\,\mathrm{d}s=(a^2+|\xi|^2)^{-1}$. The last expression is the space-time covariance quadratic form; in physical variables it pairs $G_\theta(s,x)$ with $G_\theta(t,y)$. Thus, the second Green factor in the printed source (3.5) is read with the independent variable y; see Lemma 2.3.2 and Remark 2.3.3 for the independent justification and the exact source qualification.

Lean full

Lemma 2.3.1 (Homogeneous damped norms and temporal tails)**.** *Under Hypothesis 1.2.1, the integrals in (2.3.1) are finite for every $\theta>0$, with $N_2(\theta)^2\ge 0$, and*

$$N_0(\theta)=\theta^{-2},\qquad N_1(\theta)=\theta^{\alpha+\alpha_0-2}N_1(1),\qquad N_2(\theta)^2=\theta^{-\beta}N_2(1)^2,\quad \beta=4-\alpha-\alpha_0.$$

Let

$$K_M(r) = \frac{1}{\Gamma_{\mathrm{E}}(\alpha_0)} \int_M^\infty e^{-\lambda|r|} \lambda^{\alpha_0 - 1} \,\mathrm{d}\lambda.$$

Denote by $N_1^{(M)}(1)$ *the first norm with* $\lambda > M$*, and by* $N_2^{(M)}(1)$ *the second norm with* $K_M(s-t)$ *in place of* $|s-t|^{-\alpha_0}$*. Then*

$$N_1^{(M)}(1) \longrightarrow 0, \qquad N_2^{(M)}(1) \longrightarrow 0 \quad (M \to \infty). \tag{2.3.2}$$

More precisely, let $m : \mathbb{R}^d \to [0,1]$ *be measurable and let* $S \subset S' \subset (0,\infty)$ *be measurable. Define* $N_{1,m,S}(\theta)$ *by replacing* μ *with* $m\mu$ *and restricting the* λ *integral in* N_1 *to* S*. Define* $N_{2,m,S}(\theta)^2$ *by replacing* μ *with* $m\mu$ *and the temporal kernel in* N_2^2 *with*

$$K_S(r) = \frac{1}{\Gamma_{\mathrm{E}}(\alpha_0)} \int_S e^{-\lambda|r|} \lambda^{\alpha_0 - 1} \,\mathrm{d}\lambda.$$

Then, for every $\theta > 0$*,*

$$\begin{aligned} 0 \le N_{1,m,S}(\theta) &\le N_{1,1,S'}(\theta), \\ 0 \le N_{2,m,S}(\theta)^2 &\le N_{2,1,S'}(\theta)^2. \end{aligned} \tag{2.3.3}$$

These are comparisons of spectral expressions, including full and tail domains. An arbitrary m *need not preserve Hypothesis 1.2.1; the scaling identities above are asserted for the original covariance only. Spatial Gaussian smoothing and Gaussian smoothing of the Green kernel give multipliers in this class. The separate mass identity for* N_0 *is unchanged by Gaussian smoothing of the Green kernel.*

Proof. We use radial spectral masses to bound the first norm and absolute wave estimates to control the second. Scaling gives their exact homogeneous powers. Tail convergence and multiplier comparisons are then proved from nonnegative spectral expressions after time integration.

Step 1. We bound the first norm by the homogeneous resolvent integral. Scaling the Fourier representation of Γ and using Fourier uniqueness gives $\mu(cA) = c^\alpha \mu(A)$. Radon finiteness and $\alpha > 0$ then imply $\mu(\{0\}) = 0$. In particular, $\mu(B_r) = r^\alpha V$, where $V = \mu(B_1) < \infty$. Therefore, for $a > 0$,

$$\int \frac{\mu(\,\mathrm{d}\xi)}{a^2 + |\xi|^2} = \alpha V a^{\alpha-2} \int_0^\infty \frac{u^{\alpha-1}}{1+u^2} \,\mathrm{d}u < \infty.$$

The last integral is finite since $0 < \alpha < 2$. Substitution into N_1 reduces its finiteness to $\int_0^\infty \lambda^{\alpha_0-1}(\theta+\lambda)^{\alpha-2} \,\mathrm{d}\lambda < \infty$: the conditions at zero and infinity are $\alpha_0 > 0$ and $\alpha + \alpha_0 < 2$.

Step 2. We prove absolute integrability and positivity of the second norm. For N_2 use $|\widehat{G}_s(\xi)| \le \min(s, |\xi|^{-1})$. On $|\xi| \le 1$, absolute integration is bounded by

$$V \int_0^\infty \int_0^\infty e^{-\theta(s+t)} |s-t|^{-\alpha_0} st \,\mathrm{d}s \,\mathrm{d}t < \infty.$$

On $|\xi| > 1$, use $\int_{|\xi|>1} |\xi|^{-2}\mu(\mathrm{d}\xi) = \alpha V/(2-\alpha)$ and the same time integral without st. Both time integrals are finite by splitting into $s \le t$ and $t \le s$, then using $u = \min(s,t)$ and $v = |s-t|$; the only singular factor is $v^{-\alpha_0}$, with $\alpha_0 < 1$. This proves absolute integrability of the displayed spectral formula. For each ξ, its time integral is nonnegative because the temporal kernel is positive definite. Indeed, it is a positive Laplace mixture of the kernels $e^{-\lambda|s-t|}$. This proves $N_2(\theta)^2 \ge 0$.

Step 3. We compute the homogeneous powers. The mass identity $G_s(\mathbb{R}^d) = s$ proves the formula for N_0. In N_1 change $\lambda = \theta u$ and $\xi = \theta\eta$. In N_2 change $s = u/\theta$, $t = v/\theta$ and $\xi = \theta\eta$, using $\widehat{G}_{u/\theta}(\theta\eta) = \theta^{-1}\widehat{G}_u(\eta)$. These changes give exactly the stated powers.

For N_1, the temporal measure contributes θ^{α_0}, the spatial measure contributes θ^{α}, and the resolvent contributes θ^{-2}. For N_2^2, the two time Jacobians and two wave factors contribute θ^{-4}, while the temporal kernel and spatial measure contribute $\theta^{\alpha_0+\alpha}$.

Step 4. We remove temporal tails using the absolute majorant. The first tail in (2.3.2) is a tail of the finite nonnegative $N_1(1)$ integral. For the second, $0 \le K_M(r) \le |r|^{-\alpha_0}$ and $K_M(r) \to 0$ for $r \ne 0$. The absolute majorant just proved permits dominated convergence in (s,t,ξ), giving $N_2^{(M)}(1)^2 \to 0$. The tail kernel is positive definite by the same Laplace-mixture argument, so its quadratic form is nonnegative.

Step 5. We compare nonnegative spectral quadratic forms. For the multiplier comparisons, define

$$B_\theta(\lambda,\xi) = \int_0^\infty \int_0^\infty e^{-\theta(s+t)} e^{-\lambda|s-t|} \widehat{G}_s(\xi)\overline{\widehat{G}_t(\xi)}\,\mathrm{d}s\,\mathrm{d}t.$$

For each $\lambda > 0$ and ξ, the positive definiteness of $e^{-\lambda|s-t|}$ gives $B_\theta(\lambda,\xi) \ge 0$. The absolute-integrability bound above, $0 \le m \le 1$ and $0 \le K_S \le |\cdot|^{-\alpha_0}$ justify changing the integration order:

$$N_{2,m,S}(\theta)^2 = \frac{1}{\Gamma_{\mathrm{E}}(\alpha_0)} \int_S \lambda^{\alpha_0-1} \int m(\xi) B_\theta(\lambda,\xi)\mu(\mathrm{d}\xi)\,\mathrm{d}\lambda.$$

Nonnegativity now proves the second comparison in (2.3.3). It is used after time integration, not pointwise on the oscillating product of wave Fourier kernels. The first comparison follows directly from the nonnegative integrand defining N_1. The choices $S = (0,\infty)$ or $S = (M,\infty)$ give the full or tail bounds. Gaussian spatial and Green smoothing contribute products of multipliers in $[0,1]$ depending only on ξ. Gaussian Green smoothing also preserves $G_s(\mathbb{R}^d) = s$, proving its separate assertion for N_0. This proves Lemma 2.3.1. □

Covariance pairings of translated kernels. Fix $d \in \{1,2,3\}$. Let μ be a finite positive Borel measure on $\mathbb{R}^d$ such that $\gamma(z) = \int e^{i\xi\cdot z}\mu(\mathrm{d}\xi)$ is real and nonnegative for every z. Thus, γ is bounded, continuous and even, with $0 \le \gamma(z) \le \mu(\mathbb{R}^d)$. Let ν be a positive Borel measure on $(0,\infty)$ with $\nu((0,L]) < \infty$ for every $L > 0$, and put

$$\kappa_L(t) = \int_{(0,L]} e^{-\lambda|t|}\nu(\mathrm{d}\lambda), \qquad C_L((t,x),(s,y)) = \kappa_L(t-s)\gamma(x-y).$$

For complex $L^1(\mathbb{R}\times\mathbb{R}^d)$ functions f,h, define

$$Q_L(f,h)=\int_{\mathbb{R}^2}\int_{\mathbb{R}^{2d}} f(t,x)\overline{h(s,y)}\kappa_L(t-s)\gamma(x-y)\,\mathrm{d}x\,\mathrm{d}y\,\mathrm{d}t\,\mathrm{d}s. \tag{2.3.4}$$

This integral is absolutely convergent, with $|Q_L(f,h)|\le \nu((0,L])\mu(\mathbb{R}^d)\|f\|_1\|h\|_1$. For nonnegative f,h, define $Q(f,h)=\lim_{L\to\infty}Q_L(f,h)$ as an extended nonnegative number. This positive cap limit also defines the pairing when the full temporal kernel is singular on the diagonal. The spatial covariance is fixed throughout this definition. For a nonnegative Borel function G on $(0,\infty)\times\mathbb{R}^d$, let G^0 be its zero extension to nonpositive times and put

$$N_0(G)=\int_0^\infty\int_{\mathbb{R}^d} G(t,x)\,\mathrm{d}x\,\mathrm{d}t,\qquad N_C(G)^2=Q(G^0,G^0).$$

For $(A,a)\in\mathbb{R}\times\mathbb{R}^d$, write $T_{A,a}f(t,x)=f(t-A,x-a)$. All translated pairings are over the full time line.

Lemma 2.3.2 (Translated covariance Cauchy–Schwarz)**.** *Under the preceding assumptions on μ and ν, let G_1,G_2 be nonnegative Borel functions with $N_0(G_i),N_C(G_i)<\infty$, $i=1,2$. For arbitrary origins $(A,a),(B,b)\in\mathbb{R}\times\mathbb{R}^d$,*

$$0\le Q(T_{A,a}G_1^0,T_{B,b}G_2^0)\le N_C(G_1)N_C(G_2), \tag{2.3.5}$$

and $Q(T_{A,a}G_i^0,T_{A,a}G_i^0)=N_C(G_i)^2$ for $i=1,2$. The coefficient one is independent of the origins, dimension, cap and covariance masses. Zero norms and zero measures are included.

Proof. At a finite temporal cap we represent the stationary covariance as an inner product. We use its Cauchy–Schwarz inequality together with translation invariance of each self-pairing. Positive truncation and cap limits then extend the result to the stated kernels.

Step 1. We represent the capped covariance by deterministic Hilbert features. We first prove positivity and Cauchy–Schwarz for the stationary kernel C_L at fixed finite L. For $\lambda>0$, define

$$h_\lambda(t,r)=\sqrt{2\lambda}\,e^{-\lambda(t-r)}\mathbf{1}_{\{r\le t\}}.$$

Direct integration gives

$$\int_{\mathbb{R}} h_\lambda(t,r)h_\lambda(s,r)\,\mathrm{d}r=2\lambda e^{-\lambda(t+s)}\int_{-\infty}^{\min(t,s)}e^{2\lambda r}\,\mathrm{d}r=e^{-\lambda|t-s|}.$$

In particular, $\int h_\lambda(t,r)^2\,\mathrm{d}r=1$. On the complex Hilbert space

$$\mathcal{H}_L=L^2((0,L]\times\mathbb{R}^d\times\mathbb{R},\nu(\,\mathrm{d}\lambda)\mu(\,\mathrm{d}\xi)\,\mathrm{d}r),$$

with inner product linear in its first entry, put $\Phi_L(t,x)(\lambda,\xi,r)=h_\lambda(t,r)e^{i\xi\cdot x}$. Then

$$\|\Phi_L(t,x)\|^2=m_L:=\nu((0,L])\mu(\mathbb{R}^d),\qquad \langle\Phi_L(t,x),\Phi_L(s,y)\rangle=C_L((t,x),(s,y)).$$

The scalar integrals are absolutely convergent: Cauchy–Schwarz in r bounds $\int |h_\lambda(t,r)h_\lambda(s,r)|\,\mathrm{d}r$ by one, and both remaining measures are finite on the cap.

Step 2. We identify the covariance integral as a Hilbert pairing. The map $(t,x) \mapsto \Phi_L(t,x)$ is norm-continuous, since its squared increment is $2m_L - 2\,\mathrm{Re}\,C_L((t,x),(s,y))$. Continuity of C_L follows by dominated convergence against the finite measures. Thus, the map is strongly measurable, has separable range and is bounded. For $f \in L^1$, the Bochner integral $F_L(f) = \int f(t,x)\Phi_L(t,x)\,\mathrm{d}t\,\mathrm{d}x$ exists. Bochner Fubini, justified by $m_L\|f\|_1\|h\|_1$, gives $Q_L(f,h) = \langle F_L(f), F_L(h)\rangle$. Therefore,

$$|Q_L(f,h)| \le Q_L(f,f)^{1/2} Q_L(h,h)^{1/2}.$$

This uses the original stationary covariance, rather than positivity of an independently shifted cross kernel. The feature space is deterministic and introduces no new Gaussian field.

Step 3. We compare different translates through their unchanged self norms. Changing both integration variables in (2.3.4) by the same time and spatial translation gives

$$Q_L(T_{A,a}f, T_{A,a}h) = Q_L(f,h).$$

Both differences remain unchanged. The full time line and Lebesgue translation invariance justify this equality without an origin factor. Apply Cauchy–Schwarz to the two different translates and this equality separately to their self pairings. This proves the capped form of (2.3.5).

Step 4. We pass the nonnegative kernel and temporal-cap limits. To make the passage for possibly unbounded nonnegative kernels explicit, set

$$G_{i,M}(t,x) = \min(G_i(t,x), M)\mathbf{1}_{\{0<t\le M,\ |x|\le M\}}, \qquad M \in \mathbb{N}.$$

These functions increase to G_i almost everywhere. Their zero extensions and translates are bounded compactly supported L^1 functions. Since $C_L \ge 0$, monotone convergence passes the capped inequality and common-translation identity to G_i as $M \to \infty$. Equivalently, the finite-cap passage follows from L^1 convergence and the absolute bound after (2.3.4).

Finally, positivity of ν and nonnegativity of γ give

$$Q_L(G_i^0, G_i^0) \uparrow N_C(G_i)^2, \qquad Q_L(T_{A,a}G_1^0, T_{B,b}G_2^0) \uparrow Q(T_{A,a}G_1^0, T_{B,b}G_2^0).$$

The finite self norms bound the latter limit by $N_C(G_1)N_C(G_2)$. The common-translation identity passes to the limit in the same way. No division by a norm is used, so zero norms cause no exception. No spatial Gaussian mollifier is removed in this argument. This proves Lemma 2.3.2. □

Remark 2.3.3 (Source Case 2 and the regularized inputs)**.** *(i)* In Case 2 of the proof of [17, Theorem 3.1, p. 21], the final vertices belong to two nonempty chains of lengths n_1, n_2 with $n_1 + n_2 = 2n$. Fix their predecessor origins separately:

$$(A,a) = \begin{cases} (0,0), & n_1 = 1, \\ (s_{n_1-1}, x_{n_1-1}), & n_1 > 1, \end{cases} \qquad (B,b) = \begin{cases} (0,0), & n_2 = 1, \\ (s_{2n-1}, x_{2n-1}), & n_2 > 1. \end{cases}$$

The second chain's first vertex uses its own root. An empty chain has no interchain Case 2 pair. The final-pair integral is, using evenness to fix the orientation,

$$\begin{aligned} I &= \int_A^\infty \int_B^\infty \int_{\mathbb{R}^{2d}} G_1(t-A, x-a)\kappa(t-s)\gamma(x-y)G_2(s-B, y-b)\,\mathrm{d}x\,\mathrm{d}y\,\mathrm{d}s\,\mathrm{d}t \\ &= Q(T_{A,a}G_1^0, T_{B,b}G_2^0), \end{aligned}$$

where the full temporal expression means the positive cap limit. Lemma 2.3.2 gives $0 \le I \le N_C(G_1)N_C(G_2)$ uniformly in the predecessors, so the bound can be inserted into the remaining nonnegative integrals in the source's induction. If only $u = t - A$ and $v = s - B$ are substituted, the integrand has factors

$$G_1(u, x-a)\kappa(u - v + A - B)\gamma(x-y)G_2(v, y-b). \tag{2.3.6}$$

The time difference $A - B$ must remain. The source's first Case 2 equality on physical p. 21 displays $\kappa(u-v)$ after this change of time variables, which is not an identity for general $A \neq B$. Its spatial origins remain in the two tests, so $\gamma(x-y)$ is correct in those absolute spatial variables. Changing also $x = X + a$, $y = Y + b$ gives $\gamma(X - Y + a - b)$. We use the original integral and the proved inequality, not the offset-free equality or positivity of a shifted cross kernel.

(ii) The norm $N_C(G)$ pairs $G(t,x)$ with $G(s,y)$ in (2.3.4), with independent spatial variables. The source's printed (3.5), physical p. 14, repeats x in its second Green factor. Our quadratic form states explicitly the convention used in (2.3.1); it is not a literal quotation of that display.

(iii) We use the common-prefix source convention of [17, (2.11), p. 9, and (2.24), p. 13]. Write $Y_{\epsilon,\delta}$ for its positive-width fields. Independence of disjoint Laplace-frequency increments makes the cross covariance of two prefixes their common part. Their upper limits are δ_j^{-1} and δ_h^{-1}, whose minimum is $(\delta_j \vee \delta_h)^{-1}$. Spatial heat convolution on the two fields gives $p_{\epsilon_j} * p_{\epsilon_h} = p_{\epsilon_j+\epsilon_h}$. Thus, with the original covariance amplitude,

$$\begin{aligned} \mathbb{E}[Y_{\epsilon_j,\delta_j}(s,x)Y_{\epsilon_h,\delta_h}(t,y)] &= \kappa_{\delta_j\vee\delta_h}(s-t)(p_{\epsilon_j+\epsilon_h} * \Gamma)(x-y), \\ \kappa_\delta(u) &= \frac{1}{\Gamma_{\mathrm{E}}(a)} \int_0^{\delta^{-1}} e^{-\lambda|u|}\lambda^{a-1}\,\mathrm{d}\lambda, \qquad a = \alpha_0. \end{aligned} \tag{2.3.7}$$

For generalized Γ, the spatial identity follows by testing against heat functions, or by their spectral multipliers; it requires no covariance density. The endpoint zero in the Laplace interval has zero Lebesgue measure, so $[0, L]$ and $(0, L]$ give the same integral. This verifies the covariance used on each vertexwise edge. It does not construct the coupled family from the given W alone. Its common-field realization, any prescribed auxiliary Gaussian extension, and its joint source limits remain the separate hypotheses and deductions of Lemmas 2.5.1–2.5.2; no new point-field measurability or uniqueness claim is made here. At an edge $e = \{j, h\}$, retain positive spatial widths ϵ_j, ϵ_h and use

$$\mu_e(\,\mathrm{d}\xi) = e^{-(\epsilon_j+\epsilon_h)|\xi|^2/2}\mu(\,\mathrm{d}\xi), \qquad \gamma_e = p_{\epsilon_j+\epsilon_h} * \Gamma \ge 0.$$

For $b = \epsilon_j + \epsilon_h > 0$, the radial ball masses $\mu(B_r) = Vr^\alpha$ from Lemma 2.3.1 give

$$\mu_e(\mathbb{R}^d) = \alpha V b^{-\alpha/2} \int_0^\infty u^{\alpha-1}e^{-u^2/2}\,\mathrm{d}u < \infty.$$

This uses ball masses rather than a radial density, and establishes finiteness only. It does not replace the later uniform norm bounds. Nonnegativity of the heat convolution follows from the nonnegative Radon measure Γ. This spatial covariance stays fixed during the lemma's application. For a measurable temporal domain $A_e \subset (0,\infty)$, use

$$\nu_e(\mathrm{d}\lambda) = \mathbf{1}_{A_e}(\lambda)\lambda^{\alpha_0-1}\,\mathrm{d}\lambda/\Gamma_{\mathrm{E}}(\alpha_0).$$

Since $\alpha_0 > 0$, it is finite on every $(0, L]$. This covers both bounded regularization domains and marked-tail domains after adding the finite cap, with the Gamma normalization already included. The tested kernels are $e^{-\theta t}G_t$, with positive Green smoothing in dimension three when a function is required. They have $N_0 = \theta^{-2}$, and Lemma 2.3.1 supplies the finite full and tail second-norm bounds and first-norm bounds. These are precisely the edge norm hypotheses used in Lemma 2.4.1. The Case 2 estimate contributes exactly its two second norms, with coefficient one. It changes neither a Q_2 factor nor any coefficient estimate and adds no factor depending on $A + B$. Temporal cap removal uses positivity; Green-width removal at fixed positive spatial widths and the subsequent spatial-noise limit retain their separate weak-limit arguments in Lemmas 2.5.2 and 2.5.1. No pointwise monotonicity of spatial Gaussian smoothing or general unregularized spatial-distribution version is asserted.

(iv) We prove the product estimate needed here in Lemma 2.4.1, rather than importing the remaining displayed induction. On p. 16, the empty-first-chain base caption interchanges the mass and first-norm kernel labels; their chronological order gives mass on the first kernel. On p. 18, (3.9) omits the factor two when a fused kernel occupies a first-norm slot. Retaining that factor and using the mass times first-norm convolution bound below preserves the half-bound needed in Case 3. The p. 19 mass-slot partition uses a union of the two excluded labels, not the printed intersection; its first-slot edge count excludes the fused slot. The p. 21 Case 2 offset is handled by the preceding lemma. These are explicit qualifications of the printed formulas, not corrections attributed to the source or a claim that its intended product bound is false. The finite maximum below is sufficient for all our uses; we assert no partition independent of the kernel family.

2.4 A finite product bound for two ordered chains

Fix $d \geq 1$, $0 < a < 1$ and a matching D on $2n$ labels. For each edge $e \in D$, let μ_e be finite and positive, with $\gamma_e(x) = \int e^{i\xi\cdot x}\mu_e(\mathrm{d}\xi) \geq 0$. For a measurable $A_e \subset (0,\infty)$ put

$$\nu_e(\mathrm{d}\lambda) = \Gamma_{\mathrm{E}}(a)^{-1}\mathbf{1}_{A_e}(\lambda)\lambda^{a-1}\,\mathrm{d}\lambda, \qquad \kappa_e(t) = \int e^{-\lambda|t|}\nu_e(\mathrm{d}\lambda).$$

For nonnegative $G \in L^1((0,\infty)\times\mathbb{R}^d)$ define

$$\begin{aligned} N_0(G) &= \int G(t,x)\,\mathrm{d}t\,\mathrm{d}x, \\ N_{1,e}(G) &= \int \left|\int e^{-\lambda t + i\xi\cdot x}G(t,x)\,\mathrm{d}t\,\mathrm{d}x\right| \nu_e(\mathrm{d}\lambda)\mu_e(\mathrm{d}\xi), \\ N_{2,e}(G)^2 &= \int G(s,x)G(t,y)\kappa_e(s-t)\gamma_e(x-y)\,\mathrm{d}s\,\mathrm{d}x\,\mathrm{d}t\,\mathrm{d}y. \end{aligned} \tag{2.4.1}$$

Time integrations in these definitions are positive. Denote the inner Laplace–Fourier transform by $\mathcal{L}G(\lambda,\xi)$. The last integral means its nonnegative temporal cap limit, as in the preceding covariance pairing. In particular, its spatial variables are independent.

Let $I_1=\{1,\dots,n_1\}$ and $I_2=\{n_1+1,\dots,2n\}$, where $n_1+n_2=2n$ and either chain may be empty. Each chain is ordered in its own time variables. Write $p(l)$ for its predecessor, using $(s_{p(l)},x_{p(l)})=(0,0)$ at the first vertex of each chain. Set

$$\begin{aligned} I_D(\boldsymbol{G}) = \int \prod_{\rho=1}^{2} \prod_{l\in I_\rho} G_l(s_l-s_{p(l)},x_l-x_{p(l)}) \\ \times \prod_{e=\{j,k\}\in D} \kappa_e(s_j-s_k)\gamma_e(x_j-x_k)\,\mathrm{d}\boldsymbol{s}\,\mathrm{d}\boldsymbol{x}. \end{aligned} \tag{2.4.2}$$

The domain is the product of the two positive ordered time simplices and all spatial variables.

Call (Q,ι) admissible if Q_0,Q_1,Q_2 partition the kernel labels, $|Q_0|=|Q_1|$, and the map $\iota: Q_1\cup Q_2\to D$ uses each edge once on Q_1 or twice on Q_2, never both. There is no incidence requirement between l and $\iota(l)$. These assignments form a finite nonempty set $\mathcal{A}_D$. Put

$$\mathcal{P}_{Q,\iota}(\boldsymbol{G}) = \prod_{l\in Q_0} N_0(G_l) \prod_{l\in Q_1} 2N_{1,\iota(l)}(G_l) \prod_{l\in Q_2} N_{2,\iota(l)}(G_l). \tag{2.4.3}$$

Thus, $|Q_2|$ is even and $|Q_0|+|Q_2|/2=n$.

Lemma 2.4.1 (Pairing product envelope)**.** *Suppose every G_l is nonnegative and integrable, and $N_{1,e}(G_l),N_{2,e}(G_l)<\infty$ for every l and $e\in D$. Then*

$$I_D(\boldsymbol{G}) \le \max_{(Q,\iota)\in\mathcal{A}_D} \mathcal{P}_{Q,\iota}(\boldsymbol{G}). \tag{2.4.4}$$

A maximizing assignment may depend on the kernels and edge data. No single assignment valid for all kernel families is asserted. For $n=0$, both sides are one. Zero kernels, measures and norms are allowed.

Proof. We establish convolution bounds for fused kernels, then prove a regional half-bound by induction. The endpoint configurations either give that bound directly, give two second norms, or split into two half-bounds. The finite maximum permits different assignments on the two regions.

Step 1. We work at finite temporal cap and control fused kernels. First cap every temporal domain at $L<\infty$; its measure is finite since $a>0$. The stationary covariance pairing in Lemma 2.3.2 has norm $N_{2,e}$. Its feature $h_\lambda(t,r)e^{i\xi\cdot x}$ and its proof apply in any finite dimension: their only spatial input is the finite measure μ_e. Hence, its coefficient-one Cauchy–Schwarz inequality and invariance under simultaneous time and space translation apply here. All Fourier and Bochner interchanges at this cap are justified by the finite covariance mass times the relevant L^1 masses.

For one-sided spacetime convolution $F = G * H$, positivity and the Laplace–Fourier product give

$$\begin{aligned} N_0(F) &= N_0(G)N_0(H), \\ N_{1,e}(F) &\le N_0(G)N_{1,e}(H), \\ N_{2,e}(F) &\le N_0(G)N_{2,e}(H). \end{aligned} \tag{2.4.5}$$

Indeed, $|\mathcal{L}G(\lambda,\xi)| \le N_0(G)$ for $\lambda \ge 0$ proves the first-norm estimate. For the second, zero-extend H in time. Its translates have the same covariance Hilbert norm. Express $G * H$ as their Bochner integral against G and apply Minkowski. Thus, every fused kernel satisfies all remaining edge hypotheses. No division by a norm is used.

Step 2. We prove the regional half-bound and its admissible assignments. We use induction on n, beginning with the empty product at $n = 0$. With two vertices on one chain the integral is at most $N_0(G_{\text{first}})N_{1,e}(G_{\text{last}})$; with one on each chain it is at most their two second norms by covariance Cauchy–Schwarz. These also verify both nonempty-chain orientations at $n = 1$. Assume the full bound at $n - 1$.

We first prove a half-bound on any region where an endpoint v, its predecessor p and its partner a satisfy $s_a \le s_p$. Require the region indicator to be independent of (s_v, x_v). Write $e_0 = \{a, v\}$. Since κ_{e_0} is decreasing on positive arguments, replace $\kappa_{e_0}(s_v - s_a)$ by $\kappa_{e_0}(s_v - s_p)$. Integrating the endpoint and taking the modulus of its spatial Fourier phase gives the factor

$$\int |\mathcal{L}G_v(\lambda,\xi)|\nu_{e_0}(\,\mathrm{d}\lambda)\mu_{e_0}(\,\mathrm{d}\xi) = N_{1,e_0}(G_v).$$

Now drop the region indicator by positivity. Remove v and its edge. Its partner a is unpaired. If a is terminal in its remaining chain, integrate it to $N_0(G_a)$ and apply induction. The result is one half of an admissible product, adding a to Q_0 and v to Q_1 with edge e_0.

Otherwise, let b be the immediate successor of a on its own chain. Integration at a gives exactly $F = G_a * G_b$ at b, also when a was the first vertex. Apply induction to the two reduced chains and $D \setminus \{e_0\}$. Mark the slot $i = 0, 1, 2$ occupied by F in a maximizing reduced product. Let R_0, R_1, R_2 be its other slots and B_{rest} their product, retaining every first-slot factor two. The new slots can be chosen as follows:

i	Q_0	Q_1	Q_2
0	$R_0 \cup \{a, b\}$	$R_1 \cup \{v\}$	R_2
1	$R_0 \cup \{a\}$	$R_1 \cup \{b, v\}$	R_2
2	$R_0 \cup \{a\}$	$R_1 \cup \{v\}$	$R_2 \cup \{b\}$.

For $i = 0$, $|R_0| + 1 = |R_1|$ and $|R_2|$ is even. Mass multiplicativity gives one half of the displayed new product. For $i = 1$, $|R_0| = |R_1| + 1$ and $|R_2|$ is even. If e_1 is the inherited edge, the term and its bound are

$$\begin{aligned} &N_{1,e_0}(G_v)\,[2N_{1,e_1}(F)]B_{\text{rest}} \\ &\quad \le \tfrac{1}{2}N_0(G_a)[2N_{1,e_1}(G_b)][2N_{1,e_0}(G_v)]B_{\text{rest}}. \end{aligned}$$

The inherited edge stays first exactly once; e_0 is first once. No incidence condition is needed. For $i = 2$, $|R_0| = |R_1|$ and $|R_2|$ is odd; e_1 already occurs once there. The last inequality in (2.4.5) puts its other second norm on G_b, a mass on G_a and $2N_{1,e_0}(G_v)$ on v, again with a factor one half. Every old edge retains its type and multiplicity. The displayed counts give $|Q_0| = |Q_1|$ and even $|Q_2|$ in all three cases. This proves the regional half-bound, using only the full induction hypothesis, not an assumed stronger induction.

Step 3. We treat same-chain pairs and the pair of terminal endpoints. If an endpoint is paired to a vertex in its own chain, its partner is at or before its predecessor. Hence, this half-bound applies on the entire domain. This also handles an empty chain. If both endpoints $u = n_1$ and $v = 2n$ are paired to each other, condition on their separate predecessors $(A, z), (B, w)$. The endpoint integral keeps the temporal argument $r - q + A - B$ in relative times. Here $r = s_u - A$ and $q = s_v - B$ are relative times; Lemma 2.3.2 applies with origins $(A, z), (B, w)$. The symbol q is reused as a vertex label only in the next step. The original stationary covariance Cauchy–Schwarz inequality bounds it by $N_{2,e}(G_u)N_{2,e}(G_v)$; translate each self pairing separately. Induction and adding u, v to Q_2 prove the full bound. There is no origin factor or discarded predecessor-time offset.

Step 4. We split the two distinct cross-pair configurations. It remains that both endpoint pairs are cross and distinct. Let a be the partner of v, b the partner of u, and put $p = u - 1$, $q = v - 1$. Then $a < u$ and $b < v$. On $\{s_a \le s_q\}$ remove v by the regional half-bound. Its indicator is independent of s_v, x_v. On the complementary region the chain orders give $s_p \ge s_a > s_q \ge s_b$, so remove u instead; that indicator is independent of s_u, x_u. The removed partner has a successor on its own chain in both cases. The two bounds are $P/2$ and $P'/2$ for possibly different admissible products of the original labels. Therefore, their sum is at most $(P + P')/2 \le \max(P, P')$. This proves (2.4.4) at the finite cap.

Step 5. We remove the finite cap by positivity. Finally, increase L to infinity. The diagram integrands and all norm factors increase to their declared values, by positivity and monotone convergence. There are only finitely many admissible products, so their maximum converges to the maximum of their limits. No kernel-independent or measurable maximizing choice is needed. Zero norms and measures require no exception; the positive cap convention avoids any undefined product on a singular time diagonal. This proves Lemma 2.4.1. □

Use the joint Gaussian regularizations of the source's (2.11). Write $a = (\epsilon, \delta) > 0$ for one pair of widths and $\boldsymbol{a} = (a_1, \dots, a_n)$ for vertexwise widths. Let $Y_n^{\boldsymbol{a}}(t, x)$ be the ordered terminal integral with kernel g_n in (1.4.1) and field $W_{\epsilon_j,\delta_j}(s_j, y_j)$ at vertex j; put $Y_0 = 1$. At fixed positive widths these are Gaussian-polynomial Bochner integrals. Indeed, Wick's formula bounds their product integrands in L^2 by $\sqrt{(2n-1)!!}\, V^{n/2}$, where V is the largest of the finitely many field variances. The terminal Green measure has mass $t^{2n}/(2n)!$, by induction using $G_r(\mathbb{R}^d) = r$. In dimension three these integrals use the Green measures: products and linear pushforwards of $p_\eta * G$ converge against the

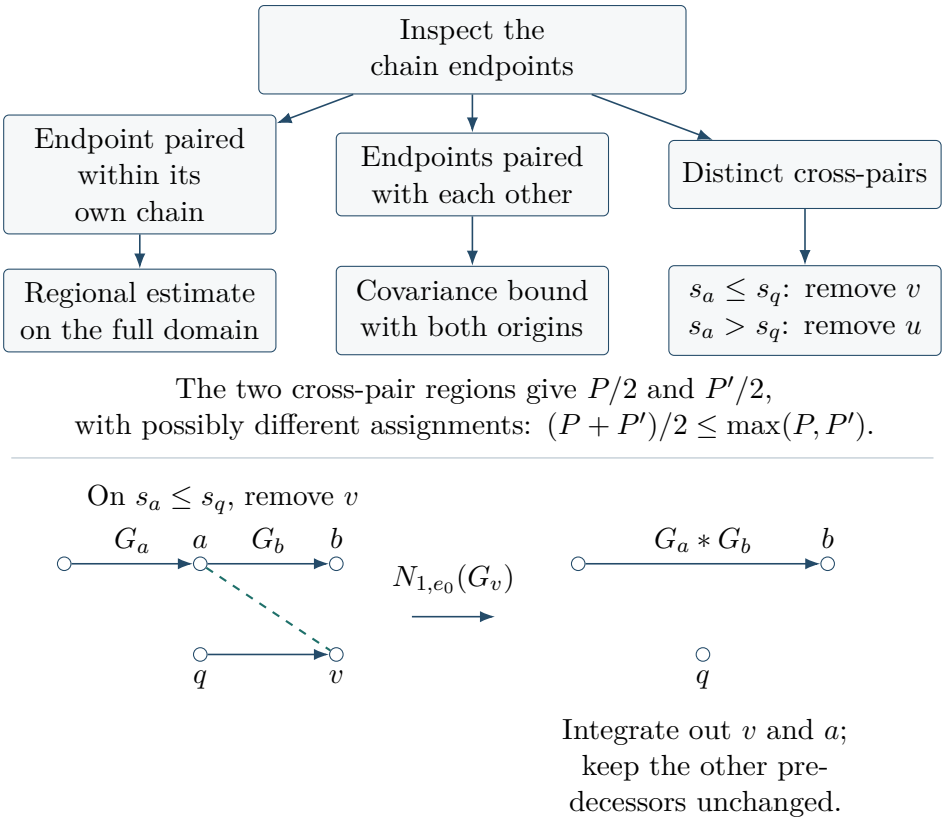

Figure 2.2: The endpoint cases in the finite two-chain product bound. The empty matching is the induction base; if only one chain is nonempty, use the within-chain case. Here u, v are the chain endpoints, a is paired with v, and q precedes v in the distinct-cross-pair case. The lower sketch shows one local fragment used in the regional fusion step, with b the immediate successor of a; other pairings are suppressed. Deleting v on $s_a \le s_q$ extracts $N_{1,e_0}(G_v)$, where $e_0 = \{a, v\}$. If the unpaired a is terminal, integrate it to $N_0(G_a)$ instead; otherwise fuse its two consecutive kernels by one-sided spacetime convolution. The mutually paired endpoint case retains both predecessor origins, including their time difference. The argument chooses a finite maximum of products; it does not produce one assignment valid for all kernel families. See Lemma 2.4.1.

bounded continuous covariance products. Mixed moments with two Green widths and the same mass bound give the L^2 limit as $\eta \downarrow 0$, before any noise width is removed.

2.5 Spatial Wick measures and fixed-order construction

Put $\gamma_b = p_b * \Gamma$, where p_b is the Brownian heat kernel. Fix $m + n = 2k \geq 2$, the two chains I_1, I_2 above and $D \in \Pi_k$. For a gap vector $\boldsymbol{r} \in (0,\infty)^{2k}$, let s_l be the sum of the gaps up to vertex l in its own chain. Similarly, for spatial increments z_l, let x_l be their cumulative sum in that chain. For positive spatial widths $\boldsymbol{\epsilon}$ define

$$J_{\boldsymbol{\epsilon},D}(\boldsymbol{r}) = \int \prod_{l=1}^{2k} G_{r_l}(\,\mathrm{d}z_l) \prod_{\{j,h\}\in D} \gamma_{\epsilon_j+\epsilon_h}(x_j - x_h), \qquad \rho_{\boldsymbol{\epsilon},D}(\,\mathrm{d}\boldsymbol{r}) = J_{\boldsymbol{\epsilon},D}(\boldsymbol{r})\,\mathrm{d}\boldsymbol{r}.$$

These are nonnegative measures. They are locally finite because the smoothed covariances are bounded and the Green masses are r_l. Write $\nu_{\boldsymbol{\epsilon},D} = e^{-\sum_l r_l}\rho_{\boldsymbol{\epsilon},D}$, and let ℓ_i be the sum of the gaps in chain i, with value zero for an empty chain.

Lemma 2.5.1 (Positive spatial Wick-measure limit)**.** *Under Hypothesis 1.2.1, the finite measures $\nu_{\boldsymbol{\epsilon},D}$ converge weakly, as all spatial widths tend to zero at arbitrary relative rates, to a finite measure ν_D. The locally finite measure $\rho_D = e^{\sum_l r_l}\nu_D$ satisfies*

$$\rho_D(cA) = c^{(4-\alpha)k}\rho_D(A), \qquad c > 0.$$

It gives zero mass to every face $r_l = 0$ and every face $\ell_i = T > 0$. Consequently, for every bounded continuous φ and $T_1, T_2 > 0$,

$$\int_{\ell_1<T_1,\,\ell_2<T_2} \varphi\,\mathrm{d}\rho_{\boldsymbol{\epsilon},D} \longrightarrow \int_{\ell_1<T_1,\,\ell_2<T_2} \varphi\,\mathrm{d}\rho_D. \tag{2.5.1}$$

Proof. We compute positive Laplace transforms and uniformly bound their masses through Brownian occupation integrals. We then recover a unique finite measure limit, exclude boundary mass, and use scaling to treat the finite-horizon faces.

Step 1. We obtain the positive Laplace transform. Orient each pair $e = \{j,h\}$ as $j < h$, and let $\eta_l(\boldsymbol{\xi})$ be the coefficient of z_l in $\sum_{e=\{j,h\}} \xi_e \cdot (x_j - x_h)$. Finite heat-weighted spectral measures and the finite damped Green masses justify Fourier and Laplace Fubini. The wave Laplace transform gives, for $\lambda_l \geq 0$,

$$\begin{aligned} L_{\boldsymbol{\epsilon},D}(\boldsymbol{\lambda}) &:= \int e^{-\sum_l \lambda_l r_l}\,\mathrm{d}\nu_{\boldsymbol{\epsilon},D} \\ &= \int \exp\left\{-\frac{1}{2}\sum_{e=\{j,h\}}(\epsilon_j+\epsilon_h)|\xi_e|^2\right\} \prod_{l=1}^{2k} \frac{1}{(1+\lambda_l)^2 + |\eta_l(\boldsymbol{\xi})|^2} \prod_{e\in D}\mu(\,\mathrm{d}\xi_e). \end{aligned} \tag{2.5.2}$$

The integrand is nonnegative. Thus, the transforms increase when any spatial width decreases. This is transform monotonicity, not pointwise monotonicity of the physical covariances.

Step 2. We bound Brownian occupation moments uniformly in the smoothing. We prove a uniform bound on their total masses. With $V = \mu(B_1)$, Fourier triangle and radial homogeneity give

$$0 \le (p_t * \gamma_b)(x) \le At^{-\alpha/2}, \qquad t, b > 0, \quad A = \alpha V \int_0^\infty u^{\alpha-1} e^{-u^2/2} \, \mathrm{d}u < \infty. \tag{2.5.3}$$

Indeed, its Fourier multiplier is $e^{-(t+b)|\xi|^2/2}$, whose integral is $A(t+b)^{-\alpha/2} \le At^{-\alpha/2}$. For a Brownian motion B put $S_b(T) = \int_0^T \int_0^T \gamma_b(B_s - B_t) \, \mathrm{d}s \, \mathrm{d}t$. For every integer $j \ge 1$,

$$\mathbb{E}_B S_b(T)^j \le \frac{(2j)![A\Gamma_{\mathrm{E}}(1-\alpha/2)]^j}{\Gamma_{\mathrm{E}}((2-\alpha/2)j+1)} T^{(2-\alpha/2)j}. \tag{2.5.4}$$

To verify this, order the $2j$ time variables in the moment integral. Condition on all but the last remaining Brownian vertex. Its pair factor has conditional mean at most A times the last remaining time gap to the power $-\alpha/2$, by (2.5.3). Remove this vertex and its partner. The remaining factors do not involve either removed vertex, and their marginal law is again the Brownian law at the remaining times. Repeat this procedure. The j selected right endpoints are distinct; each selected gap is at least the original adjacent gap at its right endpoint. On each ordered simplex the resulting bound is therefore A^j times a product of j distinct adjacent gaps to the power $-\alpha/2$. Integration over the simplex gives $\Gamma_{\mathrm{E}}(1-\alpha/2)^j T^{(2-\alpha/2)j}/\Gamma_{\mathrm{E}}((2-\alpha/2)j+1)$. There are $(2j)!$ possible orders. This proves the bound uniformly in b; the zeroth moment is one.

Step 3. We bound the two-chain transform by finite Brownian moments. Let $\epsilon_* = \min_l \epsilon_l$. The positive formula (2.5.2) bounds $L_{\boldsymbol{\epsilon},D}(0)$ by the transform with every vertex width equal to ϵ_*. The identity of finite positive measures

$$\int_0^\infty e^{-at} G_t(\, \mathrm{d}x) \, \mathrm{d}t = \frac{1}{2} \int_0^\infty e^{-a^2 u/2} p_u(x) \, \mathrm{d}u \, \mathrm{d}x$$

follows by their equal Fourier transforms $(a^2 + |\xi|^2)^{-1}$. Apply it to the $2k$ Green factors at unit damping. This writes the common-width transform as 2^{-2k} times a two-Brownian-chain integral with gap weights $e^{-\sum_l u_l/2}$ and covariance $\gamma_{2\epsilon_*}$ on every pair. If τ_i is the last Brownian time in chain i, insert

$$1 = \frac{1}{4} \int_{\tau_1}^\infty \int_{\tau_2}^\infty e^{-((a-\tau_1)+(b-\tau_2))/2} \, \mathrm{d}a \, \mathrm{d}b.$$

This also holds for an empty chain with $\tau_i = 0$. Positivity permits extension of the ordered Brownian time domains to their full cubes. At fixed paths the time integrations then factor into one occupation integral per pair. For independent Brownian paths, spectral Cauchy–Schwarz gives

$$0 \le A_{12} := \int_0^a \int_0^b \gamma_{2\epsilon_*}(B_1(s) - B_2(t)) \, \mathrm{d}s \, \mathrm{d}t \le \sqrt{S^{(1)}_{2\epsilon_*}(a) S^{(2)}_{2\epsilon_*}(b)}.$$

If the pairing has v_1, v_2 self-pairs and w cross-pairs, with $v_1 + v_2 + w = k$, its occupation product is at most

$$S_1^{v_1+w/2} S_2^{v_2+w/2} \le (1+S_1)^k (1+S_2)^k.$$

By (2.5.4), each expected factor is bounded by a fixed finite sum M_k of nonnegative powers of its horizon, independently of ϵ_*. Independence of the two paths now gives

$$\sup_{\boldsymbol{\epsilon}>0} L_{\boldsymbol{\epsilon},D}(0) \le 2^{-2k-2} \left(\int_0^\infty e^{-a/2} M_k(a)\, \mathrm{d}a \right)^2 < \infty.$$

Step 4. We identify the finite-measure limit and rule out escape of mass. Monotone convergence in (2.5.2) yields finite limits $L_D(\boldsymbol{\lambda})$ for all $\boldsymbol{\lambda} \ge 0$. The limiting integrand at zero is integrable, so dominated convergence shows continuity at zero. Here is the finite-measure Laplace argument, including possible loss of mass. Push the measures to $[0,1]^{2k}$ by $y_l = e^{-r_l}$. Uniformly bounded masses on this compact cube have weak cluster limits. Their integer monomial moments are the prescribed L_D values, so polynomial density determines a unique cluster limit. For $c > 0$ the integral of $\prod_l y_l^c$ is $L_D(c, \dots, c)$. As $c \downarrow 0$, continuity at zero and monotone convergence show that the cluster limit has no mass on the faces where any $y_l = 0$. Closed neighborhoods of the y-zero faces have limiting mass tending to zero; the portmanteau inequality bounds the approximating tail masses by these same quantities. Pulling back therefore proves weak convergence on $[0,\infty)^{2k}$. Bounded continuous test functions are handled by cutting off a neighborhood of those zero faces and then using the vanishing tail mass. Every sequence of widths tending to zero has this same limit, so the convergence is joint and independent of their relative rates.

Step 5. We exclude zero gaps and positive horizon faces. Sending just $\lambda_l \to \infty$ in the limiting positive integral (2.5.2) gives zero by domination by its integrable zero-parameter integrand. On the measure side this limit is $\nu_D\{r_l = 0\}$. Thus, every coordinate-zero face has zero mass.

Heat and wave scaling give, for Borel sets,

$$\rho_{\boldsymbol{\epsilon},D}(cA) = c^{(4-\alpha)k} \rho_{\boldsymbol{\epsilon}/c^2,D}(A).$$

This follows from $G_{cr}(c\,\mathrm{d}z) = cG_r(\,\mathrm{d}z)$, $\gamma_b(cx) = c^{-\alpha}\gamma_{b/c^2}(x)$, and the $2k$ time Jacobians. Passing to vague limits proves the stated homogeneity of ρ_D. If a compact part A of $\{\ell_i = T\}$, $T > 0$, had positive mass, its dilates cA at distinct $c \in [1,2]$ would be disjoint, have a common positive lower mass bound, and lie in one compact set. This contradicts local finiteness. Exhausting the face by compacts proves it has zero mass. For an empty chain the positive-level face is empty. The finite-horizon region is bounded, and its boundary is contained in these horizon faces and the coordinate-zero faces. Weak convergence with a compact cutoff, and the bounded continuous multiplier $e^{\sum r_l}\varphi$ there, proves (2.5.1). This proves Lemma 2.5.1. □

Lemma 2.5.1 removes only the spatial widths. We now remove the temporal widths too and construct each fixed-order term.

Lemma 2.5.2 (Joint diagram limits and fixed-order construction)**.** *Under Hypothesis 1.2.1, every two-chain diagram with $m + n = 2k \ge 2$ has a finite joint limit as all its positive vertexwise spatial and temporal widths tend to zero, at arbitrary relative rates.*

This includes unequal and empty chains. For every $n \geq 1, t > 0, x$, $Y_n^{\boldsymbol{a}}(t,x)$ has a unique joint L^2 limit, denoted $X_n(t,x)$; it is the multiple Stratonovich integral of g_n. Green smoothing in dimension three is removed before noise smoothing.

Proof. We first remove spatial smoothing at a fixed bounded temporal cutoff. A marked-edge product estimate makes the temporal error uniformly small in all spatial widths. This gives joint diagram limits, and the mixed second moments then make each fixed-order random integral Cauchy in L^2.

Step 1. We take the fixed-temporal-cutoff spatial limit. Use the gap variables and spatial measures of Lemma 2.5.1. With $s_j = s_j(\boldsymbol{r})$ define, on $\ell_1 < T_1, \ell_2 < T_2$,

$$F_{\boldsymbol{\epsilon},\boldsymbol{\delta},D} = \int \prod_{\{j,h\}\in D} \gamma^0_{\delta_j \vee \delta_h}(s_j - s_h)\, \mathrm{d}\rho_{\boldsymbol{\epsilon},D}.$$

Here γ^0_δ denotes the capped kernel κ_δ in (2.3.7); off the time diagonal, $|r|^{-\alpha_0} - \gamma^0_\eta(r) = K_{1/\eta}(r)$ is its omitted Laplace tail. At a common temporal width $\eta > 0$ the multiplier is bounded and continuous. Hence, the spatial limit exists at every $T_1, T_2 > 0$ by (2.5.1).

Step 2. We bound the temporal remainder uniformly in spatial widths. We next bound removal of that temporal cutoff uniformly in all spatial widths. Write $F_{\boldsymbol{\epsilon},0,D}$ for the integral with full factors $|s_j - s_h|^{-\alpha_0}$. It is finite at positive spatial widths: bound the spatial covariances by their finite suprema and the Green masses by their horizon bounds, then integrate the disjoint-pair time factors on the full time cube. Each factor $|s-r|^{-\alpha_0}$ is integrable since $\alpha_0 < 1$. The elementary difference-of-products inequality bounds $F_{\boldsymbol{\epsilon},0,D} - F_{\boldsymbol{\epsilon},\eta,D}$ by a sum of k nonnegative integrals, each with one marked time covariance $K_{1/\eta}$ and all other time covariances full.

Apply Lemma 2.4.1 to the damped kernels $e^{-s}G_s$. At first smooth the Green kernels in dimension three and cap the temporal Laplace domains above. Each spatial edge measure is a finite Gaussian-weighted μ with nonnegative physical covariance, and each temporal domain is a Laplace interval or its restriction. These are exactly the hypotheses of that lemma. The finite-horizon exponential loss is at most $e^{T_1+T_2}$. Lemma 2.3.1 bounds all unmarked norms independently of the smoothing parameters. The marked edge appears once in the first-norm product or twice in the second-norm product in every admissible assignment. Consequently,

$$0 \leq F_{\boldsymbol{\epsilon},0,D} - F_{\boldsymbol{\epsilon},\eta,D} \leq C_{k,T_1,T_2}\left(N_1^{(1/\eta)}(1) + N_2^{(1/\eta)}(1)^2\right), \tag{2.5.5}$$

uniformly in all spatial widths. Constants may depend on the fixed covariance and k, T_1, T_2; no uniformity in these quantities is needed. Let the upper temporal caps tend to infinity by positivity, and then remove Green smoothing at these fixed spatial widths. For the latter passage, the bounded spatial covariance products, weak convergence of Green measures and the integrable time-cube majorant just used give convergence. The bound survives both passages. Its right side tends to zero as $\eta \downarrow 0$.

Step 3. We squeeze all vertexwise cutoff choices to the same diagram limit. Denote the fixed-η spatial limit by $b_D(\eta)$. These numbers increase as η decreases, and (2.5.5) makes

them Cauchy with a finite limit b_D. If every $\delta_j < \eta$, positivity gives

$$F_{\boldsymbol{\epsilon},\eta,D} \le F_{\boldsymbol{\epsilon},\boldsymbol{\delta},D} \le F_{\boldsymbol{\epsilon},0,D}.$$

Fix η, pass to the spatial limit in the lower term, and use the uniform remainder in (2.5.5); then let $\eta \downarrow 0$. This proves the asserted joint limit b_D with arbitrary spatial/temporal rates. If one chain is empty its horizon contributes no variables, and the same proof applies.

Step 4. We obtain the joint mean-square limit from the mixed moments. At positive widths Wick's formula gives the mixed second moments of two copies of Y_n as the finite sum of these diagrams, after reversing both terminal chains at their common horizon t. Evenness of the covariances absorbs the sign changes. Every such mixed moment, including either diagonal moment, tends to the same finite sum $Q_n = \sum_{D\in\Pi_n} b_D$. Hence,

$$\|Y_n^{\boldsymbol{a}} - Y_n^{\boldsymbol{b}}\|_2^2 \longrightarrow Q_n + Q_n - 2Q_n = 0.$$

Completeness of L^2 gives a unique limit independent of all width ratios. At fixed positive noise widths the Green-width limit was already taken in the terminal construction, so the result has the required Green-before-noise convention. Restricting to common noise widths gives precisely the multiple Stratonovich definition for g_n. This proves Lemma 2.5.2. □

Since $\beta > 2$ and $\alpha + \alpha_0 < 2$, Lemma 2.3.1 gives constants $C_0 < \infty$ and $\theta_0 = 1$ such that, for $\theta \ge \theta_0$,

$$N_0(\theta) = \theta^{-2}, \qquad N_1(\theta) \le C_0, \qquad N_2(\theta) \le C_0\theta^{-1}. \tag{2.5.6}$$

Lemma 2.5.3 (Corrected crude estimate)**.** *Under Hypothesis 1.2.1, for suitable $C < \infty$ and $\theta_0 > 0$,*

$$\mathbb{E}X_n(t,x)^2 \le e^{2\theta_0 t}\frac{C^n t^{2n}}{n!} \quad (n \ge 1, t > 0), \qquad \mathbb{E}u^2(t,x) \le 2e^{2\theta_0 t + 2Ct^2}. \tag{2.5.7}$$

Proof. We first damp the two chains and apply the finite pairing envelope uniformly in the regularizations. We then choose the damping parameter as a function of the order and sum the resulting norm bounds.

Step 1. We obtain the damped pairing estimate and remove regularizations in order. On the two finite chains, the product of the exponential weights telescopes to $e^{-\theta(s_n+s_{2n})} \ge e^{-2\theta t}$. Extend the nonnegative integral to the two infinite time simplices and apply Lemma 2.4.1. For every admissible product, put $q_i = \#Q_i$. Then $q_0 = q_1$ and $q_0+q_2/2 = n$. Hence, (2.5.6) bounds each pairing by $e^{2\theta t}C^n\theta^{-2n}$. Summing the P_n pairings gives

$$\mathbb{E}X_n(t,x)^2 \le P_n e^{2\theta t}C^n\theta^{-2n}, \qquad \theta \ge \theta_0. \tag{2.5.8}$$

Equations (1.5) and (2.24) here belong to [17, (1.5), p. 3, and (2.24), p. 13]. Under Hypothesis 1.2.1, the ball growth $\mu(B_r) = Vr^\alpha$ and $\alpha + \alpha_0 < 2$ give the integrability

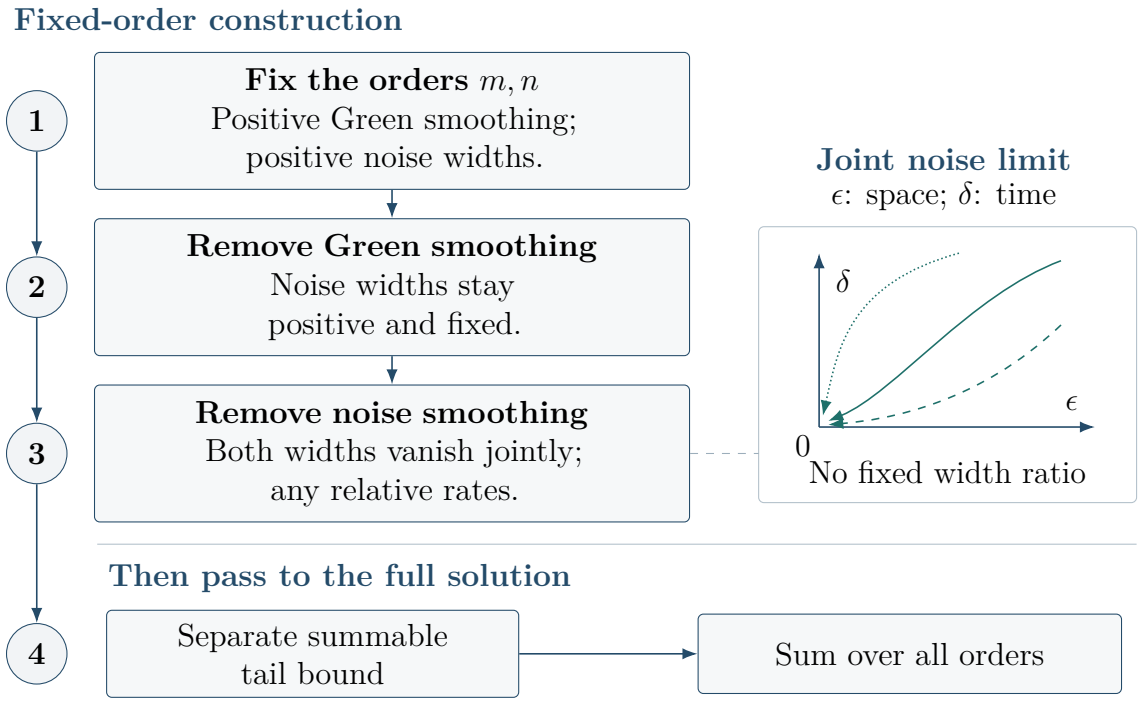

Figure 2.3: The order of the construction limits. The Green smoothing is removed while the external noise widths remain positive. Fixed-order convergence and a separate summable bound then identify the full solution. See Lemma 2.5.2 and Lemma 3.3.7. Later source limits are taken at fixed radius before the large-time limit.

in (1.5), while Remark 2.3.3(iii) directly proves finiteness of the Gaussian-weighted measure. For the finite-spectral-measure hypothesis in Lemma 2.4.1, first apply it with the spatially smoothed covariance and the temporal truncations of (2.24). The smoothed spectral measure is finite: the Gaussian multiplier is bounded by a constant times $(1+|\xi|^2)^{-(2-\alpha_0)/2}$, whose integral is finite by (1.5). This argument requires no radial density for the spectral measure. The zero norm is unchanged; the first and second norms are bounded by Lemma 2.3.1: their Gaussian multipliers can be removed in the upper bounds for the nonnegative transforms and covariance quadratic forms. The bound is uniform in these regularizations. In $d = 3$, first use $G_\eta = p_\eta * G$, as defined on pp. 13–14 of the source. Its spatial Fourier multiplier is bounded by one and its spatial mass equals that of G, so the same bounds are uniform in η as well. For each fixed noise regularization (ϵ, δ), first let $\eta \downarrow 0$ in the source's L^2 definition. The squared moments converge, so the inequality survives this first limit. Then let $(\epsilon, \delta) \to 0$ using Lemma 2.5.2. In $d = 1, 2$ only this latter limit is needed. These limits transfer a uniform inequality; no pointwise delta covariance bound is being used.

Step 2. We optimize a permitted damping parameter and sum the order bounds. Choose $\theta = \theta_0 + n/t$ in (2.5.8). Since $(2n)! \le (2n)^{2n}$, we have $P_n n^{-2n} \le 2^n/n!$. Absorb $2^n e^{2n}$ in C^n to obtain the first bound in (2.5.7). Its square roots are summable for each fixed t, by the ratio test. Thus, the norm series converges independently of Proposition 2.1.1. By Minkowski and Cauchy–Schwarz,

$$\|u(t,x)\|_2 \le e^{\theta_0 t} \sum_{n\ge 0} \frac{(\sqrt{C}t)^n}{\sqrt{n!}},$$

$$\left(\sum_{n\ge 0} \frac{z^n}{\sqrt{n!}}\right)^2 \le \left(\sum_{n\ge 0} 2^{-n}\right)\left(\sum_{n\ge 0} \frac{(2z^2)^n}{n!}\right) = 2e^{2z^2}.$$

This proves Lemma 2.5.3. □

2.6 The mild equation with the corrected bound

Lemma 2.5.3 states bounds for the limits X_n and their sum. We now bound the regularized terms uniformly in all positive vertexwise widths; Proposition 2.6.2 uses this bound.

Lemma 2.6.1 (Uniform vertexwise regularization bound)**.** *Under Hypothesis 1.2.1, there are $C < \infty$ and $\theta_0 > 0$ such that, for all positive vertexwise widths and $n \ge 1$,*

$$\|Y_n^{\boldsymbol{a}}(t,x)\|_2 \le q_n(t), \qquad q_n(t) := e^{\theta_0 t}\frac{C^{n/2}t^n}{\sqrt{n!}}. \tag{2.6.1}$$

The bound also holds for $X_n(t,x)$, with $q_0(t) = e^{\theta_0 t} \ge 1$. For each $T < \infty$,

$$\sum_{n\ge 0} \sqrt{n+1}\, q_n(T) < \infty. \tag{2.6.2}$$

Proof. We retain the separate width on every vertex while applying the edgewise product envelope. Uniform edge norms then give the factorial bound, which passes to the joint limit and supplies the weighted summability needed for multiplication.

Step 1. We identify all edge regularizations and bound their norms. Wick's formula [17, (2.19), p. 12], with the joint covariance (2.11), gives the square of $Y_n^{\boldsymbol{a}}$, with the widths copied to the second chain. Its edge covariances are

$$\gamma^0_{\delta_j\vee\delta_l}(s_j - s_l)\gamma_{\epsilon_j+\epsilon_l}(y_j - y_l).$$

On each terminal chain use $s'_j = t - s_{n+1-j}$ and $y'_j = x - y_{n+1-j}$. This reverses the chain and only permutes its vertex widths; covariance differences change sign and the kernels are even. For each pairing apply Lemma 2.4.1 to $e^{-\theta r}G_r$, first with Green smoothing if $d = 3$. The lemma permits a separate finite spectral measure and temporal truncation on each edge. These hypotheses hold here: the spatial spectral measure on an edge is $e^{-(\epsilon_j+\epsilon_l)|\xi|^2/2}\mu(\,\mathrm{d}\xi)$, which is finite by (1.5), and its temporal Laplace domain is $[0, (\delta_j \vee \delta_l)^{-1}]$.

Condition (1.5) is the source condition just identified in the preceding proof; under Hypothesis 1.2.1, finiteness of each Gaussian-weighted edge measure follows directly from Remark 2.3.3(iii). All edge norms obey (2.5.6), uniformly in their widths. For the first norm the Laplace–Fourier transform of the damped Green kernel is positive, and the spatial Gaussian multiplier and temporal truncation can only decrease its nonnegative spectral integral. For the second norm first enlarge the temporal covariance to $|s - r|^{-\alpha_0}$, using positivity of the Green kernels and the smoothed spatial covariance. Its space-time spectral expression is an integral of the squared absolute transform against nonnegative measures, so removal of the spatial Gaussian multiplier increases it. Green smoothing has multiplier at most one and unchanged mass, so the same bounds hold before its removal. These assertions follow from Lemma 2.3.1, rather than an imported normalization or large-parameter formula in the source's Appendix. The constants are independent of all the vertex widths.

Step 2. We count the norm factors and optimize the damping. Since $\#Q_0 = \#Q_1$ and $\#Q_0 + \#Q_2/2 = n$ for every admissible product, exactly as in (2.5.8) we obtain the following bound. Indeed, put $D = \max\{1, 2C_0\}$. The norm constants contribute at most $D^{\#Q_1+\#Q_2} \le D^{2n}$, so we may take $C_1 = D^2$:

$$\|Y_n^{\boldsymbol{a}}(t,x)\|_2^2 \le P_n e^{2\theta t} C_1^n \theta^{-2n}, \qquad \theta \ge \theta_0.$$

Let the Green width tend to zero at these fixed positive noise widths, and choose $\theta = \theta_0 + n/t$. The inequality $P_n n^{-2n} \le 2^n/n!$ then proves (2.6.1), after increasing C. Lemma 2.5.2 gives the joint noise-width limit X_n; the same bound passes to it. Finally,

$$\frac{\sqrt{n+2}\,q_{n+1}(T)}{\sqrt{n+1}\,q_n(T)} = \sqrt{C}\,T\frac{\sqrt{n+2}}{n+1} \longrightarrow 0.$$

The ratio test proves (2.6.2). This proves Lemma 2.6.1. □

We now show that the series of the fixed-order terms solves the mild equation.

Lean partial

Proposition 2.6.2 (Mild construction from the fixed-order limits)**.** *Under Hypothesis 1.2.1, the series $u(t,x)=\sum_{n\geq 0}X_n(t,x)$ is a mild solution in* [17, Definition 2.1 and (2.12), pp. 9–10]. *More precisely, for each $t>0$ and $x\in\mathbb{R}^d$,*

$$\lim_{\epsilon,\delta\downarrow 0}\int_0^t\int_{\mathbb{R}^d}G(t-s,x-\,\mathrm{d}y)u(s,y)W_{\epsilon,\delta}(s,y)\,\mathrm{d}s=u(t,x)-1\quad\text{in } L^2(\Omega). \tag{2.6.3}$$

The limit allows arbitrary relative rates of the two widths. In dimension three the Green-width limit precedes the noise-width limit. No uniqueness assertion is made.

For $d=3$ we read the source's generalized-integrand definition using its Green regularization, with the random factor held fixed. The proof below establishes that limit for the product $uW_{\epsilon,\delta}$.

Proof. We first control multiplication by one Gaussian variable on bounded polynomial degrees. We then identify a partially regularized terminal vertex, respecting the Green-first convention. Joint fixed-order convergence and uniform order tails finally give the full mild integral.

Step 1. We obtain the Gaussian polynomial multiplication bound. Let $\mathscr{P}_{\leq n}$ be the closed Gaussian polynomial space of total degree at most n, generated by all the coupled source fields. It includes all lower-degree contractions. The fixed-width terminal integrals lie in this space, by their Bochner construction; their fixed-order L^2 limits X_n do too.

We first record an elementary multiplication bound on these spaces. If H is any centered linear Gaussian variable and $F\in\mathscr{P}_{\leq n}$, then

$$\|HF\|_2\leq 2\sqrt{n+1}\,\|H\|_2\|F\|_2. \tag{2.6.4}$$

If $H=0$ the assertion is immediate. Otherwise take $H/\|H\|_2$ as the first coordinate of an orthonormal Gaussian basis. On normalized Hermite polynomials its creation and annihilation operators have norms at most $\sqrt{n+1}$ and $\sqrt{n}$ on total degrees at most n: the squared coefficient sums have respective weights $a_1+1\leq n+1$ and $a_1\leq n$. Their sum proves the bound for finite-coordinate polynomials. Approximation in the degree-closed space proves it for F as well. Indeed, the products of an approximating sequence are L^2 Cauchy by this bound; subsequences converging almost surely identify their limit with HF. This also proves the closedness of multiplication needed below. The argument allows F to depend on H.

Step 2. We obtain measurable fields and spatial mean-square continuity. For $t>0$, divide every ordered time and spatial Green increment by t, using $G_{tr}(t\,\mathrm{d}z)=tG_r(\,\mathrm{d}z)$; the time Jacobians and Green masses contribute t^{2n}, leaving a fixed unit-time chain domain with (t,x) in the Gaussian arguments. At $t=0$ all positive-order terms vanish. Lemma 2.6.1 proves absolute L^2 convergence of the defining series for u, locally uniformly in time in the displayed norm bounds. All fields are strongly measurable as $L^2(\Omega)$ vectors. At positive widths, rescale the ordered times and Green increments to fixed unit-time domains. The

Gaussian evaluations are jointly measurable, and their bounded moments and the finite Green masses give Bochner domination on bounded time intervals. Parameter integration therefore gives joint strong measurability in (s, y). Pointwise L^2 limits along a fixed countable sequence of widths give this property for X_n, then for the series. For later Green limits we also need spatial continuity at each fixed time. Positive-width terminal terms are L^2-continuous in space, by continuity of their bounded smoothed covariance products and dominated integration against the finite Green measures. Joint spatial stationarity of the coupled regularizations shows that

$$\|Y_n^{\boldsymbol{b}}(s, y) - X_n(s, y)\|_2 = \|Y_n^{\boldsymbol{b}}(s, 0) - X_n(s, 0)\|_2.$$

Thus, their convergence is uniform in y for fixed s. Consequently, $X_n(s, \cdot)$, and by summability $u(s, \cdot)$, have continuous L^2 representatives.

Step 3. We identify the partially regularized terminal integral. Fix an external width $a = (\epsilon, \delta) > 0$ and write $W_a = W_{\epsilon,\delta}$, with variance $V_a = \gamma_\delta^0(0)\gamma_{2\epsilon}(0) < \infty$. For $n \geq 1$ define the Bochner integral

$$I_{n,a}(t, x) = \int_0^t \int_{\mathbb{R}^d} G(t - s, x - \,\mathrm{d}y) W_a(s, y) X_{n-1}(s, y)\,\mathrm{d}s.$$

It exists because (2.6.4) gives

$$\|W_a(s, y)X_{n-1}(s, y)\|_2 \leq 2\sqrt{n}\sqrt{V_a}\, q_{n-1}(T), \qquad 0 \leq s \leq T, \tag{2.6.5}$$

and the spatial Green mass is $t - s$. At fixed a, multiplication of the inner regularizations by W_a preserves their L^2 convergence, by the same bound on degree at most $n - 1$. Their norms have the uniform domination just used. Dominated Bochner integration therefore gives

$$I_{n,a}(t, x) = \lim_{\boldsymbol{b}\downarrow 0} Y_n^{(\boldsymbol{b},a)}(t, x) \quad \text{in } L^2. \tag{2.6.6}$$

Here a is at the last, terminal vertex and $\boldsymbol{b}$ at the preceding $n - 1$ vertices. At positive widths this identity before passage to the limit is ordinary terminal-kernel Fubini; its moment bound was established before Lemma 2.6.1. For $n = 1$ there are no inner widths and the identity is exact. In particular, (2.6.1) passes to this inner limit:

$$\sup_{a>0} \|I_{n,a}(t, x)\|_2 \leq q_n(t). \tag{2.6.7}$$

Step 4. We retain the dimension-three Green-limit convention. We spell out the dimension-three convention in these steps. The product $W_a(s, y)X_{n-1}(s, y)$ is L^2-continuous in y. Apply (2.6.4) first to $W_a(s, y)(X_{n-1}(s, y) - X_{n-1}(s, y'))$ and then to $(W_a(s, y) - W_a(s, y'))X_{n-1}(s, y')$. The two factors tend to zero in the required norms, by the continuity just proved and the smoothed covariance of W_a. The bound (2.6.5) is uniform in y. Therefore, convolution against $p_\eta * G_{t-s}$ converges in L^2 to convolution against G_{t-s}: on a compact set approximate this continuous vector function by a finite continuous partition of unity times fixed vector values, use scalar weak convergence, and control the

complement by tightness and the uniform bound. The mass $t - s$ and (2.6.5) permit dominated time integration. This proves the Green-width limit at fixed external widths. The same argument applies before the inner noise limit; all $Y_n^{(\boldsymbol{b},a)}$ already use their Green limit at positive noise widths. Thus, (2.6.6) does not interchange the source's Green and noise limits.

Step 5. We remove the external width using joint convergence. For each fixed n, the joint fixed-order convergence in Lemma 2.5.2 implies

$$\lim_{a\downarrow 0} I_{n,a}(t,x) = X_n(t,x) \quad \text{in } L^2. \tag{2.6.8}$$

To see the role of joint convergence, fix $\zeta > 0$ and choose $r > 0$ so that every vertex width below r gives $\|Y_n^{(\boldsymbol{b},a)} - X_n\|_2 < \zeta$. Fix any external pair a below r and let the inner widths tend to zero in (2.6.6). Then $\|I_{n,a} - X_n\|_2 \le \zeta$. This proves the asserted limit with arbitrary relative rates; it does not assume a partial-limit theorem.

Step 6. We sum the terminal integrals and remove the final uniform tail. It remains to identify the full product integral, rather than only its finite-order terms. At fixed a, (2.6.4) and (2.6.2) imply

$$\sum_{n\ge 1} \|W_a(s,y)X_{n-1}(s,y)\|_2 \le 2\sqrt{V_a}\sum_{n\ge 1}\sqrt{n}\, q_{n-1}(T) < \infty, \qquad 0 \le s \le T.$$

Multiplication is closed: partial sums of u converge in L^2, and their products converge by this estimate, so an almost surely convergent subsequence identifies the product limit with $W_a u$. Dominated Green integration and norm summability now prove

$$I_a(t,x) := \int_0^t \int_{\mathbb{R}^d} G(t-s, x- \,\mathrm{d}y) W_a(s,y)u(s,y)\,\mathrm{d}s = \sum_{n\ge 1} I_{n,a}(t,x) \quad \text{in } L^2.$$

The sum of the product integrands is spatially L^2-continuous by uniform summability, so its Green-width limit is justified in exactly the same way. Finally, for every N,

$$\|I_a(t,x) - (u(t,x)-1)\|_2 \le \sum_{n=1}^{N} \|I_{n,a}(t,x) - X_n(t,x)\|_2 + 2\sum_{n>N} q_n(t).$$

First let $a \downarrow 0$ using (2.6.8), then let $N \to \infty$ using (2.6.2). This proves (2.6.3), hence the mild equation in the stated definition. The source's (5.3)–(5.4) and its Section 5(ii) identification proof have not been used. This proves Proposition 2.6.2. □

Thus, the exponent two enters through replacing the paired norm products by $C\theta^{-2}$, followed by the pairing count and the order summation. The sum over unequal chain lengths is not responsible for this loss: the same loss already occurs in the diagonal estimate and Minkowski's inequality.

2.7 What homogeneity recovers, and what the bound still loses

Under homogeneity the norms scale exactly in θ. We now use this scaling in place of (2.5.6).

Proposition 2.7.1 (The uniform pairing estimate)**.** *Under Hypothesis 1.2.1, there is $K > 0$ such that*

$$\mathbb{E}[X_m(t,x)X_n(t,x)] \le P_k K^k e^{2\theta t}\theta^{-\beta k}, \qquad m+n=2k\ge 2, \quad \theta>0. \tag{2.7.1}$$

Define the numerical majorant produced by applying this estimate separately at every total order by

$$B_K(t) = 1 + \sum_{k\ge 1}(2k+1)P_k K^k \inf_{\theta>0}\{e^{2\theta t}\theta^{-\beta k}\}. \tag{2.7.2}$$

Then $\mathbb{E}u^2(t,x) \le B_K(t)$ and, for some $c, C > 0$ and all large t,

$$ct^\rho \le \log B_K(t) \le Ct^\rho, \qquad \rho = \frac{\beta}{\beta-1} = \frac{4-\alpha-\alpha_0}{3-\alpha-\alpha_0} > \kappa. \tag{2.7.3}$$

The lower bound here concerns the numerical majorant B_K, not the second moment.

Proof. We use homogeneous norm scaling to bound each total order, then estimate the resulting numerical series from above and below. The lower estimate concerns that majorant only.

Step 1. We obtain the homogeneous pairing majorant. The wave kernel scales as $G(cs, c\,\mathrm{d}y) = cG(s,\mathrm{d}y)$, and the covariance has degree $-\alpha$. Changing all time and spatial variables by θ^{-1} in the norms yields

$$N_0(\theta) = \theta^{-2}, \quad N_1(\theta) = N_1(1)\theta^{\alpha+\alpha_0-2}, \quad N_2(\theta)^2 = N_2(1)^2\theta^{-\beta}. \tag{2.7.4}$$

All constants and scalings follow directly from Lemma 2.3.1. The products $2N_0N_1$ and N_2^2 therefore both have degree $-\beta$. Choose $K \ge \max\{2N_1(1), N_2(1)^2\}$, increasing it to a positive constant if needed. Lemma 2.4.1 and $q_0 + q_2/2 = k$ give $K^k\theta^{-\beta k}$ for every admissible product. The finite horizons contribute at most $e^{2\theta t}$. Apply this first to regularized moments. In $d=3$, fix (ϵ,δ) and let $\eta\downarrow 0$ in each factor's L^2 limit; Cauchy–Schwarz gives L^1 convergence of their product. Then let $(\epsilon,\delta)\to 0$ in the same way, using Lemma 2.5.2 for each chain. In $d=1,2$ only the noise limit is required. The estimates are uniform at both stages, by the multiplier bounds in Lemma 2.5.3. This proves (2.7.1). Empty-chain cases satisfy the same bound (using $e^{2\theta t}$ is harmless). Proposition 2.1.1 now gives the majorant.

Step 2. We determine the growth scale of the numerical series. The infimum in (2.7.2) is attained at $\theta = \beta k/(2t)$ and equals $e^{\beta k}(2t/(\beta k))^{\beta k}$. Put $q = \beta - 1 > 1$. The elementary estimates

$$k! \le P_k \le 2^k k!, \qquad (k/e)^k \le k! \le k^k, \qquad 2k+1 \le 3^k$$

show that, for fixed positive a, b depending only on K, β,

$$\sum_{k\geq 0} \frac{(at^\beta)^k}{(k!)^q} \leq B_K(t) \leq \sum_{k\geq 0} \frac{(bt^\beta)^k}{(k!)^q}.$$

Indeed, the additional factor $k!^\beta/k^{\beta k}$ lies between $e^{-\beta k}$ and one and can be absorbed into a^k, b^k. For $z > 0$, the right-hand series is at most $(\sum_{k\geq 0} z^{k/q}/k!)^q = e^{qz^{1/q}}$, by the elementary ℓ^q versus ℓ^1 inequality for nonnegative sequences. For a lower bound choose $k = \lfloor z^{1/q}/2 \rfloor$ and use $k! \leq k^k$; its single summand is at least 2^{qk}. These estimates prove (2.7.3). Finally, $\beta - 1 = 3 - \alpha - \alpha_0 < 3 - \alpha$, so $\rho > \kappa$. This proves Proposition 2.7.1. □

Remark 2.7.2 (Limitation of the uniform pairing estimate)**.** Since $\beta > 2$, we have $1 < \rho < 2$. Thus, Proposition 2.7.1 improves the crude quadratic time scale under homogeneity. It does not itself prove Theorem 1.5.1; Section 3.3 uses a different argument. Theorem 3.1 used through its uniform pairing estimate is *not sufficient to prove Theorem 1.5.1*: even with exact homogeneous norm scaling, the resulting majorant has exponent $\rho > \kappa$. The order coefficient has factorial denominator $(k!)^{3-\alpha-\alpha_0}$, whereas the desired scale requires $(k!)^{3-\alpha}$; the missing factor is $(k!)^{\alpha_0}$, up to exponential factors in k. Counting the $2k+1$ chain-length splits does not cause this loss, since it can be absorbed into an exponential factor. This conclusion does not rule out a more refined application retaining temporal order or grouping pairings before estimating them, and does not disprove the conjecture. In the formal boundary limit $\alpha_0 \downarrow 0$, both ρ and κ tend to $(4-\alpha)/(3-\alpha)$. This necessary time-independent calibration does not distinguish them and asserts no endpoint theorem or uniformity of constants in α_0. At $p = 1$ use the empty-chain case with $e^{\theta t}$ in place of $e^{2\theta t}$; minimizing at $\theta = \beta k/t$ changes only a constant to the power k, leaving the same factorial denominator $(k!)^{3-\alpha-\alpha_0}$. It therefore also loses the factorial power α_0 relative to $\beta/\kappa = 3 - \alpha$, the power corresponding to the target series scale. This is a comparison of scales, not a coefficient estimate asserted by the source's Theorem 1.2. The loss is not specific to the second moment. Both the crude and homogeneous upper bounds are consistent with the Jensen lower bound, being at larger time scales. No identification with the Skorohod second moment is used: its exclusion of self-pairings changes the combinatorics, already visible in the $(0, 2)$ and $(2, 0)$ terms of Lemma 2.2.1.

No-go 01 isolates this scale obstruction. The adjacent-diagram calculation in No-go 02 also explains why one cannot repair it by assigning a cubic-factorial estimate to every individual pairing.

What we now have. One solution, built from its expansion and shown to solve the mild equation (Proposition 2.6.2), with a formula for every mixed moment (Proposition 2.1.1). A single bound for all pairings misses the scale T^κ; the next chapter reaches it.

Chapter 3

An independent upper bound

Chapter 2 shows that the second moment is finite. How fast can it grow? This chapter gives a first answer, before the exact constant is known: no faster than $\exp(CT^{\kappa})$, up to a polynomial factor. This is Theorem 3.3.8, and it proves Theorem 1.5.1. Its constant is not claimed to be optimal.

The natural plan is to cut time into blocks and multiply the bounds. A wave does not allow this easily. Each block must hand on both displacement and velocity (No-go 14), and the noise in one block is correlated with the noise in the others. Sections 3.1 and 3.2 show how far independent blocks go. Section 3.3 then replaces the blocks by Gaussian fields on overlapping intervals; Figure 3.6 is the picture to keep in mind.

The model prerequisites are Hypothesis 1.2.1 and the construction of Chapter 2. On a first reading, skip the proofs of Propositions 3.1.2 and 3.2.4 and of Corollary 3.2.5: Theorem 3.3.8 uses only the lemmas of those sections and one calculation, the free-phase energy bound at the end of the proof of Proposition 3.1.2. Episode ▶ 4 of the video series follows this chapter.

3.1 A static phase estimate at first variance order

A time-block argument would have to carry both position and velocity. We establish a uniform estimate for the first variance coefficient with arbitrary deterministic initial phase. The covariance may be any member of the original three-dimensional class; no endpoint representation is assumed. The estimate below is not an all-order propagator bound. No-go 14 shows why scalar solution-value moments cannot be multiplied across blocks. No-go 15 shows why both the first random term and the second-order mean enter the phase energy coefficient.

Let $0 < \alpha < 2$, and let Γ be a nonnegative, even, positive-definite tempered Radon covariance on $\mathbb{R}^3$, satisfying $\Gamma(rA) = r^{3-\alpha}\Gamma(A)$. Its spectral convention is $\Gamma = \int e^{i\xi\cdot x}\mu(\,\mathrm{d}\xi)$. Put

$$\begin{aligned} V &= \mu(B_1), \qquad M = \Gamma(B_1), \qquad R_\alpha = \frac{\alpha\pi V}{2\sin(\pi\alpha/2)}, \\ c_\Gamma &= \frac{(3-\alpha)M}{4\pi}, \qquad b_\alpha = 2^\alpha + \frac{3^{2-\alpha}}{2-\alpha}, \qquad D_\Gamma = c_\Gamma b_\alpha. \end{aligned} \tag{3.1.1}$$

Here B_1 is the open unit ball in the relevant variable. The physical mass M and the spectral mass V are not identified. Let p_ϵ be the Brownian Gaussian density with covariance ϵI, and set $\Gamma_\epsilon = p_{2\epsilon} * \Gamma$.

Lean full

Lemma 3.1.1 (Two static contraction bounds)**.** *For $\lambda > 0$, $q \in \mathbb{R}^3$, $a > 0$, and $\epsilon > 0$,*

$$\int_{\mathbb{R}^3} \frac{\mu(\,\mathrm{d}\xi)}{\lambda^2 + |q+\xi|^2} \le R_\alpha \lambda^{\alpha-2}, \tag{3.1.2}$$

$$|T_\epsilon(a,q)| \le D_\Gamma a^{1-\alpha}, \tag{3.1.3}$$

$$T_\epsilon(a,q) := \int_{\mathbb{R}^3} e^{iq\cdot x}\Gamma_\epsilon(x) G_a(\,\mathrm{d}x) = \int_{\mathbb{R}^3} \widehat{G}_a(q+\xi) e^{-\epsilon|\xi|^2}\mu(\,\mathrm{d}\xi).$$

Proof. We first compare translated heat transforms and integrate them to obtain the resolvent bound. For the trace bound, positivity removes the Fourier phase and radial integration reduces the calculation to a spherical convolution.

Step 1. We bound the shifted resolvent. Homogeneity and Fourier uniqueness give $\mu(B_r) = Vr^\alpha$. In particular, there is no origin atom. For $s > 0$, Schwartz Fourier pairing yields

$$\int e^{-s|q+\xi|^2}\mu(\,\mathrm{d}\xi) = \int p_{2s}(x) e^{iq\cdot x}\Gamma(\,\mathrm{d}x) \le \int p_{2s}(x)\Gamma(\,\mathrm{d}x) = \int e^{-s|\xi|^2}\mu(\,\mathrm{d}\xi).$$

The integrals are finite. Evenness makes the middle integral real, and nonnegativity of Γ gives the inequality. Multiply by $e^{-\lambda^2 s}$ and integrate in s. Nonnegative Tonelli on the spectral side gives the resolvent comparison. At $q = 0$ its value is

$$\alpha V \int_0^\infty \frac{r^{\alpha-1}}{\lambda^2 + r^2}\,\mathrm{d}r = R_\alpha \lambda^{\alpha-2}.$$

This proves (3.1.2).

Step 2. We bound the regularized trace using the positive spherical integral. Since μ is tempered, its Gaussian weighting is finite. Fourier Fubini therefore gives the identity for T_ϵ. The measure $\Gamma_\epsilon(x)G_a(\,\mathrm{d}x)$ is finite and nonnegative, whence $|T_\epsilon(a,q)| \le T_\epsilon(a,0)$. The radial distribution function of Γ is $\Gamma(B_r) = Mr^{3-\alpha}$. Thus, for every nonnegative radial Schwartz function F,

$$\int F(x)\Gamma(\,\mathrm{d}x) = (3-\alpha)M\int_0^\infty F(r) r^{2-\alpha}\,\mathrm{d}r = c_\Gamma \int_{\mathbb{R}^3} F(x)|x|^{-\alpha}\,\mathrm{d}x.$$

Apply this to $F = G_a * p_{2\epsilon}$, which is radial and Schwartz. Nonnegative Fubini gives

$$T_\epsilon(a,0) = c_\Gamma[p_{2\epsilon} * (G_a * |\cdot|^{-\alpha})](0) \le c_\Gamma \sup_z (G_a * |\cdot|^{-\alpha})(z).$$

Write $r = |z|$. The spherical wave measure has mass a, and direct integration over its normal coordinate gives, for $r > 0$,

$$(G_a * |\cdot|^{-\alpha})(z) = \frac{(a+r)^{2-\alpha} - |a-r|^{2-\alpha}}{2r(2-\alpha)}.$$

For $r < a/2$, distances from z to the sphere are at least $a/2$, giving the bound $2^\alpha a^{1-\alpha}$. For $r > 2a$, they are at least a, giving $a^{1-\alpha}$. On $a/2 \le r \le 2a$, the displayed formula is at most $3^{2-\alpha}a^{1-\alpha}/(2-\alpha)$. These bounds also cover the endpoints by continuity and give (3.1.3). This proves Lemma 3.1.1. □

Let $A_\lambda = \lambda^2 - \Delta$, and equip deterministic phase pairs with the norm

$$\|(f,g)\|_\lambda^2 = \|f\|_2^2 + \|A_\lambda^{-1/2} g\|_2^2. \tag{3.1.4}$$

Let C_t be the Fourier multiplier $\cos(t|\xi|)$. On one static isonormal Gaussian space with covariance Γ, use $W_\epsilon(x) = W(p_\epsilon(x - \cdot))$. Its covariance is exactly $\Gamma_\epsilon(x-y)$, with spectral measure $\mu_\epsilon(\,\mathrm{d}\xi) = e^{-\epsilon|\xi|^2}\mu(\,\mathrm{d}\xi)$. For real Schwartz f, g, define the free position $w_0(t) = C_t f + G_t * g$ and its phase $Z_0(t) = (w_0(t), \dot{w}_0(t))$. The next two regularized static Duhamel phases are

$$Z_{j+1}(t) = \int_0^t \begin{pmatrix} G_{t-s} * (W_\epsilon Z_{j,u}(s)) \\ C_{t-s}(W_\epsilon Z_{j,u}(s)) \end{pmatrix} \mathrm{d}s, \qquad j = 0, 1, \tag{3.1.5}$$

where $Z_{j,u}$ is the position component. At fixed $\epsilon > 0$ these are Gaussian-polynomial Bochner integrals in the indicated L^2 phase space.

Proposition 3.1.2 (First variance estimate for arbitrary phase)**.** *Let $N = \|(f,g)\|_\lambda$. Uniformly in $\epsilon > 0$,*

$$\mathbb{E}\|Z_1(h)\|_\lambda^2 \le R_\alpha h^2 \lambda^{\alpha-2}(1+\lambda^2 h^2)^2 N^2, \tag{3.1.6}$$

$$\|\mathbb{E} Z_2(h)\|_\lambda \le \frac{D_\Gamma (1+\lambda^2 h^2) h^{3-\alpha}}{\lambda(2-\alpha)(3-\alpha)} N. \tag{3.1.7}$$

In particular, put $\lambda = h^{-1}$ and let K_ϵ be the coefficient of σ^2 in the finite polynomial $\mathbb{E}\|Z_0(h) + \sigma Z_1(h) + \sigma^2 Z_2(h)\|_\lambda^2$. Then

$$|K_\epsilon| \le \left(4R_\alpha + \frac{4\sqrt{e}\, D_\Gamma}{(2-\alpha)(3-\alpha)} \right) h^{4-\alpha} \|(f,g)\|_{1/h}^2. \tag{3.1.8}$$

Proof. We estimate the first random phase term and the second-order mean separately. We then retain both contributions to the variance coefficient and insert the common phase scale.

Step 1. We estimate the first random phase term. We use the unnormalized spatial Fourier transform and Plancherel measure $(2\pi)^{-3}\,\mathrm{d}\eta$. At fixed positive smoothing, Gaussian second and fourth moments make (3.1.5) integrable: G_t has finite positive mass, C_t is an L^2 contraction, and $\mathbb{E}|W_\epsilon(x) W_\epsilon(y)|^2 \le 3\Gamma_\epsilon(0)^2$. These facts, Minkowski and time integration justify the Gaussian and Fourier Fubini steps below first for Schwartz data.

Set $a_s(\eta) = \widehat{w}_0(s,\eta)$ and

$$e_\lambda(\eta) = |\widehat{f}(\eta)|^2 + \frac{|\widehat{g}(\eta)|^2}{\lambda^2 + |\eta|^2}.$$

Cauchy–Schwarz on the two initial coordinates gives

$$|a_s(\eta)|^2 \le (1+\lambda^2 s^2) e_\lambda(\eta),$$

because the squared norm of their coefficient vector is $\cos^2(sq) + (1 + \lambda^2/q^2)\sin^2(sq) \le 1 + \lambda^2 s^2$, with the continuous value at $q = 0$. For the two-component output multiplier put

$$k_\tau(r) = \left(\frac{\sin(\tau r)}{r}, \frac{\cos(\tau r)}{\sqrt{\lambda^2 + r^2}} \right).$$

Its Euclidean squared norm is

$$|k_\tau(r)|^2 = \frac{1 + \lambda^2 \sin^2(\tau r)/r^2}{\lambda^2 + r^2} \le \frac{1 + \lambda^2 h^2}{\lambda^2 + r^2}, \qquad 0 \le \tau \le h.$$

Expanding the covariance of the two copies of W_ϵ, followed by spatial Plancherel, gives exactly

$$\mathbb{E}\|Z_1(h)\|_\lambda^2 = \frac{1}{(2\pi)^3} \int \mathrm{d}\eta \int \mu_\epsilon(\,\mathrm{d}\xi) \left| \int_0^h k_{h-s}(|\eta + \xi|) a_s(\eta)\,\mathrm{d}s \right|^2.$$

Cauchy–Schwarz in time bounds the last squared norm by

$$\frac{h^2(1 + \lambda^2 h^2)^2}{\lambda^2 + |\eta + \xi|^2} e_\lambda(\eta).$$

Now $\mu_\epsilon \le \mu$ and Lemma 3.1.1 give (3.1.6).

Step 2. We estimate the contracted second-order mean. The contraction inside the mean of Z_2 is the convolution operator with kernel $G_{s-r}(\,\mathrm{d}x)\Gamma_\epsilon(x)$. Indeed, this follows directly from $\mathbb{E}[W_\epsilon(x)W_\epsilon(y)] = \Gamma_\epsilon(x - y)$ in the two Duhamel integrals. Its Fourier multiplier is $T_\epsilon(s - r, \eta)$, up to the immaterial even sign. Its L^2 operator norm is therefore at most $D_\Gamma(s - r)^{1-\alpha}$. Under the isometry $(u, v) \mapsto (u, A_\lambda^{-1/2} v)$, $\|k_\tau(|D|)\|_{L^2 \to L^2 \oplus L^2} \le \sqrt{1 + \lambda^2 h^2}/\lambda$ and $\|w_0(r)\|_2 \le \sqrt{1 + \lambda^2 h^2} N$. Minkowski and

$$\int_0^h \mathrm{d}s \int_0^s (s - r)^{1-\alpha}\,\mathrm{d}r = \frac{h^{3-\alpha}}{(2 - \alpha)(3 - \alpha)}$$

prove (3.1.7).

Step 3. We combine both terms in the phase variance coefficient. Finally, the free phase obeys $\|Z_0(h)\|_\lambda \le e^{\lambda h/2} N$. To see this, for Schwartz free data differentiate its squared norm. The $-\Delta$ terms cancel, leaving $2\lambda^2 \operatorname{Re}\langle A_\lambda^{-1} \dot{w}_0, w_0 \rangle$, whose absolute value is at most $\lambda \|Z_0\|_\lambda^2$. Gronwall gives the stated bound. The required coefficient is exactly

$$K_\epsilon = \mathbb{E}\|Z_1(h)\|_\lambda^2 + 2 \operatorname{Re}\langle Z_0(h), \mathbb{E} Z_2(h) \rangle_\lambda.$$

Substituting $\lambda = h^{-1}$ into the two estimates proves (3.1.8). This proves Proposition 3.1.2. □

The second term in K_ϵ must be retained; neither its sign nor monotonicity of the full phase energy in covariance is assumed. The estimates control both terms at this one variance order. They do not control higher Gaussian contractions, products of independent time blocks, overlapping noise levels or the temporal regularization limit. Thus, they do not yet establish Theorem 1.5.1.

3.2 All static orders with arbitrary initial phase

We now seek all static Duhamel orders, retaining the full spatial covariance class of Section 3.1. The temporal covariance is not included in this section. Static estimates alone do not identify the evolution for overlapping intervals; that step is treated in the next section.

We use one external operator theorem. From Crouzeix–Palencia [23, author preprint v1, (3), p. 1, and Theorem 6, pp. 5–6], if T is a bounded operator on a complex Hilbert space and F is holomorphic on a neighborhood of $\overline{W(T)}$, then

$$\|F(T)\| \le (1+\sqrt{2}) \sup_{w\in W(T)} |F(w)|, \qquad W(T) = \{\langle Tu, u\rangle : \|u\| = 1\}. \tag{3.2.1}$$

The theorem is imported, not proved here. All operators to which we apply it below are bounded; no unbounded-operator extension is assumed.

Lean partial

Lemma 3.2.1 (A complex phase bound)**.** *Let H be a complex Hilbert space, A_0 a bounded nonnegative selfadjoint operator, and B a bounded selfadjoint operator. Write $A_\rho = \rho^2 + A_0$. Suppose that, for $0 < a < 1$ and $d > 0$,*

$$\|A_\rho^{-1/2} B A_\rho^{-1/2}\| \le d\rho^{a-2}, \qquad \rho > 0. \tag{3.2.2}$$

Put

$$I_a = \int_0^\infty s^{-1/2}(1+s)^{(a-3)/2}\,\mathrm{d}s, \qquad \delta_a = \min\{1/4, \pi/(8I_a)\}.$$

For $\lambda > 0$ and $|z| \le \delta_a \lambda^{2-a}/d$, let $L = A_0 - zB$. The phase propagator of $u'' + Lu = 0$ satisfies

$$\|\mathcal{M}_z(h)\|_{X_\lambda \to X_\lambda} \le 100 e^{2\lambda h}, \qquad \|(f,g)\|_{X_\lambda}^2 = \|f\|^2 + \|A_\lambda^{-1/2} g\|^2, \quad h \ge 0. \tag{3.2.3}$$

The constant is independent of H, $\|A_0\|$ and $\|B\|$.

Proof. We first compare the perturbed and reference square roots through resolvents. We then enclose the numerical range and bound the three scalar functions used in the phase matrix. The bounded-operator theorem applies to those functions, after which the ordered root factors give the phase estimate.

Step 1. We obtain inverse and square-root comparisons. Set $\delta = \delta_a$ and $L_\lambda = L + \lambda^2$. For $\kappa = (\lambda^2 + t)^{1/2}$,

$$L_\lambda + t = A_\kappa^{1/2}(1 - zK_\kappa)A_\kappa^{1/2}, \qquad K_\kappa = A_\kappa^{-1/2} B A_\kappa^{-1/2}.$$

Since $a - 2 < 0$, $\|zK_\kappa\| \le \delta$. Thus, these operators are invertible and

$$\|A_\kappa^{1/2}(L_\lambda + t)^{-1}\| \le \frac{1}{(1-\delta)\kappa}.$$

Also $\mathrm{Re}\langle L_\lambda u, u\rangle \ge (1-\delta)\langle A_\lambda u, u\rangle$.

Principal inverse square roots are defined on the right half-plane. The scalar identity $w^{-1/2} = \pi^{-1} \int_0^\infty t^{-1/2}(w+t)^{-1}\,\mathrm{d}t$, and bounded holomorphic calculus, give

$$Q_z - 1 = \frac{1}{\pi}\int_0^\infty t^{-1/2} A_\lambda^{1/2}\Big[(L_\lambda + t)^{-1} - (A_\lambda + t)^{-1}\Big]\,\mathrm{d}t, \qquad Q_z = A_\lambda^{1/2} L_\lambda^{-1/2}.$$

The integrals converge in operator norm. Indeed, the resolvent identity, $\|A_\lambda^{1/2} A_\kappa^{-1/2}\| \le 1$, and the following ordered factorization give the required integrand bound:

$$\begin{aligned} &A_\lambda^{1/2}\Big[(L_\lambda + t)^{-1} - A_\kappa^{-1}\Big] \\ &\qquad = A_\lambda^{1/2} A_\kappa^{-1/2}(1 - zK_\kappa)^{-1} z K_\kappa A_\kappa^{-1/2}. \end{aligned}$$

The four factors have norms at most 1, $(1-\delta)^{-1}$, $|z| d\kappa^{a-2}$ and κ^{-1}, respectively. Thus, the integrand without $t^{-1/2}/\pi$ is bounded by

$$\frac{|z| d}{1-\delta}\kappa^{a-3}.$$

Consequently,

$$\|Q_z - 1\| \le \frac{|z| d \lambda^{a-2} I_a}{\pi(1-\delta)} \le \frac{1}{6}.$$

In particular, Q_z and Q_z^{-1} have norm at most two. Apply the same argument to $L^* = A_0 - \overline{z}B$ and take adjoints. It follows that all four operators

$$A_\lambda^{1/2} L_\lambda^{-1/2}, \quad L_\lambda^{-1/2} A_\lambda^{1/2}, \quad L_\lambda^{1/2} A_\lambda^{-1/2}, \quad A_\lambda^{-1/2} L_\lambda^{1/2} \tag{3.2.4}$$

have norm at most two. This is a quantitative comparison at the bounded cutoffs, not an assumed square-root domain identity.

Step 2. We enclose the numerical range and its square roots. We next control the numerical range. For $\|u\| = 1$ put $s = \|A_0^{1/2} u\|$. Optimizing (3.2.2) at $\rho = s$ gives $|\langle Bu, u\rangle| \le 2ds^a$. If $s = 0$, the same conclusion follows by letting $\rho \downarrow 0$. Separately, evaluating (3.2.2) at $\rho = \lambda$ gives

$$|\langle Bu, u\rangle| \le d\lambda^{a-2}(s^2 + \lambda^2), \qquad |z\langle Bu, u\rangle| \le \delta(s^2 + \lambda^2).$$

This is the estimate for the real part; the optimized estimate controls the imaginary part. Thus, for $w = x + iy = \langle Lu, u\rangle$,

$$x + \lambda^2 \ge (1-\delta)(s^2 + \lambda^2), \qquad |y| \le 2\delta\lambda^{2-a} s^a.$$

Since $s^{2a}\lambda^{2-2a} \le s^2 + \lambda^2$,

$$y^2 \le \frac{4\delta^2}{1-\delta}\lambda^2(x + \lambda^2) \le \frac{1}{3}\lambda^2(x + \lambda^2), \qquad x \ge -\lambda^2/4.$$

Squaring the positive quantity $x + 2\lambda^2$ reduces its comparison with $|w|$ to $y^2 \le 4\lambda^2(x + \lambda^2)$, while $|\operatorname{Im}\sqrt{w}|^2 = (|w| - x)/2$. Hence, $|w| \le x + 2\lambda^2$, and either square root of w has $|\operatorname{Im}\sqrt{w}| \le \lambda$.

Step 3. We apply the numerical-range theorem to holomorphic scalar functions. The scalar functions

$$C_h(w) = \cos(h\sqrt{w}), \qquad F_h(w) = \sqrt{w+\lambda^2}\frac{\sin(h\sqrt{w})}{\sqrt{w}}, \qquad H_h(w) = \frac{w}{\sqrt{w+\lambda^2}}\frac{\sin(h\sqrt{w})}{\sqrt{w}}$$

are holomorphic on a neighborhood of $\overline{W(L)}$. The values at $w = 0$ are removable; the only square-root branch required is that of $w + \lambda^2$, whose real part is positive. On the numerical range,

$$|C_h(w)| \le e^{\lambda h}, \qquad |F_h(w)| \le 2(1+\lambda h)e^{\lambda h}, \qquad |H_h(w)| \le 2e^{\lambda h}.$$

Indeed, $|\operatorname{Im}\sqrt{w}| \le \lambda$ gives $|\cos(h\sqrt{w})|, |\sin(h\sqrt{w})| \le e^{\lambda h}$. The entire identity $\sin(h\sqrt{w})/\sqrt{w} = \int_0^h \cos(r\sqrt{w})\,\mathrm{d}r$ also gives the bound $he^{\lambda h}$, including $w = 0$. If $|w| \le \lambda^2/2$, then

$$|F_h(w)| \le \sqrt{3/2}\,\lambda h e^{\lambda h}.$$

If $|w| > \lambda^2/2$, then $|w+\lambda^2|/|w| \le 3$, so $|F_h(w)| \le \sqrt{3}e^{\lambda h}$. These bounds imply the displayed estimate for F_h. Finally,

$$\frac{|w|}{|w+\lambda^2|} \le 1 + \frac{\lambda^2}{|w+\lambda^2|} \le 1 + (1-\delta)^{-1} \le 7/3,$$

and $H_h(w) = \sqrt{w}\sin(h\sqrt{w})/\sqrt{w+\lambda^2}$ gives its stated bound. All identities have their removable values at zero. Applying the imported (3.2.1) gives bounds $3e^{\lambda h}$, $6(1+\lambda h)e^{\lambda h}$ and $6e^{\lambda h}$ for these three operator functions.

Step 4. We assemble the phase blocks in their stated noncommuting order. Under the isometry $(u, v) \mapsto (u, A_\lambda^{-1/2}v)$, the four phase blocks are

$$C_h(L), \quad F_h(L)L_\lambda^{-1/2}A_\lambda^{1/2}, \quad -A_\lambda^{-1/2}L_\lambda^{1/2}H_h(L), \quad A_\lambda^{-1/2}L_\lambda^{1/2}C_h(L)L_\lambda^{-1/2}A_\lambda^{1/2}.$$

This is the usual matrix $\left(\begin{smallmatrix} C_h(L) & G_h(L) \\ -LG_h(L) & C_h(L)\end{smallmatrix}\right)$, with $G_h(w) = \sin(h\sqrt{w})/\sqrt{w}$, after weighting. In the order displayed, the four block norms are at most

$$3e^{\lambda h}, \qquad 12(1+\lambda h)e^{\lambda h}, \qquad 12e^{\lambda h}, \qquad 12e^{\lambda h}.$$

For example, the last block has two root-comparison factors of norm at most two, with $C_h(L)$ between them. Only functions of L commute; no commutation with A_λ is used in these ordered products. A block operator on $H \oplus H$ has norm at most the sum of its four block norms, by the triangle inequality and the norm-one coordinate inclusions and projections. Therefore, its norm is at most

$$(39 + 12\lambda h)e^{\lambda h} \le 39(1+\lambda h)e^{\lambda h} \le 100e^{2\lambda h}.$$

The phase operator itself is the exponential of the bounded block generator with rows $(0, 1)$ and $(-L, 0)$. It is entire in z; the intermediate square roots are used to estimate it, not to impose a branch-dependent definition of that entire operator. This proves Lemma 3.2.1. □

We use the standard Gaussian creation and annihilation algebra; see Janson [34, Section 13.2, Theorem 13.7, pp. 200–201]. The following calculation records the normalization used for the finite occupation spaces in this argument.

Lean narrower

Lemma 3.2.2 (Gaussian cutoff form bound)**.** *Retain the covariance and R_α of Section 3.1. Fix $\epsilon > 0$. Represent the smoothed real field on independent standard Gaussian coordinates as $W_\epsilon(x) = \sum_{i\ge1} g_i e_i(x)$ in $L^2(\Omega)$. Let P_N be projection onto Gaussian Hermite degrees at most N, and S_b spatial Fourier projection onto $|\eta| \le b$. For finite m, on their joint range set*

$$B_{N,m,b} = P_N S_b \Big(\sum_{i=1}^{m} g_i M_{e_i} \Big) S_b P_N, \qquad A_\rho = \rho^2 - \Delta.$$

These are bounded selfadjoint operators and, uniformly in ϵ, m, b,

$$\|A_\rho^{-1/2} B_{N,m,b} A_\rho^{-1/2}\| \le d_N \rho^{\alpha/2-2}, \qquad d_N = 2\sqrt{N+1}\sqrt{R_\alpha}. \tag{3.2.5}$$

Proof. We first estimate the column of sandwiched spatial multiplication operators. We then compose it with the Gaussian creation row, retain the annihilation adjoint, and truncate by total degree.

Step 1. We bound the spatial covariance column. Choose an orthonormal basis of the real isonormal space, which is separable, and write $e_i(x) = \mathbb{E}[W_\epsilon(x) g_i]$. Then $\sum_i e_i(x)^2 = \Gamma_\epsilon(0) =: v_\epsilon$, and $|e_i(x)| \le \sqrt{v_\epsilon}$. Thus, each multiplication M_{e_i} is bounded and selfadjoint. Put $H_i = A_\rho^{-1/2} M_{e_i} A_\rho^{-1/2}$ on spatial L^2. Gaussian isometry and spatial Plancherel give

$$\sum_i \|H_i f\|_2^2 = \frac{1}{(2\pi)^3} \int \frac{|\widehat{f}(\eta)|^2}{\rho^2 + |\eta|^2} J_{\rho,\epsilon}(\eta)\, \mathrm{d}\eta, \qquad J_{\rho,\epsilon}(\eta) = \int \frac{e^{-\epsilon|\xi|^2} \mu(\,\mathrm{d}\xi)}{\rho^2 + |\eta+\xi|^2}.$$

This is the covariance calculation for $A_\rho^{-1/2} W_\epsilon A_\rho^{-1/2} f$. By Lemma 3.1.1, $J_{\rho,\epsilon} \le R_\alpha \rho^{\alpha-2}$. Therefore, $\sum_i H_i^2 \le R_\alpha \rho^{\alpha-4} I$ in quadratic forms. Finite sums have the same upper bound. Compression to S_b preserves it: for selfadjoint H_i, $(S_b H_i S_b)^2 \le S_b H_i^2 S_b$ on its range. Both row and column variances are the same, since these operators are selfadjoint.

The compression difference $S_b H_i^2 S_b - (S_b H_i S_b)^2 = S_b H_i (I - S_b) H_i S_b$ is positive, so summing preserves the variance bound. *Step 2.* We use the Hermite creation and annihilation bounds. For completeness, use normalized Hermite polynomials, so multiplication by g_i is $a_i^* + a_i$, with $g_i h_k = \sqrt{k_i + 1}\, h_{k+e_i} + \sqrt{k_i}\, h_{k-e_i}$. On degree k, the row map $(v_i) \mapsto \sum_i a_i^* v_i$ has norm $\sqrt{k+1}$: its product with its adjoint is $\sum_i a_i^* a_i = (k+1)I$ on degree $k+1$. Composing with the column of spatial operators $S_b H_i S_b$ bounds the creation part by $\sqrt{k+1}\sqrt{R_\alpha}\rho^{(\alpha-4)/2}$. Distinct input degrees have orthogonal output degrees. The annihilation part is its adjoint, with the same bound after truncation. Adding them on degrees at most N proves (3.2.5). Boundedness of $-\Delta$ on S_b is explicit; no infinite-frequency operator theorem was used. This proves Lemma 3.2.2. □

3.2.1 Finite Gaussian products and their degree cutoffs

Lemma 3.2.2 bounds the field only on Hermite degrees at most N. We now check that this cutoff does not change the finite words that we need.

Lean full

Lemma 3.2.3 (Exact cutoffs for finite Gaussian words)**.** *Let g_{ij}, $1 \le i \le M$, $1 \le j \le m_i$, be independent standard real Gaussian coordinates, grouped by color i, and let $\mathscr{X}$ be a complex Hilbert space. On Gaussian polynomials with coefficients in $\mathscr{X}$ set*

$$J_i = \sum_{j=1}^{m_i} M_{g_{ij}} \otimes K_{ij},$$

where each K_{ij} is bounded on $\mathscr{X}$. Let $F_0, \dots, F_n$ be bounded operators acting only on $\mathscr{X}$. Fix a word $i_1, \dots, i_n$, and let r_i be the number of its occurrences of color i. If $N_i \ge r_i$ and P projects each color onto total Hermite degree at most N_i, then, for every $v \in \mathscr{X}$,

$$\begin{aligned}(I \otimes F_n)(PJ_{i_n}P)(I \otimes F_{n-1}) \cdots (PJ_{i_1}P)(I \otimes F_0)(1 \otimes v)\\ = (I \otimes F_n)J_{i_n}(I \otimes F_{n-1}) \cdots J_{i_1}(I \otimes F_0)(1 \otimes v).\end{aligned} \tag{3.2.6}$$

The equality holds for finite sums and for Bochner integrals of such words whenever the displayed vector integrals exist.

Proof. In normalized Hermite coordinates, multiplication by g_{ij} maps $h_{\boldsymbol{a}}$ to $\sqrt{a_{ij}+1}\, h_{\boldsymbol{a}+e_{ij}} + \sqrt{a_{ij}}\, h_{\boldsymbol{a}-e_{ij}}$; the second term is zero if $a_{ij} = 0$. Thus, it changes the total degree of color i by one and leaves all other color degrees unchanged. The operators $I \otimes F_l$ leave every Gaussian degree unchanged. After the first l insertions, the uncompressed word therefore has color-i degree at most $r_i(l) = |\{j \le l : i_j = i\}| \le r_i \le N_i$. This is an induction starting from degree zero in every color. Consequently, P is the identity both before and after every insertion along that word. Induction on l now proves (3.2.6). The lowering term has been retained: the assertion includes creation followed by annihilation and all resulting self-contractions. Linearity and equality of the vector integrands prove the last assertion. This is an equality of selected finite words, not of full propagators at a fixed cutoff. This proves Lemma 3.2.3. □

3.2.2 Uniform bounds for all orders

Proposition 3.1.2 controls only the first variance coefficient. We now combine Lemmas 3.2.1, 3.2.2 and 3.2.3 to bound every static Duhamel order.

Lean partial

Proposition 3.2.4 (All regularized static phase orders)**.** *Retain the full covariance class of Section 3.1. For real Schwartz f, g, let $Z_n^{\epsilon}(h)$ be the nth regularized static Duhamel phase, with the recursion (3.1.5) for every $n \ge 0$. This is an ordinary Gaussian polynomial of degree at most n, including self-contractions; it is not a pure Wick chaos. There is an explicit finite constant*

$$A_\alpha = \frac{400\sqrt{2}\, e^2}{\delta_{\alpha/2}}$$

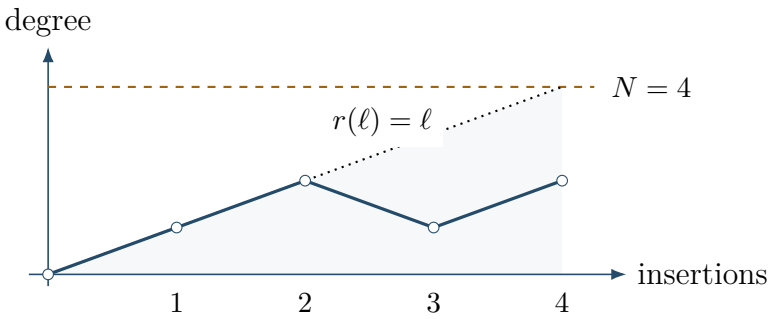

Every prefix stays below its occurrence count.
Projection changes none of
these selected finite words.

Figure 3.1: One possible degree path for four multiplications in a single Gaussian color. Multiplication is a sum of raising and lowering terms; the solid line illustrates one term, not the entire polynomial. For each color, every prefix has degree at most its occurrence count, which is at most the chosen cutoff. The result concerns selected finite words acting on the degree-zero vector, not entire propagators at a fixed cutoff. See Lemma 3.2.3.

such that, for $n \geq 1$*, uniformly in* $\epsilon > 0$*,*

$$\|Z_n^\epsilon(h)\|_{L^2(\Omega;X_{1/h})} \leq \frac{(A_\alpha\sqrt{R_\alpha})^n h^{(4-\alpha)n/2}}{(n!)^{(3-\alpha)/2}}\|(f,g)\|_{1/h}. \tag{3.2.7}$$

At every fixed positive smoothing and real coupling σ*,* $\sum_{n\geq 0}\sigma^n Z_n^\epsilon(h)$ *converges in* L^2 *phase. Its squared norm is at most*

$$(\sqrt{e}+2)^2 \exp\left\{6A_\alpha^{2/(3-\alpha)}(|\sigma|^2 R_\alpha)^{1/(3-\alpha)}h^{(4-\alpha)/(3-\alpha)}\right\}\|(f,g)\|_{1/h}^2. \tag{3.2.8}$$

Proof. We estimate the coupling coefficients at finite cutoffs, choose the phase scale by order, and then remove spatial and Gaussian cutoffs at fixed smoothing. Finally, we sum the resulting factorial estimates.

Step 1. We apply the complex phase bound at bounded cutoffs. If $R_\alpha = 0$, spectral homogeneity gives $\mu = 0$, and every positive-order term is zero. Assume $R_\alpha > 0$. First work at finite Gaussian cutoff m, degree cutoff N and spatial band b, with initial phase $S_b(f,g)$ times the Gaussian vacuum 1. All relevant operators are bounded. Lemmas 3.2.2 and 3.2.1, with $a = \alpha/2$, give a bound $100e^{2\lambda h}$ on the complex coupling circle of radius $\delta_{\alpha/2}\lambda^{2-\alpha/2}/d_N$.

The four phase entries are entire in the coupling, by the power series for $\cos(h\sqrt{L})$ and $\sin(h\sqrt{L})/\sqrt{L}$ of a bounded L. Cauchy's formula for their operator-valued series bounds the nth coefficient by

$$100e^{2\lambda h}\left(\frac{d_N}{\delta_{\alpha/2}\lambda^{2-\alpha/2}}\right)^n \|S_b(f,g)\|_\lambda.$$

The coefficient is exactly the nth Duhamel phase from the vacuum. Apply Lemma 3.2.3 with one color, $N = n$, the spatial phase Hilbert space as $\mathscr{X}$, and its free wave operators as the F_l. It identifies each cutoff Duhamel word exactly with its uncompressed word, including self-contractions. Dominated time integration preserves this identity.

Step 2. We optimize the phase scale and convert powers to factorials. Choose $\lambda = n/h$. For any phase z, $\|z\|_{1/h} \le n\|z\|_{n/h}$ and $\|(f,g)\|_{n/h} \le \|(f,g)\|_{1/h}$. Also $d_n \le 2\sqrt{2n}\sqrt{R_\alpha}$. The preceding bound is therefore at most

$$100n \left(\frac{2\sqrt{2}e^2}{\delta_{\alpha/2}}\right)^n R_\alpha^{n/2} h^{(4-\alpha)n/2} n^{-(3-\alpha)n/2} \|(f,g)\|_{1/h}.$$

Since $100n \le 200^n$ and $n! \le n^n$, this gives (3.2.7) at the cutoffs.

Step 3. We remove the cutoffs for each fixed word. We justify removal of those cutoffs at fixed ϵ and n. On Gaussian degrees at most N, the unweighted field multiplication has norm at most $2\sqrt{N+1}\sqrt{v_\epsilon}$, uniformly in m, by the same creation/annihilation argument applied pointwise in x. It follows that the noise phase insertion $(u,v) \mapsto (0, W_\epsilon u)$, between the required finite degree levels, is bounded on X_λ by this constant divided by λ. Free phase evolution is bounded by $e^{\lambda h/2}$. For finite m, $S_b \to I$ strongly and commutes with the free propagator. Each fixed Duhamel word therefore converges strongly as $b \to \infty$, by dominated time integration.

Next let $m \to \infty$ on the full Gaussian space. The truncated field multiplications converge strongly between finite degree levels. To see this, first take a vector depending on finitely many Gaussian coordinates. The annihilation tail is then zero, while the creation tail is bounded by a constant times

$$\left(\int \sum_{i>m} e_i(x)^2 \|F(x)\|^2 \,\mathrm{d}x\right)^{1/2},$$

which tends to zero by dominated convergence, since the sum is bounded by v_ϵ. Such vectors are dense; the uniform multiplication bound extends strong convergence to all vectors in those degree levels. Dominated time integration again gives convergence of every fixed word. The limit is precisely Z_n^ϵ, so the estimate survives both limits. We assert no zero-smoothing phase limit in this argument.

Step 4. We sum all regularized static orders. Finally, put $\beta = (3-\alpha)/2 \in (1/2, 3/2)$ and $x = A_\alpha |\sigma| \sqrt{R_\alpha} h^{(4-\alpha)/2}$. The elementary series satisfies

$$\sum_{n \ge 0} \frac{x^n}{(n!)^\beta} \le 2e^{3x^{1/\beta}}.$$

For $\beta \ge 1$, this follows from $\sum a_n^\beta \le (\sum a_n)^\beta$ with $a_n = x^{n/\beta}/n!$. For $\beta < 1$, apply Hölder to $((2x^{1/\beta})^n/n!)^\beta (2^{-\beta n/(1-\beta)})^{1-\beta}$. The second geometric sum is at most two. Since $\|Z_0(h)\|_{1/h} \le \sqrt{e}\|(f,g)\|_{1/h}$, absolute L^2 summation and squaring give (3.2.8). This proves Proposition 3.2.4. □

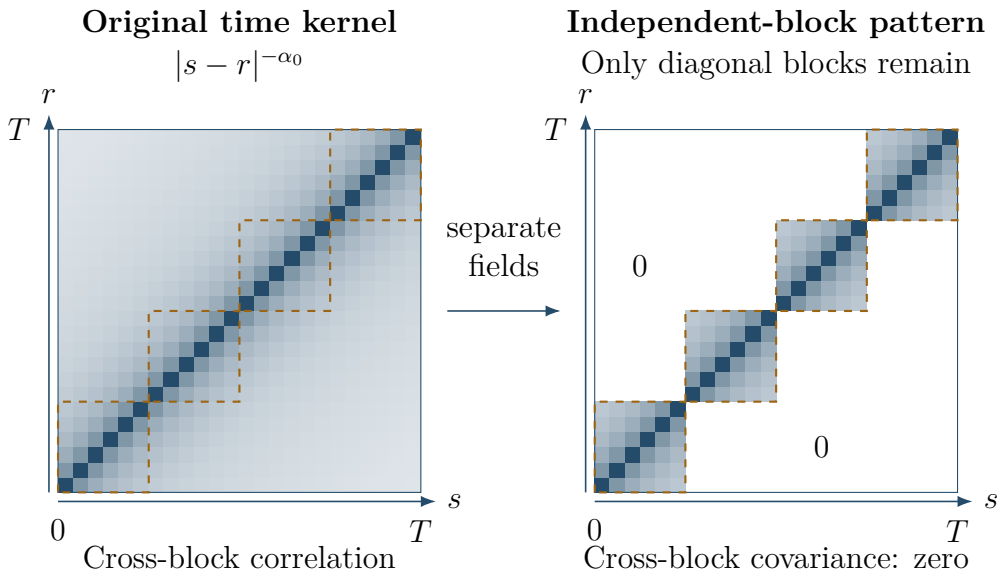

Figure 3.2: Left: the time covariance $|s-r|^{-\alpha_0}$ of the noise on $[0,T]^2$, shown for $\alpha_0 = 1/2$ with the shading capped near the diagonal; the dashed squares are the time blocks. Right: which pairs of times stay correlated when each block carries its own independent field, as in Corollary 3.2.5: only pairs in the same block. The shading inside the blocks repeats the original kernel for comparison; in the corollary each block's field is static, so its covariance is constant within a block. The product bound (3.2.11) holds for such independent blocks; it is not a bound for the original noise, whose correlation across blocks it drops.

Lean partial

Corollary 3.2.5 (Summable static interaction bounds)**.** *Let $\mathcal{S}_0(t)$ be free phase evolution and, for $\lambda h \le 1$, define the static interaction map by its convergent series*

$$\mathcal{I}^{\epsilon}_{\sigma}(h)(f,g) = \mathcal{S}_0(-h)\sum_{n\ge 0}\sigma^n Z^{\epsilon}_n(h).$$

Put $\gamma = 3-\alpha$, $B_\alpha = 3eA_\alpha^2$ and

$$L_\alpha(h,\lambda) = 4eR_\alpha h^2\lambda^{\alpha-2} + \frac{4\sqrt{e}D_\Gamma}{(2-\alpha)(3-\alpha)}\frac{h^{3-\alpha}}{\lambda},$$
$$x = B_\alpha\sigma^2 R_\alpha h^{4-\alpha},$$
$$\mathcal{E}(h,\sigma,\lambda) = \sigma^2 L_\alpha(h,\lambda) + (\lambda h)^{-2}x^2 e^{\gamma x^{1/\gamma}}.$$

Uniformly in $\epsilon > 0$,

$$\mathbb{E}\|\mathcal{I}^{\epsilon}_{\sigma}(h)(f,g)\|^2_\lambda \le [1+\mathcal{E}(h,\sigma,\lambda)]\|(f,g)\|^2_\lambda. \tag{3.2.9}$$

If $0<\alpha_0<1$ and $\alpha+\alpha_0<2$, then, for $h_j = 2^{-j}/\lambda$, $\sigma_j^2 = h_j^{-\alpha_0}$ and $T>0$,

$$\sum_{j\ge 0}\frac{T}{h_j}\mathcal{E}(h_j,\sigma_j,\lambda) < \infty. \tag{3.2.10}$$

For a finite single partition, let $\mathcal{M}_j(h_j)$ be the static phase maps with mutually independent copies of the smoothed field, real couplings σ_j, and $\lambda h_j \le 1$. They have continuous L^2 extensions to independent random initial phases. Then

$$\mathbb{E}\|\mathcal{M}_K(h_K)\cdots\mathcal{M}_1(h_1)(f,g)\|_\lambda^2 \le \exp\left\{\lambda\sum_{j=1}^K h_j + \sum_{j=1}^K \mathcal{E}(h_j,\sigma_j,\lambda)\right\}\|(f,g)\|_\lambda^2. \quad (3.2.11)$$

This concerns independent successive blocks on one partition. Formula (3.2.10) only sums individual upper bounds across dyadic levels; it does not identify a product with an evolution driven by overlapping or repeated fields.

Proof. We keep the complete first variance coefficient separate from the higher-order series. We then check dyadic summability and use independence only for successive blocks on one finite partition.

Step 1. We retain both first-variance contributions. Write $N = \|(f,g)\|_\lambda$ and $Y_n = \mathcal{S}_0(-h)Z_n^\epsilon(h)$. The free estimate from Section 3.1 holds for both time directions, since its differentiated energy was bounded in absolute value. Thus, $\|\mathcal{S}_0(-h)\|_\lambda \le \sqrt{e}$. Since $Y_0 = (f,g)$, Proposition 3.1.2 bounds the complete first variance coefficient of $\mathbb{E}\|\sum \sigma^n Y_n\|_\lambda^2$ in absolute value by $L_\alpha(h,\lambda)N^2$. In detail, its first random squared norm is bounded by e times (3.1.6), and its second-order mean cross term by $2N\sqrt{e}$ times (3.1.7).

Step 2. We bound the higher-order interaction series. For $n \ge 1$, the norm comparisons when $\lambda h \le 1$ and (3.2.7) give

$$\|Y_n\|_{L^2(\Omega;X_\lambda)} \le \frac{\sqrt{e}}{\lambda h}\frac{(A_\alpha\sqrt{R_\alpha})^n h^{(4-\alpha)n/2}}{(n!)^{\gamma/2}}N.$$

Gaussian symmetry makes $\mathbb{E}\langle Y_r, Y_s\rangle_\lambda = 0$ if $r+s$ is odd. All double series below converge absolutely by these bounds. For $r+s = 2k$, the elementary factorial inequality $r!s! \ge (k!)^2$ shows that the sum of absolute inner products is at most

$$\frac{e(2k+1)}{(\lambda h)^2}\frac{(A_\alpha^2 R_\alpha)^k h^{(4-\alpha)k}}{(k!)^\gamma}N^2, \qquad k \ge 1.$$

This includes $r = 0$ or $s = 0$, since $\lambda h \le 1$ and $\|Y_0\| = N$. The bound $e(2k+1) \le (3e)^k$ therefore controls all orders $k \ge 2$ by

$$\frac{1}{(\lambda h)^2}\sum_{k\ge 2}\frac{x^k}{(k!)^\gamma}N^2 \le \frac{x^2 e^{\gamma x^{1/\gamma}}}{(\lambda h)^2}N^2.$$

Here $\gamma > 1$, and $\sum_{j\ge 0} x^j/(j!)^\gamma \le e^{\gamma x^{1/\gamma}}$. Keeping the sharper first coefficient separately proves (3.2.9).

Step 3. We sum the dyadic budgets and estimate the independent-block product. Finally, set $\beta = 4 - \alpha - \alpha_0 > 2$. After multiplication by T/h_j, the two first-coefficient terms in (3.2.10) are constant multiples of

$$T\lambda^{\alpha-2}h_j^{1-\alpha_0}, \qquad \frac{T}{\lambda}h_j^{2-\alpha-\alpha_0}.$$

The higher-order term is

$$\frac{T(B_\alpha R_\alpha)^2}{\lambda^2} h_j^{2\beta-3} \exp\{\gamma (B_\alpha R_\alpha)^{1/\gamma} h_j^{\beta/\gamma}\}.$$

The exponential factor is bounded by its value at h_0. All three powers are positive, so their geometric series converge. For the finite partition, write $\mathcal{M}_j(h_j) = \mathcal{S}_0(h_j)\mathcal{I}_j(h_j)$. Bound (3.2.9) and $\|\mathcal{S}_0(h_j)\|_\lambda^2 \le e^{\lambda h_j}$ give a bounded linear map from deterministic X_λ to $L^2(\Omega_j; X_\lambda)$, initially on Schwartz phases and then by density. Tensoring with the past probability space extends this bound to random initial phases independent of the jth field. Iteration gives the product of $e^{\lambda h_j}(1 + \mathcal{E}(h_j, \sigma_j, \lambda))$. The inequality $1 + y \le e^y$ for $y \ge 0$ proves (3.2.11). This proves Corollary 3.2.5. □

The independent-block estimate does not use log-convexity in additive covariance amplitudes. That unrestricted interpolation principle already fails for a scalar Gaussian wave; see No-go 11.

These estimates concern individual static phase and interaction maps. Their summability alone does not identify the evolution driven by overlapping interval fields. The coefficient argument in Section 3.3 supplies the separate estimate needed for that evolution.

3.3 Interval fields and the full upper bound

The intrinsic constant is identified independently in Theorem 11.2.6.

Write

$$\nu = 3 - \alpha > 1, \qquad \beta = 4 - \alpha - \alpha_0 > 2, \qquad p = 2 - \alpha_0 > 1.$$

Thus, $\beta - \nu = 1 - \alpha_0 > 0$. In this section the spatial dimension is any admissible $d \in \{1, 2, 3\}$. The spatial covariance is the nonnegative, even, positive-definite tempered Radon measure Γ, with scaling $\Gamma(rA) = r^{d-\alpha}\Gamma(A)$ and spectral convention $\Gamma = \int e^{i\xi\cdot x}\mu(\,\mathrm{d}\xi)$. This includes $\Gamma = \delta_0$ when $d = \alpha = 1$. Set

$$R_\alpha = \frac{\alpha\pi\mu(B_1)}{2\sin(\pi\alpha/2)}, \qquad A_\rho = \rho^2 - \Delta, \qquad \|(f,g)\|_\rho^2 = \|f\|_2^2 + \|A_\rho^{-1/2} g\|_2^2.$$

Complex Hilbert inner products are linear in the first slot.

3.3.1 Contractions and complex phase estimates

The resolvent estimate in Lemma 3.1.1 and the Gaussian cutoff bound in Lemma 3.2.2 were stated for a covariance on $\mathbb{R}^3$. We now derive the needed column and finite-degree bounds for every admissible d.

Lean narrower

Lemma 3.3.1 (Dimension-independent Gaussian contractions)**.** *Uniformly in positive spatial smoothing and in finite Gaussian-mode and spatial Fourier-band cutoffs,*

$$\sum_m \|A_\rho^{-1/2} M_{e_m} f\|_2^2 \le R_\alpha \rho^{\alpha-2} \|f\|_2^2. \tag{3.3.1}$$

Here $W_\epsilon(x) = \sum_m g_m e_m(x)$ is an orthonormal-coordinate representation of $W(p_\epsilon(x-\cdot))$, whose covariance is $\Gamma_\epsilon = p_{2\epsilon} * \Gamma$. Consequently, on a Gaussian color that is initially in its vacuum, the phase insertion $(u,v) \mapsto (0, W_\epsilon u)$ has norm at most $\sqrt{R_\alpha}\rho^{(\alpha-2)/2}$ into its Gaussian L^2 phase. With Hermite degree of this color truncated at N, its sandwiched field has operator norm at most

$$2\sqrt{N+1}\sqrt{R_\alpha}\rho^{\alpha/2-2}. \tag{3.3.2}$$

Both statements remain valid tensoring with any other Hilbert factor.

Proof. We derive the spatial covariance column estimate in every admissible dimension. The vacuum insertion uses that column directly, while occupied Hermite degrees require the creation and annihilation estimate on the sandwiched operators.

Step 1. We compare translated resolvents using physical covariance positivity. Fourier uniqueness gives $\mu(B_r) = r^\alpha \mu(B_1)$. The Gaussian comparison in Lemma 3.1.1 uses no dimension-specific identity:

$$\int e^{-s|\eta+\xi|^2} \mu(\mathrm{d}\xi) = \int p_{2s}^{(d)}(x) e^{i\eta\cdot x} \Gamma(\mathrm{d}x) \le \int e^{-s|\xi|^2} \mu(\mathrm{d}\xi).$$

Evenness gives a real integral, and physical nonnegativity gives the inequality. Integrating against $e^{-\rho^2 s}\,\mathrm{d}s$ and using radial spectral homogeneity yields

$$\sup_\eta \int \frac{\mu(\mathrm{d}\xi)}{\rho^2 + |\eta+\xi|^2} \le R_\alpha \rho^{\alpha-2}.$$

No exclusion of a physical origin atom is used.

Step 2. We obtain the column bound and the new-color insertion estimate. Gaussian isometry and unnormalized spatial Plancherel give

$$\sum_m \|A_\rho^{-1/2} M_{e_m} f\|_2^2 = \frac{1}{(2\pi)^d} \int |\widehat{f}(\eta)|^2 \left(\int \frac{e^{-\epsilon|\xi|^2} \mu(\mathrm{d}\xi)}{\rho^2 + |\eta+\xi|^2} \right) \mathrm{d}\eta.$$

This proves (3.3.1). A finite mode sum is a positive sub-sum. For a Fourier-band projection S_b, which commutes with A_ρ, use $S_b A_\rho^{-1} S_b \le A_\rho^{-1}$ to obtain the same inequality for $S_b M_{e_m} S_b$. The phase assertion on a new color follows because $\sum_m g_m(0, M_{e_m} u)$ has squared norm given by the left side of (3.3.1), and its input is independent of this color.

Step 3. We obtain the finite-degree bound and retain other Hilbert factors. Substituting $A_\rho^{-1/2} f$ gives

$$\sum_m (A_\rho^{-1/2} M_{e_m} A_\rho^{-1/2})^2 \le R_\alpha \rho^{\alpha-4} I.$$

These spatial sandwiches are selfadjoint, so their row and column variances agree. The normalized Hermite creation-row norm from degree j to degree $j+1$ is $\sqrt{j+1}$, and annihilation is its adjoint, as proved in Lemma 3.2.2. Composition with the spatial column and addition of the two parts prove (3.3.2). The same positive operator identities hold with an identity on every other Hilbert factor. The calculation used only the radial mass $\mu(B_1)$, homogeneity and physical nonnegativity. Thus, R_α is the only covariance quantity in these estimates. No angular bound or unsmoothed multiplication norm has been absorbed into a constant. This proves Lemma 3.3.1. □

Lean partial

Lemma 3.3.2 (Complex sums and changing phase weights)**.** *Let A_0 be bounded, nonnegative and selfadjoint, and let V be bounded on the same complex Hilbert space. Write $A_\rho = \rho^2 + A_0$. The complex phase conclusion of Lemma 3.2.1 holds for $L = A_0 - V$ whenever V is bounded, not necessarily selfadjoint,*

$$\|A_\rho^{-1/2} V A_\rho^{-1/2}\| \le D\rho^{a-2}, \qquad \rho > 0, \quad 0 < a < 1, \quad D \le \delta_a \Lambda^{2-a}.$$

Its bound is $100e^{2\Lambda h}$ in X_Λ. If a piecewise-constant potential is the sum of connected-interval fields, assign a positive weight ω_i to each field present and put $\Lambda(t) = \lambda + \sum_i \omega_i \mathbf{1}_{I_i}(t)$. The total loss from changing between these phase norms, starting and ending in X_λ, is at most

$$\prod_i (1 + \omega_i/\lambda). \tag{3.3.3}$$

Proof. We repeat the resolvent and numerical-range estimates for a general bounded complex potential, retaining adjoint comparisons. We then count the phase-norm losses at jumps of the active interval set.

Step 1. We obtain the four ordered root comparisons without selfadjointness. The adjoint has the identical sandwich bound, since

$$A_\rho^{-1/2} V^* A_\rho^{-1/2} = (A_\rho^{-1/2} V A_\rho^{-1/2})^*.$$

The form estimate at $\rho = \Lambda$ gives $\mathrm{Re}\langle (L + \Lambda^2)u, u\rangle \ge (1 - \delta_a)\langle A_\Lambda u, u\rangle$. The shifted operator and its adjoint thus have spectra in the right half-plane, where their principal inverse roots are defined. Put $K_\kappa = A_\kappa^{-1/2} V A_\kappa^{-1/2}$ and $\kappa = (\Lambda^2 + t)^{1/2}$. The resolvent difference is exactly

$$(L + \Lambda^2 + t)^{-1} - A_\kappa^{-1} = A_\kappa^{-1/2}(1 - K_\kappa)^{-1} K_\kappa A_\kappa^{-1/2}.$$

Its product on the left with $A_\Lambda^{1/2}$ has norm at most $D\kappa^{a-3}/(1 - \delta_a)$. The inverse-root integral in Lemma 3.2.1 therefore gives the same $1/6$ bound. More explicitly, put $L_\Lambda = L + \Lambda^2$ and $Q = A_\Lambda^{1/2} L_\Lambda^{-1/2}$. Then $\|Q - I\| \le 1/6$, so $\|Q\| \le 7/6$ and $\|Q^{-1}\| \le 6/5$ by its Neumann series. Taking adjoints under the norm-convergent resolvent integral gives $(L_\Lambda^{-1/2})^* = (L_\Lambda^*)^{-1/2}$. Apply the same estimate to $L^* = A_0 - V^*$ and take adjoints. This bounds $L_\Lambda^{-1/2} A_\Lambda^{1/2}$ by $7/6$ and its inverse $A_\Lambda^{-1/2} L_\Lambda^{1/2}$ by $6/5$. Together with Q and $Q^{-1} = L_\Lambda^{1/2} A_\Lambda^{-1/2}$, these are all four ordered comparisons in (3.2.4), each at most two.

Step 2. We retain the numerical-range and phase-block bounds. For a unit vector u put $s = \|A_0^{1/2}u\|$ and $\langle Lu, u\rangle = x + iy$. The form estimate at $\rho = \Lambda$ and, separately, at $\rho = s$ gives

$$|\langle Vu, u\rangle| \le D\Lambda^{a-2}(s^2 + \Lambda^2), \qquad |\langle Vu, u\rangle| \le 2Ds^a.$$

At $s = 0$ the second bound follows by $\rho \downarrow 0$. Thus, $x + \Lambda^2 \ge (1 - \delta_a)(s^2 + \Lambda^2)$ and $|y| \le 2\delta_a\Lambda^{2-a}s^a$. These are the two inequalities used for the numerical-range parabola in Lemma 3.2.1. Its scalar bounds and the bounded-operator Crouzeix–Palencia theorem apply to L without selfadjointness. The four weighted block formulas there use only functions of L and the root comparisons just proved. Their norms are at most $3e^{\Lambda h}$, $12(1 + \Lambda h)e^{\Lambda h}$, $12e^{\Lambda h}$ and $12e^{\Lambda h}$. Their sum is at most $100e^{2\Lambda h}$. This uses neither selfadjointness of V nor commutation of A_Λ with L.

Step 3. We charge each norm loss only when an interval ends. For a common phase vector,

$$\|z\|_{\rho_{\mathrm{new}}} \le \max\{1, \rho_{\mathrm{old}}/\rho_{\mathrm{new}}\}\|z\|_{\rho_{\mathrm{old}}}.$$

At a jump, write E for ending fields, S for starting fields, and R for those remaining. The ratio is at most

$$\frac{\lambda + \sum_R \omega_i + \sum_E \omega_i}{\lambda + \sum_R \omega_i + \sum_S \omega_i} \le 1 + \sum_E \omega_i/\lambda \le \prod_E (1 + \omega_i/\lambda).$$

An initial increase of the weight has no loss. Count a final return to X_λ as an ending jump at T. Each connected interval ends once, giving (3.3.3). This proves Lemma 3.3.2. □

3.3.2 Summing the coefficient bounds

We first record an elementary bound for power series. The proof of Proposition 3.3.5 uses it to sum over the ways a total order k splits among the interval fields.

Lean full

Lemma 3.3.3 (A coefficient bound for a product with nonnegative coefficients)**.** *For $k \ge 1$, define*

$$v_i = i^{-\beta} + k^{-1}i^{-(\beta-1)} + k^{\alpha-2}i^{-p}, \qquad b_{i,l} = \frac{i^{-\beta l}(1 + li/k)^2}{(l!)^\nu}, \quad l \ge 2.$$

There is a finite $C = C(\alpha, \alpha_0)$, independent of M, k, such that

$$[z^k]\prod_{i=1}^{M}\left(1 + v_i z + \sum_{l\ge 2} b_{i,l}z^l\right) \le \frac{C^k}{(k!)^\nu}. \tag{3.3.4}$$

Proof. We evaluate the positive generating product at one order-dependent radius. We separate the third singleton term, then estimate the coarse and fine interval indices. Positivity converts the product bound back into a coefficient bound.

Step 1. We separate and bound the third singleton contribution. Evaluate the positive product at $z = \theta k^\nu$, with $\theta = 1/4$. Put $P_i = \theta k^\nu i^{-\beta}$ and $Q_i = \theta k i^{-p}$. The third singleton

term is Q_i because $\nu+\alpha-2=1$. The inequality $1+A+B\le(1+A)(1+B)$ separates the factors $1+Q_i$. For $p>1$,

$$\sum_{i\ge1}\log(1+Ai^{-p})\le\int_0^\infty\log(1+Ax^{-p})\,\mathrm{d}x=A^{1/p}\int_0^\infty\log(1+x^{-p})\,\mathrm{d}x.$$

Near zero, $\log(1+x^{-p})$ is bounded by a constant plus $p|\log x|$; at infinity it is at most x^{-p}, which is integrable for $p>1$. The last integral is finite. Hence, their logarithmic contribution is at most $Ck^{1/p}\le Ck$.

Step 2. We estimate the coarse factors by the factorial series. For $x\ge0$, the sum of the νth powers of the nonnegative terms $x^{l/\nu}/l!$ is at most the νth power of their sum, and that sum is $e^{x^{1/\nu}}$. If $i\le k$, the remaining factor is at most $S_\nu(4P_i)=\sum_{l\ge0}(4P_i)^l/(l!)^\nu$: its singleton is at most $2P_i$, and $(1+li/k)^2\le(1+l)^2\le4^l$. Since $\nu>1$, $S_\nu(x)\le e^{\nu x^{1/\nu}}$. Therefore,

$$\sum_{i\le k}\log S_\nu(4P_i)\le\nu(4\theta)^{1/\nu}k\sum_{i\ge1}i^{-\beta/\nu}\le Ck,$$

because $\beta/\nu>1$.

Step 3. We sum the fine-index tails and extract the coefficient. If $i>k$, then $P_i\le\theta$. The remaining singleton tail is at most

$$\theta\left(\frac{1}{\beta-1}+\frac{1}{\beta-2}\right)k^{\nu+1-\beta}=Ck^{\alpha_0}.$$

For $l\ge2$, $0\le P\le1/4$ and $y\ge0$, the bounds $(1+ly)^2\le2l^2(1+y^2)$ and $P^l\le P^2 4^{-(l-2)}$ leave a summable geometric series with a quadratic factor, independent of P,y. Also, uniformly for $0\le P\le1/4$ and $y\ge0$, $\sum_{l\ge2}P^l(1+ly)^2/(l!)^\nu\le CP^2(1+y^2)$. Summing this bound gives

$$Ck^{2\nu}\left(\frac{k^{1-2\beta}}{2\beta-1}+\frac{k^{-2}k^{3-2\beta}}{2\beta-3}\right)=Ck^{2\alpha_0-1}\le Ck.$$

Use $\log(1+y)\le y$ for these fine factors. The entire product is consequently at most e^{Ck}. Positivity of its coefficients bounds the kth coefficient by $\theta^{-k}k^{-\nu k}e^{Ck}\le C^k/(k!)^\nu$. This proves Lemma 3.3.3. □

Let $\mathcal{F}$ be a finite family of connected intervals I_i meeting $[0,T]$, with lengths h_i sorted decreasingly. Let W_i^ϵ be independent copies of the smoothed unit field, and suppose

$$h_i\le LT/i,\qquad\sigma_i^2\le ch_i^{-\alpha_0}.\tag{3.3.5}$$

Write $\mathcal{U}_{\mathcal{F}}^\epsilon(T;s)$ for phase evolution with potential $s\sum_i\sigma_i\mathbf{1}_{I_i}(t)W_i^\epsilon(x)$.

Lean partial

Lemma 3.3.4 (A fixed degree-split estimate)**.** *Retain the finite interval fields above, with $R_\alpha>0$ and $\sigma_i>0$. Fix integers $r_i,q_i,k_i\ge0$ with $r_i+q_i=2k_i$, and put $k=\sum_i k_i\ge1$, $\lambda=k/T$. Represent $W_i^\epsilon(x)=\sum_j g_{ij}e_{ij}(x)$ as in Lemma 3.3.1. Retain m_i Gaussian modes,*

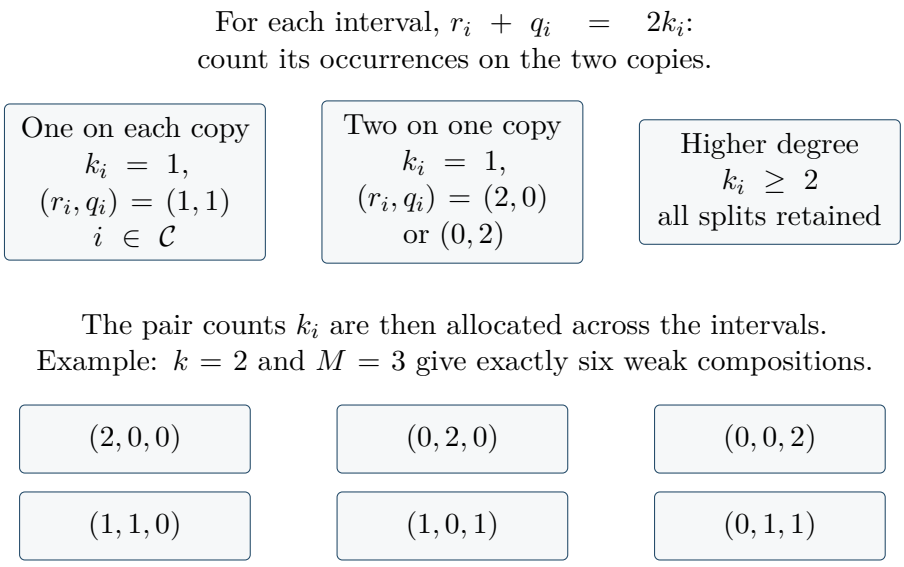

Figure 3.3: Two different counts must be kept separate. First split each interval's even total degree between two copies built from the same Gaussian fields; only distinct colors are independent. For $k_i = l$, there are $2l + 1$ possible splits. Cross singletons use one insertion on each copy; a singleton confined to one copy is estimated with the other background terms and has one ending factor, not two. Then sum the pair counts over interval indices. Ordinary positive-product coefficient extraction counts weak compositions, without an extra multinomial coefficient. The displayed $a_{i,l}$ are generic coefficients, not additional model parameters. See Lemma 3.3.4 and Lemma 3.3.3.

a spatial Fourier band S_b, and Hermite cutoff $N_i = 2k_i$ on color i. Write $P = \bigotimes_i P_{N_i}$ and set

$$B_i = PS_b \left(\sum_{j=1}^{m_i} g_{ij} M_{e_{ij}} \right) S_b P, \qquad V_{\boldsymbol{z}}(t) = \sum_i z_i \sigma_i \mathbf{1}_{I_i}(t) B_i.$$

Let $\mathcal{M}_{\boldsymbol{z}}^{\mathrm{cut}}(T)$ be the phase evolution with this bounded potential and $A_0 = -\Delta$ on the band. Define $U_{\boldsymbol{r}} v = [\boldsymbol{z}^{\boldsymbol{r}}] \mathcal{M}_{\boldsymbol{z}}^{\mathrm{cut}}(T) v$, with the projected deterministic initial phase in the Gaussian vacuum. Put

$$\mathcal{I} = \{i : k_i > 0\}, \qquad \mathcal{C} = \{i : k_i = 1,\ r_i = q_i = 1\},$$
$$\mathcal{B} = \mathcal{I} \setminus \mathcal{C}, \qquad \ell_i = \mathbf{1}_{\{r_i > 0\}} + \mathbf{1}_{\{q_i > 0\}}.$$

There is a finite $C_{\mathrm{split}} = C_{\mathrm{split}}(\alpha)$, uniform in all these cutoffs and in the finite interval family, such that

$$\begin{aligned} |\langle U_{\boldsymbol{r}} v, U_{\boldsymbol{q}} v \rangle_{L^2(\Omega; X_{1/T})}| \le k^2 C_{\mathrm{split}}^k R_\alpha^k \|v\|_{1/T}^2 \prod_{i \in \mathcal{C}} (\sigma_i^2 h_i^2 \lambda^{\alpha-2}) \\ \times \prod_{i \in \mathcal{B}} \frac{(\sigma_i^2 h_i^{4-\alpha})^{k_i}}{(k_i!)^\nu} (1 + k_i/(\lambda h_i))^{\ell_i}. \end{aligned} \tag{3.3.6}$$

In particular, a singleton used twice on one copy has $\ell_i = 1$; a higher color has at most two metric factors.

Proof. We estimate each vector coefficient on bounded cutoffs before pairing the two copies. We bound background segments on one common partition, count every change of phase norm once, and insert each cross color only from its vacuum. A cube integral and normalized vector Cauchy formula then give the coefficient with no extra permutation factor.

Step 1. We set the active colors and background amplitude radii. We give a bound for each vector coefficient before taking their inner product. Every operator below acts on the finite Gaussian-mode, Hermite and spatial-band Hilbert space in the statement. In particular, it is bounded. Its piecewise-constant evolution is a finite product of block exponentials, hence is entire in every amplitude. All coefficient extractions in this proof are ordinary power-series extractions.

An amplitude with $k_i = 0$ is evaluated at zero on both copies. If $k_i > 0$ but $I_i \cap [0, T]$ has zero length, every coefficient with a positive power of that amplitude vanishes. The claimed inner product is then zero. We may therefore assume that every active interval has a positive-length intersection $I_i^T = (a_i, b_i)$ with $(0, T)$; endpoint conventions do not affect the evolution or its time integrals. Its length is at most h_i.

Write $a = \alpha/2$, and use the positive constant δ_a in Lemma 3.2.1. For every $i \in \mathcal{B}$ put

$$\omega_i = \frac{k_i}{h_i}, \qquad d_i = 2\sqrt{2k_i + 1}\sqrt{R_\alpha}, \qquad \varrho_i = \frac{\delta_a \omega_i^{2-a}}{\sigma_i d_i}. \tag{3.3.7}$$

Fix one of the two copies. Its background set is $\mathcal{A}_r = \{i \in \mathcal{B} : r_i > 0\}$ or $\mathcal{A}_q = \{i \in \mathcal{B} : q_i > 0\}$; denote that set by $\mathcal{A}$. Evaluate every unused amplitude at zero. Colors in $\mathcal{C}$

have degree one on this copy. Put $m = |\mathcal{C}|$. Thus, there are at most k background and cross colors altogether.

Step 2. We bound background evolution on the common chronological partition. *Background segments and the common partition.* Fix $|z_i| = \varrho_i$ for $i \in \mathcal{A}$. With the cross amplitudes zero, the potential is $V_z(t) = \sum_{i\in\mathcal{A}} z_i\sigma_i \mathbf{1}_{I_i^T}(t)B_i$. Write $P_z(t,s)$ for its evolution, and set

$$\Lambda(t) = \lambda + \sum_{i\in\mathcal{A}} \omega_i \mathbf{1}_{I_i^T}(t).$$

For each $\rho > 0$, Lemma 3.3.1 gives

$$\|A_\rho^{-1/2} V_z(t) A_\rho^{-1/2}\| \le D(t)\rho^{a-2}, \qquad D(t) = \sum_{i\in\mathcal{A}} |z_i|\sigma_i d_i \mathbf{1}_{I_i^T}(t) \le \delta_a \Lambda(t)^{2-a}.$$

The last step follows from (3.3.7) and $\sum x_i^{2-a} \le (\sum x_i)^{2-a}$ for nonnegative x_i. The spatial resolvents here include the identity on every Gaussian factor. This is a deterministic operator inequality on their joint Hilbert space; the input can depend on the background fields.

For the moment fix a tuple $(t_i)_{i\in\mathcal{C}}$ with $t_i \in I_i^T$, all distinct and away from the background endpoints. The excluded tuples have Lebesgue measure zero. Form the common partition

$$0 = \tau_0 < \tau_1 < \cdots < \tau_M = T \tag{3.3.8}$$

from these times and all background endpoints in $(0,T)$. On (τ_{j-1},τ_j) let Λ_j be the constant value of Λ, and put $P_j = P_z(\tau_j,\tau_{j-1})$. There are at most $2|\mathcal{A}| + m$ interior partition points, so $M \le 2|\mathcal{A}| + m + 1 \le 3k + 1$. Lemma 3.3.2, with its adjoint bound as stated there, gives

$$\begin{aligned} \prod_{j=1}^{M} \|P_j\|_{\mathcal{H}_{\Lambda_j}\to\mathcal{H}_{\Lambda_j}} &\le 100^M \exp\left(2\sum_{j=1}^{M} \Lambda_j(\tau_j - \tau_{j-1})\right) \\ &\le 100^{3k+1} e^{4k} =: M_k, \qquad \mathcal{H}_\rho = L^2(\Omega; X_\rho). \end{aligned} \tag{3.3.9}$$

Indeed, the sum in the exponential is exactly $\lambda T + \sum_{i\in\mathcal{A}} \omega_i(b_i - a_i) \le k + \sum_{i\in\mathcal{A}} k_i \le 2k$. Insertion times refine a partition; they do not repeat this integral.

Step 3. We count the phase-metric changes. *Every identity between phase norms.* Put $\Lambda_0 = \Lambda_{M+1} = \lambda$. At τ_j let $\mathscr{I}_j$ be the identity from $\mathcal{H}_{\Lambda_j}$ to $\mathcal{H}_{\Lambda_{j+1}}$, for $0 \le j \le M$. Its norm is at most

$$q_j := \max\{1, \Lambda_j/\Lambda_{j+1}\}.$$

This follows directly from the two components of the phase norm and the spectral inequality $A_{\Lambda_{j+1}}^{-1} \le q_j^2 A_{\Lambda_j}^{-1}$. At an interior background endpoint, let E_j, S_j, R_j denote the ending, starting and remaining background colors. Then

$$\frac{\Lambda_j}{\Lambda_{j+1}} = \frac{\lambda + \sum_{R_j}\omega_i + \sum_{E_j}\omega_i}{\lambda + \sum_{R_j}\omega_i + \sum_{S_j}\omega_i} \le 1 + \sum_{E_j} \omega_i/\lambda \le \prod_{i\in E_j}(1 + \omega_i/\lambda).$$

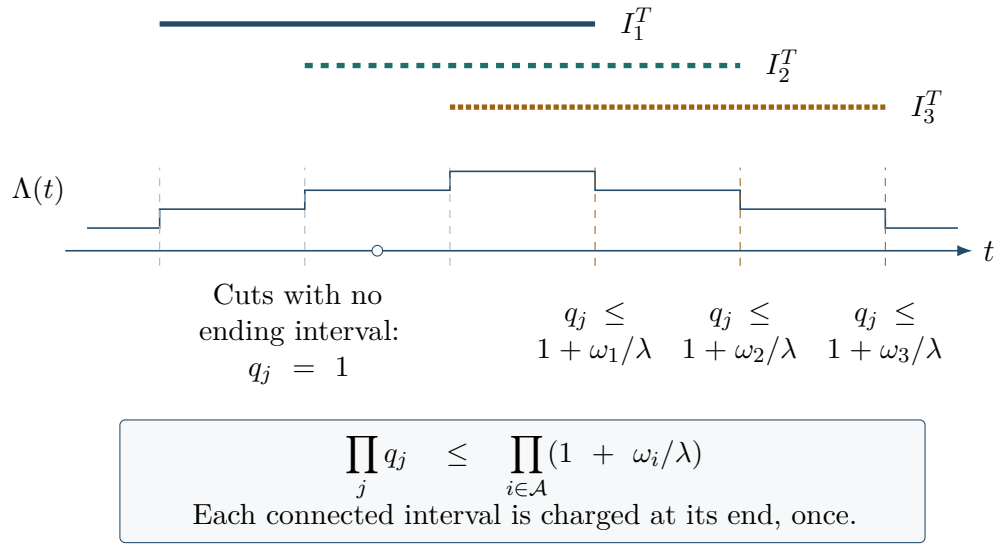

Figure 3.4: Changes of phase norm are charged at interval endpoints. The staircase illustrates $\Lambda(t) = \lambda + \sum_{i\in\mathcal{A}} \omega_i \mathbf{1}_{I_i^T}(t)$ for three overlapping intervals; its heights are schematic. The conversion satisfies $q_j = \max\{1, \Lambda_j/\Lambda_{j+1}\}$. A cut containing only starts or insertions adds no factor. At a shared ending cut, charge all ending intervals together; the final conversion at T is also included. This prevents repeating the full product at every insertion. See Lemma 3.3.4.

The last product is at least one, so it also bounds q_j. At an insertion-only cut the heights agree and $q_j = 1$. Initially $q_0 = 1$. At T the same inequality charges all intervals with $b_i = T$ as ending there. Each connected I_i^T ends at precisely one such cut. Consequently,

$$\prod_{j=0}^{M} q_j \le D_{\mathcal{A}} := \prod_{i\in\mathcal{A}} (1 + k_i/(\lambda h_i)). \tag{3.3.10}$$

This product includes the initial and final conversions. There is no new copy of $D_{\mathcal{A}}$ at an insertion time or an overlapping interval's start.

Step 4. We estimate every cross-color insertion on its actual tensor subspace. *The cross-color subspaces and the word norm.* Let $\mathscr{G}_i^{(0)}$ be the vacuum of color i and $\mathscr{G}_i^{(1)}$ its first Gaussian degree. For $S \subset \mathcal{C}$, use the tensor subspace

$$\mathscr{Z}_S = \bigotimes_{i\in\mathcal{A}} \mathscr{G}_i^{\le N_i} \otimes \bigotimes_{i\in S} \mathscr{G}_i^{(1)} \otimes \bigotimes_{i\in\mathcal{C}\setminus S} \mathscr{G}_i^{(0)},$$

with every omitted Gaussian color in its vacuum and with the common spatial band understood. Each P_j preserves the corresponding phase space over $\mathscr{Z}_S$: its potential acts only on colors in $\mathcal{A}$, and its spatial operators act identically on all cross Gaussian factors. The identities $\mathscr{I}_j$ preserve the same tensor subspace.

Define $J_i(u, w) = (0, \sigma_i B_i u)$ for $i \in \mathcal{C}$. If $i \notin S$, multiplication by its field takes its vacuum into first Gaussian degree. The Hermite cutoff $N_i = 2$ does not alter this step.

Thus, J_i maps the phase over $\mathscr{Z}_S$ into the phase over $\mathscr{Z}_{S\cup\{i\}}$. Collect all other Gaussian factors into $\mathscr{R}_i$. Every input has the form $1_i \otimes (u, w)$, with $(u, w) \in \mathscr{R}_i \otimes X_\rho$. The cutoffs on other colors are identities on its retained degrees, which multiplication by the color-i field leaves unchanged. Hence,

$$J_i(1_i \otimes (u, w)) = \sigma_i \sum_{j=1}^{m_i} g_{ij} \otimes (0, S_b M_{e_{ij}} S_b u).$$

Orthogonality $\mathbb{E}[g_{ij} g_{il}] = \mathbf{1}_{\{j=l\}}$ gives

$$\begin{aligned} \|J_i(1_i \otimes (u, w))\|^2_{\mathcal{H}_\rho} &= \sigma_i^2 \sum_{j=1}^{m_i} \|A_\rho^{-1/2} S_b M_{e_{ij}} S_b u\|^2_{\mathscr{R}_i \otimes L^2_x} \\ &\le \sigma_i^2 R_\alpha \rho^{\alpha-2} \|u\|^2_{\mathscr{R}_i \otimes L^2_x} \\ &\le \sigma_i^2 R_\alpha \rho^{\alpha-2} \|1_i \otimes (u, w)\|^2_{\mathcal{H}_\rho}. \end{aligned}$$

The first inequality is (3.3.1) tensored with $\mathscr{R}_i$ and allows arbitrary dependence on earlier colors. Thus, at the insertion time,

$$\|J_i\| \le \sigma_i \sqrt{R_\alpha} \Lambda(t_i)^{(\alpha-2)/2} \le c_i := \sigma_i \sqrt{R_\alpha} \lambda^{(\alpha-2)/2}. \tag{3.3.11}$$

Starting with $\mathscr{Z}_\varnothing$, these subspaces describe every partial word. They justify each new-color estimate even though the current vector depends on the background and earlier cross colors. No occupied-color annihilation is estimated by a vacuum bound.

Equivalently, apply Lemma 3.2.3 to the cross colors, with $\mathscr{X}$ containing the bounded background Gaussian space and the spatial phase space. Background segments act only on $\mathscr{X}$, and each cross color occurs once. Its cutoff is an exact identity on every prefix of the selected word. This does not identify an untruncated background propagator with a fixed cutoff.

At an interior cut τ_j let $B_j^{\mathrm{cut}} = J_i$ if $\tau_j = t_i$ and let B_j^{cut} be the identity otherwise. Apply B_j^{cut} after $\mathscr{I}_j$; at an insertion cut the two heights are equal. The chronological word, as a map from $\mathcal{H}_\lambda$ back to $\mathcal{H}_\lambda$, is exactly

$$\mathcal{W}_{\mathcal{A}}(z, \boldsymbol{t}) = \mathscr{I}_M P_M B_{M-1}^{\mathrm{cut}} \mathscr{I}_{M-1} P_{M-1} \cdots B_1^{\mathrm{cut}} \mathscr{I}_1 P_1 \mathscr{I}_0.$$

For $M = 1$ this means $\mathscr{I}_1 P_1 \mathscr{I}_0$. The rightmost factor acts first; no spatial operators are commuted. Multiplying their norms, using the subspaces just specified, gives the explicit bound

$$\begin{aligned} \|\mathcal{W}_{\mathcal{A}}(z, \boldsymbol{t}) v\|_\lambda &\le \left(\prod_{j=1}^{M} \|P_j\| \right) \left(\prod_{j=0}^{M} q_j \right) \left(\prod_{i \in \mathcal{C}} c_i \right) \|v\|_\lambda \\ &\le M_k D_{\mathcal{A}} \|v\|_\lambda \prod_{i \in \mathcal{C}} c_i. \end{aligned} \tag{3.3.12}$$

The background norm bound is on the joint Gaussian Hilbert space; it is not obtained by conditioning on successive fields.

Step 5. We integrate over the insertion cube and extract vector coefficients. *The insertion cube and vector Cauchy formula.* Give the cross colors amplitudes y_i and define the vector

$$\Phi_{\mathcal{A}}(z) := \left[\prod_{i\in\mathcal{C}} y_i\right] \mathcal{M}^{\mathrm{cut}}_{(z,y,0)}(T)v.$$

Variation of constants about P_z and iteration give a Dyson series. A monomial of degree one in every y_i uses exactly m insertions, with each distinct cross color used once. Hence,

$$\Phi_{\mathcal{A}}(z) = \sum_{\pi} \int_{D_\pi} \mathcal{W}_{\mathcal{A}}(z,\boldsymbol{t})v \, \mathrm{d}\boldsymbol{t}, \qquad D_\pi = \left\{ \boldsymbol{t} \in \prod_{i\in\mathcal{C}} I_i^T : t_{\pi_1} < \cdots < t_{\pi_m} \right\}. \tag{3.3.13}$$

Each ordered Dyson integral has coefficient one. The permutation simplices D_π partition the cube up to null diagonals. In particular,

$$\sum_{\pi} |D_\pi| = \prod_{i\in\mathcal{C}} |I_i^T| \le \prod_{i\in\mathcal{C}} h_i.$$

Minkowski applied to (3.3.13) and the single-word bound (3.3.12) therefore gives

$$\|\Phi_{\mathcal{A}}(z)\|_\lambda \le M_k D_{\mathcal{A}} \|v\|_\lambda \prod_{i\in\mathcal{C}} c_i h_i. \tag{3.3.14}$$

There is no factor $m!$ or $1/m!$ in this estimate. For $m = 0$, the cube has unit mass and $\Phi_{\mathcal{A}}(z) = P_z(T,0)v$.

The vector $\Phi_{\mathcal{A}}$ is entire in the background amplitudes. On the first copy its coefficient is given by the normalized formula

$$U_{\boldsymbol{r}} v = \left(\prod_{i\in\mathcal{A}_r} \varrho_i^{-r_i} \right) \int_{[0,2\pi]^{\mathcal{A}_r}} e^{-i\sum_{i\in\mathcal{A}_r} r_i\theta_i} \Phi_{\mathcal{A}_r}((\varrho_i e^{i\theta_i})_i) \prod_{i\in\mathcal{A}_r} \frac{\mathrm{d}\theta_i}{2\pi}. \tag{3.3.15}$$

This is precisely the desired coefficient because each cross exponent equals one and every omitted exponent is zero. The normalized angular measure has total mass one. Thus, (3.3.14) bounds $\|U_{\boldsymbol{r}} v\|_\lambda$ with the additional factor $\prod_{i\in\mathcal{A}_r} \varrho_i^{-r_i}$, and the identical formula bounds the second copy using $\mathcal{A}_q, q_i$. No holomorphic formula is applied to a squared norm.

Step 6. We pair the two coefficients and account for all constants. *The inner product and all constants.* Since $\lambda = k/T$ and $k \ge 1$,

$$\|w\|_{1/T} \le k\|w\|_\lambda, \qquad \|v\|_\lambda \le \|v\|_{1/T}.$$

Cauchy–Schwarz between the two vectors on the same Gaussian space now gives, before any constants are absorbed,

$$\begin{aligned} |\langle U_{\boldsymbol{r}} v, U_{\boldsymbol{q}} v\rangle_{\mathcal{H}_{1/T}}| \le k^2 M_k^2 D_{\mathcal{A}_r} D_{\mathcal{A}_q} \|v\|_{1/T}^2 \prod_{i\in\mathcal{B}} \varrho_i^{-2k_i} \\ \times \prod_{i\in\mathcal{C}} (R_\alpha \sigma_i^2 h_i^2 \lambda^{\alpha-2}). \end{aligned} \tag{3.3.16}$$

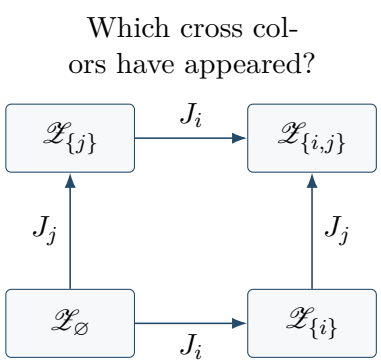

Background evolution preserves each subspace. The two paths need not give the same vector.

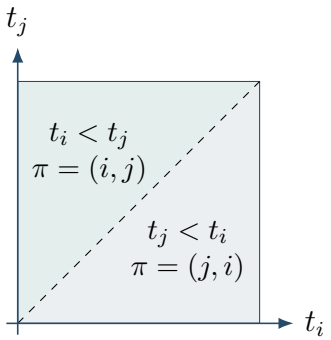

The ordered regions fill the square apart from the null diagonal.

Figure 3.5: For two distinct cross colors, each insertion starts from the vacuum in its own unused color. The left square records subspaces only; it is not a commutative operator diagram. The right picture uses identical time windows for clarity. In general the ordered regions partition $I_i^T \times I_j^T$ up to the equal-time diagonal. Each chronological operator word has coefficient one, and the total volume is $|I_i^T||I_j^T|$, without an extra 2! or 1/2!. Spatial operators are not reordered. See Lemma 3.3.4.

The radius exponent is $r_i + q_i = 2k_i$. The metric product is exactly

$$D_{\mathcal{A}_r} D_{\mathcal{A}_q} = \prod_{i \in \mathcal{B}} (1 + k_i/(\lambda h_i))^{\ell_i}.$$

In particular, a singleton on only one copy has one ending charge, not two. For every $i \in \mathcal{B}$, $d_i^2 \le 12 k_i R_\alpha$ gives

$$\begin{aligned} \varrho_i^{-2k_i} &= \left(\frac{\sigma_i^2 d_i^2}{\delta_a^2}\right)^{k_i} \left(\frac{h_i}{k_i}\right)^{(4-\alpha)k_i} \\ &\le (12\delta_a^{-2})^{k_i} (R_\alpha \sigma_i^2 h_i^{4-\alpha})^{k_i} k_i^{-(3-\alpha)k_i} \\ &\le (12\delta_a^{-2})^{k_i} \frac{(R_\alpha \sigma_i^2 h_i^{4-\alpha})^{k_i}}{(k_i!)^{3-\alpha}}. \end{aligned} \tag{3.3.17}$$

The last step uses $k_i! \le k_i^{k_i}$. Finally,

$$M_k^2 = 100^{6k+2} e^{8k} \le (100^8 e^8)^k, \qquad |\mathcal{C}| + \sum_{i \in \mathcal{B}} k_i = k.$$

Substituting these inequalities in (3.3.16) proves (3.3.6) with the explicit admissible choice

$$C_{\mathrm{split}} = 100^8 e^8 \max\{1, 12\delta_{\alpha/2}^{-2}\}. \tag{3.3.18}$$

This constant depends only on α. No permutation, Gaussian-mode, factor depending on the number of intervals or further degree factor remains. The projected initial phase has norm at most the displayed original $\|v\|_{1/T}$. This proves Lemma 3.3.4. □

Lean partial

Proposition 3.3.5 (Uniform interval coefficients)**.** *There is $C = C(\alpha, \alpha_0, L, c)$ such that, for real Schwartz phase v, every $k \geq 1$ satisfies*

$$\left|[s^{2k}]\mathbb{E}\|\mathcal{U}^{\epsilon}_{\mathcal{F}}(T;s)v\|^2_{1/T}\right| \leq \frac{C^k R_\alpha^k T^{\beta k}}{(k!)^\nu}\|v\|^2_{1/T}, \tag{3.3.19}$$

uniformly in $\epsilon > 0$ and the finite family. In particular,

$$\mathbb{E}\|\mathcal{U}^{\epsilon}_{\mathcal{F}}(T;1)v\|^2_{1/T} \leq e\exp\{CR_\alpha^{1/\nu}T^{\beta/\nu}\}\|v\|^2_{1/T}. \tag{3.3.20}$$

Proof. We first construct the ordinary coefficient series at fixed smoothing and interval family. We retain only even total degree in each color and use exact finite-word cutoffs. The fixed-split estimate and sorted interval lengths reduce the uniform sum to the inventory product, after which separate cutoff limits identify and sum the full series.

Step 1. We set up the bounded cutoffs and entire vector series. Zero noise is trivial; omit any zero σ_i. Enlarge the interval-length constant L to $\max\{1, L\}$ if necessary. The hypotheses remain true and the final constant may depend on L, so throughout this proof we may assume $L \geq 1$. Replacing (σ_i, W_i^ϵ) by $(|\sigma_i|, \operatorname{sgn}(\sigma_i)W_i^\epsilon)$ leaves the potential unchanged and preserves the joint law of the independent real Gaussian fields. Thus, we may assume $\sigma_i > 0$. We first work with finitely many Gaussian coordinates of each field and a bounded spatial Fourier band. Denote their common phase Hilbert space by $\mathcal{H}_\rho = L^2(\Omega; X_\rho)$. The initial data are projected to the band. This contracts every X_ρ norm; we keep the original $\|v\|_\rho$ on the right of the estimates. The projections converge strongly to the original data.

Ordinary coefficients and their existence. Fix $\lambda > 0$ temporarily. Give interval i its own amplitude z_i and write

$$\mathcal{U}(T;\boldsymbol{z})v = \sum_{\boldsymbol{r}\in\mathbb{N}_0^{\mathcal{F}}} \boldsymbol{z}^{\boldsymbol{r}} U_{\boldsymbol{r}} v.$$

These are ordinary power-series coefficients, without factorials incorporated in their definition. At fixed smoothing and finite interval family, put $v_{\max} = \sup_t \sum_i \sigma_i^2 \mathbf{1}_{I_i}(t)\Gamma_\epsilon(0) < \infty$. On Gaussian degrees at most n, multiplication by the instantaneous field has norm at most $2\sqrt{n+1}\sqrt{v_{\max}}$. The free-phase energy calculation at the end of the proof of Proposition 3.1.2, which uses no dimension-specific or covariance assumption, gives the bound $e^{\lambda h/2}$ in X_λ also on each spatial Fourier band. A phase insertion $(u, w) \mapsto (0, Wu)$ costs at most its unweighted multiplication norm divided by λ. Thus, on $\max_i |z_i| \leq z_*$ the total order-n phase is bounded by

$$e^{\lambda T/2}\frac{(2z_*\sqrt{n+1}\sqrt{v_{\max}}T/\lambda)^n}{n!}\|v\|_\lambda. \tag{3.3.21}$$

The series of these bounds converges for every finite z_*. Its locally uniform convergence defines an entire vector function. We also verify coefficientwise absolute convergence. Fix $z_* > 0$ and put

$$K_{2z_*} = \sup_{\max_i |z_i| \le 2z_*} \|\mathcal{U}(T;\boldsymbol{z})v\|_{\mathcal{H}_{1/T}} < \infty,$$

using the majorant with its temporary parameter $\lambda = 1/T$. Normalized vector Cauchy integration on this larger polydisc gives

$$\|U_{\boldsymbol{r}}v\|_{\mathcal{H}_{1/T}} \le K_{2z_*}(2z_*)^{-|\boldsymbol{r}|}, \qquad \sum_{\boldsymbol{r}} z_*^{|\boldsymbol{r}|}\|U_{\boldsymbol{r}}v\|_{\mathcal{H}_{1/T}} \le 2^{|\mathcal{F}|}K_{2z_*}.$$

The sum is the product of $|\mathcal{F}|$ geometric series. Cauchy–Schwarz therefore bounds the absolute energy double series by $4^{|\mathcal{F}|}K_{2z_*}^2$. This finite factor justifies the coefficient identities at fixed family and smoothing; it does not enter the uniform coefficient estimate below.

Step 2. We identify the energy coefficient and its color splits. Set $Q_{\boldsymbol{r},\boldsymbol{q}} = \langle U_{\boldsymbol{r}}v, U_{\boldsymbol{q}}v\rangle_{\mathcal{H}_{1/T}}$. Both vectors use the same Gaussian fields. Independence is between distinct colors, not between the two copies in this inner product. For real s, substitution $z_i = s$ gives the exact identity

$$[s^{2k}]\mathbb{E}\|\mathcal{U}(T;s)v\|_{1/T}^2 = \sum_{|\boldsymbol{r}|+|\boldsymbol{q}|=2k} Q_{\boldsymbol{r},\boldsymbol{q}}. \tag{3.3.22}$$

Reflection of Gaussian color i multiplies $U_{\boldsymbol{r}}v$ by $(-1)^{r_i}$. Hence, $Q_{\boldsymbol{r},\boldsymbol{q}} = 0$ unless $r_i + q_i = 2k_i$ for every i, where $\sum_i k_i = k$. If $k_i = 0$, both coefficients are obtained by setting $z_i = 0$; this removes that field exactly. There are at most k active colors. For fixed $\boldsymbol{k}$, the number of splits is $\prod_i(2k_i + 1) \le 3^k$.

Step 3. We retain the selected coefficients exactly at finite Hermite degrees. For this fixed $\boldsymbol{k}$, truncate the Hermite degree of color i at $N_i = 2k_i$. A word contributing to $U_{\boldsymbol{r}}$ has $r_i \le 2k_i$ insertions of color i, and the other copy has $q_i \le 2k_i$. Lemma 3.2.3, with the spatial phase space as $\mathscr{X}$ and free phase factors between insertions, therefore preserves both selected vector coefficients exactly. Their Duhamel time integrals and finite word sums preserve the equality. Creation followed by annihilation is retained; there is no Hermite-degree limit in this coefficient calculation.

Step 4. We convert the split estimate into the interval inventory weights. For the uniform coefficient estimate put $\lambda = k/T$. Apply Lemma 3.3.4 to each selected coefficient, retaining the original sorted interval labels in the final sum. Its factor ℓ_i is one for a singleton mean and at most two for every higher color. The separate cross factor applies only at $(r_i, q_i) = (1, 1)$. Absorb $k^2 C_{\mathrm{split}}^k 3^k c^k$ into C^k, using $k^2 \le 4^k$. After $\sigma_i^2 \le c h_i^{-\alpha_0}$, the resulting local weights, with this common per-total-order constant understood, are

case	weight in energy
$(2,0)$ or $(0,2)$	$R_\alpha h_i^\beta(1 + 1/(\lambda h_i))$
$(1,1)$	$R_\alpha \lambda^{\alpha-2} h_i^{2-\alpha_0}$
$k_i = l \ge 2$	$R_\alpha^l h_i^{\beta l}(1 + l/(\lambda h_i))^2/(l!)^\nu$.

The first metric factor occurs on only one copy; the last costs at most one factor on each copy. To justify the length substitution, expand the entire higher-degree weight, before its positive constant:

$$h^{\beta l}(1 + l/(\lambda h))^2 = h^{\beta l} + \frac{2l}{\lambda} h^{\beta l - 1} + \frac{l^2}{\lambda^2} h^{\beta l - 2}.$$

Since $\beta > 2$ and $l \geq 2$, all three powers are positive. The singleton mean likewise has powers $\beta, \beta - 1$, and the cross singleton has power $p = 2 - \alpha_0 > 0$. Thus, each whole local weight increases with h; we do not bound the inverse-length factor separately. At $h = LT/i$, $1 + l/(\lambda h) = 1 + li/(kL) \leq 1 + li/k$, since $L \geq 1$. The remaining powers of L are absorbed in the allowed C^k. For a singleton let m_i, c_i be the first and second table weights. Every one of its splits is bounded by $m_i + c_i$. The higher-degree table weight is already uniform over its splits. Hence, the previously counted $\prod_i (2k_i + 1) \leq 3^k$ bounds all split choices once, using these combined singleton weights; that is the factor absorbed into C^k above. Substituting $h_i \leq LT/i$ and $\lambda = k/T$ therefore extracts $C^k R_\alpha^k T^{\beta k}$, leaving v_i at $k_i = 1$ and $b_{i,l}$ at $k_i = l \geq 2$ from Lemma 3.3.3.

Step 5. We sum ordinary coefficients without a multinomial factor. There is no further multinomial factor: for nonnegative weights $w_{i,0} = 1$, ordinary multiplication of power series gives exactly

$$\sum_{\sum_i k_i = k} \prod_i w_{i,k_i} = [z^k] \prod_i \left(\sum_{l \geq 0} w_{i,l} z^l \right).$$

Apply this identity to the sum in (3.3.22), using the two singleton alternatives together in v_i. Lemma 3.3.3 now proves (3.3.19) at the finite cutoffs.

Step 6. We remove cutoffs at fixed coefficients and sum the uniform bound. The closed operator used below is multiplication by the measurable smoothed Gaussian field on its natural Gaussian–spatial L^2 domain. Mode sums agree with this multiplication on finite-coordinate inputs in the limit; closedness then identifies the graph limit as those inputs are approximated in L^2. *Identification and summation.* Keep positive smoothing, finite interval family and a fixed coefficient. The finite-degree multiplication bound used in (3.3.21) is uniform in mode and band cutoffs. On finite-coordinate Gaussian vectors the omitted annihilation tail is zero and the creation tail tends to zero by its omitted pointwise variances and dominated convergence. Density in each finite degree extends this strong convergence. Closedness identifies the limit with multiplication by the measurable smoothed field. Fourier projections converge strongly and commute with free evolution. Dominated time integration thus identifies every fixed Duhamel word. The selected coefficients of the local Hermite truncation were already equal to those untruncated words. The full series is constructed separately using (3.3.21), choosing a sufficient degree cutoff anew at each order. A fixed-degree truncated propagator is not identified with the full evolution. The entire majorant gives convergence uniformly on compact amplitude sets. The coefficients estimated above are therefore those of the finite-interval model, with no zero-smoothing limit at this step.

The nonuniform number $v_{\max}$ was used only for this identification. The uniform coefficient bound contains no such number. Its constants come from $\delta_{\alpha/2}$, the fixed phase bound, the interval-length bound lemma and L, c; covariance enters only through R_α^k. The zero-order energy is at most $e\|v\|_{1/T}^2$. Put $x = CR_\alpha T^\beta$ and $Y = e^{\nu x^{1/\nu}} \geq 1$. Since $\nu > 1$, $\sum_{k\geq 0} x^k/(k!)^\nu \leq Y$. Summing the coefficient bounds in absolute value gives

$$\mathbb{E}\|\mathcal{U}(T;1)v\|_{1/T}^2 \leq (e + Y - 1)\|v\|_{1/T}^2 \leq eY\|v\|_{1/T}^2.$$

Absorbing $\nu C^{1/\nu}$ into the parameter-only constant proves (3.3.20). This proves Proposition 3.3.5. □

3.3.3 Finite Gaussian models and their terminal kernels

For $n \geq 1$, define the positive terminal-chain measure

$$\mathsf{g}_n^{T,x}(\,\mathrm{d}\boldsymbol{s},\,\mathrm{d}\boldsymbol{y}) = \mathbf{1}_{[0,T]^n_<}(\boldsymbol{s})\,\mathrm{d}\boldsymbol{s}\prod_{j=1}^{n} G_{s_{j+1}-s_j}(y_{j+1} - \mathrm{d}y_j), \qquad (s_{n+1}, y_{n+1}) = (T, x). \tag{3.3.23}$$

The spatial product is read backwards from x. Explicitly, it is the pushforward of $\prod_{j=1}^n G_{s_{j+1}-s_j}(\,\mathrm{d}w_j)$ under $y_j = x - \sum_{l=j}^n w_l$. This defines the measure also in dimension three. In dimensions one and two its density is the ordered kernel g_n in (1.4.1). Set $\mathsf{g}_0^{T,x}$ equal to unit mass on the empty tuple. This definition introduces no kernel symmetrization.

Lean full

Lemma 3.3.6 (The finite terminal-chain Wick formula)**.** *Let $\mathcal{W}(s,y)$ be a centered real Gaussian field on $[0,T]\times\mathbb{R}^d$, $d = 1,2,3$, with covariance $\mathcal{K}(s,y;r,z)$. Suppose that $V = \sup_{s,y}\mathbb{E}|\mathcal{W}(s,y)|^2 < \infty$, and that the field is jointly continuous in mean square on each open cell of a finite partition of $[0,T]$, times $\mathbb{R}^d$. Define $Y_0 = 1$ and*

$$Y_n(T,x) = \int \prod_{j=1}^{n} \mathcal{W}(s_j, y_j)\,\mathsf{g}_n^{T,x}(\,\mathrm{d}\boldsymbol{s},\,\mathrm{d}\boldsymbol{y}).$$

These Bochner integrals exist in $L^2(\Omega)$ and satisfy

$$\|Y_n(T,x)\|_2 \leq \sqrt{(2n-1)!!}\,V^{n/2}\frac{T^{2n}}{(2n)!}, \qquad n \geq 1. \tag{3.3.24}$$

For $m + n = 2k$, concatenate $\boldsymbol{\tau} = (s_1,\dots,s_m,r_1,\dots,r_n)$ and $\boldsymbol{\eta} = (y_1,\dots,y_m,z_1,\dots,z_n)$. Then

$$\mathbb{E}[Y_m(T,x)Y_n(T,x)] = \sum_{D\in\Pi_k}\mathcal{T}^{\mathcal{K}}_{m,n,D}(T,x), \tag{3.3.25}$$

where, with both chains terminating at (T,x),

$$\begin{aligned}\mathcal{T}^{\mathcal{K}}_{m,n,D} = \int_{[0,T]^m_<\times[0,T]^n_<}\mathrm{d}\boldsymbol{s}\;\mathrm{d}\boldsymbol{r}\int_{(\mathbb{R}^d)^m\times(\mathbb{R}^d)^n}\\ \times\prod_{j=1}^{m}G_{s_{j+1}-s_j}(y_{j+1}-\mathrm{d}y_j)\prod_{j=1}^{n}G_{r_{j+1}-r_j}(z_{j+1}-\mathrm{d}z_j)\\ \times\prod_{\{a,b\}\in D}\mathcal{K}(\tau_a,\eta_a;\tau_b,\eta_b).\end{aligned} \tag{3.3.26}$$

Each pairing has coefficient one. If $m+n$ is odd, the expectation is zero. Empty chains and the case $m=n=0$ have the usual empty-product meaning. If $\mathcal{K}\geq 0$, every integral above is nonnegative. Consequently, entrywise comparison $0\leq\mathcal{K}_1\leq\mathcal{K}_2$ compares all finite partial-order second moments in the same direction. The series $\sum_{n\geq 0} r^n Y_n$ converges absolutely in L^2 for every real or complex r.

Proof. We establish the finite chain mass and Gaussian product integrability first. We then derive the labelled Wick formula and check symmetrization and Green smoothing. Positivity compares finite moments, while the explicit ratio test sums every fixed regularized series.

Step 1. We prove Bochner integrability of each terminal chain. The mass of G_h is h. If $M_n(T)$ is the total mass of $\mathsf{g}_n^{T,x}$, integration at the last vertex gives $M_0=1$ and $M_n(T)=\int_0^T (T-s)M_{n-1}(s)\,\mathrm{d}s$. Induction therefore yields $M_n(T)=T^{2n}/(2n)!$. Gaussian moments and Hölder's inequality give

$$\left\|\prod_{j=1}^{n}\mathcal{W}(s_j,y_j)\right\|_2\leq\prod_{j=1}^{n}\|\mathcal{W}(s_j,y_j)\|_{2n}\leq\sqrt{(2n-1)!!}\,V^{n/2}.$$

Mean-square continuity of Gaussian variables implies their continuity in every fixed finite L^p. Hence, the product is strongly measurable in L^2 on the stated pieces. The finite kernel mass and the displayed bound prove Bochner integrability and (3.3.24).

Step 2. We derive the coefficient-one Wick formula. Fubini now passes expectation through the product of the two finite kernel measures. For the $m+n$ Gaussian variables at their labelled vertices, differentiate

$$\mathbb{E}\exp\left(\sum_i t_i\mathcal{W}(\tau_i,\eta_i)\right)=\exp\left(\frac{1}{2}\sum_{i,j}t_it_j\mathcal{K}(\tau_i,\eta_i;\tau_j,\eta_j)\right)$$

once in each t_i at zero. Odd total degree gives zero. At degree $2k$ the result is the sum over unordered pair partitions, with one covariance product per pairing. Orientations and orderings of the k pairs cancel the exponential's $2^k k!$ denominator. Integration gives (3.3.25) with precisely the domains and coefficients in (3.3.26).

Step 3. We retain the ordered convention and the Green-width limit. Symmetrizing a chain measure does not change its stochastic integral: the product of its n scalar field values is invariant under relabeling. Thus, averaging the $n!$ pushforwards of $\mathsf{g}_n^{T,x}$ with coefficient $1/n!$ gives the same Y_n. There is no additional $n!$ factor in (3.3.25), or $m!n!$ in a two-chain product. This identifies the ordinary ordered regularized integrals and their symmetrized convention in (1.4.1).

In dimension three one may first replace G by $p_\eta * G$. Those positive measures have the same masses and converge weakly to G. Off the finitely many time cut points, all finite Gaussian moments are bounded continuous functions of the spatial variables. Dominated convergence for their finite Wick sums proves the same limit for the mixed second moments with two Green widths. It gives L^2 convergence to the Bochner integral above, exactly the fixed-noise Green convention used in the source.

Step 4. We compare positive diagrams and sum the regularized orders. If $\mathcal{K} \geq 0$, positivity of the Green measures makes each covariance product nonnegative. Comparing them proves the stated finite-moment monotonicity, including self-pairs and unequal chains. Finally, the ratio of successive right sides of (3.3.24), with an additional factor $|r|^n$, is $|r|\sqrt{V}T^2/((2n+2)\sqrt{2n+1})$, which tends to zero. The zero-variance case is immediate. This proves Lemma 3.3.6. □

3.3.4 Removing the regularization

Proposition 3.3.5 holds uniformly in the smoothing $\epsilon > 0$, but it concerns regularized fields only. We still have to pass to the unregularized solution.

Lean full

Lemma 3.3.7 (Uniform series tails from scaled moments)**.** *Fix (T, x). For each positive regularization pair (ϵ, δ), let $Y_n^{\epsilon,\delta}$ be the terms of Lemma 3.3.6 for a field with nonnegative covariance. Write $u^{\epsilon,\delta}(r) = \sum_{n\geq 0} r^n Y_n^{\epsilon,\delta}$. Suppose that, for some $r > 1$ and finite B_r,*

$$\sup_{\epsilon,\delta>0} \mathbb{E}|u^{\epsilon,\delta}(r)|^2 \leq B_r, \qquad Y_n^{\epsilon,\delta} \longrightarrow X_n \text{ in } L^2 \text{ for each fixed } n.$$

Then $u = \sum_{n\geq 0} X_n$ converges absolutely in L^2, $u^{\epsilon,\delta}(1) \to u$ in L^2, and

$$\|Y_n^{\epsilon,\delta}\|_2,\ \|X_n\|_2 \leq B_r^{1/2} r^{-n}, \qquad \left\|\sum_{n>N} Y_n^{\epsilon,\delta}\right\|_2, \left\|\sum_{n>N} X_n\right\|_2 \leq \frac{B_r^{1/2} r^{-(N+1)}}{1 - r^{-1}}. \tag{3.3.27}$$

If also $\mathbb{E}|u^{\epsilon,\delta}(1)|^2 \leq B_1$ uniformly, then $\mathbb{E}|u|^2 \leq B_1$.

Proof. Lemma 3.3.6 gives absolute L^2 convergence of every regularized series and nonnegative mixed moments. Its scaled second moment therefore contains the nonnegative term $r^{2n}\mathbb{E}|Y_n^{\epsilon,\delta}|^2$, so $r^{2n}\mathbb{E}|Y_n^{\epsilon,\delta}|^2 \leq B_r$. Taking the fixed-order L^2 limit proves the same bound for X_n. The geometric series and the triangle inequality give all estimates in (3.3.27), including absolute convergence.

For each N, write both full series as their first $N+1$ terms and their tails. Their distance is at most

$$\frac{2B_r^{1/2} r^{-(N+1)}}{1 - r^{-1}} + \left\|\sum_{n=0}^{N} (Y_n^{\epsilon,\delta} - X_n)\right\|_2.$$

First let $\epsilon, \delta \downarrow 0$ at fixed N, and then let $N \to \infty$. This proves convergence of the full regularized solution; it was not assumed. Continuity of the L^2 norm passes the bound B_1 to u. This proves Lemma 3.3.7. □

3.3.5 Temporal comparison and the full upper bound

The use of finitely many shifted dyadic grids is classical. For the covering principle and its antecedents, see Lerner [36, Section 2.2, p. 3162]. We give the construction, nesting check and covariance comparison needed for the time intervals below.

Theorem 3.3.8 (Full upper scale)**.** *Under Hypothesis 1.2.1, let u be the canonical expansion solution (1.4.1), constructed as a Stratonovich mild solution in Proposition 2.6.2. Put*

$$R_\alpha = \frac{\alpha\pi\mu(B_1)}{2\sin(\pi\alpha/2)}.$$

For every admissible $d = 1, 2, 3$, there is a finite $C = C(\alpha, \alpha_0)$ such that

$$\mathbb{E}u^2(T,x) \le e(T+2)^d \exp\{CR_\alpha^{1/(3-\alpha)} T^{(4-\alpha-\alpha_0)/(3-\alpha)}\}, \qquad T \ge 1. \tag{3.3.28}$$

In particular, this proves Theorem 1.5.1.

Proof. We dominate the temporal covariance by finite-depth shifted interval models with a controlled length inventory. We transfer their phase bound to constant data on a fixed observation ball, compare the positive terminal Wick integrals, and remove noise regularization using a separate uniform series-tail bound. All identifications precede the large-time conclusion.

Step 1. We construct the dyadic temporal majorant and its length inventory. Zero noise is trivial. Choose H_0 with $6T \le H_0 < 12T$. At lengths $h_j = H_0 2^{-j}$, use the three grids with endpoints $h_j(n + (-1)^j t)$, $n \in \mathbb{Z}$, $t = 0, 1/3, 2/3$. They are nested: the difference between the parent and child shifts in child units is an integer, since $3t \in \mathbb{Z}$. For $s \ne r$ in $[0,T]$, choose a scale $3|s-r| < h_j \le 6|s-r|$. Boundaries of the three grids at this scale have mutual spacing $h_j/3 > |s-r|$. Hence, at least one grid interval contains both points, including their endpoints after choosing a boundary-free grid. It follows that

$$|s-r|^{-\alpha_0} \le 6^{\alpha_0} \sum_{\text{three grids},\, |I| \le H_0} |I|^{-\alpha_0} \mathbf{1}_I(s)\mathbf{1}_I(r) =: K_\infty(s,r). \tag{3.3.29}$$

For context, the sum is at most $C_{\alpha_0}|s-r|^{-\alpha_0}$ off the diagonal: only lengths at least $|s-r|$ contribute, with at most one interval per grid and length. Endpoint values do not affect the time integrals.

Keep intervals meeting $[0,T]$ through depth J, and use independent static smoothed fields with $\sigma_I^2 = 6^{\alpha_0}|I|^{-\alpha_0}$. Their time covariance is the corresponding partial sum K_J. The decreasing interval lengths obey $h_i \le 78T/i$. Indeed, at length h_j there are at most $3(T/h_j + 2)$ intervals. Summing levels $0, \dots, j$ bounds their cumulative count by

$$6T/h_j + 6(j+1) \le 6T/h_j + 6\,2^j \le 78T/h_j,$$

since $H_0 < 12T$ and $2^j = H_0/h_j$. Each index at level j is at most that cumulative count, which gives the asserted decreasing-length bound. Thus, one may take $L = 78$ and $c = 6^{\alpha_0}$ in Proposition 3.3.5. Proposition 3.3.5 applies uniformly in J, ϵ.

Step 2. We localize constant initial data on the full backward cone. For the kept intervals, $W_{J,\epsilon}(s,y) = \sum_{I \in \mathcal{F}_J} \sigma_I 1_I(s) W_I^\epsilon(y)$, and $u_{J,\epsilon}$ is the series of its terminal terms from Lemma 3.3.6. For the compact data $(f_T, 0)$ chosen below, $u_{f_T,J,\epsilon}$ denotes the position component of the phase evolution in Proposition 3.3.5. To pass from phase data to constant initial data, choose $f_T \in C_c^\infty$ with $0 \le f_T \le 1$, equal to one on B_{T+1} and

supported in B_{T+2}, and set the velocity to zero. For $|y| + s < T + 1$, $G_s * f_T(y) = s$, so $C_s f_T(y) = 1$. The support of G_t is contained in B_t. Along a chain ending at $x \in B_1$ at time T, each earlier point (s, y) satisfies $|y| + s \le |x| + T < T + 1$. Thus, its free initial-data factor is one. Induction on Duhamel order identifies the position generated from $(f_T, 0)$ at time T on B_1 with the constant-data model $u_{J,\epsilon}$. This identity can be taken in Gaussian L^2 term by term. At fixed J, ϵ, each finite-order terminal integral is continuous in x as an $L^2(\Omega)$ vector: write its Green variables as displacements from x, and use continuity of Γ_ϵ in its mixed Wick moments. Bounded covariance products and the finite terminal Green mass permit dominated convergence. These measurable representatives identify the $L^2(\Omega; L^2_x)$ position on B_1 with the same pointwise constant-data terms. The summable bound below passes this identity to their series. At finite J, ϵ, pointwise convergence for constant data follows from the bound $\sqrt{(2n-1)!!}\, v_{\max}^{n/2} T^{2n}/(2n)!$ on the nth position term. The model is spatially stationary. Consequently,

$$|B_1|\mathbb{E}|u_{J,\epsilon}(T,0)|^2 \le \mathbb{E}\|u_{f_T,J,\epsilon}(T)\|_2^2 \le e\,|B_{T+2}|\exp\{CR_\alpha^{1/\nu}T^{\beta/\nu}\}.$$

The final inequality above is (3.3.20) with $v = (f_T, 0)$: the position L^2 norm is at most its phase norm, and $\|(f_T, 0)\|_{1/T}^2 = \|f_T\|_2^2 \le |B_{T+2}|$ because the velocity is zero and $0 \le f_T \le 1$. *Step 3.* We identify the finite interval-model Wick sums before comparison.

We now identify the interval-model Wick sums before comparing them. Its centered Gaussian noise has covariance

$$\mathbb{E}[W_{J,\epsilon}(s,y)W_{J,\epsilon}(r,z)] = \sum_{I\in\mathcal{F}_J} \sigma_I^2 \mathbf{1}_I(s)\mathbf{1}_I(r)\Gamma_\epsilon(y-z) = K_J(s,r)\Gamma_\epsilon(y-z).$$

Lemma 3.3.6 applies: at fixed J, ϵ the field has bounded variance, is mean-square continuous in space and is piecewise continuous in time. Its exact terminal kernels are (3.3.23), and every term of (3.3.26) has covariance factor $K_J(s_j, s_l)\Gamma_\epsilon(y_j - y_l)$, with coefficient one. This comparison is made before any time reversal; K_J need not be stationary in time. The position kernels and constant initial data are nonnegative. Thus, every such integral, including self-pairings and unequal chain lengths, is nonnegative. The pointwise L^2 convergence proved above identifies the full moment with their nonnegative sum. In particular, the moment of every finite partial-order sum is at most the full moment, even though samplewise partial sums need not increase.

Step 4. We compare the source model through positive terminal diagrams. From the current author version [17, (2.23)–(2.24), p. 13], the common noise regularization has covariance $\gamma_\delta^0(s-r)\Gamma_\epsilon(y-z)$, where

$$0 \le \gamma_\delta^0(t) = \Gamma(\alpha_0)^{-1}\int_0^{\delta^{-1}} e^{-q|t|}q^{\alpha_0-1}\,\mathrm{d}q \le |t|^{-\alpha_0}.$$

Here $\Gamma(\alpha_0)$ is the Euler Gamma function. At fixed positive ϵ, δ, first take the source's Green-width limit. The bounded continuous covariances, weak convergence of the positive Green measures and the dominated finite Wick calculation in Lemma 3.3.6 identify its classical measure-kernel Duhamel terms. For the source's continuous field modification,

these Bochner terms equal the pathwise smoothed integrals: writing Φ_n for the product of field values, the Gaussian bound in that lemma gives $\int \|\Phi_n\|_2 \, \mathrm{d}\mathsf{g}_n^{T,x} < \infty$. Tonelli gives pathwise integrability and Minkowski puts the integral in L^2. Fubini against every L^2 test variable and Bochner duality identify the two versions. The same argument applies before the Green-width limit in dimension three.

Write $U_N^{\epsilon,\delta}$ for the sum of source terms of orders $0, \dots, N$ after that Green limit. Write $V_{N,J}^{\epsilon}$ for the same partial-order sum of the finite interval model. Both moments are finite sums over exactly the same terminal-chain kernels and pairings; only the covariance factors differ. By (3.3.29) each source covariance factor is bounded by its K_∞ counterpart. Since $K_J \uparrow K_\infty$, nonnegative Tonelli at fixed N yields

$$\mathbb{E}|U_N^{\epsilon,\delta}(T,x)|^2 \le \lim_{J\to\infty} \mathbb{E}|V_{N,J}^{\epsilon}(T,x)|^2 \le \sup_J \mathbb{E}|u_{J,\epsilon}(T,x)|^2 \le B(T), \tag{3.3.30}$$

where $B(T)$ is the right side of (3.3.28). The middle inequality uses the positive pairing sum just identified. No Gaussian field of covariance $K_\infty\Gamma_\epsilon$ is constructed; K_∞ is used only inside these monotone limits of positive integrals. This is entrywise comparison of Wick integrals, not covariance order for arbitrary initial phases or a coupling of random solutions.

Step 5. We obtain a scaled source bound that controls all order tails. The same finite-model argument works after multiplying the source noise by any real amplitude $a > 0$. This replaces Γ by $a^2\Gamma$ and R_α by $a^2 R_\alpha$, without changing its homogeneity degree or any parameter-only constant. Thus,

$$\mathbb{E}|u^{\epsilon,\delta}(a;T,x)|^2 \le B(T;a) := e(T+2)^d \exp\{C(a^2R_\alpha)^{1/\nu}T^\kappa\}. \tag{3.3.31}$$

Here the full regularized series exists by Lemma 3.3.6; it is the ordinary Duhamel series with its order-n term multiplied by a^n. Taking the finite partial-order cutoff to infinity in (3.3.30) is justified at positive regularization by that lemma, not by a theorem about the original unsmoothed solution.

Step 6. We identify fixed orders and remove the full source regularization. Lemma 2.5.2 supplies the fixed-order construction: each $Y_n^{\epsilon,\delta}$ converges in L^2 to $X_n = S_n(g_n)$ as $\epsilon, \delta \downarrow 0$, with arbitrary relative rates. The bounded-noise Green limit and ordered-kernel convention needed to match these terms are already verified in Lemma 3.3.6.

Apply Lemma 3.3.7 with $r = 2$ and $B_r = B(T;2)$. It proves absolute L^2 convergence of the series defining u in (1.4.1) and convergence of the full regularized solution to that series. Taking the limit in (3.3.31) at $a = 1$ proves the required bound. This series-limit argument is independent of Proposition 2.1.1, Lemma 2.5.3, and the source's Section 5 convergence proof. No first-moment asymptotic or printed normalization is used. The fixed-order construction just used is proved here from the universal pairing bound and the homogeneous norm estimates; neither the source's Theorem 4.1 nor its Lemma 4.4 is imported. Proposition 2.6.2 separately proves that this same series satisfies the source's Definition 2.1: its onefold Stratonovich integral equals $u - 1$. That construction uses the corrected mixed-vertex crude bound for its product and order limits. This is a separate dependency from the sharp-scale moment estimate just proved; the source's Section 5(ii)

proof is not imported. The crude constants used for this identification may depend on the fixed covariance; they do not enter (3.3.28). No uniqueness assertion is made.

Step 7. We record the distinct cutoff limits and the parameter-only constant. *Cutoff dependence and the order of limits.* The preceding argument uses the following distinct statements.

(i) At fixed total order $2k$, the coefficient estimates are uniform in the Gaussian-mode and spatial-band cutoffs, in the finite interval family, and in positive spatial smoothing. The local Hermite cutoff $N_i = 2k_i$ preserves each selected coefficient exactly; it is an algebraic choice, not a degree limit. Lemma 3.3.4 and the interval-length bound contain no smoothing-dependent variance.

(ii) At fixed finite interval family and $\epsilon > 0$, mode and band limits identify these coefficients with the Duhamel words. The entire-series majorant in Proposition 3.3.5 may depend on this family and ϵ, through $v_{\max}$. It is used for identification, not as a uniform moment estimate. The uniform coefficient bound passes to these limits. Localization and positive covariance comparison are applied only after removing these cutoffs; positivity of a finite-mode covariance is not assumed.

(iii) For the resulting finite-depth interval model, the moment bound is uniform in J, ϵ. Fix positive source widths ϵ, δ and finite partial order N. The Green-width limit is taken first. The subsequent $J \to \infty$ comparison in (3.3.30) is monotone convergence of finite positive Wick integrals. At these fixed noise widths, $N \to \infty$ is justified by Lemma 3.3.6, yielding (3.3.31). There is no infinite-depth Gaussian field or simultaneous mode-depth limit in this step.

(iv) At each fixed T, x, Γ and order n, Lemma 2.5.2 gives qualitative L^2 convergence as $\epsilon, \delta \downarrow 0$, with arbitrary relative rates. The bound $B(T; 2)$ gives tails uniform in these two widths. Lemma 3.3.7 first uses their limit at fixed partial order, then sends that order to infinity. The final moment bound comes from $B(T; 1)$, not the larger tail bound $B(T; 2)$.

(v) All identifications above are for fixed T, x, Γ; no convergence rate uniform in T or over covariance shapes is claimed. They prove (3.3.28) for every fixed $T \geq 1$ with the same parameter-only constant. Only after this estimate is proved is $T \to \infty$ used for the growth-rate conclusion.

The constants come from $L = 78$, $c = 6^{\alpha_0}$ and the parameter-only constants of Proposition 3.3.5; covariance enters only through R_α. The volume ratio is $|B_{T+2}|/|B_1| = (T+2)^d$. This proves Theorem 3.3.8. □

Remark 3.3.9 (Claim and calibration boundary)**.** Theorem 3.3.8 asserts a nonsharp upper growth rate. It does not identify the sharp constant or require a correction of the printed first-moment normalization as an input. Its exponent tends to $(4-\alpha)/(3-\alpha)$ as $\alpha_0 \downarrow 0$. Cauchy–Schwarz and the unconditional Jensen inequality remain compatible with

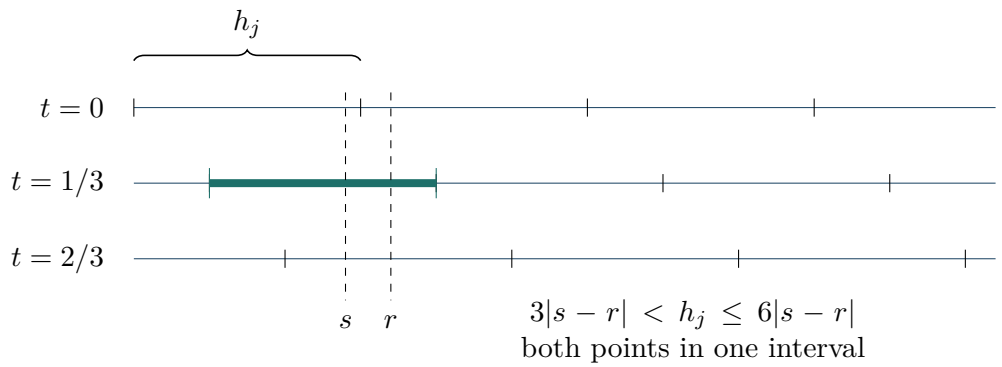

Figure 3.6: The three grids at one selected scale. Their boundaries are separated by $h_j/3 > |s-r|$, so at least one grid has no boundary between s and r. The full nested construction uses endpoints $h_j(n+(-1)^j t)$ for $t = 0, 1/3, 2/3$; the shift alternates with the level. The resulting infinite sum dominates $|s-r|^{-a}$ off the diagonal. This is not a claim that an arbitrary finite partial sum already dominates it. See Theorem 3.3.8.

the nonsharp upper constant; any numeric L_* calibration retains the source-normalization qualification stated earlier. The Skorohod exponent is compared, not used to identify constants: both Gaussian creation and annihilation were retained here. The intrinsic identification in Theorem 1.5.2 is proved in Theorem 11.2.6, using a separate argument.

What we now have. For every covariance in Hypothesis 1.2.1, the second moment is at most $\exp(CT^\kappa)$ times a polynomial in T (Theorem 3.3.8). The constant C is not claimed sharp; the next eight chapters identify the exact asymptotic constant.

Chapter 4

Covariance estimates and Gaussian approximation

A rough Gaussian potential is not a bounded multiplication operator. So what does it do to a wave? We need estimates that hold three things together: the covariance, wave propagation and spatial localization. There is one trap. An operator and its adjoint need two variance estimates, and one direction alone does not give the later Gaussian bounds.

Figure 4.1 shows a window on the potential: a physical mask is a smooth function of compact support that multiplies it in space. Section 4.1 bounds the covariance behind it. Section 4.2 carries the bounds to the full wave phase. Section 4.3 adds finite Gaussian matrix estimates and the compactness from spatial cutoffs.

The assumptions are those of Hypothesis 1.2.1. On a first reading, keep Proposition 4.2.5 and Corollary 4.3.10 and let the proofs wait. The Gaussian operator-series estimates here concern finite noise sums; fixed-vector Gaussian column limits are also constructed. Radius-explicit operator-path moment bounds come in Chapter 9. Episode ▶ 5 of the video series covers this chapter and the next two.

4.1 Covariance bounds for physically masked wave fields

We establish the covariance estimates needed for the operator construction. Throughout this section, Hypothesis 1.2.1 holds, $a = \alpha_0$, and $\Gamma \neq 0$. For zero spatial covariance, the spatial spectral measures and noise variances vanish; the purely temporal estimates remain valid independently of Γ. We use the unitary Fourier transform

$$\widehat{f}(\xi) = c_d \int_{\mathbb{R}^d} e^{-i\xi\cdot x} f(x)\,\mathrm{d}x, \qquad c_d = (2\pi)^{-d/2}.$$

The spectral convention in Hypothesis 1.2.1 means that, for every complex Schwartz test φ,

$$\int_{\mathbb{R}^d} \varphi(x)\Gamma(\,\mathrm{d}x) = \int_{\mathbb{R}^d} \left(\int_{\mathbb{R}^d} e^{i\xi\cdot x}\varphi(x)\,\mathrm{d}x \right) \mu(\,\mathrm{d}\xi). \tag{4.1.1}$$

This is an identity of distribution pairings. We will not interchange two infinite measures in the associated oscillatory expression.

A positive tempered Radon measure has polynomial mass growth. Indeed, choose a nonnegative compact smooth test that is at least one on the unit ball, and apply a defining Schwartz seminorm bound for the distribution to its dilations. Its mass on a ball of radius $R \geq 1$ is bounded by a power of R. Summation over dyadic shells then

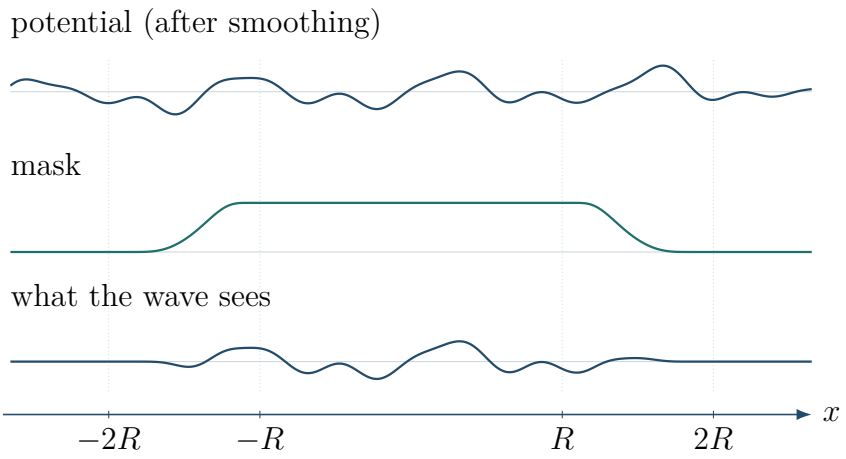

Figure 4.1: A physical mask, equal to one on a ball and zero outside a larger ball, and its product with the potential. The mask multiplies the potential in space. The covariance of the product has a mask factor at each spatial argument. The original noise and the covariance norm used for control costs remain fixed. A schematic in one space dimension: the unsmoothed potential is a distribution, not a curve.

gives integrability of $(1+|x|)^{-N}$ for some N, and hence absolute integrability of every Schwartz test. These facts apply to both Γ and μ. Smooth cutoffs converge in the Schwartz topology, so these integrals agree with the tempered pairings.

4.1.1 Translated spectral growth and physical masks

Lean full

Proposition 4.1.1 (Translated spectral mass)**.** *Put*

$$M_\Gamma = \int_{\mathbb{R}^d} e^{-|x|^2/4}\Gamma(\mathrm{d}x), \qquad C_\Gamma = \frac{eM_\Gamma}{(2\sqrt{\pi})^d}.$$

Then $0 < M_\Gamma < \infty$*, and for* $y \in \mathbb{R}^d$ *and* $r > 0$*,*

$$\int_{\mathbb{R}^d} e^{-|\xi-y|^2/r^2}\mu(\mathrm{d}\xi) = \left(\frac{r}{2\sqrt{\pi}}\right)^d \int_{\mathbb{R}^d} e^{-r^2|x|^2/4} e^{-iy\cdot x}\Gamma(\mathrm{d}x), \tag{4.1.2}$$

$$0 \le \int_{\mathbb{R}^d} e^{-|\xi-y|^2/r^2}\mu(\mathrm{d}\xi) \le \frac{r^\alpha M_\Gamma}{(2\sqrt{\pi})^d}, \qquad \mu(B(y,r)) \le C_\Gamma r^\alpha. \tag{4.1.3}$$

The ball may be open or closed.

Proof. We first compute the Gaussian transform in the stated Fourier convention. We then use positivity and homogeneity to bound it, and compare the Gaussian with the indicator of a ball.

Step 1. We compute the transform and its constant. Differentiating the Gaussian Fourier integral below is justified by its integrable first moment, and Gaussian decay makes the integration-by-parts boundary terms vanish. Temperedness gives finiteness of M_Γ. Its

positivity follows from $\Gamma \neq 0$. To check the Fourier constant, set $J(b) = \int_{\mathbb{R}} e^{-Ax^2} e^{ibx}\,\mathrm{d}x$ for $A > 0$. Squaring the real Gaussian integral and using polar coordinates gives $J(0) = \sqrt{\pi/A}$. Differentiation and integration by parts give $J'(b) = -bJ(b)/(2A)$. Therefore, $J(b) = \sqrt{\pi/A}e^{-b^2/(4A)}$. Taking products over the coordinates gives

$$\int_{\mathbb{R}^d} e^{-r^2|x|^2/4} e^{i(\xi-y)\cdot x}\,\mathrm{d}x = \left(\frac{2\sqrt{\pi}}{r}\right)^d e^{-|\xi-y|^2/r^2}.$$

Apply (4.1.1) to the single Schwartz test $e^{-r^2|x|^2/4}e^{-iy\cdot x}$ to obtain (4.1.2).

Step 2. We use positivity and homogeneity. Its left side is nonnegative. Taking the absolute value on the right removes the complex phase because Γ is nonnegative. The pushforward of Γ by $x \mapsto rx$ assigns mass $r^{\alpha-d}\Gamma(A)$ to a Borel set A. Thus,

$$\int e^{-r^2|x|^2/4}\Gamma(\mathrm{d}x) = r^{\alpha-d}M_\Gamma.$$

Multiplying the last equality by the prefactor $r^d/(2\sqrt{\pi})^d$ gives $r^\alpha M_\Gamma/(2\sqrt{\pi})^d$. This proves the Gaussian bound. On either ball $B(y,r)$ the integrand $e^{-|\xi-y|^2/r^2}$ is at least e^{-1}, proving the mass bound. This proves Proposition 4.1.1. □

Choose and fix a real nonzero Schwartz function ζ. For $R > 0$ put $\zeta_R(x) = \zeta(x/R)$, $k_R = \widehat{\zeta_R}$ and $L = \|\widehat{\zeta}\|_1$. Then $k_R(u) = R^d\widehat{\zeta}(Ru)$ and $\|k_R\|_1 = L > 0$. Define

$$\nu_R(\mathrm{d}\eta) = \rho_R(\eta)\,\mathrm{d}\eta, \qquad \rho_R(\eta) = c_d^2 L \int |k_R(\xi-\eta)|\mu(\mathrm{d}\xi). \tag{4.1.4}$$

Lean full

Proposition 4.1.2 (Auxiliary mask norm)**.** *The measure ν_R is even, tempered and Radon, with*

$$\nu_R(B(y,r)) \le c_d^2 L^2 C_\Gamma r^\alpha \tag{4.1.5}$$

for all $y \in \mathbb{R}^d$ and $r > 0$, uniformly in $R > 0$. If H is a separable complex Hilbert space and F is an H-valued Schwartz function, then

$$\int \|\widehat{\zeta_R F}(\xi)\|_H^2 \mu(\mathrm{d}\xi) \le \int \|\widehat{F}(\eta)\|_H^2 \nu_R(\mathrm{d}\eta). \tag{4.1.6}$$

For a real H, the same assertion holds after complexification.

Proof. We first establish the properties and translated growth bound of the auxiliary measure. We then prove the Fourier norm inequality by a weighted Cauchy–Schwarz estimate.

Step 1. We examine the density and its ball masses. For fixed R, translating the argument of a Schwartz function over a compact set preserves a common rapid-decay bound. Choose the decay power large enough to be integrable against the polynomially growing measure μ. Schwartz decay of k_R and polynomial growth of μ show that $\rho_R(\eta)$ is finite at every η. On compact sets of η, the integrands have a common integrable bound. Dominated convergence therefore makes ρ_R continuous, and ν_R is Radon. Since ζ is real,

$k_R(-u) = \overline{k_R(u)}$. Evenness of μ gives evenness of ρ_R. To bound a ball mass, write the density as its nonnegative integral and exchange the two integrations. For fixed ξ, set $u = \xi - \eta$. The condition $\eta \in B(y, r)$ becomes $\xi \in B(y + u, r)$ when the integrations are exchanged again. Tonelli's theorem gives

$$\nu_R(B(y, r)) = c_d^2 L \int |k_R(u)| \mu(B(y + u, r)) \, \mathrm{d}u.$$

Proposition 4.1.1 and $\|k_R\|_1 = L$ give (4.1.5). Polynomial growth on centered balls proves temperedness by the same dyadic argument as above.

Step 2. We justify the Hilbert-valued convolution identity. The finite-dimensional orthogonal projections used below have norm at most one, so their Fourier integrals have the same Schwartz majorants. Bochner Fourier integration gives

$$\widehat{\zeta_R F}(\xi) = c_d \int k_R(\xi - \eta) \widehat{F}(\eta) \, \mathrm{d}\eta.$$

The factor c_d is the product formula for the unitary Fourier transform. We justify the same identity for vector-valued functions by approximation, so that the convolution is a Bochner integral. For scalar Schwartz functions this follows by Fourier inversion and absolute integrability. It follows next for finite-rank Hilbert-valued functions. For general F, take projections onto the successive spans of a countable orthonormal basis of its separable range closure. They converge pointwise in norm. The Schwartz bounds on F dominate the Fourier integrals, proving the identity by dominated convergence. In a finite-dimensional space the full identity projection suffices; the zero space is immediate. The triangle inequality and weighted Cauchy–Schwarz yield

$$\|\widehat{\zeta_R F}(\xi)\|_H^2 \le c_d^2 L \int |k_R(\xi - \eta)| \|\widehat{F}(\eta)\|_H^2 \, \mathrm{d}\eta.$$

Step 3. We estimate the convolution in norm and integrate. Integrating against μ and applying Tonelli's theorem proves (4.1.6). Its right side is finite by Schwartz decay and temperedness of ν_R. This proves Proposition 4.1.2. □

4.1.2 Temporal completion and the original noise

The noise in (1.2.2) is also correlated in time, with kernel $|t - s|^{-a}$. We now complete the temporal tests in that form.

Lean full

Lemma 4.1.3 (Temporal covariance completion)**.** *Let $T > 0$. The form*

$$\langle f, g \rangle_a = \int_0^T \int_0^T f(t) g(s) |t - s|^{-a} \, \mathrm{d}t \, \mathrm{d}s$$

is positive semidefinite on real compact smooth tests. Its null-quotient completion H_a is separable. The inclusion of tests extends continuously from $L^2(0, T)$, with

Lean full

$$\|f\|_a^2 \le \frac{2T^{1-a}}{1 - a} \|f\|_2^2. \tag{4.1.7}$$

In its complexification the norm is given by the same double integral with $f(t)\overline{f(s)}$. In particular, bounded measurable amplitudes on a subinterval, extended by zero, belong to this completion.

Proof. We prove positivity by expressing the temporal kernel as a positive mixture of square forms. A uniform row-integral bound then gives the continuous inclusion and the completion statements.

Step 1. We prove positivity of the covariance form. For fixed t, the kernel row integral is $[t^{1-a}+(T-t)^{1-a}]/(1-a) \le 2T^{1-a}/(1-a)$; symmetry gives the same bound for columns. Write Γ_E for Euler's Gamma function. Away from the null diagonal,

$$|t-s|^{-a} = \frac{1}{\Gamma_E(a)} \int_0^\infty \lambda^{a-1} e^{-\lambda|t-s|}\, \mathrm{d}\lambda.$$

This follows by substitution in the defining Gamma integral. Moreover,

$$e^{-\lambda|t-s|} = \int_{-\infty}^{\min(t,s)} 2\lambda e^{-\lambda(t-u)} e^{-\lambda(s-u)}\, \mathrm{d}u.$$

For each $\lambda > 0$ its quadratic form is an integral of a square. All exchanges for compact smooth tests are absolutely integrable because the kernel row integral is at most $2T^{1-a}/(1-a)$. The same bound and $2|xy| \le |x|^2+|y|^2$ prove (4.1.7). A countable L^2-dense family of compact smooth tests is consequently dense in H_a, proving separability.

Step 2. We explain the row bound and the completion. The complex quadratic form is the sum of those of the real and imaginary parts, since symmetry cancels the imaginary cross term. Thus, the same bound holds after complexification. Smooth density in L^2, together with the Schur bound on the absolute bilinear form, extends the inclusion and the integral identity to L^2. This includes the stated interval amplitudes. This proves Lemma 4.1.3. □

Let $\mathcal{D}$ consist of finite sums $F(t,x) = \sum_j \tau_j(t) f_j(x)$ with real $\tau_j \in C_c^\infty(0,T)$ and real Schwartz f_j. These give H_a-valued Schwartz functions of x. Let W denote the original real isonormal noise in (1.2.2).

Lean partial

Proposition 4.1.4 (Completion on the same noise)**.** *The space $\mathcal{D}$ belongs to the original test-noise completion and*

$$\mathbb{E}W(F)^2 = (2\pi)^d \int \|\widehat{F}(\xi)\|_{H_a^{\mathbb{C}}}^2 \mu(\,\mathrm{d}\xi). \tag{4.1.8}$$

Define the auxiliary seminorm

$$N_R(F)^2 = (2\pi)^d \int \|\widehat{F}(\eta)\|_{H_a^{\mathbb{C}}}^2 \nu_R(\,\mathrm{d}\eta).$$

Then $F \mapsto W(\zeta_R F)$ extends as a contraction from the null-quotient completion for N_R into the original $L^2(\Omega)$. The extension is centered and jointly Gaussian. For finitely many real $F_1, \dots, F_m \in \mathcal{D}$, their masked covariance matrix is bounded in positive semidefinite order by the matrix of auxiliary inner products. This gives covariance comparison for every finite linear Gaussian image and every convex norm power $p \ge 1$.

Proof. We first identify the spectral norm of the original noise. We then extend masked evaluation by the auxiliary bound, and finally compare finite Gaussian vectors by adding independent Gaussian noise.

Step 1. We identify the original covariance norm. For real spatial Schwartz f, g, put $h(z) = \int f(y+z)g(y)\,\mathrm{d}y$. Fourier inversion and Parseval give

$$h(z) = \int e^{i\xi\cdot z}\widehat{f}(\xi)\overline{\widehat{g}(\xi)}\,\mathrm{d}\xi.$$

The product of the two Fourier transforms is Schwartz, so the inverse Fourier identity can be applied again. Evaluating its Fourier transform with the positive sign reflects the frequency and contributes the factor $(2\pi)^d$. Therefore,

$$\int e^{i\xi\cdot z}h(z)\,\mathrm{d}z = (2\pi)^d\widehat{f}(-\xi)\overline{\widehat{g}(-\xi)}.$$

Apply (4.1.1) to the single test h and reflect ξ using evenness of μ. The spatial covariance is thus $(2\pi)^d\int \widehat{f}(\xi)\overline{\widehat{g}(\xi)}\mu(\,\mathrm{d}\xi)$. Summing over the finitely many temporal factors gives (4.1.8). Schwartz decay, temperedness and temporal integrability justify these pairings. If W is initially given only on compact spatial tests, smooth expanding cutoffs converge in the Schwartz topology. The spectral form is continuous in that topology, admitting $\mathcal{D}$ in the same completion.

Step 2. We extend masked evaluation on the same probability space. Proposition 4.1.2, applied with $H = H_a^{\mathbb{C}}$, gives $\mathbb{E}W(\zeta_R F)^2 \le N_R(F)^2$. It annihilates auxiliary-null tests. An auxiliary Cauchy sequence thus gives a Cauchy sequence of noise evaluations in $L^2(\Omega)$, proving the contraction extension and its uniqueness. Every finite linear combination of the limits is an L^2 limit of centered Gaussian variables. Their variances converge, so their characteristic functions prove that the limits remain jointly centered Gaussian.

Step 3. We compare finite Gaussian images. The comparison uses conditional Jensen: adding an independent centered Gaussian vector leaves the conditional mean of the evaluation vector unchanged, and the pth power of a norm is convex for $p \ge 1$. For the finite family let A be the covariance matrix and B the auxiliary Gram matrix. Applying the norm inequality to $\sum_i b_i F_i$ gives $b^{\mathsf{T}}Ab \le b^{\mathsf{T}}Bb$ for every real vector b. Diagonalizing $B - A$ constructs a centered Gaussian vector Z of that covariance, independent of the evaluation vector X, on a product space. Then $X + Z$ has covariance B. Conditional Jensen gives $\mathbb{E}\|X\|^p \le \mathbb{E}\|X + Z\|^p$ for every norm and $p \ge 1$. Finite Gaussian moments ensure finiteness of both sides. This proves Proposition 4.1.4. □

The auxiliary completion depends on R and ζ. Its construction does not define multiplication by ζ_R on the original noise quotient. Nor does the finite linear Gaussian comparison assert a covariance comparison for nonlinear wave solutions. The auxiliary and original test norms need not dominate one another. No spatial representative for every auxiliary class, nonnegative physical inverse covariance for ν_R, or uniform density bound in R is asserted.

Lean narrower

Proposition 4.1.5 (A physical mask need not preserve noise-null tests)**.** *In the admissible case $d = 2$, $\alpha = 1$, $0 < a < 1$ and $\Gamma = \delta_0(\,\mathrm{d}x_1)\,\mathrm{d}x_2$, there is a real compact smooth mask ζ such that no finite C satisfies $\mathbb{E}W(\zeta F)^2 \le C\mathbb{E}W(F)^2$ for every compact smooth test F.*

Proof. We exhibit a test with zero unmasked variance and positive masked variance. This rules out any finite comparison constant.

Step 1. We identify the covariance in this example. Fourier inversion on Schwartz tests gives $\mu = (2\pi)^{-1}\,\mathrm{d}\xi_1\delta_0(\,\mathrm{d}\xi_2)$ in the stated spectral convention. The measure Γ is nonnegative, even, positive definite and tempered, with $\Gamma(cA) = c\Gamma(A)$. It therefore satisfies Hypothesis 1.2.1 with $\alpha = 1$. This is not spatial white noise in dimension two. For real compact smooth g, its spatial covariance is, by ordinary Fubini,

$$V(g) = \int_{\mathbb{R}} \left(\int_{\mathbb{R}} g(x_1, x_2)\,\mathrm{d}x_2 \right)^2 \mathrm{d}x_1.$$

Step 2. We construct the mask and a noise-null test. Choose real even $\chi \in C_c^\infty(\mathbb{R})$ equal to one on $[-1, 1]$ and zero outside $[-2, 2]$. For example, on $1 < r = |x| < 2$ use

$$\chi(x) = \frac{e^{-1/(2-r)}}{e^{-1/(2-r)} + e^{-1/(r-1)}}.$$

The endpoint exponentials vanish to every order, so the plateau pastes smoothly. Let $I_\chi = \int(\chi')^2 > 0$ and $J_\chi = \int \chi^4 > 0$. Positivity of I_χ follows because χ is not constant, and $J_\chi \ge 2$. Put $g(x) = \chi(x_1)\chi''(x_2)$ and $\zeta(x) = \chi(x_1)\chi(x_2)$. Their unmasked marginal vanishes since $\int \chi'' = 0$, whereas integration by parts gives the masked marginal $-I_\chi\chi(x_1)^2$. Thus, $V(g) = 0$ and $V(\zeta g) = J_\chi I_\chi^2 > 0$. For a nonzero nonnegative $\tau \in C_c^\infty(0, T)$, set $F(t, x) = \tau(t)g(x)$. The temporal factor $\|\tau\|_a^2$ is finite and strictly positive because its nonnegative integrand is positive on a set of positive two-dimensional measure. Consequently, the full unmasked variance is zero and the masked variance is positive. This proves Proposition 4.1.5. □

No-go 22 records the quotient interpretation of this witness: the mask separates two representatives of the same noise-null class. This is why we mask tests before constructing the auxiliary completion.

4.1.3 Temporal modulation and continuous wave factors

Write $\langle x\rangle = \sqrt{1 + x^2}$. Let $I = [s, s + h] \subset [0, T]$, with $0 < h \le 1$. Norms below are those of the complexified temporal completion in Lemma 4.1.3.

Lean full

Lemma 4.1.6 (Modulated amplitudes)**.** *Let $A \in C^1(I; \mathbb{C})$, $M = \sup_I |A|$ and $D = \sup_I |A'|$. For every real ω,*

$$\|1_I A(t)e^{i\omega t}\|_a^2 \le C_0(a)h^{2-a}(M + hD)^2\langle h\omega\rangle^{a-1}, \qquad C_0(a) = \frac{16}{1 - a}. \tag{4.1.9}$$

The bound is uniform in T, s, h, A and ω.

Proof. We express the covariance through the time difference and rescale the interval to unit length. At low frequency we use absolute values; at high frequency we separate the singular endpoint before integrating by parts.

Step 1. We express and rescale the covariance. Put $c(v) = \int_s^{s+h-v} A(u+v)\overline{A(u)}\,\mathrm{d}u$ for $0 \le v \le h$. Differentiation at the moving endpoint gives

$$c'(v) = -A(s+h)\overline{A(s+h-v)} + \int_s^{s+h-v} A'(u+v)\overline{A(u)}\,\mathrm{d}u.$$

Thus, $c(h) = 0$, $|c(v)| \le hM^2$ and $|c'(v)| \le M^2 + hMD$. Splitting the covariance square into its two conjugate triangles gives

$$\|1_I A(t)e^{i\omega t}\|_a^2 = 2\,\mathrm{Re}\int_0^h v^{-a}e^{i\omega v}c(v)\,\mathrm{d}v = 2h^{2-a}\,\mathrm{Re}\int_0^1 y^{-a}e^{i\omega hy}f(y)\,\mathrm{d}y,$$

where $f(y) = c(hy)/h$. Set $K = M + hD$. Then $f(1) = 0$ and $|f|, |f'| \le K^2$. If $K = 0$ the assertion is immediate. If $|\omega h| \le 1$, the last integral is at most $K^2/(1-a)$ in absolute value, and $\langle \omega h\rangle^{a-1} \ge 2^{(a-1)/2}$. The claimed constant is sufficient in this case.

The low-frequency constant check is $2/(1-a) \le C_0(a)2^{(a-1)/2}$, after including the factor $2h^{2-a}$. *Step 2.* We separate the singular endpoint at high frequency. Now suppose $k = |\omega h| > 1$. On $[0, 1/k]$ the integral is at most $K^2k^{a-1}/(1-a)$. On $[1/k, 1]$, integrate the exponential by parts. The endpoint at one vanishes, while the other endpoint contributes at most K^2k^{a-1}. The derivative integral, divided by k, is bounded by

$$\frac{K^2}{k}\left(a\int_{1/k}^1 y^{-a-1}\,\mathrm{d}y + \int_{1/k}^1 y^{-a}\,\mathrm{d}y\right) \le K^2k^{a-1}\left(1 + \frac{1}{1-a}\right).$$

Here $k^{-1} \le k^{a-1}$ since $a > 0$. The total is at most $4K^2k^{a-1}/(1-a)$. Finally, $k^{a-1} \le \sqrt{2}\langle\omega h\rangle^{a-1}$ and $8\sqrt{2} \le 16$. Including the factor $2h^{2-a}$ proves the bound for either sign of ω. This proves Lemma 4.1.6. □

Lemma 4.1.6 treats one exponential mode. A product of two sines or cosines is a sum of four such modes, which we bound next.

Lean full

Lemma 4.1.7 (Correlated trigonometric products)**.** *Let $r, \rho \ge 0$. Let P_r be either $\cos(rt)$ or $\sin(rt)$, and let Q_ρ be either $\cos(\rho t)$ or $\sin(\rho t)$. With the amplitude and constant above,*

$$\|1_I AP_rQ_\rho\|_a^2 \le C_0(a)h^{2-a}(M+hD)^2\mathcal{Q}_h(r,\rho), \tag{4.1.10}$$

$$\mathcal{Q}_h(r,\rho) := \langle h(r-\rho)\rangle^{a-1} + \langle h(r+\rho)\rangle^{a-1}. \tag{4.1.11}$$

Proof. Expanding the two trigonometric factors gives four complex exponential modes with frequencies $\sigma r + \tau\rho$, $\sigma, \tau \in \{-1, 1\}$, and coefficients of absolute value $1/4$. In a Hilbert space,

$$\left\|\sum_j c_j v_j\right\|^2 \le \left(\sum_j |c_j|\right)\sum_j |c_j|\|v_j\|^2.$$

This Hilbert-space inequality follows from the triangle inequality followed by scalar Cauchy–Schwarz applied to $|c_j|^{1/2}$ and $|c_j|^{1/2}\|v_j\|$.

The first coefficient sum is one. Apply Lemma 4.1.6 to each mode. Two frequencies have absolute value $|r-\rho|$ and two have absolute value $r+\rho$. This gives one half of the asserted right side, and hence the bound. Repeated or zero frequencies are permitted; no orthogonality or independence of the modes is used. This proves Lemma 4.1.7. □

Lean full

Lemma 4.1.8 (Continuous sine factors)**.** *Define* $c_r(t)=\cos(rt)$ *and*

$$b_r(t)=\langle r\rangle\frac{\sin(rt)}{r}\quad(r>0),\qquad b_0(t)=t.$$

For $F_r\in\{c_r,b_r\}$ *and* $G_\rho\in\{c_\rho,b_\rho\}$,

$$\|1_I F_r G_\rho\|_a^2\le C_1(a)(1+T)^4h^{2-a}\mathcal{Q}_h(r,\rho),\qquad C_1(a)=4\cdot 3^{1-a}C_0(a).\tag{4.1.12}$$

Proof. We replace low-frequency sine quotients by averages of cosines. The trigonometric estimate applies to each integrand; a comparison of shifted frequency weights then gives the stated constant.

Step 1. We represent each factor without a singular quotient. For $r\ge 1$, b_r is a sine times a coefficient at most $\sqrt{2}$. For $0\le r\le 1$, the fundamental theorem of calculus gives

$$b_r(t)=t\langle r\rangle\int_0^1\cos(vrt)\,\mathrm{d}v.$$

For $r>0$, integrate the derivative of $v\mapsto\sin(vrt)$ from zero to one and divide by r. At $r=0$, the right side is t, in agreement with the definition. Each low-frequency sine factor contributes one factor t and one averaging parameter; each high-frequency sine contributes a coefficient of absolute value at most $\sqrt{2}$, while a cosine contributes neither. This includes $r=0$. Hence, a product F_rG_ρ is a scalar coefficient of absolute value at most two times a normalized integral of $t^jP_{r'}(t)Q_{\rho'}(t)$, where $j\in\{0,1,2\}$ and $|r'-r|,|\rho'-\rho|\le 1$. The integral is over zero, one or two copies of $[0,1]$; with no averages, use a one-point probability space. Its parameter dependence is continuous in $L^2(0,T)$ by dominated convergence. Lemma 4.1.3 makes it continuous in H_a as well. Thus, the averages are Bochner integrals, and their H_a images agree with the pointwise averages by continuity of the inclusion. Hilbert Jensen bounds the squared norm of an average by the average of the squared norms.

Step 2. We bound each integrand and compare frequency weights. Apply Lemma 4.1.7 to each integrand with $A(t)=t^j$. For $j=0,1,2$, respectively, $M+hD$ is at most 1, $T+1$ and T^2+2T. In every case $(M+hD)^2\le(1+T)^4$. For real x,e, the triangle inequality and its reverse imply

$$\frac{\langle x\rangle}{1+|e|}\le\langle x+e\rangle\le(1+|e|)\langle x\rangle.$$

For the upper bracket comparison, view $\langle x\rangle$ as the Euclidean norm of $(1,x)$ and use the triangle inequality. Applying that same upper bound with $x+e$ and $-e$ gives the lower

comparison. The changes in $h(r \pm \rho)$ have magnitude at most two, since $h \le 1$. Because $a - 1 < 0$, each altered bracket to the power $a - 1$ is at most 3^{1-a} times the original one. Apply these comparisons, Hilbert Jensen and the squared scalar coefficient bound four to obtain (4.1.12). This proves Lemma 4.1.8. □

These estimates concern covariance forms and temporal factors. Their application to displacement and velocity is in Section 4.2; the subsequent operator, source and moment results require their separate proofs. They do not follow from covariance domination alone.

4.2 Frequency estimates and both wave variance directions

We now apply the covariance and temporal estimates of Section 4.1 to the full wave phase. We retain Hypothesis 1.2.1, write $a = \alpha_0$, and choose and fix

$$0 < \gamma < \min\left(\frac{1}{2}, \frac{2-\alpha}{2}\right). \tag{4.2.1}$$

The interval is nonempty because $\alpha + a < 2$. We use $\langle \xi \rangle = \sqrt{1 + |\xi|^2}$ and set

$$B_\alpha(h) = \begin{cases} 1, & \alpha < 1, \\ 1 + \log(1/h), & \alpha = 1, \\ h^{1-\alpha}, & \alpha > 1, \end{cases} \qquad 0 < h \le 1. \tag{4.2.2}$$

4.2.1 A scalar row estimate for a measure

Let ν be a positive Radon measure satisfying

$$\nu(B(y, r)) \le C r^\alpha, \qquad y \in \mathbb{R}^d, \quad r > 0, \tag{4.2.3}$$

where $C \ge 0$. If the estimate is initially known for open balls, apply it at radius $r + \epsilon$ and let $\epsilon \downarrow 0$ to obtain the closed-ball estimate. Neither evenness nor a density is assumed here. Using (4.1.11), define

$$\Phi_h(\xi, \eta) := \frac{\mathcal{Q}_h(|\xi|, |\eta|)}{\langle \xi \rangle \langle \eta \rangle}, \tag{4.2.4}$$

$$J_h(\xi) := \langle \xi \rangle^{2\gamma} \int_{\mathbb{R}^d} \Phi_h(\xi, \xi - \lambda) \nu(\mathrm{d}\lambda). \tag{4.2.5}$$

These are initially nonnegative extended integrals. In particular, the notation denotes a pushforward of ν, not integration against an assumed spectral density.

Lean full

Proposition 4.2.1 (Uniform scalar row)**.** *There is a finite $K = K(\alpha, a, \gamma)$, independent of d, ν, C, h and ξ, such that*

$$\sup_{\xi \in \mathbb{R}^d} J_h(\xi) \le K C B_\alpha(h), \qquad 0 < h \le 1. \tag{4.2.6}$$

Proof. We first bound the integral of the inverse Bessel weight on a ball. We then split the row integral into frequencies near and far from the origin relative to the fixed output frequency. The near bound uses the choice of γ; the far bound uses temporal decay and $\alpha + a < 2$.

Step 1. We bound the weighted mass on a ball. If $C = 0$, a countable covering by finite balls gives $\nu = 0$, and the result is immediate. Suppose $C > 0$. For each ξ, let ν_ξ be the pushforward under $\lambda \mapsto \eta = \xi - \lambda$. Then $\nu_\xi(B(0,R)) \le CR^\alpha$. For $q \ge 1$, put

$$A_\xi(q) = \int_{|\eta| \le 5q} \langle \eta \rangle^{-1} \nu_\xi(\,\mathrm{d}\eta).$$

Choose $N = \lceil \log_2(5q) \rceil$, so $5q \le 2^N < 10q$. Splitting into the unit ball and the annuli $2^j < |\eta| \le 2^{j+1}$ gives

$$A_\xi(q) \le C \left(1 + 2^\alpha \sum_{j=0}^{N-1} 2^{j(\alpha-1)} \right).$$

The geometric sum is bounded when $\alpha < 1$, is N when $\alpha = 1$, and is at most $2^{N(\alpha-1)}/(2^{\alpha-1} - 1)$ when $\alpha > 1$. Hence,

$$A_\xi(q) \le K_\alpha C \begin{cases} 1, & \alpha < 1, \\ 1 + \log q, & \alpha = 1, \\ q^{\alpha-1}, & \alpha > 1, \end{cases} \tag{4.2.7}$$

with a constant depending only on α.

Step 2. We estimate the near region. Set $q = \max(1, |\xi|)$ and $\epsilon = 1 - 2\gamma > 0$. On $|\lambda| \le 4q$ we have $|\eta| \le 5q$. Both bracket powers in $\mathcal{Q}_h$ are at most one, since $a - 1 < 0$. The contribution of this region to $J_h(\xi)$ is at most

$$2\langle \xi \rangle^{-\epsilon} A_\xi(q) \le 2q^{-\epsilon} A_\xi(q).$$

If $\alpha < 1$, this is uniformly bounded by (4.2.7). If $\alpha = 1$, the bound follows from

$$e^{-\epsilon u}(1 + u) \le 1 + \frac{1}{e\epsilon}, \qquad u = \log q \ge 0,$$

since $ue^{-\epsilon u}$ has maximum $1/(e\epsilon)$. If $\alpha > 1$, the remaining power is $q^{\alpha+2\gamma-2}$, whose exponent is negative by (4.2.1). Thus, the near contribution is at most a constant times C in all three cases.

Step 3. We use temporal decay in the far region. On the far region write $r = |\lambda| > 4q$. Then

$$|\eta| \ge \frac{3r}{4}, \qquad \big| |\eta| - |\xi| \big| \ge \frac{r}{2}, \qquad |\eta| + |\xi| \ge \frac{r}{2}.$$

Indeed, $|\xi| \le q < r/4$. The reverse triangle inequality gives $|\eta| = |\xi - \lambda| \ge r - |\xi| > 3r/4$, and then $|\eta| - |\xi| > r/2$. The sum of the two magnitudes is at least their difference. These bounds apply to both frequency arguments in $\mathcal{Q}_h$. Each oscillatory bracket is at

least $\langle hr\rangle/2$, whereas $\langle\eta\rangle^{-1} \le 4/(3r)$ and $\langle\xi\rangle^{-\epsilon} \le 1$. Consequently, the far contribution is at most

$$\frac{4}{3}\,2^{2-a}\int_{|\lambda|>4q} |\lambda|^{-1}\langle h|\lambda|\rangle^{a-1}\nu(\,\mathrm{d}\lambda).$$

Raising the lower bound on each bracket to $a-1<0$ gives an upper bound with coefficient 2^{1-a}. There are two brackets, so their sum contributes 2^{2-a}. The factor $4/3$ comes from the inverse Bessel weight of η. Enlarge the domain to $|\lambda|>1$ and split it into dyadic annuli. Applying (4.2.3) to their masses bounds this expression by a constant depending only on α, a times $CS(h)$, where

$$S(h)=\sum_{j=0}^{\infty} 2^{j(\alpha-1)}\langle h2^j\rangle^{a-1}.$$

On $2^j<|\lambda|\le 2^{j+1}$, the inverse radius is at most 2^{-j} and the decreasing bracket power is at most $\langle h2^j\rangle^{a-1}$. The mass is at most $C2^{(j+1)\alpha}$. Multiplying these bounds gives the jth term of $S(h)$ up to a constant depending only on α.

Step 4. We sum below and above the temporal scale. Choose $L=\lfloor \log_2(1/h)\rfloor \ge 0$. For $j\le L$ the bracket power is at most one. For $j\ge L+1$ it is at most $(h2^j)^{a-1}$. Since $\alpha+a-2<0$, the tail is

$$\frac{h^{a-1}2^{(L+1)(\alpha+a-2)}}{1-2^{\alpha+a-2}} \le \frac{h^{1-\alpha}}{1-2^{\alpha+a-2}}.$$

The inequality uses $2^{L+1}>1/h$ and the negative exponent. The finite sum is bounded by $1/(1-2^{\alpha-1})$ for $\alpha<1$, by $1+\log_2(1/h)$ for $\alpha=1$, and by

$$\frac{2^{\alpha-1}h^{1-\alpha}}{2^{\alpha-1}-1}$$

for $\alpha>1$. Since $h^{1-\alpha}\le 1$ in the first case, we obtain $S(h)\le K_{\alpha,a}B_\alpha(h)$. Combining the near and far bounds, and using $B_\alpha(h)\ge 1$, proves the assertion and finiteness of the original integral. All constants arose from numerical shell estimates and are independent of d. This proves Proposition 4.2.1. □

For $\alpha=1$ the profile $B_\alpha(h)$ in Proposition 4.2.1 carries a logarithm. After multiplication by h^{2-a}, we absorb it into a power of h.

Lean full

Corollary 4.2.2 (A time exponent above one half)**.** *For every*

$$\frac{1}{2}<\beta<\min\left(1-\frac{a}{2},\frac{3-a-\alpha}{2}\right), \tag{4.2.8}$$

there is a finite $K_\beta=K_\beta(\alpha,a,\gamma,\beta)$ such that

$$h^{2-a}\sup_{\xi} J_h(\xi)\le K_\beta C h^{2\beta}, \qquad 0<h\le 1. \tag{4.2.9}$$

Proof. Both upper endpoints in (4.2.8) exceed one half, by $a < 1$ and $\alpha + a < 2$. If $\alpha < 1$, use $2 - a > 2\beta$ in Proposition 4.2.1. If $\alpha > 1$, use $3 - a - \alpha > 2\beta$. For $\alpha = 1$, set $\delta = 2 - a - 2\beta > 0$ and $u = \log(1/h)$. Then

$$h^{\delta}(1 + \log(1/h)) = e^{-\delta u}(1 + u) \le 1 + \frac{1}{e\delta}.$$

For the displayed bound, $u \ge 0$, the exponential term is at most one, and $ue^{-\delta u}$ has maximum $1/(e\delta)$. Multiplying the display by $h^{2\beta}$ gives the required estimate at $\alpha = 1$. This absorbs the critical logarithm. No endpoint value of β is used. This proves Corollary 4.2.2. □

4.2.2 Forms on the full phase

Choose and fix $T > 0$. Set $\Lambda = (1 - \Delta)^{1/2}$, $s = 1/2$ and $E_r = H^r(\mathbb{R}^d) \times H^{r-1}(\mathbb{R}^d)$. On the complexification of $E = E_s$, use inner products linear in the first slot. The map

$$Jz(\xi) = \Big(\langle\xi\rangle^{1/2}\widehat{z}_1(\xi), \langle\xi\rangle^{-1/2}\widehat{z}_2(\xi)\Big)$$

is unitary onto $L^2(\mathbb{R}^d; \mathbb{C}^2)$. The full massless wave group has Fourier matrix

$$S(t, \xi) = \begin{pmatrix} \cos(t|\xi|) & \sin(t|\xi|)/|\xi| \\ -|\xi|\sin(t|\xi|) & \cos(t|\xi|) \end{pmatrix}, \tag{4.2.10}$$

where the sine quotient is t at zero. Let $B(b)(u, v) = (0, bu)$. Choose and fix a real even nonnegative $\zeta \in C_c^{\infty}(\mathbb{R}^d)$ equal to one on B_1 and zero off B_2, and put $\zeta_R(x) = \zeta(x/R)$ for $R > 0$. For $I = [t_0, t_0 + h] \subset [0, T]$, $0 < h \le 1$, and Schwartz phases z, w, put

$$v_z(t) = [S(t)z]_1, \tag{4.2.11}$$

$$G_w(t) = -\frac{\sin(t|D|)}{|D|}\Lambda w_1 + \cos(t|D|)\Lambda^{-1}w_2, \tag{4.2.12}$$

$$F_{z,w}(t, x) = 1_I(t)v_z(t, x)\overline{G_w(t, x)}, \qquad \ell_R(I; z, w) = W_{\mathbb{C}}(\zeta_R F_{z,w}), \tag{4.2.13}$$

where $W_{\mathbb{C}}(F) = W(\operatorname{Re} F) + iW(\operatorname{Im} F)$. There is no observation cutoff in this definition.

We first assume $\Gamma \ne 0$. If $\Gamma = 0$, all forms and the column maps below are zero, so their bounds hold directly. For the nonzero case, let ν_R be (4.1.4) and set

$$L_\zeta = \|\widehat{\zeta}\|_1, \qquad C_\nu = c_d^2 L_\zeta^2 C_\Gamma. \tag{4.2.14}$$

Proposition 4.1.2 gives a positive even tempered Radon measure with $\nu_R(B(y, r)) \le C_\nu r^\alpha$, uniformly in R.

Lean partial

Proposition 4.2.3 (Form and phase kernel)**.** *The tests $\zeta_R F_{z,w}$ in (4.2.13) belong to the original noise completion. The form ℓ_R is linear in z and conjugate linear in w, and uses the same W as the model. For a smooth deterministic coefficient b with common compact spatial support and bounded spatial derivatives on $[0, T]$,*

$$\langle S(-t)B(b(t))S(t)z, w\rangle_E = \int b(t, x)v_z(t, x)\overline{G_w(t, x)}\,\mathrm{d}x. \tag{4.2.15}$$

For a real compact smooth χ, multiplication D_χ on both phase entries has adjoint

$$D_\chi^{*,E} w = \left(\Lambda^{-1}\chi\Lambda w_1, \Lambda\chi\Lambda^{-1} w_2\right). \tag{4.2.16}$$

With $U = Jz$, $V = Jw$, $r = |\xi|$, $\rho = |\eta|$ and the continuous functions c_r, b_r of Lemma 4.1.8, set

$$\mathcal{K}(t;\xi,\eta) = \frac{1}{\sqrt{\langle\xi\rangle\langle\eta\rangle}} \begin{pmatrix} -b_r c_\rho & -b_r b_\rho \\ c_r c_\rho & c_r b_\rho \end{pmatrix}(t). \tag{4.2.17}$$

Then

$$\mathbb{E}|\ell_R(I;z,w)|^2 \le \int \left\| \int \sum_{i,j=1}^{2} 1_I \mathcal{K}_{ij}(\cdot;\eta+\lambda,\eta) U_j(\eta)\overline{V_i(\eta+\lambda)}\,\mathrm{d}\eta \right\|_{H_a^{\mathbb{C}}}^2 \nu_R(\,\mathrm{d}\lambda). \tag{4.2.18}$$

Proof. We first admit the masked products in the original noise completion and identify the same limits in the auxiliary norm. We then extend the comparison to complex tests, compute the phase adjoints, and write the Fourier kernel with its normalization.

Step 1. We admit the masked products in the original completion. The wave multipliers are smooth at zero through the continuous sine quotient, with polynomially bounded frequency derivatives on finite time intervals. Bessel multipliers preserve Schwartz space. Thus, v_z, G_w and their product are continuous in all Schwartz seminorms on $[0,T]$. For tests supported in a fixed compact K, the absolute spatial pairing is bounded by

$$|K|\Gamma(K-K)\|F(t)\|_\infty \|H(u)\|_\infty.$$

Indeed, only $y \in K-K$ contributes to $\int \Gamma(\,\mathrm{d}y)\int F(t,x)\overline{H(u,x-y)}\,\mathrm{d}x$. Combine this with the temporal Schur bound and approximate the interval indicator and the continuous time dependence by smooth interior temporal tests, keeping the spatial support of ζ_R. This admits the masked product in the original completion in every allowed dimension.

Step 2. We compare the limits in the two completions. We also identify its auxiliary and spectral limits. Approximate a Schwartz-valued function on I by time partitions with frozen spatial values, and then replace the finitely many indicators by compact smooth temporal functions. A diagonal sequence F_n of finite temporal tensors converges in L^2 time in every Schwartz seminorm. Fourier integration by parts and the spatial weighted supremum bounds give, for sufficiently large fixed N,

$$\|\widehat{F_n - F}(\xi)\|_{L^2(0,T)} \le \epsilon_n \langle\xi\rangle^{-N}, \qquad \epsilon_n \to 0.$$

For a fixed seminorm, continuity on the compact time interval makes a fine time partition uniformly accurate. Each frozen value is Schwartz; replacing finitely many indicators in L^2 time controls the seminorm error by a finite sum. A diagonal choice over the countable seminorms gives the sequence, and Fourier integration by parts turns those errors into the displayed frequency decay. Choose N so that the square weight is integrable against both tempered measures μ and ν_R. Lemma 4.1.3 gives convergence in their spectral H_a

norms. Multiplication by the fixed ζ_R preserves these L^2 Schwartz-seminorm limits, so the masked differences converge in the μ spectral norm too. The preceding compact-support estimate also gives convergence in the original completion. Hence, the auxiliary extension and original-noise limit agree on these products. Constants for this admission argument may depend on R; they are not the uniform variance constants below.

Step 3. We pass from real tests to complex tests. For real tensor tests f, g, the Hermitian symmetry of their spatial transforms gives

$$A(-\xi) = \overline{A(\xi)}, \qquad A(\xi) = \langle \widehat{f}(\xi), \widehat{g}(\xi) \rangle_{H_a^{\mathbb{C}}}.$$

Integration against either even μ or even ν_R cancels the imaginary mixed term. Expanding the squared norm of $\widehat{f} + i\widehat{g}$, then using the preceding approximation, extends Proposition 4.1.4 to the present complex tests:

$$\mathbb{E}|W_{\mathbb{C}}(\zeta_R F)|^2 = (2\pi)^d \int \|\widehat{\zeta_R F}(\xi)\|_{H_a^{\mathbb{C}}}^2 \mu(\,\mathrm{d}\xi) \le (2\pi)^d \int \|\widehat{F}(\lambda)\|_{H_a^{\mathbb{C}}}^2 \nu_R(\,\mathrm{d}\lambda). \tag{4.2.19}$$

This is a bound for the masked noise, not a declaration that its law is stationary. Complex linearity of $W_{\mathbb{C}}$ and linearity of v_z, G_w prove the stated sesquilinearity.

Step 4. We compute the physical adjoints. The displacement and velocity pairings carry Λ and Λ^{-1}, respectively; moving these weights onto w in $S(-t)(0, b(t)v_z(t))$ gives the negative sine and cosine terms defining G_w. The first-response integral below means $\int_I S(-t)B(b(t))S(t)z \,\mathrm{d}t$ in E; its existence allows the pointwise identity to be integrated, but is not needed for the pointwise adjoint calculation itself. Smooth multiplication is bounded on each Sobolev space: Fourier convolution, the inequality $\langle \xi \rangle^r \langle \eta \rangle^{-r} \le 2^{|r|/2} \langle \xi - \eta \rangle^{|r|}$ and weighted Schwartz decay reduce this to the $L^1 * L^2$ bound. The free matrix is strongly continuous and bounded on E on compact time intervals, directly by its weighted Fourier entries. Thus, the ordinary first-response integral exists on states. Since $S(-t)(0, f) = (-\sin(t|D|)f/|D|, \cos(t|D|)f)$, moving the real self-adjoint multipliers and the two Sobolev weights onto w proves (4.2.15). The observed form is $\ell_R(I; z, D_\chi^{*,E} w)$: applying D_χ to an output moves its phase adjoint onto the test vector w. The same weighted duality gives (4.2.16). Inserting this adjoint in G_w is the correctly observed form; D_χ need not be self-adjoint on E. This deterministic identity does not identify a positive-width source with the original noise or assert a source limit.

Step 5. We compute the normalized covariance kernel. The definitions give exactly

$$\begin{aligned} \widehat{v}_z(t, \eta) &= \langle \eta \rangle^{-1/2} [c_\rho(t) U_1(\eta) + b_\rho(t) U_2(\eta)], \\ \widehat{G}_w(t, \xi) &= \langle \xi \rangle^{-1/2} [-b_r(t) V_1(\xi) + c_r(t) V_2(\xi)]. \end{aligned}$$

In the first line, η is the input frequency and U_1, U_2 are its two weighted coordinates. In the second, ξ is the frequency paired with V_1, V_2. Multiplying the first line by the complex conjugate of the second gives four terms, indexed by input component j and output component i. The wave factors are real, so conjugation affects the coordinates but not these factors. Their product gives (4.2.17). At zero frequencies one uses the

continuous sine quotient, not division by zero; at $\xi = \eta = 0$ the matrix is $\left(\begin{smallmatrix} -t & -t^2 \\ 1 & t \end{smallmatrix}\right)$. Fourier multiplication with the conjugate yields

$$\widehat{F}_{z,w}(t,-\lambda) = c_d 1_I(t) \int \sum_{i,j=1}^{2} \mathcal{K}_{ij}(t;\eta+\lambda,\eta) U_j(\eta) \overline{V_i(\eta+\lambda)}\, \mathrm{d}\eta.$$

The product with the conjugate has frequency $\eta - \xi$. Evaluating it at $-\lambda$ therefore sets $\xi = \eta + \lambda$, explaining the shift in every kernel entry and in V_i. The spatial integral is absolutely convergent uniformly on the finite time interval by Schwartz decay. The Schur bound also makes it a Bochner $H_a^{\mathbb{C}}$ integral. Reflect λ using evenness of ν_R in (4.2.19). Since $(2\pi)^d c_d^2 = 1$, this proves (4.2.18) with no remaining Fourier factor. This proves Proposition 4.2.3. □

4.2.3 Bessel's inequality and the two variances

Proposition 4.2.3 bounds the variance of one form $\ell_R(I; z, w)$. To sum it over an orthonormal family of phases, we need a Bessel inequality with values in $H_a^{\mathbb{C}}$. Proposition 4.2.5 uses it in both directions.

Lean full

Lemma 4.2.4 (Hilbert-valued finite Bessel inequality)**.** *Let H be a separable complex Hilbert space, let $\{u_k\}$ be a finite orthonormal family in $L^2(\mathbb{R}^d;\mathbb{C}^2)$, and let $g = (g_1, g_2) \in L^2(\mathbb{R}^d; H^2)$. Then*

$$\sum_k \left\| \int \sum_{j=1}^{2} u_{k,j}(\eta) g_j(\eta)\, \mathrm{d}\eta \right\|_H^2 \le \int \sum_{j=1}^{2} \|g_j(\eta)\|_H^2\, \mathrm{d}\eta. \tag{4.2.20}$$

The same bound holds with $\overline{u_{k,j}}$ in place of $u_{k,j}$.

Proof. The nonconjugated integrand requires the conjugate orthonormal family in scalar Bessel, because the scalar inner product conjugates its second argument; complex conjugation preserves orthonormality. Expand g in a countable orthonormal basis of H. On each scalar coefficient apply scalar Bessel to the orthonormal family $\{\overline{u_k}\}$, or to $\{u_k\}$ for the conjugated version. Scalar finite Bessel follows by subtracting an orthogonal finite projection and expanding its nonnegative squared norm. Sum over the H basis and use Parseval and nonnegative Tonelli. The Bochner integrals exist by L^2 Cauchy–Schwarz. A finite-dimensional H uses its finite basis, and the zero space is immediate. No independence is involved. This proves Lemma 4.2.4. □

Lean partial

Proposition 4.2.5 (Both variance directions)**.** *There is a finite C_T, depending on the fixed model, mask, a, α, γ, T, but not on R, I or the orthonormal family, such that for every finite complex E-orthonormal Schwartz family $\{e_k\}$ and every Schwartz phase z,*

$$\sum_k \mathbb{E}|\ell_R(I; e_k, z)|^2 \le C_T h^{2-a} B_\alpha(h) \|z\|_{E_{s-\gamma}}^2, \tag{4.2.21}$$

$$\sum_k \mathbb{E}|\ell_R(I; z, e_k)|^2 \le C_T h^{2-a} B_\alpha(h) \|z\|_{E_{s-\gamma}}^2. \tag{4.2.22}$$

For every β in (4.2.8), either right side may be replaced by $C_{T,\beta} h^{2\beta} \|z\|_{E_{s-\gamma}}^2$.

Proof. We combine the temporal bound for each matrix entry with the scalar row estimate. We apply Hilbert-valued Bessel first to the input family and then to the output family, keeping both variance directions and the same constant.

Step 1. We bound the temporal kernels and their rows. Each entry in (4.2.17) is a product of two continuous wave factors times $(\langle\xi\rangle\langle\eta\rangle)^{-1/2}$, with a possible minus sign. Lemma 4.1.8 therefore gives

$$\|1_I\mathcal{K}_{ij}(\cdot;\xi,\eta)\|_{H_a^{\mathbb{C}}}^2 \le A_T h^{2-a}\Phi_h(\xi,\eta), \qquad A_T = C_1(a)(1+T)^4. \tag{4.2.23}$$

The positive even Radon measure ν_R satisfies the growth bound (4.2.14). Thus, all hypotheses of Proposition 4.2.1 hold, and

$$\int \Phi_h(\xi,\xi-\lambda)\nu_R(\,\mathrm{d}\lambda) \le KC_\nu B_\alpha(h)\langle\xi\rangle^{-2\gamma}. \tag{4.2.24}$$

No nonnegative physical inverse covariance of ν_R is needed.

Step 2. We check the hypotheses of Hilbert-valued Bessel. The kernels used in Lemma 4.2.4 belong to its stated L^2 space for each fixed λ. Indeed, $|c_r(t)| \le 1$ and $|b_r(t)| \le \sqrt{2}\max(1,T)$ on $[0,T]$, by the high- and low-frequency representations. The kernels are continuous into $L^2(0,T)$ in their frequency variables, hence into $H_a^{\mathbb{C}}$ by Schur. Separability gives strong measurability. Multiplication by shifted Schwartz components of U or V then gives the required L^2 integrability. Later λ integrals are of nonnegative functions; their finiteness follows from the estimates below.

Step 3. We sum over the input family. First fix $V = Jz$ and let $U_k = Je_k$ be the input family. In (4.2.18) set

$$g_j^\lambda(\eta) = \sum_{i=1}^{2} 1_I\mathcal{K}_{ij}(\cdot;\eta+\lambda,\eta)\overline{V_i(\eta+\lambda)}.$$

Lemma 4.2.4 and Cauchy–Schwarz over the two output components give

$$\begin{aligned}\sum_j \|g_j^\lambda(\eta)\|_{H_a^{\mathbb{C}}}^2 &\le 2\sum_{i,j}|V_i(\eta+\lambda)|^2\|1_I\mathcal{K}_{ij}(\cdot;\eta+\lambda,\eta)\|_{H_a^{\mathbb{C}}}^2\\ &\le 4A_T h^{2-a}\Phi_h(\eta+\lambda,\eta)\sum_i|V_i(\eta+\lambda)|^2.\end{aligned}$$

Under $\xi = \eta+\lambda$, the factor $\sum_i|V_i(\xi)|^2$ is independent of λ, leaving the row integral as its coefficient. Change variables $\xi = \eta+\lambda$ in the Lebesgue integral for each λ, apply Tonelli and (4.2.24), and use $\|z\|_{E_{s-\gamma}} = \|\langle\xi\rangle^{-\gamma}Jz\|_2$. This proves (4.2.21) with $C_T = 4A_TKC_\nu$.

Step 4. We sum over the output family. Next fix $U = Jz$ and let $V_k = Je_k$ be the output family. After $\eta = \xi-\lambda$ in (4.2.18), put

$$f_i^\lambda(\xi) = \sum_{j=1}^{2} 1_I\mathcal{K}_{ij}(\cdot;\xi,\xi-\lambda)U_j(\xi-\lambda).$$

Apply the conjugated version of Lemma 4.2.4. Cauchy–Schwarz over the two input components bounds its right side by

$$4A_T h^{2-a} \int \Phi_h(\xi, \xi-\lambda) \sum_j |U_j(\xi-\lambda)|^2 \, \mathrm{d}\xi.$$

After the change of variables and Tonelli, the row at fixed η is $\int \Phi_h(\eta+\lambda, \eta)\nu_R(\,\mathrm{d}\lambda)$. Reflect λ using the evenness of ν_R and then use symmetry of Φ_h. This row becomes $\int \Phi_h(\eta, \eta-\lambda)\nu_R(\,\mathrm{d}\lambda)$, which is bounded by (4.2.24) with $\xi = \eta$. This proves (4.2.22) with the same C_T.

Step 5. We obtain the time-power bounds and their uniformity. Use Corollary 4.2.2 for h^{2-a} times the row integral at the two applications above to obtain the asserted $h^{2\beta}$ bounds, including strict absorption of the critical logarithm. The constants are uniform in R, I and family size. The R-dependent admission estimate was not used as this uniform variance bound. This proves Proposition 4.2.5. □

4.2.4 Mean-square columns on the original probability space

Write E_r^{real} for the real phase space in dimension d.

Proposition 4.2.6 (Column and adjoint-column maps)**.** *On the same probability space there are deterministic bounded real linear maps*

$$m_{R,I}, n_{R,I} : E_{s-\gamma}^{\mathrm{real}} \longrightarrow L^2(\Omega; E_s^{\mathrm{real}}),$$

with squared bounds $C_T h^{2-a} B_\alpha(h)$, such that, for every fixed real Schwartz pair z, w,

$$\langle m_{R,I} z, w\rangle_E = \ell_R(I; z, w) = \langle z, n_{R,I} w\rangle_E \quad \text{in } L^2(\Omega). \tag{4.2.25}$$

Fixed-vector values and finite families of values are centered Gaussian.

Proof. We choose a real Schwartz orthonormal basis and construct the two columns by summing their scalar noise coefficients. The two variance bounds give convergence and continuous extension. We then identify the pairings and the Gaussian laws of the limits.

Step 1. We choose the basis and dense input class. Choose a countable real Schwartz orthonormal basis $\{e_k\}$ of E_s. Such a basis follows by Gram–Schmidt from a countable dense Schwartz family, discarding zero residuals. Schwartz density follows by smooth Fourier cutoff approximation in the weighted L^2 norms: approximate by compact smooth Fourier coordinates, replace $g(\xi)$ by $(g(\xi)+\overline{g(-\xi)})/2$, and apply the inverse Bessel/Fourier maps. The resulting phases are real Schwartz, and Gram–Schmidt preserves that class. The same density holds in $E_{s-\gamma}$.

Step 2. We construct the two columns in mean square. For fixed real Schwartz z, define

$$m_N(z) = \sum_{k\le N} \ell_R(I; z, e_k) e_k, \qquad n_N(z) = \sum_{k\le N} \ell_R(I; e_k, z) e_k.$$

The output-variance estimate controls $m_N(z)$, and the input-variance estimate controls $n_N(z)$. Both are finite Gaussian sums on the original W. By Proposition 4.2.5, their coefficient expected squares have finite sum. Orthogonality gives the squared tail norms as the corresponding sums of expected squares. Thus, both sequences converge in $L^2(\Omega; E_s)$ to $m(z), n(z)$ with the asserted bounds, without independence of the coefficients. Finite-sum measurability and separable E_s give strong measurability of the limits. The bounded real linear maps extend uniquely from Schwartz phases to $E_{s-\gamma}$.

Step 3. We identify the pairings and remove the basis choice. If w_N is the E_s projection of a Schwartz w onto the first N basis vectors, then $\langle m_N(z), w\rangle_E = \ell_R(I; z, w_N)$. The singleton form of (4.2.22), after normalizing $w - w_N$ in E_s, gives

$$\mathbb{E}|\ell_R(I; z, w - w_N)|^2 \le C_T h^{2-a} B_\alpha(h) \|z\|^2_{E_{s-\gamma}} \|w - w_N\|^2_{E_s}.$$

The residual is Schwartz, since the projection is a finite linear combination of Schwartz basis vectors. If it is nonzero, divide it by its E_s norm to make a singleton orthonormal family and apply the variance bound. Multiplication by the squared norm gives the displayed estimate. The zero residual is immediate. The right side tends to zero, giving the first identity in (4.2.25). For the second, project z instead and use the singleton input bound (4.2.21). A fixed countable Schwartz orthonormal basis and Parseval show basis independence of the constructed limits.

Step 4. We identify the Gaussian laws after taking limits. Continuous linear functionals of the limits, and finite linear combinations of such functionals, are L^2 limits of centered Gaussian variables with convergent variances. Their characteristic functions therefore converge to those of centered Gaussians. The same reasoning after the bounded input extension proves joint Gaussianity for arbitrary fixed inputs and finite families of the two maps. This proves Proposition 4.2.6. □

These are maps into $L^2(\Omega; E_s)$ for fixed intervals. No common uncountable almost-sure version, random bounded operator, Hilbert–Schmidt realization, time path, source convergence or new solution-moment bound is inferred by this section alone. Both variance directions are retained in Section 5.1.

4.3 Finite Gaussian moments and whole-space Sobolev compactness

We prove the finite Gaussian and compact-cutoff estimates needed to construct the wave operator path. All traces and Schatten norms in this section are unnormalized. The spatial states remain on $\mathbb{R}^d$, $d \in \{1, 2, 3\}$. Here p is an auxiliary Schatten and Gaussian-moment index. The auxiliary periodic space below is used only to factor a compactly supported multiplication operator. No infinite Gaussian series or time path is constructed in this section.

4.3.1 Finite Gaussian matrices with both variance powers

Lean full

Lemma 4.3.1 (Scalar power estimates)**.** *For $0 < \theta < 1$ and $u, v \geq 0$,*

$$u^\theta v^{1-\theta} \leq \theta u + (1-\theta)v. \tag{4.3.1}$$

Consequently, if $L > 0$ and $0 \leq q \leq L$ are integers, then for real x, y,

$$|x|^q |y|^{L-q} \leq \frac{q}{L}|x|^L + \frac{L-q}{L}|y|^L. \tag{4.3.2}$$

For nonnegative finite sequences, the usual Hölder inequality holds with exponents m and $m/(m-1)$, $m > 1$. If $Z \geq 0$ has finite expectation F and $0 < r < 1$, then $\mathbb{E}Z^r \leq F^r$.

Proof. We first prove the weighted scalar inequality and its integer-power consequence. We then use normalization to obtain the two remaining bounds.

Step 1. We prove the two scalar inequalities. If $v > 0$, divide (4.3.1) by v and put $t = u/v$. After division, the desired inequality is $t^\theta \leq \theta t + 1 - \theta$. Thus, it suffices to show that the difference of the right and left sides is nonnegative. The function $\theta t + 1 - \theta - t^\theta$ has derivative $\theta(1 - t^{\theta-1})$. Since $\theta - 1 < 0$, this derivative is negative for $0 < t < 1$ and positive for $t > 1$. The function therefore has minimum zero at $t = 1$. Continuity covers $t = 0$; if $v = 0$ the inequality is immediate.

For $0 < q < L$, apply this with $u = |x|^L$, $v = |y|^L$ and $\theta = q/L$. The left side becomes $|x|^q|y|^{L-q}$, and the coefficients on the right are q/L and $(L-q)/L$. The endpoint cases $q = 0, L$ are identities, with the ordinary integer convention $a^0 = 1$.

Step 2. We prove the finite sequence inequality. To prove finite Hölder, divide the two sequences by their respective ℓ^m and $\ell^{m/(m-1)}$ norms. If either norm vanishes, the result is immediate. Apply (4.3.1) with $\theta = 1/m$ to the corresponding normalized powers and sum; the sum of products is at most one.

Step 3. We prove the expectation bound. Finally, $F = 0$ gives $Z = 0$ almost surely. If $F > 0$, apply (4.3.1) to $u = Z/F$, $v = 1$ and $\theta = r$, and integrate. The right side has expectation one. This proves Lemma 4.3.1. □

Lean full

Lemma 4.3.2 (Two Hermitian trace bounds)**.** *Let B, Y be finite Hermitian matrices, $m \geq 2$ an integer, and $L = 2m - 2$. For integers $0 \leq q \leq L$,*

$$\operatorname{Re}\operatorname{Tr}(BY^qBY^{L-q}) \leq \operatorname{Tr}(B^2|Y|^L). \tag{4.3.3}$$

If $D \geq 0$ is Hermitian, then

$$\operatorname{Tr}(D|Y|^{2m-2}) \leq (\operatorname{Tr} D^m)^{1/m}(\operatorname{Tr}|Y|^{2m})^{(m-1)/m}. \tag{4.3.4}$$

Proof. We work in an eigenbasis of Y throughout. The first bound follows by comparing scalar powers; the second follows by finite Hölder.

Step 1. We bound the trace word. Diagonalize Y, with real eigenvalues λ_i, and write b_{ij} for the entries of B in that basis. Hermitian symmetry gives $b_{ji} = \overline{b_{ij}}$. The trace word is the real sum

$$\sum_{i,j} |b_{ij}|^2 \lambda_j^q \lambda_i^{L-q}.$$

To obtain this sum, the ith diagonal entry of the product is summed over the intermediate index j. The diagonal powers of Y contribute λ_j^q and λ_i^{L-q}, and $b_{ij}b_{ji} = |b_{ij}|^2$. All these terms are real. Bound each product by its absolute value and use (4.3.2). After interchanging i, j, the two resulting sums agree because $|b_{ij}| = |b_{ji}|$. Each equals $\sum_{i,j} |b_{ij}|^2 |\lambda_i|^L = \operatorname{Tr}(B^2|Y|^L)$. The two weights sum to one, proving (4.3.3). No commutation of B and Y is used.

Step 2. We bound the trace involving D. In the same basis put $d_i = D_{ii} \geq 0$. If θ_j are the nonnegative eigenvalues of D, a unitary change of basis gives $d_i = \sum_j |U_{ij}|^2 \theta_j$. Both row and column sums of $|U_{ij}|^2$ equal one. Finite convexity therefore yields

$$\sum_i d_i^m \leq \sum_{i,j} |U_{ij}|^2 \theta_j^m = \operatorname{Tr} D^m.$$

The row sums provide the convex weights for each d_i. The column sums then give the equality after summing over i. For completeness, the convexity step follows from $t^m \geq s^m + m s^{m-1}(t-s)$ for $s, t \geq 0$, obtained by differentiating the difference. Average this inequality with s equal to the weighted mean.

Now apply finite Hölder from Lemma 4.3.1 to $\sum_i d_i |\lambda_i|^{2m-2}$. Since $(2m-2)m/(m-1) = 2m$, we obtain the factors in (4.3.4). This proves the claimed inequality, including zero sums. This proves Lemma 4.3.2. □

The estimate below is a finite-dimensional Gaussian noncommutative Khintchine inequality. For its origins in the work of Lust-Piquard and a Gaussian integration-by-parts proof, see Tropp [45, arXiv:1504.05919v2, Proposition 2.3 and Section 7]. We include the proof and Hermitian dilation to fix the normalization and retain both variance operators.

Lean full

Proposition 4.3.3 (Finite Gaussian matrix moment)**.** *Let $A_1, \dots, A_N$ be complex o-by-n matrices, with $o, n, N \geq 1$, and let g_k be independent real standard Gaussians. Put*

$$X = \sum_k g_k A_k, \qquad V_{\mathrm{out}} = \sum_k A_k A_k^*, \qquad V_{\mathrm{in}} = \sum_k A_k^* A_k.$$

For even $p = 2m \geq 2$, with $\|A\|_{S_p}^p = \operatorname{Tr}((A^*A)^m)$,

$$(\mathbb{E}\|X\|_{S_p}^p)^{1/p} \leq \sqrt{p-1} \left(\frac{\operatorname{Tr} V_{\mathrm{out}}^m + \operatorname{Tr} V_{\mathrm{in}}^m}{2} \right)^{1/p} \tag{4.3.5}$$

$$\leq \sqrt{p-1} \max\left(\|V_{\mathrm{out}}^{1/2}\|_{S_p}, \|V_{\mathrm{in}}^{1/2}\|_{S_p} \right). \tag{4.3.6}$$

The constants are independent of o, n, N. The first inequality is an equality at $p = 2$. Empty or zero families give the zero identity.

Proof. We first prove the moment bound for Hermitian matrices by Gaussian integration by parts. We then use Hermitian dilation to treat rectangular matrices and keep track of the factor two.

Step 1. We justify Gaussian integration by parts. First suppose B_k are Hermitian and put $Y = \sum_k g_k B_k$ and $D = \sum_k B_k^2$. All polynomial moments are finite because Gaussian decay dominates every fixed power. Componentwise integration by parts against the product Gaussian density gives $\mathbb{E}[g_k P(g)] = \mathbb{E}[\partial_k P(g)]$, with zero boundary terms. It applies to complex polynomials through their real and imaginary parts; absolute polynomial integrability justifies Fubini.

For a fixed value of the other Gaussian coordinates, the derivative of the density in the kth coordinate is minus that coordinate times the density. Moving this derivative onto P gives the positive sign in the identity. At both ends of the real line, the polynomial times the Gaussian density tends to zero, so no boundary term remains.

Step 2. We estimate the Hermitian moment. For $m \geq 2$, put $F = \mathbb{E}\operatorname{Tr} Y^{2m}$ and $L = 2m - 2$. Write $\operatorname{Tr} Y^{2m} = \sum_k g_k \operatorname{Tr}(B_k Y^{2m-1})$ and differentiate the $2m - 1$ factors in their order. This gives exactly

$$F = \sum_k \sum_{q=0}^{L} \mathbb{E}\operatorname{Tr}(B_k Y^q B_k Y^{L-q}).$$

Here $\partial_k Y = B_k$. In the product rule, q counts the factors Y before the differentiated factor and $L - q$ counts those after it. The leading B_k comes from the expression for the trace before differentiation. This explains both the order of the matrices and the range $0 \leq q \leq L$. The eigenbasis calculation above shows these traces are real. The differentiated polynomial is real by conjugation and trace cyclicity. No derivative of a spectral absolute value or measurable choice of an eigenbasis is needed. The two trace bounds give

$$\begin{aligned} F &\leq (2m-1)\mathbb{E}\operatorname{Tr}(D|Y|^{2m-2}) \\ &\leq (2m-1)(\operatorname{Tr} D^m)^{1/m}\mathbb{E}(\operatorname{Tr}|Y|^{2m})^{(m-1)/m} \\ &\leq (2m-1)(\operatorname{Tr} D^m)^{1/m} F^{(m-1)/m}. \end{aligned}$$

The first inequality bounds each trace word and sums the $2m - 1$ positions of the derivative. The second applies the trace Hölder bound. Here $\operatorname{Tr}|Y|^{2m} = \operatorname{Tr} Y^{2m}$, and the last inequality is the expectation bound in Lemma 4.3.1. The matrix D is positive because each B_k^2 is positive. Also, $\operatorname{Tr}|Y|^{2m}$ is nonnegative and has finite expectation F. Thus, the expectation bound applies with $r = (m-1)/m$, which lies strictly between zero and one. If $F = 0$ the conclusion is immediate. Otherwise divide by its positive fractional power and raise to m to obtain

$$\mathbb{E}\operatorname{Tr} Y^{2m} \leq (2m-1)^m \operatorname{Tr} D^m. \tag{4.3.7}$$

For $m = 1$, independence gives directly $\mathbb{E}\operatorname{Tr} Y^2 = \sum_k \operatorname{Tr} B_k^2 = \operatorname{Tr} D$, proving the same formula as equality.

Step 3. We pass to rectangular matrices. For rectangular A_k, use the Hermitian dilation

$$B_k = \begin{pmatrix} 0 & A_k \\ A_k^* & 0 \end{pmatrix}, \qquad Y = \begin{pmatrix} 0 & X \\ X^* & 0 \end{pmatrix}, \qquad D = \operatorname{diag}(V_{\mathrm{out}}, V_{\mathrm{in}}).$$

Each B_k is Hermitian. Squaring it gives diagonal blocks $A_k A_k^*$ and $A_k^* A_k$, so its sum of squares is exactly the displayed D. Likewise, Y^2 has diagonal blocks XX^* and X^*X. Its mth power therefore has blocks $(XX^*)^m$ and $(X^*X)^m$. Finite entrywise summation proves $\operatorname{Tr}(UV) = \operatorname{Tr}(VU)$ for compatible rectangular matrices. Since $(XX^*)^m = X(X^*X)^{m-1}X^*$, it follows that

$$\operatorname{Tr} Y^{2m} = 2\operatorname{Tr}((X^*X)^m), \qquad \operatorname{Tr} D^m = \operatorname{Tr} V_{\mathrm{out}}^m + \operatorname{Tr} V_{\mathrm{in}}^m.$$

Substitute in (4.3.7), divide by two and take the pth root. This proves (4.3.5). For positive V, spectral diagonalization gives $\|V^{1/2}\|_{S_p}^p = \operatorname{Tr} V^m$, and the average of two nonnegative numbers is bounded by their maximum. At $p = 2$, $\mathbb{E}\operatorname{Tr} X^*X = \operatorname{Tr} V_{\mathrm{in}} = \operatorname{Tr} V_{\mathrm{out}}$, proving the claimed equality. This proves Proposition 4.3.3. □

Both variance directions are needed: the row-matrix example in No-go 23 rules out a dimension-independent estimate that keeps only one of them.

Lean full

Remark 4.3.4 (Both variance directions are necessary)**.** Let $n = 16$ and $A_k = e_k^{\mathsf{T}}$ be the coordinate row matrices. The only nonzero singular value of X is $(\sum_k g_k^2)^{1/2}$. Gaussian integration by parts gives $\mathbb{E}g^2 = 1$, $\mathbb{E}g^4 = 3$, and hence

$$\mathbb{E}\|X\|_{S_4}^4 = 3n + n(n-1) = n(n+2) = 288.$$

Here $V_{\mathrm{out}} = n$ and $V_{\mathrm{in}} = I_n$. Keeping only the input variance in (4.3.6) would give fourth power $9\operatorname{Tr} I_n^2 = 144$, which is false. Transposing the family refutes the corresponding output-only bound. The average and maximum bounds have fourth powers 1224 and 2304, respectively. This finite example asserts nothing about a specialized wave estimate.

4.3.2 Whole-space cutoffs through an auxiliary periodic space

Use the unitary Fourier transform with $c_d = (2\pi)^{-d/2}$ and $\Lambda = (1-\Delta)^{1/2}$. For real r, the norm on $H^r(\mathbb{R}^d)$ is $\|\langle\xi\rangle^r \widehat{u}\|_2$. The deterministic cutoff arguments allow any smoothing order $\gamma > 0$. Fix real σ and a real compact smooth χ. Singular values s_j, $j \geq 1$, are counted with multiplicity, with zeros appended when necessary. For compact K, put $\|K\|_{S_p}^p = \sum_j s_j(K)^p$.

Lemma 4.3.5 (Cutoff factorization)**.** *Choose a cube $Q_L = (-L/2, L/2)^d$ containing* $\operatorname{supp}\chi$ *in its interior, and a real $\psi \in C_c^\infty(Q_L)$ equal to one near* $\operatorname{supp}\chi$*. On the auxiliary torus $\mathbb{T}_L$ use Lebesgue measure and the orthonormal basis*

$$e_k(x) = L^{-d/2} e^{i\kappa_k \cdot x}, \qquad \kappa_k = 2\pi k/L, \qquad k \in \mathbb{Z}^d,$$

with $\|v\|^2_{H^r(\mathbb{T}_L)} = \sum_k \langle \kappa_k \rangle^{2r} |v_k|^2$. *Periodization of* ψu *and multiplication of a periodic function by* χ *extend to bounded maps*

$$\mathcal{P}_\psi : H^r(\mathbb{R}^d) \to H^r(\mathbb{T}_L), \qquad \mathcal{E}_\chi : H^r(\mathbb{T}_L) \to H^r(\mathbb{R}^d) \tag{4.3.8}$$

for every real r. *If* $\mathcal{I}_\gamma$ *denotes the identity inclusion from* $H^{\sigma+\gamma}(\mathbb{T}_L)$ *to* $H^\sigma(\mathbb{T}_L)$, *then*

$$\mathcal{E}_\chi \mathcal{I}_\gamma \mathcal{P}_\psi u = \chi u, \qquad u \in H^{\sigma+\gamma}(\mathbb{R}^d). \tag{4.3.9}$$

Proof. We have to show two things. First, the two maps in (4.3.8) are bounded for every real r. Second, the identity (4.3.9) holds on $H^{\sigma+\gamma}(\mathbb{R}^d)$. In both cases we argue first on a dense class, namely Schwartz functions on $\mathbb{R}^d$ and finite torus polynomials on $\mathbb{T}_L$, and then pass to the whole space by density. The proof has five steps. Step 1 collects three elementary facts. Step 2 recalls the mixed Schur bound. Step 3 writes the two maps as kernel operators in the Fourier variables and bounds them. Step 4 extends the maps by density. Step 5 proves the identity (4.3.9).

Step 1. We collect three elementary facts. The first fact compares the weights at two points. For $x, y \in \mathbb{R}^d$ and real r, the elementary inequality $\langle x \rangle \le \sqrt{2} \langle y \rangle \langle x - y \rangle$ gives

$$\left(\frac{\langle x \rangle}{\langle y \rangle} \right)^r \le 2^{|r|/2} \langle x - y \rangle^{|r|}. \tag{4.3.10}$$

For $r \ge 0$ we raise the elementary inequality to the power r. For negative r, we interchange x, y before raising to the power $|r|$.

The second fact is that integration by parts gives rapid decay of the Fourier transform of every compact smooth cutoff.

The third fact is a lattice sum that is bounded uniformly in its shift. For any lattice spacing $a > 0$ and $N > d$,

$$\sup_y \sum_{k \in \mathbb{Z}^d} \langle y - ak \rangle^{-N} < \infty. \tag{4.3.11}$$

Indeed, the sum does not change when y is shifted by a lattice vector. We translate y into a centered lattice cell, where $|y| \le a\sqrt{d}/2$. For $|k| \ge \sqrt{d}$ the triangle inequality gives $|y - ak| \ge a|k| - |y|$, and we have $|y - ak| \ge a|k|/2$. We treat the terms with $|k| < \sqrt{d}$ and the tail $|k| \ge \sqrt{d}$ separately. The remaining terms, those with $|k| < \sqrt{d}$, are finite: each is at most one, and their number depends only on d. The tail converges by dyadic lattice counting, since there are at most $C_d 2^{jd}$ lattice points in the jth shell $2^j \le |k| < 2^{j+1}$ in k. More precisely, for $|k| \ge \sqrt{d}$, the preceding inequality gives

$$\langle y - ak \rangle^{-N} \le \max(1, 2/a)^N \langle k \rangle^{-N}.$$

Here we use $\langle y - ak \rangle \ge \langle ak/2 \rangle \ge \min(1, a/2) \langle k \rangle$. The comparison-series terms $\langle k \rangle^{-N}$ are bounded by 2^{-jN} on each dyadic k-shell. Hence, the comparison series is bounded by the geometric sum $\sum_{j \ge 0} C_d 2^{j(d-N)}$, which converges because $N > d$. Thus, the resulting bound carries constants depending on a, d, N, as does (4.3.11).

Step 2. We recall the mixed Schur bound. We use the mixed Schur bound for a kernel whose absolute row and column integrals are bounded by M_1, M_2. It states that the

squared operator norm of the kernel operator is at most $M_1 M_2$. To prove it, we apply the weighted Cauchy–Schwarz inequality at each output point and then Tonelli's theorem. The same proof works with counting measure on one side and Lebesgue measure on the other. For counting measure inputs, use finitely supported sequences; for Lebesgue measure inputs, use smooth compactly supported functions. The estimate extends to the corresponding L^2 spaces by density. For the kernels below, the same Cauchy–Schwarz estimate on truncated inputs identifies the extension with the stated integral or sum.

Step 3. We prove the bounds in (4.3.8). We write each map as a kernel operator between the weighted Fourier variables and apply Step 2. We begin with $\mathcal{P}_\psi$. For Schwartz u, the kth coefficient of its cutoff periodization is

$$(\mathcal{P}_\psi u)_k = L^{-d/2} \int \psi(x) u(x) e^{-i\kappa_k \cdot x} \, \mathrm{d}x = L^{-d/2} \int \widehat{\psi}(\kappa_k - \xi) \widehat{u}(\xi) \, \mathrm{d}\xi.$$

In the second equality, the c_d from Fourier inversion cancels the c_d^{-1} in the ordinary Fourier integral of ψ. The norms of $H^r(\mathbb{R}^d)$ and $H^r(\mathbb{T}_L)$ carry the weights $\langle \xi \rangle^r$ and $\langle \kappa_k \rangle^r$. After weighting, that is, as a map from $\langle \xi \rangle^r \widehat{u}(\xi)$ to $\langle \kappa_k \rangle^r (\mathcal{P}_\psi u)_k$, its exact kernel is

$$L^{-d/2} \left(\frac{\langle \kappa_k \rangle}{\langle \xi \rangle} \right)^r \widehat{\psi}(\kappa_k - \xi).$$

We turn to $\mathcal{E}_\chi$. For a finite torus polynomial v, the normalized Fourier kernel of $\mathcal{E}_\chi v$ is

$$L^{-d/2} \left(\frac{\langle \xi \rangle}{\langle \kappa_k \rangle} \right)^r \widehat{\chi}(\xi - \kappa_k).$$

There is no additional c_d in this kernel.

We now bound both kernels. By (4.3.10), each is bounded in absolute value by a rapidly decreasing function of its frequency difference, times a fixed constant. For the first kernel this bound is

$$L^{-d/2} 2^{|r|/2} \langle \kappa_k - \xi \rangle^{|r|} \left| \widehat{\psi}(\kappa_k - \xi) \right|,$$

and for the second kernel it is the same expression with $\widehat{\chi}(\xi - \kappa_k)$ in place of $\widehat{\psi}(\kappa_k - \xi)$. These functions of the frequency difference decrease rapidly by the second fact of Step 1. One Schur quantity is its L^1 integral and the other a uniformly translated lattice sum, bounded by (4.3.11). Indeed, the integral over ξ at fixed k is the L^1 integral of the bounding function and does not depend on k. The sum over k at fixed ξ is a lattice sum with spacing $a = 2\pi/L$ and shift $y = \xi$. We bound the rapidly decreasing function by a constant times $\langle \cdot \rangle^{-N}$ for some $N > d$, and (4.3.11) bounds the sum uniformly in ξ. This proves (4.3.8), including negative r.

Step 4. We extend the two maps by density. We check that the two classes used in Step 3 are dense. Smooth compact approximation in weighted Fourier L^2 proves Schwartz density on $\mathbb{R}^d$. Weighted sequence truncation proves polynomial density on the torus. Hence, these maps extend uniquely. Their distributional meanings follow by testing against

compact smooth functions and density: each periodic coefficient pairs the distribution with a compact smooth test. No point sampling of a rough Fourier function is used. The same full-Lebesgue Schur argument, with Lebesgue measure on both sides, proves smooth compact multiplication bounded on every whole-space H^r.

Step 5. We prove the identity (4.3.9). We first prove the identity for Schwartz u. For Schwartz u, the periodic Fourier series of ψu converges smoothly on the cube. Its coefficients are the numbers $(\mathcal{P}_\psi u)_k$ of Step 3, and its partial sums are finite torus polynomials, on which $\mathcal{E}_\chi$ is multiplication by χ. Rapid decay of the Fourier coefficients gives convergence of these partial sums in $H^{\sigma+\gamma}(\mathbb{T}_L)$, hence also in $H^\sigma(\mathbb{T}_L)$. Boundedness of $\mathcal{E}_\chi$ gives convergence of their images to $\mathcal{E}_\chi \mathcal{I}_\gamma \mathcal{P}_\psi u$ in $H^\sigma(\mathbb{R}^d)$. Their smooth convergence on the support of χ also gives convergence of the products with χ to $\chi\psi u$ as distributions. Since Sobolev convergence implies distributional convergence for every real σ, these two limits agree. Since $\chi\psi = \chi$ and χ is supported strictly inside the cube, multiplying this series by χ recovers χu with no alias term. Since $\mathcal{I}_\gamma$ is the identity inclusion, this is (4.3.9) for Schwartz u.

It remains to pass to all of $H^{\sigma+\gamma}(\mathbb{R}^d)$. Both sides of (4.3.9) are bounded from $H^{\sigma+\gamma}(\mathbb{R}^d)$ to $H^\sigma(\mathbb{R}^d)$, using the just-proved maps, the inclusion and smooth multiplication. In detail, the left side uses $\mathcal{P}_\psi$ with $r = \sigma + \gamma$, the inclusion $\mathcal{I}_\gamma$, which is bounded because $\gamma > 0$, and $\mathcal{E}_\chi$ with $r = \sigma$. The right side uses the multiplication by χ of Step 4 with $r = \sigma$, together with the inclusion of $H^{\sigma+\gamma}(\mathbb{R}^d)$ in $H^\sigma(\mathbb{R}^d)$. Since Schwartz functions are dense in $H^{\sigma+\gamma}(\mathbb{R}^d)$ by Step 4, density proves (4.3.9) on that full domain. This proves Lemma 4.3.5. □

Proposition 4.3.6 (Whole-space cutoff singular values)**.** *For real σ and $\gamma > 0$, the initially Schwartz-defined operator $K_{\chi,\sigma,\gamma} = \Lambda^\sigma \chi \Lambda^{-\sigma-\gamma}$ extends uniquely to a compact operator on $L^2(\mathbb{R}^d)$, and*

$$s_j(K_{\chi,\sigma,\gamma}) \le C_{\chi,\sigma,\gamma,d} j^{-\gamma/d}, \qquad j \ge 1. \tag{4.3.12}$$

Consequently, $K_{\chi,\sigma,\gamma} \in S_p$ whenever $p \ge 1$ and $p\gamma > d$.

Proof. We use the cutoff factorization to approximate the operator by finite-rank operators. Their ranks and approximation errors will give the singular-value bound, which we then sum to obtain Schatten membership.

Step 1. We construct finite-rank approximations. The zero cutoff is immediate. Fix one cube and cutoff pair L, ψ as in Lemma 4.3.5. Its recovery identity gives

$$K_{\chi,\sigma,\gamma} = \Lambda^\sigma \mathcal{E}_\chi \mathcal{I}_\gamma \mathcal{P}_\psi \Lambda^{-\sigma-\gamma}.$$

The cutoff maps are bounded by the preceding lemma. Thus, the only factor we need to approximate is the torus inclusion. The rightmost Bessel map takes $L^2(\mathbb{R}^d)$ unitarily to $H^{\sigma+\gamma}(\mathbb{R}^d)$, and the leftmost takes $H^\sigma(\mathbb{R}^d)$ unitarily to $L^2(\mathbb{R}^d)$. The bounded factorization agrees with the original operator on Schwartz functions. Their density gives the unique bounded extension. In the weighted torus coordinates, $\mathcal{I}_\gamma$ is diagonal with entries $\langle \kappa_k \rangle^{-\gamma}$. Let Q_n retain $|k|_\infty \le n$. Its rank is $(2n+1)^d$, and

$$\|(1 - Q_n)\mathcal{I}_\gamma\| \le [1 + (2\pi/L)^2 (n+1)^2]^{-\gamma/2} \longrightarrow 0.$$

The weighted input coefficient has weight $\langle\kappa_k\rangle^{\sigma+\gamma}$ and the output coefficient has weight $\langle\kappa_k\rangle^{\sigma}$. The output weight divided by the input weight is $\langle\kappa_k\rangle^{-\gamma}$. Outside the retained cube, at least one integer coordinate has absolute value at least $n+1$, so $|\kappa_k| \geq (2\pi/L)(n+1)$. Taking the supremum of the remaining diagonal entries proves the norm bound. Replacing the inclusion by $Q_n\mathcal{I}_\gamma$ gives finite-rank K_n converging in norm to $K_{\chi,\sigma,\gamma}$. This proves compactness: finite-dimensional images have finite nets of each positive radius, and norm approximation transfers those nets to the limiting image of the unit ball.

Step 2. We compare approximation rank with singular-value index. Put

$$M = \|\mathcal{E}_\chi : H^\sigma(\mathbb{T}_L) \to H^\sigma(\mathbb{R}^d)\|\|\mathcal{P}_\psi : H^{\sigma+\gamma}(\mathbb{R}^d) \to H^{\sigma+\gamma}(\mathbb{T}_L)\|.$$

The outer Bessel maps are unitary. For $j \geq 3^d$, choose $n = \lfloor j^{1/d}/4 \rfloor$. Then

$$(2n+1)^d \leq (j^{1/d}/2+1)^d < j, \qquad \|K - K_n\| \leq M(2L/\pi)^\gamma j^{-\gamma/d}.$$

The strict rank inequality lets us use K_n to bound the jth singular value. The finitely many smaller indices will be treated by the operator norm. The second estimate follows from $n+1 > j^{1/d}/4$. For a compact operator, every rank less than j approximation F satisfies $s_j(K) \leq \|K - F\|$: the span of the first j right singular vectors contains a unit vector in $\ker F$, on which $\|K\cdot\| \geq s_j(K)$. If $s_j(K) = 0$ the inequality is immediate. For $j < 3^d$ use $s_j(K) \leq \|K\| \leq M$. Thus, one may take

$$C_{\chi,\sigma,\gamma,d} = M\max(3^\gamma, (2L/\pi)^\gamma).$$

Step 3. We sum the singular-value bound. Finally, $\sum_j j^{-p\gamma/d}$ converges for $p\gamma > d$. Raise the singular-value bound to p and sum over j. The resulting series bounds $\sum_j s_j(K)^p$, which is the defining Schatten norm power. This proves Proposition 4.3.6. □

No uniform support-radius constant or endpoint necessity is asserted in Proposition 4.3.6. The periodic inclusion was only a factor of the recovered whole-space operator.

4.3.3 Balanced adjoints and localized variance envelopes

For $E = H^{1/2}(\mathbb{R}^d) \times H^{-1/2}(\mathbb{R}^d)$ use the physical unitary coordinates

$$J_0(u,v) = (\Lambda^{1/2}u, \Lambda^{-1/2}v), \qquad H = L^2(\mathbb{R}^d;\mathbb{C}^2).$$

The frequency map J in Section 4.2 is $(\mathcal{F}\oplus\mathcal{F})J_0$. Let D_χ multiply both phase entries and define

$$P_\chi = J_0 D_\chi J_0^{-1}, \qquad D_\gamma = \operatorname{diag}(\Lambda^{-\gamma}, \Lambda^{-\gamma}), \tag{4.3.13}$$

$$K_{\text{out}} = P_\chi D_\gamma, \qquad K_{\text{in}} = P_\chi^* D_\gamma. \tag{4.3.14}$$

Proposition 4.3.7 (Both compact envelopes)**.** *The operator P_χ is bounded. For the unitary swap $U(v,w) = (w,v)$,*

$$P_\chi^* = UP_\chi U, \qquad K_{\text{in}} = UK_{\text{out}}U.$$

Both factors are compact and have equal S_p norms for $p \geq 1$, $p\gamma > d$. For $p \geq 2$, $p\gamma > d$, the positive compact operators

$$B_{\mathrm{out}} = P_\chi D_\gamma^2 P_\chi^* = K_{\mathrm{out}} K_{\mathrm{out}}^*, \qquad B_{\mathrm{in}} = P_\chi^* D_\gamma^2 P_\chi = K_{\mathrm{in}} K_{\mathrm{in}}^*$$

satisfy

$$\operatorname{Tr} B_{\mathrm{out}}^{p/2} = \operatorname{Tr} B_{\mathrm{in}}^{p/2} = \|K_{\mathrm{out}}\|_{S_p}^p. \tag{4.3.15}$$

Proof. We first identify the adjoint of the balanced cutoff. The swap identity then reduces both factors to the same singular values, and these values give the trace identities.

Step 1. We identify the adjoint. Put $A_\sigma = \Lambda^\sigma \chi \Lambda^{-\sigma}$. The full-Lebesgue Schur argument in Lemma 4.3.5 shows boundedness for every real σ. On Schwartz functions, self-adjointness of real multiplication and of the Bessel powers gives $A_\sigma^* = A_{-\sigma}$. Density and boundedness extend this to the Hilbert adjoints. No evenness of χ is needed. Thus,

$$P_\chi = \operatorname{diag}(A_{1/2}, A_{-1/2}), \qquad P_\chi^* = \operatorname{diag}(A_{-1/2}, A_{1/2}) = U P_\chi U.$$

Step 2. We obtain compactness and Schatten membership. The swap commutes with D_γ, giving the claimed factor identity. The blocks of K_{out} are $K_{\chi,1/2,\gamma}$ and $K_{\chi,-1/2,\gamma}$. Proposition 4.3.6 gives compactness and S_p membership. The singular values of their direct sum form the multiset union, so

$$\|K_{\mathrm{out}}\|_{S_p}^p = \|K_{\chi,1/2,\gamma}\|_{S_p}^p + \|K_{\chi,-1/2,\gamma}\|_{S_p}^p.$$

For a block diagonal operator, its adjoint times itself is block diagonal as well. The positive eigenvalues are therefore those of the two blocks, counted with multiplicity. Taking their square roots gives the asserted multiset union of singular values. Unitary conjugation preserves them.

Step 3. We compute the two traces. The products $K_{\mathrm{out}} K_{\mathrm{out}}^*$ and $K_{\mathrm{in}} K_{\mathrm{in}}^*$ are positive and compact. Their positive eigenvalues are the squared singular values of the corresponding factors. Finally, the positive eigenvalues of KK^* and K^*K agree with multiplicity: on an eigenspace with eigenvalue $\lambda > 0$, the maps $K/\sqrt{\lambda}$ and $K^*/\sqrt{\lambda}$ are inverse isometries. Indeed, K takes the λ-eigenspace of K^*K into that of KK^*, because applying KK^* after K equals applying K after K^*K. On this eigenspace, K multiplies squared norms by λ. The corresponding statement for K^* gives the inverse map after division by $\sqrt{\lambda}$.

Zero eigenvalues contribute nothing to the trace. Raising each squared singular value to $p/2$ gives its pth power. The sum is finite by the Schatten membership already proved, and the two factors have the same singular values. Thus, summing gives (4.3.15). This proves Proposition 4.3.7. □

We use the usual positive square root of a bounded positive operator and the spectral decomposition of compact positive operators. The needed order argument is recorded explicitly.

Lemma 4.3.8 (Compact positive order and trace)**.** *If A, B are bounded self-adjoint operators with $0 \le A \le B$ and B compact positive, then A is compact and its ordered eigenvalues satisfy $\lambda_j(A) \le \lambda_j(B)$, including zero padding. Consequently, for $t \ge 1$ with finite $\operatorname{Tr} B^t$,*

$$\operatorname{Tr} A^t \le \operatorname{Tr} B^t. \tag{4.3.16}$$

Proof. We first prove compactness using the square root of A. Once compactness is known, we compare Rayleigh quotients to order the eigenvalues, and then sum their powers.

Step 1. We prove compactness. Let Q_n be finite spectral projections of B whose tails tend to zero in norm. Then

$$\|(1-Q_n)A^{1/2}\|^2 = \|(1-Q_n)A(1-Q_n)\| \le \|(1-Q_n)B(1-Q_n)\| \longrightarrow 0.$$

The equality is the Hilbert-space identity that the squared norm of an operator equals the norm of its product with its adjoint. The inequality follows by applying $A \le B$ between the two projections. These products are positive, and order between positive operators implies order of their norms. The finite-rank approximants here are $Q_n A^{1/2}$; the displayed norm is precisely their error. Thus, $A^{1/2}$ is a norm limit of finite-rank operators and is compact, as is A, since $A = A^{1/2}A^{1/2}$ is a product of a compact and a bounded operator.

Step 2. We compare the eigenvalues and traces. For compact positive operators, the max-min formula for λ_j follows in an eigenbasis: the span of the first j eigenvectors gives the lower bound for the supremum over j-dimensional subspaces of their minimum Rayleigh quotient, while every such subspace meets the orthogonal complement of the first $j-1$ eigenvectors, giving the upper bound. Compare the Rayleigh quotients of A and B to obtain the eigenvalue inequality. On each fixed j-dimensional subspace, every unit vector has its Rayleigh quotient for A bounded by that for B. Taking the infimum within that subspace, and then the supremum over such subspaces, preserves the inequality. The eigenbasis argument also covers zero eigenvalues: if fewer than j positive eigenvalues exist, every such subspace meets their orthogonal complement and the infimum there is zero.

Since taking a positive scalar power preserves order, the eigenvalue comparison gives $\lambda_j(A)^t \le \lambda_j(B)^t$. Sum first over finitely many indices and then pass to the increasing limit. The finite trace of B^t bounds that limit. This proves (4.3.16). No inequality $A^t \le B^t$ is asserted. This proves Lemma 4.3.8. □

Proposition 4.3.9 (Localized finite variance bounds)**.** *Suppose finitely many bounded operators Z_ℓ on H satisfy*

$$P_\chi Z_\ell = Z_\ell = Z_\ell P_\chi, \qquad V_{\text{out}} := \sum_\ell Z_\ell Z_\ell^* \le C D_\gamma^2, \qquad V_{\text{in}} := \sum_\ell Z_\ell^* Z_\ell \le C D_\gamma^2, \tag{4.3.17}$$

with $C \ge 0$. If $p \ge 2$ and $p\gamma > d$, every Z_ℓ is compact in S_p, the two variances are

compact in $S_{p/2}$, and

$$V_{\mathrm{out}} \le CB_{\mathrm{out}}, \qquad V_{\mathrm{in}} \le CB_{\mathrm{in}}, \tag{4.3.18}$$

$$\operatorname{Tr} V_{\mathrm{out}}^{p/2}, \quad \operatorname{Tr} V_{\mathrm{in}}^{p/2} \le C^{p/2}\|K_{\mathrm{out}}\|_{S_p}^{p}. \tag{4.3.19}$$

Proof. We first use the localization identities to replace the two variance bounds by compact envelopes. We then apply the same positive-order argument to each individual operator.

Step 1. We bound the two variances. Left localization gives $V_{\mathrm{out}} = P_\chi V_{\mathrm{out}} P_\chi^*$. Apply positive congruence to the output bound in (4.3.17) to get $V_{\mathrm{out}} \le C P_\chi D_\gamma^2 P_\chi^* = CB_{\mathrm{out}}$. Right localization similarly gives $V_{\mathrm{in}} = P_\chi^* V_{\mathrm{in}} P_\chi \le CB_{\mathrm{in}}$. Positive congruence preserves order: one tests the original inequality on the adjoint of the multiplying operator applied to each vector. The exponent $t = p/2$ is at least one, and $p\gamma > d$ makes the envelope trace powers finite; scaling an envelope by C multiplies its trace power by $C^{p/2}$. Proposition 4.3.7 and Lemma 4.3.8 prove compactness and the two trace bounds with $t = p/2$. If $C = 0$, both variances and every Z_ℓ vanish, so all assertions are immediate.

Step 2. We obtain compactness of each summand. Every summand of the output variance is positive. Subtracting one summand leaves a positive sum, which gives the order comparison needed below. For each ℓ, $Z_\ell Z_\ell^* \le V_{\mathrm{out}}$ is compact by the same lemma. Its finite spectral projections Q_n give $\|(1-Q_n)Z_\ell\|^2 = \|(1-Q_n)Z_\ell Z_\ell^*(1-Q_n)\| \to 0$. Hence, Z_ℓ is compact. Its singular values squared are the nonzero eigenvalues of $Z_\ell Z_\ell^*$. The approximating operators are $Q_n Z_\ell$, whose ranges are finite dimensional. The displayed error tends to zero, proving their norm convergence. The positive-order lemma also bounds each eigenvalue of $Z_\ell Z_\ell^*$ by the corresponding one of V_{out}. Taking $p/2$ powers converts the former to pth powers of singular values. Comparing with V_{out} and summing proves $Z_\ell \in S_p$ with $\|Z_\ell\|_{S_p}^p \le \operatorname{Tr} V_{\mathrm{out}}^{p/2}$. This proves Proposition 4.3.9. □

The two localization identities are hypotheses here; a noise coefficient family has not yet been shown to satisfy them. In particular, P_χ is not assumed self-adjoint or a projection.

Corollary 4.3.10 (Finite Gaussian operators)**.** *Under (4.3.17), let g_ℓ be independent real standard Gaussians. For even $p \ge 2$ with $p\gamma > d$, the finite sum $X = \sum_\ell g_\ell Z_\ell$ satisfies*

$$(\mathbb{E}\|X\|_{S_p}^p)^{1/p} \le \sqrt{p-1}\sqrt{C}\|K_{\mathrm{out}}\|_{S_p}. \tag{4.3.20}$$

Its extended norm is measurable, with finite expectation as displayed.

Proof. We compress the operators to finite matrices, where the Gaussian moment bound is already available. We then pass to the original operators using convergence of singular values and two applications of Fatou's lemma.

Step 1. We bound the variances of the compressions. Choose finite-rank orthogonal projections Π_n from a countable orthonormal basis of H, with $\Pi_n \to I$ strongly. Put

$Z_{\ell,n} = \Pi_n Z_\ell \Pi_n$ and $X_n = \sum_\ell g_\ell Z_{\ell,n}$, viewed as matrices on $\operatorname{ran}\Pi_n$. Their output variance satisfies

$$\sum_\ell \Pi_n Z_\ell \Pi_n Z_\ell^* \Pi_n \le \Pi_n V_{\mathrm{out}} \Pi_n,$$

since the difference is $\sum_\ell \Pi_n Z_\ell (1-\Pi_n) Z_\ell^* \Pi_n \ge 0$. Each term in this difference is positive: its quadratic form is the squared norm of $(1-\Pi_n)Z_\ell^*\Pi_n$ applied to the test vector. Thus, inserting the middle projection can only decrease the variance. Lemma 4.3.8, with $t = p/2$, first bounds each compressed variance trace by the corresponding trace of $\Pi_n V \Pi_n$; the compression comparison below and (4.3.19) then bound it by $C^{p/2}\|K_{\mathrm{out}}\|_{S_p}^p$. The input inequality is identical with adjoints interchanged. Compact max-min also gives $\lambda_j(\Pi_n V \Pi_n) \le \lambda_j(V)$ for positive compact V, since Rayleigh subspaces inside $\operatorname{ran}\Pi_n$ form a subset of all subspaces. Thus, both variance trace powers of these matrices are bounded by $C^{p/2}\|K_{\mathrm{out}}\|_{S_p}^p$.

Step 2. We apply the finite matrix estimate. Proposition 4.3.3 applies to these finite complex matrices, the same real independent Gaussians and the even p. Taking the average of the two already bounded trace powers gives

$$\mathbb{E}\|X_n\|_{S_p}^p \le (p-1)^{p/2} C^{p/2} \|K_{\mathrm{out}}\|_{S_p}^p. \tag{4.3.21}$$

No factor two is added by this average.

Step 3. We pass to the limit and check measurability. This passage is pointwise in the Gaussian coordinates until the final application of Fatou in probability. For each Gaussian coordinate vector, X is a finite sum of compact operators. Strong convergence of Π_n implies $\Pi_n X \Pi_n \to X$ in operator norm: approximate X by a finite-rank F, use uniform strong convergence on the finite-dimensional ranges of F and F^*, and control the remainder using $\|\Pi_n\| \le 1$.

Singular values are norm-Lipschitz. Indeed, their formula

$$s_j(A) = \inf_{\dim L < j} \sup_{v \in L^\perp,\ \|v\|=1} \|Av\|$$

follows by choosing L to be the span of the first $j-1$ right singular vectors for the upper bound. For the lower bound, if $s_j(A) > 0$, the span of the first j right singular vectors contains a unit vector perpendicular to any L of dimension less than j. On that vector, the norm of A is at least $s_j(A)$. If $s_j(A) = 0$, the lower bound is immediate. Apply the triangle inequality inside the supremum in this formula, then take the infimum over L. This gives $s_j(A) \le s_j(B) + \|A - B\|$, and the reverse bound by interchanging A, B. Hence, $s_j(X_n) \to s_j(X)$ for each j. Fatou for the nonnegative singular-value sum gives $\|X\|_{S_p}^p \le \liminf_n \|X_n\|_{S_p}^p$, allowing extended infinity. These variables are measurable as follows. Each Z_ℓ is bounded, and there are finitely many Gaussian coordinates, so changing those coordinates changes X continuously in operator norm. The Lipschitz bound makes each singular value continuous in these coordinates. Partial sums of their nonnegative pth powers are measurable, and their increasing limit is measurable, including when it is infinite. Fatou in probability and (4.3.21) prove the bound and almost-sure finiteness. No S_p-Bochner convergence is assumed. This proves Corollary 4.3.10. □

4.3.4 A nonzero witness and the need for a compact cutoff

Proposition 4.3.9 and Corollary 4.3.10 assume (4.3.17). We check that these hypotheses admit a nonzero operator, and then test what is lost without the compact cutoff.

Proposition 4.3.11 (Whole-space cutoff tests)**.** *If χ equals one on a nonempty open set, there is a nonzero rank-one operator satisfying (4.3.17) with a finite common C. On the other hand, $\Lambda^{-\gamma}$ on $L^2(\mathbb{R}^d)$ is not compact for any $\gamma > 0$.*

Proof. We treat the two assertions separately. A rank-one operator built from test functions supported on the plateau provides the witness. Translates of a fixed function show why smoothing alone does not give compactness on the whole space.

Step 1. We construct the localized witness. Choose nonzero real $v, f \in C_c^\infty$ supported inside the plateau, and put $\widetilde{v} = (\Lambda^{1/2}v, 0)$ and $\widetilde{w} = (\Lambda^{-1/2}f, 0)$. Both are Schwartz. The block formulas give $P_\chi \widetilde{v} = \widetilde{v}$ and $P_\chi^* \widetilde{w} = \widetilde{w}$. Therefore, $Zx = \langle x, \widetilde{w}\rangle \widetilde{v}$ satisfies $P_\chi Z = Z = Z P_\chi$. Its two variances are $\|\widetilde{w}\|^2 \widetilde{v} \otimes \widetilde{v}^*$ and $\|\widetilde{v}\|^2 \widetilde{w} \otimes \widetilde{w}^*$. For any Schwartz a and any $x \in H$,

$$|\langle x, a\rangle| = |\langle D_\gamma x, D_\gamma^{-1} a\rangle| \le \|D_\gamma x\| \|D_\gamma^{-1} a\|.$$

The last inequality is Cauchy–Schwarz. The preceding equality uses self-adjointness of the multiplier and its inverse on Schwartz functions. The inverse multiplier is applied only to Schwartz a, so it belongs to H. Apply the inequality with $a = \widetilde{v}, \widetilde{w}$ to obtain the two variance bounds with

$$C = \max\left(\|\widetilde{w}\|^2 \|D_\gamma^{-1}\widetilde{v}\|^2, \|\widetilde{v}\|^2 \|D_\gamma^{-1}\widetilde{w}\|^2\right) < \infty.$$

This witness uses a plateau; no nonzero family is inferred for every compact cutoff or identified with a source family.

Step 2. We test compactness by translation. For noncompactness, take f with nonzero Gaussian Fourier transform. Then $g = \Lambda^{-\gamma} f$ is a nonzero Schwartz function. The images of translates of f are the same translates of g. With $T_h g(x) = g(x - h)$, Plancherel gives

$$\langle T_h g, g\rangle = \int e^{-i\xi\cdot h} |\widehat{g}(\xi)|^2 \, \mathrm{d}\xi = c_d^{-1} \widehat{|\widehat{g}|^2}(h).$$

The Fourier multiplier commutes with translations, so the input sequence and its image have the same translation parameters. This tends to zero because $|\widehat{g}|^2$ is Schwartz. Choose a large spacing so that any two distinct translates in the resulting sequence have image distance at least $\|g\|$. The input norms are identical, but the images have no Cauchy subsequence. This disproves compactness. This proves Proposition 4.3.11. □

The translation obstruction is restated in No-go 24: frequency decay alone does not replace compact spatial localization.

Thus, the choice $\chi = 1$ cannot be substituted into the compact-cutoff argument. No necessity at the Schatten endpoint $p\gamma = d$ is asserted. The results concern finite matrices and conditional finite operator sums. Coefficient localization, compact variance tails, an infinite Gaussian series and time regularity are proved in Section 5.1; source and Young identification are proved in Sections 5.2–6.2. They are not consequences of the finite comparison alone.

What we now have. Variance estimates for an operator and for its adjoint (Proposition 4.2.5), and bounds for finite Gaussian operator sums (Corollary 4.3.10). The next chapter builds the random operator path itself.

Chapter 5

The original noise and operator paths

The covariance estimates must now produce something random: an operator path driven by the noise of the original equation. Another Gaussian field with a convenient covariance would not do, because the later comparisons are made on the original noise (Figure 5.1).

The wave phase is a displacement in $H^{1/2}$ and a velocity in $H^{-1/2}$. For a fixed spatial mask and a finite time horizon, Section 5.1 builds the integrated interaction path on this space. Proposition 5.1.1 states its regularity and how it is approximated. Section 5.2 matches the regularized sources to the original noise and proves convergence in the path norm. The construction keeps the joint noise information that Gaussian changes of law will need.

The chapter uses the two variance directions and the compact Gaussian estimates of Chapter 4. On a first reading, keep Propositions 5.1.1 and 5.2.2 and let the proofs wait. The dependence of the operator-path bounds on the mask radius is tracked in Chapter 9. Episode ▶ 5 of the video series covers this chapter.

5.1 The Gaussian operator path

We now construct the integrated operator path in the interaction representation on the same probability space as the original noise. Retain Hypothesis 1.2.1, set $a = \alpha_0$, $s = 1/2$ and $E_r = H^r(\mathbb{R}^d) \times H^{r-1}(\mathbb{R}^d)$, and initially use real phases $E = E_s$. Let H_W be the real completion of $C_c^\infty((0,\infty) \times \mathbb{R}^d)$ modulo its covariance-null tests. The given isonormal process on it is W. If $\Gamma = 0$, the operator path and all covariance forms are zero, so the conclusions below hold directly. Assume $\Gamma \neq 0$ in the construction.

Choose and fix $R, T > 0$ and a real even nonnegative $\zeta \in C_c^\infty(\mathbb{R}^d)$ equal to one on B_1 and zero off B_2. The physical mask is $\zeta_R(x) = \zeta(x/R)$. The free group $S(t)$ and forms ℓ_R are those of Section 4.2; both phase entries and the continuous zero-frequency sine quotient are retained. Fix parameters

Lean full

$$0 < \gamma < \min\left(\frac{1}{2}, \frac{2-\alpha}{2}\right), \qquad \frac{1}{2} < \theta < \beta < \min\left(1 - \frac{a}{2}, \frac{3-a-\alpha}{2}\right). \tag{5.1.1}$$

The strict intervals are nonempty. The C^θ norm is the supremum norm plus the θ-Hölder seminorm.

Proposition 5.1.1 (Compact operator path on the original noise space)**.** *There is an orthonormal basis $\{f_j\}$ of H_W with real smooth compact test representatives, independent*

standard real Gaussians $g_j = W(f_j)$, and deterministic operators $A_j(0,t)$ on E such that

$$X_N(t) := \sum_{j \le N} g_j A_j(0,t) \longrightarrow M_R(t) \quad \text{in } L^p(\Omega; C^\theta([0,T]; \mathcal{B}(E))) \tag{5.1.2}$$

for every finite $p \ge 1$. The limit is a centered Gaussian path on the original probability space, starts at zero, and has compact values at every time on one probability-one path set. For each fixed real Schwartz pair z, w and $t \in [0,T]$,

$$\langle M_R(t)z, w\rangle_E = \ell_R((0,t); z, w) \quad \text{in } L^2(\Omega). \tag{5.1.3}$$

For long intervals, use the completed covariance test, equivalently the additive unit-interval construction justified below. Different compact smooth test bases give indistinguishable paths on the same W. For constants $C, c > 0$ depending on the fixed data but not the basis or p,

$$(\mathbb{E}\|M_R\|_{C^\theta}^p)^{1/p} \le C\sqrt{p}, \qquad \mathbb{E}\exp(c\|M_R\|_{C^\theta}^2) < \infty. \tag{5.1.4}$$

Its complexification has the corresponding sesquilinear covariance identity. Fixed-interval Schatten moments hold at the admissible even indices in (5.1.18). Arbitrary p above refers to $\mathcal{B}(E)$, not arbitrary Schatten indices or a Schatten-valued path.

5.1.1 A test basis and explicit covariance coefficients

Lemma 5.1.2 (Basis in the prescribed quotient)**.** *The nonzero space H_W is separable and infinite-dimensional. It has a real orthonormal basis with compact smooth representatives, whose evaluations by W are independent standard real Gaussians.*

Proof. We first obtain a countable dense collection of tests in the prescribed covariance norm. We then show that the quotient is infinite-dimensional and apply Gram–Schmidt within that quotient.

Step 1. We prove separability of the test completion. For tests supported in $[0,L] \times K$, with K compact, the physical covariance and the temporal Schur bound give the absolute estimate

$$|\langle F, G\rangle_{H_W}| \le |K|\Gamma(K-K)\frac{2L^{1-a}}{1-a}\|\|F(t)\|_\infty\|_{L^2(0,L)}\|\|G(t)\|_\infty\|_{L^2(0,L)}. \tag{5.1.5}$$

The spatial covariance is bounded by the product of the two spatial supremum norms, the volume $|K|$ and the mass $\Gamma(K-K)$. The temporal Schur estimate then bounds the integral of this product by the two L^2 time norms. Thus, uniform approximation on a fixed box implies approximation in the covariance seminorm. Only spatial differences in $K-K$ contribute. On each rational compact box inside positive time, rational step approximations followed by compact smooth mollifiers at rational scales give a countable uniformly dense test collection, supported in a fixed slightly larger box. The estimate proves noise-norm approximation. The union over increasing boxes is dense in the test completion. This proves separability without assuming the covariance form is injective.

Step 2. We show that infinitely many temporal tests survive the quotient. Choose $L \geq 1$ with $0 < \Gamma(B_L) < \infty$ and nonnegative compact smooth $q \geq 1$ on B_{2L+1}. Then

$$Q_{\mathrm{sp}} := \int \Gamma(\,\mathrm{d}y) \int q(x)q(x-y)\,\mathrm{d}x \geq |B_{L+1}|\Gamma(B_L) > 0,$$

and the compact-support estimate makes it finite. For every real compact smooth positive-time τ, the tensor identity is

$$\|\tau \otimes q\|_{H_W}^2 = Q_{\mathrm{sp}}\|\tau\|_a^2.$$

For $y \in B_L$ and $x \in B_{L+1}$, both x and $x-y$ lie in B_{2L+1}. Each factor in the integrand is therefore at least one on this region. Here the temporal norm is computed on any finite interval containing the support of τ. It is strictly positive for signed nonzero τ. Indeed, zero-extend this deterministic test and use the positive Laplace factorization from Lemma 4.1.3 to write

$$\|\tau\|_a^2 = \frac{1}{\Gamma_E(a)} \int_0^\infty \lambda^{a-1} E_\lambda(\tau)\,\mathrm{d}\lambda,$$
$$E_\lambda(\tau) = \int_{\mathbb{R}} 2\lambda \left| \int_r^\infty e^{-\lambda(t-r)}\tau(t)\,\mathrm{d}t \right|^2 \mathrm{d}r.$$

Signed exchanges are absolutely integrable on the test support, by the temporal Schur estimate. If the norm vanished, some $\lambda > 0$ would have $E_\lambda = 0$. Its inner integral $v(r)$ is continuous and satisfies $v' = \lambda v - \tau$. Vanishing almost everywhere makes it identically zero and forces the derivative v' to vanish as well. The identity $v' = \lambda v - \tau$ then forces $\tau = 0$. Thus, infinitely many linearly independent compact time bumps inject into H_W after multiplication by q.

Step 3. We construct the basis and its Gaussian coordinates. Apply Gram–Schmidt to a countable dense real test collection, discarding zero residuals in the given null quotient. Infinitude gives an infinite basis; each representative is a finite linear combination of compact smooth tests. The isonormal process depends only on the quotient class, so a zero residual really is a zero noise variable. The surviving normalized vectors have covariance equal to their Hilbert inner product. Thus, the isonormal identity gives $\mathbb{E}g_j g_k = \delta_{jk}$. Joint Gaussian characteristic functions then factor, giving independence and unit variances. No physical null direction is removed beyond the prescribed quotient, and no H_W-valued white Gaussian vector is used. This proves Lemma 5.1.2. □

The operator-norm topology is essential here: in dimensions two and three, No-go 21 rules out a compatible square-integrable Hilbert–Schmidt realization on a same-index Sobolev phase pair, for suitable coefficient masks and a sufficiently large observation cutoff.

Lemma 5.1.3 (Covariance coefficients)**.** *For each basis representative put*

$$H_{j,R}(t,x) = \zeta_R(x) \int_{u>0} |t-u|^{-a} \int \Gamma(\,\mathrm{d}y) f_j(u, x-y)\,\mathrm{d}u. \tag{5.1.6}$$

These functions are real smooth on finite time-space compacts, supported spatially in B_{2R}, with bounded derivatives there. For smooth compact real positive-time F, and also for the admitted wave tests of (4.2.13),

$$\mathbb{E}[W_{\mathbb{C}}(\zeta_R F)g_j] = \int H_{j,R}(t,x)F(t,x)\,\mathrm{d}t\,\mathrm{d}x. \tag{5.1.7}$$

The coefficient on $t \geq 0$ depends only on the H_W class of f_j.

Proof. We move derivatives onto the smooth basis test to avoid differentiating the singular covariance kernel. We then prove the covariance identity by approximation and show that the coefficient depends only on the noise class.

Step 1. We prove smoothness of the deterministic coefficient. Extend f_j smoothly by zero in time and substitute $v = t - u$. The unmasked expression is $\int_{\mathbb{R}} |v|^{-a} \int \Gamma(\,\mathrm{d}y) f_j(t - v, x - y)\,\mathrm{d}v$. On each compact (t,x) set, the integrand involves only bounded v and a common compact set of y. Local Radon mass and local integrability of $|v|^{-a}$ provide an integrable majorant for each derivative of the test on these fixed sets. The singular kernel is left unchanged under differentiation. Thus, every mixed derivative can move onto the smooth test. Dominated integration proves smoothness and the derivative bounds. Multiplication by ζ_R gives the stated support. Zero extension is only of a deterministic test; no negative-time noise is introduced.

Step 2. We identify the coefficient for tests and their limits. The physical covariance formula and absolute Fubini give (5.1.7) first for real compact tests. The compact difference set in Γ and integrable temporal singularity justify the exchange. For wave tests use the common-support original approximations of Proposition 4.2.3, converging in L^2 time in the spatial supremum norm after masking. The left side converges by noise Cauchy–Schwarz and the right side by the coefficient's boundedness on that support. Real and imaginary parts are treated separately because the original noise is real. Combining the two identities gives the complex evaluation defined in the preceding section. If two representatives give the same class, their Gaussian difference is zero. Testing the covariance identity against every compact smooth F makes the difference of their masked coefficients zero as a distribution for $t > 0$. Smoothness, then continuity at zero, proves the representative assertion on $t \geq 0$. This proves Lemma 5.1.3. □

5.1.2 Gain, adjoints and localization

Lemma 5.1.4 (Deterministic coefficient operators)**.** *For $I \subset [0,T]$, the statewise integral*

$$A_j(I)z = \int_I S(-t)B(H_{j,R}(t))S(t)z\,\mathrm{d}t \tag{5.1.8}$$

satisfies, for every real r,

$$\|A_j(I)\|_{\mathcal{B}(E_r,E_{r+1})} \leq C_{j,r,R,T}|I|. \tag{5.1.9}$$

Its E_s adjoint has the gain $E_{2s-r-1} \to E_{2s-r}$, so both operators act from $E_{s-\gamma}$ to E. Choose real compact smooth $\chi = 1$ on B_{2R+T+1}. On every E_r,

$$D_\chi A_j(I) = A_j(I) = A_j(I) D_\chi. \tag{5.1.10}$$

For each fixed Schwartz pair,

$$\mathbb{E}[g_j \ell_R(I; z, w)] = \langle A_j(I) z, w \rangle_E. \tag{5.1.11}$$

Proof. We establish the gain in Sobolev order and its adjoint version first. Finite propagation then gives both localization identities. Finally, the physical pairing identifies the Gaussian coefficient of each row.

Step 1. We prove the gain and the adjoint gain. The full massless wave is strongly continuous and bounded on every E_r on finite time intervals. Its normalized off-diagonal Fourier entries have sizes at most C_T and one, respectively; continuity and domination prove the strong assertion. Multiplication by $H_{j,R}(t)$ is bounded on every H^r, continuously in t, by weighted Fourier convolution and its compact smooth derivative bounds. Hence, $B(H_{j,R}(t)) : E_r \to E_{r+1}$ is bounded: its second entry is a multiplier of the displacement in H^r. The integrand in (5.1.8) is strongly continuous with values in E_{r+1} for each input in E_r, and uniformly bounded in that operator norm. Statewise Bochner integration proves (5.1.9), including the Lipschitz operator-norm primitive $A_j(0, t)$. Norm continuity of $S(t)$ is not needed.

Under the E_s pairing, the dual of E_r is isometrically E_{2s-r}, directly by the two Bessel weights. Dualizing the bound with a gain of one derivative therefore gives the asserted adjoint gain. It agrees on Schwartz phases with the bounded E_s adjoint. Since $\gamma < 1$, gain one at every index implies the two stated maps from $E_{s-\gamma}$ to E.

Step 2. We prove both localization identities by finite propagation. For smooth data the free-wave energy on a shrinking ball has nonpositive boundary flux: $v\partial_n u - (v^2 + |\nabla u|^2)/2 \le 0$. Vanishing initial displacement and velocity give zero velocity and gradient in the cone; integration of velocity from the zero displacement gives zero displacement there as well. Time reversal gives the backward assertion. Thus, both entries of $S(\pm t)$ enlarge supports by at most $|t|$. Density and testing against compact smooth functions extend this support assertion to Sobolev phases. In particular, for input $(1 - D_\chi)z$, approximate z by Schwartz phases and retain the factor $1 - D_\chi$; the approximants vanish on B_{2R+T+1}. Their free displacement vanishes on B_{2R} throughout $[0, T]$, and the same is true in the distributional limit. They contribute nothing to the integral. Its output is supported in B_{2R+T}, by the support of $H_{j,R}$ and backward finite propagation. Since $\chi = 1$ on a neighborhood of this ball, both identities in (5.1.10) follow. This uses both entries, not a scalar restart or a positivity theorem.

Step 3. We identify the covariance row. Finally, apply the physical Sobolev pairing (4.2.15) and (5.1.7) to the state integral. They give (5.1.11). In (5.1.6), the mask is after convolution; replacing it by a mask inside $\Gamma * f_j$ would change this identity. This proves Lemma 5.1.4. □

5.1.3 Finite variances and first Wiener chaos tails

Put $J_0(u,v) = (\Lambda^{1/2}u, \Lambda^{-1/2}v)$, $H_0 = L^2(\mathbb{R}^d;\mathbb{R}^2)$, $a_j = J_0 A_j(I) J_0^{-1}$ and $P_\chi = J_0 D_\chi J_0^{-1}$. The operator $D_\gamma = \mathrm{diag}(\Lambda^{-\gamma}, \Lambda^{-\gamma})$ acts on these physical coordinates. Its two compact envelopes $B_{\mathrm{out}}, B_{\mathrm{in}}$ are those of Proposition 4.3.7, after complexification when Schatten norms are used. For $I \subset [0,T]$ with $0 < h = |I| \le 1$, set

$$b_I = C_T h^{2-a} B_\alpha(h), \tag{5.1.12}$$

where C_T is the uniform-in-R constant in Proposition 4.2.5.

Lemma 5.1.5 (Both variances and their tails)**.** *For every N,*

$$V_{\mathrm{out},N} := \sum_{j\le N} a_j a_j^* \le b_I D_\gamma^2, \qquad V_{\mathrm{in},N} := \sum_{j\le N} a_j^* a_j \le b_I D_\gamma^2. \tag{5.1.13}$$

The finite families satisfy both localizations by P_χ. There are bounded positive limits $V_{\mathrm{out},\infty}, V_{\mathrm{in},\infty}$ with positive tails $T_{\mathrm{out},N}, T_{\mathrm{in},N} \to 0$ strongly, and

$$T_{\mathrm{out},N} \le b_I B_{\mathrm{out}}, \qquad T_{\mathrm{in},N} \le b_I B_{\mathrm{in}}. \tag{5.1.14}$$

For each fixed $z \in E_{s-\gamma}$, the real column maps satisfy

$$m_{R,I}(z) = \sum_j g_j A_j(I) z, \qquad n_{R,I}(z) = \sum_j g_j A_j(I)^{*,E} z \quad \text{in } L^2(\Omega;E). \tag{5.1.15}$$

Proof. We first compare finite noise projections with the original covariance forms. Summing over a phase basis gives the two variances. We then identify the column series and use their positive tails to obtain compact envelopes.

Step 1. We project scalar rows onto the noise basis. By (5.1.11), for real Schwartz z, w,

$$\langle X_N(I)z, w\rangle_E = \sum_{j\le N} g_j \mathbb{E}[g_j \ell_R(I;z,w)] = \mathcal{P}_N \ell_R(I;z,w),$$

where $\mathcal{P}_N$ is the orthogonal projection in $L^2(\Omega)$ onto the span of $g_1,\dots,g_N$. In particular,

$$\sum_{j\le N} |\langle A_j(I)z, w\rangle_E|^2 = \mathbb{E}|\langle X_N(I)z, w\rangle_E|^2 \le \mathbb{E}|\ell_R(I;z,w)|^2.$$

The variables g_j are orthonormal in $L^2(\Omega)$. Thus, the squared norm of this finite orthogonal projection is the sum of the squared coefficients and cannot exceed the squared norm of the original row. This is the contraction used in both directions below. These are projections onto the noise-test basis, not source regularizations. The two variance bounds of Proposition 4.2.5, with the mean-square columns of Proposition 4.2.6, apply to these same covariance forms and the bound (5.1.12).

Step 2. We sum the row bounds in both phase directions. Choose a real Schwartz orthonormal basis $\{e_k\}$ of E. Fix real Schwartz w. For every finite phase truncation K,

$$\begin{aligned}\sum_{k\le K}\sum_{j\le N} |\langle A_j(I)e_k, w\rangle_E|^2 &= \sum_{k\le K} \mathbb{E}|\langle X_N(I)e_k, w\rangle_E|^2 \\ &\le \sum_{k\le K} \mathbb{E}|\ell_R(I;e_k,w)|^2 \le b_I \|w\|^2_{E_{s-\gamma}},\end{aligned}$$

by (4.2.21). Let $K \to \infty$. Parseval in the phase space and nonnegative monotone convergence, with N still finite, give

$$\sum_{j\le N} \|A_j(I)^{*,E} w\|_E^2 = \mathbb{E}\|X_N(I)^{*,E} w\|_E^2 \le b_I \|w\|_{E_{s-\gamma}}^2.$$

Conversely, for fixed real Schwartz z, use (4.2.22) with the output basis varying:

$$\begin{aligned}\sum_{k\le K}\sum_{j\le N} |\langle A_j(I)z, e_k\rangle_E|^2 &= \sum_{k\le K} \mathbb{E}|\langle X_N(I)z, e_k\rangle_E|^2 \\ &\le \sum_{k\le K} \mathbb{E}|\ell_R(I; z, e_k)|^2 \le b_I \|z\|_{E_{s-\gamma}}^2.\end{aligned}$$

The same phase Parseval limit gives

$$\sum_{j\le N} \|A_j(I)z\|_E^2 = \mathbb{E}\|X_N(I)z\|_E^2 \le b_I \|z\|_{E_{s-\gamma}}^2.$$

Thus, both directions use their respective Hilbert-Bessel bounds; neither follows from retaining only one variance.

Step 3. We extend the finite bounds to the weaker input space. These inequalities extend at each finite N to the full $E_{s-\gamma}$ input space. Indeed, Lemma 5.1.4 gives $A_j : E_{s-\gamma} \to E_{s+1-\gamma} \subset E$. Its adjoint gain, at $r = s + \gamma - 1$, gives the same map for $A_j^{*,E}$. The inclusion holds since $\gamma < 1$. Approximate the input by Schwartz phases and pass each of the finitely many operator terms to the limit. The resulting constant is still b_I, independent of N; individual j-dependent gain constants were not summed. Restricting to E and using $\|z\|_{E_{s-\gamma}} = \|D_\gamma J_0 z\|_{H_0}$ gives (5.1.13) as two operator quadratic inequalities. In physical coordinates, the sum of squared adjoint norms is the quadratic form of $\sum_{j\le N} a_j a_j^*$, and the sum of squared direct norms is that of $\sum_{j\le N} a_j^* a_j$. The weaker input norm is the quadratic form of D_γ^2. This converts the two scalar inequalities into the displayed operator bounds. Both localizations follow from (5.1.10). No self-adjointness or projection property of P_χ is assumed.

Step 4. We identify the first-chaos expansions of the columns. The coordinates of $m_{R,I}(z)$, for Schwartz z, are the original covariance forms $\ell_R(I; z, e_k)$ and belong to the closed first Wiener chaos $W(H_W)$. Their coefficients against g_j are $\langle A_j z, e_k\rangle_E$. Parseval in that chaos, followed by Parseval in E and positive Tonelli, gives

$$\sum_j \|A_j z\|_E^2 = \mathbb{E}\|m_{R,I}(z)\|_E^2, \qquad m_{R,I}(z) = \sum_j g_j A_j z \quad \text{in } L^2(\Omega; E).$$

For each phase coordinate, completeness of the noise basis gives convergence in the scalar first chaos. Summing the squared coefficient tails over the phase basis gives the vector-valued mean-square error. Positive Tonelli permits this summation, and the finite total column variance forces the tails to zero. The same argument for the adjoint column gives the other expansion. Membership in this first chaos comes from linear noise tests, not merely Gaussianity. To extend to a fixed $E_{s-\gamma}$ input, approximate by Schwartz

phases. The finite inequalities extend to that space by the gain bounds and have a constant uniform in N. Apply them to the input difference, then use the Schwartz expansion and continuity of m, n. This proves (5.1.15) on the full claimed input domain.

Step 5. We pass to positive variance limits and their compact envelopes. The convergent positive quadratic sums, restricted to E and transported by J_0, define the bounded positive operators $V_{\cdot,\infty}$ by polarization and Riesz. They retain the bounds $b_I D_\gamma^2$. Their tails have quadratic forms tending to zero. Since they are uniformly bounded and positive, $\|T_N v\|^2 \le \|T_N\|\langle T_N v, v\rangle \to 0$. Passing to the limit in the finite localization identities gives

$$V_{\mathrm{out},\infty} = P_\chi V_{\mathrm{out},\infty} P_\chi^*, \qquad V_{\mathrm{in},\infty} = P_\chi^* V_{\mathrm{in},\infty} P_\chi,$$

and the same identities for their tails. Positive congruence applied to $T_N \le b_I D_\gamma^2$ proves (5.1.14).

Complexification preserves these statements and constants. The Hilbert norms split into real and imaginary squared norms; real operators extend isometrically. A real orthonormal basis complexifies to a complex orthonormal basis, preserving singular values and multiplicities. The complex column maps have the same bounds and sesquilinear row identities. This proves Lemma 5.1.5. □

Lemma 5.1.5 gives tails $T_{\mathrm{out},N}, T_{\mathrm{in},N}$ that tend to zero only strongly. They lie below the compact envelopes in (5.1.14). We now use this compact domination to improve the mode of convergence.

Lemma 5.1.6 (Compact domination of positive tails)**.** *If $0 \le T_N \le B$, with positive compact $B \in S_m$, $m \ge 1$, and $T_N \to 0$ weakly, then*

$$\|T_N\| \longrightarrow 0, \qquad \operatorname{Tr} T_N^m \longrightarrow 0. \tag{5.1.16}$$

Proof. Choose a finite spectral projection Q of B with $\|(1-Q)B(1-Q)\| < \epsilon$. Positive quadratic Cauchy–Schwarz gives, for unit x,

$$\langle T_N x, x\rangle \le 2\langle T_N Q x, Qx\rangle + 2\langle T_N(1-Q)x, (1-Q)x\rangle \le 2\|QT_NQ\| + 2\epsilon.$$

Weak convergence makes the finite-dimensional matrix QT_NQ converge in norm to zero. Letting $\epsilon \downarrow 0$ proves norm convergence. Lemma 4.3.8 gives $\lambda_j(T_N) \le \lambda_j(B)$, while each $\lambda_j(T_N) \to 0$ by norm convergence. Dominated summation of $\lambda_j(B)^m$ proves the trace limit. No order comparison of the operator powers is used. This proves Lemma 5.1.6. □

Trace powers of variances must still be turned into moments of Gaussian sums. Proposition 4.3.3 keeps the average of the two trace powers, but only for matrices. Corollary 4.3.10 bounds compact sums only through the envelope norm $\|K_{\mathrm{out}}\|_{S_p}$.

Lemma 5.1.7 (Retained finite Gaussian variance powers)**.** *Let Z_ℓ be finitely many compact operators whose two variances $V_{\mathrm{out}}, V_{\mathrm{in}}$ belong to $S_{q/2}$, for an even $q \ge 2$. With independent standard real g_ℓ,*

$$\mathbb{E}\left\|\sum_\ell g_\ell Z_\ell\right\|_{S_q}^q \le (q-1)^{q/2}\frac{\operatorname{Tr} V_{\mathrm{out}}^{q/2} + \operatorname{Tr} V_{\mathrm{in}}^{q/2}}{2}. \tag{5.1.17}$$

Proof. We retain the two variance trace powers while compressing to finite matrices. Compactness then allows passage to the original finite Gaussian sum, using Fatou twice.

Step 1. We apply the matrix estimate to the compressed sum. Compress by finite-rank orthogonal $Q_k \to I$ strongly. The compressed output variance is at most $Q_k V_{\mathrm{out}} Q_k$, since their difference is $\sum_\ell Q_k Z_\ell (1-Q_k) Z_\ell^* Q_k \geq 0$; the input inequality is the same with adjoints interchanged. Positive-order and compression max-min compare their trace powers with the uncompressed ones. Apply Proposition 4.3.3 on the finite range, retaining the average. For each finite Gaussian coordinate vector, compactness gives operator-norm convergence of the compressed sum to the original sum.

Step 2. We pass to the uncompressed sum. The singular-value norm-Lipschitz argument in the proof of Corollary 4.3.10, then Fatou over singular values and probability, proves the displayed bound. The extended norm is measurable by the same finite-coordinate continuity argument. No infinite Gaussian series or S_q-Bochner convergence is assumed. This proves Lemma 5.1.7. □

5.1.4 Interval limits on the given probability space

The two previous lemmas control tails of the series $\sum_j g_j A_j(I)$ through its two variances. We now fix one interval and use them to pass to the limit in N, without leaving the original probability space.

Lean partial

Lemma 5.1.8 (Fixed-interval operator construction)**.** *For each fixed short interval I, $X_N(I)$ converges in every finite $L^p(\Omega;\mathcal{B}(E))$ to a compact-valued centered Gaussian operator $X_R(I)$ on the original probability space. For every admissible even $q \geq 2$, $q\gamma > d$,*

$$(\mathbb{E}\|X_R(I)\|_{S_q}^q)^{1/q} \leq \sqrt{q-1}\sqrt{C_T}\, h^{1-\alpha/2} B_\alpha(h)^{1/2} \|K_\chi\|_{S_q}, \qquad K_\chi = P_\chi D_\gamma. \tag{5.1.18}$$

Its fixed Schwartz rows equal the covariance forms in L^2.

Proof. We first show that the finite sums are Cauchy using the compact variance tails. We construct their limit on the original probability space, identify its rows, and finally extend additively to long intervals.

Step 1. We obtain uniform finite moments and vanishing tails. The finite families a_j, $j \leq N$, satisfy every hypothesis of Proposition 4.3.9 and Corollary 4.3.10: both localizations, both weighted variances and the independent real g_j have been proved in Lemma 5.1.5. Thus, the coefficients are compact, and their finite Gaussian sums satisfy (5.1.18), uniformly in N. The fixed cutoff norm may depend on R, T.

Fix an admissible even $q \geq 2$, $q\gamma > d$. Both positive compact envelopes in (5.1.14) belong to $S_{q/2}$. Lemma 5.1.6 therefore gives

$$\operatorname{Tr} T_{\mathrm{out},N}^{q/2} \longrightarrow 0, \qquad \operatorname{Tr} T_{\mathrm{in},N}^{q/2} \longrightarrow 0.$$

For $M > N$, put $Y_{N,M} = \sum_{j=N+1}^{M} g_j A_j(I)$. After the unitary J_0 transport, its two finite variances are

$$V_{\mathrm{out},M} - V_{\mathrm{out},N} \leq T_{\mathrm{out},N}, \qquad V_{\mathrm{in},M} - V_{\mathrm{in},N} \leq T_{\mathrm{in},N}.$$

Lemma 5.1.7 and positive eigenvalue max-min comparison now give the uniform tail estimate

$$\sup_{M>N} \mathbb{E}\|Y_{N,M}\|_{S_q}^q \le (q-1)^{q/2} \frac{\operatorname{Tr} T_{\mathrm{out},N}^{q/2} + \operatorname{Tr} T_{\mathrm{in},N}^{q/2}}{2} \longrightarrow 0.$$

For each $M > N$, the two variances of the finite tail lie below the corresponding infinite tails. The positive-order comparison bounds their trace powers by the right side, which no longer depends on M. This is why the estimate proves a Cauchy property rather than only boundedness of the partial sums. The average of the two trace powers is retained. The comparison uses eigenvalues, not operator monotonicity of the $q/2$ power. Since $\|Y_{N,M}\| \le \|Y_{N,M}\|_{S_q}$, this proves $L^q(\Omega; \mathcal{B}(E))$ Cauchy convergence; a uniform moment bound alone would not suffice.

Step 2. We construct the operator limit on the prescribed probability space. All finite sums lie in the separable operator-norm closed real span $\mathcal{F}_I$ of the countably many deterministic $A_j(I)$. Choose N_k increasing so that $\|X_{N_{k+1}}(I) - X_{N_k}(I)\|_{L^q\mathcal{B}(E)} \le 2^{-k}$. Their L^1 norms are summable. Tonelli therefore shows that the pointwise operator-norm differences sum absolutely almost surely. Completeness gives a limit in $\mathcal{F}_I$ on the original probability space; assign it zero on the exceptional null set. It is strongly measurable as a limit of separably valued finite Gaussian sums. Fatou and the Cauchy property give convergence of the whole sequence in L^q to this limit $X_R(I)$. No new noise or probability space has been introduced. Limits constructed at different admissible even indices agree by uniqueness of convergence in probability. For each requested finite $p \ge 1$, choose an admissible even $q \ge p$ and use Lyapunov to obtain L^p operator-norm convergence to that same limit. One fixed Schatten index is not used to infer all moment orders.

Step 3. We identify compactness, moments and Gaussianity of the limit. The compact operators are norm closed, so an almost surely norm-convergent subsequence makes $X_R(I)$ compact valued. Singular-value Fatou applied to the finite uniform bound gives (5.1.18) at each admissible even q. Every continuous real linear functional of $X_R(I)$ is an L^2 limit of centered finite Gaussian sums; convergence of means, variances and characteristic functions makes it centered Gaussian. The same applies to finite linear combinations of these functionals, proving joint Gaussianity on the given space.

Step 4. We identify the rows as actual noise variables. For each fixed real Schwartz z, w, the scalar rows $\langle X_N(I)z, w\rangle_E$ are the orthogonal projections of the completed covariance form $\ell_R(I; z, w)$ onto the complete noise basis. That form lies in the original closed first Wiener chaos, so these projections converge to it in $L^2(\Omega)$. Operator-norm L^2 convergence also gives convergence to $\langle X_R(I)z, w\rangle_E$. Uniqueness of the L^2 limit identifies these two variables on the same space, not merely their laws.

Step 5. We extend the construction by finite additivity. For a fixed long interval, choose a finite partition into intervals of length at most one. Their indicator tests add to the long-interval test except at finitely many endpoints. The masked wave products have common compact spatial support, and the temporal estimate (5.1.5) makes those endpoint changes have zero original covariance norm. Covariance completion and linearity give exact additivity of the forms. The deterministic statewise coefficient integrals, hence every

X_N, add on the same partition. Passing their finite-sum L^p limits gives the corresponding operator additivity and covariance identity for matrix elements, independently of the partition by common refinement. These are statements at each fixed interval and partition; no uncountable intersection of independently selected null sets is used. No long-interval version of the short-h bound is asserted. The Schatten conclusion is a fixed-interval moment at admissible even indices, not a Schatten-valued path or arbitrary-index claim. This proves Lemma 5.1.8. □

5.1.5 Time-path convergence and Gaussian norm bounds

Lemma 5.1.8 works one interval at a time. Proposition 5.1.1 asks for more: convergence in the C^θ path norm and compact values at every time on one path event.

Lean partial

Lemma 5.1.9 (Hölder path limit)**.** *The finite paths $X_N(t) = X_N((0,t))$ converge in $L^p(\Omega; C^\theta([0,T]; \mathcal{B}(E)))$ for every finite $p \geq 1$, in a separable closed path span on the same probability space. The limit starts at zero and has compact values for all times on one path event. For sufficiently large even q_0, its C^θ norm has L^q bound $C\sqrt{q}$, uniformly over even $q \geq q_0$ and the basis.*

Proof. We first obtain a uniform moment bound on the dyadic increments in a stronger Hölder norm. Finite-grid convergence then gives uniform convergence, and interpolation gives the desired Hölder convergence. We construct the limit in a separable path span.

Step 1. We bound increments and the dyadic sum. Corollary 4.2.2 bounds the budget b_I by $C|t-u|^{2\beta}$ for $I = (u,t)$; substitute this in (5.1.13) and apply Corollary 4.3.10 to the finite increment sum. Choose $\theta < \eta < \beta$ and an even $q_0 \geq 2$ with $q_0\gamma > d$ and $\beta - \eta - 1/q_0 > 0$. For $q \geq q_0$, the singular-value sequence gives $\|K_\chi\|_{S_q} \leq \|K_\chi\|_{S_{q_0}}$: if the latter is nonzero, normalize by it, so every singular value is at most one, and sum its qth powers. The zero case is immediate. Apply the finite Gaussian operator estimate with the time-refined variances from Proposition 4.2.5. This gives, uniformly in N and even $q \geq q_0$,

$$\|X_N(t) - X_N(u)\|_{L^q(\mathcal{B}(E))} \leq C\sqrt{q}\,|t-u|^\beta, \qquad |t-u| \leq 1. \tag{5.1.19}$$

The constant includes the fixed S_{q_0} cutoff norm and does not depend on q. Longer increments are finite sums of unit increments, with constants depending on T.

Let $D_n(F)$ be the maximum of adjacent increments on the grid $kT2^{-n}$, $0 \leq k \leq 2^n$. At fine levels $T2^{-n} \leq 1$, the elementary bound for a finite maximum yields

$$\|D_n(X_N)\|_{L^q} \leq 2^{n/q} C\sqrt{q}\,(T2^{-n})^\beta.$$

The qth power of a maximum is at most the sum of the qth powers. There are 2^n adjacent increments, so taking the qth root contributes $2^{n/q}$. Each increment has length $T2^{-n}$, which yields the displayed estimate. No independence of these increments is used. The finitely many coarse levels are controlled by unit partitions. Minkowski and a geometric sum therefore give

$$\sup_N \left\| \sum_{n \geq 0} 2^{n\eta} D_n(X_N) \right\|_{L^q} \leq C_\eta \sqrt{q}, \tag{5.1.20}$$

since the fine-level ratio is at most $2^{-(\beta-\eta-1/q_0)} < 1$.

Step 2. We control the stronger Hölder norm by dyadic increments. For a continuous Banach-valued F starting at zero, this weighted dyadic sum controls its C^η norm. Approximate two times by dyadic points at a scale comparable to their separation. The two grid points differ by at most two adjacent increments, and each endpoint's finer binary corrections are bounded by the tail sum of D_n. Multiplying by the separation to the power $-\eta$ bounds that total by the weighted sum, up to a constant depending on T, η. Continuity identifies the endpoint limits and also controls the supremum norm from $F(0) = 0$. The finite paths are Lipschitz by (5.1.9). Thus, (5.1.20) gives uniform $L^q C^\eta$ bounds, and the triangle inequality gives the same bound for their differences.

Step 3. We prove convergence in the required Hölder norm. On a fixed finite time grid, Lemma 5.1.8 gives L^q convergence of every point value. For continuous F,

$$\|F\|_\infty \le \max_k \|F(t_k)\| + C(\text{mesh})^\eta \|F\|_{C^\eta}.$$

Apply this to $X_N - X_M$, send $N, M \to \infty$ at a fixed grid, and then send the mesh to zero. The uniform C^η bound proves sup-norm L^q Cauchy convergence. The deterministic interpolation inequality

$$\|F\|_{C^\theta} \le C\|F\|_\infty^{1-\theta/\eta} \|F\|_{C^\eta}^{\theta/\eta} \tag{5.1.21}$$

follows by bounding each increment by both $2\|F\|_\infty$ and its C^η bound, and splitting at their balancing scale. Its supremum term is controlled too. Scalar Hölder in probability proves the $L^q C^\theta$ Cauchy property. For any requested finite p, choose an even $q \ge \max(p, q_0)$ and use Lyapunov.

Step 4. We choose the measurable limit and one path event. The full Hölder/operator space need not be separable. Nevertheless, every finite path lies in the span of the countably many deterministic Lipschitz paths $A_j(0, \cdot)$. Their C^θ-closed real span is a separable Banach space. In it the same elementary Cauchy/subsequence construction as in Lemma 5.1.8 gives a strongly measurable limit M_R on the original space. Different p limits agree by uniqueness of convergence in probability in the path norm. An almost surely C^θ-convergent subsequence converges uniformly in operator norm. Finite paths have compact values on short intervals, and on long ones by finite additivity. Therefore, the limit has compact values at every time on that single path set. It starts at zero. Passing the uniform bounds from (5.1.20) through the path convergence proves the asserted $C\sqrt{q}$ bound. This proves Lemma 5.1.9. □

Proof of Proposition 5.1.1. We assemble the interval and path constructions, then verify basis independence. The uniform square-root moment bound gives the exponential norm estimate by summing its power series.

Step 1. We identify the path and its covariance rows. Lemmas 5.1.2–5.1.9 construct the stated finite sums and their path limit, with no new probability space. Evaluation at a fixed time agrees with the interval limit by uniqueness in probability. Its covariance identity for matrix elements is (5.1.3), by Lemma 5.1.8, including the long-interval

interpretation. The same additivity identifies each fixed increment with $X_R(I)$, proving its stated Schatten moment bound.

The finite paths are Gaussian linear combinations of deterministic paths. Every continuous linear functional on their closed path span converges in L^2 to a centered Gaussian; finite linear combinations do as well. Thus, M_R is a centered Gaussian path. The four real pair identities give its complexified sesquilinear row identity.

Step 2. We compare paths built from different noise bases. The construction used only compact smooth representatives, orthonormality and completeness, so it applies to any such noise basis. Compare two constructions using a fixed countable dense Schwartz phase collection and rational times. Both rows equal the same covariance forms. A countable null-set union, boundedness of the operators, phase density and path continuity give equality at all times on one probability-one set. This proves indistinguishability without an assumed common event for uncountably many original evaluations.

Step 3. We deduce all finite moments and exponential integrability. For $p \geq 1$, choose even $q \geq \max(p, q_0)$ with $q \leq p + q_0 + 2 \leq (q_0 + 3)p$. Lemma 5.1.9 and Lyapunov give the first bound in (5.1.4). Write its resulting constant as C_1; Lyapunov and $q \leq (q_0+3)p$ absorb the passage from even q into the constant C_1. Now let $Y = \|M_R\|_{C^\theta}$. If $C_1 = 0$, then $Y = 0$ almost surely and the exponential bound is immediate. Otherwise, $\mathbb{E}Y^{2m} \leq (C_1\sqrt{2m})^{2m}$. Since $m! \geq (m/e)^m$, as follows by integrating $\log x$ from one to m, the mth term in the exponential series is at most $(2ecC_1^2)^m$. For $0 < c < 1/(2eC_1^2)$, positive Tonelli and the geometric series prove the second bound. This proves Proposition 5.1.1. □

All constants here may depend on R, T and the fixed admissible parameters. No uniform-in-R path-norm estimate or $C^\theta S_q$-valued path is asserted. This constructs the local masked integrated operator on the original noise. Source-cutoff convergence, Young evolution, canonical initial data and solution-moment asymptotics remain separate parts of the argument.

5.2 Convergence of the regularized Gaussian operator paths

We match the heat normalization, Laplace prefix and joint source law in the author version [17, (1.20), (1.21), (2.9), (2.11), pp. 5–6, 8–9]. Preservation of the given noise retention, the Radon implementation and the operator-path conclusions are proved here. No first-moment variational theorem is an input.

Retain Hypothesis 1.2.1, the fixed R, T, ζ_R, E and parameters of (5.1.1), and the original noise space H_W. Write $\mathscr{B}_\theta = C^\theta([0,T]; \mathcal{B}(E))$. Fix one original test basis f_j and its coefficient paths $A_j(t)$ from Proposition 5.1.1. Thus, $M_N = \sum_{j \leq N} W(f_j)A_j \to M_R$ in every finite $L^p(\mathscr{B}_\theta)$. Zero covariance gives zero noises and operator paths throughout; assume $\Gamma \neq 0$ in the construction.

5.2.1 Gaussian transfer in the full path norm

Lean full

Lemma 5.2.1 (Finite Gaussian linear images)**.** *Let $v_1, \dots, v_N$ lie in a real Banach space and let ξ be a centered Gaussian vector with covariance bounded by CI, $C \geq 0$. For independent standard real g_j and $p \geq 1$,*

$$\left(\mathbb{E} \left\| \sum_j \xi_j v_j \right\|^p \right)^{1/p} \leq \sqrt{C} \left(\mathbb{E} \left\| \sum_j g_j v_j \right\|^p \right)^{1/p}. \tag{5.2.1}$$

Proof. The function $\varphi(x) = \| \sum_j x_j v_j \|^p$ is continuous and convex, even when the linear image gives only a seminorm on $\mathbb{R}^N$. Its Gaussian expectations are finite by the finite-sum bound. On an auxiliary space take an independent centered Gaussian Z of covariance $CI - \operatorname{Cov} \xi$. The covariance difference is positive semidefinite by hypothesis, so its diagonalization constructs such a Gaussian vector even if it is degenerate. Independence and centering give conditional mean ξ for $\xi + Z$ given ξ. Convexity therefore applies to this conditional expectation. Conditional Jensen gives $\mathbb{E}\varphi(\xi) \leq \mathbb{E}\varphi(\xi + Z)$. The latter vector has the law of $\sqrt{C}\, g$, proving the claim. The case $C = 0$ is immediate. This auxiliary comparison changes neither the coupling of ξ nor any nonlinear wave solution. This proves Lemma 5.2.1. □

Lemma 5.2.1 compares two finite Gaussian sums with the same vectors. We apply it to the coefficient paths A_j, keeping the original basis f_j and replacing $W(f_j)$ by the evaluations of another Gaussian noise.

Proposition 5.2.2 (Gaussian transfer and stability)**.** *Let Y be a centered Gaussian linear noise on smooth compact positive-time tests, on a common coupled space, with*

$$\operatorname{Var} Y(F) \leq C \|F\|_{H_W}^2. \tag{5.2.2}$$

It extends to H_W. The finite paths $M_{Y,N} = \sum_{j \leq N} Y(f_j) A_j$ converge in every finite $L^p(\mathscr{B}_\theta)$ to a centered Gaussian path M_Y with compact values at all times on one path event, and

$$\|M_Y - M_{Y,N}\|_{L^p \mathscr{B}_\theta} \leq \sqrt{C} \|M_R - M_N\|_{L^p \mathscr{B}_\theta}, \tag{5.2.3}$$

$$\|M_Y\|_{L^p \mathscr{B}_\theta} \leq \sqrt{C} \|M_R\|_{L^p \mathscr{B}_\theta}. \tag{5.2.4}$$

For a fixed real Schwartz pair and time,

$$\langle M_Y(t) z, w \rangle_E = Y(h_{R,t;z,w}) \quad \text{in } L^2, \tag{5.2.5}$$

where $h_{R,t;z,w}$ is the explicit original test class $\zeta_R 1_{(0,t)} v_z G_w$ with the adjoint from (4.2.12). The path is basis-independent up to indistinguishability, is linear in jointly Gaussian noise families, and complexifies sesquilinearly.

If (W, Y_n) are jointly centered Gaussian, Y_n and $D_n = W - Y_n$ have uniform bounds of the form (5.2.2), and $\operatorname{Var} D_n(F) \to 0$ on every smooth compact test, then $M_{Y_n} \to M_R$ in every finite $L^p(\mathscr{B}_\theta)$.

Proof. We first transfer finite path sums and their tails using the Gaussian comparison. We then identify the transferred rows on the given coupling. For stability, we make the common tail small before sending the finitely many remaining noise errors to zero.

Step 1. We extend the noise and compare its finite coordinate vectors. The variance bound annihilates covariance-null tests and extends Y as a bounded linear map into its L^2 space. Completion preserves Gaussian finite-dimensional laws. For each finite original orthonormal family, the covariance of its Y evaluations is bounded by CI, by applying the variance bound to every real linear combination. Independence of $Y(f_j)$ is not assumed.

Step 2. We construct the transferred path and its bounds. Apply Lemma 5.2.1 with $v_j = A_j(\cdot)$ in $\mathscr{B}_\theta$, also to finite tails. The standard comparison vector has the law of the original $W(f_j)$. The already-proved original path convergence makes $M_{Y,N}$ Cauchy in every L^p. It lies in the same separable closed span of the countably many deterministic paths. The elementary Cauchy/subsequence construction of Lemma 5.1.9 gives a strongly measurable limit on the space of Y. Different p limits agree by convergence in probability. Passing to limits in the finite inequalities gives both displayed bounds. An almost surely uniformly convergent subsequence gives compact values for all times. Functional L^2 limits of Gaussian linear combinations prove that the path is Gaussian.

Step 3. We identify the rows and remove dependence on the basis. For real Schwartz z, w, the coefficient identity is

$$\langle A_j(t)z, w\rangle_E = \mathbb{E}[W(h_{R,t;z,w})W(f_j)] = \langle h_{R,t;z,w}, f_j\rangle_{H_W}.$$

Therefore, the finite transferred row is $Y(P_N h)$, with P_N the original H_W orthogonal projection. Since $P_N h \to h$, the noise bound gives $Y(P_N h) \to Y(h)$ in L^2. Operator-path L^2 convergence proves (5.2.5). Long intervals use the same covariance completion and endpoint nullity as in Lemma 5.1.8. No filter is commuted through a physical mask or wave group. Four real pair identities give the complex assertion. Countably many dense Schwartz phases and rational times, followed by phase density and path continuity, prove basis indistinguishability.

Step 4. We prove linearity and stability of the transfer. For jointly Gaussian Y, Z, their real linear combinations have an original variance bound by the L^2 triangle inequality. The finite sums are linear in the noise, hence so are the path limits. In the stability assertion D_n is centered Gaussian by the joint hypothesis. Its uniform bound gives

$$\|M_{D_n} - M_{D_n,N}\|_{L^p\mathscr{B}_\theta} \le \sqrt{C_D}\|M_R - M_N\|_{L^p\mathscr{B}_\theta}.$$

The right side of this bound is independent of n and tends to zero as N increases. We can therefore select the tail cutoff before considering convergence of the finite coordinate vector. For fixed N, the covariance matrix of $(D_n(f_j))_{j\le N}$ is positive and bounded by $s_N(n)I$, where $s_N(n) = \sum_{j\le N} \operatorname{Var} D_n(f_j) \to 0$. Every eigenvalue of a positive finite matrix is at most its trace, so the scalar $s_N(n)$ bounds that covariance matrix in positive order. Thus, the finite comparison gives $\|M_{D_n,N}\|_{L^p\mathscr{B}_\theta} \le \sqrt{s_N(n)}\|M_N\|_{L^p\mathscr{B}_\theta}$. Choose N large for

the uniform tail, then n large for the finite head. Linearity identifies $M_{D_n} = M_R - M_{Y_n}$. The same argument proves a multiparameter limit whenever each fixed test error tends to zero, with no relation between parameter rates. This proves Proposition 5.2.2. □

5.2.2 The spatial covariance space and an extension preserving the given noise

Proposition 5.2.2 reduces source-path convergence to uniform variance domination and vanishing residual variance on each test, for noises jointly Gaussian with W. We now construct such regularized sources, beginning with the spatial covariance space and heat regularization.

Lean full

Lemma 5.2.3 (Original spatial space and heat)**.** *Let H_Γ be the real test-null completion with*

$$B_\Gamma(f,g) = \int \Gamma(\,\mathrm{d}y) \int f(x)g(x-y)\,\mathrm{d}x = (2\pi)^d \int \widehat{f}(\xi)\overline{\widehat{g}(\xi)}\mu(\,\mathrm{d}\xi).$$

It is separable and includes Schwartz tests. With

$$p_\varepsilon(x) = (2\pi\varepsilon)^{-d/2} e^{-|x|^2/(2\varepsilon)}, \qquad C_\varepsilon f = p_\varepsilon * f, \tag{5.2.6}$$

heat is a positive self-adjoint contraction on H_Γ, $I - C_\varepsilon$ is a contraction, and $C_\varepsilon \to I$ strongly.

Proof. The spectral normalization is the spatial computation in Proposition 4.1.4; its integral is real on real tests by evenness of μ. The local bound $|B_\Gamma(f,g)| \le |K|\Gamma(K-K)\|f\|_\infty\|g\|_\infty$ on a common compact support gives separability by countable smooth approximation. Expanding smooth cutoffs of a Schwartz test converge in Schwartz seminorms, and its covariance correlation pairing converges against tempered Γ. Thus, Schwartz tests enter the same completion. The Fourier multiplier of C_ε is $m_\varepsilon(\xi) = e^{-\varepsilon|\xi|^2/2}$. On dense Schwartz tests, the displayed norm represents heat by multiplication by the real function m_ε, which satisfies $0 \le m_\varepsilon \le 1$. The multiplier of $I - C_\varepsilon$ is $1 - m_\varepsilon$, also between zero and one. Thus, the displayed norm gives positivity, self-adjointness and both contraction bounds. Dominated convergence gives strong convergence there; uniform boundedness extends it to the completion. This uses no physical mask operator on a noise quotient. This proves Lemma 5.2.3. □

Set $\nu_a(\,\mathrm{d}\lambda) = \lambda^{a-1}\,\mathrm{d}\lambda/\Gamma_E(a)$ and

$$\mathcal{G} = L^2((0,\infty)_\lambda \times \mathbb{R}_r, \nu_a(\,\mathrm{d}\lambda)\,\mathrm{d}r; H_\Gamma).$$

This is a real separable Hilbert space: countable simple functions on rational rectangles with a countable dense spatial collection suffice.

Lemma 5.2.4 (Feature isometry preserving the given noise)**.** *On finite smooth temporal-spatial tensors define*

$$\Phi F(\lambda, r) = \sqrt{2\lambda} \int_{\substack{t>0\\ t\ge r}} e^{-\lambda(t-r)} F(t,\cdot)\,\mathrm{d}t. \tag{5.2.7}$$

It extends to an isometry $\Phi : H_W \to \mathcal{G}$ with closed range, and the formula represents smooth compact tests almost everywhere. On a product extension retaining the original W, there is an isonormal $\mathcal{I}$ on $\mathcal{G}$ with

$$\mathcal{I}(\Phi h) = W(h) \quad \text{in } L^2 \quad \text{for each } h \in H_W. \tag{5.2.8}$$

Proof. We first prove the feature map is an isometry and identify its formula on completed tests. We then extend the given noise only on the orthogonal complement of the feature range, preserving every original evaluation.

Step 1. We identify the feature norm with the original covariance norm. The identity

$$\int_{-\infty}^{\min(t,u)} 2\lambda e^{-\lambda(t+u-2r)}\,\mathrm{d}r = e^{-\lambda|t-u|}$$

and the original Laplace formula give $\|\Phi F\|_{\mathcal{G}}^2 = \|F\|_{H_W}^2$. Indeed, integrating the two exponential time features over r gives the displayed kernel. Integrating that kernel against ν_a gives $|t-u|^{-a}$. The spatial inner product is the original B_Γ, so these two integrations reproduce the original covariance. All signed exchanges for finite tensors are absolutely integrable: compact temporal factors give integrals of $|\tau(t)\sigma(u)||t-u|^{-a}$, finite for $a < 1$, times fixed finite spatial inner products. No oscillatory infinite-measure Fubini is used. Smooth time partitions on one compact support approximate a general smooth spacetime test uniformly by finite tensors. The local covariance bound (5.1.5) proves their density in H_W. Hence, the isometry extends with closed range.

Step 2. We identify the integral formula for general compact tests. For a general smooth compact F, those approximants also converge uniformly in spatial H_Γ norm in time, by local Radon mass. For fixed λ, r, their integrals in (5.2.7) converge in H_Γ. Meanwhile the isometry gives convergence in $\mathcal{G}$, with an almost everywhere convergent subsequence. Its two limits agree, proving the stated formula. The coordinate r is auxiliary; no value of original negative-time noise has been assigned.

Step 3. We extend the isonormal process while retaining the given noise. Let P project orthogonally onto ΦH_W. On a product extension take an independent isonormal J on $(\Phi H_W)^\perp$, built from independent real standard Gaussians on a finite or countable basis. Define

$$\mathcal{I}(g) = W(\Phi^{-1}Pg) + J((I-P)g).$$

The two summands use orthogonal feature components and independent Gaussian processes. Their variances are $\|Pg\|_{\mathcal{G}}^2$ and $\|(I-P)g\|_{\mathcal{G}}^2$, whose sum is $\|g\|_{\mathcal{G}}^2$. If $g = \Phi h$, the second component vanishes and the first is the original $W(h)$. Orthogonality and independence make it isonormal on $\mathcal{G}$ and prove (5.2.8) with the original random variable, not only its law. For the countable fixed original basis, these equalities hold on one common probability-one set. Thus, the original finite paths and their L^p limits are precisely pullbacks of the already constructed original operator path. Cutoff fields may use J; they are not asserted to be functions of W alone. This proves Lemma 5.2.4. □

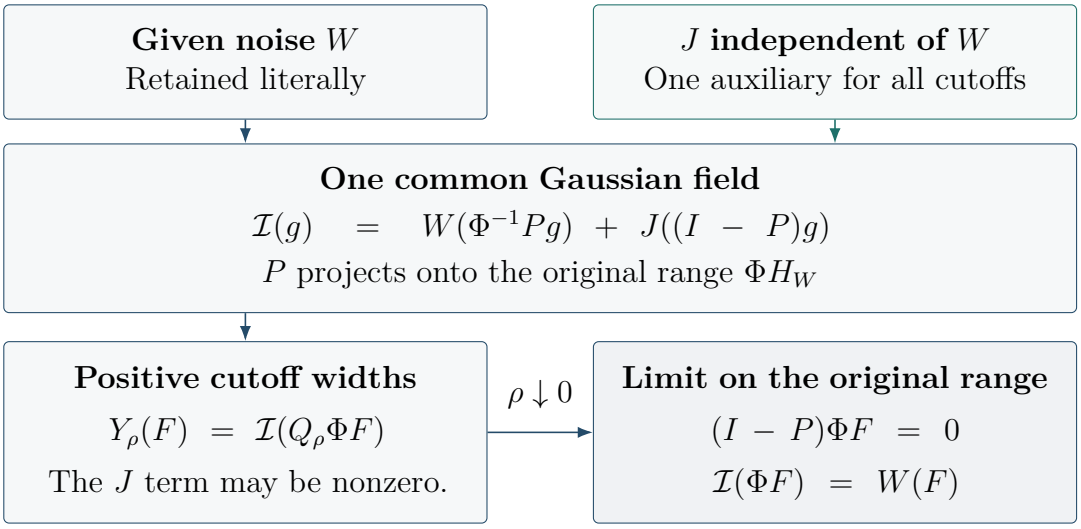

Figure 5.1: One coupling for every cutoff. The sources may depend on the auxiliary noise J, but the limiting noise and operator path retain the given W. A new independent copy is not chosen at each cutoff. Here P projects onto ΦH_W; it is not a time cutoff. See Lemma 5.2.4 and Proposition 5.2.5.

The auxiliary component can be nonzero: No-go 32 constructs an orthogonal witness for every positive finite cutoff point feature at positive time. Proposition 6.2.7 later proves that the tested fixed-mask limit is W-measurable, using the operator-path and Young-flow convergence.

5.2.3 Exact joint source law and convergence

Let P_η multiply $\mathcal{G}$ by $1_{\{\lambda \le \eta^{-1}\}}$. Let C_ε act fiberwise on H_Γ. These commute. For $\rho = (\varepsilon, \eta) > 0$, define

$$Q_\rho = C_\varepsilon P_\eta, \qquad Y_\rho(F) = \mathcal{I}(Q_\rho \Phi F), \qquad D_\rho(F) = \mathcal{I}((I - Q_\rho)\Phi F) = W(F) - Y_\rho(F). \tag{5.2.9}$$

The last equality uses the coupling preserving the given noise. Define

$$\Gamma_e(x) = (p_e * \Gamma)(x), \qquad K_\eta(v) = \frac{1}{\Gamma_E(a)} \int_0^{\eta^{-1}} e^{-\lambda|v|} \lambda^{a-1} \, \mathrm{d}\lambda. \tag{5.2.10}$$

The temporal operation is a Laplace prefix, not temporal convolution.

Proposition 5.2.5 (Canonical sources on the extended space containing the given noise)**.** *The noises in* (5.2.9) *have random field realizations with joint covariance*

$$\mathrm{Cov}(Y_{\varepsilon,\eta}(t,x), Y_{\varepsilon',\eta'}(s,y)) = K_{\max(\eta,\eta')}(t-s)\Gamma_{\varepsilon+\varepsilon'}(x-y). \tag{5.2.11}$$

Mean-square random field integration agrees with $Y_\rho(F)$ on tests. Both source and full residual obey

$$\operatorname{Var} Y_\rho(F), \quad \operatorname{Var} D_\rho(F) \le \|F\|_{H_W}^2, \tag{5.2.12}$$

and $\operatorname{Var} D_\rho(F) \to 0$ *for every* $F \in H_W$ *as* $\varepsilon, \eta \downarrow 0$ *at arbitrary relative rates. Consequently, for every finite* $p \ge 1$,

$$M_R^\rho := M_{Y_\rho} \longrightarrow M_R \quad \text{in } L^p(\mathscr{B}_\theta), \qquad M_{D_\rho} = M_R - M_R^\rho. \tag{5.2.13}$$

The source and residual have uniform local Gaussian operator-path moments and square-exponential norms, with constants for fixed R, T *and exponents.*

Proof. We compute the joint law from the point features, including the two heat widths and the common Laplace range. We then identify field integrals, bound both filters, and apply Gaussian transfer to the vanishing residual.

Step 1. We compute the spatial covariance and point-feature covariance. Apply the spatial distribution identity to a single shifted heat test:

$$\Gamma_e(x) = \int e^{i\xi\cdot x} e^{-e|\xi|^2/2} \mu(\mathrm{d}\xi).$$

Gaussian spectral moments of every order are finite for tempered μ. Thus, this is smooth with bounded derivatives. Since $\widehat{p_\varepsilon(x-\cdot)} = c_d e^{-i\xi\cdot x} e^{-\varepsilon|\xi|^2/2}$, the two heat factors in the spatial inner product cancel $(2\pi)^d$ exactly, giving

$$B_\Gamma(p_\varepsilon(x-\cdot), p_{\varepsilon'}(y-\cdot)) = \Gamma_{\varepsilon+\varepsilon'}(x-y). \tag{5.2.14}$$

The product of the two heat multipliers is $e^{-(\varepsilon+\varepsilon')|\xi|^2/2}$. The product of their Fourier normalization factors is c_d^2, and $(2\pi)^d c_d^2 = 1$. This gives the sum of widths without any remaining Fourier factor. Evenness of μ removes the reflected argument.

For each positive ρ and point (t, x) put

$$v_{\rho;t,x}(\lambda, r) = 1_{\{\lambda \le \eta^{-1}\}} \sqrt{2\lambda} e^{-\lambda(t-r)} 1_{\{r \le t\}} p_\varepsilon(x-\cdot). \tag{5.2.15}$$

Its squared $\mathcal{G}$ norm is $K_\eta(0)\Gamma_{2\varepsilon}(0) < \infty$. Define $Y_\rho(t,x) = \mathcal{I}(v_{\rho;t,x})$. The common λ range for two such vectors is $\lambda \le \min(\eta^{-1}, \eta'^{-1}) = \max(\eta, \eta')^{-1}$. Integrating r gives $e^{-\lambda|t-s|}$, and (5.2.14) gives the spatial factor. This proves (5.2.11) with the prescribed widths and original amplitudes, also for singular Radon and white covariances.

Step 2. We identify the mean-square field integral with the filtered noise. The representing vector is continuous in $\mathcal{G}$ norm, directly from this continuous covariance. Its norm is bounded on compact parameter sets. Hence, for a smooth compact spacetime F, its Bochner integral against $v_{\rho;t,x}$ exists. Integrate the heat translates in x, then the time feature, to obtain exactly $Q_\rho \Phi F$. Applying the bounded map $\mathcal{I} : \mathcal{G} \to L^2$ proves the random field-test identity on the same space. Common-support indicator tests follow by covariance completion and L^1 approximation; bounded point-feature norms and the domination below give the same L^2 limit.

Step 3. We bound the source and the full residual. Orthogonality of the two λ ranges gives, for $g \in \mathcal{G}$,

$$\|(I - Q_\rho)g\|_{\mathcal{G}}^2 = \|(I - P_\eta)g\|_{\mathcal{G}}^2 + \|P_\eta(I - C_\varepsilon)g\|_{\mathcal{G}}^2 \leq \|g\|_{\mathcal{G}}^2.$$

On the retained range, $I - C_\varepsilon$ is a contraction by the heat lemma. Hence, its squared norm is bounded by $\|P_\eta g\|_{\mathcal{G}}^2$. Adding the omitted-range norm gives at most the full squared norm, because these two ranges are orthogonal. Also $\|Q_\rho g\|_{\mathcal{G}} \leq \|g\|_{\mathcal{G}}$. Together with the isometry these prove both variance bounds. Disjoint λ ranges are independent; the full heat residual need not be independent of the source.

Step 4. We send both regularization parameters to zero. The L^2 tail integral gives $P_\eta \to I$ strongly. Fiberwise heat converges strongly on simple $\mathcal{G}$ functions by Lemma 5.2.3, then on all of $\mathcal{G}$ by the contraction bound. The estimate

$$\|(I - Q_\rho)g\|_{\mathcal{G}} \leq \|(I - C_\varepsilon)g\|_{\mathcal{G}} + \|(I - P_\eta)g\|_{\mathcal{G}} \longrightarrow 0$$

holds at arbitrary relative rates. Indeed, the two terms on the right depend on separate parameters, and each tends to zero by strong convergence. Therefore, there is no need to compare the rates at which the heat width and the Laplace cutoff are removed. Thus, the residual variance tends to zero for every original F. Proposition 5.2.2 gives (5.2.13) without commuting a filter through ζ_R or a wave group.

Step 5. We retain the uniform Gaussian path bounds. The same comparison gives $\|M_R^\rho\|_{L^p\mathscr{B}_\theta}, \|M_{D_\rho}\|_{L^p\mathscr{B}_\theta} \leq \|M_R\|_{L^p\mathscr{B}_\theta}$. The original $\sqrt{p}$ estimate and its even-moment exponential-series argument give uniform Gaussian operator path bounds. They are statements about L^p equivalence classes on the extension preserving the given noise, not a simultaneous path event for all uncountably many cutoffs. This proves Proposition 5.2.5. □

5.2.4 Regularized random fields and the ordinary first response

Lemma 5.2.6 (Regularity for each fixed cutoff)**.** *For each fixed $\rho > 0$, the random field has a version continuous in time and smooth in space, with every spatial derivative jointly continuous on compact time-space rectangles.*

Proof. We first differentiate the point features and bound their increments. A dyadic construction gives jointly continuous versions for all spatial derivative fields. The feature-space fundamental theorem then identifies those fields as actual derivatives of one version.

Step 1. We construct derivative fields and bound their increments. For each spatial multiindex b, differentiate (5.2.15) in x as a $\mathcal{G}$ vector. All derivatives exist because their spatial squared norms are the finite heat moments

$$\int \xi^{2b} e^{-\varepsilon|\xi|^2} \mu(\,\mathrm{d}\xi),$$

and the next moments dominate difference quotients. Set $Z_b(t,x) = \mathcal{I}(\partial_x^b v_{\rho;t,x})$. At fixed x, use $1 - e^{-\lambda h} \le \lambda h$ in the finite λ integral; at fixed t, use $|e^{i\xi\cdot x} - e^{i\xi\cdot y}| \le |\xi||x-y|$ and the next heat moment. The squared triangle inequality gives

$$\mathbb{E}|Z_b(t,x) - Z_b(s,y)|^2 \le C_{\rho,b}(|t-s| + |x-y|^2). \tag{5.2.16}$$

For fixed cutoff, the temporal integral is over a bounded range of λ, so its extra factor λ remains integrable. The heat factor controls the extra powers of ξ needed for the spatial increment. Splitting a general increment into a time increment and a spatial increment gives the displayed sum of bounds. This computation uses (5.2.11), including its spatial width, and applies to singular spectral measures without a density assumption.

Step 2. We construct the jointly continuous versions. The maximum of finitely many increments has its L^q norm bounded by the qth root of the sum of their qth moments, without independence. Here is a direct continuity construction. In $m = d+1$ parameter dimensions on a compact rectangle, even Gaussian qth increment moments have root bounded by $C\sqrt{q}$ times the parameter distance to the power $1/2$ at small distances. The dyadic grid has at most $C_m 2^{nm}$ adjacent edges at level n. Their maximum has L^q norm at most $C\sqrt{q}\,2^{-n(1/2-m/q)}$, with constants for this rectangle and fixed ρ, b. Choose q large and $0 < h_0 < 1/2 - m/q$. The sum of these maxima weighted by 2^{nh_0} has finite L^q norm. Binary refinement, using a fixed number of adjacent edges per coordinate at each scale, gives a continuous extension from dyadic points. At each fixed parameter the extension agrees with the given Gaussian variable in L^2, by (5.2.16); it is a modification. Use countably many nested compact rectangles and all multiindices. The versions agree on overlaps on countable dense sets, hence everywhere there by continuity, so they patch.

Step 3. We identify the continuous fields as spatial derivatives. They are derivatives. The $\mathcal{G}$-valued fundamental theorem gives, along a coordinate segment,

$$\partial_x^b v(t, x + he_i) - \partial_x^b v(t,x) = \int_0^h \partial_x^{b+e_i} v(t, x + ue_i)\,\mathrm{d}u.$$

Apply bounded linear $\mathcal{I}$ and L^2 integration. The continuous versions give the same ordinary integral by their Riemann sums, which converge both pathwise and in L^2. Enforce these identities first on countably many rational t, x, h and multiindices, then use joint continuity to extend them to every segment in the compact rectangles. The ordinary fundamental theorem yields $\partial_i Z_b = Z_{b+e_i}$. Thus, all spatial derivatives exist and are jointly continuous with time. The versions are for this fixed ρ, not a common path event over uncountably many source parameters. This proves Lemma 5.2.6. □

Proposition 5.2.7 (Ordinary source response)**.** *For each fixed $\rho > 0$, on its regularity event, put $b_\rho(t,x) = \zeta_R(x) Y_\rho(t,x)$. The statewise integral*

$$L_\rho(t)z = \int_0^t S(-u)B(b_\rho(u))S(u)z\,\mathrm{d}u \tag{5.2.17}$$

defines an operator-norm Lipschitz path on E, and $L_\rho = M_R^\rho$ for all $t \in [0,T]$ on one probability-one set. In particular, it has the strongly measurable path version supplied by the Gaussian construction.

Proof. We first construct the ordinary integral path using the samplewise smooth coefficient. We then identify its scalar rows with the transferred noise evaluations and use countability and continuity to obtain equality of paths.

Step 1. We construct the ordinary response on its regularity event. The coefficient is compact smooth in space and continuous in time in every spatial derivative norm. Multiplication estimates and strong continuity of the full free group show that the statewise integral exists on every E_r. Its operator increments $E_r \to E_{r+1}$ are bounded by a finite sample constant times $|t-s|$, exactly by the statewise gain argument of Lemma 5.1.4. This proves Lipschitz continuity in $\mathcal{B}(E)$, without requiring norm continuity or an operator-norm derivative of $S(t)$.

Step 2. We identify its rows by physical duality and test approximation. The row calculation is (4.2.15) of Proposition 4.2.3, with G_w from (4.2.12), applied at the fixed time u to the spatial coefficient $b_\rho(u,\cdot)$. At each fixed u, the Sobolev duality calculation uses only spatial smoothness of $b_\rho(u,\cdot)$. From $S(-u)(0,f)$ and the two Bessel weights, for real Schwartz phases,

$$\langle S(-u)B(b_\rho(u))S(u)z, w\rangle_E = \int b_\rho(u,x)[S(u)z]_1(x)G_w(u,x)\,\mathrm{d}x.$$

Thus, no prior hypothesis of smoothness in time is invoked for this instantaneous identity. For complex pairs conjugate the second factor. For the approximation below, Cauchy–Schwarz on the fixed finite time interval converts L^2 time error to L^1 error, and the common compact spatial support contributes only its fixed volume. Integrating gives the ordinary source-field integral against the specified wave test for the original covariance $h_{R,t;z,w}$. For smooth tests, the point-feature integral has already been identified with $Y_\rho(F)$. The continuous random field version has the same integral: compact Riemann sums converge pathwise and in L^2 to the ordinary and feature integrals, respectively. Approximate the indicator wave test in the covariance completion with common compact spatial support and L^2-time spatial supremum error tending to zero. Its L^1 error also tends to zero. The point-feature norms are bounded on that support, so their integrals converge in $\mathcal{G}$; the original variance domination gives the same L^2 limit on the test side. Consequently,

$$\langle L_\rho(t)z, w\rangle_E = Y_\rho(h_{R,t;z,w}) = \langle M_R^\rho(t)z, w\rangle_E \quad \text{in } L^2.$$

Step 3. We obtain equality at every time on one event. Compare a countable dense Schwartz phase collection and rational times. Boundedness and the path continuity of both sides extend this equality to all states and all times on one probability-one set. The equality is on the coupled space, not only in law. The set is for fixed ρ; the L^p limit in (5.2.13) needs no simultaneous version for every source parameter. This proves Proposition 5.2.7. □

The regularized noise laws above match the pinned author definitions. The author's page 9 redefinition keeps the law; the extension preserving the given noise was proved in Lemma 5.2.4. The derivative estimate here was derived from the correct joint covariance,

not from the differing spatial index in the author's page 8 increment display. No source correction is adopted. All limits are at fixed finite R, T. The nonlinear Young flow, canonical initial datum $(1, 0)$ and its solution-moment transfer remain separate parts of the argument.

What we now have. An operator path driven by the original noise, for a fixed mask and a finite horizon (Proposition 5.1.1); the regularized sources converge to it in the path norm (Section 5.2). The next chapter lets this path drive a wave.

Chapter 6

Fixed masks and wave evolution

An operator path describes the forcing. Which wave does it drive? The initial data hide a catch: the constant displacement does not lie in the Sobolev phase of the operator estimates. So we carry the constant coordinates explicitly, with displacement and velocity.

This chapter has no figure. Section 6.1 compares the regularized solutions and their tested moments. Section 6.2 builds the Young evolution on the enlarged phase space (Proposition 6.2.4) and identifies it with the physical wave. Section 6.3 studies compact families of nonnegative potentials with a common negative trial value. Their positive ground states and uniform gap (Proposition 6.3.1) control growth in the lower bound.

The inputs are the paths of Chapter 5 and the canonical expansion of Chapter 2. On a first reading, keep Propositions 6.2.4 and 6.3.7 and let the proofs wait. The masks are fixed before source and time limits; none grows with observation time here. Episode ▶ 5 of the video series covers this chapter.

6.1 Fixed masks and displacement moments

We retain Hypothesis 1.2.1, data $(1, 0)$, and all its original dimensions and covariance amplitudes. Fix $\rho = (\epsilon, \eta) > 0$ and the source Y_ρ of Proposition 5.2.5. For each fixed ρ use the continuous-time, smooth-space version in Lemma 5.2.6. Source fields can use the auxiliary extension preserving the given noise; their law and the given noise remain those already constructed. Let $m \in C_c^\infty(\mathbb{R}^d)$ be real with $0 \le m \le 1$. It multiplies the physical source after regularization.

Write $X^m_{\rho,n}(t, x)$ for the ordinary ordered displacement integral with coefficient mY_ρ, and $X_{\rho,n}$ for its unmasked version; both order-zero terms are one. We first construct these integrals. The positive Green measures $G_d(r, \mathrm{d}z)$ have mass r and support in B_r, including the sphere measure in $d = 3$. These are the source kernels [17, (2.1), (2.3)–(2.5), p. 7]; the ordered convention and Gaussian pairing formula are [17, (2.13)–(2.16), p. 10; (2.19), p. 12]. We use all pair partitions, including self-pairings.

Lemma 6.1.1 (Chains and mixed-order comparison)**.** *The finite ordered integrals are Bochner L^2 integrals. For all $n, k \ge 0$, fixed t, x, y and positive ρ,*

$$0 \le \mathbb{E}[X^m_{\rho,n}(t, x) X^m_{\rho,k}(t, y)] \le \mathbb{E}[X_{\rho,n}(t, x) X_{\rho,k}(t, y)]. \tag{6.1.1}$$

Both expectations vanish when $n + k$ is odd. With q_n from Lemma 2.6.1,

$$\|X^m_{\rho,n}(t, x)\|_2 \le q_n(t), \qquad \|X_{\rho,n}(t, x)\|_2 \le q_n(t). \tag{6.1.2}$$

Proof. We construct the ordered integrals using finite positive chain measures and Gaussian moment bounds. We then identify the Green-regularization limit and compare every Wick diagram before summing over pairings.

Step 1. We construct the finite chain integrals. Let $\nu_n^{t,x}$ be the positive time-space chain measure on $0 < s_1 < \cdots < s_n < t$, with successive spatial factors $G_d(s_{j+1} - s_j, \mathrm{d}z_j)$ and $s_{n+1} = t$, recovering positions backwards from x. It uses measures rather than sphere densities. The order-zero measure has mass one. Integrating the latest vertex gives the recursion $f_n(t) = \int_0^t (t-r) f_{n-1}(r)\,\mathrm{d}r$; hence,

$$\nu_n^{t,x}(1) = \frac{t^{2n}}{(2n)!}. \tag{6.1.3}$$

In the covariance and mask factors below, z_i denotes the vertex position recovered backwards from the terminal point, not the Green increment used to construct the chain measure. Starting from mass one at order zero, the recursion integrates the mass of the last Green factor, $t-r$, against the previous mass. Substituting $f_{n-1}(r) = r^{2n-2}/(2n-2)!$ gives the displayed mass by elementary integration. In particular, the measure is finite at each fixed order. Measurability follows by representing $G_d(r)$ as r times the dilation by r of its unit-time probability measure.

The covariance is

$$C_\rho(s, z; r, w) = K_\eta(s-r)\Gamma_{2\epsilon}(z-w), \qquad 0 \le C_\rho \le c_\rho := K_\eta(0)\Gamma_{2\epsilon}(0) < \infty.$$

Positivity uses the nonnegative Radon measure Γ and positive heat and Laplace kernels. The upper bound also follows by Gaussian Cauchy–Schwarz. Hölder's inequality and scalar Gaussian moments bound the absolute expectation of any fixed number of source factors, uniformly over their vertices. Applied to $2n$ factors this bounds the L^2 norm of each n-fold product. The field is measurable and continuous, so integration against the finite chain measure defines a Bochner L^2 integral and permits stochastic Fubini between two chains.

The bound on the L^2 norm of each product is uniform over the integration variables at fixed ρ, n. Its integral against the finite chain measure is therefore finite. This is the Bochner integrability condition, and applying the same argument to two products gives the absolute integrability needed to exchange expectation and the two chain integrals.

Step 2. We identify the integrals obtained by Green smoothing. These are the canonical regularized terminal integrals at common noise widths. The unmasked $X_{\rho,n}(t,x)$ is $Y_n^{\boldsymbol{a}}(t,x)$ from Lemma 2.6.1 with every vertexwise noise width in $\boldsymbol{a}$ set equal to ρ, so its bound is $q_n(t)$. Here is the Green-width identification needed in dimension three. At fixed positive ρ, replace every Green measure by its convolution with a positive heat approximate identity. At fixed times the measures converge weakly, preserving masses. Every Wick covariance product is bounded by a power of c_ρ and is spatially continuous by Lemma 5.2.6. Thus, its spatial integrals converge. The chain mass integrands from (6.1.3) give an integrable time majorant. Square and cross moments between smoothed and unsmoothed integrals converge to the same diagram sum; therefore, the random integrals

converge in L^2. This is precisely the Green-before-noise limit in Lemma 2.5.2. It also applies in dimensions one and two if Green smoothing is used. No samplewise source bound on heat-kernel tails is needed. Consequently, Lemma 2.6.1 applies to the unmasked integrals.

Step 3. We compare each masked Wick diagram with its unmasked diagram. If $n+k$ is odd, Gaussian centering gives zero. If $n+k=2l$, each pair partition D contributes the nonnegative finite integral

$$\int \prod_{\{i,j\}\in D} C_\rho(s_i,z_i;s_j,z_j)\,\mathrm{d}(\nu_n^{t,x}\otimes\nu_k^{t,y}).$$

The masked integrand has the additional factor $\prod_{i=1}^{2l} m(z_i)\in[0,1]$. Every vertex appears exactly once, irrespective of its chain or partner. Summing gives (6.1.1), including unequal and empty chains and every self-pairing. At $n=k=0$ both sides are one. Taking $k=n$, $y=x$ and then applying the unmasked bound gives (6.1.2). This is a statement about expected displacement diagrams; no samplewise solution order or Gaussian covariance order is used. This proves Lemma 6.1.1. □

Proposition 6.1.2 (Ordinary solutions and tested moments)**.** *The sums $u_\rho^m=\sum_{n\ge0}X_{\rho,n}^m$ and $u_\rho=\sum_{n\ge0}X_{\rho,n}$ converge absolutely in L^2 and have locally continuous versions that are the unique locally continuous ordinary mild solutions with coefficients mY_ρ and Y_ρ, respectively, and data $(1,0)$. For every nonnegative $\phi\in C_c^\infty(\mathbb{R}^d)$,*

$$0\le\mathbb{E}[u_\rho^m(t,x)u_\rho^m(t,y)]\le\mathbb{E}[u_\rho(t,x)u_\rho(t,y)], \tag{6.1.4}$$

$$\mathbb{E}\left|\int\phi(x)u_\rho^m(t,x)\,\mathrm{d}x\right|^2\le\|\phi\|_1^2\,\mathbb{E}|u_\rho(t,0)|^2. \tag{6.1.5}$$

The spatial integral is a Bochner L^2 integral.

Proof. We first identify the mean-square series with the continuous Picard solution on each compact observation region. We then pass the mixed-order comparison through the series and integrate it against the nonnegative spatial test.

Step 1. We construct and identify the ordinary mild solutions. Put $Q_T=\sum_{n\ge0}q_n(T)<\infty$, using (2.6.2). Lemma 6.1.1 proves absolute L^2 convergence uniformly in space and widths. To identify the sums pathwise, fix ρ, a compact observation set and a finite horizon T. On the source regularity event the coefficient is bounded by a finite sample-dependent M on the compact backward-cone enlargement. Finite propagation and (6.1.3) bound each Picard term there by $M^nT^{2n}/(2n)!$. This series converges uniformly. Each term is continuous by the unit-time Green representation and dominated integration. Summing the Volterra recursion gives the ordinary mild equation with initial displacement one and velocity zero. Iterating the difference equation between two continuous solutions bounds its value on the observation set by $BM^nT^{2n}/(2n)!$, where B bounds their difference on the larger compact cone. Letting $n\to\infty$ proves uniqueness.

Step 2. We identify the continuous version with the Bochner series. Ordinary Fubini and the absolute product integrability in the preceding lemma identify each Bochner term

with the pathwise chain integral at a fixed terminal point, simultaneously over countably many orders. An almost surely convergent subsequence of the L^2 partial sums then identifies its limit with the continuous Picard version at that point. These versions define the solution for all terminal points at this fixed ρ; no common event over uncountably many widths is needed.

Step 3. We sum the expected two-point comparison. For either masked or unmasked terms, Cauchy–Schwarz gives

$$\sum_{n,k\geq 0} \mathbb{E}|X^{(m)}_{\rho,n}(t,x)X^{(m)}_{\rho,k}(t,y)| \leq Q_t^2.$$

For the unmasked stationary field, Cauchy–Schwarz bounds its two-point expectation by the geometric mean of two equal point second moments. Products of partial sums converge in L^1. Thus, the preceding lemma passes termwise to (6.1.4). The unmasked source law is spatially stationary, and its finite Picard integrals commute with translations. Their L^2 limits inherit stationarity, so $\mathbb{E}[u_\rho(t,x)u_\rho(t,y)] \leq \mathbb{E}|u_\rho(t,0)|^2$. Stationarity is not required of the masked solution.

Step 4. We form the tested spatial average. Translating every recovered vertex position by x identifies $\nu_n^{t,x}$ with the translate of $\nu_n^{t,0}$; on this fixed increment measure, varying x changes only the arguments of the source factors and, in the masked case, of m. Each finite Bochner term is L^2-continuous in x by source increment continuity on compact cones and dominated Gaussian product moments. Uniform q_n tails pass this property to the full sum. Its separable L^2 image and bound Q_t give the Bochner average. Absolute Fubini is justified by $\|\phi\|_1^2 Q_t^2$. Integrating the two-point inequality against $\phi(x)\phi(y)$ proves (6.1.5). This proves Proposition 6.1.2. □

Proposition 6.1.3 (Canonical point-moment limit and conditional transfer)**.** *At every fixed t, at arbitrary relative rates of the two widths,*

$$\lim_{\epsilon,\eta\downarrow 0} \mathbb{E}|u_\rho(t,0)|^2 = \mathbb{E}|u(t,0)|^2, \tag{6.1.6}$$

where u is the original canonical Stratonovich solution. If the masked averages in (6.1.5) converge in L^2 to $Z_m(t,\phi)$, either at arbitrary rates or along a specified sequence with both widths tending to zero, then

$$\mathbb{E}|Z_m(t,\phi)|^2 \leq \|\phi\|_1^2\, \mathbb{E}|u(t,0)|^2. \tag{6.1.7}$$

Proof. We first pass to the canonical limit at each pair of chain orders. A summable double majorant then gives the full point moment. The conditional masked transfer follows by passing to the limit in the tested source inequality.

Step 1. We identify the limit for fixed orders. The relabelling r below reverses the vertex order separately within each chain. At every fixed pair of orders the common-width source law is the vertexwise law in Lemma 2.5.2. At terminal $(t,0)$ reverse each chain by $s'_j = t - s_{n+1-j}$, $z'_j = -z_{n+1-j}$, and likewise for the other chain. Even covariances preserve

the reversed differences. Relabeling vertices sends each pairing $\{i, j\}$ to $\{r(i), r(j)\}$, giving the exact initial-chain convention in Proposition 2.1.1, also for an empty chain. The preceding Green-width identification removes Green smoothing first. Lemma 2.5.2 then gives the canonical limit of each diagram at arbitrary relative noise-width rates. Odd mixed moments stay zero. Hence, at fixed n, k,

$$\mathbb{E}[X_{\rho,n}(t,0)X_{\rho,k}(t,0)] \longrightarrow \mathbb{E}[X_n(t,0)X_k(t,0)].$$

Step 2. We pass from finitely many orders to the full moment. All absolute mixed moments, before and after the limit, are bounded by $q_n(t)q_k(t)$. Given $\delta > 0$, choose a finite square of orders with the double majorant outside it less than δ. On the square the finitely many limits hold jointly; off it both tails are bounded by δ. Proposition 2.1.1 identifies the canonical sum, proving (6.1.6). This argument uses the single-width diagram laws, without assigning a new pathwise realization of the entire canonical solution family.

Step 3. We transfer the bound under the stated masked-limit premise. Finally, L^2 convergence of the masked averages implies convergence of their second moments by

$$|\mathbb{E}|B|^2 - \mathbb{E}|A|^2| \le \|B - A\|_2(\|B\|_2 + \|A\|_2).$$

The inequality follows by factoring the difference of squared norms and applying Cauchy–Schwarz. Convergence in L^2 also bounds both norms on the right, so this difference tends to zero. Thus, both sides of the source inequality have the limits needed for the comparison. Take the same source limit in (6.1.5) and use (6.1.6). Existence of the masked limit remains an explicit premise here; the next section constructs it on a phase containing the constant data. This proves Proposition 6.1.3. □

6.2 Young evolution with constant initial data

We use the fixed $R, T, E, \gamma, \theta, \beta$ of (5.1.1), and choose the allowed even mask $m = \zeta_R$ with $0 \le m \le 1$. All constants in this section can depend on these fixed data, the model and the auxiliary physical cutoffs. There is no uniform estimate as R or T grows.

6.2.1 The distributional phase and its free evolution

Define the real Hilbert space

$$F = E \oplus \mathbb{R}^2, \qquad \|(e, c_1, c_2)\|_F^2 = \|e\|_E^2 + c_1^2 + c_2^2, \qquad e_0 = (0, 1, 0). \tag{6.2.1}$$

Its distributional interpretation is $(e, c_1, c_2) \mapsto (e_1 + c_1, e_2 + c_2)$. Let $i : E \to F$ denote $e \mapsto (e, 0, 0)$ and let $\pi_C : F \to \mathbb{R}^2$ be the constant-coordinate projection.

Lemma 6.2.1 (Constants and finite propagation)**.** *The distributional interpretation of F is continuous and injective. The space is complete and separable, and iE is closed and proper. For every real $\psi \in C_c^\infty(\mathbb{R}^d)$,*

$$L_\psi(e, c_1, c_2) = \psi e + (c_1\psi, c_2\psi) \tag{6.2.2}$$

is bounded from F to E. The free wave group on F is

$$S_F(t)(e, c_1, c_2) = (S(t)e, c_1 + tc_2, c_2). \tag{6.2.3}$$

It is strongly continuous and bounded on finite horizons and has finite propagation for the total distributional data, including local cancellation between e and the constants.

Proof. We first separate constant distributions from the Sobolev phase and prove the cutoff bound. We then identify the free group as convolution on the total distributional data, which gives finite propagation even when the two parts cancel locally.

Step 1. We prove injectivity and the basic Hilbert-space properties. A nonzero constant has Fourier transform a nonzero multiple of δ_0. Every H^σ Fourier transform is locally L^2 near zero, since its weight is bounded above and below there. A locally L^2 function f cannot represent δ_0: testing against $\varphi(\xi/\varepsilon)$, with $\varphi(0) = 1$ and φ compactly supported in B_1, bounds its integral by

$$\|f\|_{L^2(B_\varepsilon)}\varepsilon^{d/2}\|\varphi\|_2 \longrightarrow 0,$$

whereas δ_0 gives one. Thus, constants lie in neither $H^{1/2}$ nor $H^{-1/2}$; the interpretation is injective. Sobolev duality and the two test integrals prove continuity into distributions, uniformly on bounded families of compact tests. Completeness, separability and the closed proper inclusion follow from the Hilbert direct sum.

Step 2. We bound localization from the extended phase to the Sobolev phase. Multiplication by ψ is bounded on both Sobolev entries. Indeed, the Peetre inequalities give $\langle\xi\rangle^\sigma\langle\eta\rangle^{-\sigma} \le 2^{|\sigma|/2}\langle\xi-\eta\rangle^{|\sigma|}$. In the unitary Fourier convention its weighted kernel is therefore bounded by convolution with the L^1 function $2^{|\sigma|/2}c_d|\widehat{\psi}(q)|\langle q\rangle^{|\sigma|}$, where $c_d = (2\pi)^{-d/2}$. The $L^1 * L^2$ bound applies at $\sigma = \pm 1/2$; the two constant columns are also in E. This proves boundedness of (6.2.2).

Step 3. We identify the free group and finite propagation. The finite-dimensional block in (6.2.3) and the strong, finite-horizon bound for $S(t)$ from Lemma 5.1.4 prove the group assertions. To verify its physical meaning, for $t > 0$ consider the matrix of compactly supported distributions

$$\begin{pmatrix} \partial_t G_d(t) & G_d(t) \\ \Delta G_d(t) & \partial_t G_d(t) \end{pmatrix}.$$

The source Green convention gives $\widehat{G}_d(t)(\xi) = c_d \sin(t|\xi|)/|\xi|$; hence its convolution multiplier is the sine quotient, and the differentiated multipliers are $\cos(t|\xi|)$ and $-|\xi|\sin(t|\xi|)$. The matrix agrees with $S(t)$ on Schwartz phases. Convolution by a compact distribution is continuous on tempered distributions: its transpose convolves a Schwartz test with the reflected compact distribution, continuously in all Schwartz seminorms. Schwartz approximation in E extends the identity to E. The masses of the four entries are $1, t, 0, 1$, so constants give exactly (6.2.3). Time reversal handles $t < 0$ with the same support bound. The support property concerns the total distribution, not its chosen decomposition. Each entry is supported in $B_{|t|}$, also for the three-dimensional sphere

kernel. If the total initial distribution vanishes on an enlarged region, each translated kernel tests zero there, so the evolved total distribution vanishes on the smaller cone. This argument permits cancellation between its Sobolev and constant parts. This proves Lemma 6.2.1. □

6.2.2 The two columns for constant initial data

Choose real $\chi \in C_c^\infty$, equal to one on B_{2R+T+1} and supported in B_{2R+T+2}, and choose real compact smooth $\psi = 1$ on a neighborhood of $\operatorname{supp}\chi$. Write $M_E = M_R$ and $M_E^\rho = M_{Y_\rho}$ for the paths already constructed, with the same original deterministic coefficients.

Proposition 6.2.2 (Extended operator path)**.** *As identities of continuous operator paths,*

$$D_\chi M_E = M_E = M_E D_\chi, \tag{6.2.4}$$

and the same holds for each fixed ρ. Define

$$A_E = M_E L_\psi, \qquad A = iA_E, \qquad A_E^\rho = M_E^\rho L_\psi, \qquad A^\rho = iA_E^\rho. \tag{6.2.5}$$

These are independent of ψ, have compact values, and satisfy $Ai = iM_E$, $\pi_C A = 0$ and their source counterparts. In every finite L^pC^θ, $A^\rho \to A$ at arbitrary relative source-width rates. Their norms have uniform $\sqrt{p}$ moment bounds and a common finite square-exponential moment. The original A is measurable with respect to the given W.

Proof. We pass both localizations from the deterministic coefficients to the path limits. Right localization then removes the choice of the auxiliary cutoff, while bounded composition transfers convergence, compactness and moment estimates to the larger phase.

Step 1. We pass the localization identities to the path limits. Lemma 5.1.4 gives both localizations for every deterministic $A_j(0,t)$. The original finite sums retain them. Proposition 5.2.2 constructs the source finite sums with exactly these coefficients and correlated $Y_\rho(f_j)$. Their C^θ limits preserve both identities. A uniformly convergent subsequence, or rational times and continuous paths, gives (6.2.4) for all t on one event. Use a separate event for each fixed ρ.

Step 2. We define the extended path independently of the auxiliary cutoff. For two choices ψ, ψ', $(L_\psi - L_{\psi'})z \in E$ and $D_\chi(L_\psi - L_{\psi'})z = 0$. The right localization kills this difference. For $z = ie$, $D_\chi D_\psi e = D_\chi e$ and hence $Ai = iM_E$. The constant columns are precisely $iM_E(\psi, 0)$ and $iM_E(0,\psi)$; they are retained. The range of i has zero constant coordinates, which also gives $\pi_C A = 0$.

Step 3. We transfer the path bounds and measurability. Bounded composition preserves compactness and transfers (5.2.13) and the Gaussian norm bounds to (6.2.5). If $\|X\|_{L^p} \le C\sqrt{p}$, then $\mathbb{E}X^{2n} \le C^{2n}(2n)^n$. Since $n! \ge (n/e)^n$, the exponential series gives $\mathbb{E}e^{cX^2} < \infty$ uniformly when $2ecC^2 < 1$. Finally, A is a deterministic bounded transform of the original W-measurable operator path. This proves Proposition 6.2.2. □

Lemma 6.2.3 (Ordinary response on all of F)**.** *For fixed ρ put $b(r) = mY_\rho(r)$ and define*

$$B_F(b)(e, c_1, c_2) = (0, b(e_1 + c_1)) \in E.$$

Then

$$A_E^\rho(t)z = \int_0^t S(-r)B_F(b(r))S_F(r)z\,\mathrm{d}r \tag{6.2.6}$$

as a statewise strong integral. Its primitive is Lipschitz in $\mathcal{B}(F, E)$ and the identity holds for all states and times on one event for this fixed ρ.

Proof. We first bound the ordinary coefficient operator on the full phase, including the constant displacement. We then use finite propagation to replace each initial state by its localized Sobolev representative near the coefficient support.

Step 1. We construct the statewise integral and its Lipschitz bound. The source regularity gives one compact spatial support for b, continuity in L^∞ and L^2, and bounded spatial derivatives on the horizon. Since $e_1 \in L^2$ and $\|\cdot\|_{H^{-1/2}} \le \|\cdot\|_2$,

$$\|B_F(b)\|_{\mathcal{B}(F,E)} \le \|b\|_\infty + \|b\|_2.$$

Strong continuity and finite-horizon bounds of both free groups make the integrand strongly continuous on each state and uniformly bounded as an operator. Integrating its bound proves operator-norm Lipschitz increments without assuming a Banach-valued operator derivative.

Step 2. We identify the ordinary response for every extended state. The total initial distributions of z and $iL_\psi z$ agree on the entire enlarged ball where $\psi = 1$. Lemma 6.2.1 gives equality of the free displacements near $\operatorname{supp} m$ for $0 \le r \le T$. Multiplication by $b(r)$ kills the difference. Apply Proposition 5.2.7 to the E state $L_\psi z$ to obtain (6.2.6). Separability and rational times, followed by boundedness and continuity, give its path identity. This proves the constant columns directly; no density of E in F is used. This proves Lemma 6.2.3. □

6.2.3 The exact linear Young equation

We use Young's integration theory [49] in its Banach-space form. The estimate is stated by Friz and Hairer [30, Sections 1.4–1.5, 4.1, (4.3), pp. 13, 61–62]. For D, V with exponent $\theta > 1/2$ and bounded bilinear multiplication, left composition gives

$$\left\| \int_s^t \mathrm{d}D(r)V(r) - D(s,t)V(s) \right\| \le C_\theta [D]_\theta [V]_\theta |t - s|^{2\theta}. \tag{6.2.7}$$

The Banach spaces here are $\mathcal{B}(F)$, and multiplication is bounded with constant one. We derive the linear solution and stability estimates below rather than invoke a nonlinear bounded-vector-field theorem.

Proposition 6.2.4 (Linear Young evolution)**.** *For every $D \in C^\theta([0,T];\mathcal{B}(F))$ with $D(0)=0$ there is a unique C^θ solution, in the terminal variable, of*

$$U_D(t,s) = I + \int_s^t \mathrm{d}D(r)U_D(r,s). \tag{6.2.8}$$

It has the composition law, invertible values and joint operator-norm continuity on $0 \le s \le t \le T$. The map $D \mapsto U_D$ is locally Lipschitz into the uniform time-triangle norm, and

$$\sup_{s\le t\le T} \|U_D(t,s)\| \le C_T \exp\Big(C_T(1+\|D\|_{C^\theta})^{1/\theta}\Big). \tag{6.2.9}$$

Proof. We solve the equation by contraction on short intervals in a scaled Hölder norm. We compare two such solutions on the same partition, then patch the intervals to obtain the global bound, composition law and invertibility.

Step 1. We construct the solution on a short interval. On an interval $[a, a+\ell]$ use the complete scaled norm $N_\ell(V) = \sup\|V\| + \ell^\theta [V]_\theta$ and put $I_D(V)(t) = \int_a^t \mathrm{d}D\,V$. Applying (6.2.7) to every subinterval gives

$$\begin{aligned} \sup\|I_D(V)\| &\le [D]_\theta \ell^\theta \sup\|V\| + C_\theta [D]_\theta \ell^{2\theta}[V]_\theta, \\ [I_D(V)]_\theta &\le [D]_\theta \sup\|V\| + C_\theta [D]_\theta \ell^\theta [V]_\theta. \end{aligned}$$

For the supremum estimate, use the Young remainder bound between a and t. For the seminorm estimate, apply it to each subinterval and divide by its length to the power θ. Multiplying the second estimate by ℓ^θ and adding it to the first gives the scaled-norm estimate. Thus, with $c_\theta = 2\max(1, C_\theta)$,

$$N_\ell(I_D(V)) \le c_\theta [D]_\theta \ell^\theta N_\ell(V). \tag{6.2.10}$$

Take $K \ge 1$, $[D]_\theta \le K$, and choose ℓ with $c_\theta K \ell^\theta \le 1/4$. The map $V \mapsto V_a + I_D(V)$ is a contraction on the complete affine space of paths starting at V_a. Its solution satisfies $N_\ell(V) \le (4/3)\|V_a\| \le 2\|V_a\|$.

Subtracting two images of the fixed-point map removes the initial value, so its Lipschitz constant is at most $1/4$. The image starts at V_a because the integral vanishes at the left endpoint. Finally, the fixed-point equation gives $N_\ell(V) \le \|V_a\| + N_\ell(V)/4$, which yields the factor $4/3$.

Step 2. We compare solutions driven by two paths. To compare D, D', require both seminorms at most K and write $\delta = \|D - D'\|_{C^\theta}$, $W = V - V'$. Subtracting gives $W = W_a + I_D(W) + I_{D-D'}(V')$. Absorbing the factor $1/4$ yields

$$N_\ell(W) \le 2\|W_a\| + 2c_\theta \ell^\theta \delta N_\ell(V'). \tag{6.2.11}$$

In the difference equation, the first integral contains the unknown difference W and has coefficient at most $1/4$. Move it to the left. The remaining integral is bounded by the same local estimate with driver $D - D'$, whose seminorm is at most δ. Replacing $4/3$ by two gives the displayed bound. Cover $[s,T]$ by at most $n_{K,T}$ such pieces. If the second

initial norm is B, its norm on piece j, indexed from zero, is at most $2^{j+1}B$. With E_j the difference at its left endpoint, induction gives

$$E_{j+1} \le 2E_j + 2^{j+2}c_\theta \ell^\theta \delta B, \qquad E_j \le 2^j E_0 + j2^{j+1}c_\theta \ell^\theta \delta B.$$

Equation (6.2.11) gives the same bound inside each piece; a shorter final piece only reduces the coefficient. For evolutions, $E_0 = 0$ and $B = 1$. The number of pieces is uniform in s, t, proving local Lipschitz dependence in the full triangle norm.

Step 3. We patch the intervals and prove the flow properties. Now choose $K = 1 + \|D\|_{C^\theta}$. At most $C_T(1 + \|D\|_{C^\theta}^{1/\theta})$ pieces suffice. Each multiplies the norm by at most two, giving (6.2.9). The product of these factors is bounded by an exponential in the number of pieces. Uniqueness patches the solutions; right multiplication by the preceding evolution gives the composition law. On a small piece (6.2.10) gives $\|U_D - I\|_\infty \le 1/3$, so a Neumann series proves local invertibility, then products give global invertibility. Finally, $U_D(t,s) = U_D(t,0)U_D(s,0)^{-1}$ proves joint norm continuity, since $U_D(\cdot,0)$ is continuous and inversion is continuous on invertible operators. This proves Proposition 6.2.4. □

Proposition 6.2.4 concerns one deterministic operator path. We now apply it to the random paths A and A^ρ of (6.2.5) and pass to the physical flow on F.

Proposition 6.2.5 (Gaussian Young and physical flows)**.** *Apply Proposition 6.2.4 to A, A^ρ. The resulting flows are strongly measurable in uniform triangle norm, have every finite norm moment and satisfy*

$$U_{A^\rho} \longrightarrow U_A \quad \text{in every finite } L^p\left(\sup_{0\le s\le t\le T} \|\cdot\|_{\mathcal{B}(F)}\right). \tag{6.2.12}$$

They preserve the interaction constant coordinates:

$$\pi_C U_A(t,s) = \pi_C, \qquad (U_A(t,s) - I)F \subset iE, \tag{6.2.13}$$

and likewise for the source. The physical flow is

$$P_A(t,s) = S_F(t)U_A(t,s)S_F(-s). \tag{6.2.14}$$

It has composition and strong continuity on states, physical constant block $(c_1, c_2) \mapsto (c_1 + (t-s)c_2, c_2)$, all finite moments and the analogous uniform L^p source convergence. Its difference from the free flow has range in iE.

Proof. We first obtain measurability and the constant-coordinate identities. Local stability gives convergence in probability after restricting to bounded driver norms. Gaussian tails give the moments needed to strengthen this to L^p convergence, and bounded free-group composition transfers it to the physical flow.

Step 1. We obtain measurable flows and their range identities. The original paths lie in separable closed path spans by their Gaussian construction. Bounded composition in (6.2.5) and the continuous Young map preserve strong measurability into $C(\Delta_T; \mathcal{B}(F))$,

where $\Delta_T = \{(t,s) : 0 \le s \le t \le T\}$ has the uniform norm. Indeed, the continuous image of the separable space of operator paths has separable closure in this triangle space. Applying π_C to Young Riemann sums gives the first identity in (6.2.13). Each increment applied to any state lies in iE; closedness of this subspace passes the property through sums and limits, giving the second identity.

Step 2. We prove convergence in probability of the Young flows. Write $X_\rho = \|A^\rho\|_{C^\theta}$ and $X_0 = \|A\|_{C^\theta}$. Proposition 6.2.2 supplies $c_0 > 0$ and $H_0 < \infty$ such that

$$\sup_\rho \mathbb{E} e^{c_0 X_\rho^2} \le H_0, \qquad \mathbb{E} e^{c_0 X_0^2} \le H_0.$$

For $K \ge 1$, let L_K be the Lipschitz constant of Proposition 6.2.4 on the ball of operator paths of radius K, in the whole time-triangle norm. On $\{X_\rho \le K,\ X_0 \le K\}$ it gives

$$\|U_{A^\rho} - U_A\|_\infty \le L_K \|A^\rho - A\|_{C^\theta}.$$

Consequently, for $\varepsilon > 0$ and any finite $q \ge 1$, Markov and the union bound give

$$\mathbb{P}(\|U_{A^\rho} - U_A\|_\infty > \varepsilon) \le 2H_0 e^{-c_0 K^2} + (L_K/\varepsilon)^q \mathbb{E}\|A^\rho - A\|_{C^\theta}^q.$$

The exceptional event is contained in the union where either driver norm exceeds K. Markov applied to each square exponential bounds this union by the first term. On its complement, the local Lipschitz estimate and the ordinary moment form of Markov give the second term. At fixed K the second term tends to zero at arbitrary relative source-width rates. Only then let $K \to \infty$ to obtain convergence in probability. No independence of the original, source and residual operator paths is required.

Step 3. We obtain flow moments and strengthen convergence to L^p. Put $\nu = 1/\theta < 2$. For each finite $r \ge 1$ and $c > 0$, there is $C_{r,c} < \infty$ such that

$$r C_T (1+x)^\nu \le c x^2 + C_{r,c}, \qquad x \ge 0.$$

This follows because $(1+x)^\nu / x^2 \to 0$ as $x \to \infty$, while the remainder is bounded on compact intervals. Use $c \le c_0$ and (6.2.9) to obtain

$$\sup_\rho \mathbb{E}\|U_{A^\rho}\|_\infty^r < \infty, \qquad \mathbb{E}\|U_A\|_\infty^r < \infty.$$

In particular, for fixed finite $p \ge 1$ and $V_\rho = \|U_{A^\rho} - U_A\|_\infty$, the $2p$ moments of V_ρ are uniformly bounded. For every $\varepsilon > 0$,

$$\mathbb{E} V_\rho^p \le \varepsilon^p + (\mathbb{E} V_\rho^{2p})^{1/2} \mathbb{P}(V_\rho > \varepsilon)^{1/2}.$$

Split the expectation into $V_\rho \le \varepsilon$ and its complement. On the first event the integrand is at most ε^p. On the second, Cauchy–Schwarz pairs V_ρ^p with the indicator, giving the displayed probability factor. The uniform $2p$ moment bound therefore supplies uniform integrability. The second term tends to zero by convergence in probability; then let $\varepsilon \downarrow 0$.

This proves (6.2.12). The square-exponential bound used here is an operator path bound; no square-exponential flow bound is needed.

Step 4. We transfer the conclusions to the physical flow. The free group is strongly continuous and bounded on the horizon. Define $\mathcal{B}_\infty(\Delta_T;\mathcal{B}(F))$ to be the Banach space of all bounded operator families on Δ_T. The deterministic map

$$\mathcal{L}(V)(t,s) = S_F(t)V(t,s)S_F(-s)$$

is bounded linear from $C(\Delta_T;\mathcal{B}(F))$ into this bounded-family space, with norm at most C_T^2, where $C_T \geq \sup_{|r|\leq T}\|S_F(r)\|$. Hence, it preserves strong measurability on the separable ranges and gives, in particular,

$$\|P_{A^\rho} - P_A\|_\infty \leq C_T^2\|U_{A^\rho} - U_A\|_\infty.$$

For the range identity below, the rightmost free-group factor changes the input, while the leftmost factor preserves iE. Thus, composing $U_A(t,s)-I$ with these factors preserves its range inclusion in iE. All finite moments and uniform L^p convergence therefore transfer to the physical flows. This does not place those flows in the norm-continuous triangle space or assert operator-norm continuity of the free group. For each fixed state, joint continuity follows by splitting a physical-flow difference into the norm-continuous U difference and two strong free-group differences, using the uniform group bound. Group cancellation gives composition. The finite constant block $J_t(c_1,c_2) = (c_1+tc_2,c_2)$ satisfies $J_tJ_{-s} = J_{t-s}$, which gives the asserted physical constant coordinates from $\pi_C U_A = \pi_C$. Finally,

$$P_A(t,s) - S_F(t-s) = S_F(t)(U_A(t,s)-I)S_F(-s)$$

has range in iE, since $S_F(t)iE = iE$. This proves Proposition 6.2.5. □

6.2.4 Ordinary source solutions and the original tested observable

So far P_{A^ρ} is defined through Young integrals, not through the source equation of Proposition 6.1.2. We now connect the two at a fixed source width ρ.

Lemma 6.2.6 (Identification with the ordinary source equation)**.** *For fixed ρ, the displacement distribution of $P_{A^\rho}(t,0)e_0$ is the locally continuous ordinary source solution $u_\rho^m(t,\cdot)$ from Proposition 6.1.2.*

Proof. We first identify the Young integral with the ordinary interaction integral for fixed regularization. We then compare the phase Picard terms with the scalar Green-chain terms by distributional testing and pass to their limits.

Step 1. We identify the statewise Young equation with the ordinary equation. In (6.2.6) let $C(r) = S(-r)B_F(b(r))S_F(r)$. The primitive is A_E^ρ. For left endpoints $r_j = t_j$, the Young sums applied to a state v are

$$\sum_j \int_{t_j}^{t_{j+1}} iC(r)U_{A^\rho}(r_j,s)v\,\mathrm{d}r.$$

Uniform continuity of U and the uniform bound for C make these converge to the strong integral with $U(r,s)v$. Thus, the Young equation is precisely the ordinary interaction integral on states. Multiplying by free groups gives the Duhamel equation for displacement and velocity. Its unique $C([0,T];F)$ solution follows by the bounded-coefficient Picard argument with the strongly continuous, bounded free group. No operator-norm derivative of S_F is used.

Step 2. We construct the phase Picard series. More explicitly, put $W_0(t) = e_0$ and, for $n \geq 1$,

$$W_n(t) = \int_0^t S_F(t-r) i B_F(b(r)) W_{n-1}(r)\,\mathrm{d}r.$$

The ordered n-fold time simplex has volume $T^n/n!$. If $B_T = \sup_r \|B_F(b(r))\|_{\mathcal{B}(F,E)}$, induction on the time simplex gives $\sup_t \|W_n(t)\|_F \leq C_T^{n+1} B_T^n T^n/n!$. We take $C_T \geq \max(1, \sup_{|t|\leq T} \|S_F(t)\|)$, which also supplies the bound at order zero. The series converges in $C([0,T];F)$. The Duhamel map there has norm at most $C_T B_T T$, so its sum solves the same integral equation and equals the ordinary phase by uniqueness.

Step 3. We identify the displacement of each term and then of the sum. Let $X_0(t,x) = 1$ and $X_n(t) = \int_0^t G_d(t-r) * (b(r) X_{n-1}(r))\,\mathrm{d}r$. At fixed n these are continuous in time and smooth in space. Derivatives fall on the smooth compact factor bX_{n-1}; Green mass $t-r$ bounds the integrals, while the unit-time measure representation gives time continuity. This is induction using only finitely many bounded derivatives for each fixed derivative order. At $n=0$ the phase displacement is X_0. If the equality holds at $n-1$, multiplication by smooth b identifies the forcing with $(0, f_r)$, where $f_r = b(r)X_{n-1}(r)$ is smooth and compactly supported. For a compact smooth test φ, continuous distributional testing of the phase integral yields

$$\langle [W_n(t)]_1, \varphi \rangle = \int_0^t \int f_r(y) \int G_d(t-r,\,\mathrm{d}z)\varphi(y+z)\,\mathrm{d}y\,\mathrm{d}r = \langle X_n(t), \varphi \rangle.$$

Absolute Fubini follows from $\|\varphi\|_\infty \|f_r\|_1 (t-r)$, integrable on the horizon because f_r has one compact support and continuous L^1 norm. This also covers sphere measures in $d=3$. Iterating the scalar recursion gives exactly $X^m_{\rho,n}$, with chronological order and all physical mask factors. The scalar compact-cone factorial bound gives locally uniform convergence to u^m_ρ, whereas the phase series converges in F and hence in distributions. Their displacement limits agree. This proves Lemma 6.2.6. □

Lemma 6.2.6 holds at each fixed ρ. To reach the original noise we test against a fixed ϕ and use the source limit (6.2.12).

Proposition 6.2.7 (Original average and original point moment)**.** *Let real $\phi \in C_c^\infty(\mathbb{R}^d)$ be nonnegative with integral one. The bounded functional and original random variable*

$$O_\phi(e, c_1, c_2) = \langle e_1, \phi \rangle + c_1, \qquad Z_m(t,\phi) = O_\phi P_A(t,0) e_0 \tag{6.2.15}$$

are well defined, and Z_m is W-measurable. At arbitrary relative source-width rates, for every finite p,

$$\int \phi(x) u^m_\rho(t,x)\,\mathrm{d}x \longrightarrow Z_m(t,\phi) \quad \text{in } L^p. \tag{6.2.16}$$

In particular,

$$\mathbb{E}|Z_m(t,\phi)|^2 \le \mathbb{E}|u(t,0)|^2. \tag{6.2.17}$$

Proof. We first identify the ordinary tested source observable with the phase functional. We then show that it is the same random variable as the Bochner average. This allows the flow convergence to supply the masked-limit premise for the original moment comparison.

Step 1. We identify the phase functional and the ordinary source average. Sobolev duality gives $\|O_\phi\| \le (\|\phi\|^2_{H^{-1/2}} + 1)^{1/2}$. The original operator path is W-measurable, and the Young and deterministic maps above are continuous or bounded measurable on their separable ranges. Thus, Z_m is W-measurable and does not depend on the auxiliary J used in source realizations. At each fixed ρ, Lemma 6.2.6 identifies the displacement as a distribution with the ordinary source solution. Testing by this same ϕ, with $\int \phi = 1$, therefore gives the almost sure identity

$$O_\phi P_{A^\rho}(t,0)e_0 = C_\phi := \int \phi(x) u^m_\rho(t,x)\,\mathrm{d}x.$$

This uses the displacement pairing and its constant displacement coordinate in (6.2.15); it takes no point trace of an $H^{1/2}$ state. All identities here are at one fixed ρ, so no uncountable intersection of source-version events is used.

Step 2. We identify the ordinary and Bochner averages in L^2. We verify that C_ϕ equals the Bochner L^2 average B_ϕ from Proposition 6.1.2. That proposition gives the spatially uniform bound $\|u^m_\rho(t,x)\|_2 \le Q_t$, with Q_t also independent of source widths. Scalar Fubini gives

$$\mathbb{E}\int |\phi(x)u^m_\rho(t,x)|\,\mathrm{d}x \le Q_t\|\phi\|_1 < \infty.$$

Thus, the ordinary spatial integral exists almost surely. Weighted Cauchy–Schwarz and scalar Fubini also give

$$\mathbb{E}|C_\phi|^2 \le \|\phi\|_1 \int |\phi(x)|\mathbb{E}|u^m_\rho(t,x)|^2\,\mathrm{d}x \le Q_t^2\|\phi\|_1^2.$$

For every bounded real random variable Ξ on the fixed source space, $V \mapsto \mathbb{E}[\Xi V]$ is a continuous functional on L^2. It therefore commutes with the Bochner integral, while scalar Fubini is justified by $\|\Xi\|_\infty Q_t\|\phi\|_1$. Consequently,

$$\mathbb{E}[\Xi B_\phi] = \int \phi(x)\mathbb{E}[\Xi u^m_\rho(t,x)]\,\mathrm{d}x = \mathbb{E}[\Xi C_\phi].$$

Both averages are real L^2 variables. Taking $\Xi = \operatorname{sign}(B_\phi - C_\phi)$ yields $\mathbb{E}|B_\phi - C_\phi| = 0$, so the two averages agree almost surely.

Step 3. We pass to the original tested observable and moment bound. Proposition 6.2.5 now gives, for every finite p,

$$\|B_\phi - Z_m(t,\phi)\|_{L^p} \le \|O_\phi\|\|e_0\|\Big\|\|P_{A^\rho} - P_A\|_\infty\Big\|_{L^p} \longrightarrow 0.$$

This is (6.2.16), including its L^2 case, for the masked Bochner average, with arbitrary relative source-width rates. It supplies the conditional convergence premise of Proposition 6.1.3 at the same fixed mask, horizon, original covariance and observable. Since $\phi \geq 0$ and $\|\phi\|_1 = 1$, that proposition gives (6.2.17). Zero covariance gives the free constant solution and equality. All source limits are at fixed mask and horizon, before time asymptotics. This proves Proposition 6.2.7. □

So far the operator path comes from the noise alone. Section 6.3 also needs a deterministic potential.

Proposition 6.2.8 (Compact deterministic base)**.** *Let $h \in C([0,T]; C_c^\infty(K))$ be real for one fixed compact K, with all spatial derivatives continuous on that support. The statewise primitive*

$$A_h(t) = \int_0^t iS(-r)B_F(h(r))S_F(r)\,\mathrm{d}r$$

is Lipschitz in $\mathcal{B}(F)$, takes values with range in iE, and has a bound $C_T \sup_r(\|h(r)\|_\infty + \|h(r)\|_2)$. The flow conclusions above, including moments, source convergence and ordinary-source identification, hold for $A_h + gA$ and $A_h + gA^\rho$, uniformly on bounded displayed deterministic bounds and bounded real g. No Cameron-shift identity is asserted here.

Proof. We bound the deterministic primitive and then add it to the Gaussian driver. Its bounded shift preserves the required exponential control, so the preceding stability and ordinary-source arguments apply.

Step 1. We bound the shifted driver and its moments. The estimate for B_F and the strong free groups prove the primitive and its Lipschitz bound exactly as in Lemma 6.2.3. If $\|A_h\|_{C^\theta} \leq H$, $|g| \leq G$ and $X = \|A\|_{C^\theta}$, then $\|A_h + gA\|_{C^\theta} \leq H + GX$. If $\mathbb{E}e^{cX^2}$ is bounded, choose $c' \leq c/(2(1+G^2))$ to obtain

$$\mathbb{E}e^{c'\|A_h+gA\|_{C^\theta}^2} \leq e^{2c'H^2}\mathbb{E}e^{2c'G^2X^2} < \infty.$$

The elementary inequality $(H+GX)^2 \leq 2H^2 + 2G^2X^2$ gives the displayed exponential comparison. The choice of c' ensures that the coefficient of X^2 stays below the available Gaussian exponential constant. The deterministic factor is uniform when H and G are bounded. Alternatively $pC(1+H+Gx)^{1/\theta} \leq cx^2 + C_{p,H,G,c}$ transfers the Young growth estimate directly to all finite moments.

Step 2. We transfer convergence and the ordinary-source identification. Source operator-path convergence, local Young stability and uniform integrability give the same flow convergence. The state-integral and Picard-to-chain arguments apply to $h + gmY_\rho$, whose spatial support lies in one fixed compact union. These are individual estimates and versions, without an uncountable common-parameter event. Only $h = 0$, $g = 1$ enters (6.2.17). This proves Proposition 6.2.8. □

6.3 Compact mean families and the spectral gap for wave evolution

Let $I = [0,1]$, let $K_x \subset \mathbb{R}^d$ be compact, and let $\sigma \mapsto V_\sigma$ be continuous from I into $C_c^\infty(K_x)$, real and nonnegative. The index σ is a family parameter, distinct from physical propagation time t. Assume that one real $w \in H^1(\mathbb{R}^d)$ with $\|w\|_2 = 1$ satisfies

$$\|\nabla w\|_2^2 - \int V_\sigma w^2 \le -\varepsilon \quad \text{for all } \sigma \in I, \qquad \varepsilon > 0. \tag{6.3.1}$$

Put $M = \sup_I \|V_\sigma\|_\infty$ and $H_\sigma = -\Delta - V_\sigma$. The phases E, F, inclusion i, data e_0 and observable O_ϕ are exactly those of Section 6.2. Proposition 6.2.8, with deterministic coefficient $h = V_\sigma$ and noise amplitude zero, gives the ordinary physical flow $P_\sigma(t)$ on F. Its E restriction is $P_\sigma^E(t)$. Uniqueness of the Duhamel solution makes finite-horizon constructions agree on overlaps; integer horizons and autonomy give the same semigroup for every $t \ge 0$.

We import the following statements from the *second edition* of [44]: Theorem 10.2, p. 258, gives the self-adjoint H^2 operator, lower bound, essential spectrum $[0,\infty)$ and compact smooth core for real compact smooth potentials in the dimensions considered here. Theorem 10.13, p. 273, gives a simple positive ground state *if the spectral bottom is an eigenvalue*. Theorem 4.12 and Corollary 4.13, pp. 140–141, give max–min and form monotonicity, with the essential threshold used after discrete eigenvalues end and with the quadratic-form domain allowed. Uniformity, fractional norms and all applications to F are proved below.

6.3.1 The ground family and the global phase

Proposition 6.3.1 (Ground states and a uniform rate gap)**.** *The common form domain of H_σ is H^1 with form $q_\sigma(u) = \|\nabla u\|_2^2 - \int V_\sigma |u|^2$. Its bottom $E_1(\sigma)$ is a simple eigenvalue with a unique real positive-a.e. normalized ground state p_σ. Let $E_2(\sigma)$ be the second max–min level, set to zero when there is no second negative eigenvalue. Then*

$$-M \le E_1(\sigma) \le -\varepsilon, \qquad E_1(\sigma) < E_2(\sigma) \le 0, \tag{6.3.2}$$

$$|E_j(\sigma) - E_j(\tau)| \le \|V_\sigma - V_\tau\|_\infty, \qquad j = 1, 2. \tag{6.3.3}$$

The map $\sigma \mapsto p_\sigma$ is continuous into H^2 and bounded there. With $\lambda_\sigma = \sqrt{-E_1(\sigma)}$ and $\mu_\sigma = \sqrt{-E_2(\sigma)}$,

$$\sqrt{\varepsilon} \le \lambda_\sigma \le \sqrt{M}, \qquad d_0 := \inf_I (\lambda_\sigma - \mu_\sigma) > 0. \tag{6.3.4}$$

Proof. We first identify the common form domain and place the spectral bottom below the essential threshold. We then use simplicity and continuity to obtain a uniform gap, and compare ground states to prove their continuity in H^2.

Step 1. We identify the common form domain. The imported Theorem 10.2 applies to $-V_\sigma$, which is real, compactly supported and in L^2 for $d \le 3$. It gives the stated self-adjoint

operator on H^2 and essential threshold zero. Write $c = 1 + M$ and $A_\sigma = H_\sigma + c \geq 1$. On H^2, integration by parts and the spectral theorem give

$$\|A_\sigma^{1/2} u\|_2^2 = q_\sigma(u) + c\|u\|_2^2, \qquad \|u\|_{H^1}^2 \leq \|A_\sigma^{1/2} u\|_2^2 \leq c\|u\|_{H^1}^2.$$

Since $0 \leq V_\sigma \leq M$ and $c = 1 + M$, the shifted potential term $c - V_\sigma$ lies between one and c. This gives the two form bounds on H^2. The issue is then to identify their completions, rather than assume the form domain from the formal expression. Spectral cutoffs $1_{[1,n]}(A_\sigma)u$ show that H^2 is a core for the half-power form norm. Fourier cutoffs show it is dense in H^1. The two equivalent completions are therefore $D(A_\sigma^{1/2})$ and H^1. Both norms dominate L^2 and give the same L^2 limit, so these are equal as subspaces, with the displayed form. This verifies the form domain used below.

Step 2. We obtain the isolated simple ground state. The form lower bound and (6.3.1) give $-M \leq E_1 \leq -\varepsilon$ by the imported form max–min principle. The bottom belongs to the spectrum and lies below the essential threshold, so it is an isolated eigenvalue of finite multiplicity. Only now apply the imported Theorem 10.13: it is simple with a positive ground state. Conjugation preserves the real operator; positivity and unit L^2 norm fix its real representative.

Step 3. We make the spectral and rate gaps uniform. Simplicity, isolation and threshold zero give $E_1 < E_2 \leq 0$. For every common unit form test, $|q_\sigma(u) - q_\tau(u)| \leq \|V_\sigma - V_\tau\|_\infty$. Taking the same infima over orthogonal complements and suprema in the source max–min formula proves (6.3.3), including passage of E_2 to the threshold. Compactness gives $\Delta_* := \min_I(E_2 - E_1) > 0$. Thus,

$$\lambda_\sigma - \mu_\sigma = \frac{E_2(\sigma) - E_1(\sigma)}{\lambda_\sigma + \mu_\sigma} \geq \frac{\Delta_*}{2\sqrt{M}} > 0.$$

Here $M \geq \varepsilon > 0$, and no division by μ_σ occurs.

Step 4. We prove continuity of the positive normalized ground state. Put $d_V = \|V_\sigma - V_\tau\|_\infty$ and decompose $p_\tau = a p_\sigma + r$, with $r \perp p_\sigma$ and $0 < a \leq 1$. The variational bound gives $q_\sigma(p_\tau) \leq E_1(\sigma) + 2d_V$, whereas the complementary spectral bound gives $q_\sigma(p_\tau) \geq E_1(\sigma) + \Delta_* \|r\|_2^2$. Hence,

$$\|p_\tau - p_\sigma\|_2^2 = 2(1 - a) \leq 2(1 - a^2) \leq 4d_V/\Delta_*. \tag{6.3.5}$$

Positivity of both ground states gives $a = \langle p_\tau, p_\sigma \rangle > 0$. Orthogonality gives $a^2 + \|r\|_2^2 = 1$. The upper form bound follows by changing the potential and then the lowest eigenvalue, each at cost at most d_V. The complementary lower bound uses the uniform gap on r. Combining them gives $\|r\|_2^2 \leq 2d_V/\Delta_*$ and hence the displayed distance estimate. The eigenfunction equation is

$$(1 - \Delta)p_\sigma = (1 - \lambda_\sigma^2 + V_\sigma)p_\sigma.$$

Its right side is continuous in L^2 and bounded there by $1 + 2M$. The inverse of $1 - \Delta$ is an isometry from L^2 to the Bessel H^2 space, proving the asserted H^2 continuity and bound. This proves Proposition 6.3.1. □

The rate gap (6.3.4) is a statement about the spectrum of H_σ. The wave on E is measured in the fixed norm of E, so we first compare the two.

Lemma 6.3.2 (Uniform fractional phase norms)**.** *Let $B = 1 - \Delta$, $c = 1 + M$ and $A_\sigma = H_\sigma + c$. The quarter-power domain is $H^{1/2}$ and*

$$\|B^{1/4}u\|_2 \le \|A_\sigma^{1/4}u\|_2 \le c^{1/4}\|B^{1/4}u\|_2. \tag{6.3.6}$$

The norm

$$\|(u,z)\|_{E_\sigma}^2 = \|A_\sigma^{1/4}u\|_2^2 + \|A_\sigma^{-1/4}z\|_2^2 \tag{6.3.7}$$

is uniformly equivalent to the fixed norm on $E = H^{1/2} \times H^{-1/2}$, interpreting the negative entry by completion.

Proof. We prove the needed fractional order comparison from resolvents. The resulting quarter-power norm comparison identifies the positive phase entry, and duality identifies the negative entry with uniform constants.

Step 1. We compare the quarter-power norms and their domains. In the resolvent supremum below, increasing the quadratic form decreases every term being maximized over the common form domain, reversing the order. On the common form domain H^1, $B \le A_\sigma \le cB$ and all three operators are at least one. For positive self-adjoint T, S with common form domain, $T \le S$ implies $(T+t)^{-1} \ge (S+t)^{-1}$ for $t > 0$. Indeed,

$$\langle f, (T+t)^{-1}f\rangle = \sup_u \{2\,\mathrm{Re}\langle f, u\rangle - q_T(u) - t\|u\|_2^2\};$$

completing the square in the closed form norm proves the identity, and comparison of the suprema proves the order. Consequently, $I - t(T+t)^{-1} \le I - t(S+t)^{-1}$. The scalar identity

$$\sqrt{x} = \frac{1}{\pi}\int_0^\infty t^{-1/2}\frac{x}{x+t}\,\mathrm{d}t$$

follows by $t = xr^2$ and $\int_0^\infty (1+r^2)^{-1}\,\mathrm{d}r = \pi/2$. Spectral integration and positive Tonelli, first over finite intervals and then by monotone convergence, give $T^{1/2} \le S^{1/2}$ as forms, including domain inclusions. Apply this to $B \le A_\sigma \le cB$ to obtain (6.3.6): the form of $A_\sigma^{1/2}$ is the squared norm of $A_\sigma^{1/4}$. The lower and upper comparisons give both domain inclusions, so they also give equality of the quarter-power domains with $H^{1/2}$.

Step 2. We identify the negative phase norm by duality. Under the L^2 pairing the dual norm of $\|A_\sigma^{1/4}u\|_2$ at $z \in L^2$ is $\|A_\sigma^{-1/4}z\|_2$. Cauchy–Schwarz gives the upper bound, and a scalar multiple of $A_\sigma^{-1/2}z$ attains it. Comparison of these dual norms preserves the comparison with reversed inequalities. The constants remain uniform because the positive norm constants depend only on c. Completion and (6.3.6) identify this negative space with $H^{-1/2}$, uniformly in σ. Adding the squared norms proves the claim. This proves Lemma 6.3.2. □

Proposition 6.3.3 (The complementary wave on E)**.** *Put*

$$e_\sigma^E = (p_\sigma, \lambda_\sigma p_\sigma), \qquad \ell_\sigma^E(u,z) = \frac{\langle p_\sigma, u\rangle + \langle p_\sigma, z\rangle/\lambda_\sigma}{2}, \qquad \Pi_\sigma^E = e_\sigma^E \ell_\sigma^E.$$

These are bounded real objects, continuous in their respective norms, with $\ell_\sigma^E(e_\sigma^E) = 1$, *and*

$$P_\sigma^E(t)e_\sigma^E = e^{\lambda_\sigma t}e_\sigma^E, \qquad \ell_\sigma^E P_\sigma^E(t) = e^{\lambda_\sigma t}\ell_\sigma^E, \tag{6.3.8}$$

$$\|P_\sigma^E(t)(I - \Pi_\sigma^E)\|_{\mathcal{B}(E)} \le C(1+t)e^{\mu_\sigma t}, \qquad t \ge 0. \tag{6.3.9}$$

The constant is uniform over $\sigma \in I$.

Proof. We estimate the spectral wave matrix in the uniformly equivalent phase norm, separating the complementary spatial spectrum from the two ground-state branches. We then identify this spectral matrix with the ordinary physical flow.

Step 1. We write the spectral wave and its complementary spatial bound. Define real spectral functions $C_t(h), S_t(h)$ by $\cos(t\sqrt{h}), \sin(t\sqrt{h})/\sqrt{h}$ for $h > 0$, by $1, t$ at zero, and by $\cosh(t\sqrt{-h}), \sinh(t\sqrt{-h})/\sqrt{-h}$ for $h < 0$. The spectral wave matrix is

$$\begin{pmatrix} C_t(H_\sigma) & S_t(H_\sigma) \\ -H_\sigma S_t(H_\sigma) & C_t(H_\sigma) \end{pmatrix}. \tag{6.3.10}$$

Real potentials, their resolvents and spectral resolutions commute with conjugation. All these real functions and positive A_σ powers preserve the real phases.

The spatial projection $Q_\sigma^{\mathrm{sp}} = I - |p_\sigma\rangle\langle p_\sigma|$ commutes with H_σ, A_σ and is contractive on both entries of (6.3.7). On its support $h \ge E_2 = -\mu_\sigma^2$, the phase isometry gives scalar matrix entries

$$C_t(h), \quad \sqrt{h+c}\,S_t(h), \quad -hS_t(h)/\sqrt{h+c}, \quad C_t(h).$$

The isometry multiplies the displacement by $(h+c)^{1/4}$ and the velocity by $(h+c)^{-1/4}$. Conjugating the two off-diagonal entries by these weights produces the displayed factors $\sqrt{h+c}$ and its reciprocal. Thus, an ordinary scalar matrix bound gives an operator bound in the spectral phase norm. For $h \ge 0$, use $|S_t(h)| \le \min(t, h^{-1/2})$ and split $h \le 1$ from $h \ge 1$; the lower off-diagonal entry is at most one. For $-\mu_\sigma^2 \le h < 0$, use $|C_t(h)| \le e^{\mu_\sigma t}$ and $|S_t(h)| \le te^{\mu_\sigma t}$, with $|h| \le M$ and $1 \le h + c \le c$. Thus, the complementary spatial matrix has norm at most $C(1+t)e^{\mu_\sigma t}$, including $\mu_\sigma = 0$.

Step 2. We retain the decaying ground branch in the phase complement. The two spatial ground branches are $(p_\sigma, \pm\lambda_\sigma p_\sigma)$. Besides Π_σ^E, their projections include the decaying branch

$$(p_\sigma, -\lambda_\sigma p_\sigma)\frac{\langle p_\sigma, u\rangle - \langle p_\sigma, z\rangle/\lambda_\sigma}{2}.$$

Their sum is the spatial ground projection on both phase entries. Both projection norms are uniformly bounded in the spectral phase norm because $\sqrt{\varepsilon} \le \lambda_\sigma \le \sqrt{M}$ and $1 \le c - \lambda_\sigma^2 \le c$. The decaying branch has factor $e^{-\lambda_\sigma t}$ and remains in $I - \Pi_\sigma^E$. The fractional norm equivalence now proves the stated complement estimate for the spectral matrix.

Step 3. We identify the spectral matrix with the ordinary flow. We identify this matrix with the physical flow. The same scalar bounds at graph levels $(A_\sigma u, A_\sigma^{1/2} z)$ give

continuous solutions in $H^2 \times H^1$. These graph norms are uniformly equivalent to the Sobolev norms: the H^1 case was proved above, and $A_\sigma - B = M - V_\sigma$ is bounded by M while $A_\sigma, B \geq 1$. Spectral cutoffs give $u_t = z$ in H^1 and $z_t = -H_\sigma u$ in L^2, with continuous derivatives there. The free Fourier group is used at these graph levels so that the interaction-picture derivative is justified in $H^1 \times L^2$. This derivative is not an operator-norm derivative on the whole phase. The free Fourier group on $H^1 \times L^2$ has, after its Bessel isometry, the same bounded weighted entries and is strongly continuous by dominated Fourier convergence. Its generator is $(z, \Delta u)$ on $H^2 \times H^1$, as the Fourier multipliers show. For compact smooth initial data, differentiating the free interaction picture at these graph levels gives Duhamel with force $(0, V_\sigma u)$. The identity also holds in E. Multiplication by V_σ maps $H^{1/2}$ into L^2 and then $H^{-1/2}$ with bound M, so Picard uniqueness identifies the spectral solution with the ordinary E flow on these data. Density within E and finite-horizon boundedness extend equality to all E. No density of E in F is used. Finally, the ground branches give (6.3.8); their pairings are continuous because $p_\sigma \in H^2$. Continuity and uniform bounds of the displayed vectors and duals follow from Proposition 6.3.1. This proves Proposition 6.3.3. □

6.3.2 The growing projection and its complementary wave evolution

For the constant coordinates write $C(t)(c_1, c_2) = (c_1 + tc_2, c_2)$ and $D_\sigma(c_1, c_2) = (0, V_\sigma c_1) \in E$. The data $e_0 = (0, 1, 0)$ lie entirely in these constant coordinates, outside iE. So we follow the flow on all of F, where D_σ couples the constants to E.

Proposition 6.3.4 (The growing projection on the wave phase space)**.** *The physical flow satisfies*

$$P_\sigma(t)(e, c) = \left(P_\sigma^E(t)e + \int_0^t P_\sigma^E(t - r) D_\sigma C(r) c \, \mathrm{d}r, \; C(t)c \right). \tag{6.3.11}$$

Set

$$f_\sigma = \frac{\int V_\sigma p_\sigma}{2\lambda_\sigma} > 0, \qquad \ell_\sigma^C(c) = f_\sigma \left(\frac{c_1}{\lambda_\sigma} + \frac{c_2}{\lambda_\sigma^2} \right), \tag{6.3.12}$$

$$e_\sigma = i e_\sigma^E, \qquad \ell_\sigma(e, c) = \ell_\sigma^E(e) + \ell_\sigma^C(c), \qquad \Pi_\sigma = e_\sigma \ell_\sigma, \quad Q_\sigma = I - \Pi_\sigma. \tag{6.3.13}$$

These vectors, duals and rank-one projections are norm-continuous and uniformly bounded, and

$$\ell_\sigma(e_\sigma) = 1, \qquad P_\sigma(t)\Pi_\sigma = \Pi_\sigma P_\sigma(t) = e^{\lambda_\sigma t}\Pi_\sigma. \tag{6.3.14}$$

For every fixed nonnegative smooth compact ϕ of integral one,

$$\inf_I \ell_\sigma(e_0) > 0, \qquad \inf_I O_\phi(e_\sigma) > 0. \tag{6.3.15}$$

Proof. We derive the block formula by variation of constants in E. We then compute the constant-coordinate contribution to the growing dual, combine its finite-time contribution with an exponential tail, and obtain uniform positive margins by compactness.

Step 1. We derive the block formula for the full phase. The constant coordinates obey $C(t)$ because the potential force has range in iE. To justify variation of constants on the E component, let g be a continuous E force and substitute the ordinary free-Duhamel equation for $P_\sigma^E(t-r)g(r)$ in its time integral. With $B_\sigma^E(u,z) = (0, V_\sigma u)$, strong E-valued Fubini gives

$$\begin{aligned}\int_0^t \int_r^t S(t-s)B_\sigma^E P_\sigma^E(s-r)g(r)\,\mathrm{d}s\,\mathrm{d}r \\ = \int_0^t S(t-s)B_\sigma^E \left[\int_0^s P_\sigma^E(s-r)g(r)\,\mathrm{d}r\right]\,\mathrm{d}s.\end{aligned}$$

The integration region is the triangle $0 \le r \le s \le t$. Reversing the order changes the outer variable from r to s, with $0 \le r \le s$ in the inner integral. This is exactly the forcing term in the free-Duhamel equation for the proposed E component. All norms are bounded on the finite triangle, so this exchange is absolute in E. Thus, $Y(t) = P_\sigma^E(t)e + \int_0^t P_\sigma^E(t-r)g(r)\,\mathrm{d}r$ solves free Duhamel with force $B_\sigma^E Y + g$. Take $g(r) = D_\sigma C(r)c$ and adjoin the constant block. This is the same F Duhamel equation as the ordinary flow; uniqueness proves (6.3.11). Its finite-horizon bounds are uniform since the family has bounded L^∞ and L^2 norms on one compact support.

Step 2. We compute the growing dual on the constant coordinates. The integral defining f_σ is finite by L^2 Cauchy–Schwarz and positive because V_σ is nonzero by the common trial and $p_\sigma > 0$ a.e. Its coefficients are continuous and uniformly bounded by the H^2 continuity and positive lower bound for the rate; no $p_\sigma \in L^1$ assumption is used. Directly,

$$\begin{aligned}\ell_\sigma^E D_\sigma C(r)c &= f_\sigma(c_1 + rc_2),\\ \ell_\sigma^C(c) &= \int_0^\infty e^{-\lambda_\sigma r} f_\sigma(c_1 + rc_2)\,\mathrm{d}r,\\ \ell_\sigma^C(C(t)c) &= \int_t^\infty e^{\lambda_\sigma(t-r)} f_\sigma(c_1 + rc_2)\,\mathrm{d}r.\end{aligned}$$

The first integral uses $\int_0^\infty e^{-\lambda_\sigma r}\,\mathrm{d}r = 1/\lambda_\sigma$ and $\int_0^\infty re^{-\lambda_\sigma r}\,\mathrm{d}r = 1/\lambda_\sigma^2$. The last identity follows by translating the integration variable by t and using $C(t)c = (c_1 + tc_2, c_2)$. These integrals converge absolutely. Applying ℓ_σ to (6.3.11), the finite integral and this tail combine to give $\ell_\sigma P_\sigma(t) = e^{\lambda_\sigma t}\ell_\sigma$. The ground mode also gives $P_\sigma(t)e_\sigma = e^{\lambda_\sigma t}e_\sigma$ and $\ell_\sigma(e_\sigma) = 1$, proving (6.3.14). Bounded bilinear multiplication and the preceding continuous coefficients prove norm continuity of all objects. Finally, $\ell_\sigma(e_0) = f_\sigma/\lambda_\sigma > 0$ and $O_\phi(e_\sigma) = \int \phi p_\sigma > 0$. Nonnegativity and positive integral of ϕ give a set of positive measure on which $\phi > 0$. Since $p_\sigma > 0$ almost everywhere, its pairing with ϕ is strictly positive. Both are continuous on compact I, proving (6.3.15). Positivity is in integrals, without a point trace or a one-dimensional ODE. This proves Proposition 6.3.4. □

Proposition 6.3.4 isolates the growing part Π_σ. It remains to bound the flow on the complement Q_σ. The proof of Lemma 7.2.4 uses the normalized form of this bound.

Proposition 6.3.5 (Complementary wave evolution and parameter dependence)**.** *Uniformly over σ and $t \ge 0$,*

$$\|P_\sigma(t)Q_\sigma\|_{\mathcal{B}(F)} \le C(1+t)^3 e^{\mu_\sigma t}. \tag{6.3.16}$$

For every fixed $0 < \eta < d_0$,

$$\|e^{-\lambda_\sigma t} P_\sigma(t) Q_\sigma\| \le C_\eta e^{-\eta t}. \tag{6.3.17}$$

For every finite T_0,

$$\sup_{0\le t\le T_0} \|P_\sigma(t) - P_\tau(t)\|_{\mathcal{B}(F)} \le C_{T_0}\Big(\|V_\sigma - V_\tau\|_\infty + \|V_\sigma - V_\tau\|_2\Big). \tag{6.3.18}$$

Proof. We use the block formula to keep track of the growing response to the constant coordinates when subtracting the projection. We estimate the remaining integral and absorb its polynomial factor into the rate gap. Finally, we compare two potentials through their Duhamel equations.

Step 1. We bound the complementary flow on the full phase. The growing forcing component equals

$$e_\sigma^E \int_0^t e^{\lambda_\sigma (t-r)} f_\sigma(c_1 + r c_2)\,\mathrm{d}r = e_\sigma^E\Big(e^{\lambda_\sigma t}\ell_\sigma^C(c) - \ell_\sigma^C(C(t)c)\Big).$$

Its first term cancels the constant-coordinate contribution of $e^{\lambda_\sigma t}\Pi_\sigma(e,c)$, leaving the negative term in the complement formula below. Write $Q_\sigma^E = I - \Pi_\sigma^E$. Split D_σ into its growing and complementary parts in (6.3.11) and use the two tail integrals in the preceding proof. The exact E component of $P_\sigma(t)Q_\sigma(e,c)$ is

$$P_\sigma^E(t)Q_\sigma^E e + \int_0^t P_\sigma^E(t-r)Q_\sigma^E D_\sigma C(r)c\,\mathrm{d}r - e_\sigma^E \ell_\sigma^C(C(t)c), \tag{6.3.19}$$

and the constant component is $C(t)c$. The final subtraction retains the growing response to constants in the projection. Since $\|Q_\sigma^E D_\sigma C(r)\| \le C(1+r)$, the integral in (6.3.19) has norm at most

$$Ce^{\mu_\sigma t}|c| \int_0^t (1+t-r)(1+r)\,\mathrm{d}r = Ce^{\mu_\sigma t}(t + t^2 + t^3/6)|c|.$$

The integrand has one factor $1+t-r$ from the complementary E flow and one factor $1+r$ from the free constant block. Its exponential is bounded by $e^{\mu_\sigma t}$ because $\mu_\sigma \ge 0$. Integrating the product of the two linear factors gives the displayed cubic polynomial. The first term is bounded by $C(1+t)e^{\mu_\sigma t}\|e\|_E$; the final term and constant component by $C(1+t)|c|$. Since $\mu_\sigma \ge 0$ this proves (6.3.16). The boundedness of $(1+t)^3 e^{-(d_0-\eta)t}$ proves (6.3.17). In particular, the constant-velocity polynomial is included in this estimate.

Step 2. We prove finite-horizon dependence on the potential. Put $\mathcal{B}_\sigma = iB_F(V_\sigma)$ and $d_{\sigma,\tau} = \|V_\sigma - V_\tau\|_\infty + \|V_\sigma - V_\tau\|_2$. The bound for B_F gives $\|\mathcal{B}_\sigma - \mathcal{B}_\tau\| \le d_{\sigma,\tau}$. Subtract the two free-Duhamel equations on states. Their difference is the sum of the integral with $S_F(t-r)\mathcal{B}_\sigma(P_\sigma(r) - P_\tau(r))$ and that with $S_F(t-r)(\mathcal{B}_\sigma - \mathcal{B}_\tau)P_\tau(r)$. The uniform finite-horizon bounds control the second integral by a constant times $d_{\sigma,\tau}$. The first integral is bounded by a constant times the time integral of the unknown flow difference. Thus, the finite-horizon bounds and scalar Gronwall prove (6.3.18). The operator norm is measurable: separability of F expresses it as the supremum over a countable dense set of unit states, each with continuous image. Hence, Gronwall applies without a $\mathcal{B}(F)$-valued derivative or operator-norm continuity of the free group. This proves Proposition 6.3.5. □

6.3.3 The original nonnegative control and a common trial

So far V_σ was any continuous family satisfying (6.3.1). We now produce such a family from a nonnegative test Ψ and the original covariance Γ, in two steps.

Lemma 6.3.6 (The original mean and variance)**.** *Let $\Gamma \neq 0$ satisfy Hypothesis 1.2.1, let $a = \alpha_0$, and let real nonnegative nonzero $\Psi \in C_c^\infty((0,1) \times \mathbb{R}^d)$ be arbitrary, without a separability assumption. Define*

$$h_\sigma(x) = \int_0^1 |\sigma - u|^{-a} (\Gamma * \Psi(u, \cdot))(x) \, \mathrm{d}u, \qquad \overline{q}(x) = \int_0^1 \Psi(u, x) \, \mathrm{d}u, \qquad Z = W(\Psi). \tag{6.3.20}$$

Then h is smooth in time and space on compact sets, and

$$0 < v_\Psi := \mathbb{E}Z^2 = \int_0^1 \int \Psi(\sigma, x) h_\sigma(x) \, \mathrm{d}x \, \mathrm{d}\sigma < \infty. \tag{6.3.21}$$

Against every smooth compact positive-time test F_0,

$$\mathbb{E}[W(\Psi) W(F_0)] = \int F_0(s, x) h_s(x) \, \mathrm{d}x \, \mathrm{d}s.$$

Moreover, on I,

$$h_\sigma \geq \Gamma * \overline{q}, \qquad v_\Psi \geq Q(\overline{q}) := \int \Gamma(\, \mathrm{d}z) \int \overline{q}(x) \overline{q}(x - z) \, \mathrm{d}x > 0. \tag{6.3.22}$$

For every fixed mask, $V_\sigma = m_R h_\sigma$ is a smooth compact family, Lipschitz in σ in L^∞ and L^2.

Proof. We identify the original covariance mean and show its cost is finite. Positivity and homogeneity give a nonnegative, nonzero time-independent lower profile and a strictly positive covariance cost. We then differentiate the test, rather than the singular time kernel, to obtain regularity.

Step 1. We identify the mean and bound its covariance cost. Choose $A \geq 1$ containing the spatial support of Ψ in B_A. The original covariance identity and absolute Fubini give the stated mean pairing: the two compact tests restrict spatial differences to a compact set of finite Γ mass, and the time singularity is locally integrable since $a < 1$. This identifies the linear covariance mean without evaluating noise at a point. The same calculation gives (6.3.21). Its spatial integrand is bounded in integral by $\|\Psi\|_\infty^2 |B_A| \Gamma(\overline{B}_{2A})$, and $\int_0^1 \int_0^1 |\sigma - u|^{-a} \, \mathrm{d}u \, \mathrm{d}\sigma = 2/((1-a)(2-a))$, proving finiteness.

Step 2. We obtain strict positivity and the uniform mean floor. Nonnegative nonzero smooth Ψ has positive integral, so $\overline{q} \neq 0$. Nonzero Γ charges some ball, and homogeneity gives $\Gamma(B_1) = r^{\alpha - d} \Gamma(B_r) > 0$. Thus, every origin-centered ball B_r, $r > 0$, has positive finite mass. The continuous compact autocorrelation $\int \overline{q}(x) \overline{q}(x - z) \, \mathrm{d}x$ is positive at zero and bounded below on some ball. This proves $0 < Q(\overline{q}) < \infty$. Since $|\sigma - u|^{-a} \geq 1$ on the unit time square, positive Tonelli gives both inequalities in (6.3.22).

Step 3. We prove smoothness and the fixed-mask Lipschitz bounds. Extend Ψ by zero in time and write

$$h_s(x) = \int_{\mathbb{R}} |r|^{-a} \int \Gamma(\,\mathrm{d}z)\Psi(s-r, x-z)\,\mathrm{d}r.$$

On compact s, x sets the relevant r, z range over fixed compact sets; $|r|^{-a}$ is integrable there. Every derivative falls on the smooth test, not on the singular time kernel. Dominated differentiation gives smoothness and continuity of all derivatives on compacts. Multiplication by m_R now gives the claimed compact family and its fixed-R Lipschitz bounds. This proves Lemma 6.3.6. □

Lemma 6.3.6 gives a smooth compact family for every fixed mask, but not yet the common negative trial (6.3.1).

Proposition 6.3.7 (Binding with the original control and cost fixed)**.** *For every Ψ in Lemma 6.3.6, a sufficiently large finite mask m_R gives $V_\sigma = m_R h_\sigma$ a common negative trial (6.3.1). Thus, all preceding ground, projection, positive-margin and complementary-wave conclusions apply. The rate is Lipschitz on I and has $\lambda_0 > 0$. The original test Ψ, original variable Z and variance v_Ψ are unchanged by this choice. The mask can additionally cover any fixed compact variational test supports.*

Proof. We dilate a fixed trial function and choose the mask to contain its support. Homogeneity gives a potential contribution of order $L^{-\alpha}$, which dominates the kinetic contribution of order L^{-2}. We then apply the ground-family estimates at this fixed mask.

Step 1. We bound the potential contribution of the dilated trial. Choose a real unit L^2 function $\psi \in C_c^\infty(B_2)$ with $\psi \geq c_0 > 0$ on B_1, and put $\psi_L(x) = L^{-d/2}\psi(x/L)$, $D_\psi = \|\nabla\psi\|_2^2$, where $L \geq \max(1, 2A)$. Choose the even mask with $R \geq 2L$, so $V_\sigma = h_\sigma$ on $\operatorname{supp}\psi_L$. This is the allowed real mask $0 \leq m_R \leq 1$, equal to one on B_R and with support in $\overline{B}_{2R}$. Positive Tonelli and (6.3.22) give

$$\begin{aligned}
\int V_\sigma \psi_L^2 &\geq c_0^2 L^{-d} \int_{B_L} (\Gamma * \overline{q})(x)\,\mathrm{d}x \\
&= c_0^2 L^{-d} \int \overline{q}(y)\Gamma(B_L - y)\,\mathrm{d}y \\
&\geq c_0^2 L^{-d}\Gamma(B_{L/2}) \int \overline{q} = C_\Gamma L^{-\alpha}, \qquad (6.3.23)\\
C_\Gamma &= c_0^2 2^{\alpha-d}\Gamma(B_1) \int \overline{q} > 0.
\end{aligned}$$

On B_L, the dilated trial has squared value at least $c_0^2 L^{-d}$.

Homogeneity gives $\Gamma(B_{L/2}) = (L/2)^{d-\alpha}\Gamma(B_1)$, yielding the displayed constant. Here $B_{L/2} \subset B_L - y$ for $|y| \leq A$ and $L \geq 2A$. All covariance masses in the argument are compact and finite. The kinetic energy is $D_\psi L^{-2}$. Since $\alpha < 2$, choose L large enough that $\varepsilon_R := C_\Gamma L^{-\alpha} - D_\psi L^{-2} > 0$. Then

$$\|\nabla\psi_L\|_2^2 - \int V_\sigma \psi_L^2 \leq -\varepsilon_R \quad \text{for every } \sigma \in I.$$

Step 2. We fix a negative trial and obtain the rate regularity. Fix this finite R before invoking Proposition 6.3.1. Its level bound and the mean Lipschitz estimate give

$$|\lambda_\sigma - \lambda_\tau| \le \frac{\|V_\sigma - V_\tau\|_\infty}{2\sqrt{\varepsilon_R}} \le C_R|\sigma - \tau|.$$

The lowest eigenvalue remains at most $-\varepsilon_R$ for every parameter. Factoring the difference of its negative square roots gives a denominator $\lambda_\sigma + \lambda_\tau \ge 2\sqrt{\varepsilon_R}$. The level comparison then gives the displayed Lipschitz estimate. The positive mean integrates the entire time test, so $\lambda_0 > 0$ even though $\Psi(0,\cdot) = 0$. Only the trial and mask have grown; the original test, its variable and (6.3.21) were fixed first. Enlarging R to contain additional fixed compact test supports preserves the trial and gives equality of masked and unmasked potential energies on those supports. This includes singular invariant-direction covariances and the one-dimensional white case. It is not an all-strength binding assertion for one fixed compact potential. Masks are fixed before source or time asymptotics; a later supremum over controls must follow their individual bounds. This proves Proposition 6.3.7. □

What we now have. The Young evolution and its physical-wave identification (Proposition 6.2.5 and Lemma 6.2.6), together with positive ground states and a uniform gap for compact potential families satisfying the common negative trial condition (Proposition 6.3.1). The next chapter uses both for the lower bound.

Chapter 7

Scaling and the point lower bound

To bound a moment from below, push the Gaussian noise toward a deterministic potential that makes the wave grow, and pay for the push. The noise is correlated in time, so the cost of one control is charged once, in the original covariance space. It is not a sum over independent time blocks (Figure 7.1).

Section 7.1 turns long time into small noise by an equality in law. Section 7.2 proves, block by block in time, a pointwise lower bound for each nonnegative smooth control (Proposition 7.2.7). Section 7.3 removes the spatial mask and optimizes over controls, including those that do not factor into time and space (Figure 7.2).

We start from the canonical solution of Chapter 2 and the phase and ground states of Chapter 6. On a first reading, keep Lemma 7.1.1 and Proposition 7.3.6, and let the proofs wait. The result is a variational lower value; only Chapter 11 proves that it equals the upper value. Episode ▶ 6 of the video series covers this chapter and the next.

7.1 Exact scaling of the canonical solution

We first rewrite the second moment at a large time T as a second moment at time one, for an equation with the small parameter $\delta = T^{-\kappa}$. The proof of Proposition 7.2.6 uses this for the final equality in (7.2.13).

Lean partial

Lemma 7.1.1 (Canonical law scaling)**.** *Under Hypothesis 1.2.1, put $a = \alpha_0$, $\kappa = (4-\alpha-a)/(3-\alpha)$, and, for $T > 0$,*

$$\delta = T^{-\kappa}, \qquad r_T = T\delta = T^{(a-1)/(3-\alpha)}.$$

The law of $u(Tt, r_T x)$ is the canonical expansion solution $V_\delta(t,x)$ with data $(1,0)$ of

$$\delta^2 \partial_t^2 V_\delta = \Delta V_\delta + \sqrt{\delta}\, \dot{W} V_\delta, \tag{7.1.1}$$

where $\dot{W}$ has the original covariance. In particular,

$$T^{-\kappa} \log \mathbb{E}|u(T,0)|^2 = \delta \log \mathbb{E}|V_\delta(1,0)|^2. \tag{7.1.2}$$

The assertion is equality in law; it assumes no pathwise uniqueness for a full rough solution.

Proof. We first scale the regularized noise and the Green measure. We check that the coefficient at each ordered vertex is the one in the fast equation. We then pass the finite-order law identities to the canonical series at fixed dilation.

Step 1. We scale the source covariance and the Green measure. For the scalar powers below, substituting $r_T = T\delta$ and $(3-\alpha)\kappa = 4-\alpha-a$ with $\delta = T^{-\kappa}$ gives $T^{1-a/2} r_T^{1-\alpha/2} = \delta^{-1/2}$; multiplying by δ gives the companion identity used for the noise coefficient $\sqrt{\delta}$. At each vertex the time substitution contributes the Jacobian T, the Green-measure scaling contributes r_T, and the single Gaussian source factor contributes the square root $T^{-a/2} r_T^{-\alpha/2}$ of its covariance amplitude. At positive widths, time and space dilation of the Gaussian source gives covariance amplitude $T^{-a} r_T^{-\alpha}$. This follows distributionally from the homogeneous Radon covariance, including spatial white noise. Its source cutoffs transform by $K_\eta(Ts) = T^{-a} K_{\eta/T}(s)$ and $\epsilon \mapsto \epsilon / r_T^2$; the joint maximum-time and summed-space width laws are preserved at every vertex. The Green measure has the scaling

$$G_d(T\tau, r_T \,\mathrm{d}z) = r_T G_d(\tau/\delta, \,\mathrm{d}z).$$

It follows from its degree $1-d$ distributional scaling, also for the sphere measure in dimension three. Each terminal Duhamel vertex thus contributes $T r_T T^{-a/2} r_T^{-\alpha/2}$. Substitution of the displayed positive real powers gives

$$T^{-a/2} r_T^{2-\alpha/2} = \sqrt{\delta}, \qquad T^{1-a/2} r_T^{1-\alpha/2} = \delta^{-1/2}.$$

Step 2. We match the scaled vertex with the fast-equation vertex. The Green kernel for the forcing in (7.1.1) is $\delta^{-1} G_d((t-s)/\delta)$; after multiplication by $\sqrt{\delta}$ it gives exactly that vertex factor. Therefore, every finite list of fixed-order coefficients has the same joint law under the dilation, including all self-pairings, unequal orders and empty chains. At fixed T, r_T, remove Green smoothing first in dimension three, with its width divided by r_T^2 on the scaled side. Lemma 2.5.2 and the absolute L^2 summability in Lemma 2.6.1 pass the identities to the canonical series and its second moment. No large-time and source limit are interchanged. Finally, evaluate the law identity at $t = 1, x = 0$ and use $T^{-\kappa} = \delta$ to obtain the logarithmic moment identity. This proves the law assertion and (7.1.2). This proves Lemma 7.1.1. □

7.2 Time blocks for the original noise and the pointwise lower bound

Fix a nonzero covariance from Hypothesis 1.2.1 and any real nonnegative nonzero $\Psi \in C_c^\infty((0,1) \times \mathbb{R}^d)$. Retain the *original* $Z = W(\Psi)$, $v = v_\Psi > 0$ and mean h_s of Lemma 6.3.6. Choose one finite even mask $m_R \in [0,1]$, equal to one on B_R and supported in $\overline{B}_{2R}$, as in Proposition 6.3.7. Then $V_s = m_R h_s$ has the ground family, rate λ_s and full F projection of Section 6.3. Set

$$I_R = \int_0^1 \lambda_s \,\mathrm{d}s, \qquad Q_2 = \liminf_{T\to\infty} T^{-\kappa} \log \mathbb{E}|u(T,0)|^2.$$

We will prove $Q_2 \geq 2I_R - v/2$, for this same control and covariance. Fix a real nonnegative smooth compact ϕ of integral one, the bounded observable O_ϕ, and the data

$e_0 = (0, 1, 0) \in F$. Both displacement and velocity are retained. This is the same physical profile $m_R = \zeta_R$ used in the operator path and compact mean; no mask is changed in a covariance identity. The semiscaled W below is the given-law noise. The comparison to the unscaled solution uses equality in law, not samplewise identities on one probability space for every T.

7.2.1 The common original noise and its exact Gaussian shift

Choose an integer $B \geq 1$, later fixed by the cone estimate, and take $0 < \delta < \min(1, 1/B)$. Define

$$N = \left\lfloor \frac{1}{\delta B} \right\rfloor \geq 1, \quad s_m = m\delta B \ (0 \leq m \leq N), \quad \tau = \delta^{-1} - NB \in [0, B), \quad g_\delta = \delta^{(1-a)/2}. \tag{7.2.1}$$

For a smooth compact positive-fast-time test f, extended by zero, put

$$T_{\delta,m} f(s, x) = \delta^{a/2-1} f((s - s_m)/\delta, x), \qquad W_{\delta,m}(f) = W(T_{\delta,m} f). \tag{7.2.2}$$

Write $W_{\mathrm{fast}} = W_{\delta,0}$. Use the same admissible γ, θ, β as (5.1.1). Write $A_R(W_{\delta,m})$ for the F integrated operator obtained by the bounded extension (6.2.5), on the local horizon $[0, B]$, and set

$$X_m = g_\delta A_R(W_{\delta,m}), \qquad H_m(u) = \int_0^u S_F(-r) i B_F(V_{s_m+\delta r}) S_F(r) \, \mathrm{d}r. \tag{7.2.3}$$

The convolution formula for h extends smoothly to $s \in [0, 2]$, covering these means. Ground templates will only use $s_m \in [0, 1]$.

Lean partial

Lemma 7.2.1 (Coupled Gaussian block inputs)**.** *Each $T_{\delta,m}$ is an isometry of the original test completion, respecting covariance-null tests. All $W_{\delta,m}$ and Z are on the same given noise space, without an independence assertion. Let $\mathcal{K}(F)$ have the operator norm and let $\mathscr{B}_0 = h_0^\theta([0, B]; \mathcal{K}(F))$ be the C^θ closure of zero-initial polygonal compact-operator paths. It is a separable Banach space. In $\mathscr{B}_\delta = \mathscr{B}_0^{N+1}$ with maximum norm, (X, Z), $X = (X_m)_{m=0}^N$, is jointly centered Gaussian and*

$$b := \mathbb{E}[XZ] = \sqrt{\delta}\, H, \qquad H = (H_m)_{m=0}^N. \tag{7.2.4}$$

Moreover,

$$\|X_m\|_{L^p \mathscr{B}_0} \leq C_{R,B} \sqrt{p}\, g_\delta, \qquad p \geq 1. \tag{7.2.5}$$

Proof. We first check the time pullbacks in the original covariance norm. We then place the operator paths in a separable space and compute their joint covariance with the single original Gaussian variable.

Step 1. We check the common-space pullback identities. Substituting $s = s_m + \delta u$, $t = s_m + \delta r$ in the original covariance gives the factor $\delta^{a-2}\delta^2\delta^{-a} = 1$. Thus, the maps extend isometrically through the null quotient. Direct test substitution gives $W_{\delta,m}(f) = W_{\mathrm{fast}}(f(\cdot - mB, \cdot))$. These are explicit common-space identities.

Step 2. We identify a separable path space for the Gaussian variables. The pullback isometry gives $W_{\delta,m}$ the same Gaussian law as W, so Proposition 6.2.2 supplies the path convergence and Gaussian norm bound on $[0, B]$, with the same $C_{R,B}$ for every m, δ. Finite-rank rational matrices in a countable real Hilbert basis are dense in $\mathcal{K}(F)$: for compact T, $P_n T P_n \to T$ in norm by compactness of T, T^*, and finite entries admit rational approximation. Polygonal paths with rational breakpoints and such matrices give separability of $\mathscr{B}_0$. To approximate breakpoints, use uniform convergence, uniform Lipschitz bounds and $[f]_\theta \le (2\|f\|_\infty)^{1-\theta} \operatorname{Lip}(f)^\theta$. The same inequality puts every zero-initial Lipschitz compact-valued path in $\mathscr{B}_0$ by polygonal approximation. The finite original coefficient paths $iA_j L_\psi$ have these properties. Their Gaussian sums converge in $L^p C^\theta$ and hence in the closed space $\mathscr{B}_0$. Their laws and the parent Gaussian norm bound give (7.2.5). Every finite joint coefficient list with Z is Gaussian on the same W. Scalar continuous functionals pass through the L^2 limits, preserving Gaussianity by convergence of variances and characteristic functions. Thus, (X, Z) is the asserted Banach Gaussian variable. Cauchy–Schwarz gives $\mathbb{E}\|XZ\| \le \|X\|_2 \sqrt{v} < \infty$, so its Bochner covariance exists.

Step 3. We compute the covariance direction of the operator paths. The time substitution in the mean pairing contributes a Jacobian δ, changing the pullback factor $\delta^{a/2-1}$ to $\delta^{a/2}$. The original covariance and the test pullback give

$$\mathbb{E}[W_{\delta,m}(f) Z] = \delta^{a/2} \int f(u, x) h_{s_m+\delta u}(x) \, \mathrm{d}x \, \mathrm{d}u. \tag{7.2.6}$$

Absolute Fubini uses compact supports, local Radon mass and $a < 1$. This identity extends to the explicit matrix-element tests for the operator path on E: their time indicator is approximated by smooth bounded tests on one compact support, converging in the original covariance norm by dominated convergence against $|u - r|^{-a}\Gamma$; their mean pairings converge as well. Insert the matrix-element test $\zeta_R 1_{(0,u)} v_z G_w$ in (7.2.6): the mask multiplying the mean is $V_{s_m+\delta r}$, and (5.1.11) identifies the resulting integral with the row of H_m. For constant inputs, the free displacement from $(c_1\psi, c_2\psi)$ equals $c_1 + r c_2$ on B_{2R} for $r \le B$, since $\psi = 1$ on the enlarged ball; multiplying by $V_{s_m+\delta r}$ therefore gives the same constant-column forcing in H_m. The Sobolev adjoint is the one in (5.1.11). Hence, the path covariance is $g_\delta \delta^{a/2} H_m = \sqrt{\delta}\, H_m$ on real Schwartz E pairs. For constant inputs the two columns are the same L_ψ inputs $(\psi, 0)$ and $(0, \psi)$, and total finite propagation identifies their deterministic response. The span of E and both constant coordinates is dense in F; E alone is not. Boundedness, rational times and path continuity prove (7.2.4) on all F. In particular, $H = b/\sqrt{\delta} \in \mathscr{B}_\delta$. This proves Lemma 7.2.1. □

The next identity is the covariance-direction Cameron–Martin formula; see Janson [34, Theorem 14.1(v), pp. 216–217]. We prove it on the norm-Borel space used here to verify the measurable realization and its deterministic translate.

Proposition 7.2.2 (Change of law on the whole norm-Borel space)**.** *For every nonnegative norm-Borel j on all of $\mathscr{B}_\delta$,*

$$\mathbb{E} j(X) = \mathbb{E}\left[e^{-Z/\sqrt{\delta} - v/(2\delta)} j(X + H) \right]. \tag{7.2.7}$$

The equality is valid also as an extended nonnegative integral.

Proof. We prove the change of measure first for finitely many continuous coordinates, allowing singular covariance matrices. We then show that these coordinates generate the norm-Borel sets and extend the identity to nonnegative functions.

Step 1. We shift the finite Gaussian coordinate vectors. For real s, the density $e^{-sZ-s^2v/2}$ defines an equivalent probability measure Q_s by completing the square in the $N(0,v)$ density. For any finite list ℓ of continuous real coordinates on $\mathscr{B}_\delta$, the Gaussian vector $(\ell(X), Z)$ is equal in law to $(TG, z \cdot G)$ for a finite standard Gaussian vector G. A positive covariance square root gives this representation even when singular; no inverse is used. Here $Tz = \ell(b)$ and $|z|^2 = v$. Substitution $G' = G + sz$ in its density gives $\mathbb{E}_{Q_s} f(\ell(X + sb)) = \mathbb{E} f(\ell(X))$ for every bounded Borel f.

Step 2. We pass from coordinates to the full norm-Borel space. The matrix entries of each block in a real Hilbert basis at rational times, together with $0, B$, generate the norm-Borel sigma-field. To see the operator-norm point, for a countable dense set $\mathcal{D}$ of unit vectors obtained from normalized rational finite basis combinations, $\|T\| = \sup_{u,w\in\mathcal{D}} |\langle Tu, w\rangle|$. These pairings are finite linear combinations of matrix entries. Supremum and Hölder norms of continuous paths are suprema over rational times and pairs. Thus, distance to every fixed element of $\mathscr{B}_\delta$ is coordinate-measurable. Open balls are measurable by rational closed-ball approximation, and separability makes every open set a countable union of balls from dense centers. Conversely the coordinates are continuous. The cylinder sets form a generating pi-system; uniqueness of probability measures extends the finite-coordinate equality to all norm-Borel sets. Simple functions and monotone convergence give the identity for nonnegative j. Finally, take $s = \delta^{-1/2}$ and use $sb = H$ from (7.2.4). The map and its deterministic translate are defined on the entire input space; there is no translated exceptional-domain assumption. This proves Proposition 7.2.2. □

The identity retains the random shifted input $X + H$. Replacing its expected contribution by evaluation at the deterministic mean can lose the exponential constant, even in a scalar Gaussian calculation; see No-go 16. Positive semidefinite residual covariance does not justify discarding that residual: No-go 19 gives an admissible parent model whose rank-one projection has a larger small-coupling wave mean.

7.2.2 Small noisy blocks and a cone in the displacement-velocity space

For any $x \in \mathscr{B}_0$ define $D_x(u) = S_F(u)U_x(u,0)$ by the everywhere-defined linear Young map of Proposition 6.2.4. Write $D^0_m = D_{X_m}$ and $D^+_m = D_{X_m+H_m}$. The latter retains both the mean and the residual noise.

The shifted blocks D^+_m are random. We now show that their largest distance from the deterministic P_{s_m} of (6.3.11), over all blocks $m \le N$, tends to zero in every finite L^q.

Lemma 7.2.3 (Uniform block error)**.** *Let $M_\delta = \max_{m\le N} \|X_m\|_{\mathscr{B}_0}$, including its factor g_δ. Then $M_\delta \to 0$ in every finite L^q, and, for some $c > 0$,*

$$\sup_\delta \mathbb{E} e^{cM_\delta^2} < \infty. \tag{7.2.8}$$

With the deterministic P_s in (6.3.11),

$$E_{\mathrm{op},\delta} := \max_{m\le N} \sup_{0\le u\le B} \|D_m^+(u) - P_{s_m}(u)\|_{\mathcal{B}(F)} \longrightarrow 0 \quad \text{in every finite } L^q. \tag{7.2.9}$$

Proof. We control the largest scaled Gaussian block by a moment bound and its exponential series. We then compare shifted drivers on a fixed ball and use uniform higher moments to pass from convergence in probability to convergence in every finite L^q.

Step 1. We bound the scaled maximum and its exponential moment. The maximum and (7.2.5), with $N + 1 \le 2/\delta$, give

$$\|M_\delta\|_p \le (N+1)^{1/p} C\sqrt{p}\, g_\delta \le C'\sqrt{p}\, \delta^{(1-a)/2-1/p}.$$

For a finite family, the pth power of the maximum is at most the sum of the pth powers. This gives the factor $(N+1)^{1/p}$ without independence. For fixed q, choose $p > \max(q, 2/(1-a))$ to prove the first limit. No independence is needed. Choose an integer n_0 with $n_0(1-a) \ge 1$. For $n \ge n_0$,

$$\mathbb{E} M_\delta^{2n} \le 2C^{2n}(2n)^n \delta^{n(1-a)-1} \le 2C^{2n}(2n)^n.$$

For $1 \le n < n_0$, Lyapunov bounds the moment by the appropriate power of the $2n_0$ moment. These finitely many terms are bounded. For the remaining exponential series, $n! \ge (n/e)^n$ gives a geometric tail $2\sum_{n\ge n_0}(2ecC^2)^n$ for small c. This proves (7.2.8); no such assertion is made for the unscaled maximum.

Step 2. We compare each noisy block with its frozen deterministic flow. Let H_m^{stat} be the primitive for constant potential V_{s_m}. The primitive estimate is Proposition 6.2.8 on horizon B, applied to $V_{s_m+\delta r}$, V_{s_m} and their difference, in the L^∞ and L^2 coefficient norms. The frozen flow is $P_{s_m}(u) = S_F(u)U_{H_m^{\mathrm{stat}}}(u,0)$; Proposition 6.2.4 compares it with the driver $X_m + H_m$, whose distance from H_m^{stat} is at most $M_\delta + C\delta$ on the fixed driver ball. Compact mean smoothness on $[0,2]$ and the statewise primitive bound give

$$\sup_m \max(\|H_m\|_{C^\theta}, \|H_m^{\mathrm{stat}}\|_{C^\theta}) \le H_0, \qquad \sup_m \|H_m - H_m^{\mathrm{stat}}\|_{C^\theta} \le C\delta.$$

Indeed, the potential difference is at most $C\delta B$ in L^∞ and L^2; integration of the bounded free groups gives its Lipschitz primitive bound on this fixed horizon. On $\{M_\delta \le 1\}$, local Young stability on the fixed ball of radius $H_0 + 1$ gives $E_{\mathrm{op},\delta} \le C(M_\delta + \delta)$. This proves convergence in probability. The global Young bound also gives

$$\max_m \sup_{u\le B} \|D_m^+(u)\| \le C_B \exp\Big(C_B(1 + H_0 + M_\delta)^{1/\theta}\Big).$$

Since $1/\theta < 2$, every finite power of this bound is dominated by a constant times the exponential in (7.2.8). Uniform higher moments yield uniform integrability, proving (7.2.9). Suprema are measurable: on a countable dense set of unit states each difference is continuous in u, so rational times and those states suffice. Operator-norm continuity of the physical free group is not used. Only $s_m \le 1$ supplies the ground templates. This proves Lemma 7.2.3. □

Lemma 7.2.3 bounds the distance of each shifted block from P_{s_m}. It says nothing about the product of the blocks. The next lemma is deterministic and holds for every $N \ge 1$. If each factor D_m is within ϵ_{op} of P_{σ_m}, and adjacent indices σ_m are within ω, then the product satisfies the lower bound (7.2.10).

Lean partial

Lemma 7.2.4 (Indexed cone and terminal displacement)**.** *Fix $0 < \varrho < 1/2$. There are an integer $B \ge 1$ and positive $\omega, \epsilon_{\mathrm{op}}, c_*$ such that the following holds for every $N \ge 1$. If $\sigma_0, \dots, \sigma_N \in I$ have adjacent distances at most ω and real bounded operator families $D_m(u)$, $0 \le u \le B$, satisfy*

$$\max_{m \le N} \sup_{0 \le u \le B} \|D_m(u) - P_{\sigma_m}(u)\| \le \epsilon_{\mathrm{op}},$$

then, for $0 \le u \le B$,

$$O_\phi D_N(u) D_{N-1}(B) \cdots D_0(B) e_0 \ge c_*(1-\varrho)^{N-1} \exp\left(B \sum_{m<N} \lambda_{\sigma_m} + u\lambda_{\sigma_N} \right) > 0. \quad (7.2.10)$$

No positivity, composition or independence assumption on the D_m is required.

Proof. We choose the cone aperture before the block length and perturbation tolerances. We prove entrance, rebase at each changing index, and finally bound the terminal observable even when the last interval is short.

Step 1. We choose the margins in an order independent of the number of blocks. Proposition 6.3.4 and (6.3.15) give the positive margins below and norm continuity of e_s, ℓ_s, Π_s; compactness of I makes their bounds finite and their continuity uniform. From (6.3.17) fix $C_{\mathrm{gap}} \ge 1$, $\eta_{\mathrm{gap}} > 0$ so the normalized complementary norm is at most $C_{\mathrm{gap}} e^{-\eta_{\mathrm{gap}} t}$. Define positive margins and finite bounds

$$a_* = \inf_I \ell_s(e_0), \quad j_* = \inf_I O_\phi(e_s), \quad M_e = \max(1, \sup_I \|e_s\|), \quad M_\ell = \max(1, \sup_I \|\ell_s\|).$$

Also put $M_P = \max(1, \sup_I \|\Pi_s\|)$, $M_Q = 1 + M_P$, $M_z = M_e + 1$, $E_0 = \|e_0\| = 1$ and $H_{\mathrm{obs}} = \max(1, \|O_\phi\|)$. Choose the aperture *first*: $\vartheta = \min(1, j_*/(16 H_{\mathrm{obs}} C_{\mathrm{gap}})) > 0$. Next choose integer $B \ge 1$ with

$$q_B := C_{\mathrm{gap}} e^{-\eta_{\mathrm{gap}} B} \le \min\left(\frac{1}{8}, \frac{\vartheta a_*}{8 M_Q E_0} \right).$$

Choose $\nu > 0$ such that $\nu M_z \le \min(\varrho/2, \vartheta, 1/4)$. Uniform continuity of ℓ_s, Π_s supplies $\omega > 0$ for which adjacent distances at most ω give both norm differences at most ν. Finally, choose $\epsilon_{\mathrm{op}} > 0$ satisfying all five smallness conditions

$$M_\ell \epsilon_{\mathrm{op}} M_z \le \varrho/2, \qquad M_Q \epsilon_{\mathrm{op}} M_z \le \vartheta/4,$$
$$M_\ell \epsilon_{\mathrm{op}} E_0 \le a_*/2, \qquad M_Q \epsilon_{\mathrm{op}} E_0 \le \vartheta a_*/8, \qquad H_{\mathrm{obs}} \epsilon_{\mathrm{op}} M_z \le j_*/8.$$

All denominators are positive. This order of choices uses the normalized complement rather than a growing terminal norm.

Step 2. We prove entrance into the first cone. The identities in (6.3.14) give $\ell_s P_s(B) = e^{\lambda_s B}\ell_s$ and $Q_s P_s(B) = P_s(B) Q_s$, so the unperturbed normalized entrance amplitude is $\ell_s(e_0)$ and its residual is at most $q_B M_Q E_0$; perturbation errors use $e^{-\lambda_s B} \le 1$. The cone at s consists of $z = Ae_s + r$, with $A = \ell_s(z) > 0$, $\ell_s(r) = 0$ and $\|r\|_F \le \vartheta A$. In particular, $r = Q_s z$ and $\|z\| \le M_z A$. For entrance, $z_1 = D_0(B)e_0$, with $b = \sigma_0$, has normalized amplitude at least $a_* - M_\ell \epsilon_{\mathrm{op}} E_0 \ge a_*/2$. Its normalized residual is at most $q_B M_Q E_0 + M_Q \epsilon_{\mathrm{op}} E_0 \le \vartheta a_*/4$. Thus, it enters the cone with residual ratio at most $\vartheta/2$ and amplitude at least $e^{\lambda_b B} a_*/2$.

Step 3. We rebase the cone and propagate it through each full block. For an old-cone state $z = Ae_b + r$ and an adjacent index c, rebase before using the complementary estimate:

$$\ell_c(z) \ge (1 - \nu M_z)A, \qquad \|Q_c z\| \le \|Q_b z\| + \|(\Pi_b - \Pi_c)z\| \le (\vartheta + \nu M_z)A.$$

Since $Q_c - Q_b = \Pi_b - \Pi_c$, the change in the residual is controlled by the projection difference times $\|z\|$. Likewise, $\ell_c(z) - \ell_b(z)$ is controlled by the dual difference times $\|z\|$. Using $\|z\| \le M_z A$ gives the two rebasing errors in the display. For the next full block D close to $P_c(B)$, put $x = e^{-\lambda_c B}\ell_c(Dz)$ and $y = e^{-\lambda_c B}\|Q_c D z\|$. Since $\lambda_c > 0$, the perturbation and smallness conditions give

$$x \ge (1 - \nu M_z - M_\ell \epsilon_{\mathrm{op}} M_z)A \ge (1 - \varrho)A > A/2,$$

and

$$y \le [q_B(\vartheta + \nu M_z) + M_Q \epsilon_{\mathrm{op}} M_z]A \le \vartheta A/2.$$

The last inequality uses $q_B \le 1/8$, $0 \le \nu M_z \le \vartheta$ and $M_Q \epsilon_{\mathrm{op}} M_z \le \vartheta/4$. Together with $\varrho < 1/2$, these give $y \le \vartheta x$. These are precisely the finite residual and cone-conversion margins; the old residual was not assumed to lie in the new kernel. Each full block therefore preserves the new cone and multiplies its amplitude by at least $e^{\lambda_c B}(1 - \varrho)$.

Step 4. We bound the observable on the final partial block. For the terminal $0 \le u \le B$, rebase once more to $c = \sigma_N$. The same bounds give $\ell_c(z) \ge 3A/4$ and $\|Q_c z\| \le 2\vartheta A$. Consequently,

$$e^{-\lambda_c u} O_\phi(P_c(u)z)/A \ge 3j_*/4 - 2H_{\mathrm{obs}} C_{\mathrm{gap}} \vartheta.$$

The normalized growing component contributes at least $3j_*/4$. The rebased residual has norm at most $2\vartheta A$, and the normalized complementary flow is at most C_{gap} for every nonnegative terminal time. Applying the observable norm gives the subtracted

residual term, uniformly even at $u = 0$. The perturbation changes this by at most $H_{\mathrm{obs}}\epsilon_{\mathrm{op}}M_z \le j_*/8$. Since $16H_{\mathrm{obs}}C_{\mathrm{gap}}\vartheta \le j_*$, the result is at least $j_*/2$. Combine entrance, all $N-1$ intermediate full blocks and this terminal estimate to obtain (7.2.10), with $c_* = a_*j_*/4$. The induction is empty for $N = 1$ and the estimate includes $u = 0$. This proves Lemma 7.2.4. □

7.2.3 Source restart and comparison with the original point

So far the blocks D_m^0 and D_m^+ are defined one at a time, from the local operator paths X_m and $X_m + H_m$. We now show that each family forms the successive pieces of its corresponding global flow, and that its finite products are source limits in L^2 at fixed δ, N. The proof of Proposition 7.2.6 uses this to verify the source-limit premise of the masked comparison.

Lean partial

Lemma 7.2.5 (Composition over time blocks and regularized products)**.** *Fix δ, B, N and let $L = \delta^{-1}$, $L_{\mathrm{ext}} = (N+1)B \ge L$. On this global fast horizon define $A_{\mathrm{glob}} = g_\delta A_R(W_{\mathrm{fast}})$. Its physical flow obeys*

$$P_{\mathrm{glob}}(mB + u, mB) = D_m^0(u), \qquad 0 \le u \le B. \tag{7.2.11}$$

The analogous identity holds with the deterministic mean $V_{\delta t}$ added globally and local operator paths $X_m + H_m$. Their finite block products, including the last remainder τ, are source limits in L^2, at this fixed δ, N.

Proof. We use a single regularized slow noise to realize every fast and local source together. An ordinary change of variables gives the restart identity. We pass it through the fixed-horizon source limit and control the finite products by a telescoping estimate.

Step 1. We construct coupled global and local regularizations. Take one regularized slow noise preserving the given noise $Y_{\epsilon,\eta}$ on the extension of the given W constructed in Section 5.2. Define the fast and local noises by

$$Y_{\mathrm{fast}}(f) = Y_{\epsilon,\eta}(T_{\delta,0}f), \qquad Y_m(f) = Y_{\epsilon,\eta}(T_{\delta,m}f).$$

The pullback isometry and (5.2.12) give source and residual variance bounds by $\|f\|^2_{H_W}$. The residual tends to zero on each transformed smooth compact test at fixed δ, m. Joint Gaussianity is retained. Proposition 5.2.2 therefore gives the L^pC^θ operator-path limits on $[0, L_{\mathrm{ext}}]$ and on $[0, B]$, including both constant columns.

The field-test integral identity of Proposition 5.2.5 passes through these test pullbacks by change of variables; the proof of Lemma 6.2.3 then identifies the ordinary primitives using spatial smoothness and total finite propagation. Their random fields are $Y_{\mathrm{fast}}(u, x) = \delta^{a/2}Y_{\epsilon,\eta}(\delta u, x)$ and $Y_m(u, x) = Y_{\mathrm{fast}}(mB+u, x)$. Indeed, these follow by change of variables in their test integrals. The temporal law is $K_{\eta/\delta}$ because $\delta^a K_\eta(\delta r) = K_{\eta/\delta}(r)$; the spatial heat law and all joint width rules are unchanged. They are continuous in time and smooth in space. Their ordinary primitives equal their Gaussian operator paths: their matrix entries are $Y_m(h_R)$, by the indicator approximation used in (7.2.6) and the point-test integral identity. Total finite propagation extends this identity to both constant

columns. This does not assume a separately chosen extension preserving the given noise automatically commutes with time dilation.

Step 2. We identify the restart relation before and after removing the source widths. Changing the ordinary source integration variable and composing the free groups gives the exact identity on F

$$S_F(mB)\Big[A^{\mathrm{src}}_{\mathrm{glob}}(mB+u)-A^{\mathrm{src}}_{\mathrm{glob}}(mB)\Big]S_F(-mB)=X^{\mathrm{src}}_m(u).$$

No physical mask is commuted through a wave group. Restriction, difference and conjugation are bounded maps on these fixed-horizon C^θ spaces. Passing the source limits gives the same identity for A_{glob}, X_m. For the finitely many m, a convergent subsequence or rational times and path continuity gives simultaneous identities in u. Conjugation norms need only be finite at this fixed δ.

Step 3. We identify the local Young equations and compose the blocks. Conjugate the global interaction Young equation on $[mB, mB+u]$ by $S_F(mB)$. Bounded linearity of its Riemann sums and that original identity give the local equation driven by X_m. Uniqueness identifies it with U_{X_m}, proving (7.2.11). The ordinary deterministic primitive for $V_{\delta t}$ has the identical cocycle with local H_m. Composition now identifies the full product, with terminal τ.

Step 4. We pass finite products through the source limit. For the unshifted factors use Proposition 6.2.5 on the fixed horizon $[0, L_{\mathrm{ext}}]$; for the shifted factors use Proposition 6.2.8 with $g = g_\delta$ and the fixed mean $V_{\delta t}$, followed by the restart identity. For completeness, source convergence of these finite products requires no growing-product stability assertion. At fixed δ, N let $C \geq 1$ be the maximum norm of their source and original factors, and let e_{src} be the maximum factor difference. The parent Young convergence gives every finite moment of C uniformly in source widths and $e_{\mathrm{src}} \to 0$ in every finite L^p. If $d(n)$ is the difference of the first n ordered products, then

$$d(n+1) \leq Cd(n) + C^n e_{\mathrm{src}}, \qquad d(0) = 0.$$

Subtract the next pair of products by adding and subtracting the source factor times the old partial product. One term is at most C times the previous difference; the other is at most e_{src} times the norm of an old product of n factors, bounded by C^n. This gives the displayed recurrence without commuting factors. Extend both finite sequences by identities so the recurrence holds for all natural n. The finite error-accumulation estimate gives $d(N+1) \leq (N+1)C^{N+1}e_{\mathrm{src}}$. Hölder, using C in $L^{4(N+1)}$ and the error in L^4, proves L^2 convergence. This is only a fixed-δ source limit. Shifted source products may use the fixed original mean plus the regularized noise; no finite-source Cameron mean is substituted. This proves Lemma 7.2.5. □

Proposition 7.2.6 (The square observable and canonical comparison)**.** *Define the signed averages without and with the deterministic mean*

$$U_{\delta,B} = O_\phi D^0_N(\tau)D^0_{N-1}(B)\cdots D^0_0(B)e_0, \qquad Y_{\delta,B} = O_\phi D^+_N(\tau)D^+_{N-1}(B)\cdots D^+_0(B)e_0.$$

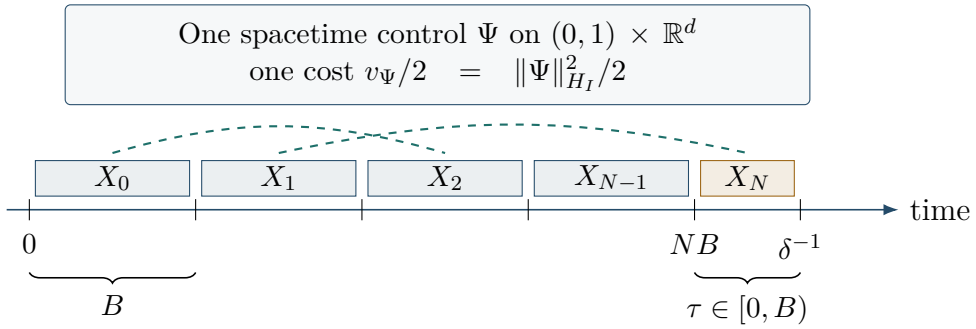

Correlated blocks; ordered evolution carries $(u, \partial_t u)$.
The last block may be empty. Example: $N = 4$.

Figure 7.1: The true partition in fast time. Here $N = \lfloor 1/(\delta B) \rfloor$ and $\tau = \delta^{-1} - NB$. All blocks come from the same noise and a single control on the whole time interval. The change-of-law density has cost $v_\Psi/(2\delta)$; the displayed $v_\Psi/2$ is its normalized cost. The proof does not multiply independent block probabilities or add separate Gaussian costs. See Lemma 7.2.1 and Proposition 10.2.4.

They have all finite unweighted moments, and

$$\mathbb{E}U^2_{\delta,B} = \mathbb{E}\left[e^{-Z/\sqrt{\delta}-v/(2\delta)} Y^2_{\delta,B}\right], \tag{7.2.12}$$

$$\mathbb{E}U^2_{\delta,B} \le \mathbb{E}|V_\delta(1,0)|^2 = \mathbb{E}|u(T,0)|^2, \qquad \delta = T^{-\kappa}. \tag{7.2.13}$$

The variance v in the density is the original slow original variance.

Proof. We first apply the exact Gaussian change of law to the squared observable on the whole path space. We then verify the source-limit premise for the unshifted masked product and compare it with the canonical point moment at the scaled amplitude.

Step 1. We apply the Gaussian identity to an everywhere-defined squared observable. On all of $\mathscr{B}_\delta$ put

$$j_\delta(x) = |O_\phi D_{x_N}(\tau) D_{x_{N-1}}(B) \cdots D_{x_0}(B) e_0|^2.$$

The everywhere-defined continuous Young map, fixed-time bounded free groups, finite products and bounded O_ϕ make j_δ continuous and nonnegative on the whole input space. Apply Proposition 7.2.2 directly to these original paths. Since $X + H$ is its exact translate, this proves (7.2.12) with the single original $Z = W(\Psi)$ and its variance v. Finite products of the local Young flows have every finite unweighted moment by their Gaussian path bounds and Hölder, at fixed δ, N. The Gaussian identity itself did not require prior integrability of j_δ. No source convergence under its exponential density is used.

Step 2. We identify the amplitude-rescaled original model. To apply the masked comparison at the amplitude, put $\Gamma_\delta = g_\delta^2 \Gamma$ and $W' = g_\delta W_{\text{fast}}$. This is a nonzero member of the same admissible covariance class, with unchanged degree α and temporal parameter a. Its integrated operator is g_δ times the original one: the original matrix forms are linear

in noise, and basis-independent Gaussian transfer and the bounded F extension retain both constant columns. The nth source chain is multiplied by g_δ^n. Thus, this is exactly the model without the deterministic mean at that amplitude.

Step 3. We pass the unshifted source product to its masked limit. We verify the source-limit premise of the masked comparison. Keep δ, B, N fixed and use the single regularized noise preserving the given noise of Lemma 7.2.5. For $m < N$ let $F_m = D_m^0(B)$ and put $F_N = D_N^0(\tau)$; write $F_{m,\rho}$ for the corresponding ordinary source factors, where both source widths in ρ tend to zero. Lemma 7.2.5 and Proposition 6.2.5 give factor convergence in every finite L^q and uniform bounds for every finite moment of their norms. These statements are on the fixed finite horizons $[0,(N+1)B]$ and $[0,B]$, and include both constant-response columns. Set $n = N+1$ and

$$C_\rho = \max\left(1, \max_{m\le N}\|F_{m,\rho}\|, \max_{m\le N}\|F_m\|\right), \qquad e_\rho = \max_{m\le N}\|F_{m,\rho} - F_m\|.$$

Then $\sup_\rho \|C_\rho\|_q < \infty$ for every finite q, and $\|e_\rho\|_q \to 0$. Telescoping the ordered products gives

$$\|F_{N,\rho}\cdots F_{0,\rho} - F_N\cdots F_0\| \le nC_\rho^n e_\rho.$$

Each term in the telescoping difference contains one factor error and at most $n-1$ factors bounded by C_ρ. There are n such terms. Since $C_\rho \ge 1$, replacing C_ρ^{n-1} by C_ρ^n gives the displayed bound. Therefore, Hölder with exponents $4n$ and 4 gives

$$\left\|F_{N,\rho}\cdots F_{0,\rho} - F_N\cdots F_0\right\|_{L^2} \le n\|C_\rho\|_{L^{4n}}^n\|e_\rho\|_{L^4} \longrightarrow 0.$$

No uniform estimate in the growing number N is needed: this source limit is completed at each fixed δ, N. The physical source identification in Lemma 6.2.6, with the same m_R and initial state e_0, identifies the source product with the tested ordinary masked solution at fast time $L = 1/\delta$. Boundedness of O_ϕ and $\|e_0\| = 1$ thus identify $U_{\delta,B}$ as its L^2 limit. The sources $g_\delta Y_{\text{fast}}$ have the correct law, contraction and original-test limit by Lemma 7.2.5.

Step 4. We apply the masked moment comparison at the fixed amplitude. At positive source widths, $0 \le m_R \le 1$ multiplies each nonnegative displacement Wick integrand by the product of its vertex masks. Positive Green measures and covariance retain this comparison for unequal, self and empty chains as well. Proposition 6.1.2 gives the tested comparison, and the just-proved L^2 convergence discharges the premise of Proposition 6.1.3 at Γ_δ. Its canonical unmasked moment limit uses the fixed-order joint source limits and the absolutely summable order bounds. Since $\phi \ge 0$ and $\int \phi = 1$, these facts give

$$\mathbb{E}U_{\delta,B}^2 \le \mathbb{E}|u_{\Gamma_\delta}(L,0)|^2.$$

Only the source products without the deterministic mean were needed for this passage. The shifted original product is already the everywhere-defined $j_\delta(X+H)$ in the Gaussian identity; no tilted source limit or change of the original slow Ψ, Z, v has been made.

Step 5. We identify the canonical fast-time moment with the large-time moment. The ordinary change from fast u to slow $t = \delta u$, with phase $(V, \delta V_t)$, transforms the unmasked

source equation into the regularized version of (7.1.1), with slow terminal time one. Indeed, $g_\delta Y_{\mathrm{fast}}(u) = \sqrt{\delta}\, Y_{\epsilon,\eta}(\delta u)$, and its fast cutoff is η/δ. The canonical fixed-order and absolutely convergent series construction passes this law identity at fixed δ to the original moment, preserving every mixed, unequal, self and empty chain. Lemma 7.1.1 gives the final equality in (7.2.13). The physical scale $r_T = T\delta$ is distinct from the fixed mask radius R. The mask need not contain the growing backward cone: the comparison is a moment inequality, not equality of masked and full fields. All source limits preceded this large-time comparison. This proves Proposition 7.2.6. □

Proposition 7.2.6 bounds $\mathbb{E}|u(T,0)|^2$ from below by the weighted second moment of $Y_{\delta,B}$ in (7.2.12). We still need a lower bound for $Y_{\delta,B}$ itself. The proof below obtains one on an event whose probability tends to one. It uses the estimates of Lemma 7.2.3 and the cone bound of Lemma 7.2.4.

Lean partial

Proposition 7.2.7 (Original point lower rate at the Gaussian quadratic cost)**.** *For every original positive Ψ and eligible fixed mask R chosen above, and every fixed $x \in \mathbb{R}^d$,*

$$\liminf_{T\to\infty} T^{-\kappa} \log \mathbb{E}|u(T,x)|^2 \geq 2\int_0^1 \lambda_s \,\mathrm{d}s - \frac{\upsilon_\Psi}{2}. \tag{7.2.14}$$

Proof. We fix the cone constants before taking the small-parameter limit. A single high-probability event controls every block and the original Gaussian variable. On that event the cone bound and a Riemann sum give the growth rate, while the linear Gaussian penalty vanishes after normalization.

Step 1. We fix the rate tolerance and bound the coupled block maximum. Fix $e_{\mathrm{rate}} > 0$. Choose $0 < \varrho < 1/2$ with $\log(1-\varrho) > -e_{\mathrm{rate}}/3$, then choose the cone constants, including an integer B fixed independently of δ, from Lemma 7.2.4. The control Ψ and eligible mask R remain fixed throughout.

Choose a finite $p > 2/(1-a)$ and put $\gamma_p = p(1-a)/2 - 1 > 0$. From (7.2.5) and $N+1 \leq 2/\delta$, Markov and the union bound give, for $\eta > 0$,

$$\begin{aligned}\mathbb{P}(M_\delta > \eta) &\leq \eta^{-p} \sum_{m=0}^{N} \mathbb{E}\|X_m\|_{C^\theta}^p \\ &\leq A_p \eta^{-p} \delta^{\gamma_p}, \qquad A_p = 2(C_{R,B}\sqrt{p})^p < \infty.\end{aligned}$$

This estimate concerns the coupled blocks; no independence is needed. At these fixed data A_p is independent of δ.

Step 2. We choose a deterministic block tolerance and one common good event. We also specify the deterministic tolerance used with this bound. The primitive estimates in Lemma 7.2.3 give, for the constant-potential primitives H_m^{stat},

$$\max_m \max(\|H_m\|_{C^\theta}, \|H_m^{\mathrm{stat}}\|_{C^\theta}) \leq H_0, \qquad \max_m \|H_m - H_m^{\mathrm{stat}}\|_{C^\theta} \leq C_B\delta.$$

Apply Proposition 6.2.4 on the fixed ball of operator paths of radius $H_0 + 1$ and use the bounded free groups on $[0,B]$. There is $L_B \geq 1$, depending on these fixed R, B, Ψ and the admissible exponents, such that on $\{M_\delta \leq 1\}$,

$$E_{\mathrm{op},\delta} \leq L_B(M_\delta + \delta).$$

Set $\eta = \min(1, \epsilon_{\mathrm{op}}/(2L_B)) > 0$. If $\delta \le \epsilon_{\mathrm{op}}/(2L_B)$, then $M_\delta \le \eta$ implies $E_{\mathrm{op},\delta} \le \epsilon_{\mathrm{op}}$. Thus, for the measurable event on the original common space

$$E_\delta = \{E_{\mathrm{op},\delta} \le \epsilon_{\mathrm{op}}\} \cap \{|Z| \le \delta^{-1/4}\}, \qquad p_\delta = \mathbb{P}(E_\delta),$$

Chebyshev for the same single $Z = W(\Psi)$, with $\mathbb{E}Z^2 = v$, gives

$$p_\delta \ge 1 - A_p \eta^{-p} \delta^{\gamma_p} - v\delta^{1/2} \longrightarrow 1.$$

This is one union bound, with no independence between blocks or from Z and no product of block probabilities.

Step 3. We make the block and Riemann-sum errors smaller than the fixed tolerance. Let C_λ be a Lipschitz bound for $s \mapsto \lambda_s$. Take δ small enough, in addition to $0 < \delta < \min(1, 1/B)$, that

$$\begin{aligned} \delta B \le \omega, \qquad \delta \le \epsilon_{\mathrm{op}}/(2L_B), \qquad C_\lambda \delta B \le e_{\mathrm{rate}}/3, \\ \delta |\log c_*| \le e_{\mathrm{rate}}/3, \qquad A_p \eta^{-p} \delta^{\gamma_p} + v\delta^{1/2} \le 1/2. \end{aligned}$$

Every constant has been fixed before this choice. The condition involving C_λ is vacuous if that constant is zero. All source limits in Proposition 7.2.6 have already been completed at each such fixed δ.

The indices $s_m = m\delta B$ lie in I with adjacent gaps at most ω. On E_δ the shifted full-F blocks therefore satisfy Lemma 7.2.4, retaining both phase entries and the final remainder τ. In particular, $Y_{\delta,B} > 0$, and

$$\delta \log Y_{\delta,B} \ge \delta \log c_* + \delta(N-1)\log(1-\varrho) + \delta B \sum_{m<N} \lambda_{s_m} + \delta\tau\lambda_{s_N}.$$

Since $s_N + \delta\tau = 1$, the last two terms are the left Riemann sum for I_R on the entire interval, including its last interval of length $\delta\tau$, with mesh at most δB. Its error is at most $C_\lambda \delta B$. Also $0 \le \delta(N-1) \le 1/B \le 1$, so the logarithmic loss is at least $\log(1-\varrho) > -e_{\mathrm{rate}}/3$. The two other losses are each at most $e_{\mathrm{rate}}/3$ by the choices above. Hence,

$$Y_{\delta,B} \ge \exp((I_R - e_{\mathrm{rate}})/\delta) \quad \text{on } E_\delta,$$

including the $N = 1$ and $\tau = 0$ cases of the cone estimate.

Step 4. We use the same event in the shifted second-moment identity. The integrand in (7.2.12) is nonnegative. On the same E_δ its linear Gaussian term satisfies $-Z/\sqrt{\delta} \ge -\delta^{-3/4}$. Restriction to this event and (7.2.13) therefore give the explicit bound for the original point moment

$$\mathbb{E}|u(T,0)|^2 \ge \mathbb{E}U_{\delta,B}^2 \ge p_\delta \exp\left(\frac{2I_R - 2e_{\mathrm{rate}} - v/2}{\delta} - \delta^{-3/4}\right), \qquad \delta = T^{-\kappa}.$$

Here $p_\delta \ge 1/2$ for small δ, so $-\delta\log 2 \le \delta \log p_\delta \le 0$. Multiplying the logarithm of the preceding inequality by δ yields

$$\delta \log \mathbb{E}|u(T,0)|^2 \ge 2I_R - 2e_{\mathrm{rate}} - v/2 - \delta^{1/4} + \delta \log p_\delta.$$

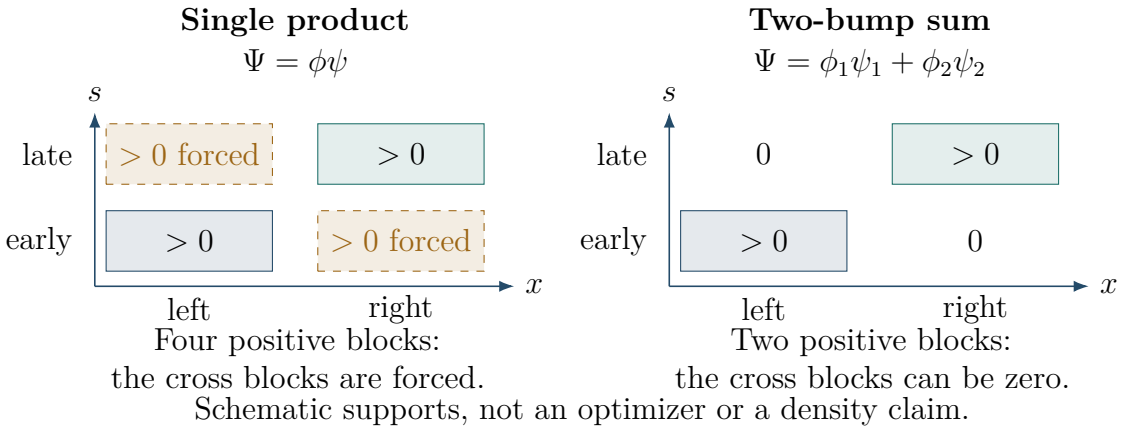

Figure 7.2: The full control class allows spatial profiles to change with time, as in this sum of two smooth nonnegative product bumps that no single time–space product can represent. The full class is infinite-dimensional; see Theorem 11.2.6.

Thus, the normalized linear penalty is $\delta\delta^{-3/4} = \delta^{1/4} \to 0$, and $\delta \log p_\delta \to 0$. The quadratic Gaussian cost is precisely half the original variance v. Since $\kappa > 0$, $\delta = T^{-\kappa}$ is a bijection between all sufficiently large T and all sufficiently small δ. This gives the full continuous-time liminf $Q_2 \geq 2I_R - 2e_{\mathrm{rate}} - v/2$. For each e_{rate} the argument first fixed its own $B = B(e_{\mathrm{rate}})$ and then took $\delta \downarrow 0$. The original point rate Q_2 is independent of B; only now let $e_{\mathrm{rate}} \downarrow 0$. No choice $B = B(\delta)$ is made.

Step 5. We extend the point bound by translation. Finally, spatial translation of all positive-width vertices preserves the original noise law, Green kernels and constant initial data. The fixed-order L^2 and absolute-series limits preserve equality of point second moments. Hence, zero can be replaced by every fixed x in (7.2.14). Every control and mask were fixed before asymptotics; a supremum over them may follow their individual inequalities. This proves Proposition 7.2.7. □

7.3 The unmasked Rayleigh rate and nonnegative controls

Fix a nonzero covariance satisfying Hypothesis 1.2.1, including its original amplitude, and set $a = \alpha_0$. Define the full class

$$\mathcal{C}_{\mathrm{pos}} = \{\Psi \in C_c^\infty((0,1) \times \mathbb{R}^d; \mathbb{R}) : \Psi \geq 0,\ \Psi \neq 0\}. \tag{7.3.1}$$

It includes nonseparable tests. It is nonempty: if $b(z) = e^{-1/(1-z^2)}$ on $|z| < 1$ and zero otherwise, then $b(4s-2)\prod_{j=1}^d b(x_j)$ belongs to this class. All boundary derivatives vanish because exponential decay dominates every power of $(1-z^2)^{-1}$. For each Ψ retain the original mean $h_{\Psi,s}$ and original variance $v_\Psi = \mathbb{E}W(\Psi)^2$ from (6.3.20)–(6.3.21). Neither the test nor its covariance is changed by a physical mask. We write h_s when Ψ is fixed.

7.3.1 Global bounds and the unmasked spectral bottom

We first record a bound for the covariance smoothed by the heat kernel. The proof of Lemma 7.3.2 uses it to bound $\Gamma * |D\Psi(t,\cdot)|$ uniformly in t, x.

Lean full

Lemma 7.3.1 (Gaussian envelope for the original covariance)**.** *For the normalized heat kernel $p_\epsilon(x) = (2\pi\epsilon)^{-d/2} e^{-|x|^2/(2\epsilon)}$,*

$$(\Gamma * p_\epsilon)(x) = \int e^{i\xi\cdot x} e^{-\epsilon|\xi|^2/2} \mu(\,\mathrm{d}\xi), \qquad 0 \le (\Gamma * p_\epsilon)(x) \le (\Gamma * p_\epsilon)(0) < \infty. \tag{7.3.2}$$

The value at zero is strictly positive.

Proof. We first use temperedness to make all Gaussian pairings finite. We identify the convolution and spectral expressions as continuous distributions, then use positivity to obtain the bound by the value at zero.

Step 1. We obtain integrable majorants for the Gaussian weights. In the dyadic summation below, mass growth 2^{jN} times weight decay 2^{-jL} is summable for $L > N$; Gaussian derivatives decrease faster than each such polynomial weight. A positive tempered Radon measure has polynomial ball growth. Indeed, evaluate its tempered bound on a nonnegative smooth cutoff equal to one on B_1, dilated by $R \ge 1$. Its finitely many Schwartz seminorms are bounded by CR^N, so positivity gives a ball-mass bound CR^N. Summing dyadic annuli shows that $(1+|x|)^{-L}$ is integrable for $L > N$. Apply this separately to Γ and μ. Gaussian weights are therefore integrable against both measures. The classical convolution on the left is finite and smooth locally in x: on compact x sets its translated Gaussian derivatives are bounded by any fixed sufficiently fast polynomial weight in the integration variable.

Step 2. We identify the two continuous expressions and bound their common value. Pair the convolution with a Schwartz test φ. Absolute Fubini is justified by these weights. The resulting pairing is that of Γ with $p_\epsilon * \varphi$. Applying the spectral convention in Hypothesis 1.2.1 and the identity $\int p_\epsilon(y) e^{-i\xi\cdot y}\,\mathrm{d}y = e^{-\epsilon|\xi|^2/2}$ gives exactly the right side of (7.3.2) as a distribution. The heat kernel is even, so either Fourier sign gives that same Gaussian multiplier. Its spectral integral is absolutely finite and continuous in x by dominated convergence. Thus, equality of the two continuous distributions gives equality at every x, without an extra normalization factor. The physical convolution is nonnegative. Evenness of μ makes the spectral integral real, and its absolute value is bounded by its total Gaussian mass, the value at zero. Finally, $\Gamma \ne 0$ and $p_\epsilon > 0$ give strict positivity there. This proves Lemma 7.3.1. □

Lean full

Lemma 7.3.2 (Global regularity of the original mean)**.** *Every mixed time and space derivative of h_s is globally bounded in space, uniformly on compact time intervals. In particular, for $I = [0,1]$ there are finite constants M, C_Ψ such that*

$$0 \le h_s(x) \le M, \qquad \|h_s - h_t\|_\infty \le C_\Psi |s-t|, \qquad s,t \in I. \tag{7.3.3}$$

Proof. Extend Ψ by zero in time; its compact support inside $(0,1)$ makes this a smooth extension. For any mixed derivative $D\Psi$, a fixed $\epsilon > 0$ and compactness of its common spatial support give $|D\Psi(t,x)| \le C_D p_\epsilon(x)$ for all t, x. Here the heat kernel has a positive minimum on that support. Lemma 7.3.1 consequently bounds $\Gamma * |D\Psi(t,\cdot)|$ uniformly in t, x. Ordinary local differentiation against the Radon measure gives the corresponding derivatives of the convolution. After the change $r = s - t$,

$$h_s(x) = \int_{\mathbb{R}} |r|^{-a} (\Gamma * \Psi(s - r, \cdot))(x) \, \mathrm{d}r.$$

For s in a compact interval the relevant r lie in a fixed bounded interval. The preceding global bound times $|r|^{-a}$ is integrable since $a < 1$. Every derivative thus falls on the smooth test and passes through the integral by dominated convergence, with the claimed global spatial bounds. Nonnegativity follows from positive kernels. The bounded time derivative proves the Lipschitz estimate. No directional decay of the mean has been inferred. This proves Lemma 7.3.2. □

Lemma 7.3.2 shows that h_s is bounded by M for $s \in I$ and is Lipschitz in s in the supremum norm. We now use these two bounds to define the rate $\lambda_{\Psi,s}$ of the potential h_s without a mask and to show that it is Lipschitz on I.

Lean narrower

Proposition 7.3.3 (The unmasked Rayleigh rate)**.** *On complex $L^2(\mathbb{R}^d)$, the operator $H_s = -\Delta - h_s$ is self-adjoint on H^2, with form domain H^1 and form $q_s(f) = \|\nabla f\|_2^2 - \int h_s |f|^2$. Its spectral bottom E_s is uniformly negative on I. The positive rate $\lambda_{\Psi,s} = \sqrt{-E_s}$ satisfies*

$$\lambda_{\Psi,s}^2 = \sup_{\substack{f \in H^1(\mathbb{R}^d;\mathbb{R}) \\ \|f\|_2 = 1}} \left(\int h_s f^2 - \|\nabla f\|_2^2 \right). \tag{7.3.4}$$

It is Lipschitz on I, and $I_\Psi := \int_0^1 \lambda_{\Psi,s} \, \mathrm{d}s$ is positive and finite. No eigenstate at the unmasked bottom is asserted.

Proof. We construct the unmasked self-adjoint operator using bounded perturbation and identify its form domain. The spectral theorem gives the real Rayleigh formula; the common compact trial makes its bottom uniformly negative and its square-root rate Lipschitz.

Step 1. We prove self-adjointness on the stated operator domain. The Fourier Laplacian $A = -\Delta$ is self-adjoint on H^2, being multiplication by $|\xi|^2$ with its maximal domain. Multiplication $B_s = -h_s$ is bounded self-adjoint with norm at most M. Thus, $H_s = A + B_s$ is densely defined, symmetric and closed on H^2; the two graph norms are equivalent under a bounded perturbation. For real $b > M$,

$$H_s - ib = (I + B_s(A - ib)^{-1})(A - ib).$$

The first factor has a Neumann inverse because $\|B_s(A - ib)^{-1}\| \le M/b < 1$, and the same holds with $+ib$. To check self-adjointness directly, for $u \in D(H_s^*)$ solve

$(H_s - ib)v = (H_s^* - ib)u$ with $v \in D(H_s)$. Then $u - v \in \ker(H_s^* - ib) = \mathrm{Ran}(H_s + ib)^\perp = \{0\}$. Hence, $D(H_s^*) = D(H_s)$.

Step 2. We identify the form domain by equivalent completions. Set $c_{\mathrm{shift}} = 1 + M$ and $J_s = H_s + c_{\mathrm{shift}} \geq 1$. Integration by parts on H^2 gives

$$\|J_s^{1/2} f\|_2^2 = q_s(f) + c_{\mathrm{shift}} \|f\|_2^2, \qquad \|f\|_{H^1}^2 \leq \|J_s^{1/2} f\|_2^2 \leq c_{\mathrm{shift}} \|f\|_{H^1}^2.$$

Spectral cutoffs $1_{[1,n]}(J_s)$ show that $H^2 = D(J_s)$ is a core for the half-power norm; Fourier cutoffs give its density in H^1. Completion in the equivalent norms identifies $D(J_s^{1/2})$ and H^1 as L^2 subspaces, since both norms dominate L^2. This proves the stated form domain.

Step 3. We obtain the real Rayleigh formula without an eigenstate assumption. The spectral lower bound gives one direction of the Rayleigh identity. For the reverse, nonzero spectral projections in $[E_s, E_s + \epsilon]$ give unit H^2 vectors with Rayleigh values at most $E_s + \epsilon$. The bottom is finite because the operator is bounded below and has finite Rayleigh tests. Let $\epsilon \downarrow 0$. Real tests give the same infimum: $q_s(u + iv) = q_s(u) + q_s(v)$, so the quotient is the norm-weighted average of the nonzero real quotients. This proves the Rayleigh identity with $-E_s$ on the left. The following negative upper bound justifies writing that value as $\lambda_{\Psi,s}^2$ in (7.3.4).

For a complex vector $f = u + iv$ with real-valued u, v, its quadratic form and squared norm are sums of the corresponding values for u and v. At least one of the nonzero components has quotient no greater than their norm-weighted average.

Step 4. We obtain strict negativity and uniform rate continuity. Proposition 6.3.7 supplies, for this original Ψ, one unit compactly supported w and a finite plateau mask with a common strictly negative upper bound $\epsilon_0 > 0$. Its trial has support in B_{2L}; choose its plateau radius $R_0 \geq 2L$. The unmasked form on this same w is no larger. Consequently, $-M \leq E_s \leq -\epsilon_0 < 0$, and $\sqrt{\epsilon_0} \leq \lambda_{\Psi,s} \leq \sqrt{M}$. Comparing identical unit form tests gives $|E_s - E_t| \leq \|h_s - h_t\|_\infty$ and therefore

$$|\lambda_{\Psi,s} - \lambda_{\Psi,t}| \leq \frac{C_\Psi}{2\sqrt{\epsilon_0}} |s - t|.$$

This also proves positivity and finiteness of I_Ψ. No compact-potential spectral theorem was applied to H_s. This proves Proposition 7.3.3. □

7.3.2 Removing masks from the numerical lower rate

Proposition 7.2.7 gives the lower bound with the rate of the masked potential $m_R h_s$, for one fixed mask. We now let the mask radius R tend to infinity and replace this rate by the rate $\lambda_{\Psi,s}$ of Proposition 7.3.3.

Lean partial

Proposition 7.3.4 (Monotone rates and the original point moment)**.** *There is an increasing family of admissible radial masks m_R tending to one, for which the compact ground rates satisfy $\lambda_{R,s} \uparrow \lambda_{\Psi,s}$ uniformly on I as $R \to \infty$, with the compact ground statements used for $R \geq R_0(\Psi)$. For the original canonical solution and any fixed x,*

$$\liminf_{T \to \infty} T^{-\kappa} \log \mathbb{E}|u(T, x)|^2 \geq 2I_\Psi - \frac{\upsilon_\Psi}{2}. \tag{7.3.5}$$

Proof. We choose nested physical masks, compare their Rayleigh suprema with the unmasked supremum, and prove uniform convergence in the time parameter. We then take a numerical supremum of already established fixed-mask bounds.

Step 1. We construct the nested masks. Put $F(t) = e^{-1/t}$ for $t > 0$ and zero otherwise, and define

$$\chi(r) = \frac{F(2-r)}{F(2-r) + F(r-1)}, \qquad m_R(x) = \chi(|x|/R).$$

The denominator is positive. The numerator decreases and the second denominator term increases; thus χ is nonincreasing, equals one on $r \le 1$, and zero on $r \ge 2$. Flatness of F at zero gives smoothness. Since χ is constant near zero, m_R is smooth also at the spatial origin. These even $[0,1]$ masks increase pointwise to one.

Step 2. We pass the Rayleigh values and rates to their unmasked limits. For each fixed unit form test f, the mask-removal argument uses the integrable majorant Mf^2 for $m_R h_s f^2$. The compact-family input is Proposition 6.3.1, with the common trial supplied by Proposition 6.3.7: its rate obeys $\lambda_{R,s}^2 = -E_1$, the negative form bottom of $-\Delta - m_R h_s$ on H^1. Choose R_0 so the preceding common trial lies in the plateau. Every $R \ge R_0$ has the same negative margin. For each fixed R, the compact-family theorem applies to $m_R h_s$. Its real Rayleigh formula follows from the same real/complex quotient argument as (7.3.4). The rates are continuous, positive, at most $\sqrt{M}$ and monotone in R. For every fixed real unit $f \in H^1$, dominated convergence gives $\int m_R h_s f^2 \to \int h_s f^2$. Hence,

$$\sup_{R \ge R_0} \lambda_{R,s}^2 = \sup_{\|f\|_2 = 1,\ f \in H^1(\mathbb{R}^d;\mathbb{R})} \sup_{R \ge R_0} \left(\int m_R h_s f^2 - \|\nabla f\|_2^2 \right) = \lambda_{\Psi,s}^2.$$

Only two numerical suprema were interchanged. Positive square roots give the pointwise rate convergence. For $R_n = R_0 + n$ and $\epsilon > 0$, the increasing open sets $\{s : \lambda_{\Psi,s} - \lambda_{R_n,s} < \epsilon\}$ cover compact I. A finite subcover lies in the largest one, proving uniform convergence. Monotonicity extends it to all real $R \to \infty$. Therefore, $\int_I \lambda_{R,s}\, \mathrm{d}s \uparrow I_\Psi$.

Step 3. We take the supremum of fixed-mask moment lower bounds. At each fixed R use this very same mask in the operator path and mean when applying Proposition 7.2.7. It gives the lower bound with $2\int_I \lambda_{R,s}\, \mathrm{d}s - v_\Psi/2$ for the same original point liminf. Taking the numerical supremum over these individual bounds proves (7.3.5). There is no $R(T)$, unmasked noisy wave, uniform-in-mask Gaussian estimate or exchange of source and time limits. This proves Proposition 7.3.4. □

7.3.3 Full-class dilation and finite variational values for nonnegative controls

The bound (7.3.5) holds for each $\Psi \in \mathcal{C}_{\mathrm{pos}}$ separately. Before we take the supremum over Ψ, we record how $h_{\Psi,s}$, v_Ψ, $\lambda_{\Psi,s}$ and I_Ψ change under a spatial dilation of the control. The proof of Proposition 7.3.6 uses this to relate the variational values for different coefficients c.

Lean narrower

Lemma 7.3.5 (Radon and Rayleigh dilation)**.** *For $r > 0$ the map*

$$(D_r\Psi)(s,x) = r^{d+2-\alpha}\Psi(s,rx) \tag{7.3.6}$$

is a bijection of $\mathcal{C}_{\mathrm{pos}}$, with inverse $D_{1/r}$. With the same original covariance,

$$h_{D_r\Psi,s}(x) = r^2 h_{\Psi,s}(rx), \qquad v_{D_r\Psi} = r^{4-\alpha}v_\Psi, \qquad \lambda_{D_r\Psi,s} = r\lambda_{\Psi,s}, \quad I_{D_r\Psi} = rI_\Psi. \tag{7.3.7}$$

Proof. We apply the homogeneous Radon pushforward to the covariance mean and the Lebesgue Jacobian to its cost. We then dilate the unit Rayleigh tests to identify the rate and its time integral.

Step 1. We scale the original mean and covariance cost. Positive dilation preserves the full smooth positive nonzero class; multiplication of its amplitude powers gives the stated inverse. Homogeneity of the physical Radon measure gives, for every nonnegative measurable G,

$$\int G(ry)\Gamma(\,\mathrm{d}y) = r^{\alpha-d}\int G(z)\Gamma(\,\mathrm{d}z).$$

Indeed, its left pushforward measure on a Borel set A is $\Gamma(A/r) = r^{\alpha-d}\Gamma(A)$. Positive Tonelli applies this identity inside the temporal convolution, giving $h_{D_r\Psi,s}(x) = r^2 h_{\Psi,s}(rx)$. Now use the *Lebesgue* substitution $z = rx$ in the original pairing:

$$v_{D_r\Psi} = r^{d+2-\alpha}r^2 r^{-d}v_\Psi = r^{4-\alpha}v_\Psi.$$

This distinguishes the Radon pushforward from the spatial volume factor; it includes singular covariances and white noise.

Step 2. We scale the full set of Rayleigh tests. The map $U_r f(x) = r^{d/2}f(rx)$ is a unitary bijection on real L^2, preserving H^1, H^2 as sets under its inverse. Weak derivatives give $\|\nabla U_r f\|_2^2 = r^2\|\nabla f\|_2^2$ and $\int h_{D_r\Psi,s}(U_r f)^2 = r^2\int h_{\Psi,s}f^2$. The real Rayleigh bijection proves the squared rate identity; the rates are positive, so their square roots and integrals give (7.3.7). On H^2 this is also $H_{D_r\Psi,s}U_r = r^2 U_r H_{\Psi,s}$. Time has not been rescaled. For compact masks the corresponding identity uses $m_R(rx) = m_{R/r}(x)$; a fixed mask radius is not invariant. This proves Lemma 7.3.5. □

Lean narrower

Proposition 7.3.6 (Intrinsic variational lower bounds)**.** *For $c > 0$, the set of variational values $\{cI_\Psi - v_\Psi/2 : \Psi \in \mathcal{C}_{\mathrm{pos}}\}$ is nonempty and bounded above. Its finite real supremum S_c^{pos} is positive and satisfies*

$$S_c^{\mathrm{pos}} = c^{(4-\alpha)/(3-\alpha)}S_1^{\mathrm{pos}}, \qquad Q_2 \geq S_2^{\mathrm{pos}}, \tag{7.3.8}$$

where Q_2 is the original point liminf. The coefficient-one value is an auxiliary variational value; no first-moment or source-constant identification is asserted.

Proof. We first construct a positive coefficient-one value and scale the entire class of values. We use the independently proved point upper bound to show these sets are bounded above before taking their finite real suprema.

Step 1. We exhibit a positive value. Write $k = 3 - \alpha > 0$, $q = 4 - \alpha = k + 1$ and $m = q/k > 1$. Fix one Ψ_0 from the nonempty class and put $I_0 = I_{\Psi_0} > 0$, $v_0 = v_{\Psi_0} > 0$. Positivity of the latter is Lemma 6.3.6. For $r_0 = (I_0/v_0)^{1/k} > 0$, which need not be less than one, the exact real-power identity gives

$$I_{D_{r_0}\Psi_0} - v_{D_{r_0}\Psi_0}/2 = r_0 I_0 - r_0^q v_0/2 = r_0 I_0/2 > 0.$$

The definition of r_0 gives $r_0^k = I_0/v_0$. Since $q = k + 1$, it follows that $r_0^q v_0 = r_0 I_0$. Thus, subtracting half the cost leaves exactly half of the positive linear term. This positive value is obtained from a smooth nonnegative control.

Step 2. We scale the whole coefficient-one set bijectively. For $c > 0$ put $r_c = c^{1/k}$ and $K_c = c^m > 0$. Lemma 7.3.5 and the exact scalar powers give, for every Ψ,

$$cI_{D_{r_c}\Psi} - v_{D_{r_c}\Psi}/2 = K_c(I_\Psi - v_\Psi/2). \tag{7.3.9}$$

The two scalar factors agree: $cr_c = c^{1+1/k} = c^{q/k} = K_c$ and $r_c^q = c^{q/k} = K_c$. Consequently, dilation multiplies the linear reward and the quadratic cost by the same factor for this choice of r_c. Since D_{r_c} is a bijection of the entire class, the whole set of variational values with coefficient c is K_c times the whole coefficient-one set of variational values.

Step 3. We bound the sets using the original point upper estimate. We prove boundedness before taking finite-real suprema. The independent Theorem 3.3.8, for the *same canonical solution*, gives

$$\mathbb{E}|u(T,0)|^2 \le e(T+2)^d e^{C_{\mathrm{up}}T^\kappa}, \qquad T \ge 1, \quad C_{\mathrm{up}} < \infty.$$

Its prefactor is negligible: choose $\epsilon = \kappa/2 > 0$, use $\log T \le (T^\epsilon - 1)/\epsilon$ and $\log(T+2) \le \log T + \log 3$ for $T \ge 1$, and divide by T^κ. Thus, the original point limsup is at most C_{up}. One fixed test/mask lower bound gives a finite lower bound for Q_2, so Q_2 is finite. By (7.3.5) every coefficient-two variational expression is at most this same $Q_2 \le C_{\mathrm{up}}$, uniformly in Ψ. Equation (7.3.9) at $c = 2$ consequently bounds all coefficient-one variational values by C_{up}/K_2. The nonempty set has a finite real supremum $S_1^{\mathrm{pos}} > 0$ by the positive test above.

Step 4. We take finite real suprema and retain their interpretation. For general c, set equality and $K_c > 0$ show that $K_c S_1^{\mathrm{pos}}$ is the supremum: it is an upper bound, and every smaller number is exceeded by K_c times a coefficient-one variational expression within the corresponding positive distance of its supremum. This proves finiteness, positivity and the first identity in (7.3.8). Taking the numerical supremum of the coefficient-two lower bounds proves the second. Although $2^m > 2$, the resulting $S_2^{\mathrm{pos}} > 2S_1^{\mathrm{pos}}$ is only a comparison of auxiliary variational values. It is not a Jensen improvement without a first-moment identification. This proves Proposition 7.3.6. □

For $\Gamma = 0$, the mean, original variance and Rayleigh rate are zero. Set all these variational values to zero; the free canonical solution $u = 1$ has the corresponding zero moment rate. Strict positivity above is restricted to nonzero covariance. Matching an upper variational rate and identifying an exact pointwise limit remain later steps.

What we now have. The lower bound $Q_2 \geq S_2^{\mathrm{pos}}$ (Proposition 7.3.6). The upper bound takes the next three chapters.

Chapter 8

Spatial controls and Gaussian means

The lower bound used smooth controls. The upper bound must also handle controls completed in the Gaussian covariance norm, where pointwise formulas may no longer exist. So we need to know how such a control, the deterministic mean it induces, and the wave operators generated by that mean are related.

Figure 8.1 is the picture to keep in mind. Section 8.1 computes a temporal equilibrium density. Section 8.2 extends the physical spatial pairings and defines the class of time-dependent spatial profiles used in the later energy bounds. Section 8.3 builds the compact map from a Gaussian control to its mean on time blocks. Section 8.4 estimates perturbations of the Young evolution while keeping the deterministic endpoint.

The chapter uses the variational value of Section 7.3 and the wave phase of Section 6.2. On a first reading, keep Propositions 8.2.5, 8.3.5 and 8.3.7 and let the proofs wait. The spatial radius is still fixed; the next chapter decides which bounds survive as it grows. Episode ▶ 6 of the video series covers this chapter.

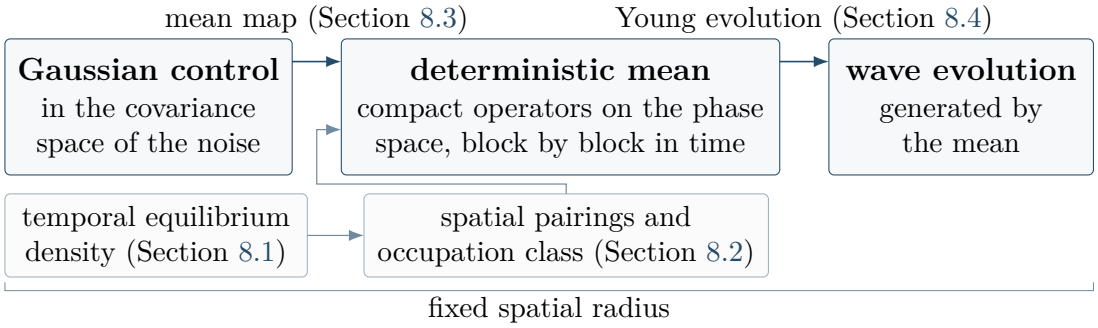

Figure 8.1: How this chapter is organized. The arrows show the order of construction only, and the spatial radius is fixed throughout.

8.1 The temporal equilibrium density

The density in Lemma 8.1.2 is the classical interval Riesz equilibrium density. Its probability-normalized form on $[-1,1]$ is recalled by Calef and Hardin [10, p. 1]. We prove the potential identity with the normalization used here.

We use Euler's function $\Gamma_E(x) = \int_0^\infty u^{x-1}e^{-u}\,\mathrm{d}u$, $x>0$, and $\mathrm{Beta}(x,y) = \int_0^1 t^{x-1}(1-t)^{y-1}\,\mathrm{d}t$, $x,y>0$. Both integrals are positive and finite.

Lean full

Lemma 8.1.1 (Gamma and Beta identities)**.** *For positive arguments,*

$$\begin{aligned}\Gamma_E(x+1) &= x\Gamma_E(x),\\ \operatorname{Beta}(x,y) &= \frac{\Gamma_E(x)\Gamma_E(y)}{\Gamma_E(x+y)},\\ \Gamma_E(2x) &= \frac{2^{2x-1}\Gamma_E(x)\Gamma_E(x+1/2)}{\sqrt{\pi}}.\end{aligned}$$

Proof. Integration by parts gives the recurrence, with vanishing boundary terms. In the positive product Gamma integral, use $(u,v)=(Rt,R(1-t))$, with Jacobian R; Tonelli gives the Beta–Gamma identity. For the last identity, symmetry, then $t=(1+v)/2$ and $v^2=w$, give $\operatorname{Beta}(x,x)=2^{1-2x}\operatorname{Beta}(1/2,x)$. Also $\Gamma_E(1/2)=\int_{\mathbb{R}} e^{-z^2}\,\mathrm{d}z=\sqrt{\pi}$: the substitution $u=z^2$ gives the first equality, and squaring the positive Gaussian integral and using polar coordinates gives $2\pi\int_0^\infty re^{-r^2}\,\mathrm{d}r=\pi$. Substituting these into the Beta–Gamma identity proves duplication. This proves Lemma 8.1.1. □

Lean full

Lemma 8.1.2 (Exact potential and mass)**.** *For $0<a<1$ put $r=(1-a)/2$ and, for $0<t<1$,*

$$f_a(t)=\frac{[t(1-t)]^{-r}}{\Gamma_E(r)\Gamma_E(1-r)}. \tag{8.1.1}$$

This positive function belongs to $L^1(0,1)\cap L^2(0,1)$, and

$$\int_0^1 |s-t|^{-a} f_a(t)\,\mathrm{d}t = 1 \qquad \text{for every } s\in[0,1], \tag{8.1.2}$$

$$M_a := \int_0^1 f_a(t)\,\mathrm{d}t = \frac{\Gamma_E((1+a)/2)}{\Gamma_E(1+a)\Gamma_E((1-a)/2)} > 0. \tag{8.1.3}$$

Proof. We first justify the positive series used in the integral calculation. We compute the two halves of the potential through an incomplete Beta integral, treat the endpoints directly, and then compute the mass and integrability.

Step 1. We justify the positive binomial expansion. The positive binomial series $(1-z)^{-p}=\sum_{n\ge0}(p)_n z^n/n!$, $p>0$, $0\le z<1$, follows directly as follows. Its coefficient ratio gives uniform convergence on compact subintervals, including for its derivative. Termwise differentiation gives $(1-z)y'=py$, $y(0)=1$; hence $(1-z)^p y$ is constant one. Here $(p)_0=1$, $(p)_n=p(p+1)\cdots(p+n-1)$. All terms used below are nonnegative, so Tonelli applies.

Step 2. We compute the potential at interior points and endpoints. For $0<s<1$ split the integral of $|s-t|^{2r-1}[t(1-t)]^{-r}$ into left and right parts. In the left part, $t=su$ gives

$$\begin{aligned}L(s) &= s^r\int_0^1 (1-u)^{2r-1}u^{-r}(1-su)^{-r}\,\mathrm{d}u\\ &= \operatorname{Beta}(1-r,2r)s^r\sum_{n\ge0}\frac{(r)_n(1-r)_n s^n}{(1+r)_n n!}.\end{aligned}$$

The Beta ratio follows from the Gamma recurrence. Since $(r)_n/(1+r)_n = r/(r+n)$, expanding the incomplete Beta integral gives

$$L(s) = r\,\mathrm{Beta}(1-r,2r)B_s(r,r), \qquad B_s(r,r) = \int_0^s u^{r-1}(1-u)^{r-1}\,\mathrm{d}u.$$

Expanding $(1-u)^{r-1}$ in $B_s(r,r)$ gives coefficient $(1-r)_n/n!$ and integral $s^{r+n}/(r+n)$. Multiplication by $r\,\mathrm{Beta}(1-r,2r)$ therefore gives exactly the coefficients of $L(s)$. Reflection makes the right part $L(1-s)$, while symmetry gives $B_s(r,r) + B_{1-s}(r,r) = \mathrm{Beta}(r,r)$. The full integral is therefore $r\,\mathrm{Beta}(1-r,2r)\,\mathrm{Beta}(r,r) = \Gamma_E(r)\Gamma_E(1-r)$. All integrals are finite because $-r > -1$ and $2r-1 > -1$. At $s=0$ the integral is directly $\mathrm{Beta}(r,1-r) = \Gamma_E(r)\Gamma_E(1-r)$; $s=1$ follows by reflection. This proves (8.1.2), including the endpoints without a limiting argument there.

Step 3. We verify both integrability classes and the stated mass. Integrability and square integrability follow from $-r > -1$ and $-2r = a - 1 > -1$. Finally,

$$M_a = \frac{\mathrm{Beta}(1-r,1-r)}{\Gamma_E(r)\Gamma_E(1-r)} = \frac{\Gamma_E(1-r)}{\Gamma_E(2-2r)\Gamma_E(r)},$$

which is (8.1.3). Its time mass has not been renormalized. This proves Lemma 8.1.2. □

8.2 Physical spatial pairings and the full occupation class

Retain a nonzero original covariance from Hypothesis 1.2.1 with its amplitude. Set $a = \alpha_0$, $k = 3-\alpha > 1$, $q = 4-\alpha = k+1$ and $D = q - 2a > 0$. The scalar D is fixed. All profiles are real. The original positive temporal exponent and threshold imply $\alpha < 2$; this is the strict inequality used in the scalar powers and concavity. The finite variational value over nonnegative controls S_1^{pos} is that of Proposition 7.3.6.

Lean full

Lemma 8.2.1 (The physical two-point integral)**.** *The positive measure $\nu(\mathrm{d}x, \mathrm{d}y) = \mathrm{d}x\,\Gamma(\mathrm{d}y)$ is sigma-finite. For nonnegative functions define*

$$B_\Gamma(f,h) = \int f(x)h(x-y)\nu(\mathrm{d}x, \mathrm{d}y) \tag{8.2.1}$$

initially as an extended nonnegative integral, using finite Borel representatives of Lebesgue classes. Its value is representative independent. Lebesgue-a.e. convergence transfers to ν-a.e. convergence at both positions x and $x-y$.

Proof. Local finiteness of Γ gives sigma-finiteness on exhausting balls, and Lebesgue measure is sigma-finite. If N is Borel and Lebesgue null, Tonelli applied first in x gives $\nu\{x \in N\} = 0$ and $\nu\{x - y \in N\} = 0$, because every fixed translate of N is null. An arbitrary Lebesgue null set has a Borel null superset. Thus, arbitrary versions are measurable in the ν completion with the same value, and the same observation applies to the exceptional sets of a.e. convergence. Signed pairings will be used only after absolute convergence. This proves Lemma 8.2.1. □

Put $A_{\mathrm{sp}}(g) = B_\Gamma(g^2, g^2)$ and $b(g) = \|\nabla g\|_2^2$ on H^1; initially A_{sp} is used only for smooth compact profiles before the extension below. For smooth compact z, write $U_z = \Gamma * z$ in its usual pointwise sense.

Lean narrower

Lemma 8.2.2 (Smooth temporal controls)**.** *For every nonnegative nonzero $z \in C_c^\infty(\mathbb{R}^d)$, let*

$$\lambda_z(c)^2 = \sup_{\substack{g \in H^1(\mathbb{R}^d;\mathbb{R}) \\ \|g\|_2 = 1}} \left(c \int U_z g^2 - b(g) \right), \qquad c > 0.$$

This is positive and finite, and λ_z is Lipschitz on every compact positive c interval. With the exact M_a in (8.1.3),

$$S_1^{\mathrm{pos}} \geq \lambda_z(1) - \frac{M_a}{2} B_\Gamma(z, z). \tag{8.2.2}$$

Proof. We first obtain the static Rayleigh rate from an admissible smooth control. We then approximate the exact temporal equilibrium by increasing compact smooth controls and pass their rewards and original covariance costs to the limit separately.

Step 1. We obtain the static rate and its local Lipschitz bound. Choose nonnegative nonzero $f \in C_c^\infty(0,1)$ and $s_0 = 1/2$. Let $k_f(s_0) = \int_0^1 |s_0 - t|^{-a} f(t)\,\mathrm{d}t > 0$. The smooth test $\Psi(t,x) = cf(t)z(x)/k_f(s_0)$ has mean cU_z at s_0. Proposition 7.3.3 gives boundedness of this potential, the displayed real Rayleigh formula, and a positive rate for every $c > 0$. Comparing identical unit tests makes $\lambda_z(c)^2$ Lipschitz with constant $\|U_z\|_\infty$. On a positive compact interval its rate has a positive floor by monotonicity, giving the square-root Lipschitz bound.

Step 2. We approximate the equilibrium density by admissible controls. Use the nonincreasing smooth cutoff χ constructed in the proof of Proposition 7.3.4. For integers $n \geq 4$, set on $(0,1)$

$$f_n(t) = f_a(t)\chi(1/(nt))\chi(1/(n(1-t))), \qquad k_n(s) = \int_0^1 |s-t|^{-a} f_n(t)\,\mathrm{d}t.$$

Extend f_n by zero. It is smooth compact, vanishes near both endpoints, is nonzero, and increases to f_a. Thus, $\Psi_n = f_n \otimes z$ is a positive smooth control. Monotone convergence and (8.1.2) give $k_n(s) \uparrow 1$ for every $s \in [0,1]$. Since the kernel is at least one on the unit square off its null diagonal, $0 < c_0 := \int_0^1 f_4 \leq k_n(s) \leq 1$. The mean is $k_n(s)U_z$; hence its rate is $\lambda_z(k_n(s))$, converging to $\lambda_z(1)$ and bounded by that finite number. Dominated convergence gives $I_{\Psi_n} \to \lambda_z(1)$.

Step 3. We pass the covariance cost and the score to the limit. The Gaussian cost is exactly the nonnegative Tonelli pairing

$$v_{\Psi_n} = B_\Gamma(z,z) \int_0^1 f_n(s)k_n(s)\,\mathrm{d}s.$$

Its time integrand increases to f_a, so the cost tends to $M_a B_\Gamma(z,z)$. The spatial factor is finite and positive: its smooth compact autocorrelation is positive near zero, and homogeneity scales any origin-centered ball of positive Γ mass to every other positive

radius. Such a ball exists by exhaustion. Take the limit of the individual inequalities $S_1^{\mathrm{pos}} \geq I_{\Psi_n} - v_{\Psi_n}/2$. The variational expression differences need not increase. No control depends on original large time and no rough stochastic evolution has been used. This proves Lemma 8.2.2. □

The next estimate also allows zero covariance and does not use the finiteness of S_1^{pos}.

Lean full

Lemma 8.2.3 (Deterministic Fourier bound for the spatial energy)**.** *Under Hypothesis 1.2.1, allowing* $\Gamma = 0$*, let* $g \in C_c^\infty(\mathbb{R}^d;\mathbb{R})$ *satisfy* $\|g\|_2 = 1$ *and put* $b = \|\nabla g\|_2^2$*. Then* $b > 0$ *and*

$$0 \leq A_{\mathrm{sp}}(g) \leq 2^{1+\alpha} R_\alpha b^{\alpha/2}, \tag{8.2.3}$$

where R_α *is defined in* (1.5.1)*.*

Proof. We identify the spatial energy spectrally without assuming a measure density. A mass bound and a derivative bound on the Fourier transform give a resolvent majorant, whose homogeneous integral supplies the desired constant.

Step 1. We identify the energy as a finite spectral integral. If $b = 0$, smoothness makes $\nabla g = 0$ everywhere. Thus, g is constant, and compact support forces $g = 0$, contrary to $\|g\|_2 = 1$. Put $Q = g^2$ and use the unnormalized Fourier transform

$$\mathcal{F}_0 Q(\xi) = \int_{\mathbb{R}^d} e^{-i\xi\cdot x} Q(x)\,\mathrm{d}x.$$

In the unitary convention of Section 4.1, this is $c_d^{-1}\widehat{Q}$, with $c_d = (2\pi)^{-d/2}$. The autocorrelation

$$c_Q(y) = \int_{\mathbb{R}^d} Q(x)Q(x-y)\,\mathrm{d}x$$

is smooth and compactly supported. Apply the distributional spectral identity (4.1.1) to this Schwartz function. Its inner Fourier integral is $|\mathcal{F}_0 Q(\xi)|^2$, since Q is real. Hence

$$A_{\mathrm{sp}}(g) = \int c_Q(y)\Gamma(\,\mathrm{d}y) = \int |\mathcal{F}_0 Q(\xi)|^2 \mu(\,\mathrm{d}\xi).$$

Both integrals are finite: c_Q is compactly supported and Γ is Radon, while $|\mathcal{F}_0 Q|^2$ is Schwartz and μ is tempered. No density of either measure is required.

Step 2. We bound the Fourier transform by a resolvent weight. Since $\|Q\|_1 = 1$, we have $|\mathcal{F}_0 Q| \leq 1$. Integration by parts and the Cauchy–Schwarz inequality give

$$|\xi|\,|\mathcal{F}_0 Q(\xi)| \leq \|\nabla Q\|_1 \leq 2\|g\|_2\|\nabla g\|_2 = 2\sqrt{b}.$$

Splitting into $|\xi|^2 \leq 4b$ and $|\xi|^2 > 4b$ therefore yields

$$|\mathcal{F}_0 Q(\xi)|^2 \leq \frac{8b}{4b + |\xi|^2}.$$

In the region $|\xi|^2 \leq 4b$, the right side of the preceding display is at least one, so the mass bound applies. In the other region, the derivative bound gives $4b/|\xi|^2$, which is at most

$8b/(4b + |\xi|^2)$ because $4b \le |\xi|^2$. Thus, the two estimates give one majorant over the whole spectrum.

Step 3. We integrate the majorant and keep the original spectral normalization. The scalar integral in that resolvent calculation is

$$\int_0^\infty \frac{u^{\alpha-1}}{1+u^2}\,\mathrm{d}u = \frac{1}{2}\,\mathrm{Beta}(\alpha/2, 1-\alpha/2) = \frac{\pi}{2\sin(\pi\alpha/2)},$$

by the Beta integral and Euler's reflection identity. In the following resolvent formula, q is a free positive argument, separate from the fixed exponent $q = 4 - \alpha$ used elsewhere in this section. The deterministic resolvent calculation in the proof of Lemma 2.3.1, together with (1.5.1), gives, for $q > 0$,

$$\mathcal{R}_\Gamma(q) := \int \frac{\mu(\,\mathrm{d}\xi)}{q^2 + |\xi|^2} = q^{\alpha-2} R_\alpha < \infty.$$

Consequently,

$$A_{\mathrm{sp}}(g) \le 8b\mathcal{R}_\Gamma(2\sqrt{b}) = 2^{1+\alpha} R_\alpha b^{\alpha/2}.$$

Nonnegativity follows from the spectral identity. If $\Gamma = 0$, then $\mu = 0$ and both sides of (8.2.3) vanish. This proves Lemma 8.2.3. □

Lemma 8.2.2 gives a lower bound for each nonzero, nonnegative smooth spatial control of compact support. We now scale and dilate a single profile and optimize. The resulting bound depends on the profile only through the ratio of A_{sp} to a power of b.

Lean narrower

Proposition 8.2.4 (The finite smooth spatial ratio)**.** *For real unit $g \in C_c^\infty(\mathbb{R}^d)$ put $R(g) = A_{\mathrm{sp}}(g)/b(g)^{\alpha/2}$. Its supremum R_0 over these profiles is a positive finite real number, and*

$$S_1^{\mathrm{pos}} \ge k\left[\frac{R(g)\alpha^{\alpha/2}}{8M_a q^{q/2}}\right]^{1/k}. \tag{8.2.4}$$

Proof. We first bound the smooth spatial ratio. We then vary the amplitude of a squared dilated profile so that its Rayleigh test has a prescribed positive value, and optimize the resulting one-variable score.

Step 1. We prove positivity and finiteness of the ratio supremum. The gradient energy $b(g)$ is positive: a nonzero L^2 function with zero weak gradient would have Fourier transform supported only at zero, and hence would vanish. Its square is nonnegative nonzero smooth compact, so the autocorrelation argument in the proof of Lemma 8.2.2 gives $0 < A := A_{\mathrm{sp}}(g) < \infty$. Lemma 8.2.3 gives $R(g) \le 2^{1+\alpha} R_\alpha$ for every such profile. A normalized compact bump supplies a positive ratio. Thus, $0 < R_0 < \infty$, independently of the finiteness of S_1^{pos}. It remains to prove the score inequality. With $U_\ell g(x) = \ell^{d/2} g(\ell x)$, the physical changes of variables give

$$A_{\mathrm{sp}}(U_\ell g) = \ell^\alpha A, \qquad b(U_\ell g) = \ell^2 b(g). \tag{8.2.5}$$

The factors in the first identity are ℓ^{2d} from the two squares, ℓ^{-d} from $\mathrm{d}x$, and $\ell^{\alpha-d}$ from the Radon pushforward.

Step 2. We choose the amplitude and spatial scale of a single control. For $\theta, \ell > 0$ choose the smooth control $z = \theta(U_\ell g)^2$. The Rayleigh test $U_\ell g$ gives $\lambda_z(1)^2 \geq \theta\ell^\alpha A - \ell^2 b$, while $B_\Gamma(z,z) = \theta^2\ell^\alpha A$. For any $L > 0$, put $u = \alpha/q > 0$ and choose

$$\ell^2 = uL^2/b, \qquad \theta = (1+u)L^2/(\ell^\alpha A).$$

In the cost, substituting these same choices gives $\theta^2\ell^\alpha A = (1+u)^2L^4/(\ell^\alpha A)$; replacing $\ell^\alpha A$ by $u^{\alpha/2}L^\alpha R(g)$ yields the coefficient C below. The radicand is L^2. Lemma 8.2.2 consequently gives

$$S_1^{\mathrm{pos}} \geq L - CL^q, \qquad C = \frac{M_a(1+u)^2}{2R(g)u^{\alpha/2}} > 0.$$

Its maximum occurs at $L^k = 1/(qC)$ and is $(k/q)(qC)^{-1/k}$. Since $1 + u = 4/q$, $1/(q^qC) = R(g)\alpha^{\alpha/2}/(8M_aq^{q/2})$, proving (8.2.4). This argument retains the finite real value S_1^{pos} fixed at the start of the section; only the proof of $R_0 < \infty$ is independent of that input. This proves Proposition 8.2.4. □

So far A_{sp} has been used only for smooth compact profiles. Proposition 8.2.8 needs it and the square pairings for real H^1 profiles, so we extend them with the same constant R_0.

Lean full

Proposition 8.2.5 (The physical four-linear extension)**.** *For real $f \in H^1(\mathbb{R}^d)$ define $N(f) = \|f\|_2^{1-\alpha/4}\|\nabla f\|_2^{\alpha/4}$. Every physical square pairing is finite and*

$$A_{\mathrm{sp}}(f) \leq R_0 N(f)^4, \tag{8.2.6}$$

$$0 \leq B_\Gamma(f^2, h^2) \leq \sqrt{A_{\mathrm{sp}}(f)A_{\mathrm{sp}}(h)}. \tag{8.2.7}$$

The signed integral $C_4(f_1,f_2,f_3,f_4) = B_\Gamma(f_1f_2, f_3f_4)$ is absolutely convergent and jointly continuous on $(H^1)^4$, with

$$\int |f_1(x)f_2(x)f_3(x-y)f_4(x-y)|\,\mathrm{d}\nu \leq R_0 \prod_{j=1}^4 N(f_j). \tag{8.2.8}$$

The ratio supremum R_{sp} over all real unit H^1 profiles equals R_0. Every nonzero H^1 profile has $A_{\mathrm{sp}}(f) > 0$.

Proof. We first obtain the square-pair bound for smooth profiles and extend it by Fatou. We then use ordinary Cauchy–Schwarz under the physical measure to prove an absolutely convergent four-linear bound. That bound, rather than Fatou alone, gives continuity and the full-class ratio identity.

Step 1. We establish the smooth square-pair estimates. For smooth compact f, normalization in R_0 proves (8.2.6), including $f = 0$. All exponents in N are positive and

$N(f) \le \|f\|_{H^1}$. For smooth compact signed Q, P, the absolute correlation is compactly supported and bounded by $\|Q\|_2\|P\|_2$. Local finiteness of Γ therefore makes its physical integral finite. Smooth signed covariance is positive: with the ordinary transform $\widehat{Q}_{\mathrm{ord}}(\xi) = \int e^{i\xi\cdot x}Q(x)\,\mathrm{d}x$, the model convention gives

$$B_\Gamma(Q,Q) = \int |\widehat{Q}_{\mathrm{ord}}(\xi)|^2 \mu(\,\mathrm{d}\xi) \ge 0, \qquad Q \in C_c^\infty(\mathbb{R}^d;\mathbb{R}).$$

Pair Γ with the smooth compact correlation to obtain this identity; rapid Fourier decay and tempered μ give finiteness. Evenness of Γ and $(x,y) \mapsto (x-y,-y)$ give symmetry. The quadratic polynomial for $Q + tP$ gives covariance Cauchy–Schwarz. In particular, for smooth real f, h,

$$0 \le B_\Gamma(f^2,h^2) \le R_0 N(f)^2 N(h)^2.$$

The squares of signed smooth profiles are already smooth and nonnegative.

Step 2. We approximate Sobolev profiles and obtain finite physical pairings. Smooth compact functions are dense in H^1. Cutoffs equal to one on the radius-R ball, vanishing beyond $2R$ and with gradient at most C/R, converge by the function and gradient tails and the bound $C\|f\|_2/R$ for the extra gradient term. Mollification then converges in H^1 by L^2 translation continuity of the function and its weak gradients. The space is separable through its closed isometric image $f \mapsto (f, \nabla f)$ in $L^2(\mathbb{R}^d)^{d+1}$.

For arbitrary $f, h \in H^1$ take smooth approximants converging in H^1 and along a common subsequence Lebesgue-a.e. Lemma 8.2.1 transfers this convergence at both positions to ν-a.e. convergence. Fatou and continuity of N give $B_\Gamma(f^2,h^2) \le R_0 N(f)^2 N(h)^2 < \infty$, including the diagonal bound. At this stage Fatou supplies an inequality, not continuity.

Step 3. We prove the four-linear estimate and continuity. Apply ordinary Cauchy–Schwarz under the positive measure ν to $f_1(x)f_3(x-y)$ and $f_2(x)f_4(x-y)$. The two squared integrals are finite by the last bound; their square root is at most $R_0 \prod_j N(f_j)$. This proves (8.2.8), absolute convergence and multilinearity. Telescoping a difference one argument at a time and using $N(f) \le \|f\|_{H^1}$ proves joint continuity. Thus, A_{sp} and the square pairings are continuous. PSD for smooth compact profiles passes to finite linear combinations of H^1 squares by this continuity, and its two-profile Cauchy–Schwarz gives (8.2.7). This completes the physical pairing argument beyond Fatou.

Step 4. We identify the full ratio supremum and strict positivity. As in Lemma 6.3.6, nonzero Γ gives positive mass to some origin-centred ball, and homogeneity rescales that ball to every positive radius. Every real unit H^1 profile has positive gradient energy by the Fourier argument above. The homogeneous bound gives $R_{\mathrm{sp}} \le R_0$, and smooth inclusion gives the reverse. Normalized smooth approximations preserve the ratio by continuity. Finally, for nonzero f, choose a bounded set E of finite positive measure where $|f| \ge c > 0$. The correlation of 1_E is continuous and positive near zero by L^2 translation continuity. An origin-centered ball there has positive Γ mass, so $A_{\mathrm{sp}}(f) \ge c^4 B_\Gamma(1_E, 1_E) > 0$. This uses a nonnegative integral, not an H^1 claim for 1_E. Finiteness was already proved. This proves Proposition 8.2.5. □

By Proposition 8.2.5, the ratio supremum is the same over smooth and over H^1 profiles. We now express it through an energy and restate the score bound in those terms.

Lean narrower

Proposition 8.2.6 (The spatial energy and static lower variational expression)**.** *Over all real unit H^1 profiles define the energy*

$$\mathcal{E}_{\mathrm{sp}} = \sup_{\|g\|_2=1} \left(A_{\mathrm{sp}}(g) - \frac{b(g)}{2} \right).$$

Then

$$\mathcal{E}_{\mathrm{sp}} = \frac{2-\alpha}{2} \alpha^{\alpha/(2-\alpha)} R_{\mathrm{sp}}^{2/(2-\alpha)} \in (0, \infty). \tag{8.2.9}$$

In particular,

$$S_1^{\mathrm{pos}} \geq M_a^{-1/k} F_0(\mathcal{E}_{\mathrm{sp}}), \qquad F_0(z) = k \left[\frac{(2z/(2-\alpha))^{(2-\alpha)/2}}{8q^{q/2}} \right]^{1/k}, \quad z > 0. \tag{8.2.10}$$

The subscript in F_0 labels this scalar map; the covariance retains its original temporal exponent a.

Proof. We optimize spatial dilation for a fixed profile, then take the supremum over all profiles. The resulting identity expresses the ratio constant in terms of the energy and lets us rewrite the static score bound.

Physical change of variables, or smooth approximation and Proposition 8.2.5, extends (8.2.5) to real H^1 profiles. For fixed unit g, with $A, b > 0$, the maximum of $\ell^\alpha A - \ell^2 b/2$ occurs at $\ell^{2-\alpha} = \alpha A/b$ and equals

$$\frac{2-\alpha}{2} \alpha^{\alpha/(2-\alpha)} R(g)^{2/(2-\alpha)}.$$

Differentiating the scalar expression gives $\alpha A \ell^{\alpha-1} - b\ell$. Its positive zero satisfies the stated equation. At that point, $b\ell^2 = \alpha A \ell^\alpha$, so the value is $(1-\alpha/2) A \ell^\alpha$. Substitution of the critical scale gives the displayed power of $R(g)$. Dilation preserves the whole unit class and includes $\ell = 1$. Taking both numerical suprema, then profiles with ratio tending to R_{sp}, proves (8.2.9). No optimizer is assumed. Smooth ratios also approach R_{sp} by Proposition 8.2.5. Pass them through (8.2.4) and substitute

$$R_{\mathrm{sp}} \alpha^{\alpha/2} = \left(\frac{2\mathcal{E}_{\mathrm{sp}}}{2-\alpha} \right)^{(2-\alpha)/2}.$$

This gives (8.2.10). This proves Proposition 8.2.6. □

8.2.1 The kernel row and full occupation energy

Define, for $u \neq 0$,

$$K_\star(u) = \frac{1}{\Gamma_E(a)} \int_0^\infty e^{-(\lambda + \lambda^2/(2D))|u|} \lambda^{a-1} \, \mathrm{d}\lambda, \tag{8.2.11}$$

and set $K_\star(0) = 0$ for time integration. The spatial estimates above concern individual H^1 profiles. To apply them to time-dependent families, we first compute the exact row bound for this time kernel.

Lean full

Lemma 8.2.7 (Exact row maximum)**.** *The kernel is even, positive off zero, locally integrable, decreasing on $(0,\infty)$, and $K_\star(u) \le |u|^{-a}$ off zero. Its exact row maximum on $[0,1]$ is*

$$\max_{s\in[0,1]} \int_0^1 K_\star(s-t)\,\mathrm{d}t = R_\star := 2\int_0^{1/2} K_\star(u)\,\mathrm{d}u \in (0,\infty). \tag{8.2.12}$$

Proof. Dropping the positive quadratic damping bounds the mixture by the Gamma integral $|u|^{-a}$. Positivity and monotonicity follow directly from the integrand, and $a < 1$ gives local integrability. Put $\Phi(t) = \int_0^t K_\star(u)\,\mathrm{d}u$. It is concave because its integrand is decreasing on positive arguments. The row is $\Phi(s) + \Phi(1-s) \le 2\Phi(1/2)$, with equality at $s = 1/2$. The diagonal value changes no time integral. This proves Lemma 8.2.7. □

Let $\mathcal{O}$ be the full class of strongly $H^1(\mathbb{R}^d;\mathbb{R})$-measurable fields $s \mapsto g_s$ on $(0,1)$ with $\|g_s\|_2 = 1$ a.e. and $T(g) = \int_0^1 b(g_s)\,\mathrm{d}s < \infty$. No time smoothness, common compact support or optimizer condition is imposed.

Lean full

Proposition 8.2.8 (The full physical occupation class)**.** *The pairings $(s,t) \mapsto B_\Gamma(g_s^2, g_t^2)$ are measurable, representative independent and equal to their physical integrals. With*

$$J(g) = \int_0^1 \int_0^1 K_\star(s-t) B_\Gamma(g_s^2, g_t^2)\,\mathrm{d}s\,\mathrm{d}t,$$

every $g \in \mathcal{O}$ satisfies

$$0 \le J(g) \le R_\star R_{\mathrm{sp}} T(g)^{\alpha/2} < \infty. \tag{8.2.13}$$

The energy over exactly this full class satisfies

$$0 < \mathcal{E}_\star^{\mathcal{O}} := \sup_{g\in\mathcal{O}} \big(J(g) - T(g)/2\big) \le R_\star^{2/(2-\alpha)} \mathcal{E}_{\mathrm{sp}} < \infty. \tag{8.2.14}$$

Proof. We first identify measurable physical pairings for the full occupation class. We bound the time integral by the kernel row estimate and then compare its energy with the spatial energy, retaining the full class throughout.

Step 1. We identify measurable representatives and their pairings. The map $s \mapsto b(g_s)$ is measurable by continuity of the squared gradient norm. Also $\int_0^1 \|g_s\|_{H^1}^2\,\mathrm{d}s = 1 + T(g)$. Use a separably valued strong representative and replace exceptional null times by one fixed real unit compact bump. Joint measurable spatial representatives exist: approximate this Bochner L^2 field by simple H^1-valued functions with summable $L^2(0,1;H^1)$ errors, and choose measurable spatial versions for their countably many values. A subsequence has a measurable spacetime L^2 limit, and for a.e. s its spatial L^2 class is g_s. Lemma 8.2.1 makes every pairing independent of the spatial versions. The continuous pairing map on the separable space $H^1 \times H^1$ from Proposition 8.2.5 consequently gives a measurable function of (s,t) agreeing a.e. with the nonnegative physical integral.

Step 2. We apply the spatial bound and the temporal row estimate. Set $F(s) = b(g_s)^{\alpha/4}$. Equations (8.2.6) and (8.2.7) give $B_\Gamma(g_s^2, g_t^2) \le R_{\mathrm{sp}} F(s)F(t)$. Since $0 < \alpha/2 < 1$, concavity on the unit time interval yields $\int_0^1 F^2 = \int_0^1 b(g_s)^{\alpha/2}\,\mathrm{d}s \le T(g)^{\alpha/2}$. Now use $2F(s)F(t) \le F(s)^2 + F(t)^2$ and the exact row bound (8.2.12), whose column bound is the same because $K_\star$ is even, to obtain (8.2.13). Positive Tonelli is valid before finiteness is known. Null-time modifications affect only a product-null set, so they cannot change J.

Step 3. We bound the energy and show that it is positive. The scalar maximum of $R_\star R_{\mathrm{sp}} T^{\alpha/2} - T/2$ over $T \ge 0$ is $R_\star^{2/(2-\alpha)} \mathcal{E}_{\mathrm{sp}}$, by the same differentiation as (8.2.9). This bounds the occupation supremum from above. For positivity take a constant-in-time unit compact profile and its spatial dilation U_ℓ. Its J is $J_0 \ell^\alpha A_{\mathrm{sp}}(g)$, where $J_0 = \int_0^1 \int_0^1 K_\star(s-t)\,\mathrm{d}s\,\mathrm{d}t \in (0,\infty)$, while $T = \ell^2 b(g)$. For sufficiently small $\ell > 0$, $\alpha < 2$ makes $J - T/2 > 0$. Thus, the nonempty supremum is a positive finite real number. This is a comparison bound; no attaining profile or equality in it has been asserted. No spatial point trace or rough stochastic evolution was used. This proves Proposition 8.2.8. □

For zero covariance all spatial pairings vanish and set $R_{\mathrm{sp}} = 0$. The spatial and occupation energies are zero suprema of $-b/2$ and $-T/2$: small spatial dilations of one fixed unit compact profile make these energies tend to zero, with the profile constant in time for the latter. No zero-gradient unit state is used. The temporal identities remain valid, and the moment model is the free case already treated.

8.3 The compact mean and Cameron map on time blocks

Retain the nonzero original covariance in Hypothesis 1.2.1, its amplitude, $a = \alpha_0$, and the real phases $E = H^{1/2} \times H^{-1/2}$ and $F = E \oplus \mathbb{R}^2$. Write $\Lambda = (1-\Delta)^{1/2}$. The form B_Γ and constant R_{sp} are those of Section 8.2. Let H_{sp} be the real covariance-null completion of $C_c^\infty(\mathbb{R}^d)$ with inner product B_Γ, and H_t the analogous completion of $C_c^\infty(I)$, $I = (0,1)$, with time kernel $|s-t|^{-a}$. Let $H = H_I$ be the completion of smooth tests supported inside $I \times \mathbb{R}^d$. It embeds isometrically as a closed subspace of the given H_W. We retain the given W restricted to it.

Fix $R > 0$ and real even $\eta_R \in C_c^\infty(\mathbb{R}^d)$ with $0 \le \eta_R \le 1$, equal to one on the radius-R ball and supported in the closed radius-$2R$ ball. The physical mask is $m_R = \eta_R^2$. Every operator path below takes its mask argument equal to m_R: at this fixed radius the base profile $\zeta(y) = m_R(Ry)$ meets the earlier hypotheses. The root η_R factors state tests; it does not multiply an original noise class. All compactness conclusions here fix R.

8.3.1 Fractional products and the compact spatial map

The four-linear estimate (8.2.8) needs H^1 factors. The first component of a state in E lies only in $H^{1/2}$, so we first extend that estimate to fractional Sobolev factors.

Lemma 8.3.1 (Fractional covariance products)**.** *For $\alpha/4 < s < 1/2$, products of real H^s functions define elements of H_{sp}, with*

$$\|fg\|_{H_{\mathrm{sp}}} \le C_s^2 \sqrt{R_{\mathrm{sp}}} \|f\|_{H^s} \|g\|_{H^s}. \tag{8.3.1}$$

Their Hilbert pairings equal their physical integrals. In particular,

$$\int |f_1(x) f_2(x) f_3(x-y) f_4(x-y)| \, \mathrm{d}x \, \Gamma(\mathrm{d}y) \le C_s^4 R_{\mathrm{sp}} \prod_{j=1}^{4} \|f_j\|_{H^s}. \tag{8.3.2}$$

Proof. We first define covariance products for H^1 factors. We then decompose each fractional Sobolev factor into real Fourier bands and sum the absolute four-linear bounds, identifying the completed products with their physical pairings.

Step 1. We obtain the product map on H^1 factors. First approximate real H^1 factors by compact smooth ones. The absolute four-linear bound (8.2.8) and covariance PSD make their products Cauchy in H_{sp}, with norm at most $\sqrt{R_{\mathrm{sp}}} N(f) N(g)$. Expanding product differences proves independence of approximation; physical continuity identifies all pairings. PSD for products also follows from $fg = ((f+g)^2 - (f-g)^2)/4$.

Step 2. We sum the band bounds for fractional Sobolev factors. Use real radial Fourier bands $D_0 = 1_{\{|\xi|<1\}}$ and $D_j = 1_{\{2^{j-1} \le |\xi| < 2^j\}}$, $j \ge 1$. For $f \in H^s$ put $f_j = D_j f$. Each block is real and in H^1. Frequency support, Parseval and weighted Cauchy–Schwarz give

$$N(f_j) \le 2^{j\alpha/4} \|f_j\|_2, \qquad \sum_{j \ge 0} N(f_j) \le C_s \|f\|_{H^s}. \tag{8.3.3}$$

On band j, the gradient norm is at most $2^j \|f_j\|_2$. Substituting into N gives the first inequality. Write $2^{j\alpha/4} \|f_j\|_2$ as $2^{-j(s-\alpha/4)} (2^{js} \|f_j\|_2)$ and apply Cauchy–Schwarz to the two sequences. Indeed, $\sum_j 2^{-2j(s-\alpha/4)} < \infty$, while $\sum_j 2^{2js} \|f_j\|_2^2 \le 2^{2s} \|f\|_{H^s}^2$. The low block has factor one. No L^p multiplier result is used. Also $\sum_j \|f_j\|_2 < \infty$ since $s > 0$. Thus, $\sum_j |f_j|$ lies in L^2 by Minkowski and monotone convergence, and the series is absolutely convergent a.e. with sum f.

Step 3. We identify the physical and Hilbert-space product series. Apply the absolute H^1 four-linear estimate to each band quadruple. The sum of its absolute integrals is at most $R_{\mathrm{sp}} \prod_{\ell=1}^4 \sum_j N((f_\ell)_j) < \infty$. Tonelli and the null-set transfer at both spatial positions in Lemma 8.2.1 identify the physical product series, proving (8.3.2). The double series $\sum_{j,k} f_j g_k$ is also absolutely convergent in H_{sp} by the H^1 product bound. Its partial sums are products of H^1 functions. The absolute quadruple calculation identifies their limiting physical pairings and gives (8.3.1). Compact smooth functions are dense in H^s: approximate in Fourier space by real Schwartz functions, then cut each off compactly in H^1 and hence in H^s. This also proves uniqueness of the bilinear extension. This proves Lemma 8.3.1. □

With these products in H_{sp}, we can extend the spatial mean map from smooth tests to all of H_{sp}.

Proposition 8.3.2 (Compact spatial mean map)**.** *The smooth-test map*

$$T_{\mathrm{sp}}q = iB_F(m_R(\Gamma * q))$$

extends to a compact linear map $T_{\mathrm{sp}} : H_{\mathrm{sp}} \to \mathcal{K}(F)$, where $\mathcal{K}(F)$ has the operator norm. For $z = (z_1, z_2, c_1, c_2)$ and $w = (w_1, w_2, d_1, d_2)$ set $w' = \Lambda^{-1}w_2$. Its exact row identity is

$$\langle T_{\mathrm{sp}}qz, w\rangle_F = \langle q, k(z, w)\rangle_{H_{\mathrm{sp}}}, \qquad k(z, w) = (\eta_R z_1 + c_1\eta_R)(\eta_R w'). \tag{8.3.4}$$

Proof. We identify the spatial row and use compactness of localized fractional factors to bound it uniformly. We first extend the map with compact operator values, then approximate the map itself by finite-dimensional spatial projections.

Step 1. We identify the physical and covariance row. Fix s with $\alpha/4 < s < 1/2$; this interval is nonempty because the original threshold implies $\alpha < 2$. For smooth compact q, $\Gamma * q$ is locally smooth by differentiation under the compactly restricted Radon integral. The masked potential is smooth compact. The velocity pairing in E has weight Λ^{-1}; hence physical Fubini gives (8.3.4) on smooth states. Evenness of Γ changes $B_\Gamma(k, q)$ to $B_\Gamma(q, k)$. For general states the localized products are L^1, and $\Gamma * q$ is bounded on their compact support. L^2 state approximation passes the physical integral to the limit, while Lemma 8.3.1 passes the H_{sp} pairing. This proves the row.

Step 2. We obtain compact families of row tests. The velocity test satisfies $w_2 \in H^{-1/2}$ and $w' = \Lambda^{-1}w_2 \in H^{1/2}$, so it has the same localization regularity as the displacement test. Multiplication by η_R maps bounded $H^{1/2}$ sets to precompact H^s sets by Proposition 4.3.6, with gain $1/2 - s > 0$. This applies to z_1 and w'. The $c_1\eta_R$ family is finite dimensional and compact. The closures of both factor families for unit z, w are compact, so their products have compact closure $\mathcal{L}$ in H_{sp} by the fractional product bound. The row identity gives $\|T_{\mathrm{sp}}q\| \le \sup_{k\in\mathcal{L}} \|k\|\|q\|$. Null covariance classes therefore map to zero.

Step 3. We extend the map with compact operator values. For smooth q, multiplication by its potential is compact $H^{1/2} \to H^{-1/2}$ by the same whole-space cutoff result with gain one. Its extra c_1 column is finite rank, and the instantaneous c_2 column is zero. Thus, the smooth images lie in $\mathcal{K}(F)$, and so does the bounded extension by operator-norm closure.

Step 4. We prove compactness of the map itself. On each fixed compact support, local Radon finiteness bounds the covariance norm by a constant times the supremum norm. Countable uniformly dense families of smooth tests on exhausting compact supports therefore give a countable dense set in H_{sp}. Choose a complete smooth-test orthonormal basis of H_{sp} by countable compact-support approximation and Gram–Schmidt, omitting null classes. Let Q_n project onto its first n terms. The row identity yields

$$\|T_{\mathrm{sp}}(I - Q_n)\| \le \sup_{k\in\mathcal{L}} \|(I - Q_n)k\|_{H_{\mathrm{sp}}} \longrightarrow 0.$$

Strong projection convergence is uniform on compact $\mathcal{L}$ by a finite-net argument and $\|I - Q_n\| \le 1$. Each $T_{\mathrm{sp}}Q_n$ has finite-dimensional range; their operator-norm limit is a compact map. This is compactness of the map, in addition to compact values. This proves Proposition 8.3.2. □

8.3.2 The supported tensor and temporal mean

Proposition 8.3.2 treats the spatial variable alone. A control in H depends on time and space, so we first split H into a time factor and a spatial factor.

Lemma 8.3.3 (Supported original tensor space)**.** *Canonically $H = H_t \otimes H_{\mathrm{sp}}$ as real Hilbert spaces. It is separable and admits a complete orthonormal basis e_j with smooth test representatives supported inside $I \times \mathbb{R}^d$. Projection P_J onto its first J elements is also an orthogonal projection on H_W by the same finite formula.*

Proof. On separated smooth tests, absolute Fubini makes the original inner product exactly the tensor product after both null quotients. Finite sums are dense: approximate a smooth compact spacetime test uniformly by smooth time partitions times its spatial slices, on one common compact support inside $I \times \mathbb{R}^d$. A uniform error ϵ on spatial compact A has squared original covariance norm at most

$$\epsilon^2 |A| \Gamma(A - A) \int_I \int_I |s - t|^{-a} \, \mathrm{d}s \, \mathrm{d}t < \infty.$$

This also gives countable smooth-test density on exhausting compact sets, both here and in H_{sp}. Gram–Schmidt skipping zeros preserves smooth compact support. The isometric embedding into H_W has closed image by completeness; its finite orthonormal projection formula remains orthogonal there. It is not multiplication by a time indicator and gives no independence of disjoint time intervals. This proves Lemma 8.3.3. □

It remains to treat the time factor H_t, whose kernel is $|s - t|^{-a}$. Proposition 8.3.5 then combines the two maps.

Proposition 8.3.4 (The compact temporal mean, without trace class)**.** *Let K on $L^2(I)$ have kernel $|s - t|^{-a}$. It is compact, self-adjoint, strictly positive and injective. The map $\iota : f \mapsto K^{1/2} f$ extends isometrically from H_t onto $L^2(I)$, and the temporal mean*

$$C_t = K^{1/2} \iota : H_t \longrightarrow L^r(I) \tag{8.3.5}$$

is bounded and compact for every $2 < r < 2/a$. The displayed formula first has its $L^2(I)$ meaning; the same completed map is then shown to take values compactly in $L^r(I)$. The operator K is not trace class and $C_t : H_t \to L^2(I)$ is not Hilbert–Schmidt.

Proof. We prove compactness and strict positivity of the temporal operator before identifying the covariance completion. We then obtain the stronger L^r bound by duality, use interpolation for compactness, and test cell indicators to rule out trace class.

Step 1. We prove positivity, injectivity and compactness of the kernel operator. Schur bounds K by its finite row and column integrals. The Gamma representation of $|s - t|^{-a}$ and zero extension of $f \in L^2(I)$ give strict positivity directly: the kernel $e^{-\lambda |v|}$ has quadratic form

$$\int_{\mathbb{R}} \frac{2\lambda}{\lambda^2 + \xi^2} |\widehat{f}(\xi)|^2 \, \mathrm{d}\xi > 0 \quad (f \neq 0, \ \lambda > 0)$$

in the unitary Fourier convention. Absolute Fubini is justified by Schur applied to $|f(s)f(t)|$. Integrating with positive weight $\lambda^{a-1}/\Gamma_E(a)$ proves positivity and injectivity. Symmetry gives self-adjointness. The deterministic truncated kernel $K_\epsilon = K1_{\{|s-t|\geq\epsilon\}}$ is square integrable, so finite separated-kernel approximations make it compact. The Schur norm of $K - K_\epsilon$ is at most $2\epsilon^{1-a}/(1-a)$, proving compactness of K. These truncations are not used as Gaussian covariances. Its positive square root is compact by the compact spectral theorem.

Step 2. We identify the covariance completion with the square-root range. On tests $\|K^{1/2}f\|_2 = \|f\|_{H_t}$. Smooth-test L^2 density and $\ker K = 0$ imply that its range is dense, so the isometry extends onto $L^2(I)$. On tests $C_t f = Kf$, and (8.3.5) first gives compactness into L^2.

Step 3. We bound the temporal mean in L^r and obtain compactness there. The restriction $r < 2/a$ gives $ar/2 < 1$, ensuring integrability of the kernel power at zero. Extend $K_a(v) = |v|^{-a}1_{\{|v|\leq 1\}}$ to the line. It lies in $L^{r/2}$. Scalar Young convolution gives

$$\|g\|_{H_t}^2 \leq \|K_a\|_{r/2}\|g\|_{r'}^2, \qquad r' = r/(r-1).$$

To verify the needed Young inequality, take $u = r/2$, $v = r'$, so $u, v < r$ and $1/u + 1/v = 1 + 1/r$. Split the absolute convolution integrand into $(|f|^u|h|^v)^{1/r}$, $|f|^{1-u/r}$ and $|h|^{1-v/r}$. Hölder with exponents r, $(1/u - 1/r)^{-1}$ and $(1/v - 1/r)^{-1}$, followed by integration and Tonelli, gives $\|f * h\|_r \leq \|f\|_u\|h\|_v$. Covariance Cauchy–Schwarz and L^r duality now imply $\|Kf\|_r \leq C_{a,r}\|f\|_{H_t}$ on tests. Their Kf are bounded by the integrable-kernel row, making duality legitimate before completion. Density extends the estimate, with L^2 value equal to (8.3.5). Choose $r < r_2 < 2/a$. Compactness into L^2 and boundedness into L^{r_2} give compactness into L^r by $\|u\|_r \leq \|u\|_2^\tau\|u\|_{r_2}^{1-\tau}$ with $1/r = \tau/2 + (1-\tau)/r_2$.

Step 4. We test the trace by orthonormal cell indicators. Finally, the orthonormal cell indicators $N^{1/2}1_{(j/N,(j+1)/N)}$, $0 \leq j < N$, have K quadratic forms summing to $2N^a/((1-a)(2-a)) \to \infty$. On a cell of length $1/N$, the double kernel integral is $2N^{a-2}/((1-a)(2-a))$. The squared normalization of its indicator contributes N, and summing over the N cells gives the stated N^a divergence. For a positive trace-class operator every such finite orthonormal sum is bounded by its trace, so this divergence excludes trace class. Thus, positive K has infinite trace, and $K^{1/2}\iota$ is not Hilbert–Schmidt into L^2. No instantaneous L^2-valued Gaussian has been introduced. This proves Proposition 8.3.4. □

No-go 27 explains the upper endpoint of this compactness range: temporal concentration makes the mean map unbounded above $2/\alpha_0$ and noncompact at $2/\alpha_0$. The endpoint witness does not refute boundedness there.

Proposition 8.3.5 (The compact time-space mean)**.** *Fix one $2 < r < 2/a$ throughout this proposition. For finite tensors with orthonormal spatial labels define*

$$\mathcal{U}\left(\sum_j f_j \otimes q_j\right)(s) = \sum_j (Kf_j)(s)q_j.$$

It extends to a bounded map $H \to L^r(I; H_{\mathrm{sp}})$ with dimension-free bound. The map

$$T\Phi(s) = T_{\mathrm{sp}}(\mathcal{U}\Phi(s)) : H \longrightarrow L^r(I; \mathcal{K}(F)) \tag{8.3.6}$$

is compact. For smooth supported Φ, it is the multiplier $iB_F(m_R h_\Phi(s))$, where $h_\Phi = |\cdot|^{-a} * (\Gamma * \Phi)$. For the supported projections of Lemma 8.3.3,

$$\epsilon_J := \|T(I - P_J)\|_{H \to L^r(\mathcal{K}(F))} \longrightarrow 0. \tag{8.3.7}$$

Proof. We first prove a dimension-free temporal estimate on finite tensors and identify its physical mean. We then combine spatial finite-rank approximation with temporal compactness, and use compactness of the combined map to control supported projection tails.

Step 1. We bound and extend the time-only tensor map. For a finite-dimensional spatial field g, positivity of the time kernel and scalar Young give

$$\|g\|^2_{H_t \otimes H_{\mathrm{sp}}} \le \int_I \int_I |s-t|^{-a} \|g_s\| \|g_t\| \, \mathrm{d}s \, \mathrm{d}t \le C^2_{a,r} \|g\|^2_{L^{r'}(H_{\mathrm{sp}})}.$$

Hilbert Cauchy–Schwarz and finite-dimensional L^r duality give $\|\mathcal{U}\Phi\|_{L^r(H_{\mathrm{sp}})} \le C_{a,r}\|\Phi\|_H$. The duality can be checked by the pointwise direction $\|\mathcal{U}\Phi\|^{r-2}\mathcal{U}\Phi$ and smooth coefficient approximation in $L^{r'}$, controlled by the displayed estimate. No dimension factor occurs. Tensor density and completeness extend this to a strongly measurable Bochner field. This time-only map still contains spatial vectors in the covariance space. Spatial covariance is applied once, by T_{sp}.

Step 2. We identify the completed map on smooth controls. The multiplier estimate used here is $\|B_F(b)\| \le \|b\|_\infty + \|b\|_2$ from Lemma 6.2.3; on the fixed support of m_R, the L^2 error is at most the square root of its volume times the supremum error. The physical mean identity on separated tests follows from (8.3.4). For a smooth spacetime test use the separated compact-support approximations in the tensor proof. Their uniform errors give uniformly small masked mean errors, using the finite time row and locally finite spatial covariance on the relevant compact differences. The multiplier bound by $L^\infty + L^2$ then gives uniform operator convergence, identifying the L^r mean in (8.3.6). General H controls denote completed operator fields, without a pointwise-potential assertion.

Step 3. We combine temporal and spatial compactness. Let Q_n be the spatial projections in the compact-map proof. The maps $T_n\Phi = T_{\mathrm{sp}}Q_n\mathcal{U}\Phi$ approximate T in operator norm by the dimension-free bound and $\|T_{\mathrm{sp}}(I - Q_n)\| \to 0$. For fixed n, each spatial coordinate extraction $H \to H_t$ has norm at most one and its image under C_t is precompact in L^r. Finite combination with the compact operators $T_{\mathrm{sp}}q_j$ makes T_n compact. Hence, T is compact. Scalar time compactness alone tensored with an infinite identity would not prove this.

Step 4. We obtain the supported projection-tail bound. To prove (8.3.7), if it failed choose unit v_J on a subsequence with $\|T(I-P_J)v_J\|$ bounded below. The vectors $(I-P_J)v_J$ tend weakly to zero, since their pairings with fixed h are bounded by $\|(I-P_J)h\|$. Compactness gives a norm-convergent image subsequence with weak limit zero, a contradiction. This proves Proposition 8.3.5. □

The radius remains fixed in this approximation. No-go 25 shows that translated white-noise controls prevent these fixed smooth projections from giving tails uniform over growing radii.

8.3.3 The noise residual and its Cameron operator

Choose integer $B \geq 1$ and $0 < \delta < \min(1, 1/B)$. Put $N = \lfloor 1/(\delta B) \rfloor$, $s_m = m\delta B$, $\ell_m = B$ for $m < N$ and $\ell_N = \delta^{-1} - NB \in [0, B)$. The intervals $I_m = [s_m, s_m + \delta\ell_m]$ partition $[0, 1]$ up to endpoints. With $Q_J = I - P_J$ on H_W and the explicit pullback (7.2.2), define

$$Y_{m,J}(f) = W(Q_J T_{\delta,m} f), \qquad g_\delta = \delta^{(1-a)/2}.$$

Fix parameters

$$\frac{1}{2} < \theta < \min\left(1 - \frac{a}{2}, \frac{3 - a - \alpha}{2}\right), \qquad \frac{1}{1-\theta} < r < \frac{2}{a}, \qquad \frac{1}{\theta} \leq p < 2 < r. \tag{8.3.8}$$

These intervals are nonempty.

Lemma 8.3.6 (Supported residual paths)**.** *Gaussian transfer with mask m_R and its F extension constructs the centered Gaussian paths*

$$X_{m,J}(u) = g_\delta A_{m_R}(Y_{m,J})(\min(u, \ell_m)), \qquad 0 \leq u \leq B.$$

Their finite tuple lies in the separable space $\mathscr{B}_0^{N+1}$, where $\mathscr{B}_0 = h_0^\theta([0, B]; \mathcal{K}(F))$. Every continuous linear statistic $\ell(X)$ is $W(k_\ell)$ for some $k_\ell \in H_I$. An empty last interval gives zero.

Proof. We construct the stopped residual paths by Gaussian transfer. We then identify the supported slow-time tests in every observed row, so that each continuous path statistic lies in the original first chaos over H_I.

Step 1. We construct the stopped paths in the separable little Hölder space. For $Y = Y_{m,J}$, the notation $A_{m_R}(Y)$ means $iM_Y L_\psi$ from (6.2.5), where M_Y is the transferred E path. The two localizations are (6.2.4), passed from the common deterministic coefficients to this path by bounded multiplication. Isometry of the pullback and orthogonality of Q_J give $\operatorname{Var} Y_{m,J}(f) \leq \|f\|_{H_W}^2$. Proposition 5.2.2 therefore applies. Its finite sums retain both deterministic localizations, and their limits retain the true F extension and constant columns. Choose $\theta < \beta < \beta_2$ below the upper threshold in (8.3.8); read the operator-path construction at exponent β with auxiliary β_2. Constant stopping preserves compact values and C^β bounds, hence gives paths in the little C^θ closure by polygonal approximation. Its separability is Lemma 7.2.1.

Step 2. We identify the supported first-chaos tests for the path statistics. The projection P_J has range in H_I, so subtracting it from a vector already in H_I keeps that vector in H_I. Consequently, once an observed slow-time row is shown to belong to H_I, its residual row has the same support-space membership. This is a Hilbert-subspace statement, not multiplication of the original noise by a time indicator. As in Lemma 7.2.1, every observed

row's slow pullback belongs to H_I: its time support is in $[0,1]$, and approximating its indicator inside I converges in original covariance norm by dominated convergence against the integrable time kernel and locally finite Γ on the common compact support. This includes endpoints. Schwartz E states and both true constant columns supply the identities, then boundedness extends them to F. Let P_H be the orthogonal projection onto closed H_I. Transfer for the noise $f \mapsto W(P_H Q_J T_{\delta,m} f)$ leaves each observed row unchanged, since its residual slow test already lies in H_I. Countable states and rational times identify the same operator paths. This projected-transfer series has coefficient tests in H_I. Applying ℓ gives an L^2 limit in the closed isonormal image $W(H_I)$, proving the assertion. Original global-basis tests were not assumed individually supported. No time-support independence or Hilbert-valued noise is used. This proves Lemma 8.3.6. □

Proposition 8.3.7 (Cameron covariance and averaged bound)**.** *The covariance map* $L_{\delta,J}\Phi = \mathbb{E}[XW(\Phi)]$ *is*

$$(L_{\delta,J}\Phi)_m(u) = \sqrt{\delta}\int_0^{\min(u,\ell_m)} S_F(-v)T(Q_J\Phi)(s_m+\delta v)S_F(v)\,\mathrm{d}v, \qquad \Phi \in H. \tag{8.3.9}$$

This is a compact-operator Bochner integral. Define the exact norm and constants

$$\|x\|_{\delta,p} = \left(\delta\sum_{m=0}^{N}\|x_m\|_{C^\theta}^p\right)^{1/p}, \quad G_B = \sup_{|v|\le B}\|S_F(v)\|, \quad C_B = G_B^2[B^{1-1/r}+B^{1-1/r-\theta}]. \tag{8.3.10}$$

Then the Gaussian Cameron embedding satisfies

$$\|L_{\delta,J}\Phi\|_{\delta,p} \le \sqrt{\delta}\,C_B(2/B)^{1/p-1/r}\epsilon_J\|\Phi\|_H. \tag{8.3.11}$$

Convergence $\epsilon_J \to 0$ *fixes* R *and is independent of* δ*.*

Proof. We compute the covariance direction first on smooth supported controls and justify its compact-operator integral. We then extend to all controls, identify the Cameron preimage norm, and sum the local primitive estimates with the exact time weights.

Step 1. We compute the covariance direction and its factor $\sqrt{\delta}$. Insert the wave-row tests of (5.2.5) in the scalar covariance below; Proposition 8.3.5 identifies the resulting masked mean with $T(Q_J\Phi)$, and the row calculation of Lemma 7.2.1 gives its conjugated primitive on F. For smooth supported Φ, $Q_J\Phi$ is another such test. The explicit pullback covariance (7.2.6) gives

$$\mathbb{E}[Y_{m,J}(f)W(\Phi)] = \delta^{a/2}\int f(v,x)h_{Q_J\Phi}(s_m+\delta v,x)\,\mathrm{d}x\,\mathrm{d}v.$$

Absolute Fubini also holds for signed compact tests. Multiplying by g_δ gives $\sqrt{\delta}$. Explicit rows and (8.3.4) give (8.3.9). The constant-velocity input acquires displacement v under $S_F(v)$; the constant displacement remains one. Both columns are included.

Step 2. We justify the compact-operator Bochner integral. Both S_F and its adjoint are strongly continuous on Hilbert F. In Bessel-unitary E coordinates the Fourier matrix is

$$\begin{pmatrix} \cos(v|\xi|) & \langle\xi\rangle\sin(v|\xi|)/|\xi| \\ -|\xi|\sin(v|\xi|)/\langle\xi\rangle & \cos(v|\xi|)\end{pmatrix}.$$

Its continuous zero quotient and common bound $C(1+B)$ apply also to its adjoint; dominated convergence proves the assertion. The constant block is finite dimensional. For compact A, conjugation $S_F(-v)AS_F(v)$ is norm continuous: strong convergence is uniform on compact images, and the right factor follows by adjoints. Joint norm continuity in (v, A) and uniform bounds give Bochner measurability for the conjugated strongly measurable compact-operator field. No norm continuity of the free group itself is assumed.

Step 3. We bound each stopped primitive and extend the covariance identity. Write $M = TQ_J\Phi$. Hölder and the primitive increment estimate give

$$\|(L_{\delta,J}\Phi)_m\|_{C^\theta} \le \sqrt{\delta}\, C_B \delta^{-1/r} \|M\|_{L^r(I_m)}. \tag{8.3.12}$$

Hölder in the fast variable bounds an increment by G_B^2 times its length to the power $1-1/r$, multiplied by the pulled-back L^r norm. The latter is $\delta^{-1/r}\|M\|_{L^r(I_m)}$. For the supremum use length at most B; for the θ seminorm divide by the increment length to the power θ. The two remaining powers of B are exactly those in C_B. Its primitive exponent is $1-1/r > \theta$. Simple compact-operator integrand approximation in L^r puts the primitive in $\mathscr{B}_0$; constant stopping does not increase the Hölder norm. Affine pullback preserves null sets. For fixed δ, J the covariance map is bounded by Bochner Cauchy–Schwarz and finite tuple L^2 moments. The integral is bounded by the displayed estimate, so equality on smooth controls extends by density to all H. Dense states and rational times make it a full operator-path identity.

Step 4. We identify the Cameron embedding norm. Let H_{seen} be the closed span of the k_ℓ from Lemma 8.3.6. Then $\ell(L_{\delta,J}\Phi) = \langle k_\ell, \Phi\rangle_H$ and $\ker L_{\delta,J} = H_{\mathrm{seen}}^{\perp}$. The first Wiener chaos definition of the Cameron space is therefore $L_{\delta,J}(H_{\mathrm{seen}})$ with the minimum H preimage norm. Extra directions are removed by orthogonal projection, without an inverse covariance. A bound in the original H norm is thus the embedding bound.

Step 5. We combine the block estimates using the true partition. Put $t_m = \|M\|_{L^r(I_m)} \ge 0$ and $n = N+1 \ge 2$. Finite power mean at exponent $r/p > 1$, applied to t_m^p, gives

$$\left(\sum_m t_m^p\right)^{1/p} \le n^{1/p-1/r} \left(\sum_m t_m^r\right)^{1/r}.$$

The true partition gives $\sum_m t_m^r = \|M\|_{L^r(I)}^r$, including an empty last interval, and $n \le 2/(\delta B)$. Hence, the exact δ-weighted norm gives

$$\|L_{\delta,J}\Phi\|_{\delta,p} \le \sqrt{\delta}\, C_B (\delta n)^{1/p-1/r} \|M\|_{L^r} \le \sqrt{\delta}\, C_B (2/B)^{1/p-1/r} \epsilon_J \|\Phi\|_H.$$

The B factor remains explicit; covariance and mask occur once. This proves Proposition 8.3.7. □

These conclusions fix the radius and make no uniform-radius projection tail assertion. No concentration estimate or original moment upper bound follows from this section alone.

8.4 Young perturbations retaining the deterministic endpoint

Let $\mathcal{X}$ be any nonzero real Banach space, with its induced operator norm on $\mathcal{B}(\mathcal{X})$. Fix $B \geq 1$, $1/2 < \theta < 1$ and $\nu = 1/\theta < 2$. All operator paths start at zero and have norm $\|D\|_\theta = \sup_t \|D(t)\| + [D]_\theta$ on $[0, B]$. Let $U_D = I + \int \mathrm{d}D\, U_D$ be the left Young evolution. The construction in Proposition 6.2.4 applies: its proof needs completeness and operator multiplication of norm one, with no Hilbert-space assumption. The primary estimate is [30, Section 1.5, p. 13; Section 4.1, (4.1)–(4.3), pp. 61–62].

Lemma 8.4.1 (Refined growth and uniform inverse control)**.** *With dimension-free constants,*

$$\sup_{t \leq B} \|U_D(t)\| \leq \exp\{c_{\theta,B}(d + d^\nu)\}, \qquad d = \|D\|_\theta. \tag{8.4.1}$$

For $\|H\|_\theta \leq K$, $K \geq 1$,

$$\|U_H\|_{C^\theta} + \|U_H^{-1}\|_{C^\theta} \leq L_{\theta,B,K} < \infty. \tag{8.4.2}$$

Proof. We separate small drivers, where one contraction gives a linear logarithmic bound, from larger drivers, where a partition gives the power bound. We then use a fixed partition on a bounded driver ball to control both the evolution and its inverse in the Hölder norm.

Step 1. We prove the refined growth bound in the two driver-size regimes. The derivative of $x \mapsto -\log(1-x)$ is at most two on $[0, 1/4]$, giving the linear logarithmic bound in the small-driver case below. Let $c_\theta = 2\max(1, C_\theta)$ for the primary Young constant. The complete scaled norm $N_\ell(V) = \sup \|V\| + \ell^\theta [V]_\theta$ satisfies $N_\ell(\int_a^{\cdot} \mathrm{d}D\, V) \leq c_\theta [D]_\theta \ell^\theta N_\ell(V)$, as in (6.2.10). If $c_\theta d B^\theta \leq 1/4$, whole-interval contraction gives $\sup \|U_D\| \leq (1 - c_\theta d B^\theta)^{-1}$ and hence $\log \sup \|U_D\| \leq 2 c_\theta B^\theta d$. Otherwise take $n_D = \lceil B(4c_\theta d)^\nu \rceil$ equal pieces. Their contraction ratios are at most $1/4$ and local norms at most $4/3$. The expression inside the ceiling exceeds one, so $n_D \leq 2B(4c_\theta d)^\nu$. Composition gives the d^ν bound. At $d = 0$, $U_D = I$, proving (8.4.1) without a prefactor.

Step 2. We bound the global evolution and inverse on a fixed driver ball. On the ball $\|H\|_\theta \leq K$ choose one uniform equal partition with ratio at most $1/4$. Each local evolution Q has $N_\ell(Q) \leq 4/3$ and $\sup \|Q - I\| \leq 1/3$. Its Neumann inverse is bounded by $3/2$. Products give uniform global sup bounds. The same scaled estimate bounds local Hölder seminorms. Pairs crossing a boundary at distance below ℓ split into at most two pieces; use $h_1^\theta + h_2^\theta \leq 2^{1-\theta}(h_1 + h_2)^\theta$. For larger distances use $2 \sup \|U_H\| / \ell^\theta$. This gives its global C^θ bound. Finally,

$$U_H^{-1}(t) - U_H^{-1}(s) = -U_H^{-1}(t)(U_H(t) - U_H(s))U_H^{-1}(s)$$

bounds the inverse seminorm. This proves Lemma 8.4.1. □

The linear term in (8.4.1) cannot simply be dropped: No-go 26 gives a scalar commuting counterexample. Its second observation also distinguishes an averaged block budget from a uniform bound on every block.

Proposition 8.4.2 (Multiplicative upper perturbation)**.** *If $K \geq 1$, $\|H\|_\theta \leq K$, $x = \|X\|_\theta$ and $A \in \mathcal{B}(\mathcal{X})$, then*

$$\|AU_{H+X}(t)\| \leq \|AU_H(t)\| \exp\{C_{\theta,B,K}(x + x^\nu)\}, \qquad 0 \leq t \leq B. \tag{8.4.3}$$

This includes noninvertible A and $A = 0$ with no extra factor when $x = 0$.

Proof. We conjugate the perturbation by the deterministic evolution to form a new Young driver. We verify the resulting product identity directly from increments, preserving the left multiplication order, and then apply the refined growth bound only to the perturbation driver.

Step 1. We form the conjugated perturbation driver. Put $U = U_H$, $R = U^{-1}$ and $G(s)Z = R(s)ZU(s)$. Lemma 8.4.1 makes G a C^θ path of bounded linear maps on $\mathcal{B}(\mathcal{X})$, uniformly bounded on the fixed ball. Thus, the Banach Young integral

$$Z(t) = \int_0^t R(s)\,\mathrm{d}X(s)U(s)$$

exists, with $\|Z\|_\theta \leq L'_{\theta,B,K}x$ and $Z_{s,t} = R(s)X_{s,t}U(s) + O(|t-s|^{2\theta})$. Put $V = U_Z$. Its and U's Young remainders are $V_{s,t} = Z_{s,t}V(s) + O(|t-s|^{2\theta})$ and $U_{s,t} = H_{s,t}U(s) + O(|t-s|^{2\theta})$. The exact increment of $P = UV$ includes a cross term of order 2θ. Substitution in the stated left order gives

$$P_{s,t} = H_{s,t}P(s) + U(s)R(s)X_{s,t}U(s)V(s) + O(|t-s|^{2\theta}) = (H+X)_{s,t}P(s) + O(|t-s|^{2\theta}).$$

Step 2. We identify the product as the full Young evolution. Each interval length to the power 2θ is at most that length times the mesh to the power $2\theta - 1$, so summing bounds the remainder by the total length times that mesh power. On any partition the remainder sum is bounded by a constant times B mesh$^{2\theta-1} \to 0$. Left sums converge to the Young integral, so uniqueness yields $U_{H+X} = U_H U_Z$. This proves the product identity without assuming smooth density in the full Hölder norm.

Step 3. We retain the deterministic endpoint factor in the norm bound. At $x = 0$, the driver Z is zero and $U_Z = I$. Apply (8.4.1) to Z, then left multiply by A and use submultiplicativity. No inverse or lower bound for A is required. This proves Proposition 8.4.2. □

What we now have. The compact map from a Gaussian control to its mean, at a fixed spatial radius (Propositions 8.3.5 and 8.3.7). The next chapter lets the radius grow.

Chapter 9

Bounds as the spatial radius grows

Finite propagation makes spatial localization useful, but the region we need grows with the observation time (Figure 10.2, in the next chapter). A bound with an uncontrolled constant in the radius is useless for long time. This chapter sorts the estimates into two kinds: those uniform in the radius, and stochastic ones that must display it.

Section 9.1 gives uniform mean and Cameron bounds on the displacement–velocity Sobolev phase; it claims nothing of the kind for the additional constant coordinates. Section 9.2 tracks the radius in the Gaussian path moments and estimates averages over time blocks. Section 9.3 builds the physical wave for completed static mean potentials of either sign, so the upper argument keeps all its Gaussian controls.

We use the covariance and phase constructions of Chapters 4–6 and the mean maps of Chapter 8. On a first reading, keep Propositions 9.1.4 and 9.3.4, and let the proofs wait. The restriction to nonnegative controls enters later, through a separate variational comparison. Episode ▶ 7 of the video series covers this chapter and the next.

Estimate	Result	Dependence on the radius R
Completed mean: norm and tail	Proposition 9.1.4	none, uniform for $R \geq 1$
Cameron embedding of the block paths	Proposition 9.1.5	none, uniform for $R \geq 1$
Compact envelopes of the cutoff	Proposition 9.2.2	displayed: $\rho^{d/q}$
Moments of the operator path	Proposition 9.2.3	displayed: $R^{d/Q}$
Expected weighted norm of block paths	Proposition 9.2.5	$g_\delta R^{d/Q} \to 0$ at $R_\delta = \delta^{-1} + 2$ if $Q > 2d/(1-\alpha_0)$

All rows concern the Sobolev phase $E = H^{1/2} \times H^{-1/2}$, not the additional constant columns on F. In the last two rows, fix the exponents and even Q as in (9.2.1)–(9.2.2). The last limit fixes B, p, Q before $\delta \downarrow 0$.

9.1 Mean and Cameron bounds uniform in the spatial radius

Retain the original nonzero covariance, amplitude and real spaces of Section 8.3. Fix $\alpha/4 < s < 1/2$ and put $\beta = 1/2 - s > 0$. Write $A_s = C_s^2 \sqrt{R_{\mathrm{sp}}}$ for the constant in (8.3.1). Choose a real even smooth compact η, equal to one on the unit ball, with $0 \leq \eta \leq 1$ and support in the closed radius-two ball. For $R \geq 1$ set $\eta_R(x) = \eta(x/R)$ and $m_R = \eta_R^2$. In this section the mean acts on $E = H^{1/2} \times H^{-1/2}$. The constant data columns belong to F, outside E. All uniform-radius claims below concern E. The spatial map $T_R : H_{\mathrm{sp}} \to \mathcal{K}(E)$ is the E restriction of Proposition 8.3.2. Its explicit row is

$$\langle T_R q z, w \rangle_E = \langle q, k_R(z,w) \rangle_{H_{\mathrm{sp}}}, \qquad k_R(z,w) = (\eta_R z_1)(\eta_R \Lambda^{-1} w_2). \tag{9.1.1}$$

Thus, the physical mask occurs once, after covariance convolution.

9.1.1 Uniform multiplier and spatial tails

We first bound the row k_R in (9.1.1) uniformly in $R \geq 1$. Both factors of this row carry the cutoff η_R, so we start with its multiplier norm on H^σ.

Lemma 9.1.1 (Uniform cutoff and physical mean)**.** *For every real σ, multiplication by η_R on H^σ has norm at most*

$$M_\sigma = 2^{|\sigma|/2}(2\pi)^{-d/2} \int_{\mathbb{R}^d} |\widehat{\eta}(p)| \langle p \rangle^{|\sigma|} \, \mathrm{d}p,$$

independently of $R \geq 1$. With $M = M_{1/2}$ and $M_0 = A_s M^2$,

$$\|k_R(z,w)\|_{H_{\mathrm{sp}}} \leq M_0 \|z\|_E \|w\|_E, \qquad \|T_R\|_{H_{\mathrm{sp}} \to \mathcal{L}(E)} \leq M_0. \tag{9.1.2}$$

Proof. Peetre's inequality bounds the weighted Fourier kernel for multiplication by η_R by convolution with

$$2^{|\sigma|/2}(2\pi)^{-d/2} |\widehat{\eta_R}(q)| \langle q \rangle^{|\sigma|}.$$

Here $\widehat{\eta_R}(q) = R^d \widehat{\eta}(Rq)$. Substitution $p = Rq$ and $\langle p/R \rangle \leq \langle p \rangle$ bound its L^1 norm by M_σ. The $L^1 * L^2$ inequality proves the assertion on Schwartz functions and density extends it to H^σ. The map $w_2 \mapsto \Lambda^{-1} w_2$ is an isometry from $H^{-1/2}$ to $H^{1/2}$, and $H^{1/2} \hookrightarrow H^s$ has norm one. Apply the cutoff bound at $\sigma = 1/2$ and Lemma 8.3.1 to the two factors in (9.1.1). Hilbert Cauchy–Schwarz then gives the operator bound. This is the existing completed physical map: the row agrees on smooth controls and hence on their completion. Its compact values at each fixed R are retained. This proves Lemma 9.1.1. □

Lemma 9.1.1 bounds T_R on all of H_{sp}. The approximation in Proposition 9.1.4 also needs T_R to be small on high frequencies, uniformly in $R \geq 1$. We obtain this from a bound on $T_R(I - C_\varepsilon)$ for the heat contraction C_ε.

Lemma 9.1.2 (Uniform heat and frequency tails)**.** *Let C_ε be the covariance-Hilbert heat contraction with Fourier multiplier $e^{-\varepsilon|\xi|^2/2}$. There is a real orthogonal projection P_K on H_{sp} corresponding to the closed frequency ball $\{|\xi| \leq K\}$. It commutes with heat. For $K \geq 1$, $\varepsilon > 0$ and $R \geq 1$,*

$$\|T_R(I - C_\varepsilon)\| \leq M_h \varepsilon^{\beta/2}, \qquad M_h = 4A_s M^2 \mathbb{E}|G_d|^\beta, \tag{9.1.3}$$

$$\|T_R(I - P_K)\| \leq M_f K^{-\beta}, \qquad M_f = \frac{M_h}{1 - e^{-1/2}}, \tag{9.1.4}$$

where G_d is a standard real d-dimensional normal vector. Operator norms are from H_{sp} to $\mathcal{L}(E)$. The projection P_K is allowed to have infinite rank.

Proof. We estimate translations of each covariance row and average them against heat. We then construct the frequency projection on the actual Fourier image and use the heat error to bound its high-frequency tail.

Step 1. We bound translations of the localized row. Translations $\tau_h f(x) = f(x-h)$ extend to strongly continuous isometries of the H_{sp}. Indeed, in its covariance Fourier isometry they multiply by $e^{-i\xi\cdot h}$; dominated convergence gives continuity on tests, then density and isometry give it on the completion. The real subspace is preserved. The inequalities $|e^{-it}-1| \le 2\min(1,|t|^\beta)$ and $|\xi|^\beta\langle\xi\rangle^s \le \langle\xi\rangle^{1/2}$ show that

$$\|\tau_h f - f\|_{H^s} \le 2\min(1,|h|^\beta)\|f\|_{H^{1/2}}.$$

Use this for $f = \eta_R z_1$ and $g = \eta_R \Lambda^{-1} w_2$. The product identity

$$\tau_h(fg) - fg = (\tau_h f - f)\tau_h g + f(\tau_h g - g)$$

holds in H_{sp}, first for smooth factors and then by the continuous fractional product extension. Lemma 9.1.1 gives

$$\|\tau_h k_R(z,w) - k_R(z,w)\|_{H_{\mathrm{sp}}} \le 4A_s M^2 \min(1,|h|^\beta)\|z\|_E\|w\|_E. \tag{9.1.5}$$

Step 2. We average the translation bound to obtain the heat error. The Bochner integral $\int p_\varepsilon(h)\tau_h k \,\mathrm{d}h$ exists, since the translation orbit is strongly continuous and bounded in the separable covariance Hilbert space. Its Fourier image is $e^{-\varepsilon|\xi|^2/2}\widehat{k}$: ordinary Gaussian integration proves this on tests and contraction extends it to all k. It is therefore the C_ε of the source construction. Heat has variance ε here; there is no additional Fourier normalization factor. Integrating (9.1.5) with $h = \sqrt{\varepsilon}G_d$ bounds $\|(I-C_\varepsilon)k_R(z,w)\|$ by $M_h\varepsilon^{\beta/2}\|z\|_E\|w\|_E$. Here C_ε is selfadjoint on H_{sp}, since its Fourier multiplier is real; the row identity therefore gives

$$\langle T_R(I-C_\varepsilon)qz, w\rangle_E = \langle q, (I-C_\varepsilon)k_R(z,w)\rangle_{H_{\mathrm{sp}}}.$$

Selfadjointness in (9.1.1) proves (9.1.3).

The two terms in the product difference each use one translation error and one bounded factor. The fractional product bound therefore contributes $2A_sM^2$ twice. Averaging $\min(1,|h|^\beta) \le |h|^\beta$ with $h = \sqrt{\varepsilon}G_d$ gives $\varepsilon^{\beta/2}\mathbb{E}|G_d|^\beta$.

Step 3. We construct the projection without assuming Fourier surjectivity. To construct P_K, let V be the closed image of the covariance Fourier isometry into $L^2(\mu)$, including its fixed $(2\pi)^{d/2}$ factor. No surjectivity is assumed. Its formula extends to Schwartz functions: compact cutoff approximation converges in Schwartz seminorms, and temperedness of μ controls the Fourier error in $L^2(\mu)$. Choose real even radial smooth χ_n, equal to one on the closed ball of radius K, zero outside radius $K+1/n$, and between zero and one. For real Schwartz f, the function $\chi_n\widehat{f}$ is the transform of another real Schwartz function and so lies in V. Dominated convergence against $|\widehat{f}|^2\mu$ gives $1_{\{|\xi|\le K\}}\widehat{f} \in V$. The pointwise limit includes the boundary sphere, even if μ charges it. Test density and contraction extend this assertion to all of V. Indicator multiplication is selfadjoint and idempotent on V; pulling it back defines the asserted real orthogonal P_K. All Fourier multipliers here commute.

Step 4. We compare the frequency tail with a heat residual. On $|\xi| > K$ one has $1 - e^{-|\xi|^2/(2K^2)} \geq 1 - e^{-1/2}$, whence

$$\|(I - P_K)k\|_{H_{\mathrm{sp}}} \leq (1 - e^{-1/2})^{-1} \|(I - C_{K^{-2}})k\|_{H_{\mathrm{sp}}}.$$

Apply the row heat bound and selfadjointness of P_K in (9.1.1) to obtain (9.1.4). No density of μ, periodic state space or finite rank was used. This proves Lemma 9.1.2. □

9.1.2 Tensor products and mean approximation

We first record a tensor extension bound for maps into $L^r(I)$. The proof of Proposition 9.1.4 uses it to pass from a scalar time map to the Hilbert-valued time map without a dimension factor.

Lemma 9.1.3 (Dimension-free Hilbert tensor extension)**.** *If H_0, G are real Hilbert spaces, $2 \leq r < \infty$ and $A : H_0 \to L^r(I)$ is bounded, then*

$$\|A \otimes I_G\|_{H_0 \otimes G \to L^r(I;G)} \leq \|A\|.$$

The tensor extension need not be compact when A is compact.

Proof. We use finite Gaussian sums to estimate the Hilbert-valued tensor norm with the scalar operator constant. We then extend by density and check why the same argument does not imply compactness.

Step 1. We compare the Gaussian norm moment with its total variance. For a finite tensor write $v = \sum_{j=1}^n f_j \otimes e_j$ with (e_j) orthonormal. Its squared norm is $\sum_j \|f_j\|^2$. Let γ_j be independent standard real normals and $m_r = \mathbb{E}|\gamma_1|^r$. Finite covariance diagonalization gives

$$\mathbb{E}\left\|\sum_j \gamma_j f_j\right\|_{H_0}^r \leq m_r \left(\sum_j \|f_j\|_{H_0}^2\right)^{r/2}.$$

In fact, if λ_l are the covariance eigenvalues and $L = \sum_l \lambda_l$, the squared norm has law $\sum_l \lambda_l \zeta_l^2$ for independent standard ζ_l. For $L > 0$, convexity at exponent $r/2 \geq 1$ bounds $(\sum_l (\lambda_l/L)\zeta_l^2)^{r/2}$ by $\sum_l (\lambda_l/L)|\zeta_l|^r$. Taking expectations proves the inequality; $L = 0$ is immediate. Also $L = \sum_j \|f_j\|^2$.

Step 2. We apply the scalar operator estimate and cancel the Gaussian moment. Choose measurable representatives of the finitely many Af_j. Scalar Gaussian moments and Tonelli give

$$m_r \int_I \left(\sum_j |Af_j(t)|^2\right)^{r/2} \mathrm{d}t = \mathbb{E}\left\|A\sum_j \gamma_j f_j\right\|_{L^r}^r \leq \|A\|^r m_r \left(\sum_j \|f_j\|^2\right)^{r/2}.$$

For each fixed t, the scalar sum of the $Af_j(t)$ with independent Gaussian coefficients has variance $\sum_j |Af_j(t)|^2$. Its rth absolute moment is that variance to the power $r/2$

times m_r. This explains the same factor m_r on both sides, so no dimension-dependent factor remains after cancellation. Cancel the finite positive m_r and take the rth root. Finite tensor density and Bochner completeness give the extension. The zero space is trivial. If $Af \neq 0$ and G has an infinite orthonormal sequence (e_j), the images of the bounded sequence $f \otimes e_j$ have pairwise distance $\sqrt{2}\|Af\|_{L^r}$. They have no convergent subsequence, even when the scalar map A is compact. Only finite auxiliary Gaussians were used in the estimate. This proves Lemma 9.1.3. □

Recall the supported identity $H_I = H_t \otimes H_{\mathrm{sp}}$, the compact scalar covariance map $C_t : H_t \to L^r(I)$, $2 < r < 2/a$, and its completed tensor $U = C_t \otimes I_{H_{\mathrm{sp}}}$ from Section 8.3. On finite smooth tensors U agrees with the earlier $\mathcal{U}$; density gives equality of their completed maps. For block applications fix the same r as in (8.3.8). All c_t, ε_J and mean norms below use that one choice. Choose a smooth-test orthonormal basis of H_t and let π_J be its first-J orthogonal projection, with $\pi_0 = 0$. Put

$$c_t = \|C_t\|, \qquad \varepsilon_J = \|C_t(I - \pi_J)\|_{H_t \to L^r(I)}, \qquad \mathcal{T}_R = T_R U.$$

Proposition 9.1.4 (Uniform approximation of the completed mean)**.** *On H_I the operators*

$$P_{\mathrm{ret}} = \pi_J \otimes P_K, \qquad Q_{J,K} = I - P_{\mathrm{ret}}$$

are real orthogonal projections, and $\varepsilon_J \to 0$. The mean is a strongly measurable $L^r(I; \mathcal{K}(E))$ field and satisfies, uniformly for $R \geq 1$,

$$\|\mathcal{T}_R\| \leq M_0 c_t, \qquad \|\mathcal{T}_R Q_{J,K}\| \leq M_0 \varepsilon_J + M_f c_t K^{-\beta}. \tag{9.1.6}$$

These norms have domain H_I and target $L^r(I; \mathcal{L}(E))$.

Proof. We transfer the compact scalar temporal tail to Hilbert-valued functions. We then decompose the residual projection into a temporal tail and a spatial-frequency tail, estimating these terms separately.

Step 1. We control the temporal projection tail. The tensor projections are selfadjoint, idempotent and contractive on finite tensors and hence on their Hilbert completion. For the scalar tail, failure of convergence would supply unit v_J with $\|C_t(I - \pi_J)v_J\|$ bounded below on a subsequence. But $(I - \pi_J)v_J$ tends weakly to zero, since its pairing with h is bounded by $\|(I - \pi_J)h\|$. Compactness supplies a norm-convergent image subsequence; bounded linear scalar observables show its limit is zero, a contradiction. Lemma 9.1.3 transfers this scalar tail norm to the Hilbert-valued time map without a dimension factor.

Step 2. We decompose and bound the completed mean residual. For $\Phi \in H_I$, Lemma 9.1.3 applied to $A = C_t$ gives $\|U\Phi\|_{L^r(I;H_{\mathrm{sp}})} \leq c_t \|\Phi\|_{H_I}$. Applying (9.1.2) pointwise in time then bounds $\|T_R U\Phi\|_{L^r(I;\mathcal{L}(E))}$ by $M_0 c_t \|\Phi\|_{H_I}$. For fixed R, T_R is bounded into the separable compact-operator space on E. Composition with the Bochner field $U\Phi$ gives the stated mean and its first bound. The exact decomposition is

$$Q_{J,K} = (I - \pi_J) \otimes I + \pi_J \otimes (I - P_K).$$

The first term is bounded by $M_0\varepsilon_J$. For the second term use the intertwining identity

$$U(\pi_J \otimes (I - P_K)) = (I_{L^r} \otimes (I - P_K))(C_t\pi_J \otimes I).$$

It holds first on finite tensors, then by continuity. Apply (9.1.4) pointwise, followed by Lemma 9.1.3 for $C_t\pi_J$, whose norm is at most c_t. This proves (9.1.6). Infinite spatial rank is allowed throughout; neither tensor compactness nor uniform-radius compactness has been asserted. This proves Proposition 9.1.4. □

9.1.3 The block Cameron embedding for the given noise

Use $B, \delta, N, s_m, \ell_m, I_m$ and θ, r, p exactly as in (8.3.8) and its preceding block partition. Let $i_I : H_I \to H_W$ be the isometric closed inclusion. On the full original noise space set

$$P_{\text{full}} = i_I P_{\text{ret}} i_I^*, \qquad Q_{\text{full}} = I - P_{\text{full}}.$$

These are orthogonal projections on H_W. Define the residual fast noise and stopped E operator path by

$$Y_m(f) = W(Q_{\text{full}} T_{\delta,m} f), \qquad X_m(u) = g_\delta A_{m_R}(Y_m)(\min(u, \ell_m)), \qquad g_\delta = \delta^{(1-a)/2}. \tag{9.1.7}$$

Here $T_{\delta,m}$ is the explicit original isometry (7.2.2), and A_{m_R} takes its E restriction. Its isometry is proved in Lemma 7.2.1. The symbol H_{fast} below denotes this same original covariance norm in fast coordinates, carried isometrically into H_W. The E little Hölder space means the closure of Lipschitz compact-operator paths starting at zero in C^θ norm. Compact operators on separable E and polygonal approximation make this closure separable. The last interval can be empty, in which case $X_N = 0$.

Proposition 9.1.5 (Uniform-radius Cameron bound)**.** *The tuple $X = (X_m)_{m=0}^N$ is a centered Gaussian variable in the separable little Hölder compact-operator path space on E. Its Bochner covariance $Lh = \mathbb{E}[XW(h)]$, $h \in H_W$, is*

$$(Lh)_m(u) = \sqrt{\delta} \int_0^{\min(u,\ell_m)} S_E(-v)\mathcal{T}_R(Q_{J,K} i_I^* h)(s_m + \delta v) S_E(v)\, \mathrm{d}v. \tag{9.1.8}$$

In the exact norm $\|x\|_{\delta,p} = (\delta \sum_m \|x_m\|_{C^\theta}^p)^{1/p}$, its Cameron embedding has the uniform-radius bound

$$\|Lh\|_{\delta,p} \le \sqrt{\delta}\, C_{B,E}(2/B)^{1/p-1/r}[M_0\varepsilon_J + M_f c_t K^{-\beta}]\|h\|_{H_W}, \qquad C_{B,E} \le 18B^{3-1/r}. \tag{9.1.9}$$

All spatial constants are independent of $R \ge 1$.

Proof. We construct the residual paths on the given noise, identify their supported covariance rows, and estimate the resulting primitive. The true block partition then gives the averaged Cameron bound with its exact radius-independent constants.

Step 1. We construct the residual paths and their first-chaos coordinates. Orthogonality and original pullback isometry give $\operatorname{Var} Y_m(f) \le \|f\|_{H_{\text{fast}}}^2$. Gaussian transfer, Proposition 5.2.2, therefore constructs the operator paths on the given W, with finite path

moments at each fixed R, B, δ, J, K. Choose an admissible Hölder exponent strictly above θ as in Lemma 8.3.6; constant stopping puts the paths in the separable little C^θ closure. Finite-coefficient constructions and their L^2 limits show that every continuous linear coordinate is in the first chaos of the given W.

Step 2. We identify the covariance direction on the supported subspace. Every explicit observed row, pulled back to slow time, belongs to H_I. This is the supported-row approximation from Lemma 8.3.6, also valid before any projection; approximate endpoints inside I against the integrable time kernel and locally finite spatial covariance. For such a row k, exact orthogonality gives

$$\langle Q_{\mathrm{full}} T_{\delta,m} k, h\rangle_{H_W} = \langle T_{\delta,m} k, i_I Q_{J,K} i_I^* h\rangle_{H_W}.$$

In the earlier construction $P_0 = 0$, so $Y_{m,0}(f) = W(T_{\delta,m} f)$. The preceding pairing therefore reduces the present covariance to that unprojected identity with control $\Phi = Q_{J,K} i_I^* h \in H_I$. Directions perpendicular to H_I disappear from this pairing. Apply the completed $J = 0$ identity (8.3.9) to $Q_{J,K} i_I^* h$, and restrict its input and output to E. The free F group preserves E and restricts to S_E; the mean restricts to $\mathcal{T}_R$. This proves (9.1.8). Its amplitude is exactly $g_\delta \delta^{a/2} = \sqrt{\delta}$, on the noise W. Arbitrary projected controls are covered by the completed mean identity; no smoothness or finite rank of P_K is required. Compact operator values and strong continuity of S_E and its adjoint make conjugation norm continuous on compact operators, as in Proposition 8.3.7. Thus, the integral is Bochner measurable. Fixed-parameter L^2 covariance continuity, dense states and rational times identify the entire operator path.

Step 3. We estimate the free group and each local primitive. For explicit free constants, the Bessel-unitary Fourier matrix of $S_E(v)$ is the matrix displayed in that proposition. For $|v| \le B$, $B \ge 1$, the upper off-diagonal entry is at most $\sqrt{2}B$: use $|\sin(vk)| \le Bk$ for $k \le 1$ and $\langle k\rangle/k \le \sqrt{2}$ for $k \ge 1$. The lower entry is at most one, as are both diagonal entries; at zero the sine quotient has value v. Its Frobenius bound is $\sqrt{3 + 2B^2} \le 3B$. Hence, $G_{B,E} = \sup_{|v|\le B} \|S_E(v)\| \le 3B$. With

$$\mathcal{M}_h(t) = \mathcal{T}_R(Q_{J,K} i_I^* h)(t), \qquad t_m = \|\mathcal{M}_h\|_{L^r(I_m;\mathcal{L}(E))},$$

the primitive increment bound and the affine time change give

$$\|(Lh)_m\|_{C^\theta} \le \sqrt{\delta}\, C_{B,E} \delta^{-1/r} t_m, \qquad C_{B,E} = G_{B,E}^2 [B^{1-1/r} + B^{1-1/r-\theta}] \le 18 B^{3-1/r}.$$

Here $1 - 1/r > \theta$, constant stopping preserves the bound, and the empty block contributes zero.

Step 4. We combine the local estimates with the block weights. Put $n = N + 1 \ge 2$. The finite power-mean inequality at exponent $r/p > 1$ with nonnegative inputs t_m^p gives

$$\left(\sum_m t_m^p\right)^{r/p} \le n^{r/p-1} \sum_m t_m^r, \qquad \left(\sum_m t_m^p\right)^{1/p} \le n^{1/p-1/r} \left(\sum_m t_m^r\right)^{1/r}.$$

By (9.1.6) and $\|i_I^*\| \le 1$, the field $\mathcal{M}_h = \mathcal{T}_R Q_{J,K} i_I^* h$ satisfies $\|\mathcal{M}_h\|_{L^r} \le [M_0\varepsilon_J + M_f c_t K^{-\beta}]\|h\|_{H_W}$. Raising nonnegative terms uses only positive powers, including when $t_m = 0$. The true partition gives $\sum_m t_m^r = \|\mathcal{M}_h\|_{L^r(I)}^r$ and $\delta n \le 2/B$. The exact δ weight therefore yields

$$\|Lh\|_{\delta,p} \le \sqrt{\delta}\, C_{B,E}(\delta n)^{1/p-1/r}\|\mathcal{M}_h\|_{L^r} \le \sqrt{\delta}\, C_{B,E}(2/B)^{1/p-1/r}[M_0\varepsilon_J + M_f c_t K^{-\beta}]\|h\|_{H_W}.$$

The local factor $\delta^{-1/r}$ is multiplied by the averaged norm's factor $\delta^{1/p}$. Finite power mean contributes $n^{1/p-1/r}$, so their product is $(\delta n)^{1/p-1/r}$. Since $p < r$, this power is increasing, and $\delta n \le 2/B$ gives the claimed bound. The two powers in the primitive constant are each at most $B^{1-1/r}$ because $B \ge 1$, giving $18B^{3-1/r}$ from $G_{B,E} \le 3B$.

Step 5. We apply the bound to the minimum-norm Cameron representative. Finally, let H_{seen} be the closed span in H_W of all coefficient tests k_ℓ with $\ell(X) = W(k_\ell)$. The first Wiener chaos Cameron identification in Proposition 8.3.7 applies on H_W: L kills $H_{\text{seen}}^\perp$ and its Cameron space is $L(H_{\text{seen}})$ with minimum norm of a preimage in the original covariance space. Thus, $\|Lh\|_{\text{CM}} = \|P_{\text{seen}}h\|_{H_W}$. Applying the bound to this minimum-norm representative gives precisely the Cameron embedding bound, without an inverse covariance or finite-dimensional density. This proves Proposition 9.1.5. □

The orthogonal P_{full} and Q_{full} Gaussian fields are independent; residual time blocks can remain correlated. The retained spatial head may have infinite rank. Heat filtering alone would not give this orthogonal decomposition. These linear bounds do not bound the expected residual path norm uniformly on growing masks, nor perform conditioning or integration over the infinite sum. The remaining stochastic, product and pointwise upper estimates require their own proofs.

9.2 Bounds for the operator path with explicit radius dependence

Retain every original covariance and amplitude in Hypothesis 1.2.1, with $a = \alpha_0$, and the real phase $E = H^{1/2} \times H^{-1/2}$. Use the fixed cutoff profile η of Section 9.1 and physical mask $m_R = \eta(\cdot/R)^2$, $R \ge 1$. In the variance construction the base mask is $\zeta = \eta^2$. The balanced unitary is $J_0(u,v) = (\Lambda^{1/2}u, \Lambda^{-1/2}v)$. Fix a finite horizon $B \ge 1$ and parameters

$$0 < \gamma < \min\left(\frac{1}{2}, \frac{2-\alpha}{2}\right), \qquad \frac{1}{2} < \theta < \eta_t < \beta_t < \min\left(1 - \frac{a}{2}, \frac{3-a-\alpha}{2}\right). \tag{9.2.1}$$

The strict subcritical assumptions make these intervals nonempty. Fix one even integer $Q \ge 2$ such that

$$Q\gamma > d, \qquad \beta_t - \eta_t - \frac{1}{Q} > 0, \qquad Q > \frac{2d}{1-a}. \tag{9.2.2}$$

Such a Q exists because all three lower thresholds are finite. It stays fixed as δ tends to zero. Constants below may depend on the model, B, Q, these exponents and the

fixed auxiliary cutoff profiles. They are independent of the spatial radius, noise-basis truncation, moment index and deterministic residual projection unless explicitly stated otherwise.

9.2.1 Uniform outer factors and the exact whole-space envelope

Fix real $\chi_0 \in C_c^\infty(\mathbb{R}^d)$, equal to one on B_1 and supported in the closed ball of radius two. Choose real $\psi_0 \in C_c^\infty(\mathbb{R}^d)$, equal to one on a neighbourhood of $\operatorname{supp}\chi_0$ and supported inside B_3. For $\rho \geq 1$ put $\chi_\rho(x) = \chi_0(x/\rho)$, $\psi_\rho(x) = \psi_0(x/\rho)$ and $L = 2\pi\rho$. Since $3 < \pi$, both cutoffs are supported strictly inside the cube of side L. The auxiliary torus has unnormalized $L^2(Q_L, \mathrm{d}x)$, orthonormal modes $L^{-d/2}e^{ik\cdot x/\rho}$ and Sobolev weights $\langle k/\rho\rangle^r$.

Lemma 9.2.1 (Uniform rescaled outer maps)**.** *The cutoff periodization and recovery maps from Lemma 4.3.5 satisfy, for every real r,*

$$\|\mathcal{P}_{\psi_\rho} : H^r(\mathbb{R}^d) \to H^r(\mathbb{T}_L)\| \leq C_{\psi_0,r}, \qquad \|\mathcal{E}_{\chi_\rho} : H^r(\mathbb{T}_L) \to H^r(\mathbb{R}^d)\| \leq C_{\chi_0,r},$$

independently of $\rho \geq 1$.

Proof. We rescale the exact Fourier kernels and bound their integral and lattice-sum norms separately. The radius powers cancel in the mixed Schur estimate, after which density gives the full Sobolev maps.

The exact weighted Fourier kernels are

$$L^{-d/2}\left(\frac{\langle k/\rho\rangle}{\langle \xi\rangle}\right)^r \widehat{\psi_\rho}(k/\rho - \xi),$$
$$L^{-d/2}\left(\frac{\langle \xi\rangle}{\langle k/\rho\rangle}\right)^r \widehat{\chi_\rho}(\xi - k/\rho).$$

There is no additional $(2\pi)^{-d/2}$: it cancels between Fourier inversion and the ordinary integral in the first kernel, while the torus normalization gives the second. For either base profile ϕ_0, $\widehat{\phi_\rho}(t) = \rho^d\widehat{\phi_0}(\rho t)$. Peetre's inequality (4.3.10), also for negative r, and $\langle(\rho\xi - k)/\rho\rangle \leq \langle\rho\xi - k\rangle$ bound the relevant kernel by

$$C_r\rho^{d/2}F_r(k - \rho\xi), \qquad F_r(t) = |\widehat{\phi_0}(\pm t)|\langle t\rangle^{|r|}.$$

The bracket comparison uses $\rho \geq 1$; consequently, the constants multiplying the explicit radius powers in the two Schur bounds depend only on the fixed ϕ_0, r, d. The nonnegative F_r is integrable and bounded by arbitrarily high inverse powers of $\langle t\rangle$. At fixed k, integration in ξ gives a bound $C\rho^{-d/2}$. At fixed ξ, summation in k gives $C\rho^{d/2}$: translate $\rho\xi$ into a unit lattice cell and sum a power tail of order greater than d, as in (4.3.11). This lattice spacing is one and has no remaining ρ dependence. The mixed Schur estimate bounds the operator norm by the square root of the product of those two quantities. Their radius powers cancel. For recovery the row and column roles are reversed.

In the integral bound, the substitution $\rho\xi - k$ contributes ρ^{-d}. Multiplying by the kernel's factor $\rho^{d/2}$ gives $\rho^{-d/2}$. Bounded kernel extension from Schwartz functions and

torus polynomials gives the full Sobolev maps by density. Their distributional meanings are the same cutoff maps as in Lemma 4.3.5; no point sampling of a rough Fourier function is used. This includes negative indices. This proves Lemma 9.2.1. □

Lemma 9.2.1 bounds the two outer maps independently of $\rho \geq 1$. The proof below places a diagonal inclusion on the torus between them. We now sum the qth powers of the singular values of this inclusion and take the qth root, which produces the factor $\rho^{d/q}$.

Proposition 9.2.2 (Radius-explicit compact envelopes)**.** *For real σ, $\gamma > 0$ and $q \geq 1$ with $q\gamma > d$,*

$$\|\Lambda^{\sigma}\chi_{\rho}\Lambda^{-\sigma-\gamma}\|_{S_q} \leq C_{\sigma,\gamma,q,d,\chi_0,\psi_0}\rho^{d/q}. \tag{9.2.3}$$

In the balanced coordinates of (4.3.14),

$$\|K_{\mathrm{in}}\|_{S_q} = \|K_{\mathrm{out}}\|_{S_q} \leq C_q\rho^{d/q}. \tag{9.2.4}$$

Proof. We factor the cutoff through the auxiliary torus. We compare the diagonal inclusion sum with a Euclidean integral and then use finite-rank approximations to transfer that sum to the whole-space operator.

Step 1. We use the full-domain recovery factorization. The exact recovery identity, with $\chi_{\rho}\psi_{\rho} = \chi_{\rho}$, gives

$$\Lambda^{\sigma}\chi_{\rho}\Lambda^{-\sigma-\gamma} = \Lambda^{\sigma}\mathcal{E}_{\chi_{\rho}}\mathcal{I}_{\gamma}\mathcal{P}_{\psi_{\rho}}\Lambda^{-\sigma-\gamma}.$$

Here $\mathcal{I}_{\gamma} : H^{\sigma+\gamma}(\mathbb{T}_L) \to H^{\sigma}(\mathbb{T}_L)$ has diagonal singular values $\langle k/\rho\rangle^{-\gamma}$. The outer Bessel maps are unitary on their indicated Sobolev domains. The preceding lemma bounds both other outer maps uniformly in ρ. This is an equality on the full whole-space domain by the recovery proof and density, including negative σ.

Step 2. We bound the diagonal sum by a volume integral. Put $u = q\gamma > d$. If $x \in k + [-1/2, 1/2]^d$, then

$$\langle x/\rho\rangle \leq \sqrt{2}\langle k/\rho\rangle\langle (x-k)/\rho\rangle \leq c_d'\langle k/\rho\rangle, \qquad c_d' = \sqrt{2(1+d/4)}.$$

Integrate over the unit cubes to obtain

$$\sum_{k\in\mathbb{Z}^d}\langle k/\rho\rangle^{-u} \leq (c_d')^u\rho^d\int_{\mathbb{R}^d}\langle y\rangle^{-u}\,\mathrm{d}y \leq C_{d,u}\rho^d. \tag{9.2.5}$$

The integral is finite: dyadic annuli outside the unit ball give a geometric series with terms bounded by $C_d 2^{j(d-u)}$.

The unit cubes partition Euclidean space and each has volume one. The preceding weight comparison bounds the constant cube value $\langle k/\rho\rangle^{-u}$ by $(c_d')^u\langle x/\rho\rangle^{-u}$. Summing the cube integrals and substituting $y = x/\rho$ gives the factor ρ^d. Taking a qth root later gives $\rho^{d/q}$.

Step 3. We transfer the singular-value bound to the two whole-space envelopes. Arrange the inclusion's diagonal values in decreasing order (λ_j). They tend to zero. Retaining its first $j-1$ coordinates has rank less than j and error λ_j. Compose this approximation

with the bounded outer factors. The singular-value approximation argument in Proposition 4.3.6 gives $s_j \le C_{\chi_0,\sigma} C_{\psi_0,\sigma+\gamma} \lambda_j$. Finite-rank approximation also proves compactness. Summing qth powers and using (9.2.5) proves (9.2.3). No separate Schatten ideal theorem is needed.

The two blocks of $K_{\mathrm{out}} = P_{\chi_\rho} D_\gamma$ are the whole-space operators with $\sigma = 1/2, -1/2$. Their qth power norms add, proving its bound. Proposition 4.3.7 gives $K_{\mathrm{in}} = V K_{\mathrm{out}} V$ for the unitary coordinate swap $V(z_1, z_2) = (z_2, z_1)$, so their norms agree. In (9.2.1), $\gamma < 1/2$ and $q\gamma > d$ force $q > 2d \ge 2$; there is no Hilbert–Schmidt conclusion. Neither P_{χ_ρ} nor its adjoint is assumed selfadjoint or idempotent. This proves Proposition 9.2.2. □

9.2.2 The operator path and covariance contractions

Write $M_R(W) = A_{m_R}(W)$ for the E interaction operator path starting at zero on $[0, B]$ from Proposition 5.1.1. The phase remains the whole-space E throughout.

Proposition 9.2.3 (Radius-explicit path moments)**.** *Under* (9.2.1)–(9.2.2)*, for every finite* $v \ge 1$*,*

$$\|M_R(W)\|_{L^v(C^\theta([0,B];\mathcal{L}(E)))} \le C_{Q,B} \sqrt{v}\, R^{d/Q}, \qquad R \ge 1. \tag{9.2.6}$$

The constant does not depend on v *or* R*. This is an* E *operator-path estimate; the two constant columns on* F *require their own estimates. Any later projection used in a Cameron comparison must also satisfy its orthogonality and covariance hypotheses.*

Proof. We keep the physical noise mask fixed while choosing a larger localization envelope. We use only one fixed Schatten index to extract the radius factor, then apply the dyadic path estimate uniformly over all higher moment indices.

Step 1. We choose a localization envelope covering the propagated support. Use the given smooth-test basis from Lemma 5.1.2, $g_j = W(f_j)$, and its finite paths $M_N = \sum_{j \le N} g_j A_j$. These coefficient paths use the same given noise as in Lemma 5.1.9, not source approximations. Choose

$$\rho = 2R + B + 2 \le (B+4)R, \qquad \chi = \chi_0(\cdot/\rho).$$

The plateau covers B_{2R+B+1}. Thus, both explicit localization identities (5.1.10) hold for this envelope. The physical noise mask remains m_R. Both envelopes $K_{\mathrm{in}}, K_{\mathrm{out}}$ here use this same χ_ρ.

Step 2. We estimate increments using both variance bounds. For an interval $I \subset [0, B]$ of length $0 < h \le 1$, Proposition 4.2.5 and Lemma 5.1.5 give both finite weighted variances with bound $V_{B,\mathrm{var}} h^{2-a} B_\alpha(h)$, uniformly in R, N, I. In particular, the base mask is the same fixed η^2 required by that variance theorem. Corollary 4.3.10, applied in the balanced coordinates, gives for every even $q \ge Q$

$$\|M_N(I)\|_{L^q(S_q)} \le \sqrt{q-1} \sqrt{V_{B,\mathrm{var}}}\, h^{1-a/2} B_\alpha(h)^{1/2} \|K_{\mathrm{out}}\|_{S_q},$$

where $B_\alpha(h)$ is 1, $1 + \log(1/h)$ or $h^{1-\alpha}$ according as $\alpha < 1$, $\alpha = 1$ or $\alpha > 1$. Both variances and both localizations have been checked; individual basis-dependent coefficient bounds are not summed.

Step 3. We extract the radius factor at the fixed index. For $q \geq Q$, the unnormalized Schatten norms obey $\|K_{\mathrm{out}}\|_{S_q} \leq \|K_{\mathrm{out}}\|_{S_Q}$. Indeed, normalize a nonzero singular-value sequence by its ℓ^Q norm; each entry is at most one, so its qth power sum is at most its Qth power sum. The zero case is immediate. Apply (9.2.4) only at the fixed index Q. Use $\|A\| \leq \|A\|_{S_q}$ and $\sqrt{q-1} \leq \sqrt{q}$. The balanced Hilbert complexification has the same operator norm as its real restriction, and $\rho^{d/Q} \leq (B+4)^{d/Q} R^{d/Q}$. Since β_t is strictly below the corresponding short-time power, it follows that

$$\|M_N(t) - M_N(u)\|_{L^q(\mathcal{L}(E))} \leq C_{Q,B} \sqrt{q}\, R^{d/Q} |t-u|^{\beta_t}, \qquad |t-u| \leq 1. \tag{9.2.7}$$

At $\alpha = 1$, the factor $\sqrt{1 + \log(1/h)}$ is absorbed by the strict gap $1 - a/2 - \beta_t > 0$. For $\alpha > 1$, the power is $(3 - a - \alpha)/2$. These power/log constants are independent of R, N, q. Longer increments are finite sums of increments of length at most one, with constants depending only on the fixed B.

Step 4. We sum dyadic increments and pass to the path limit. Let $D_n(F)$ be the largest adjacent increment on the grid $kB2^{-n}$ of $[0, B]$. For fine levels $B2^{-n} \leq 1$, the finite-maximum bound gives

$$\|D_n(M_N)\|_{L^q} \leq 2^{n/q} C_{Q,B} \sqrt{q}\, R^{d/Q} (B2^{-n})^{\beta_t}.$$

No independence of increments is used. The sum after multiplication by $2^{n\eta_t}$ converges uniformly for even $q \geq Q$, because its geometric ratio is at most $2^{-(\beta_t - \eta_t - 1/Q)} < 1$. The finitely many coarse levels are controlled by unit partitions. The deterministic dyadic chaining argument in Lemma 5.1.9 therefore bounds the $L^q C^{\eta_t}$ norms by $C_{Q,B}\sqrt{q}\, R^{d/Q}$. Each finite path is continuous and starts at zero, as required there. The fixed-horizon embedding $C^{\eta_t} \hookrightarrow C^\theta$ gives the same estimate in C^θ.

For each fixed R, Lemma 5.1.9 identifies $M_R(W)$ as the all-finite-moment C^θ limit of these very M_N. Pass the uniform finite-N estimate to this limit. Uniform convergence in R is unnecessary: the limiting bound has its explicit radius dependence at every R. For arbitrary $v \geq 1$, choose an even $q \geq \max(v, Q)$ with $q \leq v + Q + 2 \leq (Q+3)v$. Lyapunov's inequality gives (9.2.6), absorbing $\sqrt{Q+3}$ into the fixed constant. This proves Proposition 9.2.3. □

Proposition 9.2.3 concerns the path $M_R(W)$ of the noise W itself. Proposition 9.2.5 works instead with residual noises Y_m, obtained from W through a deterministic orthogonal projection. We now transfer the moment bound to such noises.

Corollary 9.2.4 (Deterministic covariance residuals)**.** *Let Y be a centered Gaussian linear noise on the coupled space, with $\operatorname{Var} Y(f) \leq C\|f\|^2_{H_W}$, $C \geq 0$. Its transferred operator path satisfies*

$$\|M_R(Y)\|_{L^v(C^\theta)} \leq \sqrt{C}\, C_{Q,B} \sqrt{v}\, R^{d/Q}.$$

In particular, this holds with $C = 1$ for $Y_m(f) = W((I - \Pi)T_{\delta,m} f)$, for any deterministic orthogonal projection Π on the slow H_W. Its rank may be infinite and it may depend on δ, R.

Proof. Proposition 5.2.2 is a linear Gaussian covariance contraction theorem for this same physical mask and these same deterministic coefficient maps. It bounds the path norm by $\sqrt{C}$ times the reference isonormal operator-path norm. The reference has the canonical operator-path law used in Proposition 9.2.3; the Y is not replaced in this comparison. The zero case gives zero directly. This proves the first assertion. For the second, the original isometry (7.2.2), proved in Lemma 7.2.1, and $\|I - \Pi\| \le 1$ give $\operatorname{Var} Y_m(f) \le \|f\|_{H_W}^2$, where the right side is the original norm in fast coordinates. The joint residuals retain the given slow W and may be correlated. They need not lie in the span of an individual fast noise, which is not a hypothesis of Gaussian transfer. No random noise-dependent projection is used. This proves Corollary 9.2.4. □

9.2.3 The growing-radius expected-norm anchor

Corollary 9.2.4 bounds each residual path with the growing factor $R^{d/Q}$. We now average over the time blocks with the amplitude g_δ. The last condition in (9.2.2) makes $g_\delta R^{d/Q}$ tend to zero at the radius $R_\delta = \delta^{-1} + 2$.

Lean partial

Proposition 9.2.5 (Averaged block mean tends to zero)**.** *Fix integer $B \ge 1$ and use the true block partition B, δ, N, ℓ_m of Section 8.3, with $0 < \delta < \min(1, 1/B)$ and $N = \lfloor 1/(\delta B) \rfloor$. For Y_m as in Corollary 9.2.4, put*

$$X_m(u) = g_\delta M_R(Y_m)(\min(u, \ell_m)), \qquad Z_\delta = \left(\delta \sum_{m=0}^{N} \|X_m\|_{C^\theta}^p \right)^{1/p}, \qquad g_\delta = \delta^{(1-a)/2},$$

for any fixed $p \ge 1$. Then

$$\mathbb{E} Z_\delta \le (2/B)^{1/p} C_{Q,B} \sqrt{p}\, g_\delta R^{d/Q}. \tag{9.2.8}$$

In particular, for $R_\delta = \delta^{-1} + 2$,

$$2\mathbb{E} Z_\delta \le 2(2/B)^{1/p} C_{Q,B} \sqrt{p}\, 3^{d/Q} \delta^{e_{\text{anchor}}} \longrightarrow 0, \qquad e_{\text{anchor}} = \frac{1-a}{2} - \frac{d}{Q} > 0. \tag{9.2.9}$$

Both bounds are uniform in the deterministic orthogonal projection.

Proof. Stopping an interaction primitive starting at zero and extending it constantly to B does not increase its supremum or Hölder seminorm. An empty last interval gives the zero path. Probability normalization and Lyapunov give

$$\begin{aligned} \mathbb{E} Z_\delta \le (\mathbb{E} Z_\delta^p)^{1/p} &= \left(\delta \sum_{m=0}^{N} \mathbb{E} \|X_m\|_{C^\theta}^p \right)^{1/p} \\ &\le [\delta(N+1)]^{1/p} g_\delta C_{Q,B} \sqrt{p}\, R^{d/Q}. \end{aligned}$$

This is linearity for a finite sum; no time-block independence or maximum over blocks is used. Since $\delta B < 1$, we have $N \ge 1$ and $N + 1 \le 2/(\delta B)$, proving (9.2.8).

Now $R_\delta \le 3/\delta$ because $\delta < 1$. The last condition in (9.2.2) is equivalent to $Q(1-a) > 2d$. Dividing by $2Q > 0$ gives $e_{\text{anchor}} > 0$. Substitute this radius into (9.2.8) to obtain (9.2.9). The estimate holds at each fixed B, p, Q and model, uniformly in every deterministic residual projection. This proves Proposition 9.2.5. □

These bounds concern the expected operator-path norm on E. They do not give an F estimate with constant initial-data columns. The radius substitution is numerical; cone coverage and source-to-point transfer require their separate arguments. No concentration, integration over an infinite sequence of Gaussian coordinates or nonlinear moment upper bound follows from this section alone. The constants need not be uniform as Q, B tend to infinity or as model parameters approach an endpoint. For zero covariance, the operator paths and stochastic bounds vanish directly.

9.3 Signed rough static potentials and the physical wave

Fix the original nonzero covariance and a finite physical mask m_R as in Section 8.3. For real $q \in C_c^\infty(\mathbb{R}^d)$ put $V_q = m_R(\Gamma * q)$ and $L_q(u, v, c_1, c_2) = (0, V_q(u + c_1), 0, 0)$ on $F = E \oplus \mathbb{R}^2$. Let $\mathcal{V}_R$ be the operator-norm closure of these operators in $\mathcal{K}(F)$. It is a closed real linear space. No positivity is imposed on q.

Lemma 9.3.1 (The limiting multiplier)**.** *Every $L \in \mathcal{V}_R$ determines a unique real $V \in H^{-1/2}$ supported in* $\operatorname{supp} m_R$*. It has the multiplier action $L(u, v, c_1, c_2) = (0, Vu + c_1 V, 0, 0)$, where multiplication extends from tests to $H^{1/2} \to H^{-1/2}$. For $k = \|L\|$, its symmetric pairing obeys*

$$|v_V(u, w)| \le k\|u\|_{H^{1/2}}\|w\|_{H^{1/2}}. \tag{9.3.1}$$

Proof. The form $v_V(u, w)$ is the duality pairing $\langle Vu, w\rangle_{H^{-1/2}, H^{1/2}}$. Once the multiplier bound $\|Vu\|_{H^{-1/2}} \le k\|u\|_{H^{1/2}}$ is obtained below, duality gives (9.3.1). Choose $L_{q_n} \to L$. The constant-displacement vector has norm one, so $\|V_{q_n} - V_{q_j}\|_{H^{-1/2}} \le \|L_{q_n} - L_{q_j}\|$. Thus, $V_{q_n} \to V$ in $H^{-1/2}$. Testing outside the fixed compact mask support preserves that support. Every zero column of L_{q_n} remains zero. Its displacement multipliers converge in $\mathcal{L}(H^{1/2}, H^{-1/2})$ to a map of norm at most k. For compact smooth u, smooth multiplication is bounded on $H^{-1/2}$ by Lemma 4.3.5. Hence, $V_{q_n}u \to Vu$ there, identifying the limiting map on tests and then uniquely on $H^{1/2}$ by density. The constant column recovers V and proves uniqueness. On compact smooth u, w, the pairing is $\langle V, uw\rangle$, denoted $v_V(u, w)$, so it is symmetric. Its bound and symmetry extend by density. Complexification preserves the operator norm by splitting real and imaginary parts in the Hilbert norms. The pairing extends sesquilinearly to a Hermitian form; its diagonal is the sum of the real and imaginary diagonal values. This proves Lemma 9.3.1. □

The bound (9.3.1) controls the pairing v_V on $H^{1/2}$. We now use it to define a self-adjoint operator H_V from the quadratic form q_V on H^1. We also compare the quarter power of its shift A with the $H^{1/2}$ norm.

Lean partial

Proposition 9.3.2 (Closed form and quarter-power phase)**.** *Let $K \ge \max(1, \|L\|)$ and $c = 2 + K^2$. On complexified L^2 the form*

$$q_V(u) = \|\nabla u\|_2^2 - v_V(u, u), \qquad Q(q_V) = H^1,$$

represents a unique self-adjoint H_V. With $A = H_V + c$ and $L_K = 3(1 + K^2)$,

$$A \geq 1, \qquad D(A^{1/2}) = H^1, \tag{9.3.2}$$

$$\tfrac{1}{2}\|u\|_{H^1}^2 \leq q_V(u) + c\|u\|_2^2 \leq L_K\|u\|_{H^1}^2, \tag{9.3.3}$$

$$D(A^{1/4}) = H^{1/2}, \qquad 2^{-1/4}\|u\|_{H^{1/2}} \leq \|A^{1/4}u\|_2 \leq L_K^{1/4}\|u\|_{H^{1/2}}. \tag{9.3.4}$$

The negative dual completion is $H^{-1/2}$. No H^2 operator domain is asserted.

Proof. We first bound the signed potential form by the Sobolev norm and identify its closed representation. We then derive the quarter-power comparison from resolvents, and use duality to identify the negative phase.

Step 1. We make the shifted form coercive and closed. Put $b = \|u\|_2$, $z = \|u\|_{H^1}$. Fourier Cauchy–Schwarz and (9.3.1) give

$$\|u\|_{H^{1/2}}^2 \leq bz, \qquad |v_V(u,u)| \leq Kbz \leq \tfrac{1}{2}z^2 + \tfrac{1}{2}K^2b^2.$$

The last scalar inequality is the weighted arithmetic–geometric mean inequality at weights $1/2, 1/2$ and nonnegative bases $z^2, (Kb)^2$, including zero norms. Since $q_V = z^2 - b^2 - v_V(u,u)$, it follows that

$$q_V + cb^2 \geq \tfrac{1}{2}z^2 + (1 + K^2/2)b^2, \qquad q_V + cb^2 \leq \tfrac{3}{2}z^2 + (1 + 3K^2/2)b^2 \leq L_K z^2.$$

The lower bound dominates both $z^2/2$ and b^2. Thus, this densely defined Hermitian form is semibounded and its shifted norm is equivalent to the complete H^1 norm. It is closed in the definition of [44, p. 80]. From [44, Theorem 2.14, p. 81, (2.63)], it represents a unique self-adjoint H_V. This representation is independent of the admissible shift. From that book's Theorem 3.6 and (3.51)–(3.53), p. 109, applied after shifting, we obtain (9.3.2). Here $A \geq 1$ is initially its form lower bound. A bounded spectral slice below one would produce a unit $D(A)$ test contradicting that form bound; hence it is also the spectral lower bound. Lemma 9.3.3 records the full bottom argument.

Step 2. We compare fractional powers through resolvent order. Set $B_0 = 1 - \Delta$. On the common form domain, $\frac{1}{2}B_0 \leq A \leq L_K B_0$. We prove the needed square-root comparison rather than assuming an order rule for arbitrary operator powers. For $T_0, S_0 \geq 1$ with common form domain and $q_{T_0} \leq q_{S_0}$, completing the square in the shifted form norm gives

$$\langle f, (T_0 + t)^{-1}f\rangle = \sup_u\{2\,\mathrm{Re}\langle f, u\rangle - q_{T_0}(u) - t\|u\|^2\} \geq \langle f, (S_0 + t)^{-1}f\rangle, \quad t > 0.$$

The scalar identity $\sqrt{x} = \pi^{-1}\int_0^\infty t^{-1/2}x/(x + t)\,\mathrm{d}t$ follows by $t = xv^2$. Positive spectral integration and Tonelli now imply $T_0^{1/2} \leq S_0^{1/2}$ as forms, with their domain inclusions: $I - t(T_0 + t)^{-1} \leq I - t(S_0 + t)^{-1}$. Apply this to $(B_0, 2A)$ and $(A, L_K B_0)$. Both operators in each pair are at least one. The resulting inequalities give (9.3.4), including equality of its domains. For $v \in L^2$ the L^2-duality norm against $\|A^{1/4}u\|_2$ is $\|A^{-1/4}v\|_2$: Cauchy–Schwarz gives the upper bound, and $u = A^{-1/2}v$ gives equality after normalization. Duality and completion therefore identify the negative phase. Uniqueness of the form, resolvent and spectral calculus makes these constructions commute with real conjugation. This proves Proposition 9.3.2. □

Proposition 9.3.2 gives the operator H_V and compares the norms built from $A^{1/4}$ with those of E. We now locate the bottom of the spectrum of H_V and bound the wave that its spectral calculus defines on E. The bound allows exponential growth at the rate $\lambda(V)$.

Lemma 9.3.3 (The bottom and spectral wave)**.** *Write P_V^E for the evolution in (9.3.6), and S_E for the free restriction from Lemma 6.2.1. Put*

$$\beta(V) = \inf_{\substack{u\in H^1\\ \|u\|_2=1}} q_V(u), \qquad \lambda(V) = \sqrt{-\beta(V)}.$$

Then $\beta(V) = \inf \operatorname{spec} H_V$ and $-K^2 \le \beta(V) \le 0$. The spectral wave on E has the bound

$$\|P_V^E(t)\| \le 8(1+K)^2(1+t)e^{\lambda(V)t}, \qquad t \ge 0. \tag{9.3.5}$$

Proof. We identify the form infimum with the spectral bottom and use the compact support to show that it is nonpositive. We then estimate the spectral wave matrix in its adapted phase norm and transfer the estimate to the fixed Sobolev phase.

Step 1. We locate the spectral bottom. For unit u, $z = \|u\|_{H^1} \ge 1$ gives $q_V(u) \ge z^2/2 - 1 - K^2/2 \ge -(1+K^2)/2 \ge -K^2$. Conversely dilate a unit compact smooth bump and translate its whole support outside $\operatorname{supp} m_R$. Its potential pairing is zero and its kinetic energy tends to zero. Thus, $\beta \le 0$. Real and complex form infima agree because a complex diagonal splits into the two real diagonals. The spectral form formula in [44, (3.52)–(3.53)] identifies this form infimum with the spectral bottom. For clarity, a bounded spectral slice below the form lower bound would give a unit form test violating that bound. Conversely the form integral is bounded below by the spectral infimum. The spectrum is nonempty: a unit vector's scalar spectral measure has mass one and a support point, and normalized projections onto arbitrarily small bounded neighborhoods give approximate eigenvectors, excluding a bounded inverse there. Conversely, off the closed PVM support Σ the Borel function $(h-z)^{-1}$, set to zero off Σ, is bounded for real $z \notin \Sigma$, as is $h/(h-z)$ on Σ. Its calculus maps into $D(H_V)$ and is a two-sided resolvent inverse on the appropriate domains. Thus, the spectrum is precisely Σ. Hence, $\lambda \le K$ and every spectral value h has $h + c \ge 2$.

Step 2. We estimate the spectral matrix in an equivalent phase norm. Use the phase norm $\|(u,v)\|_{E_A}^2 = \|A^{1/4}u\|_2^2 + \|A^{-1/4}v\|_2^2$. With $M_K = L_K^{1/4}$, the preceding proposition and its dual give $M_K^{-1}\|z\|_E \le \|z\|_{E_A} \le M_K\|z\|_E$. The condition-number cost is $M_K^2 = \sqrt{3(1+K^2)} \le 2(1+K)$. Define $C_t(h), S_t(h)$ by $\cos(t\sqrt{h}), \sin(t\sqrt{h})/\sqrt{h}$ for $h > 0$, by $1, t$ at zero, and by $\cosh(t\sqrt{-h}), \sinh(t\sqrt{-h})/\sqrt{-h}$ for $h < 0$. In the E_A isometry the wave matrix is

$$\begin{pmatrix} C_t(h) & \sqrt{h+c}\, S_t(h) \\ -hS_t(h)/\sqrt{h+c} & C_t(h) \end{pmatrix}. \tag{9.3.6}$$

The isometry is $(u,v) \mapsto (A^{1/4}u, A^{-1/4}v)$ onto $L^2 \times L^2$, with the negative-power map extended to the completed velocity space. The displayed matrix is the conjugate, initially

on bounded spectral cutoffs, of the spectral solution

$$P_V^E(t)\begin{pmatrix}u\\v\end{pmatrix}=\begin{pmatrix}C_t(H_V)u+S_t(H_V)v\\-H_VS_t(H_V)u+C_t(H_V)v\end{pmatrix}.$$

For $h\geq 0$, the entries are bounded using $|C_t|\leq 1$, $|S_t|\leq \min(t,h^{-1/2})$, $\sqrt{h+c}|S_t|\leq 1+\sqrt{c}\,t$ and $|hS_t|/\sqrt{h+c}\leq 1$; at zero the off-diagonals are $\sqrt{c}\,t,0$. For $\beta\leq h<0$, they are bounded using $|C_t|\leq e^{\lambda t}$, $|S_t|\leq te^{\lambda t}$, $\sqrt{h+c}|S_t|\leq\sqrt{c}\,te^{\lambda t}$ and $|hS_t|/\sqrt{h+c}\leq Ke^{\lambda t}$. There is no division by λ. Since $\sqrt{c}\leq 2K$, each entry is at most $2(1+K)(1+t)e^{\lambda t}$. Bounded Borel calculus from [44, Theorem 3.1, pp. 102–103, (3.18)–(3.21)], the two-by-two matrix norm bound and the condition-number cost give (9.3.5). Functions can be set to zero off the spectral support. Spectral dominated convergence gives strong continuity, and scalar addition identities give the group property. The same matrix and bounds apply on the weighted graph levels $D(A^{1/2})\times L^2$ and $D(A)\times D(A^{1/2})$. Spectral cutoffs justify their extensions and continuity there. For negative spectral values, the lower off-diagonal estimate can be read without dividing by λ: its absolute value is $\sqrt{-h}\sinh(t\sqrt{-h})/\sqrt{h+c}$. The bounds $\sqrt{-h}\leq K$ and $h+c\geq 2$ make this at most $Ke^{\lambda t}$. Thus, the estimate also remains meaningful when the bottom rate is zero. This proves Lemma 9.3.3. □

Lemma 9.3.3 bounds a wave defined by spectral calculus, and only on E. We still have to identify it with the physical wave and to include the two constant columns of F.

Proposition 9.3.4 (Identification with the physical wave)**.** *The spectral wave in Lemma 9.3.3 is the bounded-perturbation, equivalently Young, physical wave on E. Its extension on F satisfies*

$$\|P_V(t)\|_{\mathcal{L}(F)}\leq 16(1+K)^4(1+t)^3e^{\lambda(V)t},\qquad t\geq 0. \tag{9.3.7}$$

Both constant response columns are included.

Proof. We first embed the form operator domain into the free generator domain. The spectral solution then satisfies the physical Duhamel identity on dense graph data. We extend that identity and include the constant columns by variation of constants.

Step 1. We obtain the graph-continuous embedding. The imported form representation [44, Theorem 2.14, p. 81, (2.63)], tested against compact smooth functions, gives $H_Vu=-\Delta u-Vu$ in distributions for $u\in D(H_V)$. Such u lies in H^1 and $Vu\in H^{-1/2}$. Consequently, $(1-\Delta)u=H_Vu+Vu+u\in H^{-1/2}$, so $D(H_V)\hookrightarrow H^{3/2}$. The embedding is graph-continuous: by (9.3.3), $\|u\|_{H^1}^2\leq 2\langle Au,u\rangle\leq\|Au\|_2^2+\|u\|_2^2$, and the distributional equation bounds the $H^{3/2}$ norm by this graph norm.

Step 2. We identify the free generator and apply the interaction identity. The generator of the free E group is $A_0(u,v)=(v,\Delta u)$ on $H^{3/2}\times H^{1/2}$. Indeed, differentiate its Fourier matrix after a frequency cutoff, dominate by that graph norm and remove the cutoff. Conversely any strong generator derivative has those distributional components; they

require $v \in H^{1/2}$ and $\Delta u \in H^{-1/2}$, hence $u \in H^{3/2}$. No operator-norm differentiability of the group is used.

Start spectral data in $D(A) \times D(A^{1/2}) = D(H_V) \times H^1$. The preceding graph-level estimates give continuous graph trajectories and C^1 trajectories in $H^1 \times L^2$, with $u_t = v$, $v_t = -H_V u$. This follows first on bounded spectral cutoffs and then uniformly on finite horizons in the graph norms by spectral dominated convergence and [44, Theorem 3.2, p. 104, (3.29)–(3.33)]. The projections $1_{[1,n]}(A)$ approximate every graph datum and the same weighted matrix bounds control all cutoff tails on those horizons. Graph embedding gives continuity in $D(A_0)$ and $z_t = A_0 z + L_E z$ in E, where $L_E = L|_E$. The strong-group chain rule on this domain yields

$$S_E(-t)z(t) = z(0) + \int_0^t S_E(-s)L_E z(s)\,\mathrm{d}s.$$

Graph data are dense in E: spectral cutoffs make $D(A)$ dense in $D(A^{1/2}) = H^1$, and H^1 is dense in both $H^{1/2}$ and $H^{-1/2}$. Boundedness on finite horizons extends this identity to all E. Volterra uniqueness by Picard iteration identifies the physical wave. No $D(A^{3/4}) = H^{3/2}$ assertion is needed.

Step 3. We identify the ordinary and Young flows on the extended phase. On F, bounded L and strongly continuous S_F similarly define a unique Duhamel flow. On $[0,T]$, the nth Volterra term has bound $C_T^{n+1}\|L\|^n T^n/n!$. Uniqueness makes horizons consistent and gives composition. Its interaction primitive is $\int_0^t S_F(-s)LS_F(s)\,\mathrm{d}s$. Compactness of L, and strong continuity of the group and its adjoint, give norm-continuity of the conjugated compact operator, as in Proposition 8.3.7. Thus, this primitive is Lipschitz and its ordinary equation is exactly the Young equation.

Step 4. We bound both constant response columns. For initial (e, c_1, c_2) the constant coordinates are $(c_1 + tc_2, c_2)$ and the E component is

$$P_V^E(t)e + \int_0^t P_V^E(t-s)(0, V(c_1 + sc_2))\,\mathrm{d}s.$$

The bounded E-valued Fubini argument proving (6.3.11) applies: substitute the E Duhamel formula under this integral and interchange the absolutely bounded finite time triangle. It solves the full system, and uniqueness identifies it. No ground positivity or gap is used. The forcing norm is at most $K(1+s)|(c_1,c_2)|$. Since $\lambda \geq 0$ and $\int_0^t (1+t-s)(1+s)\,\mathrm{d}s \leq (1+t)^3$, the full norm is at most

$$(1+t)^3 e^{\lambda t}\{8(1+K)^2\|e\| + [8K(1+K)^2+1]|(c_1,c_2)|\}.$$

The coefficient of $\|e\|$ is bounded by $8(1+K)^3$. The coefficient of the constant-coordinate norm is at most $9(1+K)^3$, since $K \leq 1+K$ and $1 \leq (1+K)^3$. Cauchy–Schwarz on these two scalar components therefore gives the factor $\sqrt{8^2+9^2}$ in the following estimate. Scalar Cauchy–Schwarz and $\sqrt{8^2+9^2} < 13$ bound this by $13(1+K)^3(1+t)^3 e^{\lambda t}\|(e,c_1,c_2)\|_F$. This implies the stated sufficient bound. This proves Proposition 9.3.4. □

What we now have. Mean bounds uniform in the radius (Proposition 9.1.4) and the physical wave for signed static means (Proposition 9.3.4).

Chapter 10

Gaussian estimates for the point upper bound

The lower bound needed only the favorable shifts of the noise. The upper bound must account for every Gaussian fluctuation. It must also control the moment at one point of space while the region of propagation grows (Figure 10.2). The Gaussian cost stays in the original covariance norm.

Section 10.1 sets up the symplectic and norm properties of the wave evolution. Section 10.2 is the heart of the chapter: Gaussian enlargement turns a probabilistic estimate into growth under deterministic mean controls (Figure 10.1). Section 10.3 makes this compatible with the growing radius. Section 10.4 returns to the original point moment. Section 10.5 controls the Gaussian tail.

The prerequisites are the mean estimates of Chapter 8, the radius bounds of Chapter 9 and the exact scaling in Section 7.1. The chapter delivers Proposition 10.5.4: an upper variational expression over signed controls. The next chapter matches it to the lower value. Episode ▶ 7 of the video series covers this chapter.

10.1 The symplectic form and mean evolution on time blocks

Retain the original model, covariance amplitude, physical mask m_R and real $E = H^{1/2} \times H^{-1/2}$. Fix finite $R, T > 0$ and admissible exponents as in (5.1.1). Let $M = M_R(W)$ be the from the given noise first interaction path on E, and M^ρ its regularized paths from Proposition 5.2.2 and the source construction. Here ρ is the positive heat/Laplace smoothing pair. The construction preserving the given noise and ordinary rows are those of Lemma 5.2.4, Lemma 5.2.6 and Proposition 5.2.7. The full F operator path and Young evolution are fixed by Proposition 6.2.2 and Proposition 6.2.4; their E restrictions are used here. Complexifications commute with conjugation, so these real restrictions are the physical phases. For fixed Φ in the full positive-time original H_W and real c set

$$\begin{aligned} Z &= W(\Phi), \qquad D_\Phi = \mathbb{E}[ZM], \qquad D_\Phi^\rho = \mathbb{E}[ZM^\rho], \\ D &= cM + D_\Phi, \qquad D^\rho = cM^\rho + D_\Phi^\rho. \end{aligned} \tag{10.1.1}$$

All these are operator paths on E. The covariance mean is not a pointwise original potential. Write U_D for left Young evolution and $P_D(t,s) = S_E(t) U_D(t,s) S_E(-s)$.

Lean partial

Lemma 10.1.1 (Free wave form and compact Young baseline)**.** *There is a bounded isometric skew-adjoint J_E on E, with $J_E^2 = -I$, such that*

$$\omega(z,w) = \langle z, J_E w \rangle_E = \langle u, g \rangle_{H^{1/2}, H^{-1/2}} - \langle f, v \rangle_{H^{1/2}, H^{-1/2}}, \quad z = (u,v), \quad w = (f,g).$$

The free group preserves ω. For bounded real smooth b, the force $B(b)(u,v) = (0, bu)$ obeys $\omega(B(b)z, w) + \omega(z, B(b)w) = 0$.

Let $1/2 < \theta < 1$ and let $X \in C^\theta([0,T]; \mathcal{K}(E))$ start at zero, with U_X its left Young evolution. Then

$$U_X(t,s) - I \in \mathcal{K}(E), \qquad \|S_E(t)U_X(t,s)S_E(-s)\| \geq \|S_E(t-s)\| \geq 1, \qquad 0 \leq s \leq t \leq T. \tag{10.1.2}$$

More generally, for finitely many such paths X_j starting at zero on $[0,B]$ and lengths $0 \leq \ell_j \leq B$, put $P_j = S_E(\ell_j)U_{X_j}(\ell_j, 0)$. Then

$$P_N \cdots P_0 - S_E\Big(\sum_{j=0}^{N} \ell_j\Big) \in \mathcal{K}(E), \qquad \|P_N \cdots P_0\| \geq \left\|S_E\Big(\sum_{j=0}^{N} \ell_j\Big)\right\| \geq 1. \tag{10.1.3}$$

These norm bounds require neither Gaussian nor Hamiltonian operator paths.

Proof. We identify the symplectic form in balanced coordinates and check free-wave preservation. We then show that compact Young perturbations remain compact at the endpoint. Translation to spatial infinity gives the required norm lower bound, including finite products.

Step 1. We identify the form and its preservation by the free group. The balanced map $C_{\mathrm{bal}}(u,v) = (\Lambda^{1/2}u, \Lambda^{-1/2}v)$ is an onto real isometry to $L^2 \times L^2$. Define $J_{\mathrm{symp}}(q,p) = (p,-q)$ and $J_E = C_{\mathrm{bal}}^{-1} J_{\mathrm{symp}} C_{\mathrm{bal}}$. This gives all stated operator properties and $J_E(f,g) = (\Lambda^{-1}g, -\Lambda f)$. The two displayed dualities follow from the balanced L^2 pairing. No L^2 pairing of a general distributional velocity is taken.

In balanced Fourier coordinates, the free matrix is

$$W_t(\xi) = \begin{pmatrix} \cos(tk) & \langle\xi\rangle \sin(tk)/k \\ -k\sin(tk)/\langle\xi\rangle & \cos(tk) \end{pmatrix}, \qquad k = |\xi|.$$

At zero it is $\left(\begin{smallmatrix} 1 & t \\ 0 & 1 \end{smallmatrix}\right)$, by the continuous sine quotient. Direct matrix multiplication gives $W_t^{\mathsf{T}} J_{\mathrm{symp}} W_t = J_{\mathrm{symp}}$, since its determinant is $\cos^2(tk) + \sin^2(tk) = 1$, also at zero. The entries are real, even and bounded on finite time horizons. Integrating the identity against real-phase Fourier vectors with Hermitian symmetry is legitimate by L^2 Cauchy–Schwarz. It gives $\omega(S_E(t)z, S_E(t)w) = \omega(z,w)$ on all E. Equivalently one may first use Schwartz phases and then density. No rough generator derivative or frequency-zero trace is used.

Step 2. We verify force skewness and compactness of Young endpoint differences. Finally, $\|bu\|_{H^{-1/2}} \leq \|bu\|_2 \leq \|b\|_\infty \|u\|_{H^{1/2}}$. Duality for these L^2 functions gives the absolutely integrable cancellation $-\int fbu + \int ubf = 0$. This is skewness for ω, not for the E Hilbert inner product. The Young construction of Proposition 6.2.4 applies on $\mathcal{L}(E)$: its proof uses completeness and operator multiplication of norm one, exactly as on $\mathcal{L}(F)$. For fixed s,t, each left Young sum

$$\sum_j \Big(X(t_{j+1}) - X(t_j)\Big) U_X(t_j, s)$$

is compact. The sums converge in operator norm to $U_X(t,s) - I$, so closedness of the compact ideal gives the first assertion in (10.1.2). Bounded composition then shows that the physical endpoint differs from $S_E(t-s)$ by a compact operator.

Step 3. We bound the norm of a compact perturbation by the free norm. We prove the required compact-perturbation bound for this whole-space phase. Translations τ_y on both entries are isometries on E and commute with $S_E(h)$. For fixed $z, w \in E$, their translated pairing is the Fourier transform of an L^1 function: the two weighted Fourier products are integrable by Cauchy–Schwarz in the Bessel norms. Approximation of that function in L^1 by compact smooth functions, followed by integration by parts for the approximants, proves $\langle \tau_y z, w\rangle_E \to 0$ as $|y| \to \infty$. Thus, $\tau_y z$ tends weakly to zero. For compact K, $\|K\tau_y z\| \to 0$: otherwise compactness supplies a norm-convergent subsequence with nonzero norm, while bounded linear testing makes its limit zero. For unit z it follows that

$$\|S_E(h) + K\| \geq \liminf_{|y|\to\infty} \|(S_E(h) + K)\tau_y z\| \geq \|S_E(h)z\|.$$

Since translations commute with the free group and preserve the norm, $\|S_E(h)\tau_y z\| = \|S_E(h)z\|$. The compact term tends to zero on this weakly vanishing family. The reverse triangle inequality therefore gives the second inequality in the display for each fixed unit vector, before the supremum over vectors is taken. Taking the supremum over z gives $\|S_E(h) + K\| \geq \|S_E(h)\|$. The isometric velocity reversal $\mathcal{R}(u,v) = (u,-v)$ satisfies $S_E(-h) = \mathcal{R}S_E(h)\mathcal{R}$ by the full free Fourier matrix. The group law yields $1 \leq \|S_E(-h)\|\|S_E(h)\| = \|S_E(h)\|^2$. This proves (10.1.2).

Step 4. We retain the compact difference through finite ordered products. Finally, $P_j - S_E(\ell_j)$ is compact. Telescoping the finite ordered product against its free product gives a finite sum of bounded–compact–bounded products, hence a compact difference. Only the free factors are combined by the group law; no noisy factors are commuted. The same translation argument proves (10.1.3). A zero length gives $P_j = I$. All assertions are at fixed finite horizons and products; no uniform compact approximation in a radius, horizon or number of factors is asserted. This proves Lemma 10.1.1. □

Lemma 10.1.2 (Covariance means and source primitives)**.** *The expectations in* (10.1.1) *are Bochner defined and*

$$\|D_\Phi^\rho - D_\Phi\|_{C^\theta} \leq \|\Phi\|_{H_W}\|M^\rho - M\|_{L^2C^\theta} \longrightarrow 0. \tag{10.1.4}$$

For each positive ρ, there is a deterministic real time-continuous, spatially smooth h_Φ^ρ such that

$$D_\Phi^\rho(t) = \int_0^t S_E(-r)B(m_R h_\Phi^\rho(r))S_E(r)\,\mathrm{d}r. \tag{10.1.5}$$

This is the statewise primitive and defines a Lipschitz operator path. The combined source coefficient is $b^\rho = m_R(cY^\rho + h_\Phi^\rho)$.

Proof. We bound the Bochner covariance means by path moments. At positive source widths, the feature representation gives a smooth deterministic coefficient, whose ordinary rows identify the covariance primitive.

Step 1. We bound the covariance mean and its source error. Use (5.2.13) for $M^\rho \to M$ in L^2C^θ, and (5.2.4) with $C = 1$ from (5.2.12) for $\|M^\rho\|_{L^2C^\theta} \le \|M\|_{L^2C^\theta}$. Separable Gaussian path moments give $\mathbb{E}\|ZM\|_{C^\theta} \le \|\Phi\|_{H_W}\|M\|_{L^2C^\theta}$, and the same holds for sources. Bochner Cauchy–Schwarz gives (10.1.4). Covariance contraction also gives the uniform source bound $\|D^\rho_\Phi\|_{C^\theta} \le \|\Phi\|_{H_W}\|M\|_{L^2C^\theta}$.

Step 2. We identify the regularized deterministic coefficient. The construction preserving the given noise has an isometry $j_{\mathrm{src}} : H_W \to \mathcal{G}$ and an isonormal process $\mathcal{I}$ with $\mathcal{I}(j_{\mathrm{src}}h) = W(h)$. Its source random field is $Y^\rho(t,x) = \mathcal{I}(v_{\rho;t,x})$, with continuous $\mathcal{G}$-valued spatial derivatives at positive widths. Consequently,

$$h^\rho_\Phi(t,x) = \mathbb{E}[W(\Phi)Y^\rho(t,x)] = \langle j_{\mathrm{src}}\Phi, v_{\rho;t,x}\rangle_{\mathcal{G}}$$

has the claimed regularity. Bounded linear testing commutes with those derivatives. After multiplication by m_R the coefficient has one compact support and bounded derivatives on $[0,T]$.

Step 3. We identify its ordinary primitive with the source covariance mean. Proposition 5.2.7 identifies M^ρ with the ordinary source primitive; the approximation here extends smooth time tests to the indicator wave tests in (5.2.5), with both limits taken in the original covariance completion. On Schwartz states, the row of the right side of (10.1.5) is the integral of h^ρ_Φ against the explicit masked source wave product. Ordinary Fubini is justified by $\mathbb{E}|ZY^\rho(t,x)| \le \|\Phi\|_{H_W}\sqrt{\mathbb{E}|Y^\rho(t,x)|^2}$ and bounded point variance on this fixed compact set at positive widths. The source test and indicator approximation extends this to the completed rows by Gaussian Cauchy–Schwarz and covariance contraction. Hence, this row is the row of $\mathbb{E}[ZM^\rho(t)]$. Countable dense states and rational times, then continuity, identify the operator path. The uniformly bounded integrand gives its Lipschitz bound. This identifies the combined source coefficient exactly. The combined source is generally noncentered and the mask occurs once. This proves Lemma 10.1.2. □

Proposition 10.1.3 (Source conservation)**.** *At each fixed positive ρ, on one probability-one set for the fixed c, Φ, R, T, the physical source flow satisfies*

$$P_{D^\rho}(t,s)^* J_E P_{D^\rho}(t,s) = J_E, \qquad 0 \le s \le t \le T.$$

Proof. Intersect the source coefficient regularity event with the event identifying its first primitive with the ordinary primitive for all times and states. The source construction supplies both at this fixed ρ. On their intersection b^ρ has a common compact support, is continuous in supremum norm and is uniformly bounded on $[0,T]$. Thus, $C_b(r) = S_E(-r)B(b^\rho(r))S_E(r)$ is uniformly bounded and strongly continuous on states. Lemma 10.1.1 gives $\omega(C_b(r)z,w) + \omega(z,C_b(r)w) = 0$ for all r,z,w.

Free preservation transfers the force identity to its interaction conjugate: applying $S_E(r)$ to both arguments turns the two terms with $C_b(r)$ into the two skew-force terms with $B(b^\rho(r))$. Their sum is zero. This uses the symplectic form, not skew-adjointness in the phase Hilbert norm. The source and mean primitive identities identify the Young

state equation with $U(t,s)e = e + \int_s^t C_b(r)U(r,s)e\,\mathrm{d}r$. Indeed, replace each operator path increment in a Young sum by its statewise integral. The error is bounded by the uniform coefficient bound times the uniform continuity error of U on the partition. Each state trajectory is therefore C^1, with derivative $C_b(t)U(t,s)e$, by the strong-integral difference quotient. Differentiating the bounded bilinear form $\omega(U(t,s)e, U(t,s)f)$ gives zero. This holds on the same path set for all states and time pairs, since the bounded ordinary evolution is defined there on all E. Free conjugation gives the displayed physical identity. No uncountable intersection of state-dependent null sets or derivative of the free generator on a rough state was used. This proves Proposition 10.1.3. □

Proposition 10.1.3 concerns the regularized flow P_{D^ρ} at a fixed positive ρ. We now prove the same conservation identity for the flow P_D itself, together with a lower bound on its norm.

Proposition 10.1.4 (Conservation, inverse and a lower norm bound)**.** *For the fixed parameters in* (10.1.1)*, on one probability-one set,*

$$P_D(t,s)^* J_E P_D(t,s) = J_E, \qquad \|P_D(t,s)\| \geq 1, \qquad 0 \leq s \leq t \leq T. \tag{10.1.6}$$

The flow is invertible. For $c = 0$ these assertions are deterministic for every fixed Φ.

Proof. We first show that every driver increment satisfies the same closed linear symplectic constraint. We pass that constraint to the Gaussian path and its covariance mean, then prove conservation by summing Young remainder estimates. Invertibility comes separately from the Young construction.

Step 1. We identify the closed constraint for the coefficient paths. We first identify a closed real linear constraint on the operator path. Write

$$\mathfrak{g}_J = \{A \in \mathcal{L}(E) : A^* J_E + J_E A = 0\}.$$

The coefficient $H_{j,R}$ in (5.1.6) is real and smooth. Free conservation gives $S_E(-r)^* J_E = J_E S_E(r)$ and $J_E S_E(-r) = S_E(r)^* J_E$. Lemma 10.1.1 therefore makes $S_E(-r)B(H_{j,R}(r))S_E(r)$ belong to $\mathfrak{g}_J$. Testing the statewise integral in (5.1.8) against two states shows $A_j(0,t) \in \mathfrak{g}_J$ for every j, t. No operator-norm derivative of the free group is taken. The real finite sums in (5.1.2) obey the same constraint. The map $A \mapsto A^* J_E + J_E A$ is bounded on the path space, so their L^2C^θ limit M obeys it at all times on one probability-one path set.

Step 2. We pass the constraint to the combined driver. The mean is a Bochner expectation since $\mathbb{E}\|W(\Phi)M\|_{C^\theta} \leq \|\Phi\|_{H_W}\|M\|_{L^2C^\theta} < \infty$. Bounded real linear maps commute with this expectation, hence $D_\Phi(t) \in \mathfrak{g}_J$ for every t. Thus, $D = cM + D_\Phi$ starts at zero and is a C^θ path in $\mathfrak{g}_J$ on that path set. Complex Gaussian coefficients are not used. All these variables remain on the given W.

Step 3. We prove conservation from the Young increment expansion. The proof of Proposition 6.2.4 applies on $\mathcal{L}(E)$, with multiplication of norm one. Fix any s and put $V(r) = U_D(r,s)$ for $r \geq s$. The Young remainder on $[u,v] \subset [s,T]$ gives

$$V(v) - V(u) = D_{u,v}V(u) + R_{u,v}, \qquad \|R_{u,v}\| \leq C|v-u|^{2\theta}.$$

The exact increment of V^*J_EV has first-order term $V(u)^*(D_{u,v}^*J_E + J_ED_{u,v})V(u) = 0$. Its remaining terms have norm at most $C'|v-u|^{2\theta}$, using the bounded C^θ norm of V. Their sum on a partition is at most $C'(t-s)\,\mathrm{mesh}^{2\theta-1}$, which tends to zero. Therefore, $U_D(t,s)^*J_EU_D(t,s) = J_E$. This deterministic argument applies to every time pair on the same operator path; it requires no state-dependent null sets. Free conservation in Lemma 10.1.1 gives (10.1.6), including $1 = \|J_E\| \le \|P_D(t,s)\|^2$.

Step 4. We retain the independent justification of invertibility. Invertibility comes from the local Young Neumann pieces and their finite products, followed by the free inverse; it is not inferred from conservation in infinite dimension. For $c = 0$ the path and the argument are deterministic for each Φ. Zero covariance gives the free flow directly. At each fixed δ one may take the given reference $W \circ T_{\delta,0}$, $R = \delta^{-1} + 2$, $T = \delta^{-1}$, $c = g_\delta$ and $\Phi = 0$. No uniform-radius or uniform bound for controls assertion follows. This proves Proposition 10.1.4. □

Proposition 10.1.5 (The exact completed block mean)**.** *Use the true partition $B, \delta, N, s_m, \ell_m$ of Section 8.3, with integer $B \ge 1$. Let $i_I : H_I \to H_W$ be the supported closed inclusion and $T_m = T_{\delta,m} : H_{\mathrm{fast}} \to H_W$ the original isometry; H_{fast} has the same original covariance in fast coordinates. For $\Phi \in H_I$ set*

$$W_m(f) = W(T_mf), \qquad \phi_m = \delta^{-a/2}T_m^*i_I\Phi, \qquad \mathcal{T}_E\Phi = i^*T\Phi\, i,$$

where T is the full F mean of Proposition 8.3.5. Define

$$H_{m,E}(\Phi)(u) = \int_0^{\min(u,\ell_m)} S_E(-v)\mathcal{T}_E\Phi(s_m + \delta v)S_E(v)\,\mathrm{d}v. \tag{10.1.7}$$

With $M_m = M_R(W_m)$ and $D_{\phi_m}(u) = \mathbb{E}[M_m(u)W_m(\phi_m)]$, one has

$$D_{\phi_m}(\min(u,\ell_m)) = H_{m,E}(\Phi)(u), \qquad 0 \le u \le B. \tag{10.1.8}$$

Consequently, the pure-mean endpoint obeys

$$\|S_E(\ell_m)U_{H_{m,E}(\Phi)}(\ell_m,0)\| \ge 1.$$

Proof. We define the fast covariance direction using the adjoint of the original isometry. We identify the stopped completed mean by bounded compression, then remove the orthogonal complement of the fast first chaos from its covariance pairing.

Step 1. We define the fast control and its completed mean path. The original pullback (7.2.2) has covariance factor $\delta^{a-2}\delta^2\delta^{-a} = 1$, hence respects nulls and extends isometrically from fast to slow original space. Its Hilbert adjoint is a contraction. Thus, $\|\phi_m\| \le \delta^{-a/2}\|\Phi\|$ is finite at fixed δ, without a uniform control-radius assertion. The fast noise remains on the same given W.

The compact-conjugation and primitive estimates are those in Proposition 8.3.7, including (8.3.12), restricted from F to E: compactness gives norm-continuous conjugation and Hölder integration gives exponent $1 - 1/r$. The mean $T\Phi$ has range in closed iE. By

Proposition 8.3.5, bounded compression passes its strong measurability, L^r bound and compact operator values to $\mathcal{T}_E\Phi \in L^r(I;\mathcal{K}(E))$. Choose the full parameter choices (8.3.8). Its intervals are nonempty because $\theta < 1 - a/2$ and $\theta > 1/2$; p only instantiates that package here. The compact-conjugation argument makes (10.1.7) a Bochner integral, and the L^r primitive estimate gives C^θ, since $1 - 1/r > \theta$. Affine pullback preserves null sets. Its integrand is compact valued almost everywhere; closedness of $\mathcal{K}(E)$ under Bochner integration makes $H_{m,E}(\Phi)$ a compact-valued path starting at zero, also after constant stopping.

Step 2. We compute the unscaled covariance by compressing the full phase. Here $A_{F,m}$ is the full F interaction operator path from Proposition 6.2.2, and $H_{m,F}$ is its stopped completed mean primitive in (8.3.9). The completed identity (8.3.9) at original projection rank zero gives, for $0 \le u \le \ell_m$,

$$\mathbb{E}[g_\delta A_{F,m}(u)W(i_I\Phi)] = \sqrt{\delta}\, H_{m,F}(\Phi)(u).$$

Compress through i using the operator path intertwining, $S_F i = iS_E$, and the mean range in iE preserved by S_F. Bochner expectation commutes with this bounded compression. The constant columns are retained in the full F operator path and mean until this compression; they are inactive only on the iE inputs. Since $g_\delta\delta^{a/2} = \sqrt{\delta}$ and $g_\delta > 0$, division gives the unscaled covariance

$$\mathbb{E}[M_m(u)W(i_I\Phi)] = \delta^{a/2}H_{m,E}(\Phi)(u), \qquad u \le \ell_m. \tag{10.1.9}$$

The factor here is $\delta^{a/2}$, not $\sqrt{\delta}$. Completion in the earlier covariance identity permits every $\Phi \in H_I$, without positivity or smoothness.

Step 3. We identify the covariance direction in the fast noise space. The operator $T_mT_m^*$ is the orthogonal projection onto the original isometry's closed range. Thus, $W((I - T_mT_m^*)i_I\Phi)$ is orthogonal to the entire fast first chaos. Every continuous linear coordinate of M_m is an L^2 limit of finite W_m-basis sums. Its covariance with this difference vanishes. Bochner covariance exists by L^2 path moments, and bounded linear functionals separate its values. Hence,

$$\mathbb{E}[M_m(u)W(i_I\Phi)] = \mathbb{E}[M_m(u)W_m(T_m^*i_I\Phi)].$$

Multiply by $\delta^{-a/2}$ and use (10.1.9) to obtain (10.1.8) on $[0,\ell_m]$, then stop both sides. No unstopped equality beyond ℓ_m is asserted.

Step 4. We apply the compact endpoint lower bound. Apply Lemma 10.1.1 directly to the compact-valued path $H_{m,E}(\Phi)$ starting at zero on $[0,B]$. Its physical endpoint has norm at least $\|S_E(\ell_m)\| \ge 1$. If $\ell_m = 0$, the endpoint is the identity and its norm is one. The radius may be chosen $\delta^{-1} + 2$ after fixing δ; all identities are fixed-parameter instances. This proves Proposition 10.1.5. □

For zero covariance the operator paths and covariance means vanish, and the claims reduce directly to the free identity in Lemma 10.1.1. These results give a lower bound on the operator norm and its exact completed mean application. They provide no uniform bound on the control radius, stochastic moment upper bound or nonlinear product ratio by themselves.

10.2 Gaussian enlargement and the Rayleigh comparison

We first state the Gaussian geometry with its exact covariance scale. Let H be real separable Hilbert, W its given isonormal process, and X a strongly measurable centered Gaussian variable in a real separable Banach space $\mathscr{B}$, with $\mathbb{E}\|X\|^2 < \infty$. Assume every continuous linear coordinate has the form $\ell(X) = W(k_\ell)$, $k_\ell \in H$. Fix $0 < \delta < 1$ and write

$$Ch = \mathbb{E}[XW(h)] = \sqrt{\delta}\,\mathcal{M}_\delta h, \qquad H_{\mathrm{seen}} = \overline{\mathrm{span}\{k_\ell\}}, \qquad E_0 = \overline{C(H)}. \tag{10.2.1}$$

Assume $\mathcal{M}_\delta : H \to \mathscr{B}$ is compact. All Hilbert balls below are closed.

10.2.1 The Wiener-space realization

The Gaussian isoperimetric theorem that we import in Section 10.2.2 is stated for an abstract Wiener space. We first show that the law of X on E_0 is of this kind, and we identify its Cameron space.

Proposition 10.2.1 (First Wiener chaos realization on the support)**.** *The variable X lies in E_0 almost surely, with a centered Radon Gaussian law of full support there. Its Cameron space and norm are*

$$H_{\mathrm{CM}} = C(H_{\mathrm{seen}}), \qquad \|Ch\|_{\mathrm{CM}} = \|P_{\mathrm{seen}}h\|_H. \tag{10.2.2}$$

This support triple is an abstract Wiener realization, including the measurable-norm condition.

Proof. We reconstruct the Gaussian variable from its finite original-noise coordinates. We identify its Cameron image and support, and then verify the measurable-norm condition required by the imported abstract Wiener theorem.

Step 1. We recover the variable from finite Gaussian regressions. The zero law has $C = 0$ and $E_0 = \{0\}$ and is immediate. A countable norming family exists in $\mathscr{B}^*$: choose a dense sequence on the unit sphere and apply Hahn–Banach at each point. Approximation gives $\|x\| = \sup_j |\ell_j(x)|$. Norms of differences from a countable dense set show that these coordinates generate the Borel sets. Consequently, X is measurable in the completion of $\sigma(W(H))$. Fix an orthonormal basis (e_j) of H and set $\mathcal{G}_j = \sigma(W(e_1), \dots, W(e_j))$. In finite dimension these sums and projections stabilize at the dimension. Bochner conditional expectations need no Radon–Nikodym property here: define them first on finite-valued simple variables using scalar conditional expectations, then extend by the L^2 norm contraction. Simple approximation supplies their scalar testing identities. Gaussian regression and the countable norming family give

$$X_j = \mathbb{E}[X \mid \mathcal{G}_j] = \sum_{l \le j} W(e_l) C e_l, \qquad X_j \longrightarrow X \quad \text{in } L^2(\mathscr{B}). \tag{10.2.3}$$

To justify convergence, finite-coordinate scalar events approximate all events in the generated sigma field: the class of events whose indicators are approximable in L^2 is a monotone class containing the finite-coordinate algebra. Approximate a Bochner variable by simple variables and use the conditional L^2 contraction.

Step 2. We identify the Cameron image and the closed support space. Bounded testing gives $\ell(Ch) = \langle k_\ell, h\rangle$. Thus, $\ker C = H_{\text{seen}}^{\perp}$, and C is injective on H_{seen}. The closed first Wiener chaos generated by X is exactly $W(H_{\text{seen}})$. Its covariance image therefore has the first Wiener chaos norm in (10.2.2); unused directions are removed by the orthogonal projection, without an inverse covariance. This is the Cameron image under the first Wiener chaos definition. The finite sums in (10.2.3) lie in E_0, so L^2 convergence and an almost-sure subsequence put X in that closed space almost surely. Functionals on E_0 extend to $\mathscr{B}$ by Hahn–Banach, so restriction preserves the scalar laws and first chaos.

Step 3. We prove the Radon and full-support assertions. Its law is tight. For each radius 2^{-j} choose a finite union of balls of mass greater than $1 - \varepsilon 2^{-j-1}$, using a countable cover of the separable space. The intersection of the corresponding finite closed unions is closed and totally bounded and has mass at least $1 - \varepsilon$. Completeness makes it compact. Metric Borel regularity on these compact sets, followed by tightness, gives a Radon law. To prove full support, the tail $X - X_j$ is independent of the finite Gaussian sum: every tail coordinate has label $(I - P_j)k_\ell$, orthogonal to $e_1, \dots, e_j$. Joint Gaussianity and countable Borel coordinates give Banach tail independence. Given h and $\varepsilon > 0$, choose j with $\|CP_j h - Ch\| < \varepsilon/3$ and $\mathbb{P}(\|X - X_j\| < \varepsilon/3) > 0$. The finite sum has positive probability in every ball about $CP_j h$, even if its covariance is singular: the preimage under its finite linear map contains an open ball about the coefficient vector of $P_j h$. Independence proves positivity of every ball about Ch. Closure proves that the support is all of E_0.

Step 4. We verify the finite-dimensional tail criterion for the measurable norm. We check the measurable norm explicitly. In H_{seen} put $V_j = \operatorname{span}\{P_{\text{seen}} e_l : l \le j\}$. Any finite orthonormal family (h_k) in $V_j^{\perp}$ is also orthogonal to $e_1, \dots, e_j$. The same regression and Bochner Jensen argument gives

$$\mathbb{E}[X - X_j \mid W(h_k),\ \text{all } k] = \sum_k W(h_k) C h_k, \qquad \mathbb{E}\left\| \sum_k W(h_k) C h_k \right\|^2 \le \mathbb{E}\|X - X_j\|^2.$$

For any $\varepsilon > 0$ choose j so that the right side is less than ε^3. Markov bounds the probability that this finite sum has norm exceeding ε by ε, uniformly over every such finite orthonormal family. Since $C : H_{\text{seen}} \to H_{\text{CM}}$ is isometric, the excluded finite-dimensional Cameron subspace is $C(V_j)$. This is the measurable-norm tail condition for the dense Hilbert image, whose Banach completion is E_0. The characteristic functional of the law is $\mathbb{E}e^{i\ell(X)} = \exp(-\|k_\ell\|_H^2/2)$. These facts give the stated abstract Wiener realization. The zero space has the direct zero-law interpretation. This proves Proposition 10.2.1. □

10.2.2 Closed Gaussian enlargements and the quadratic cost

The Gaussian isoperimetric theorem is due to Borell and, independently, Sudakov–Tsirelson [9, 39]. We use its set-enlargement form from Friz and Hairer [30, Theorem 11.6, p. 190], with footnote 3 on p. 190; p. 191 supplies the following context. For an abstract Wiener space, a Borel A of positive mass and its Cameron unit ball $\mathcal{K}$, it states

$$\mu((A + t\mathcal{K})^c) \le \overline{\Phi}_{\mathrm{N}}(\widehat{a} + t), \qquad \widehat{a} = \Phi_{\mathrm{N}}^{-1}(\mu(A)), \quad t \ge 0.$$

Here Φ_{N} is the standard normal distribution function; the same page gives $\overline{\Phi}_{\mathrm{N}}(y) \le e^{-y^2/2}$ for $y \ge 0$. This theorem is imported, not proved here. It concerns Gaussian input sets, not Gaussianity of a nonlinear wave. We verify Borel measurability of every enlargement we use.

Lemma 10.2.2 (Compact images and attained tube radii)**.** *Suppose the law of X is nonzero and put*

$$b_\delta = 2\mathbb{E}\|X\|, \qquad A_\delta = \{x \in E_0 : \|x\| \le b_\delta\}, \qquad \mathcal{T}_r = A_\delta + \mathcal{M}_\delta(\overline{B}_H(r)).$$

Every $\mathcal{T}_r$ is closed. The extended distance $d_\delta(x) = \inf\{r \ge 0 : x \in \mathcal{T}_r\}$ satisfies

$$\{d_\delta \le r\} = \mathcal{T}_r, \qquad \mathbb{P}(d_\delta(X) > r) \le e^{-r^2/(2\delta)}, \quad r \ge 0. \tag{10.2.4}$$

In particular, d_δ is lower semicontinuous and finite almost surely.

Proof. We first prove that compact control images make the tubes closed. Weak compactness also attains every finite infimal radius. We then apply Gaussian enlargement at the covariance scale fixed in the statement.

Step 1. We prove closedness and attainment of finite radii. A compact map from a separable Hilbert space sends a closed bounded ball to a compact set, including closedness of the image. Indeed, diagonal orthonormal coordinates and Fatou give a weakly convergent subsequence of any bounded sequence, with limit still in the ball. Compactness gives norm-convergent image subsequences, and bounded scalar testing identifies every limit with the image of that weak limit. This proves sequential compactness. Closed A_δ plus a compact image is closed: along a converging sequence of sums, extract the compact component and pass the residual into the closed base set.

Membership in $\mathcal{T}_r$ implies $d_\delta \le r$. Conversely, if $d_\delta(x) \le r$, choose h_j with $\|h_j\| \le r + 1/j$ and $x - \mathcal{M}_\delta h_j \in A_\delta$. A weak subsequence has limit h of norm at most r; compactness gives $\mathcal{M}_\delta h_j \to \mathcal{M}_\delta h$. Closedness of the residual proves membership in $\mathcal{T}_r$. This also covers $r = 0$ and proves least finite-radius attainment. Closed sublevels give lower semicontinuity and Borel measurability.

Step 2. We use the exact Cameron scale in the enlargement inequality. The nonzero law has $b_\delta > 0$, and Markov gives $\mu(A_\delta) \ge 1/2$. Projection onto H_{seen} removes all unused directions in the original covariance space, so (10.2.2) gives the exact set identities

$$\mathcal{K} = C(\overline{B}_H(1)) = \sqrt{\delta}\,\mathcal{M}_\delta(\overline{B}_H(1)), \qquad \mathcal{T}_r = A_\delta + (r/\sqrt{\delta})\mathcal{K}.$$

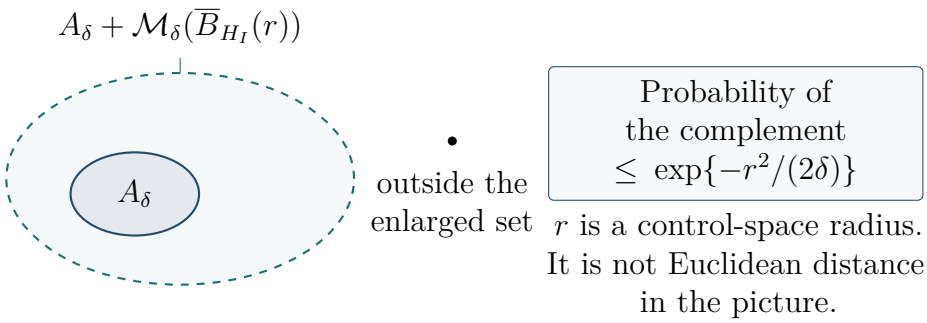

Figure 10.1: A schematic finite-dimensional projection of enlargement for the nonzero Gaussian law in the cited lemma. The map $\mathcal{M}_\delta$ is compact, so the image of a closed control ball is compact; the set A_δ itself need not be compact. No ambient Lebesgue density or Euclidean distance formula is being assumed. The cost uses one global control norm. See Lemma 10.2.2 and Proposition 10.2.3.

These are Borel enlargements by the preceding closedness. The imported theorem applies to the realization in Proposition 10.2.1. Since $\widehat{a} \geq 0$, it yields (10.2.4). The value $\widehat{a} = +\infty$ is allowed when $\mu(A_\delta) = 1$. The tail tends to zero, proving almost-sure finiteness. The Cameron embedding does not change the factor one half in the Gaussian cost. This proves Lemma 10.2.2. □

Lemma 10.2.2 bounds the tail of the tube distance $d_\delta(X)$. We now convert this tail bound into a bound for $\mathbb{E}e^{F(X)/\delta}$, for a functional F that satisfies $F \leq G(r)$ on each tube $\mathcal{T}_r$.

Lean supplied

Proposition 10.2.3 (Comparison with the Rayleigh integral, including jumps and zero law)**.** *Let $F : E_0 \to \mathbb{R}$ be Borel and let $G : [0,\infty) \to \mathbb{R}$ be Borel and nondecreasing. If $F(x) \leq G(r)$ for every $x \in \mathcal{T}_r$ and every $r \geq 0$, then*

$$\mathbb{E}e^{F(X)/\delta} \leq \int_0^\infty \frac{r}{\delta} \exp\left(\frac{G(r) - r^2/2}{\delta}\right) \mathrm{d}r. \tag{10.2.5}$$

For zero law use $E_0 = \{0\}$, $C = \mathcal{M}_\delta = 0$; the same conclusion holds when $F(0) \leq G(0)$.

Proof. We compare upper-level probabilities with those of the scalar Rayleigh law, treating both open and closed endpoints. Layer cake then gives the exponential integral bound, with attained radius removing the need for a measurable control choice.

The auxiliary Rayleigh variable $\mathcal{R}_\delta$ with density $(r/\delta)e^{-r^2/(2\delta)}$, $r > 0$, has mass one and survival function $e^{-r^2/(2\delta)}$ by direct integration. It is a scalar stochastic dominator, not a norm of a Gaussian variable in the covariance Hilbert space. For every level $t \geq 0$, the upper level set of $e^{G(r)/\delta}$ is an upper interval, possibly empty or the whole halfline. An open endpoint is controlled by (10.2.4). At a positive closed endpoint c, let $s \uparrow c$:

$$\mathbb{P}(d_\delta(X) \geq c) = \lim_{s \uparrow c} \mathbb{P}(d_\delta(X) > s) \leq e^{-c^2/(2\delta)} = \mathbb{P}(\mathcal{R}_\delta \geq c).$$

Rayleigh has no atoms, and at the closed endpoint zero both probability bounds are one. On the null event $\{d_\delta(X) = \infty\}$ define $e^{G(d_\delta(X))/\delta}$ to be one. No value of G at infinity is needed and no expectation changes. Layer cake and Tonelli therefore order the expectations of $e^{G(d_\delta(X))/\delta}$ and $e^{G(\mathcal{R}_\delta)/\delta}$, even when G jumps or expectations are infinite. Least-radius attainment gives $F(X) \le G(d_\delta(X))$ almost surely. No measurable selection of a control or residual is needed. This proves (10.2.5). For zero law, $X = 0$ and $F(0) \le G(0) \le G(r)$; normalization of the Rayleigh density proves the claim directly. In particular, $F(0)$ need not be zero. This proves Proposition 10.2.3. □

10.2.3 The wave tuple and its globally defined endpoint

Retain all original covariances and amplitudes. Use the exponents and fixed even Q in (9.2.1)–(9.2.2); put $\nu = 1/\theta$ and choose $(1-\theta)^{-1} < r_t < 2/a$, $\nu \le p < 2 < r_t$. All these intervals are nonempty by the strict subcritical assumptions. Fix integer $B \ge 1$ and the true partition δ, N, s_m, ℓ_m from Section 8.3. Set $L_\delta = \delta^{-1}$ and eventually $R_\delta = L_\delta + 2$. On the same given slow W define the full, unprojected input

$$W_m(f) = W(T_{\delta,m} f), \qquad X_m(u) = g_\delta M_R(W_m)(\min(u, \ell_m)), \qquad g_\delta = \delta^{(1-a)/2}. \tag{10.2.6}$$

Write $P^R_{\delta,E}$ for the physical E flow driven by $g_\delta M_R(W \circ T_{\delta,0})$ on the global fast horizon $[0, L_\delta]$. Let $\mathscr{B}_\delta$ be the finite product of little $C^\theta([0,B]; \mathcal{K}(E))$ spaces of paths starting at zero, with exact norm

$$\|x\|_{\delta,p} = \left(\delta \sum_{m=0}^{N} \|x_m\|^p_{C^\theta} \right)^{1/p}.$$

Proposition 10.2.4 (Eligibility of the E law)**.** *The tuple $X_\delta = (X_m)$ satisfies the preceding Gaussian hypotheses with $H = H_I$ and*

$$(\mathcal{M}_\delta \Phi)_m(u) = \int_0^{\min(u,\ell_m)} S_E(-v) \mathcal{T}_R \Phi(s_m + \delta v) S_E(v) \, \mathrm{d}v, \tag{10.2.7}$$

$$\mathbb{E}[X_\delta W(\Phi)] = \sqrt{\delta}\, \mathcal{M}_\delta \Phi. \tag{10.2.8}$$

Its support is $E_{0,\delta} = \overline{C_\delta(H_I)} \subset \mathscr{B}_\delta$, where $C_\delta \Phi = \mathbb{E}[X_\delta W(\Phi)] = \sqrt{\delta}\, \mathcal{M}_\delta \Phi$. The map $\mathcal{M}_\delta$ is compact at each fixed radius and parameters. At $R = R_\delta$,

$$b_\delta = 2\mathbb{E}\|X_\delta\|_{\delta,p} \le C_{Q,B,p} \delta^{(1-a)/2 - d/Q} \longrightarrow 0. \tag{10.2.9}$$

Proof. We check the separable Gaussian tuple and compact completed mean at fixed parameters. We then identify its covariance on the supported original Hilbert space and apply the explicit radius moment bound to its typical norm.

Step 1. We check the measurable Gaussian state space. Compact operators on separable Hilbert E form a separable operator-norm space: finite-rank rational matrices in an orthonormal basis are dense. Polygonal paths give separability of the little Hölder closure. The construction is a C^θ limit of Lipschitz finite coefficient paths starting at zero; stopping at ℓ_m and extending constantly preserves this space and gives zero for

an empty final interval. Gaussian transfer retains the given W for all finitely many blocks. Every finite collection of linear statistics is an L^2 limit of joint first Wiener chaos Gaussians, hence jointly centered Gaussian. The finite tuple has finite L^2 norm by the fixed-parameter path moments in Corollary 9.2.4. The original Hilbert space H_I is separable by Lemma 8.3.3. No separability of all $\mathcal{L}(E)$ or full C^θ is claimed.

Step 2. We prove compactness of the fixed-parameter mean map. The E mean field $\mathcal{T}_R$ is the compression of Proposition 8.3.5; it is compact into $L^{r_t}(I;\mathcal{K}(E))$ at fixed R. Proposition 9.1.4 gives $\|\mathcal{T}_R\| \le C_{\mathrm{mean}} = M_0\|C_t\|$ independently of $R \ge 1$. Compact conjugation, affine time pullback and $1-1/r_t > \theta$ make the primitive in (10.2.7) bounded from that field space to $\mathscr{B}_\delta$, with constant stopping. Composition proves compactness of $\mathcal{M}_\delta$. There is no uniform-radius compactness assertion.

Step 3. We identify the supported covariance and typical radius. The rank-zero identity (8.3.9), compressed to E as in Proposition 10.1.5, gives (10.2.8). Its scale is exactly $g_\delta\delta^{a/2} = \sqrt{\delta}$. Every stopped row's slow pullback lies in H_I by the inside-I endpoint approximation of Lemma 8.3.6. Countable matrix coordinates and rational times identify the tuple in the closed first Wiener chaos $W(H_I)$, so every linear statistic has its label there. Equivalently, apply that lemma at $J = 0$ on F and compose any E-tuple statistic with the bounded E-compression. This is same-W covariance, without a block-independence assumption or a time-indicator multiplier on the covariance space. Proposition 10.2.1 therefore applies to this exact law on its support. Finally, Proposition 9.2.5, with zero residual projection, gives (10.2.9). The third fixed-Q condition $Q > 2d/(1-a)$ makes this exponent positive; the first two supply the path moments and chaining. Fast directions used for the symplectic baseline do not replace this global H_I action or get summed as separate costs. Zero covariance gives zero operator paths and means directly. This proves Proposition 10.2.4. □

Lemma 10.2.5 (The endpoint functional)**.** *For every $x \in \mathscr{B}_\delta$ define*

$$P_m(x_m) = S_E(\ell_m)U_{x_m}(\ell_m, 0), \qquad \mathcal{P}_\delta(x) = P_N(x_N)\cdots P_0(x_0),$$
$$F_\delta(x) = 2\delta \log\max(1, \|\mathcal{P}_\delta(x)\|).$$

This is a finite continuous functional on all tuples. For the input it satisfies

$$\mathcal{P}_\delta(X_\delta) = P^R_{\delta,E}(L_\delta, 0), \qquad e^{F_\delta(X_\delta)/\delta} = \|P^R_{\delta,E}(L_\delta, 0)\|^2. \tag{10.2.10}$$

These are almost-sure identities for each fixed admissible δ, R, B, without a simultaneous event over all parameter choices.

Proof. We define the endpoint functional on the entire tuple space, including inputs outside any Gaussian full-measure set. We then use the common-source restart identity and the compact-product lower bound to identify its value on the actual input.

Step 1. We obtain continuity and the deterministic endpoint lower bound. Generic Young evolution is globally defined and locally Lipschitz in every C^θ operator path. Finite products, fixed-time free factors, norm and $\log\max(1,\cdot)$ preserve continuity. Thus, F_δ is

defined even off every Gaussian full-measure set. Every x_m in this ambient space is a compact-valued C^θ path starting at zero. The finite-product assertion of Lemma 10.1.1 gives, for every such tuple,

$$\|\mathcal{P}_\delta(x)\| \geq \Big\| S_E\Big(\sum_{m=0}^{N} \ell_m \Big) \Big\| \geq 1.$$

Step 2. We identify the global endpoint from the coupled local factors. Lemma 7.2.5, in its case without the deterministic mean, applies to this same full input with base physical profile η^2. To check the exact objects, use its single regularized slow noise preserving the given noise and pull it back by $T_{\delta,0}$ and $T_{\delta,m}$. At fixed δ the global fast source random field is $\delta^{a/2} Y^\rho(\delta u, x)$ and its local restriction is its time shift by mB. Their ordinary Duhamel flows have the same massless free groups, amplitude g_δ and mask m_R. Source limits are taken on the fixed finite extended horizon $(N+1)B$ and on each local B before composing the finitely many factors. The original cocycle from that lemma therefore gives the ordered physical F product with the true remainder. The full operator paths and free groups intertwine through the closed isometry $i : E \to F$, including the source limits. Restricting the product and using injectivity of i gives the first identity in (10.2.10). Both fast velocity and displacement remain in each factor. No mask was commuted through a free group, and the time blocks remain correlated on the same W. For zero covariance every input is zero and the ordered factors are $S_E(\ell_m)$, whose product is $S_E(L_\delta)$.

The lower bound already established for every tuple removes the maximum at X_δ. Together with the first identity, this proves the second identity in (10.2.10). No fixed-radius Gaussian-operator rate or source-to-point result is an input to this restart argument. This proves Lemma 10.2.5. □

10.2.4 Uniform coarse envelope and the exact radial integral

To apply Proposition 10.2.3 to the endpoint functional F_δ of Lemma 10.2.5, we need a nondecreasing Borel function that dominates F_δ on every tube. We take the supremum of F_δ over each tube and bound its growth in the radius, uniformly in δ and $R \geq 1$.

Proposition 10.2.6 (Coarse tube envelope and operator moment)**.** *On the support $E_{0,\delta}$ let A_δ be its closed ball of radius b_δ and put*

$$G_\delta(r) = \sup_{\substack{a \in A_\delta \\ \|\Phi\|_{H_I} \leq r}} F_\delta(a + \mathcal{M}_\delta \Phi).$$

This is finite, nondecreasing and Borel. There is $C_{\mathrm{env}} < \infty$, independent of δ and $R \geq 1$, such that

$$G_\delta(r) \leq C_{\mathrm{env}}(1 + b_\delta^\nu + r^\nu), \qquad \mathbb{E}\|P^R_{\delta,E}(L_\delta, 0)\|^2 \leq \int_0^\infty \frac{r}{\delta} e^{(G_\delta(r) - r^2/2)/\delta} \, \mathrm{d}r. \tag{10.2.11}$$

Proof. We first bound the sum of deterministic mean primitive norms. We combine this with the generic Young growth estimate and the exact weighted power means to obtain a finite monotone tube envelope, then apply the Rayleigh comparison.

Step 1. We bound the deterministic mean primitives on the true partition. Put $G_B = \sup_{|v|\le B} \|S_E(v)\|$ and $C_{\mathrm{pr}} = G_B^2[B^{1-1/r_t} + B^{1-1/r_t-\theta}]$. The lower bound $G_B \ge 1$ follows directly from $S_E(0) = I$. Proposition 9.1.5 gives $1 \le G_B \le 3B$, $C_{\mathrm{pr}} \le 18B^{3-1/r_t}$. Its primitive estimate, now without the covariance factor $\sqrt{\delta}$, gives

$$\delta \sum_m h_m^{r_t} \le (C_{\mathrm{pr}} C_{\mathrm{mean}})^{r_t} \|\Phi\|_{H_I}^{r_t}, \qquad h_m = \|(\mathcal{M}_\delta \Phi)_m\|_{C^\theta}. \tag{10.2.12}$$

Indeed, each primitive norm is at most $C_{\mathrm{pr}}\delta^{-1/r_t}\|\mathcal{T}_R\Phi\|_{L^{r_t}(I_m)}$. Raising to r_t cancels the δ weight, and the true partition sums to the full field norm, including an empty cell.

Step 2. We control the endpoint on every tube. The generic Banach Young bound supplies $c_Y = c_Y(B,\theta) > 0$ with $\log\|U_d(u,0)\| \le c_Y(1 + \|d\|_{C^\theta}^\nu)$ for $u \le B$. This follows from (8.4.1) and (6.2.9) by $d \le 1 + d^\nu$ and $(1+d)^\nu \le 2^{\nu-1}(1+d^\nu)$. It applies on $\mathcal{L}(E)$ with multiplication norm one, without Gaussian, positivity or Hamiltonian assumptions on d. For $a \in A_\delta$ put $v_m = \|a_m\|_{C^\theta}$ and $n = N + 1$. Convexity and submultiplicativity give

$$F_\delta(a + \mathcal{M}_\delta\Phi) \le 2\delta n(\log G_B + c_Y) + 2^\nu c_Y \delta \sum_m (v_m^\nu + h_m^\nu).$$

The upper expression is nonnegative, so it also bounds the logarithm with the maximum at one. The exact finite weighted power-mean inequalities are

$$\delta \sum_m v_m^\nu \le (\delta n)^{1-\nu/p}\|a\|_{\delta,p}^\nu,$$

$$\delta \sum_m h_m^\nu \le (\delta n)^{1-\nu/r_t}\left(\delta \sum_m h_m^{r_t}\right)^{\nu/r_t}.$$

They use exponents $p/\nu \ge 1$, $r_t/\nu > 1$ and nonnegative inputs v_m^ν, h_m^ν, followed by positive powers. Zero norms and empty cells cause no negative powers; $\delta > 0$ and $n \ge 2$, including the case $p = \nu$. Since $\delta n \le 2/B$, these bounds and (10.2.12) give $F_\delta(a + \mathcal{M}_\delta\Phi) \le D_0 + D_1 b_\delta^\nu + D_2 r^\nu$, where

$$D_0 = 2(2/B)(\log G_B + c_Y),$$
$$D_1 = 2^\nu c_Y (2/B)^{1-\nu/p},$$
$$D_2 = 2^\nu c_Y (2/B)^{1-\nu/r_t}(C_{\mathrm{pr}} C_{\mathrm{mean}})^\nu.$$

Hence, $C_{\mathrm{env}} = 1 + D_0 + D_1 + D_2$ is independent of δ, R and proves the coarse bound for every admissible δ, not just when b_δ is small. The supremum sets are nonempty and this bound makes their suprema finite. Monotonicity gives Borel measurability without asserting attainment of these suprema. The definition bounds F_δ on every closed tube. Apply Proposition 10.2.3 and (10.2.10) to obtain the operator-moment bound. For zero law its direct case applies, with no assumption that the free endpoint norm is one. This proves Proposition 10.2.6. □

Lean narrower

Lemma 10.2.7 (Exact Rayleigh tail bound)**.** *Suppose G is Borel and $G(r) \le A_0 + Cr^\nu$, $C \ge 0$, $1 < \nu < 2$. If $M > 0$ and $4C \le M^{2-\nu}$, then*

$$\int_M^\infty \frac{r}{\delta} e^{(G(r)-r^2/2)/\delta}\,\mathrm{d}r \le 4e^{(A_0-M^2/4)/\delta}. \tag{10.2.13}$$

In particular, the operator-moment bound in (10.2.11) is finite at fixed parameters.

Proof. The finite scalar cutoff inequality gives, for $r \ge M$, $Cr^\nu - r^2/2 \le -M^2/8 - r^2/8$. Its exact conditions are $M > 0$, $r \ge M$, $C \ge 0$, $1 < \nu < 2$ and $4C \le M^{2-\nu}$. Indeed, $r^{2-\nu} \ge M^{2-\nu} \ge 4C$ gives $Cr^\nu \le r^2/4$, while $r^2 \ge M^2$ splits the remaining $-r^2/4$ into the two displayed negative terms. Analytically, $-\frac{\mathrm{d}}{\mathrm{d}r}[4e^{-r^2/(8\delta)}] = (r/\delta)e^{-r^2/(8\delta)}$. Integrating gives the front factor $4e^{-M^2/(8\delta)}$; multiplication by $e^{(A_0-M^2/8)/\delta}$ proves (10.2.13). Such a cutoff exists since $2 - \nu > 0$. On $[0, M]$ the growth bound gives $G(r) \le A_0 + CM^\nu$, so the integral is finite there as well. Apply this to $A_0 = C_{\mathrm{env}}(1 + b_\delta^\nu)$ and $C = C_{\mathrm{env}}$ in the preceding proposition. No infinite-dimensional Gaussian density is used. This proves Lemma 10.2.7. □

Lean full

Lemma 10.2.8 (Supremum with the Gaussian quadratic cost)**.** *For finite $J : H \to \mathbb{R}$ bounded above on every original ball, let $g_J(r) = \sup_{\|h\|\le r} J(h)$. In the extended reals,*

$$\sup_{r\ge 0}\{g_J(r) - r^2/2\} = \sup_{h\in H}\{J(h) - \|h\|_H^2/2\}.$$

Proof. For the lower inequality take $r = \|h\|$. For the upper inequality, every $\|h\| \le r$ gives $J(h) - r^2/2 \le J(h) - \|h\|^2/2$. Take first the ball supremum and then the radius supremum. Each ball is nonempty with finite supremum, so no infinity-minus-infinity expression occurs. No compactness, rank or density assumption is needed. This proves Lemma 10.2.8. □

The Gaussian comparison retains one half of the squared norm of the single control. The coarse envelope is not the sharp spectral/product envelope. Its application to the original canonical point moment, and the sharp envelope and variational comparison, require their separate proofs.

10.3 Uniform spectral rates and phase products

Retain every original covariance and amplitude. Set $E = H^{1/2} \times H^{-1/2}$, $F = E \oplus \mathbb{R}^2$, and $m_R = \eta(\cdot/R)^2$, $R \ge 1$, with the same fixed cutoff profile. Choose

$$\frac{1}{2} < \theta < \min(1 - a/2, (3 - a - \alpha)/2), \qquad \nu = 1/\theta,$$
$$(1 - \theta)^{-1} < r < 2/a, \qquad \nu \le p < 2 < r.$$

Choose auxiliary exponents $0 < \gamma < \min(1/2, (2 - \alpha)/2)$ and $\theta < \beta < \min(1 - a/2, (3 - a - \alpha)/2)$ for the phase construction. The original strict threshold makes these intervals

nonempty. Write $i_I : H_I \to H_W$ for the supported closed inclusion. For nonzero covariance the field is

$$\mathcal{T}_R = T_R(C_t \otimes I_{H_{\mathrm{sp}}}), \qquad \|\mathcal{T}_R\|_{H_I \to L^r(I;\mathcal{K}(E))} \le C_{\mathrm{mean}} = M_0\|C_t\|,$$

by Proposition 9.1.4. For zero covariance set $H_{\mathrm{sp}} = H_I = \{0\}$ and $M_0 = C_{\mathrm{mean}} = 0$. Means and their rates are then zero, and mean flows are free; no nonzero-noise estimate is needed for that case. The residual comparisons below still act on the nonzero phase E.

10.3.1 The operator class on E and its spectral constants

For real smooth compact q let $V_q = m_R(\Gamma * q)$, $M_q : H^{1/2} \to H^{-1/2}$ be its multiplier and $L_q^E(u,v) = (0, M_q u)$. Let $\mathcal{V}_{E,R}$ be their operator-norm closure in $\mathcal{K}(E)$.

Lemma 10.3.1 (Unique potential and fixed-radius lift)**.** *Each $L \in \mathcal{V}_{E,R}$ has the form $L(u,v) = (0, Mu)$, with $\|L\| = \|M\| =: k$, and determines a unique real $V \in H^{-1/2}$ supported in* $\operatorname{supp} m_R$*. The symmetric pairing satisfies*

$$|v_V(u,w)| \le k\|u\|_{H^{1/2}}\|w\|_{H^{1/2}}. \tag{10.3.1}$$

It has a lift L_F in the exact class of Section 9.3, with $L_F i = iL$. Lift constants may depend on R and are used only for identification. Here $v_V(u,w) = \langle Vu, w\rangle_{H^{-1/2},H^{1/2}}$ on real states, with its Hermitian extension on complex states.

Proof. For zero covariance, $L = M = V = L_F = 0$ gives the claims directly. If $L_n^E \to L$, the zero columns persist and $M_n \to M$ in $\mathcal{L}(H^{1/2}, H^{-1/2})$, with the stated norm equality. At fixed R choose real compact smooth $\chi_R = 1$ near $\operatorname{supp} m_R$. Since $M_n\chi_R = V_n$, $\|V_n - V_j\|_{H^{-1/2}} \le \|\chi_R\|_{H^{1/2}}\|M_n - M_j\|$. Thus, $V_n \to V$, with the same support by testing outside it. Smooth multiplication on $H^{-1/2}$ identifies $Mu = Vu$ on compact tests, then on $H^{1/2}$ by density. The identity $M\chi_R = V$ gives uniqueness; symmetry and (10.3.1) pass to the limit.

The original F operators are $(u, v, c_1, c_2) \mapsto (0, M_n u + c_1 V_n, 0, 0)$. Their differences are bounded by $(1+\|\chi_R\|_{H^{1/2}})\|M_n - M_j\|$. They therefore converge in the old F class and give the lift. This bound is allowed to grow with R; it will enter no uniform estimate. Dense smooth original controls and bounded completion of T_R also show that all completed mean fields lie in $\mathcal{V}_{E,R}$ almost everywhere. Bochner averages preserve this closed linear class. Complexification preserves k by the Hilbert real/imaginary splitting. The real symmetric pairing becomes Hermitian and its diagonal splits into the two real diagonals. This proves Lemma 10.3.1. □

Proposition 10.3.2 (Spectral rate in E)**.** *For $L \in \mathcal{V}_{E,R}$ put*

$$\beta(V) = \inf_{\substack{u \in H^1 \\ \|u\|_2 = 1}} \{\|\nabla u\|_2^2 - v_V(u,u)\}, \qquad \lambda(L) = \sqrt{-\beta(V)}.$$

If $K \ge \max(1,k)$, the physical wave satisfies, for $t \ge 0$,

$$-K^2 \le \beta(V) = \inf \operatorname{spec} H_V \le 0, \qquad \|P_V^E(t)\| \le 8(1+K)^2(1+t)e^{\lambda(L)t}. \tag{10.3.2}$$

If two such operators have norms at most K, then

$$|\beta(V)-\beta(W)|\le (K+2)\|L_V-L_W\|,\qquad |\lambda(L_V)-\lambda(L_W)|\le \sqrt{(K+2)\|L_V-L_W\|}. \tag{10.3.3}$$

Every quantitative constant here uses the E norm alone.

Proof. We derive the form and spectral bounds using only the E multiplier norm. We use the fixed-radius lift only to identify the physical flow. Finally, approximate minimizers give continuity of the spectral rate without assuming an eigenfunction at the bottom.

Step 1. We obtain the closed form with constants measured on E. We derive the bounds without transferring a quantitative F bound. With $b=\|u\|_2$, $z=\|u\|_{H^1}$, Fourier Cauchy–Schwarz gives $\|u\|_{H^{1/2}}^2\le bz$. Equation (10.3.1) and the half-weight arithmetic–geometric mean inequality give $|v_V(u,u)|\le Kbz\le z^2/2+K^2b^2/2$. The weights are $1/2,1/2$, bases $z^2,(Kb)^2\ge 0$; positive powers include zero norms. For $q_V=\|\nabla u\|_2^2-v_V(u,u)$ and $c=2+K^2$,

$$\tfrac12 z^2+(1+K^2/2)b^2\le q_V(u)+cb^2\le \tfrac32 z^2+(1+3K^2/2)b^2\le 3(1+K^2)z^2. \tag{10.3.4}$$

This is a densely defined closed semibounded Hermitian form on full H^1: its shifted norm is equivalent to the complete H^1 norm. The lower bound dominates $2b^2$, since $z\ge b$ and $K\ge 1$. From [44, Theorem 2.14, p. 81, (2.63)] and Theorem 3.6, p. 109, (3.51)–(3.53), it represents a unique self-adjoint H_V with $A=H_V+c\ge 2$ and $D(A^{1/2})=H^1$. Closedness uses the definition on that book's p. 80. The spectral meaning of $A\ge 2$ follows from bounded spectral slices: a nonzero slice below two would give a unit vector in $D(A)$ contradicting the form lower bound. The bottom argument below uses the same representation.

Step 2. We compare the spectral phase with the fixed Sobolev phase. Put $B_0=1-\Delta$ and $L_K=3(1+K^2)$. The common forms obey $\frac12 B_0\le A\le L_KB_0$. For positive self-adjoint $T,S\ge 1$ with ordered forms, completing the square gives

$$\langle f,(T+t)^{-1}f\rangle=\sup_u\{2\,\mathrm{Re}\langle f,u\rangle-q_T(u)-t\|u\|^2\}\ge\langle f,(S+t)^{-1}f\rangle.$$

The identity $\sqrt{x}=\pi^{-1}\int_0^\infty t^{-1/2}x/(x+t)\,\mathrm{d}t$ follows by $t=xv^2$. Positive spectral integration and Tonelli give square-root form order, with domain inclusions, from $I-t(T+t)^{-1}\le I-t(S+t)^{-1}$. Apply this to $(B_0,2A)$ and (A,L_KB_0), both pairs at least one:

$$D(A^{1/4})=H^{1/2},\qquad 2^{-1/4}\|u\|_{H^{1/2}}\le\|A^{1/4}u\|_2\le L_K^{1/4}\|u\|_{H^{1/2}}.$$

Under the L^2 pairing the dual norm is $\|A^{-1/4}v\|_2$, by Cauchy–Schwarz and the equality test $u=A^{-1/2}v$. Completion gives $H^{-1/2}$. Thus, with $M_K=L_K^{1/4}$, the phase norm $\|(u,v)\|_{E_A}^2=\|A^{1/4}u\|_2^2+\|A^{-1/4}v\|_2^2$ lies between $M_K^{-2}\|(u,v)\|_E^2$ and $M_K^2\|(u,v)\|_E^2$. The condition cost is $M_K^2=\sqrt{3(1+K^2)}\le 2(1+K)$.

Step 3. We identify and bound the spectral bottom. For unit L^2 data, $b=1$ and $z\ge 1$. The form bound gives $q_V\ge z^2/2-1-K^2/2\ge -K^2$. A dilated compact unit bump

translated wholly off the potential support has zero potential pairing and kinetic energy tending to zero, so $\beta \le 0$. Complex form infima agree with real ones: dividing each complex diagonal by its squared norm is the convex combination of the two normalized real diagonals, omitting zero parts. The spectral form formulas identify β with the spectral bottom by bounded spectral slices. There are support points because scalar spectral measures of unit vectors have mass one; their arbitrarily small bounded slices give approximate eigenvectors and the reverse form bound. If Σ denotes the closed PVM support and real $z \notin \Sigma$, the Borel function $f_z(h) = (h - z)^{-1}$ on Σ, zero outside, is bounded, as is $hf_z(h)$. Its calculus has range in $D(H_V)$ and supplies both inverse identities for $H_V - z$ on their respective domains. Thus, no such z is spectral; the approximate eigenvectors give the other inclusion. Hence, $\lambda \le K$ and $h + c \ge 2$ on the spectrum.

Step 4. We estimate the spectral wave matrix. Define $\mathrm{Cos}_t(h), \mathrm{Sin}_t(h)$ by $\cos(t\sqrt{h}), \sin(t\sqrt{h})/\sqrt{h}$ for $h > 0$, by $1, t$ at zero and by $\cosh(t\sqrt{-h}), \sinh(t\sqrt{-h})/\sqrt{-h}$ for $h < 0$. In the E_A isometry the matrix is

$$\begin{pmatrix} \mathrm{Cos}_t(h) & \sqrt{h+c}\,\mathrm{Sin}_t(h) \\ -h\,\mathrm{Sin}_t(h)/\sqrt{h+c} & \mathrm{Cos}_t(h) \end{pmatrix}.$$

For $h \ge 0$, its off-diagonals have bounds $1 + \sqrt{c}\,t$ and one; at zero their values are $\sqrt{c}\,t, 0$. For $\beta \le h < 0$, the entries are bounded using $|\,\mathrm{Cos}_t\,| \le e^{\lambda t}$, $|\,\mathrm{Sin}_t\,| \le te^{\lambda t}$, upper off-diagonal at most $\sqrt{c}\,te^{\lambda t}$, and lower at most $Ke^{\lambda t}$. Since $\sqrt{c} \le 2K$, each entry is at most $2(1 + K)(1 + t)e^{\lambda t}$. Set these entries to zero off the closed spectral support before applying bounded Borel calculus. From [44, Theorems 3.1–3.2, pp. 102–104, (3.18)–(3.33)], their matrix norm is at most twice that entry bound, and the condition cost gives (10.3.2). Spectral dominated convergence and scalar addition give the group.

Step 5. We identify the physical wave without importing the lift norm. Denote the spectral matrix evolution by $P_V^E(t)$. It is the physical E wave. The fixed-R lift in Lemma 10.3.1 belongs to the precise class in Proposition 9.3.4. Its form is this same q_V and has the same self-adjoint representative by uniqueness, regardless of the lift's larger shift. On dense bounded spectral cutoffs the two waves have the same $\mathrm{Cos}, \mathrm{Sin}$ functions of H_V. Boundedness extends equality to all E. The old graph-core Duhamel identification therefore applies; no lift norm or χ_R constant entered the bounds above. Conjugation commutes with the real structures, so real restrictions are the phases. For compact L, finite-rank approximation and strong continuity of the free group and its adjoint make $v \mapsto S_E(-v)LS_E(v)$ norm continuous on finite intervals. Its primitive is Lipschitz. Its Young equation is therefore the ordinary bounded-interaction equation by Proposition 6.2.4. This identifies the averaged static baseline without transferring any lift norm into the uniform bounds.

The static baseline is the identity

$$S_E(t)U_H(t,0) = P_V^E(t), \qquad H(u) = \int_0^u S_E(-v)LS_E(v)\,\mathrm{d}v,$$

for the constant multiplier L just considered; a cell average uses this identity with its frozen multiplier.

Step 6. We compare rates by approximate form minimizers. Finally, take a unit ε-minimizer for W, $0 < \varepsilon \le 1$. Since $\beta(W) \le 0$, it has $q_W \le 1$. Thus, $z^2 - 1 - Kz \le 1$, which forces $z \le K + 2$. The multiplier difference changes its form by at most $\|L_V - L_W\|\|u\|^2_{H^{1/2}} \le (K+2)\|L_V - L_W\|$. Take infima, let $\varepsilon \downarrow 0$ and reverse V, W. The square-root inequality on nonnegative $-\beta$ gives (10.3.3). For zero covariance the class is $\{0\}$, $H_V = -\Delta$ and $\beta = \lambda = 0$; the free wave gives the claims directly. This proves Proposition 10.3.2. □

10.3.2 Scalar-time averaging and mean bounds

Proposition 10.3.2 bounds the wave of one fixed operator $L \in \mathcal{V}_{E,R}$ through the rate $\lambda(L)$. The mean field $\mathcal{T}_R\Phi$ depends on the time variable. We now average it over the cells of the partition and bound the resulting change in the integrated rate, uniformly in $R \ge 1$.

Proposition 10.3.3 (Uniform completed-field averaging)**.** *Use the true slow partition I_m with mesh at most δB. Let $\mathcal{A}_\delta$ average over each positive-length cell; an empty final cell is ignored. Put $\omega_\delta = \|(\mathcal{A}_\delta - I)C_t\|_{H_t \to L^r(I)}$. At fixed B, $\omega_\delta \to 0$. For $M \ge 0$, if $\|\Phi\|_{H_I} \le M$, $W_R = \mathcal{T}_R\Phi$, $\overline{W}_R = \mathcal{A}_\delta W_R$ and $Z = C_{\mathrm{mean}}M$, then*

$$\|W_R\|_{L^r},\ \|\overline{W}_R\|_{L^r} \le Z, \qquad \|\overline{W}_R - W_R\|_{L^r} \le M_0 M\omega_\delta =: \Omega_\delta(M), \tag{10.3.5}$$

$$\mathrm{Rate}_R(\Phi) = \int_I \lambda(\mathcal{T}_R\Phi(s))\,\mathrm{d}s, \tag{10.3.6}$$

$$\int_I |\lambda(\overline{W}_R) - \lambda(W_R)|\,\mathrm{d}s \le \sqrt{3 + 2Z}\sqrt{\Omega_\delta(M)} =: \Lambda_\delta(M) \to 0. \tag{10.3.7}$$

These errors are uniform in $R \ge 1$. The rate is finite, nonnegative and continuous on H_I.

Proof. We approximate the scalar time map by cell averages uniformly on its compact image. The dimension-free tensor bound transfers this to the completed operator field. A pointwise rate comparison followed by Cauchy–Schwarz gives the integrated rate error.

Step 1. We obtain uniform scalar-time averaging on the compact image. Bochner averaging is a contraction on $L^r(I; \mathscr{Z})$ for any Banach $\mathscr{Z}$, by Jensen. For continuous fields on $[0,1]$, its error is bounded by the modulus of continuity at the mesh. Simple-field approximation, followed by continuous approximation of scalar indicators in L^r, proves density of those fields. The contraction gives strong convergence for every Bochner field. In the scalar case it is uniform on the compact closure of C_t's unit-ball image, by a finite net and $\|\mathcal{A}_\delta - I\| \le 2$. This proves $\omega_\delta \to 0$.

Step 2. We transfer the estimate to the full mean field. On finite tensors, integration commutes with the fixed bounded T_R:

$$\mathcal{A}_\delta^{\mathcal{K}(E)} T_R(C_t \otimes I)\Phi = T_R((\mathcal{A}_\delta C_t) \otimes I)\Phi.$$

The dimension-free Hilbert tensor bound in Lemma 9.1.3, and $\|T_R\| \le M_0$, extend this identity to the completed H_I. Applying it to the difference gives (10.3.5). Averages

remain in the same closed E operator class. Only scalar-time compactness was used; the tensor map is not claimed compact. Nor does this assert noncompactness of a composite spatial family: each fixed-radius completed mean is compact.

Step 3. We estimate the integrated rate difference. For any two such fields, apply (10.3.3) with the pointwise bound

$$K(s) = \max(1, \|W_1(s)\|, \|W_2(s)\|).$$

The bound $K(s) + 2 \le 3 + \|W_1(s)\| + \|W_2(s)\|$ controls the first factor in the pointwise square-root estimate. Cauchy–Schwarz gives

$$\int_I |\lambda(W_1) - \lambda(W_2)| \le \sqrt{3 + \|W_1\|_{L^1} + \|W_2\|_{L^1}}\, \sqrt{\|W_1 - W_2\|_{L^1}}.$$

Continuity of λ on the class makes these quantities measurable. Since $|I| = 1$, this proves (10.3.7). It also proves rate continuity, while $\lambda(L) \le \max(1, \|L\|)$ gives $\mathrm{Rate}_R(\Phi) \le 1 + C_{\mathrm{mean}}\|\Phi\|$. For zero covariance the fields and rate errors are zero directly. This proves Proposition 10.3.3. □

For the remaining proofs use the full parameter choices and the $B, \delta, N, \ell_m, I_m$ partition of Section 8.3. For $W_R = \mathcal{T}_R\Phi$ define

$$H_m(u) = \int_0^{\min(u,\ell_m)} S_E(-v) W_R(s_m + \delta v) S_E(v)\, \mathrm{d}v, \qquad P_m^{\mathrm{mean}} = S_E(\ell_m) U_{H_m}(\ell_m, 0).$$

Lemma 10.3.4 (Explicit physical primitive and growth bounds)**.** *Write* $G_B = \sup_{|v|\le B} \|S_E(v)\|$ *and* $C_B = G_B^2[B^{1-1/r} + B^{1-1/r-\theta}]$. *Then* $1 \le G_B \le 3B$, $C_B \le 18B^{3-1/r} \le 32B^{3-1/r}$ *and* $C_B B^{1/r} \ge B$. *The stopped primitives lie in the little Hölder space of paths starting at zero and*

$$\|H_m\|_\theta \le a_m := C_B \delta^{-1/r} \|W_R\|_{L^r(I_m)}, \qquad \delta \sum_m a_m^r \le C_B^r \|W_R\|_{L^r}^r. \tag{10.3.8}$$

There is a fixed $C_{\mathrm{gr}} = C_{\mathrm{gr}}(\theta) > 0$ *such that*

$$\log \|S_E(\ell) U_D(\ell, 0)\| \le C_{\mathrm{gr}} B (1 + \|D\|_\theta^\nu), \qquad 0 \le \ell \le B. \tag{10.3.9}$$

Here D *is any* $C^\theta([0, B]; \mathcal{L}(E))$ *path starting at zero; no Gaussian or Hamiltonian hypothesis is imposed on this growth bound. The mean endpoints have* $\|P_m^{\mathrm{mean}}\| \ge 1$.

Proof. We compute the free-group and primitive constants explicitly. We then count short contraction intervals for the generic Young growth bound and use compactness only for the lower bound on mean endpoint norms.

Step 1. We estimate the free group and the physical primitive. The balanced free matrix has upper entry $\langle k\rangle \sin(vk)/k$ and lower $-k \sin(vk)/\langle k\rangle$. Splitting $k \le 1$ and $k \ge 1$ bounds the upper by $\sqrt{2}B$, while the lower and diagonals have bound one. At zero the off-diagonals are $v, 0$. The Frobenius bound gives $G_B \le \sqrt{3 + 2B^2} \le 3B$; $S_E(0) = I$ gives

$G_B \geq 1$. The stated C_B inequalities follow, including $C_B B^{1/r} = G_B^2(B + B^{1-\theta}) \geq B$. Hölder in time with $1 - 1/r > \theta$, the affine time change, compact conjugation and constant stopping prove (10.3.8); the true partition sums the rth powers, with zero on an empty cell.

Step 2. We make the generic Young growth constant independent of radius. For the explicit Young bound put $d = \|D\|_\theta$ and $c_\theta = 2\max(1, C_{\mathrm{Young}})$, as in the local estimate proving Lemma 8.4.1. If $c_\theta d B^\theta \leq 1/4$, whole-interval contraction gives $\log\sup\|U_D\| \leq \log(4/3) < 1/2$. Otherwise at most $2B(4c_\theta d)^\nu$ contraction pieces have norm at most $4/3$. Combine their logarithms with $\log G_B \leq \log(4B)$. For example $C_{\mathrm{gr}} = 4 + \log 4 + 2(4c_\theta)^\nu$ gives (10.3.9), since $B \geq 1$. This is the generic algebra argument on $\mathcal{L}(E)$ with multiplication norm one, not an unspecified radius-dependent bound.

Step 3. We retain the compact endpoint lower bound. Finally, Proposition 9.1.4 gives $W_R \in L^r(I; \mathcal{K}(E))$ for each fixed R, Φ. The compact conjugation and stopped Bochner primitive used above therefore make each H_m a compact-valued C^θ path starting at zero. Lemma 10.1.1 gives $\|P_m^{\mathrm{mean}}\| \geq \|S_E(\ell_m)\| \geq 1$, deterministically for each Φ. This norm bound needs no fast covariance direction or action estimate. An empty endpoint is I; zero covariance gives the free endpoint. This proves Lemma 10.3.4. □

10.3.3 Full blocks, the true last cell and polynomial control balls

Proposition 10.3.5 (Finite-mesh physical mean-product bound)**.** *Fix B as above, $M \geq 0$ and $K \geq 1$, and put $Z = C_{\mathrm{mean}} M$. Uniformly for $R \geq 1$, $\|\Phi\| \leq M$,*

$$\delta \sum_{m=0}^{N} \log\|P_m^{\mathrm{mean}}\| - \mathrm{Rate}_R(\Phi) \leq \frac{L_{B,K}}{B} + C_{\mathrm{gr}} 32^r Z^r B^{3r}(K^{-r} + K^{\nu-r}) + \Lambda_\delta(M) + C(\theta, B, K)E_\delta + \mathrm{Last}_\delta, \tag{10.3.10}$$

where $L_{B,K} = \log 16 + 4\log(1+K) + 3\log(1+B)$ and

$$E_\delta = (2/B)^{1-1/r} C_B \Omega_\delta(M) + (2/B)^{1-\nu/r} C_B^\nu \Omega_\delta(M)^\nu,$$
$$\mathrm{Last}_\delta = C_{\mathrm{gr}} B[\delta + C_B^\nu Z^\nu \delta^{1-\nu/r}].$$

The last three terms vanish as $\delta \downarrow 0$ at fixed B, K, M.

Proof. We freeze each positive-length cell at its own mean. Good full blocks use the spectral baseline and the multiplicative perturbation bound; bad full blocks use their L^r budget. We estimate the true final cell separately, avoiding division by its possibly small length.

Step 1. We control the mean-freezing errors and primitive budgets. On each positive-length cell use its own Bochner average $\overline{M}_m$; set it to zero on an empty cell and form the constant-field primitive $\overline{H}_m$. Put $e_m = C_B \delta^{-1/r} \|W_R - \overline{W}_R\|_{L^r(I_m)}$. Jensen and (10.3.8) give

$$\|\overline{H}_m\|_\theta \leq a_m, \quad \|H_m - \overline{H}_m\|_\theta \leq e_m, \quad \delta\sum e_m^r \leq C_B^r \Omega_\delta(M)^r, \quad \delta\sum a_m^r \leq D_M := C_B^r Z^r.$$

Finite power mean at exponents r and $r/\nu > 1$, with nonnegative inputs e_m, e_m^ν, gives $\delta \sum_m (e_m + e_m^\nu) \le E_\delta$. Here $n = N + 1 \ge 2$, $\delta > 0$ and $\delta n \le 2/B$; all subsequent powers are positive and zero errors are allowed.

Step 2. We use the spectral baseline on good full blocks. On full cells only, $\|\overline{M}_m\| \le (\delta B)^{-1/r} \|W_R\|_{L^r(I_m)} = a_m/(C_B B^{1/r}) \le a_m/B$. Split full indices $m < N$ into good $a_m \le K$ and bad $a_m > K$. On a good block, Proposition 8.4.2 applies with base $\overline{H}_m$, perturbation $H_m - \overline{H}_m$ and the left multiplier $S_E(B)$. The baseline is the static wave of $\overline{M}_m$ by Proposition 10.3.2. Here $\|\overline{M}_m\| \le K/B \le K$, whereas $\|\overline{H}_m\|_\theta \le a_m \le K$. The spectral estimate gives

$$\|S_E(B) U_{\overline{H}_m}(B, 0)\| \le 8(1 + K)^2 (1 + B) e^{B\lambda(\overline{M}_m)}.$$

Consequently,

$$\log \|P_m^{\mathrm{mean}}\| \le L_{B,K} + B\lambda(\overline{M}_m) + C(\theta, B, K)(e_m + e_m^\nu).$$

This sufficient prefactor follows from the bound in E, $8(1 + K)^2(1 + B)$, by enlarging it. Since $\delta N \le 1/B$, the prefactors sum to at most $L_{B,K}/B$. Nonnegativity of λ gives $\delta \sum_{\mathrm{good}} B\lambda(\overline{M}_m) \le \int_I \lambda(\overline{W}_R) \le \mathrm{Rate}_R(\Phi) + \Lambda_\delta(M)$. Bad and last rate cells can be dropped in this upper bound.

Step 3. We control bad full blocks by the higher-power budget. On bad full cells (10.3.9) gives $C_{\mathrm{gr}} B(1 + a_m^\nu)$. Because $a_m > K \ge 1$ and $r > \nu$, $1 + a_m^\nu \le (K^{-r} + K^{\nu - r}) a_m^r$. Their weighted sum is bounded by $C_{\mathrm{gr}} B C_B^r Z^r (K^{-r} + K^{\nu - r})$. The inequality $C_B \le 32 B^{3 - 1/r}$ yields the displayed bad-block term.

Step 4. We bound the final remainder directly. If $\ell_N = 0$, the last endpoint is I and $\log \|I\| = 0$. Otherwise use the stopped path, not its frozen full-cell formula. Since $a_N \le C_B \delta^{-1/r} Z$, its weighted logarithm is at most Last_δ by (10.3.9). This tends to zero because $\nu < r$, even for arbitrarily short last cells; no division by that cell length occurs. Combining these estimates proves (10.3.10). All constants are independent of R. This proves Proposition 10.3.5. □

Corollary 10.3.6 (Every polynomial control radius)**.** *For $c_{\mathrm{ball}} > 0$, $\kappa_{\mathrm{ball}} \ge 0$ put $M_B = c_{\mathrm{ball}} B^{\kappa_{\mathrm{ball}}}$. Then*

$$\limsup_{\substack{B \to \infty \\ B \in \mathbb{N}}} \limsup_{\delta \downarrow 0} \sup_{\substack{R \ge 1 \\ \|\Phi\| \le M_B}} \left\{ \delta \sum_m \log \|P_m^{\mathrm{mean}}\| - \mathrm{Rate}_R(\Phi) \right\} \le 0.$$

Proof. Choose $s > r(3 + \kappa_{\mathrm{ball}})/(r - \nu)$ and $K_B = B^s$. At each fixed B, the inner δ limit has a fixed finite radius and threshold, so the last three errors in (10.3.10) vanish first. Its bad terms become

$$C_{\mathrm{gr}} 32^r C_{\mathrm{mean}}^r c_{\mathrm{ball}}^r \{ B^{r(3 + \kappa_{\mathrm{ball}}) - sr} + B^{r(3 + \kappa_{\mathrm{ball}}) + s(\nu - r)} \}.$$

Both exponents are negative: the second by choice and the first because $s > 3 + \kappa_{\mathrm{ball}}$. Also $L_{B,K_B}/B \le [\log 16 + 7 \log 2 + (4s + 3) \log B]/B \to 0$. Thus, the outer integer-B

limit gives the claim. No diagonal choice B_δ, M_δ is asserted. At fixed parameters all primitive maps are bounded linear into separable little Hölder products. Young local dependence and positive endpoint norms make the displayed logarithms continuous; the rate is continuous by Proposition 10.3.3. Growth bounds make each control-ball supremum finite. A countable dense subset of each closed Hilbert ball has the same supremum. Supremum over R is an ordinary deterministic real supremum, not a random measurability or compact-family claim. This proves Corollary 10.3.6. □

10.3.4 Arbitrary small residual paths and the ordered product

Corollary 10.3.6 compares the sum of the logarithms $\log\|P_m^{\mathrm{mean}}\|$ with the rate, for the mean primitives H_m alone. We now add compact-operator paths x_m to the H_m and bound the norm of the ordered product of the perturbed endpoints when these paths are small.

Proposition 10.3.7 (Residual comparison and the integrated rate)**.** *Let x_m be arbitrary little C^θ compact-operator paths starting at zero on $[0,B]$, put $v_m = \|x_m\|_\theta$ and $Y = (\delta\sum_m v_m^p)^{1/p}$. Define*

$$P_m^{\mathrm{pert}} = S_E(\ell_m)U_{H_m+x_m}(\ell_m,0), \qquad z_{\mathrm{rat}} = \prod_m \frac{\|P_m^{\mathrm{pert}}\|}{\|P_m^{\mathrm{mean}}\|}.$$

For fixed integer $B \geq 1$, $M \geq 0$ and every $K_{\mathrm{res}} \geq 1$,

$$\begin{aligned}\delta \log\max(1, z_{\mathrm{rat}}) \leq C_{K_{\mathrm{res}}}[(2/B)^{1-1/p}Y + (2/B)^{1-\nu/p}Y^\nu] \\ + c_B D_M(K_{\mathrm{res}}^{-r} + K_{\mathrm{res}}^{\nu-r}),\end{aligned} \tag{10.3.11}$$

uniformly in $R \geq 1$, $\|\Phi\| \leq M$. The finite constants may be written $C_{K_{\mathrm{res}}} = C(\theta, B, K_{\mathrm{res}})$ and $c_B = 2^{\nu-1}C_{\mathrm{gr}}B$. Here $D_M = C_B^r(C_{\mathrm{mean}}M)^r$. If $b_\delta \geq 0$ is any deterministic function of δ tending to zero at each fixed B, M_B is as in Corollary 10.3.6, and $\mathcal{F} = 2\delta\log\max(1, \|P_N^{\mathrm{pert}}\cdots P_0^{\mathrm{pert}}\|)$, then

$$\limsup_{\substack{B\to\infty\\ B\in\mathbb{N}}} \limsup_{\delta\downarrow 0} \sup_{\substack{R\geq 1,\ \|\Phi\|\leq M_B\\ Y\leq b_\delta}} \{\mathcal{F} - 2\,\mathrm{Rate}_R(\Phi)\} \leq 0. \tag{10.3.12}$$

No Gaussian, Cameron or Hamiltonian condition on the residuals is imposed.

Proof. We compare perturbed and mean endpoints separately on good and bad primitive blocks. We then use the mean norm lower bound to compare the ordered product, taking the residual threshold limit only after the small-parameter limit.

Step 1. We estimate endpoint norm ratios and sum the residual budgets. All endpoint norms are positive by the Young and free inverses. On every cell with $a_m \leq K_{\mathrm{res}}$ apply Proposition 8.4.2 with base H_m, perturbation x_m and left multiplier $S_E(\ell_m)$. It gives logarithmic ratio at most $C(\theta, B, K_{\mathrm{res}})(v_m + v_m^\nu)$. On cells with $a_m > K_{\mathrm{res}}$ use (10.3.9), $(a_m + v_m)^\nu \leq 2^{\nu-1}(a_m^\nu + v_m^\nu)$ and the mean denominator $\|P_m^{\mathrm{mean}}\| \geq 1$. The logarithmic

ratio is at most $c_B(1 + a_m^\nu + v_m^\nu)$, with c_B independent of $K_{\mathrm{res}}, R, \delta, \Phi, M$. Increase $C_{K_{\mathrm{res}}}$ to dominate both good and bad residual constants. Summation gives a nonnegative bound

$$\log \max(1, z_{\mathrm{rat}}) \le C_{K_{\mathrm{res}}} \sum_m (v_m + v_m^\nu) + c_B \sum_{a_m > K_{\mathrm{res}}} (1 + a_m^\nu).$$

The bad sum times δ is at most $D_M(K_{\mathrm{res}}^{-r} + K_{\mathrm{res}}^{\nu-r})$. Finite power mean at exponents $p \ge 1$ and $p/\nu \ge 1$, with nonnegative inputs v_m, v_m^ν, gives $\delta \sum v_m \le (2/B)^{1-1/p} Y$ and $\delta \sum v_m^\nu \le (2/B)^{1-\nu/p} Y^\nu$. This includes $p = \nu$, zero entries and the true empty block, with no singular powers. It proves (10.3.11).

Step 2. We compare the ordered product and take the limits in order. The product $A_{\mathrm{prod}} = \prod_m \|P_m^{\mathrm{mean}}\|$ is at least one. Since $A_{\mathrm{prod}} \ge 1$, the inequality $\max(1, A_{\mathrm{prod}} z_{\mathrm{rat}}) \le A_{\mathrm{prod}} \max(1, z_{\mathrm{rat}})$ preserves the product bound when taking the maximum with one. Submultiplicativity, without commutation, gives

$$\max(1, \|P_N^{\mathrm{pert}} \cdots P_0^{\mathrm{pert}}\|) \le A_{\mathrm{prod}} \max(1, z_{\mathrm{rat}}),$$
$$\mathcal{F} - 2\delta \sum_m \log \|P_m^{\mathrm{mean}}\| \le 2\delta \log \max(1, z_{\mathrm{rat}}).$$

At fixed B, M, K_{res} the residual terms vanish on $Y \le b_\delta$. Let $\delta \downarrow 0$ first and then $K_{\mathrm{res}} \to \infty$. Since $r > \nu$, the residual excess has limsup at most zero, uniformly in R, Φ. Now take $M = M_B$ at each fixed B and combine with Corollary 10.3.6; a supremum of sums is no larger than the sum of the suprema. The outer integer-B limit proves (10.3.12). The endpoint functional is continuous on all tuples by generic Young local dependence, including nonphysical residuals. Nothing was multiplied as scalar displacement moments. This proves Proposition 10.3.7. □

These are uniform deterministic E-phase product estimates. Their Gaussian Rayleigh application, original point transfer and signed-variational value over nonnegative controls comparison are proved separately in Sections 10.2–11.2.

10.4 The original point moment and the growing-cone phase

Retain all original covariances and amplitudes. Write $a = \alpha_0$, $\kappa = (4 - \alpha - a)/(3 - \alpha) > 1$. Fix the auxiliary parameters of the preceding Gaussian and product sections once, in their strict admissible gaps. For $0 < \delta < 1$ put

$$L = \delta^{-1}, \quad R = L + 2, \quad T_\delta = \delta^{-1/\kappa}, \quad g = \delta^{(1-a)/2}, \quad \Gamma_\delta = g^2 \Gamma.$$

Use the same real even root η, set $\psi = \eta(\cdot/R)$, $m = \psi^2$, $z = (\psi, 0) \in E$, $D = B_1(0)$ and $v_d = |D| > 0$. Let $W_{\mathrm{fast}} = W \circ T_{\delta,0}$ on the given slow probability space, and let P_δ be the physical E endpoint at time L driven by $gM_R(W_{\mathrm{fast}})$, with physical noise mask m once. The datum ψ is not the auxiliary cutoff used to extend the operator path to constant columns on F.

Lemma 10.4.1 (Restriction and fixed-parameter finiteness)**.** *For nonzero covariance, the E flow and its source flows are the closed isometric restrictions of their F extensions. Their operator norms and differences are measurable, and*

$$1 \le \mathbb{E}\|P_\delta\|^2_{\mathcal{L}(E)} < \infty. \tag{10.4.1}$$

Proof. We first identify the E flow as a closed isometric restriction of the extended phase flow. We then apply the fixed-parameter Gaussian tube estimate and compact endpoint lower bound to this exact original endpoint.

Step 1. We identify restrictions and measurable endpoint norms. Let $A_F = gA_{F,R}(W_{\text{fast}})$ be the scaled full operator path. Linearity and Proposition 6.2.2 give $A_F i = iD_E$, with $D_E = gM_R(W_{\text{fast}})$, and $S_F(t)i = iS_E(t)$. The extension uses a cutoff $\widetilde{\psi} = 1$ near its larger localization, not the datum ψ. Applying i to the state Young sums and using uniqueness gives $U_F(t,s)i = iU_E(t,s)$, then $P_F(t,s)i = iP_E(t,s)$. The same argument applies to sources. Closedness and isometry imply $\|P_E\| \le \|P_F\|$ and the analogous difference bound; density of E in F is neither true nor used. The continuous Young map on its separable path span, followed by bounded physical conjugation and restriction, gives measurable endpoint norms and uniform time-triangle difference norms. No operator-norm continuity of the free group is assumed. Young Neumann pieces and the free inverse also give invertibility.

Step 2. We prove finiteness and the lower endpoint norm bound. The clock condition is $0 < \delta < \min(1, 1/B)$ from Section 8.3, which reduces to $0 < \delta < 1$ at $B = 1$. We check a direct finiteness input, without a fixed-mask asymptotic rate. Take $B = 1$ in Propositions 10.2.4 and 10.2.6 and Lemma 10.2.7. Every $0 < \delta < 1$ satisfies their clock condition. The global endpoint in (10.2.10) is exactly this P_δ: the same given W_{fast}, amplitude g, root η, one mask m, massless E phase, and horizon δ^{-1}. We use the same admissible θ and operator path version. Explicit row identities, rational times and Young uniqueness identify versions if a smaller common admissible exponent is used. Thus, the finite radial bound applies to this endpoint, not merely an equal-law copy. At these fixed parameters the operator path $gM_R(W_{\text{fast}})$ is a compact-valued $C^\theta([0,L];\mathcal{K}(E))$ path starting at zero on its path event. Lemma 10.1.1 gives $\|P_\delta\| \ge \|S_E(L)\| \ge 1$ almost surely, proving (10.4.1). This use requires no F-norm rate along growing radii. Source convergence and source uniform integrability are checked next, separately from this original endpoint finiteness. This proves Lemma 10.4.1. □

Lemma 10.4.2 (The same regularized fast noises preserving the given noise)**.** *At each fixed δ, take one regularized slow noise preserving the given noise $Y_{\epsilon,\tau}$ and define*

$$Y_{\text{fast}}(t,x) = \delta^{a/2} Y_{\epsilon,\tau}(\delta t, x).$$

Its physical E flows $P_E^{\epsilon,\tau}$ with coefficient mgY_{fast} satisfy

$$\mathbb{E} \sup_{0\le s\le t\le L} \|P_E^{\epsilon,\tau}(t,s) - P_E(t,s)\|^2 \longrightarrow 0 \quad \text{as } (\epsilon,\tau) \to (0,0). \tag{10.4.2}$$

The unmasked field gY_{fast} has the canonical source law for covariance Γ_δ, spatial width ϵ and temporal width τ/δ.

Proof. We pull one regularized slow noise into fast coordinates and transfer its operator paths on the original coupling. We identify the ordinary response and compute the exact temporal width and covariance amplitude.

Step 1. We prove convergence of the source flow at fixed dilation. Testwise this field is $Y_{\epsilon,\tau}(T_{\delta,0}f)$. The original isometry and source domination give source and residual variances bounded by $\|f\|^2_{H_{\mathrm{fast}}}$, with residual variance tending to zero at fixed δ on every smooth compact test. The Gaussian transfer Proposition 5.2.2 therefore gives operator-path convergence in every finite L^pC^θ, retaining W_{fast} literally. Multiplication by fixed g and the bounded F extension preserve it. The transfer bound and Proposition 5.1.1 also give uniform source $\sqrt{p}$ path moments at these fixed δ, R, L. The moment-series argument yields square-exponential path norms. Young local dependence gives convergence in probability on balls of operator paths; the growth exponent $1/\theta < 2$ and those tails give uniform flow moments of every finite order and uniform integrability. The proof of Proposition 6.2.5 applies to this very pullback family. Restriction from F then proves (10.4.2). No uniform-in-δ source bound or exchange of limits is asserted.

Step 2. We identify the source primitive on the same states. This source is also the ordinary response for all E data. On Schwartz states its first primitive has row $gY_{\mathrm{fast}}(h_R)$. The source indicator approximation and bounded point variances at positive widths identify it with the statewise integral $\int_0^t S_E(-r)B(mgY_{\mathrm{fast}}(r))S_E(r)\,\mathrm{d}r$. Fubini uses $\mathbb{E}|ZY| \le \|Z\|_2\|Y\|_2$ when Gaussian testing is needed. Countable dense states, rational times and continuity give the full ordinary-primitive identity, as in Proposition 5.2.7. Lemma 6.2.6 and Proposition 10.1.3 then identify the Young equation with the ordinary interaction equation on E.

Step 3. We compute the transformed source law. In the temporal kernel $K_\tau(v) = \Gamma_{\mathrm{E}}(a)^{-1}\int_0^{\tau^{-1}} e^{-\lambda|v|}\lambda^{a-1}\,\mathrm{d}\lambda$, substitution $\lambda' = \delta\lambda$ gives

$$\delta^a K_\tau(\delta v) = K_{\tau/\delta}(v).$$

The change of variable contributes δ^{-1} from $d\lambda$ and δ^{1-a} from λ^{a-1}. These cancel the prefactor δ^a, while the upper cutoff becomes δ/τ. Thus, the new temporal width is τ/δ, with the original temporal covariance amplitude unchanged before multiplication by g^2. Hence, gY_{fast} has covariance $K_{\tau/\delta}(t-s)(p_{2\epsilon} * \Gamma_\delta)(x-y)$. The shared-width maximum and spatial heat-sum conventions persist for two sources. Positive multiplication by g^2 preserves every original covariance class, including spatial white noise. At fixed δ, $(\epsilon, \tau/\delta) \to (0,0)$. The full source point-moment limit in Proposition 6.1.3 thus applies to this single-source law and its continuous version; no newly reconstructed auxiliary family for Γ_δ is required. This proves Lemma 10.4.2. □

Lemma 10.4.3 (Compact-data source identification)**.** *For fixed δ, ϵ, τ, the displacement $v_{\epsilon,\tau}(t,x) = (\mathrm{pr}_1\, P_E^{\epsilon,\tau}(t,0)z)(x)$ has a jointly measurable continuous version and satisfies the ordinary scalar mild equation with coefficient $b = mgY_{\mathrm{fast}}$ and initial data $(\psi, 0)$.*

Proof. At positive source widths we solve in a sufficiently regular Sobolev phase, identify that solution with the E flow by uniqueness, and then use Fourier embedding and Green testing to recover the continuous scalar mild solution.

Step 1. We construct the high-regularity phase solution. On the fixed source regularity event, b is smooth in space, has common compact support in B_{2R}, and is continuous in time in every bounded spatial derivative norm on $[0, L]$. Choose integer $k > d/2 + 1$ and $E_k = H^k \times H^{k-1}$. Its Bessel-unitary free matrix is

$$\begin{pmatrix} \cos(t|\xi|) & \langle\xi\rangle \sin(t|\xi|)/|\xi| \\ -|\xi| \sin(t|\xi|)/\langle\xi\rangle & \cos(t|\xi|) \end{pmatrix}.$$

The zero sine quotient is t; finite-horizon bounds and dominated Fourier convergence give a strongly continuous group on E_k. Leibniz and the derivative-norm equivalence, obtained by expanding $(1 + |\xi|^2)^{k-1}$ and Parseval, give

$$\|b(t)f\|_{H^{k-1}} \le C_k \max_{|j|\le k-1} \|\partial^j b(t)\|_\infty \|f\|_{H^{k-1}}.$$

Thus, $B(b(t))$ is a norm-continuous bounded force on E_k, with a finite uniform sample bound B_L. For $Z_0 = S(t)z$ and $Z_{n+1}(t) = \int_0^t S(t-r)B(b(r))Z_n(r)\,\mathrm{d}r$,

$$\sup_{t\le L} \|Z_n(t)\|_{E_k} \le C_L^{n+1} B_L^n L^n \|z\|_{E_k}/n!.$$

This series converges in $C_t E_k$. Iterating a homogeneous Volterra difference proves uniqueness. Its continuous embedding into E and ordinary E uniqueness identify the sum with $P_E^{\epsilon,\tau}(t, 0)z$.

Step 2. We obtain continuous measurable displacement and velocity. Fourier Cauchy–Schwarz gives $\|\widehat{f}\|_1 \le \|f\|_{H^k} (\int \langle\xi\rangle^{-2k}\,\mathrm{d}\xi)^{1/2} < \infty$. Fourier inversion and dominated convergence imply continuous bounded displacement, and the same holds for velocity since $k - 1 > d/2$. The source derivatives on the compact support form a measurable $C_t C_x^{k-1}$ random element, by countable evaluations and continuity. Picard iteration and local norm estimates make its phase sum measurable in $C_t E_k$; the Fourier embedding gives joint measurability. These high norms are used only at positive source widths.

Step 3. We identify the scalar Green equation. The first component of Duhamel is, distributionally,

$$v(t) = \cos(t\sqrt{-\Delta})\psi + \int_0^t G_d(t-r) * [b(r)v(r)]\,\mathrm{d}r.$$

Here $G_d(h)$ is the positive Green measure of mass h and support in B_h, including the sphere measure for $d = 3$. The product bv is continuous compactly supported, with finite uniform L^1 and supremum bounds. Against a compact smooth ϕ, absolute Fubini is bounded by $\int_0^t \|\phi\|_\infty \|b(r)v(r)\|_1 (t-r)\,\mathrm{d}r < \infty$. Writing $G_d(h)$ as h times the dilation of its unit-time probability measure proves continuity of the convolution term. The free term is continuous by the Fourier embedding. Thus, the distributional identity agrees everywhere with the pointwise continuous mild versions. No Green density in $d = 3$ or original Sobolev point trace is used. This proves Lemma 10.4.3. □

The displacement $v_{\epsilon,\tau}$ of Lemma 10.4.3 has the masked coefficient mgY_{fast} and the data $(\psi, 0)$. The unmasked source solution has the coefficient gY_{fast} and the data $(1, 0)$. We now show that the two agree on a cone that contains D at time L.

Proposition 10.4.4 (Cone identity and an average of squares)**.** *Let $u^{\mathrm{full}}_{\epsilon,\tau}$ be the unmasked source solution with coefficient gY_{fast} and data $(1, 0)$. At the fixed parameters, almost surely,*

$$v_{\epsilon,\tau} = u^{\mathrm{full}}_{\epsilon,\tau} \quad \text{on } \mathcal{C} = \{(t, x) : 0 \le t \le L,\ |x| \le 1 + L - t\}.$$

Consequently,

$$\mathbb{E}\| \operatorname{pr}_1 P_E^{\epsilon,\tau}(L, 0)z\|^2_{L^2(D)} = v_d\, \mathbb{E}|u^{\mathrm{full}}_{\epsilon,\tau}(L, 0)|^2 < \infty. \tag{10.4.3}$$

Proof. We compare the compact-data and constant-data source equations on one causally closed cone. Their free terms agree there by total finite propagation, and iteration of the homogeneous difference equation gives equality before taking the terminal spatial square average.

Step 1. We identify the common source law and the causally closed cone. Proposition 6.1.2, applied through the exact source law of Lemma 10.4.2, gives the locally continuous measurable full solution and its L^2 point Picard sum. The pathwise cone argument uses the realized pullback field; the point second moments depend only on its Gaussian covariance through those Bochner chain sums. We place no global unmasked field in E or F. The cone is causally closed: a predecessor at distance at most $t - s$ has norm at most $1 + L - s$. Its spatial projection lies a positive distance inside the plateau of both ψ and m.

Step 2. We compare both initial phase components on the cone. The total initial difference $(\psi - 1, 0)$ is represented in E plus constants by $(\psi, 0) + (-1, 0)$. Every entry of the full free phase kernel is a compactly supported distribution in B_t, and the top-left is $\partial_t G_d(t)$. Since $|x| + t \le 1 + L = R - 1$ on the cone, its entire translated kernel support lies in the region where this total datum vanishes. Lemma 6.2.1 therefore gives $\cos(t\sqrt{-\Delta})\psi(x) = 1$ there. Testing the E and constant summands separately would not give this total finite-propagation statement.

Step 3. We prove uniqueness of the two restrictions on the cone. The two mild equations have the same coefficient on the cone. For their difference w, causal closure gives the homogeneous Green integral equation there. Put $H = \sup_{\mathcal{C}} |w|$ and $M = \sup_{\mathcal{C}} |gY_{\mathrm{fast}}|$, both finite sample constants. Iteration with the positive Green measures gives $|w(t, x)| \le HM^n t^{2n}/(2n)!$. Indeed, the mass recursion is $f_0 = 1$, $f_{n+1}(t) = \int_0^t (t - r) f_n(r)\, \mathrm{d}r = t^{2n+2}/(2n + 2)!$. The factorial ratio forces this bound to zero on the fixed cone. No positivity of the sample coefficient or expectation of a global source supremum is required.

Step 4. We take the terminal average of squares. At time L the cone contains D. Tonelli and spatial stationarity of the unmasked single-source law give (10.4.3). Finiteness is the full source point-moment bound. This is an integral of squares, not a squared average or a covariance comparison with a masked model. Events are for each fixed δ, ϵ, τ. This proves Proposition 10.4.4. □

Agreement on the terminal observation set alone would not suffice: both initial phase components must agree on its backward cone. No-go 31 gives a smooth free-wave counterexample when the velocity guard is omitted, and a separate phase example explaining why operator growth alone does not imply growth for every initial state.

Proposition 10.4.4 holds at fixed positive ϵ, τ and for the scaled covariance Γ_δ. We now remove the regularization and undo the scaling to reach the original point moment $\mathbb{E}|u_\Gamma(T_\delta, 0)|^2$.

Proposition 10.4.5 (Exact original point transfer and polynomial cost)**.** *For every original model, including zero covariance,*

$$\begin{aligned} \mathbb{E}|u_\Gamma(T_\delta,0)|^2 &= v_d^{-1}\mathbb{E}\| \operatorname{pr}_1 P_\delta z\|^2_{L^2(D)}, && (10.4.4)\\ &\le v_d^{-1}\|\psi\|^2_{H^{1/2}}\mathbb{E}\|P_\delta\|^2, \\ \limsup_{T\to\infty} T^{-\kappa}\log \mathbb{E}|u_\Gamma(T,x)|^2 &\le \limsup_{\delta\downarrow 0}\delta\log\mathbb{E}\|P_\delta\|^2 \quad \textit{for every fixed } x. && (10.4.5)\end{aligned}$$

Proof. We remove source regularization at fixed dilation, then use the canonical law scaling to identify the original point moment. The compact initial datum costs only a polynomial factor, which disappears after logarithmic normalization.

Step 1. We pass the source square identity to the original operator endpoint. Assume nonzero covariance until the last paragraph, and fix δ. Equation (10.4.2) gives convergence of the source displacement in $L^2(\Omega; L^2(D))$, since $\|\operatorname{pr}_1 e\|_{L^2(D)} \le \|e\|_E$. Expected squared norms converge by Cauchy–Schwarz applied to their difference times their sum. Separately, the full source point-moment limit (6.1.6) at covariance Γ_δ gives convergence of the right side of (10.4.3) to $v_d\mathbb{E}|u_{\Gamma_\delta}(L,0)|^2$. Both cutoffs $(\epsilon, \tau/\delta)$ tend to zero at fixed δ. Thus, the two limits in the equal prelimit moments give

$$\mathbb{E}|u_{\Gamma_\delta}(L,0)|^2 = v_d^{-1}\mathbb{E}\|\operatorname{pr}_1 P_\delta z\|^2_{L^2(D)}.$$

Step 2. We identify the original moment by the canonical time change. The law normalization is the consequence of Lemma 7.1.1 and the canonical-series time change proved in Proposition 7.2.6. Explicitly, for $\delta = T^{-\kappa}$ and $r_T = T\delta$, V_δ has the law of $u_\Gamma(Tt, r_T x)$ and equation (7.1.1). At positive source widths, $U(t,x) = V_\delta(\delta t, x)$ has coefficient $\sqrt{\delta}\, Y_{\epsilon,\tau}(\delta t, x) = gY_{\mathrm{fast}}(t,x)$. The fixed-order and absolutely convergent canonical-series argument passes this time change to the point moment at fixed δ. Hence, $\mathbb{E}|u_\Gamma(T_\delta,0)|^2 = \mathbb{E}|u_{\Gamma_\delta}(L,0)|^2$. This is a law/moment identity, not a pathwise identity on the same noise. It preserves all mixed, unequal, self and empty Stratonovich chains and the Green-before-noise convention in $d = 3$. The shrinking r_T is not the mask radius R; no spatial Jacobian occurs at point zero. The phase/operator inequality now proves (10.4.4).

Step 3. We control the initial-data norm and its logarithmic cost. Parseval and the inhomogeneous Bessel weights give, for $R \ge 1$,

$$\|\psi\|^2_{H^{1/2}} \le \|\psi\|^2_{H^1} = R^d\|\eta\|_2^2 + R^{d-2}\|\nabla\eta\|_2^2 \le C_\eta R^d, \quad C_\eta = \|\eta\|_2^2 + \|\nabla\eta\|_2^2 > 0.$$

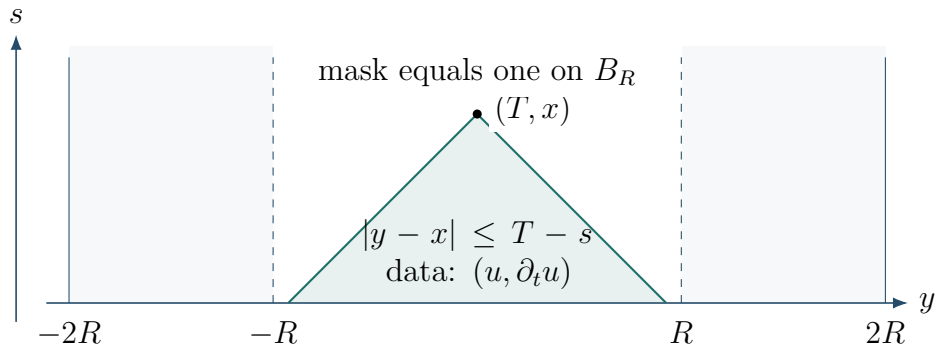

Figure 10.2: A spatial cross-section of finite propagation. The entire backward cone is chosen inside the region where the mask equals one; the mask vanishes outside $\overline{B}_{2R}$. The drawing is schematic and does not prescribe a value of R/T. Shading indicates the domain of dependence, not a Green density; in dimension three the Green measure is supported on a sphere. In the point-moment comparison, $L = \delta^{-1}$, $R = L + 2$ and $x \in B_1$. Both displacement and velocity must be passed between time intervals. See Lemma 7.2.5 and Proposition 10.4.5.

This includes the negative $d - 2$ power in $d = 1$. For $\mathrm{DataPref}_\delta = v_d^{-1} C_\eta (\delta^{-1} + 2)^d$,

$$\delta \log \mathrm{DataPref}_\delta = \delta \log(C_\eta / v_d) + d\delta[\log(1 + 2\delta) - \log \delta] \to 0.$$

The nontrivial term follows by $t = -\log \delta$ and $te^{-t} \to 0$, since $e^t \ge t^2/2$. The original point moment is at least one: its nonnegative full pairing expansion contains the unit empty pair of chains. It is finite by (10.4.4) and (10.4.1). Thus, logs are defined without subtracting infinite quantities. Since $\alpha < 2 < 3$, $a < 1$, we have $\kappa > 1$ and $\delta \mapsto T_\delta$ is a decreasing bijection $(0, 1) \to (1, \infty)$ with inverse $\delta = T^{-\kappa}$. Taking logs and this change of parameter proves (10.4.5) at zero. Original canonical spatial stationarity, proved in Proposition 7.2.7, extends it to every fixed x; no stationarity of the masked operator is assumed.

Step 4. We verify the free zero-covariance case directly. For zero covariance, $u = 1$, all operator paths vanish and $P_\delta = S_E(L)$. The same total free cone argument gives the spatial-square identity. Lemma 10.1.1 gives $\|S_E(L)\| \ge 1$, and its Fourier matrix gives $\|S_E(L)\| \le C(1 + L)$. Thus, $0 \le \delta \log \|S_E(\delta^{-1})\|^2 \to 0$ and both claims hold directly without a nonzero-noise import. This proves Proposition 10.4.5. □

10.5 An upper bound from a signed variational expression

Keep all auxiliary choices fixed as in the Gaussian tube construction, including $\alpha/4 < s_{\mathrm{sp}} < 1/2$, the admissible θ, ν, r, p, and the three fixed even-Q conditions. The mean bound C_{mean} is independent of R, B, δ; it may depend on those fixed auxiliary parameters

and the model. The space H_I has the original covariance Γ. Its norm is not reweighted by g and is not a sum of fast block costs. Let $R_\delta = \delta^{-1} + 2$ and $M_\delta = \mathbb{E}\|P_\delta\|^2_{\mathcal{L}(E)}$. For every fixed integer B the Gaussian block tuple has typical radius $b_{\delta,B} = 2\mathbb{E}\|X_{\delta,B}\|_{\delta,p} \to 0$. Its endpoint is the same P_δ for every B by Lemma 10.2.5, not a B-dependent surrogate. Write $\mathcal{M}_{\delta,B,R}$ for the normalized mean tuple in (10.2.7), with the indicated block length and radius. Write $\mathcal{F}_{\delta,B}$ for the everywhere-defined endpoint functional F_δ of Lemma 10.2.5.

Lemma 10.5.1 (Signed variational expression and quantitative radial envelope)**.** *For $R \geq 1$ define the variational expression*

$$\mathcal{S}_R = \sup_{\Phi \in H_I} \{2\,\mathrm{Rate}_R(\Phi) - \|\Phi\|^2_{H_I}/2\}, \qquad V_{\mathrm{up}} = \limsup_{\delta \downarrow 0} \mathcal{S}_{R_\delta}. \tag{10.5.1}$$

Then $0 \leq \mathcal{S}_R, V_{\mathrm{up}} \leq 2 + 2C^2_{\mathrm{mean}} < \infty$. The tube envelope $G_{\delta,B}$ of Proposition 10.2.6 satisfies, uniformly in $R \geq 1$ (in particular at the radius R_δ),

$$G_{\delta,B}(\rho) \leq A_0 + A_1 B^{3\nu}\rho^\nu + \eta_B b^\nu_{\delta,B}, \tag{10.5.2}$$

for $0 < \delta < \min(1, 1/B)$ and every $\rho \geq 0$, where

$$\begin{aligned} A_0 &= 4C_{\mathrm{gr}}, \\ A_1 &= 2^{\nu+1-\nu/r} C_{\mathrm{gr}} 32^\nu C^\nu_{\mathrm{mean}}, \\ \eta_B &= 2^{\nu+1-\nu/p} C_{\mathrm{gr}} B^{\nu/p}. \end{aligned}$$

The variational expression is not identified here with a constant in the cited source or a variational value over nonnegative controls.

Proof. We bound the signed score by completing the square in the control norm. We then use the explicit physical Young growth bound and weighted block estimates to compute the radial envelope constants, keeping their dependence on B.

Step 1. We obtain a finite uniform ceiling for the signed score. The mean is linear, so $\mathcal{T}_R 0 = 0$. Its free form has nonnegative gradient energy and spectral bottom zero; thus $\mathrm{Rate}_R(0) = 0$. Proposition 10.3.3 gives $\mathrm{Rate}_R(\Phi) \leq 1 + C_{\mathrm{mean}}\|\Phi\|$. With $q = \|\Phi\| \geq 0$,

$$2\,\mathrm{Rate}_R(\Phi) - q^2/2 \leq 2 + 2C_{\mathrm{mean}} q - q^2/2 = 2 + 2C^2_{\mathrm{mean}} - (q - 2C_{\mathrm{mean}})^2/2.$$

The coarser inequality also follows from half-weight arithmetic–geometric mean at bases $q^2, (2C_{\mathrm{mean}})^2$, with nonnegative weights and bases, including zeros. The zero control gives the lower bound. No optimizer, finite rank, positive control or convergence of $\mathcal{S}_{R_\delta}$ is assumed. The finite ceiling is auxiliary-parameter dependent and need not be sharp.

Step 2. We compute the block-length dependence of the tube envelope. For $\|a\|_{\delta,p} \leq b_{\delta,B}$, $\|\Phi\| \leq \rho$ set $v_m = \|a_m\|_\theta$ and $h_m = \|(\mathcal{M}_{\delta,B,R}\Phi)_m\|_\theta$. The quantitative physical bound (10.3.9), already including the free factor, and convexity give

$$\mathcal{F}_{\delta,B}(a + \mathcal{M}_{\delta,B,R}\Phi) \leq 2C_{\mathrm{gr}} B\delta n + 2^\nu C_{\mathrm{gr}} B\delta \sum_m (v^\nu_m + h^\nu_m).$$

Its upper expression is nonnegative, so it controls the maximum at one. The true primitive estimate and weighted power mean give

$$\delta \sum v_m^\nu \le (2/B)^{1-\nu/p} b_{\delta,B}^\nu,$$
$$\delta \sum h_m^\nu \le (2/B)^{1-\nu/r} (32 B^{3-1/r} C_{\mathrm{mean}} \rho)^\nu.$$

The exponents are $p/\nu \ge 1$, $r/\nu > 1$, inputs nonnegative, $n = N + 1 \ge 2$, $\delta > 0$, and $\delta n \le 2/B$. Zeros and $p = \nu$ are legal. The first constant is $4C_{\mathrm{gr}}$. In the mean term the factors $B^{\nu/r}$ and $B^{-\nu/r}$ cancel exactly, leaving $B^{3\nu}$. These computations give the displayed coefficients and (10.5.2), uniformly for all radii. They use no unspecified $c_Y(B)$ or quantitative F estimate. This proves Lemma 10.5.1. □

Lemma 10.5.1 bounds the envelope $G_{\delta,B}$ at every radius ρ. We now split the radial integral in (10.2.11) at a radius M. Below M we compare the exponent with $\mathcal{S}_{R_\delta}$, and above M we use Lemma 10.2.7.

Proposition 10.5.2 (Finite-delta bulk and exact tail)**.** *For fixed integer $B \ge 1$, $0 < \delta < \min(1, 1/B)$ and $M > 0$, define the deterministic number*

$$\mathcal{E}_{\delta,B,M} = \max\left(0, \sup_{\substack{R\ge 1,\ \|\Phi\|\le M \\ \|x\|_{\delta,p} \le b_{\delta,B}}} [\mathcal{F}_{\delta,B}(x + \mathcal{M}_{\delta,B,R}\Phi) - 2\,\mathrm{Rate}_R(\Phi)]\right).$$

It is finite. For every polynomial $M_B = c_{\mathrm{ball}} B^{\kappa_{\mathrm{ball}}}$, with $c_{\mathrm{ball}} > 0$, $\kappa_{\mathrm{ball}} \ge 0$, one has

$$e_B := \limsup_{\delta\downarrow 0} \mathcal{E}_{\delta,B,M_B} \text{ finite and nonnegative}, \qquad e_B \longrightarrow 0. \tag{10.5.3}$$

If $4A_1 B^{3\nu} \le M^{2-\nu}$, then

$$M_\delta \le \frac{M^2}{2\delta} e^{(\mathcal{S}_{R_\delta} + \mathcal{E}_{\delta,B,M})/\delta} + 4e^{(A_0 + \eta_B b_{\delta,B}^\nu - M^2/4)/\delta}. \tag{10.5.4}$$

Proof. We first identify the vanishing deterministic error on polynomial control balls. We then split the exact radial integral at M: the bulk uses the signed variational score, and the tail uses the explicit subquadratic envelope.

Step 1. We control the deterministic product error. The polynomial envelope and nonnegative rate make this supremum finite. It is an ordinary deterministic real number, not a random uncountable-radius supremum. At fixed R the inner functions are continuous in controls and paths; no measurable maximizing selector or joint δ, R measurability is needed. The zero control and zero path have rate zero and $\mathcal{F}_{\delta,B}(0) \ge 0$, so the untruncated supremum is already nonnegative. The anchor $b_{\delta,B} \to 0$ at fixed B satisfies Proposition 10.3.7 exactly. Its polynomial-radius conclusion gives $\limsup_B e_B \le 0$. At fixed B, the polynomial envelope bounds the inner limsup by a finite number, and $e_B \ge 0$ then proves (10.5.3).

Step 2. We split the radial integral and keep both prefactors. The exact Gaussian-enlargement bound is

$$M_\delta \le \int_0^\infty \frac{\rho}{\delta} e^{(G_{\delta,B}(\rho)-\rho^2/2)/\delta}\,\mathrm{d}\rho.$$

For every $\rho \le M$, every base-ball a and $\|\Phi\| \le \rho$,

$$\mathcal{F}_{\delta,B}(a + \mathcal{M}_{\delta,B,R_\delta}\Phi) - \rho^2/2 \le 2\,\mathrm{Rate}_{R_\delta}(\Phi) - \|\Phi\|^2/2 + \mathcal{E}_{\delta,B,M} \le \mathcal{S}_{R_\delta} + \mathcal{E}_{\delta,B,M}.$$

Taking suprema and integrating ρ/δ over $[0, M]$ gives the first term of (10.5.4), even if $M^2/(2\delta) < 1$. This used $\rho^2 \ge \|\Phi\|^2$, not equality or an optimizer. For the tail apply Lemma 10.2.7 with $C = A_1 B^{3\nu}$ and intercept $A_0 + \eta_B b_{\delta,B}^\nu$. All cutoff conditions hold: $M > 0$, $\rho \ge M$, $C \ge 0$, $1 < \nu < 2$, $4C \le M^{2-\nu}$. Its analytic integration retains both the front factor four and the exponent $-M^2/4$. Adding bulk and tail proves the finite-delta bound. No infinite-dimensional density or Laplace principle is used. This proves Proposition 10.5.2. □

Proposition 10.5.3 (Two limits on the same moment)**.** *The global operator moment obeys*

$$0 \le \liminf_{\delta\downarrow 0} \delta \log M_\delta \le \limsup_{\delta\downarrow 0} \delta \log M_\delta \le V_{\mathrm{up}} \le 2 + 2C_{\mathrm{mean}}^2.$$

Proof. We choose a polynomial cutoff large enough for the quadratic tail to dominate. We first take the small-parameter limit at fixed block length, and only then send the block length to infinity, keeping the same endpoint moment on the left.

Step 1. We choose a polynomial tail cutoff and bound the logarithm of the sum. Choose any $c_{\mathrm{ball}} > 0$ and $\kappa_{\mathrm{ball}} > 3\nu/(2-\nu)$, and set $M_B = c_{\mathrm{ball}} B^{\kappa_{\mathrm{ball}}}$. The cutoff in Proposition 10.5.2 holds for all sufficiently large integers B. For $A_1 = 0$ this is immediate; otherwise its side ratio is

$$\frac{M_B^{2-\nu}}{4A_1 B^{3\nu}} = \frac{c_{\mathrm{ball}}^{2-\nu}}{4A_1} B^{\kappa_{\mathrm{ball}}(2-\nu)-3\nu} \longrightarrow \infty.$$

Both constants and the strictly positive exponent are retained. At such a fixed B, a positive sum is at most twice its larger term. Taking $\delta \log$ of (10.5.4) therefore gives

$$\begin{aligned}\delta \log M_\delta \le \delta \log 2 + \max\{&\mathcal{S}_{R_\delta} + \mathcal{E}_{\delta,B,M_B} + \delta \log(M_B^2/(2\delta)),\\ &A_0 + \eta_B b_{\delta,B}^\nu - M_B^2/4 + \delta \log 4\}.\end{aligned}$$

Step 2. We take the small-parameter limit before the block-length limit. At fixed B, $b_{\delta,B} \to 0$. All logarithmic normalizers vanish, including $\delta \log(M_B^2/(2\delta)) = \delta \log(M_B^2/2) - \delta \log \delta \to 0$. The last limit follows from $te^{-t} \le 2/t$ for $t = -\log \delta > 0$. Finite variational expression and error bounds permit limsup subadditivity, giving

$$\limsup_{\delta\downarrow 0} \delta \log M_\delta \le \max\{V_{\mathrm{up}} + e_B,\ A_0 - M_B^2/4\}.$$

The lower bound $M_\delta \ge 1$ used here is (10.4.1) of Lemma 10.4.1. The left side has no B: restart identifies every block product with this same P_δ. Now let integer $B \to \infty$.

We have $e_B \to 0$, $M_B \to \infty$ and finite $V_{\mathrm{up}} \geq 0$. This gives the asserted upper bound, while $M_\delta \geq 1$ gives the nonnegative lower bound. The order was δ first at fixed block length, ball and thresholds, then B; no diagonal or limit of $\mathcal{S}_{R_\delta}$ was assumed. This proves Proposition 10.5.3. □

Proposition 10.5.4 (Pointwise upper bound from the signed variational expression)**.** *For every original admissible model and every fixed x,*

$$\limsup_{T\to\infty} T^{-\kappa} \log \mathbb{E}|u_\Gamma(T,x)|^2 \leq \limsup_{\delta\downarrow 0} \mathcal{S}_{\delta^{-1}+2} \leq 2 + 2C_{\mathrm{mean}}^2.$$

For zero covariance the two normalized moments and the signed variational expression have rate zero.

Proof. Proposition 10.4.5 bounds the original point moment by $\mathrm{DataPref}_\delta\, M_\delta$, with $\delta \log \mathrm{DataPref}_\delta \to 0$. Its proof, which removes the regularization first, keeps the full chain and works with the canonical law, is the input here, not an original E point trace. The decreasing bijection $T_\delta = \delta^{-1/\kappa}$ has inverse $\delta = T^{-\kappa}$. Take logs, normalized limsup and Proposition 10.5.3. Original canonical spatial stationarity from Proposition 7.2.7 gives every fixed x. The moment is at least one by its full expansion and finite by the bound, so no logarithm or difference of infinite quantities is hidden.

For $\Gamma = 0$ set $C_{\mathrm{mean}} = 0$ directly. Then $H_I = \{0\}$, $\mathrm{Rate}_R = \mathcal{S}_R = V_{\mathrm{up}} = 0$, $u = 1$ and $P_\delta = S_E(\delta^{-1})$. The free lower and upper bounds give $0 \leq \delta \log M_\delta \leq 2\delta \log[C(1+\delta^{-1})] \to 0$. This direct proof needs no nonzero Gaussian or nondegenerate Cameron assumption; the free functional at zero may exceed zero. The formal $a \downarrow 0$ exponent is $(4-\alpha)/(3-\alpha)$, with no new endpoint-in-a theorem asserted. The Jensen and lower bounds remain valid. This proves Proposition 10.5.4. □

The varying variational expression remains a signed variational value for the original covariance. Its positive-control comparison, exact limit and identification of the derived constant require the subsequent variational arguments.

Chapter 11

The constant and its consequences

The lower and the upper bound now concern the same point moment, but their variational problems differ. The lower bound uses nonnegative smooth controls (Section 7.3). The upper bound allows signed controls in a completed covariance space (Section 10.5). Do the two optimizations have the same value?

Section 11.1 solves a finite optimization problem whose Gram matrix has nonnegative entries (Figure 11.1). Section 11.2 applies this to the physical means, removes the spatial cutoff and reaches Theorem 11.2.6. For the limit alone, stop there.

The remaining sections study the constant. Section 11.3 gives occupation and spatial-energy bounds. For spatial white noise in one dimension, Section 11.4 evaluates the spatial energy and obtains explicit moment bounds. These are bounds: the full supremum is not evaluated, and the auxiliary value with coefficient one is not identified with the actual first-moment constant. Section 11.5 lists what is established and what is open. Episode ▶ 8 of the video series covers this chapter.

11.1 Finite optimization with nonnegative Gram entries

Let H be any real Hilbert space, $\mathcal{I}$ a finite index set, $k_i \in H$, $\ell_i > 0$ and $b_i \geq 0$. Write $C_{ij} = \langle k_i, k_j \rangle$ and assume $C_{ij} \geq 0$ for every pair. The Gram matrix is symmetric and positive semidefinite, since $\sum_{i,j} a_i C_{ij} a_j = \| \sum_i a_i k_i \|^2$. Put $t_+ = \max(t, 0)$ and define

$$\mathfrak{F}_C(\Phi) = 2 \sum_{i \in \mathcal{I}} \ell_i \sqrt{(\langle \Phi, k_i \rangle - b_i)_+} - \|\Phi\|^2/2, \qquad \mathscr{S}(C) = \sup_{\Phi \in H} \mathfrak{F}_C(\Phi). \tag{11.1.1}$$

Let $\mathcal{J} = \{i : k_i \neq 0\} = \{i : C_{ii} > 0\}$. Zero vectors contribute zero because $b_i \geq 0$. Empty index sets, singular Grams and $H = \{0\}$ are allowed. For nonempty $A \subset \mathcal{J}$ and $w_i > 0$, set

$$D_A^C(w) = \sum_{i \in A} \frac{\ell_i^2}{w_i} - \sum_{i \in A} b_i w_i + \frac{1}{2} \sum_{i,j \in A} w_i C_{ij} w_j, \qquad d_A^C = \inf_{w_i > 0} D_A^C(w). \tag{11.1.2}$$

Set $d_\varnothing^C = 0$.

Lean full

Lemma 11.1.1 (Scalar and Hilbert identities)**.** *For real ℓ, $w > 0$ and $t \geq 0$,*

$$2\ell\sqrt{t} \leq \ell^2/w + wt. \tag{11.1.3}$$

For $\Phi, z \in H$,

$$\langle \Phi, z \rangle - \|\Phi\|^2/2 = \|z\|^2/2 - \|\Phi - z\|^2/2 \leq \|z\|^2/2. \tag{11.1.4}$$

For finite real w_i, $\| \sum_i w_i k_i \|^2 = \sum_{i,j} w_i C_{ij} w_j$.

Proof. Since $\sqrt{w} > 0$ and $\sqrt{wt} = \sqrt{w}\sqrt{t}$,

$$0 \le (\ell/\sqrt{w} - \sqrt{wt})^2 = \ell^2/w + wt - 2\ell\sqrt{t}.$$

This includes $t = 0$. If $\ell, t > 0$, equality holds for $w = \ell/\sqrt{t}$. Expanding $\|\Phi - z\|^2$ proves (11.1.4). Bilinearity of the real inner product proves the finite Gram identity. These identities use neither compactness of a Hilbert ball nor an inverse covariance matrix. This proves Lemma 11.1.1. □

Lemma 11.1.2 (Interior dual minimum)**.** *Each nonempty $A \subset \mathcal{J}$ has a unique positive minimizer w^A of D_A^C. At this minimizer,*

$$\sum_{j \in A} C_{ij} w_j^A - b_i = \frac{\ell_i^2}{(w_i^A)^2} > 0, \qquad i \in A. \tag{11.1.5}$$

Proof. We bound each coordinate of a minimizing sequence away from both zero and infinity. This gives an attained interior minimum. Strict positivity of the Hessian then gives uniqueness and the stationarity equations.

Step 1. We confine a nonempty sublevel to a compact positive box. Put $c_i = C_{ii} > 0$ and $K_A = \sum_{i \in A} b_i^2/c_i$. Nonnegative entries and positive weights give

$$D_A^C(w) \ge \sum_i \left(\ell_i^2/w_i - b_i w_i + c_i w_i^2/2 \right).$$

Completing the square in $c_i w_i^2/4 - b_i w_i$ yields

$$D_A^C(w) \ge \sum_i \ell_i^2/w_i + \frac{1}{4} \sum_i c_i w_i^2 - K_A. \tag{11.1.6}$$

Thus, no coordinate can approach zero or infinity in a bounded sublevel while a different negative term hides its growth. Take $w^0 = (1, \dots, 1)$, $d_0 = D_A^C(w^0)$ and $L_A = d_0 + K_A$. Equation (11.1.6) at w^0 gives $L_A \ge \sum_i \ell_i^2 + \sum_i c_i/4 > 0$. Every w with $D_A^C(w) \le d_0$ satisfies

$$\ell_i^2/L_A \le w_i \le \sqrt{4L_A/c_i}.$$

The sublevel is nonempty and closed inside this compact box, which lies in the open positive orthant. A minimizing sequence chosen in the sublevel has a convergent subsequence there. Continuity attains its infimum. Outside this sublevel the values exceed d_0, so the minimum is global on the entire positive orthant.

Step 2. We prove uniqueness and compute the interior critical equations. The function is smooth in that orthant. Its Hessian on a nonzero vector ξ has value

$$\sum_i \frac{2\ell_i^2}{w_i^3} \xi_i^2 + \sum_{i,j} \xi_i C_{ij} \xi_j > 0.$$

The first term is strictly positive and the second is a squared Hilbert norm. Restriction to any nonconstant line segment is strictly convex, proving uniqueness. Each coordinate permits both signs of a small perturbation at the interior minimum. Differentiation gives $-\ell_i^2/w_i^2 - b_i + \sum_j C_{ij} w_j = 0$. This is (11.1.5). This proves Lemma 11.1.2. □

Lean partial

Proposition 11.1.3 (Positive conic maximizer)**.** *The finite real value in* (11.1.1) *satisfies*

$$\mathscr{S}(C) = \max_{A \subset \mathcal{J}} d_A^C. \tag{11.1.7}$$

If a maximizing subset is empty, $\Phi = 0$ attains the supremum. If a maximizing subset A is nonempty, a maximizer is $\Phi_A = \sum_{i \in A} w_i^A k_i$ with strictly positive coefficients. No uniqueness of the primal maximizer or maximizing subset is asserted.

Proof. We bound each primal value using its own active set. We then evaluate the restricted objective at the corresponding dual minimizer, where both scalar and Hilbert inequalities are equalities, and use the nonnegative omitted rewards.

Step 1. We bound the primal objective by a finite active-set dual value. For arbitrary Φ, let $A(\Phi) = \{i : \langle \Phi, k_i \rangle > b_i\}$. It is contained in $\mathcal{J}$. All other terms in the objective vanish, including equality at the threshold. If $A(\Phi)$ is empty, $\mathfrak{F}_C(\Phi) = -\|\Phi\|^2/2 \le 0$. Otherwise, for any positive w on $A = A(\Phi)$, set $t_i = \langle \Phi, k_i \rangle - b_i > 0$ and $z = \sum_{i \in A} w_i k_i$. Lemma 11.1.1 gives

$$\mathfrak{F}_C(\Phi) \le \sum_i \ell_i^2 / w_i - \sum_i b_i w_i + \langle \Phi, z \rangle - \|\Phi\|^2/2 \le D_A^C(w).$$

This holds for every positive w, so $\mathfrak{F}_C(\Phi) \le d_A^C$. There are finitely many subsets and their values are finite by Lemma 11.1.2. Taking the supremum bounds $\mathscr{S}(C)$ above by their maximum.

Step 2. We realize the maximum of the dual values by a nonnegative conic control. Conversely, $\mathfrak{F}_C(0) = 0 = d_\varnothing^C$. For nonempty A, take its dual minimizer. Equation (11.1.5) makes every vector in A strictly active at Φ_A, with $\sqrt{\langle \Phi_A, k_i \rangle - b_i} = \ell_i / w_i^A$. Both inequalities in the preceding display are then equalities for the sum restricted to A, since $z = \Phi_A$. This restricted objective equals d_A^C. All omitted vectors contribute nonnegative terms to the full objective, hence $\mathfrak{F}_C(\Phi_A) \ge d_A^C$, even if this value is negative. Maximizing over A, including the empty set, proves (11.1.7) and the asserted attainment. For a maximizing nonempty subset the upper and lower bounds force $\mathfrak{F}_C(\Phi_A) = d_A^C$; no outside inactivity was assumed. All-zero vectors give $\mathscr{S}(C) = 0$ directly. This proves Proposition 11.1.3. □

No-go 29 gives the three finite counterexamples behind this formulation: the empty active set cannot be omitted, the primal objective need not be concave, and entrywise matrix order is not positive semidefinite order.

Lemma 11.1.4 (Real Gram realization)**.** *Every finite real symmetric positive semidefinite matrix is the Gram matrix of vectors in a finite-dimensional real Hilbert space. When its entries are nonnegative, the value $\mathscr{S}(C)$ is independent of its realization.*

Proof. Induct on the size, with the empty matrix realized in $\{0\}$. Diagonal entries are nonnegative. If all vanish, testing on $e_i + te_j$ gives $2tC_{ij} \ge 0$ for every real t, hence $C = 0$, realized by zero vectors. Otherwise permute a positive diagonal c into the first position

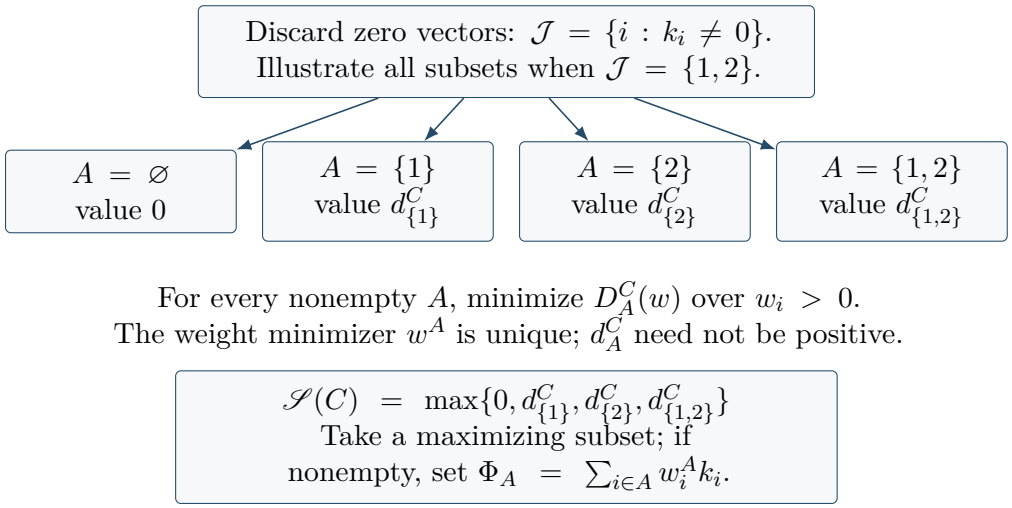

Figure 11.1: The finite-subset identity includes the empty set with value zero. For each nonempty subset the inner problem is a strictly convex minimization in positive weights, followed by a maximum over subsets. This does not assert global concavity of the original objective, uniqueness of its maximizer, or an effective algorithm. No inverse Gram matrix is used, so coincident vectors and singular Gram matrices remain allowed. See Lemma 11.1.2 and Proposition 11.1.3.

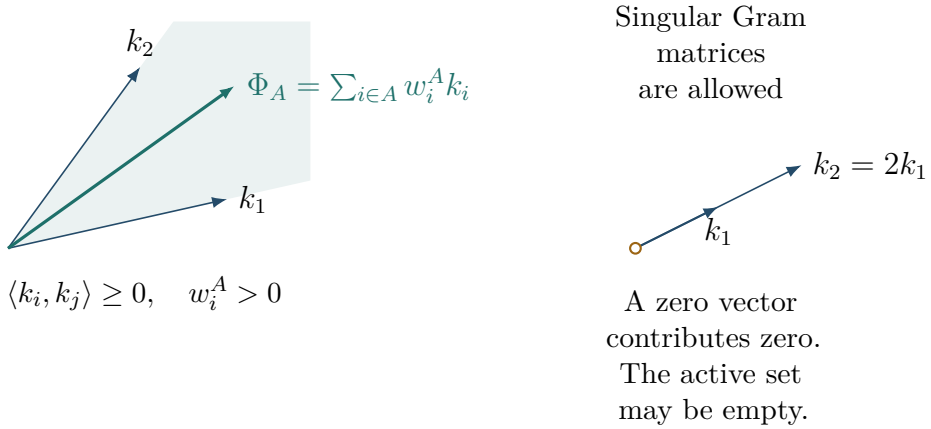

Figure 11.2: Finite positive combinations, not an inverse covariance formula. For a nonempty maximizing active set, a maximizer has positive coefficients on its selected vectors. The right panel shows why linear independence must not be imposed. The drawing is in a finite-dimensional span and does not restrict the ambient Hilbert space. Neither the maximizing subset nor the maximizer is asserted to be unique. See Proposition 11.1.3.

and write $C = \left[\begin{smallmatrix} c & v^{\mathsf{T}} \\ v & A \end{smallmatrix}\right]$. The Schur complement $B = A - vv^{\mathsf{T}}/c$ is positive semidefinite: test the original quadratic form on $(-v^{\mathsf{T}}y/c, y)$. Realize B by vectors u_i using the induction hypothesis. Then $k_1 = (\sqrt{c}, 0)$ and $k_i = (v_i/\sqrt{c}, u_i)$ for the other indices realize C. Undo the permutation. The inner products are $\langle k_1, k_i\rangle = v_i$ and $\langle k_i, k_j\rangle = v_iv_j/c + B_{ij} = A_{ij}$, while $\|k_1\|^2 = c$. Entries of B need not be nonnegative; this construction requires neither nonnegative coordinates nor complete positivity.

In any realization, $C_{ii} = 0$ means $k_i = 0$, so its entire row vanishes. Formula (11.1.7) depends only on C, ℓ, b and these eligible indices. It therefore proves realization independence whenever the entries are nonnegative, which is the scope in which $\mathscr{S}(C)$ is used. This proves Lemma 11.1.4. □

By Lemma 11.1.4, $\mathscr{S}(C)$ depends only on the matrix C and the data ℓ, b. We can therefore compare two Gram matrices directly.

Lean partial

Proposition 11.1.5 (Entrywise Gram comparison)**.** *Let C, D be real symmetric positive semidefinite matrices on the same finite index set, with $0 \le C_{ij} \le D_{ij}$. With the same $\ell_i > 0, b_i \ge 0$,*

$$\mathscr{S}(C) \le \mathscr{S}(D).$$

No positive-semidefinite order on $D - C$ is required.

Proof. Lemma 11.1.4 defines both values. Their eligible sets satisfy $\mathcal{J}_C \subset \mathcal{J}_D$. For nonempty $A \subset \mathcal{J}_C$ and positive weights,

$$D_A^D(w) - D_A^C(w) = \frac{1}{2}\sum_{i,j\in A} w_i(D_{ij} - C_{ij})w_j \ge 0.$$

Taking infima gives $d_A^C \le d_A^D$. The empty values are both zero. Taking maxima and using the inclusion of eligible families proves the claim by Proposition 11.1.3. This includes the appearance of previously zero vectors. This proves Proposition 11.1.5. □

Remark 11.1.6 (Exact checks and scope)**.** The empty value is essential: for one vector with $C = 1$, $\ell = 1/10, b = 4$, the nonempty dual has $D(4) = -3199/400 < 0$, whereas the primal objective at zero is zero. Global concavity is unavailable: for $k = \ell = b = 1$ the objective $2\sqrt{(\phi-1)_+} - \phi^2/2$ decreases on $[0,1]$ and has infinite positive right slope at one. For $k = \ell = 1, b = 0$, differentiation on $\phi > 0$ gives the maximum $3/2$ at $\phi = 1$; on $\phi \le 0$ the objective is nonpositive. Doubling the cost changes the positive critical point to $2^{-2/3}$ and the maximum to $3\,2^{-4/3}$. Finally, $C = I_2$, $D = \left[\begin{smallmatrix} 1 & 1/2 \\ 1/2 & 1 \end{smallmatrix}\right]$ are nonnegative positive semidefinite Grams but $D - C$ has eigenvalues $1/2, -1/2$. These are finite analytic checks, not a covariance-order theorem for physical waves.

The scalar, finite Gram, conditional active upper and half-quadratic entrywise deductions have existing local Lean certificates at their exact hypotheses. Dual coercivity, calculus, attainment, realization and the infimum/maximum argument above remain analytic proofs. No new kernel fact or formalization of the physical application follows merely from these certificates.

11.2 A variational formula for the second-moment limit

Retain every original covariance and amplitude. Write $a = \alpha_0$, $I = (0,1)$, $K(s,t) = |s-t|^{-a}$ and $H_I = H_t \otimes H_{\mathrm{sp}}$ for the original covariance. Keep the uniform E mean $\mathcal{T}_R = T_R(C_t \otimes I)$ and $C_{\mathrm{mean}} = M_0\|C_t\|$ of Section 10.3, with exactly the fixed r chosen there. In particular, $2 < r < 2/a$. To distinguish it from the map below, write $J_R = T_R$. For a bounded multiplier $V : H^{1/2} \to H^{-1/2}$ write $B_E(V)(u,v) = (0, Vu)$, the E operator of Lemma 10.3.1. The physical mask is $m_R = \eta(\cdot/R)^2$, used once. Let $\mathcal{C}_{\mathrm{pos}}$ be the full nonseparable class in (7.3.1). For Ψ in that class, retain its unmasked mean $h_{\Psi,s}$, original variance v_Ψ, integrated full-gradient rate I_Ψ and variational values for nonnegative controls S_c^{pos} from Section 7.3. The value with coefficient one is not identified with a first-moment limit or a constant in the cited source. We assume $\Gamma \neq 0$ through the following comparison lemmas. The theorem treats zero covariance directly.

Lean narrower

Lemma 11.2.1 (Inclusion into the covariance space and the smooth mean)**.** *For any real Hilbert space G there is a bounded map $J_G : L^2(I;G) \to H_t \otimes G$ with*

$$\|J_G F\|^2 = \int_{I^2} K(s,t)\langle F(s), F(t)\rangle_G \,\mathrm{d}s\,\mathrm{d}t \le K_0 \|F\|^2_{L^2(I;G)}, \qquad K_0 = \frac{2^a}{1-a}. \tag{11.2.1}$$

The natural inclusion puts every $\Psi \in \mathcal{C}_{\mathrm{pos}}$ in H_I, with

$$\|\Psi\|^2_{H_I} = v_\Psi, \qquad \mathcal{T}_R\Psi(s) = B_E(m_R h_{\Psi,s}) \quad \text{a.e. } s. \tag{11.2.2}$$

For each fixed smooth Ψ the right side gives a canonical version for every $R \ge 1$ and every $s \in I$.

Proof. We construct the covariance inclusion from the temporal Schur bound and identify its completed temporal mean. We then use common compact spatial supports to identify a smooth positive test with its original covariance class and physical masked mean.

Step 1. We construct the Hilbert-valued covariance inclusion. Direct integration and concavity of x^{1-a} give

$$\int_I K(s,t)\,\mathrm{d}t = \frac{s^{1-a} + (1-s)^{1-a}}{1-a} \le K_0.$$

For scalar $f \ge 0$, Cauchy–Schwarz against $K(s,t)\,\mathrm{d}t$ and then Tonelli give $\|Kf\|_2 \le K_0\|f\|_2$. The same estimate for absolute values bounds the bilinear integral by $K_0\|f\|_2\|g\|_2$. Approximate scalar $L^2(I)$ functions by real $C_c^\infty(I)$ functions. This bound makes their original test-null classes Cauchy in H_t, defines the bounded inclusion, and identifies its pairing with the integral. Finite G-valued tensors then give (11.2.1). Simple fields are dense in Bochner $L^2(I;G)$; the same bound on differences extends J_G. Absolute bilinear continuity extends the integral identity as well.

Step 2. We identify the temporal integral with the completed tensor map. For $G = H_{\mathrm{sp}}$, the Bochner integral $\int_I K(s,t)F(t)\,\mathrm{d}t$ exists almost everywhere: its norm is bounded by

$K\|F\|(s)$, which belongs to L^2. Simple-field approximation and the Schur estimate give a strongly measurable L^2 version and a bounded map of norm at most K_0. On smooth finite tensors it agrees with $(C_t \otimes I)J_G$ by the covariance definition. Approximation by such tensors converges in $L^2(I;G)$. The integral converges there by Schur; the completed tensor map converges in $L^r(I;G)$ by Lemma 9.1.3 and (11.2.1), hence also in L^2. Uniqueness of the L^2 limit identifies these versions. In particular, the integral belongs to L^r.

Step 3. We identify the original norm of a smooth spacetime test. Choose a closed ball B containing all spatial supports of Ψ. For real smooth q supported there, the physical covariance gives

$$\|q\|_{H_{\mathrm{sp}}}^2 \le |B|\,\Gamma(B-B)\|q\|_\infty^2. \tag{11.2.3}$$

Indeed, in $\int \mathrm{d}x \int \Gamma(\mathrm{d}y) q(x)q(x-y)$ only $x \in B, y \in B-B$ contribute. Absolute values and local finiteness prove the bound, including white and singular Radon covariances. Thus, $t \mapsto \Psi_t$ is continuous, bounded and compactly supported as an H_{sp}-valued field, and belongs to L^2. Its image under $J_{H_{\mathrm{sp}}}$ is the original test class of Ψ. Indeed, the separated compact smooth approximants in Lemma 8.3.3 converge uniformly on one common compact support. The local bound above and the temporal Schur estimate give convergence both in $L^2(I;H_{\mathrm{sp}})$ and in the original covariance norm. Their finite tensor identifications therefore have this same limit. Formula (11.2.1) and absolute Fubini give

$$\|\Psi\|_{H_I}^2 = \int_{I^2} K(s,t)\langle \Psi_s, \Psi_t\rangle_{H_{\mathrm{sp}}}\,\mathrm{d}s\,\mathrm{d}t = \int_{I\times\mathbb{R}^d} \Psi(s,x)h_{\Psi,s}(x)\,\mathrm{d}x\,\mathrm{d}s = v_\Psi.$$

The compact spatial supports and (11.2.3) make all these absolute integrals finite.

Step 4. We identify its masked operator mean on all phase states. Test the spatial row (9.1.1) first with displacement f and dual second component Λg, with f, g compact smooth. The row product is $m_R fg$, so the preceding temporal identity gives

$$\left\langle \int_I K(s,t)\Psi_t\,\mathrm{d}t, m_R fg \right\rangle_{H_{\mathrm{sp}}} = \int m_R h_{\Psi,s} fg.$$

This Fubini step has two fixed compact supports and integrable time kernel. Both resulting operators are bounded on E: the left by the mean theorem, the right by the bounded smooth $h_{\Psi,s}$ and compact smooth mask. Dense states extend the identity to E. For this fixed Ψ the temporal integral exists at every s, with norm at most $K_0 \sup_t \|\Psi_t\|_{H_{\mathrm{sp}}}$. Applying J_R gives the explicit version in (11.2.2) for every R, s. For each R it agrees with the completed L^r mean class. This makes no simultaneous-version assertion over all rough controls. This proves Lemma 11.2.1. □

Proposition 10.5.4 bounds the original point limsup by a limsup of the signed values $\mathcal{S}_R$. Proposition 7.3.6 bounds the original point liminf below by S_2^{pos}. To close this gap in Theorem 11.2.6 we compare $\mathcal{S}_R$ with S_2^{pos}. We start with finite Gram matrices, with and without the mask.

Lean narrower

Lemma 11.2.2 (Finite covariance vectors and entrywise order)**.** *Take a finite partition of I with nonempty cells I_i, lengths $\ell_i > 0$ and $\sum_i \ell_i = 1$, and real $f_i \in C_c^\infty(\mathbb{R}^d)$ with $\|f_i\|_2 = 1$. Put*

$$h_i = \mathbf{1}_{I_i}/\ell_i, \quad b_i = \|\nabla f_i\|_2^2, \quad k_i^R = h_i \otimes (m_R f_i^2), \quad k_i^\infty = h_i \otimes f_i^2.$$

These are elements of H_I. If v_L is the multiplier form of (10.3.1), then for every $\Phi \in H_I$,

$$\langle \Phi, k_i^R \rangle_{H_I} = \ell_i^{-1} \int_{I_i} v_{\mathcal{T}_R\Phi(s)}(f_i, f_i)\, \mathrm{d}s. \tag{11.2.4}$$

The Grams $C_{ij}^R = \langle k_i^R, k_j^R \rangle$ and $D_{ij} = \langle k_i^\infty, k_j^\infty \rangle$ satisfy $0 \le C_{ij}^R \le D_{ij}$ entrywise.

Proof. We realize the cell labels in the original tensor Hilbert space and identify their rows by completion. We then compare their Gram entries through the nonnegative temporal and physical spatial integrands.

Step 1. We identify the finite label rows. Lemma 11.2.1 puts h_i in H_t. The compact smooth spatial factors lie in H_{sp} by its test definition and (11.2.3). On a smooth finite tensor, use (9.1.1) with $z = (f_i, 0)$ and $w = (0, \Lambda f_i)$. Its row is $(\eta_R f_i)(\eta_R \Lambda^{-1} \Lambda f_i) = m_R f_i^2$. Temporal integration gives the pairing with h_i. This proves (11.2.4) on dense tensors. Its right side is a bounded original functional, with bound $\ell_i^{-1/r} C_{\mathrm{mean}} \|\Phi\| \|f_i\|_{H^{1/2}}^2$ by Hölder and (9.1.6). The left side is bounded by Hilbert Cauchy–Schwarz. Thus, the identity extends to the completed H_I. The form is the displacement form by Lemma 10.3.1.

Step 2. We compare the physical Gram integrands entrywise. Each Gram is symmetric positive semidefinite. Its entries factor into the temporal pairing of nonnegative h_i, h_j and the physical spatial covariance pairing. The kernels K, Γ and f_i^2, f_j^2 are nonnegative; $0 \le m_R \le 1$. Tonelli therefore gives the entrywise order. The physical pairing already contains Γ, and the row cancellation introduces no additional Fourier factor. Zero labels are permitted. All hypotheses of Proposition 11.1.5 are met, without assuming $D - C^R$ is positive semidefinite. This proves Lemma 11.2.2. □

By Proposition 11.1.3, the unmasked finite problem has a maximizer built from the k_i^∞. Their time factors h_i are scaled indicators, so this maximizer is in general not a test in $\mathcal{C}_{\mathrm{pos}}$. We also need a bound on the controls that holds uniformly in R.

Lemma 11.2.3 (Uniform optimizer norm and positive smoothing)**.** *Put $M = 4C_{\mathrm{mean}} + 4$. The supremum defining $\mathcal{S}_R$ may be restricted to $\|\Phi\| \le M$, uniformly in R. For every finite trial family in Lemma 11.2.2, the unmasked finite variational expression has a maximizer Φ_D with $\|\Phi_D\| \le M$. It is zero or is a positive conic combination of the k_i^∞. In the latter case it is approximable in H_I by tests in $\mathcal{C}_{\mathrm{pos}}$.*

Proof. We first restrict the signed score to a uniform control ball. We prove that the finite unmasked optimizer lies in that same ball before using any averaging estimate. Finally, its positive conic structure permits nonnegative smooth approximation with convergent cost and rate.

Step 1. We restrict the signed optimization to a fixed ball. Put $C = C_{\mathrm{mean}}$ and $q = \|\Phi\|$. Proposition 10.3.3 gives

$$2\,\mathrm{Rate}_R(\Phi) - q^2/2 \le 2 + 2Cq - q^2/2 < 2 - 2q < 0 \quad (q > M).$$

The zero control gives zero, proving the restriction.

Step 2. We bound the finite unmasked optimizer uniformly. Denote the finite unmasked objective by $\mathfrak{F}_D$. Proposition 11.1.3 supplies an attained maximum at zero or a positive conic sum Φ_D. Choose a finite $R' \ge 1$ whose plateau contains all supports of f_i. Then $k_i^{R'} = k_i^{\infty}$. Write $W_i = \ell_i^{-1} \int_{I_i} \mathcal{T}_{R'}\Phi(s)\,\mathrm{d}s$. The row identity and real Rayleigh formula imply, for every Φ,

$$\begin{aligned}\mathfrak{F}_D(\Phi) &\le 2\sum_i \ell_i \lambda(W_i) - q^2/2 \\ &\le 2 + 2\sum_i \ell_i \|W_i\| - q^2/2 \le 2 + 2Cq - q^2/2.\end{aligned}$$

For fixed f_i, the map $L \mapsto v_L(f_i, f_i)$ is bounded linear; hence the form of the Bochner average is the average form. Here $\lambda(L) \le \max(1, \|L\|) \le 1 + \|L\|$, the norm of an average is bounded by the average norm, and the L^1 mean norm is at most its L^r norm. No time-averaging error or concavity of the positive-part square root enters this estimate. Since the maximum is nonnegative, its optimizer lies in the same ball of radius M, independently of the partition, profiles and R'.

Step 3. We smooth the positive temporal factors without changing the limit class. On a nonzero branch write $\Phi_D = \sum_{i\in A} w_i h_i \otimes f_i^2$, with $w_i > 0$. Extend h_i by zero, convolve with a nonnegative compact smooth approximate identity, and multiply by smooth cutoffs $0 \le \chi_j \le 1$ compactly supported in I, tending pointwise to one. The resulting nonnegative $h_{i,j} \in C_c^{\infty}(I)$ converge to h_i in L^2: the error is bounded by the convolution error plus $\|(\chi_j - 1)h_i\|_2$, which tends to zero by domination. Set $\Psi_j = \sum_{i\in A} w_i h_{i,j} f_i^2$. Finite tensor estimates and (11.2.1) give $\Psi_j \to \Phi_D$ in H_I. The positive conic sum has positive squared norm, since at least one eligible diagonal is positive and all Gram entries are nonnegative. Thus, $\Psi_j \ne 0$ eventually, so $\Psi_j \in \mathcal{C}_{\mathrm{pos}}$. Costs converge. The integrated rate continuity proved in Proposition 10.3.3 gives

$$|\,\mathrm{Rate}_{R'}(\Psi_j) - \mathrm{Rate}_{R'}(\Phi_D)| \le \sqrt{3 + C\|\Psi_j\| + C\|\Phi_D\|}\sqrt{C\|\Psi_j - \Phi_D\|} \longrightarrow 0. \quad (11.2.5)$$

This estimate is uniform in R'. It asserts no uniform derivative bound on the smooth approximants. The zero branch will use $S_2^{\mathrm{pos}} \ge 0$ directly. This proves Lemma 11.2.3. □

Lemma 11.2.2 orders the masked and unmasked Grams entrywise. Lemma 11.2.3 keeps the unmasked optimizer in a fixed ball and, when it is nonzero, approximates it by nonnegative tests. The time averaging of Proposition 10.3.3 links these finite problems to the rate.

Proposition 11.2.4 (Signed variational values bounded by the variational value over nonnegative controls)**.** *For every $R \ge 1$,*

$$\mathcal{S}_R \le S_2^{\mathrm{pos}}. \quad (11.2.6)$$

Proof. We approximate each integrated signed rate by a finite collection of smooth Rayleigh trials. Entrywise Gram comparison replaces the optimized masked value by an unmasked positive conic optimizer. Its uniform norm bound allows the same averaging error to be used again, after which positive smoothing gives the nonnegative-control bound.

Step 1. We approximate the integrated rate uniformly on the fixed control ball. Use uniform partitions with $n \geq 2$ cells of length $1/n$. They are the $B = 1, \delta = 1/n$ partitions in Proposition 10.3.3, with the empty last cell omitted. That proposition gives $e_n \to 0$, independent of R, such that

$$\left|\mathrm{Rate}_R(\Phi) - \sum_i \ell_i \lambda\left(\ell_i^{-1} \int_{I_i} \mathcal{T}_R \Phi(s)\,\mathrm{d}s\right)\right| \leq e_n \quad (\|\Phi\| \leq M).$$

Step 2. We choose finitely many near-maximizing spatial trials. Fix R, Φ, n, with $\|\Phi\| \leq M$, and denote these averages by W_i. Real compact smooth unit trials are dense in the real H^1 unit sphere: truncate by cutoffs tending to one, whose gradient errors tend to zero, then mollify in H^1 and normalize in L^2. Continuity of the multiplier form in $H^{1/2}$ and hence H^1 proves

$$\lambda(W_i) = \sup_{\substack{f \in C_c^\infty(\mathbb{R}^d;\mathbb{R}) \\ \|f\|_2 = 1}} \sqrt{(v_{W_i}(f,f) - \|\nabla f\|_2^2)_+}.$$

The real Rayleigh supremum is nonnegative by Proposition 10.3.2, so the positive part does not change its supremum. For $\varepsilon > 0$ choose one near-maximizing f_i per cell with error at most ε in the square root. This is a finite choice, not a measurable continuum optimizer. Since $\sum_i \ell_i = 1$, the weighted trial error contributes 2ε to the next inequality. Lemma 11.2.2 gives

$$2\,\mathrm{Rate}_R(\Phi) - \|\Phi\|^2/2 \leq \mathfrak{F}_{C^R}(\Phi) + 2e_n + 2\varepsilon.$$

Step 3. We compare optimized Gram values and return to an integrated rate. Optimize this finite objective and use entrywise Gram comparison:

$$\mathfrak{F}_{C^R}(\Phi) \leq \mathscr{S}(C^R) \leq \mathscr{S}(D) = \mathfrak{F}_D(\Phi_D).$$

This compares optimized values, not the same individual control. Lemma 11.2.3 proves $\|\Phi_D\| \leq M$ before time averaging is used again. Choose R' covering the finite supports as in that lemma. The label row, Rayleigh bound and the same uniform averaging estimate give

$$\mathfrak{F}_D(\Phi_D) \leq 2\,\mathrm{Rate}_{R'}(\Phi_D) - \|\Phi_D\|^2/2 + 2e_n. \tag{11.2.7}$$

Step 4. We pass through nonnegative smooth controls and remove the two finite errors. If $\Phi_D = 0$, its finite variational expression is zero. Otherwise use its positive smooth approximants Ψ_j. Lemma 11.2.1 identifies their mean with $B_E(m_{R'} h_{\Psi_j,s})$ and their

Gaussian cost with v_{Ψ_j}. Since $h_{\Psi_j,s} \geq 0$ and $0 \leq m_{R'} \leq 1$, real H^1 form order gives $\mathrm{Rate}_{R'}(\Psi_j) \leq I_{\Psi_j}$. Thus, $2\,\mathrm{Rate}_{R'}(\Psi_j) - \|\Psi_j\|^2/2 \leq S_2^{\mathrm{pos}}$. Rate and cost convergence pass this inequality to Φ_D. Together with (11.2.7) and the separate zero branch this yields

$$2\,\mathrm{Rate}_R(\Phi) - \|\Phi\|^2/2 \leq S_2^{\mathrm{pos}} + 4e_n + 2\varepsilon.$$

All finite choices were made after fixing n, R, Φ. The right side is independent of those choices. Let $\varepsilon \downarrow 0$, take the supremum over the original ball, use Lemma 11.2.3, and then let $n \to \infty$. This proves (11.2.6). Finiteness of the variational value over nonnegative controls was already proved from the independent canonical upper bound in Proposition 7.3.6, not from this conclusion. This proves Proposition 11.2.4. □

Proposition 11.2.4 bounds $\mathcal{S}_R$ above for every R. For the limit we still need a lower bound as the mask is removed.

Proposition 11.2.5 (Cutoff removal for the optimized variational expression)**.** *The possibly nonmonotone mask family satisfies*

$$\lim_{R\to\infty} \mathcal{S}_R = S_2^{\mathrm{pos}}.$$

Proof. We fix one smooth positive control and use compactly supported Rayleigh tests to remove the mask from its rate. We then approximate the already finite supremum by one such fixed control; the uniform signed comparison supplies the opposite bound.

Fix $\Psi \in \mathcal{C}_{\mathrm{pos}}$ before taking R or moment limits. Use the explicit mean version of Lemma 11.2.1. Its rate $\lambda_R(s)$ obeys $0 \leq \lambda_R(s) \leq \lambda_{\Psi,s}$ by real form order. For each real compact smooth unit f, $m_R = 1$ on its support for every sufficiently large R. The Rayleigh formula therefore gives

$$\liminf_{R\to\infty} \lambda_R(s)^2 \geq \int h_{\Psi,s} f^2 - \|\nabla f\|_2^2.$$

Compact trial density and (7.3.4) identify the supremum of the right side as $\lambda_{\Psi,s}^2$. Hence, $\lambda_R(s) \to \lambda_{\Psi,s}$ for these versions. The global smooth-source bound $H_\Psi = \sup_{s,x} h_{\Psi,s}(x) < \infty$ gives $\lambda_R(s) \leq \sqrt{H_\Psi}$. Dominated convergence yields $\mathrm{Rate}_R(\Psi) \to I_\Psi$. Neither monotonicity of m_R nor an unmasked ground eigenfunction was used.

The original representative and cost $\|\Psi\|^2 = v_\Psi$ are independent of R. Thus, $\liminf_R \mathcal{S}_R \geq 2I_\Psi - v_\Psi/2$ for each fixed test. Given $\varepsilon > 0$, choose one fixed test with variational expression greater than $S_2^{\mathrm{pos}} - \varepsilon$; the finite supremum admits such a test. Take the liminf and then $\varepsilon \downarrow 0$. Proposition 11.2.4 supplies the reverse limsup. This proves Proposition 11.2.5. □

This passage from cutoff scores to their suprema needs the comparison just proved. No-go 30 shows why pointwise convergence and bounded control costs alone would not justify it.

Theorem 11.2.6 (Intrinsic original second-moment constant)**.** *For every original admissible model with data* $(1,0)$ *and fixed* x*,*

$$\lim_{T\to\infty} T^{-(4-\alpha-a)/(3-\alpha)} \log \mathbb{E}|u_\Gamma(T,x)|^2 = C_2(\Gamma,a) = S_2^{\mathrm{pos}} = 2^{(4-\alpha)/(3-\alpha)} S_1^{\mathrm{pos}}. \tag{11.2.8}$$

Its complete variational formula over nonnegative controls is

$$C_2(\Gamma,a) = \sup_{\Psi\in\mathcal{C}_{\mathrm{pos}}} \left\{ 2\int_I \sqrt{\sup_{\substack{f\in H^1(\mathbb{R}^d;\mathbb{R})\\ \|f\|_2=1}} \left(\int h_{\Psi,s} f^2 - \|\nabla f\|_2^2 \right)} \,\mathrm{d}s - \frac{v_\Psi}{2} \right\}, \tag{11.2.9}$$

$$h_{\Psi,s}(x) = \int_I |s-t|^{-a} (\Gamma * \Psi_t)(x)\,\mathrm{d}t, \qquad v_\Psi = \int_{I\times\mathbb{R}^d} \Psi(s,x) h_{\Psi,s}(x)\,\mathrm{d}x\,\mathrm{d}s.$$

Here $\mathcal{C}_{\mathrm{pos}}$ *consists of all nonzero nonnegative real* $C_c^\infty(I\times\mathbb{R}^d)$ *tests, including nonseparable ones. The covariance retains its amplitude, the kinetic term has coefficient one, and the Gaussian action is* $v_\Psi/2$*. For nonzero covariance* $0 < C_2 < \infty$*. For* $\Gamma = 0$ *the constant and moment rate are zero.*

Proof. We compare the upper and lower rates for the same canonical solution, then identify the variational expression and its homogeneity. The zero-covariance case is handled directly.

Step 1. We match the two finite bounds for nonzero covariance. Assume first $\Gamma \neq 0$. Proposition 10.5.4, followed by Proposition 11.2.5 with $R = \delta^{-1} + 2$, bounds the original point limsup by S_2^{pos}. The radius $\delta^{-1} + 2$ tends to infinity, so cutoff-score convergence applies along this radius without a separate exchange of limits. Proposition 7.3.6 bounds the original point liminf below by this same value. Both are for the same canonical Stratonovich solution, exponent, original covariance and variance-half action. Their identifications, made with the regularization removed first, retain all mixed, unequal, self and empty chains and both phase components with initial data $(1,0)$. The original spatial stationarity proved in Proposition 7.2.7 extends both bounds to every fixed x. Thus, the limit exists and equals S_2^{pos}. Its homogeneity, positivity and finiteness are Proposition 7.3.6. Formula (7.3.4) and the definition of the original variance give (11.2.9).

The factor relating S_2^{pos} to S_1^{pos} is the control-dilation factor, not an identification with a first-moment constant.

Step 2. We verify zero covariance directly. If $\Gamma = 0$, $H_I = \{0\}$, all means, variances and rates vanish, $\mathcal{S}_R = S_c^{\mathrm{pos}} = 0$, and $u = 1$. Both formulas are direct zero identities. This proves Theorem 11.2.6. □

The variational value with coefficient one is auxiliary; the theorem does not identify it with a first-moment limit or with Chen's printed constants. It neither repairs a source energy normalization nor asserts a Jensen improvement. The exponent formally tends to $(4-\alpha)/(3-\alpha)$ as $a \downarrow 0$; no interchange with the static moment limit is claimed. The explicit bounds and full calibration are separate from this identification.

11.3 Occupation bounds for the intrinsic constant

Retain all original models and amplitudes, put $a = \alpha_0$, $q = 4-\alpha > 2$, $k = 3-\alpha = q-1 > 1$ and $m = q/k$. The temporal kernel is $K(s,t) = |s-t|^{-a}$ on $I = (0,1)$; its diagonal value may be set to zero. Let $\mathcal{O}$ be the full strongly H^1-measurable unit-profile class defined before Proposition 8.2.8. Here we use the *original* kernel, defining

$$\begin{aligned} A(g) &= \int_{I^2} K(s,t) B_\Gamma(g_s^2, g_t^2)\,\mathrm{d}s\,\mathrm{d}t, \\ C_{\mathrm{occ}} &= \sup_{g\in\mathcal{O}} \frac{A(g)}{T(g)^{\alpha/2}}, \qquad\qquad \mathcal{E}_\zeta^{\mathcal{O}} = \sup_{g\in\mathcal{O}}\{A(g) - \zeta T(g)\}, \qquad \zeta > 0. \end{aligned} \tag{11.3.1}$$

The scalar penalty ζ is not a spatial mask. These objects differ from the earlier damped-kernel energy. Assume $\Gamma \neq 0$ until the direct zero case below.

Lean narrower

Lemma 11.3.1 (Full-profile squares in the original space)**.** *There is a continuous map $Q : H^1(\mathbb{R}^d;\mathbb{R}) \to H_{\mathrm{sp}}$ with*

$$\langle Q(f), Q(h)\rangle_{H_{\mathrm{sp}}} = B_\Gamma(f^2, h^2), \qquad \|Q(f)\|^2 = A_{\mathrm{sp}}(f).$$

For $g \in \mathcal{O}$, the element $\rho_g = J_{H_{\mathrm{sp}}}(s \mapsto Q(g_s))$ belongs to the original H_I and satisfies

$$\|\rho_g\|_{H_I}^2 = A(g), \qquad \langle \Psi, \rho_g\rangle_{H_I} = \int_I \int_{\mathbb{R}^d} h_{\Psi,s}(x) g_s(x)^2\,\mathrm{d}x\,\mathrm{d}s \tag{11.3.2}$$

for every $\Psi \in \mathcal{C}_{\mathrm{pos}}$. In particular,

$$\langle \Psi, \rho_g\rangle_{H_I} \le \sqrt{v_\Psi A(g)}.$$

Proof. We complete the square map in the spatial covariance Hilbert space. Its norm bound makes a measurable occupation an L^2 covariance-valued field, so the temporal inclusion applies. We then identify the physical pairing with a smooth control and use Hilbert Cauchy–Schwarz.

Step 1. We define the continuous square map by Sobolev approximation. Approximate f in H^1 by real compact smooth f_n. Proposition 8.2.5 gives

$$\|f_n^2 - f_l^2\|_{H_{\mathrm{sp}}}^2 = C_4(f_n - f_l, f_n + f_l, f_n - f_l, f_n + f_l) \le R_{\mathrm{sp}} N(f_n - f_l)^2 N(f_n + f_l)^2 \to 0.$$

Here N is continuous on H^1 and $N(f) \le \|f\|_{H^1}$. Completeness defines $Q(f)$; interlacing two approximating sequences proves independence. Passing the physical four-linear continuity and Hilbert pairings to limits proves the first identities. The same difference bound, first for smooth approximants and then by passage to the limit, proves continuity of Q.

Step 2. We construct the occupation vector in the original covariance space. Thus, $F_g(s) = Q(g_s)$ is strongly measurable. Writing $b_s = \|\nabla g_s\|_2^2$, the unit norm and $0 < \alpha/2 < 1$ give

$$\int_I \|F_g(s)\|^2\,\mathrm{d}s \le R_{\mathrm{sp}} \int_I b_s^{\alpha/2}\,\mathrm{d}s \le R_{\mathrm{sp}} T(g)^{\alpha/2} < \infty.$$

Lemma 11.2.1 now constructs ρ_g and identifies its squared norm with the physical $A(g)$. Joint measurability and representative independence follow from the continuous physical pairing on $(H^1)^2$. Absolute time integrability follows from the same Schur bound.

Step 3. We identify its pairing with the original smooth control. Choose one compact smooth χ equal to one on all spatial supports of Ψ_t. For real $f \in H^1$, smooth approximation gives

$$\langle \Psi_t, Q(f)\rangle_{H_{\mathrm{sp}}} = \lim_n B_\Gamma(\Psi_t, f_n^2) = C_4(\chi, \Psi_t, f, f) = B_\Gamma(\Psi_t, f^2).$$

Proposition 8.2.5 justifies these absolute integrals and limits. Polarizing (11.2.1) gives

$$\langle \Psi, \rho_g\rangle = \int_{I^2} K(s,t)\langle \Psi_t, Q(g_s)\rangle_{H_{\mathrm{sp}}}\,\mathrm{d}t\,\mathrm{d}s.$$

The absolute integrand is bounded by the product of two H_{sp} norms against K, integrable by Schur and L^2 Cauchy–Schwarz. Evenness of Γ and Tonelli for the nonnegative physical integrands yield (11.3.2). Hilbert Cauchy–Schwarz with $\|\Psi\|^2 = v_\Psi$ proves the bound. No rough occupation is inserted into a stochastic flow. This proves Lemma 11.3.1. □

Lean full

Proposition 11.3.2 (Original occupation energy and dilation)**.** *With* $K_0 = 2^a/(1-a)$,

$$0 < C_{\mathrm{occ}} \le K_0 R_{\mathrm{sp}} < \infty.$$

Moreover,

$$\mathcal{E}_\zeta^{\mathcal{O}} = D_\zeta C_{\mathrm{occ}}^{2/(2-\alpha)}, \qquad D_\zeta = \frac{2-\alpha}{2}\left(\frac{\alpha}{2\zeta}\right)^{\alpha/(2-\alpha)}, \tag{11.3.3}$$

$$C_{\mathrm{occ}} = \left(\frac{2\mathcal{E}_\zeta^{\mathcal{O}}}{2-\alpha}\right)^{(2-\alpha)/2}\left(\frac{2\zeta}{\alpha}\right)^{\alpha/2}. \tag{11.3.4}$$

In particular, $\mathcal{E}_\zeta^{\mathcal{O}} > 0$ *is finite and equals* $\zeta^{-\alpha/(2-\alpha)}\mathcal{E}_1^{\mathcal{O}}$.

Proof. We bound the occupation ratio with the original temporal row bound and show it is positive. We then dilate the whole occupation class and optimize the resulting scalar energy to recover the exact penalty dependence.

Step 1. We prove a positive finite occupation ratio. A unit H^1 profile has positive gradient energy: a zero weak gradient makes it constant, and an L^2 constant on $\mathbb{R}^d$ is zero. Hence, $0 < T(g) < \infty$. Spatial covariance Cauchy–Schwarz gives $B_\Gamma(g_s^2, g_t^2) \le R_{\mathrm{sp}} b_s^{\alpha/4} b_t^{\alpha/4}$. Schur with row bound K_0, then concavity, proves

$$0 \le A(g) \le K_0 R_{\mathrm{sp}} T(g)^{\alpha/2}. \tag{11.3.5}$$

A fixed compact smooth unit profile, constant in time, belongs to $\mathcal{O}$ and has positive A by Proposition 8.2.5. This proves positivity and finiteness of C_{occ}.

Step 2. We optimize spatial dilation over the same occupation class. The map $(U_\ell g)_s(x) = \ell^{d/2} g_s(\ell x)$ is an H^1 isomorphism preserving unit mass and strong measurability. It has inverse $U_{1/\ell}$ and is a bijection on $\mathcal{O}$. The physical Radon change of variables gives

$$A(U_\ell g) = \ell^\alpha A(g), \qquad T(U_\ell g) = \ell^2 T(g).$$

Indeed, the two densities contribute ℓ^{2d}, $\mathrm{d}x$ contributes ℓ^{-d}, and the pushforward of Γ contributes $\ell^{\alpha-d}$. Approximation extends the identity to full H^1. Taking the union over g, ℓ leaves the class unchanged. For fixed $A, T > 0$, the derivative of $A\ell^\alpha - \zeta T \ell^2$ has the sign of $\alpha A - 2\zeta T \ell^{2-\alpha}$. Its global maximum occurs at $\ell = (\alpha A/(2\zeta T))^{1/(2-\alpha)}$ and equals $D_\zeta [A/T^{\alpha/2}]^{2/(2-\alpha)}$. For $A = 0$ the supremum is zero as $\ell \downarrow 0$. Bounding every ratio by C_{occ} gives one inequality in (11.3.3). Fixed ratios approaching its positive supremum give the other by continuity of the positive power. Algebra gives (11.3.4) and the penalty scaling. No optimizer or minimax interchange is assumed. This proves Proposition 11.3.2. □

Lean narrower

Lemma 11.3.3 (Countable Rayleigh near-occupations)**.** *For fixed $\Psi \in \mathcal{C}_{\mathrm{pos}}$ and every $\varepsilon > 0$ there is $g_\varepsilon \in \mathcal{O}$ such that*

$$I_\Psi^2 + T(g_\varepsilon) \le \sqrt{v_\Psi A(g_\varepsilon)} + \varepsilon. \tag{11.3.6}$$

Proof. We choose near-maximizing Rayleigh tests from one countable dense family. A first-index rule makes the chosen occupation strongly measurable; the bounded potential controls its kinetic energy and allows the physical covariance pairing estimate.

Step 1. We choose a measurable near-maximizing occupation. The real H^1 space is separable, for example by its isometric embedding $f \mapsto (f, \nabla f)$ into a finite product of L^2 spaces. Compact smooth density therefore supplies a countable real family. Discard zero and normalize each member in L^2 to obtain f_j dense in the L^2-unit H^1 class. Normalization preserves convergence because the approximating L^2 norms tend to one. Put $b_j = \|\nabla f_j\|_2^2$ and $R_j(s) = \int h_{\Psi,s} f_j^2 - b_j$. Bounded-potential form continuity and Proposition 7.3.3 give $\lambda_{\Psi,s}^2 = \sup_j R_j(s)$. The canonical functions are measurable, indeed continuous. Let $U_j = \{s : R_j(s) > \lambda_{\Psi,s}^2 - \varepsilon\}$, $A_1 = U_1$ and $A_j = U_j \setminus \bigcup_{i<j} U_i$. These first-index cells are Borel and cover I. Put $g_\varepsilon(s) = f_j$ on A_j. Finite-valued truncations using f_1 on the remaining cells converge pointwise in H^1, proving strong measurability. A null-set representative may be filled by f_1.

Step 2. We bound its kinetic energy and integrate the Rayleigh inequality. With $H_\Psi = \sup_{s,x} h_{\Psi,s}(x) < \infty$, the selection implies

$$b(g_\varepsilon(s)) < \int h_{\Psi,s} g_\varepsilon(s)^2 - \lambda_{\Psi,s}^2 + \varepsilon \le H_\Psi + \varepsilon.$$

Thus, it belongs to the $\mathcal{O}$. Integrating the near-Rayleigh inequality, using Lemma 11.3.1, gives

$$\int_I \lambda_{\Psi,s}^2 \,\mathrm{d}s + T(g_\varepsilon) \le \langle \Psi, \rho_{g_\varepsilon} \rangle + \varepsilon \le \sqrt{v_\Psi A(g_\varepsilon)} + \varepsilon.$$

Time Cauchy–Schwarz on the unit interval gives $I_\Psi^2 \le \int_I \lambda_{\Psi,s}^2 \, \mathrm{d}s$. This proves (11.3.6). No eigenvector, continuum selector or limiting occupation is required. This proves Lemma 11.3.3. □

For $0 \le b < q/2$ define $F_b(0) = 0$ and

$$F_b(z) = k \left[\frac{(q-2b)^{(q-2b)/2}}{8(q-b)^{q-b}} \left(\frac{2z}{2-\alpha} \right)^{(2-\alpha)/2} \right]^{1/k}, \qquad z > 0. \tag{11.3.7}$$

At $b = 0$ this is exactly the map in (8.2.10). The display parameter b does not change the temporal exponent a.

Lean narrower

Theorem 11.3.4 (The computed occupation ceiling)**.** *For every variational value over nonnegative controls coefficient* $\mathfrak{c}$*,*

$$\begin{aligned} S_{\mathfrak{c}}^{\mathrm{pos}} \le U_{\mathfrak{c}} &:= \mathfrak{c}^m k \left[\frac{\alpha^{\alpha/2} C_{\mathrm{occ}}}{8 q^{q/2}} \right]^{1/k} \\ &= \mathfrak{c}^m (2\zeta)^{\alpha/(2k)} F_0(\mathcal{E}_\zeta^{\mathcal{O}}), \qquad \zeta > 0. \end{aligned} \tag{11.3.8}$$

In particular, the original moment constant satisfies $C_2(\Gamma, a) \le U_2$ *for every original model. This ceiling is not asserted to be attained or equal to* C_2*.*

Proof. We first optimize the kinetic budget in the near-occupation inequality to bound the integrated rate by a power of the original variance. We then optimize that variance in the reward-minus-cost expression and rewrite the result using the occupation energy.

Step 1. We optimize the kinetic budget before removing the selection error. Fix Ψ and write $v = v_\Psi$, $C = C_{\mathrm{occ}}$ and $\beta = \alpha/4$. Take $T = T(g_\varepsilon) > 0$ from the selected occupation; by the definition of C_{occ}, $A(g_\varepsilon) \le C_{\mathrm{occ}} T^{\alpha/2}$, which converts its covariance term into $\sqrt{vC}\, T^\beta$. At the positive critical point T_* of the scalar maximization below, $T_* = \beta\sqrt{vC}\, T_*^\beta$, so the value is $(1-\beta)\sqrt{vC}\, T_*^\beta$. Lemma 11.3.3 gives $I_\Psi^2 \le \sqrt{vC} T^\beta - T + \varepsilon$ for some $T > 0$. Bound it by the supremum over all $T \ge 0$ before sending $\varepsilon \downarrow 0$. If $v = 0$, that supremum is zero. If $v > 0$, the derivative $\beta\sqrt{vC} T^{\beta-1} - 1$ strictly decreases from infinity to -1. Its unique positive zero is $T_* = (\beta\sqrt{vC})^{1/(1-\beta)}$. The global maximum equals $(q/4)(\alpha/4)^{\alpha/q}(vC)^{2/q}$. In both cases,

$$I_\Psi \le D v^{1/q}, \qquad D = \sqrt{q/4}\,(\alpha/4)^{\alpha/(2q)} C^{1/q}.$$

Step 2. We optimize the variance and keep the exact Gaussian half-cost. For the constant computation below, $4^{-\alpha/2} = 2^{-\alpha}$ and absorbing the outside factor $1/2$ into the $1/k$ power contributes 2^{-k}, whose product is 2^{-3} because $k + \alpha = 3$. The scalar function $\mathfrak{c} D v^{1/q} - v/2$ vanishes at zero, tends to minus infinity, and has strictly decreasing derivative. Its unique positive maximum is at $v_* = (2\mathfrak{c}D/q)^{q/k}$, with value $k v_*/2$. Direct positive-power algebra gives

$$(2D/q)^q = q^{-q/2} (\alpha/4)^{\alpha/2} C.$$

Since $k+\alpha=3$, the maximum is precisely $U_{\mathfrak{c}}$ in (11.3.8), with denominator eight. Substitution of (11.3.4) gives the second form, retaining the factor $(2\zeta)^{\alpha/(2k)}$. Take the supremum over the smooth positive-control class. Theorem 11.2.6 identifies $C_2=S_2^{\mathrm{pos}}$, proving the moment ceiling. The penalty factor cancels its energy scaling, so the ceiling is independent of ζ. This proves Theorem 11.3.4. □

Lean narrower

Corollary 11.3.5 (A common spatial-energy bracket)**.** *With the same original covariance and M_a of (8.1.3),*

$$2^m M_a^{-1/k} F_0(\mathcal{E}_{\mathrm{sp}}) \le C_2(\Gamma,a) \le 2^m K_0^{1/k} F_0(\mathcal{E}_{\mathrm{sp}}). \tag{11.3.9}$$

For $\Gamma\neq 0$ there is also the comparison of the energies defined here

$$C_2 \le 2^m F_0(\mathcal{E}^{\mathcal{O}}_{1/2}) < 2^m F_a(\mathcal{E}^{\mathcal{O}}_{1/2}).$$

Proof. We combine the spatial ratio estimate with the occupation ceiling for the common-energy bracket. We then compare the scalar maps by strict convexity, keeping the kinetic penalty normalization explicit.

Insert $C_{\mathrm{occ}}\le K_0 R_{\mathrm{sp}}$ into (11.3.8) and use (8.2.9). This gives the upper bracket; the lower is (8.2.10) multiplied by 2^m, using Theorem 11.2.6. Both concern one common spatial energy, not an assumed first moment.

For completeness put

$$\Delta = \tfrac{1}{2}[q\log q + (q-2a)\log(q-2a)] - (q-a)\log(q-a) > 0.$$

Here $a>0$ and $q-2a>2-a>1$. The scalar inequality for the difference of logarithms applies at exactly these conditions, without $q\ge 3$. Equivalently the strict midpoint convexity of $x\log x$ on positive arguments, whose second derivative is $1/x$, gives the sign. Subtracting logarithms in (11.3.7) gives

$$\log(F_a(z)/F_0(z)) = \Delta/k, \qquad \frac{\mathfrak{c}^m F_a(\mathcal{E}^{\mathcal{O}}_{\zeta})}{U_{\mathfrak{c}}} = \exp\!\left(\frac{\Delta-(\alpha/2)\log(2\zeta)}{k}\right).$$

At $\zeta=1/2$ this and the ceiling prove the strict comparison. At $\zeta=1$ the comparison is not universally favorable. For $\alpha=5/4, a=1/2, d=2$,

$$8[\Delta-(\alpha/2)\log 2] = \log\frac{11^{11}7^7}{2^5 9^{18}} < 0,$$

since $11^{11}7^7 = 234966429149994773$ and $2^5 9^{18} = 4803028329503971872$. This contrasts computed bounds; it refutes no moment inequality. This proves Corollary 11.3.5. □

The kinetic normalization matters in this comparison. No-go 28 shows that changing it can reverse an ordering between the computed ceiling and a comparison value. That example makes no claim about the ordering of the actual moment constant.

For $\Gamma=0$, all original means and variational values vanish and $C_2=0$. Here $Q=0$, $A=0$ and $C_{\mathrm{occ}}=0$. The supremum of $-\zeta T(g)$ is zero: dilate a fixed unit compact profile by $\ell^{d/2}f(\ell x)$ and let $\ell\downarrow 0$. The same argument gives $\mathcal{E}_{\mathrm{sp}}=0$ and the earlier damped energy zero, without using a zero vector as a unit profile. With $F_b(0)=0$, every non-strict bound above is the zero identity. These energies are not identified with Chen's printed energies.

11.4 Spatial white noise: energy and explicit moment bounds

Take $d = \alpha = 1$ and $\Gamma = c\delta_0$, $c \geq 0$, with temporal kernel $|s-t|^{-a}$, $0 < a < 1$, and data $(1, 0)$. The parameter c is covariance mass; the coefficient of unit noise would be $\sqrt{c}$. No additional temporal normalization is inserted. The wave kinetic coefficient is one. For real unit $f \in H^1(\mathbb{R})$ put $A = \int_{\mathbb{R}} f^4$ and $b = \int_{\mathbb{R}} (f')^2$. The physical covariance is $A_{\mathrm{sp}}(f) = cA$.

The next calculation recovers the sharp one-dimensional interpolation inequality recorded by Sz.-Nagy [41, (2), p. 64, and (4), p. 65], now commonly called a Gagliardo–Nirenberg inequality, and its hyperbolic-secant optimizer. We give the proof to fix the normalization of the spatial energy.

Lemma 11.4.1 (A square identity for the distribution function)**.** *Every such f has $A < \infty$. With $\mathsf{F}(x) = \int_{-\infty}^{x} f(y)^2 \, \mathrm{d}y$, for every real z,*

$$0 \leq \int_{\mathbb{R}} [f' - zf(1 - 2\mathsf{F})]^2 = b - 2zA + z^2/3. \tag{11.4.1}$$

Proof. We first obtain a continuous representative with a bounded square and zero limits at infinity. We then integrate the derivative of its product with the distribution function and expand the square, with all terms absolutely integrable.

Step 1. We identify the representative and its endpoint decay. On a bounded interval the weak derivative f' is L^1 by Cauchy–Schwarz. Its integral primitive has weak derivative f' by Fubini. Subtracting it from f gives a function of weak derivative zero, hence constant almost everywhere: test against derivatives of compact smooth primitives of all zero-integral test functions. The resulting locally absolutely continuous representatives patch on overlaps, giving one continuous representative. Thus, $\rho = f^2$ is locally absolutely continuous with $\rho' = 2ff' \in L^1(\mathbb{R})$, while $\rho \geq 0$ and $\int \rho = 1$. Integrability of ρ' makes ρ Cauchy on each infinite tail, so it has finite limits at both ends. Its L^1 integrability forces both limits to be zero. It is therefore bounded, and $A = \int \rho^2 \leq \|\rho\|_\infty \int \rho < \infty$.

Step 2. We compute the two integrals in the square expansion. Now $0 \leq \mathsf{F} \leq 1$, $\mathsf{F}' = \rho$ continuously, and its limits are zero and one. The derivative of $\rho(1 - 2\mathsf{F})$ is $\rho'(1 - 2\mathsf{F}) - 2\rho^2 \in L^1$. Its endpoint limits vanish. Since $\rho' = 2ff'$, dividing the integrated derivative identity by two gives the cross term with a positive sign. Integrating on $[-R, R]$ and sending $R \to \infty$ gives

$$\int_{\mathbb{R}} f' f(1 - 2\mathsf{F}) = A.$$

The polynomial $P(y) = y - 2y^2 + (4/3)y^3$ has derivative $(1 - 2y)^2$. The chain rule and the endpoints of F give

$$\int_{\mathbb{R}} f^2 (1 - 2\mathsf{F})^2 = P(1) - P(0) = 1/3.$$

Absolute integrability holds since this integrand is bounded by f^2. For each real z, both terms in the square in (11.4.1) are in L^2, and their cross product is absolutely integrable. Expansion and the two preceding identities prove the formula. Neither positivity of f nor strict increase of its CDF is required. This proves Lemma 11.4.1. □

One choice of z in Lemma 11.4.1 gives an inequality between A and b. We use it to evaluate the spatial ratio R_{sp} and the energy $\mathcal{E}_{\mathrm{sp}}$ of Proposition 8.2.6 for white noise.

Lean partial

Proposition 11.4.2 (Exact white spatial energy)**.** *For $c > 0$,*

$$R_{\mathrm{sp}} = c/\sqrt{3}, \qquad \mathcal{E}_{\mathrm{sp}} = c^2/6.$$

Both values are zero at $c = 0$.

Proof. We minimize the CDF square in its scalar parameter to bound the ratio. We then evaluate the hyperbolic-secant profiles, which attain both the ratio and the completed-square energy bound at the stated scale.

Step 1. We obtain the sharp ratio upper bound. Substitution $z = 3A$ into (11.4.1) gives $3A^2 \le b$. This is the exact premise and conclusion of the existing conditional WhiteCDF square deduction. Here $A > 0$, since $A = 0$ would imply $f = 0$ a.e. Also $b > 0$: zero derivative makes its continuous representative constant and hence zero in L^2, contradicting unit mass. Thus, $A/\sqrt{b} \le 1/\sqrt{3}$.

Step 2. We evaluate an attaining family and the original covariance energy. For $\ell > 0$ use the real smooth H^1 profile $f_\ell(x) = \sqrt{\ell/2}\,\mathrm{sech}(\ell x)$, with $f_\ell' = -\ell \tanh(\ell x) f_\ell$. Set $t = \tanh(\ell x)$, so $\mathrm{d}t = \ell\,\mathrm{sech}^2(\ell x)\,\mathrm{d}x$. Direct integration gives

$$\int f_\ell^2 = \frac{1}{2}\int_{-1}^{1} \mathrm{d}t = 1, \quad \int f_\ell^4 = \frac{\ell}{4}\int_{-1}^{1}(1-t^2)\,\mathrm{d}t = \ell/3, \quad \int (f_\ell')^2 = \frac{\ell^2}{2}\int_{-1}^{1} t^2\,\mathrm{d}t = \ell^2/3.$$

The ratio is attained, proving $R_{\mathrm{sp}} = c/\sqrt{3}$. The physical Dirac measure introduces no Fourier constant or nonintegrable kernel $|x|^{-1}$. The existing conditional energy deduction applies to $3A^2 \le b$:

$$cA - b/2 \le cA - \tfrac{3}{2}A^2 = c^2/6 - \tfrac{3}{2}(A - c/3)^2 \le c^2/6.$$

The coefficient is covariance mass c in the physical pairing, not a noise coefficient of size c. At $\ell = c > 0$ the profile attains $c^2/6$. These are full H^1 energy profiles; compact approximation equality is Proposition 8.2.5, not a claim that the noncompact profile itself is a compact stochastic control. At $c = 0$ the ratio is zero and the energy is $\sup(-b/2) = 0$, approached by f_ℓ as $\ell \downarrow 0$. No zero-scale profile is used as a unit vector. The CDF, integral and attainment arguments remain analytic; the two finite conditional deductions do not formalize them. This proves Proposition 11.4.2. □

Corollary 11.3.5 bounds C_2 above and below through the spatial energy $\mathcal{E}_{\mathrm{sp}}$. With its white value, both bounds become explicit.

Lean partial

Theorem 11.4.3 (Explicit white moment bounds)**.** *For the same original point limit,*

$$\frac{2}{3}\sqrt{\frac{c}{M_a}} \le C_2(c,a) \le \frac{2}{3}\sqrt{cK_0(a)}, \qquad K_0(a) = \frac{2^a}{1-a}, \quad M_a = \frac{\Gamma_E((1+a)/2)}{\Gamma_E(1+a)\Gamma_E((1-a)/2)}. \tag{11.4.2}$$

Its time exponent is $(3-a)/2$*. These are bounds, not a numerical evaluation of the intrinsic supremum.*

Proof. Here $q = 3, k = 2, m = 3/2$. Formula (8.2.10) gives

$$F_0(z) = 2\left[\frac{(2z)^{1/2}}{8\,3^{3/2}}\right]^{1/2}.$$

For $c > 0$, $\sqrt{2\mathcal{E}_{\mathrm{sp}}} = c/\sqrt{3}$, hence $F_0(\mathcal{E}_{\mathrm{sp}}) = \sqrt{c}/(3\sqrt{2})$ and $2^m F_0(\mathcal{E}_{\mathrm{sp}}) = (2/3)\sqrt{c}$. Substitution into Corollary 11.3.5 proves (11.4.2) in the original units. All Gamma factors are positive finite for $0 < a < 1$. At $c = 0$, $u = 1$ and $C_2 = 0$ by Theorem 11.2.6; both displayed bounds vanish. This proves Theorem 11.4.3. □

For $c > 0$, both formulas in (11.4.2) are multiples of $\sqrt{c}$. Their ratio depends only on a.

Lean full

Corollary 11.4.4 (Uniform relative width of the bound formulas)**.** *For $c > 0$, the ratio of the upper and lower formulas is*

$$\sqrt{K_0(a)M_a} \le \left[\frac{\sqrt{\pi}}{2\Gamma_E(5/4)^2}\right]^{1/2},$$

with equality at $a = 1/2$.

Proof. Duplication and recurrence from Lemma 8.1.1 give

$$\Gamma_E(1+a) = \frac{2^a\Gamma_E((1+a)/2)\Gamma_E(1+a/2)}{\sqrt{\pi}}, \qquad (1-a)\Gamma_E((1-a)/2) = 2\Gamma_E((3-a)/2).$$

Therefore,

$$K_0(a)M_a = \frac{\sqrt{\pi}}{2\Gamma_E(1+a/2)\Gamma_E((3-a)/2)}.$$

Put $x = 1 + a/2$, $y = (3-a)/2$, so $x, y > 0$ and $x + y = 5/2$. In Euler's Gamma integral the $L^2(0,\infty)$ functions $t^{(x-1)/2}e^{-t/2}$ and $t^{(y-1)/2}e^{-t/2}$ have squared norms $\Gamma_E(x), \Gamma_E(y)$ and inner product $\Gamma_E(5/4)$. Cauchy–Schwarz, positivity, inversion and the increasing square root prove the bound. At $a = 1/2$, $x = y = 5/4$, giving equality. Replacing a by $1 - a$ exchanges these two arguments, so only this ratio of bound formulas is symmetric, not the moment constant or exponent. This proves Corollary 11.4.4. □

This example retains the all-model theorem rather than replacing its scope. The formal static exponent is $3/2$ as $a \downarrow 0$; no interchange of long-time and temporal-endpoint limits is asserted. Jensen holds for the same canonical solution, while S_1^{pos} remains auxiliary. The read-only Skorohod comparison at strict spatial Riesz exponent below one does not cover this spatial-white endpoint. A separate white-time problem cannot be substituted for $0 < a < 1$. No new Skorohod result, source correction or certified decimal enclosure is claimed.

11.5 Established steps and open questions

1. **The mixed expansion and the first obstruction.** Chapter 2 proves the complete nonnegative mixed expansion and an independent convergent solution series. It corrects the time-uniformity issue in the source's intermediate estimate. The common-per-pairing majorant has exponent $\rho > \kappa$ and cannot give the desired scale. This is a restriction on that majorant, not on the model or all uses of the source's Theorem 3.1.

2. **Calibrations.** Section A.1 gives the finite white and Riesz coefficients. As $\alpha_0 \downarrow 0$, the target exponent becomes $(4-\alpha)/(3-\alpha)$, the static exponent. Proposition 1.4.4 is unconditional; its numerical $2L_*$ specialization requires the stated first-moment premise. Comparisons with the Skorohod model identify time exponents only.

3. **The full upper scale.** Section B.1 gives explicit bounds when $\alpha \leq 1$. Section 3.3 proves the full homogeneous-covariance upper scale by independent interval fields, local Gaussian-degree estimates and dyadic covariance domination. The latter proof does not assume an endpoint representation of the spatial covariance.

4. **The intrinsic constant.** Sections 5.1–11.2 construct the phase/source framework and prove matching original point-moment bounds. The upper variational expression uses the original covariance norm and its Gaussian quadratic cost. Finite Gram optimization and positive smoothing identify it with the full positive-control lower value. The auxiliary coefficient-one variational quantity is not identified with the first-moment limit of the solution or Chen's printed constants.

5. **Computed bounds and the white example.** Section 11.3 bounds the same constant using the full occupation class and a common spatial energy. Section 11.4 evaluates that energy for $\Gamma = c\delta_0$ and gives explicit moment bounds and the relative width of their formulas. It does not evaluate the intrinsic supremum numerically or assert equality at either bound.

6. **Source comparisons and scope.** The source first-moment normalization remains a qualified comparison question. Chapter 12 collects the failed approaches and explains their precise scope and the constructions that replace them. They are not new premises of the intrinsic-limit proof.

Chapter 12

Obstructions and failed approaches

12.1 How to read the negative results

The proof of the main results did not follow one route from beginning to end. Several plausible steps lost the required time scale, changed the covariance class, discarded part of the wave state, or asserted uniformity that was not available. This chapter explains those failures as mathematical results. Each entry starts with the reason the approach was attractive, states a precise obstruction, and supplies its argument. It then separates what fails from what survives and specifies what a replacement would need to establish.

Where to begin. For pairing arguments, start with the two-chain expansion in Proposition 2.1.1; for covariance and phase arguments, recall Hypothesis 1.2.1 and the displacement–velocity state. The topology section states its own spaces, and the finite examples need only Gaussian moments and elementary optimization. Each entry gives more specific prerequisites and points to the part of the positive proof it explains. The five groups below can be read independently.

The stable records NG-01 to NG-33 are printed below as No-go 01 to No-go 33. Their numbers do not change when related examples are placed together. Some restate results proved earlier in the book; others give the retained counterexample in full. They are records of attempted approaches, not a count of independent discoveries. No-go 33 groups three elementary errors found in review arguments.

The scope of a counterexample. Unless an entry specifies a different model, the covariance and initial data are those of Hypothesis 1.2.1 and the canonical Stratonovich equation with data $(1, 0)$. We write $a = \alpha_0$. Scalar ordinary differential equations, finite matrices and abstract Hilbert-space examples are identified as such. They test the general principles stated in those entries; an example outside Hypothesis 1.2.1 does not refute a theorem restricted to that hypothesis. A numerical majorant growing too quickly is an obstruction to its use in a proof, not a lower bound on the actual moment.

The status of the evidence. The historical record distinguishes arguments already in the book, arguments that received a review, and author-side diagnostics. These descriptions are not interchangeable. A review may have occurred without meeting its required acceptance threshold, as happened for the earlier NG-09 record. The proofs below are the present mathematical account; the original reports and their grades remain unchanged. Where an earlier computation was only formal, the necessary analytic justification is given explicitly rather than attributed to that earlier computation.

Obstruction	What the book keeps explicit	Entries
Pairing and coefficient estimates	Temporal order, spatial support and the quantifiers on constants	01–07, 10, 17, 18
Covariance comparisons	The actual covariance class and the correct order of comparison	08, 09, 11–13, 19
Phase and Gaussian controls	Velocity, the second-order mean and the full tilted law	14–16, 20, 31
Operator spaces and limits	The specified topology, radius dependence and control of variational suprema	21, 22, 24–27, 30, 32
Finite optimization and review	Both variances, active sets and exact algebraic factors	23, 28, 29, 33

The main text cites these entries where they explain a choice in the proof. The entries also point back to the construction or estimate that survives. This is intended to let a reader begin with an attempted approach, understand its obstruction, and then follow the successful replacement.

Tao has observed that negative results are underreported, which can make the public account of AI-assisted mathematics appear more successful than the underlying research process [43, first paragraph]. The purpose here is to make these particular failures usable. Separate source-paper qualifications and failures of the checking process retain their own records; they are not silently added to the 33 mathematical identifiers below.

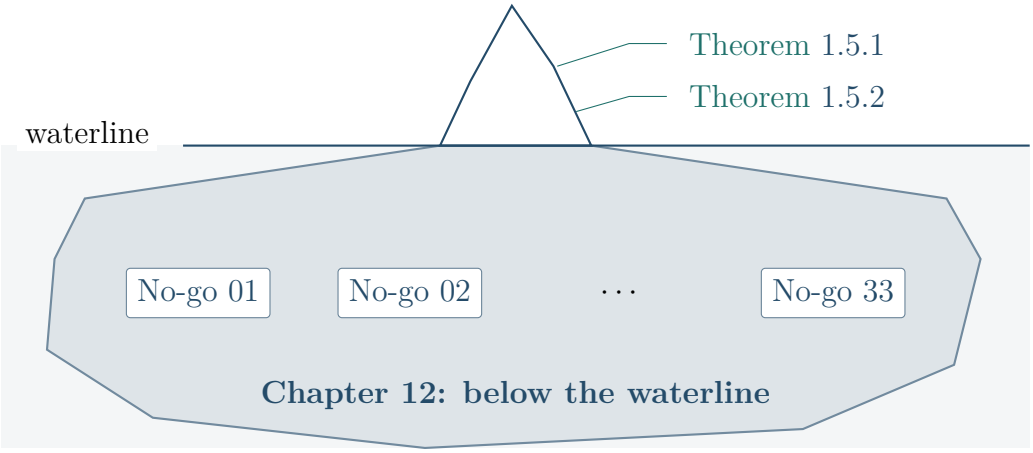

Figure 12.1: The results stated in Chapter 1, Theorems 1.5.1 and 1.5.2, are what shows above the waterline. This chapter is what lies below it: the 33 numbered obstructions and failed approaches, each kept with the reason it was tried and the argument that stops it.

12.2 Pairings, ordering, and comparison kernels

The second moment contains two ordered chains and all their Gaussian pairings, including pairs within a chain. This structure offers several natural reductions: estimate each pairing separately, compare with a single chain, or copy the first-moment clock. The obstructions below distinguish loss of scale from failure of an inequality. A majorant can be too large even when every step used to obtain it is valid.

Throughout this section write $a = \alpha_0$ and $\beta = 4 - \alpha - a$. Let X_n denote the ordered Stratonovich term of degree n, and put

$$a_k = \mathbb{E}X_{2k}(1,x), \qquad A_k = \sum_{m+n=2k} \mathbb{E}[X_m(1,x)X_n(1,x)], \qquad b_1 = \mathbb{E}X_1(1,x)^2.$$

Thus $A_1 = 2a_1 + b_1$. Homogeneity supplies the factor $t^{\beta k}$. The nonnegative convergent moment expansions used here are those of Proposition 2.1.1; they include unequal chain lengths. In dimension one we use $G_s(z) = \frac{1}{2}\mathbf{1}_{\{|z|<s\}}$.

12.2.1 NG-01: one common estimate loses a factorial power

Chen's author version [17, Theorem 3.1, (3.6)] bounds regularized two-chain integrals for arbitrary pairings under its finite-measure and norm hypotheses. Proposition 2.7.1 gives the application under Hypothesis 1.2.1. Applying one common norm bound to every pairing is an attractive first attempt at the upper exponent. The issue is what happens after optimization and summation.

No-go 01 (The common-parameter majorant has the wrong scale)**.** Under Hypothesis 1.2.1, let $P_k = (2k)!/(2^k k!)$ and $K > 0$. The numerical majorant

$$B_K(t) = 1 + \sum_{k\geq 1} (2k+1) P_k K^k \inf_{\theta>0} e^{2\theta t}\theta^{-\beta k}$$

satisfies $\log B_K(t) \asymp t^{\beta/(\beta-1)}$ as $t \to \infty$. Since $\beta/(\beta-1) > \kappa = \beta/(3-\alpha)$, this majorant cannot establish a finite upper constant on the scale t^κ.

Proof. The infimum equals $e^{\beta k}(2t/(\beta k))^{\beta k}$. The inequalities $k! \leq P_k \leq 2^k k!$ and $e^{-k} \leq k!/k^k \leq 1$ show that B_K lies between two series

$$\sum_{k\geq 0} \frac{(ct^\beta)^k}{(k!)^q}, \qquad q = \beta - 1 > 1,$$

with different positive constants c. For $z > 0$, this series is at most $\exp(qz^{1/q})$, by the ℓ^q–ℓ^1 inequality. Its term with $k = \lfloor z^{1/q}/2 \rfloor$ is at least 2^{qk} for large z. This proves the two-sided growth. Finally, $\beta - 1 = 3 - \alpha - a < 3 - \alpha$. This proves No-go 01. □

This restates the obstruction in Proposition 2.7.1 and Remark 2.7.2. The lower estimate is for B_K, not for the moment. The valid upper estimate improves the crude

quadratic exponent, but its factorial denominator misses $(k!)^a$. The split count $2k+1$ costs only an exponential factor in k; removing it does not repair the loss. The same calculation for one chain, with $e^{\theta t}$, has the same defect. Reopening requires an estimate retaining ordering or grouping pairings before taking this common bound. Section 3.3 provides such a different argument.

12.2.2 NG-02: a single adjacent diagram is too large

There are roughly an exponential factor times $k!$ pairings of $2k$ vertices. In white space, a uniform denominator $(k!)^3$ for each diagram would therefore give the desired denominator $(k!)^2$ after summation. The following example explains why that convenient sufficient estimate is stronger than the problem permits.

No-go 02 (No uniform cubic factorial denominator per diagram)**.** Let $d = 1$, $\Gamma = \delta_0$ and $0 < a < 1$. For the split $(0, 2k)$ and adjacent matching $\{(1,2),(3,4),\dots,(2k-1,2k)\}$, its contribution is

$$J_{\mathrm{adj}}(t) = \left[\frac{\Gamma_{\mathrm{E}}(1-a)}{2}\right]^k \frac{t^{(3-a)k}}{\Gamma_{\mathrm{E}}(1+(3-a)k)}.$$

Consequently, there is no finite $C = C(a)$ bounding every diagram by $C^k t^{(3-a)k}/(k!)^3$ for all k and $t > 0$.

Proof. We compute the adjacent diagram after its white contractions and justify that fixed-order limit. Its Dirichlet integral then shows why a uniform cubic factorial denominator is impossible.

Step 1. We identify the adjacent-pair integral and its smoothing limit. Use root-forward increments $h_1, \dots, h_{2k} > 0$ with $\sum h_i < t$. Each adjacent contraction evaluates the even Green factor at zero, giving $1/2$, and integration of the preceding free increment gives mass h_{2j-1}. The temporal factor is h_{2j}^{-a}. Therefore,

$$J_{\mathrm{adj}}(t) = 2^{-k} \int_{\sum h_i < t} \prod_{j=1}^{k} h_{2j-1} h_{2j}^{-a} \, \mathrm{d}h.$$

Here delta contractions mean limits of Gaussian approximate identities. For completeness, fix k and a strictly positive increment vector. After convolution the paired positions approach equality. The even Green factors are continuous at zero; the remaining indicator boundaries are finitely many hyperplanes in the k free positions and have measure zero. The limit is thus the stated diagonal integral. All positions in the original chain lie in $[-t, t]$. Uniformly in the smoothing widths, replacing its Green indicators by one bounds the spatial integral by $2^{-2k}(2t)^k$: each disjoint smoothed pair has integral at most $2t$ over $[-t,t]^2$. The temporal factors on the full time cube are a product of k disjoint factors $|s-r|^{-a}$, each integrable because $a < 1$. Dominated convergence justifies the fixed-order spatial limit through the time integration, and also temporal truncation limits.

Step 2. We compare its growth with the proposed factorial bound. The Dirichlet simplex formula, with parameters 2 and $1-a$ for each pair, now gives the asserted expression. Stirling's formula yields

$$\log\Big((k!)^3 J_{\mathrm{adj}}(1)\Big) = ak\log k + O(k).$$

This exceeds $k\log C$ eventually for every fixed C. This proves No-go 02. □

The adjacent matching is only one diagram. Its denominator is, up to exponential factors, $(k!)^{3-a}$, which is stronger than the desired summed denominator $(k!)^2$. Hence, this witness does not obstruct the summed bound. A viable successor must retain the number of large diagrams, or sum before estimating; it cannot assign the same cubic denominator to all of them.

12.2.3 NG-03: doubled variance does not give the proposed squared mean

A positive mixture of exponentials of linear Gaussian functionals would satisfy a useful comparison between the second moment and the mean at noise amplitude $\sqrt{2}$. Such a representation must be established for the wave rather than inferred from a parabolic analogy.

No-go 03 (Failure of the all-time comparison with unit prefactor)**.** For the admissible Riesz case $d=1$, $\Gamma(x)=|x|^{-1/2}$ and $a=1/2$,

$$\mathbb{E}u(t,x)^2 > \Big(\mathbb{E}u_{\sqrt{2}}(t,x)\Big)^2$$

for all sufficiently small $t>0$, where u_λ uses noise amplitude λ and the same initial data.

Proof. We compare the first nonconstant coefficients in the proposed inequality. We then bound both series remainders to turn that coefficient discrepancy into a strict small-time failure.

Step 1. We compare the two first-order contributions. More generally, for $\Gamma(x)=c|x|^{-\alpha}$, $0<\alpha<1$, direct integration of the length-two chain gives

$$a_1 = \frac{c}{(1-\alpha)(2-\alpha-a)(3-\alpha-a)(4-\alpha-a)}.$$

Indeed the spatial integral is $ch_1h_2^{1-\alpha}/(1-\alpha)$ and its temporal factor is h_2^{-a}; integrate over $h_1+h_2<1$. At $\alpha=a=1/2$, $c=1$, this gives $a_1=1/3$. For independent uniforms U on $[-s,s]$ and V on $[-r,r]$, $0<r\le s$,

$$\mathbb{E}|U-V| = \frac{s}{2} + \frac{r^2}{6s} \le \frac{2s}{3}.$$

Jensen's inequality for $z \mapsto z^{-\alpha}$ implies

$$\int G_s(x)G_r(y)|x-y|^{-\alpha}\,\mathrm{d}x\,\mathrm{d}y \geq (3/2)^{\alpha}s^{1-\alpha}r.$$

Integrating on the two temporal triangles gives

$$b_1 \geq \frac{2(3/2)^{\alpha}}{(1-a)(2-a)(4-\alpha-a)} = \frac{8}{9}\sqrt{\frac{3}{2}} > \frac{2}{3} = 2a_1.$$

Step 2. We justify the strict inequality for sufficiently small positive time. The comparison is a finite-time failure, not just a formal coefficient test. Put $z = t^{\beta}$. The two nonnegative series under comparison have expansions

$$\mathbb{E}u(t,x)^2 = 1 + (2a_1 + b_1)z + O(z^2), \qquad (\mathbb{E}u_{\sqrt{2}}(t,x))^2 = 1 + 4a_1 z + O(z^2).$$

To justify the remainders, choose any fixed positive z_0 at which these series converge, using the moment expansion also at amplitude $\sqrt{2}$. For each nonnegative coefficient sequence (c_j), $\sum_{j\geq 2} c_j z^j \leq (z/z_0)^2 \sum_{j\geq 2} c_j z_0^j$ when $0 \leq z \leq z_0$. Apply this to both series, including the nonnegative Cauchy product for the squared mean. Their difference therefore has the strictly positive leading coefficient $b_1 - 2a_1$. This proves No-go 03. □

For a deterministic nonnegative mixture of Gaussian exponentials, the inequality follows by Tonelli and $\|h+k\|^2/2 \leq \|h\|^2 + \|k\|^2$, provided the same mixture represents all amplitudes in the comparison. That proposed mechanism is excluded by the example. White noise, an eventual large-time comparison, or a prefactor larger than one is not excluded. Reopening requires a restriction or a new comparison that removes the contradicted first-coefficient requirement; it cannot merely assert this positive-mixture representation.

12.2.4 NG-04: a coefficient constant cannot be uniform at the time boundary

Comparing A_k with a_k retains the self-pairings of the Stratonovich problem and would transfer a first-moment bound to the second moment. However, a prescribed asymptotic constant must not be imposed on every low-order coefficient without checking parameter uniformity.

No-go 04 (Divergence of the first coefficient ratio)**.** Fix $0 < \alpha < 1$ and $c > 0$, with $\Gamma(x) = c|x|^{-\alpha}$ in $d = 1$. Then

$$\lim_{a\uparrow 1}(1-a)\frac{A_1}{a_1} = 2^{2-\alpha}(1-\alpha) > 0.$$

In particular no constant depending on α alone, including $2^{4-\alpha}$, can satisfy $A_k \leq C^k a_k$ for every $k \geq 1$ and every $0 < a < 1$ at this fixed spatial covariance.

Proof. We isolate the contribution near equal times and compute its boundary divergence. Dividing by the finite limiting single-chain coefficient shows why no constant uniform in the temporal exponent can work.

Step 1. We identify the diagonal time contribution. Let $K(s,r) = \int G_s(x)G_r(y)c|x-y|^{-\alpha}\,\mathrm{d}x\,\mathrm{d}y$. This is continuous on $[0,1]^2$ by local integrability of the Riesz kernel and dominated convergence on a fixed square. Direct integration gives

$$K(s,s) = \frac{c\,2^{1-\alpha}s^{2-\alpha}}{(1-\alpha)(2-\alpha)}.$$

Writing $v = s - r$, define the continuous function $H(v) = 2\int_v^1 K(s, s-v)\,\mathrm{d}s$. Then

$$b_1 = \int_0^1 v^{-a}H(v)\,\mathrm{d}v, \qquad H(0) = \frac{c\,2^{2-\alpha}}{(1-\alpha)(2-\alpha)(3-\alpha)}.$$

Step 2. We take the boundary limit of the coefficient ratio. For any continuous H on $[0,1]$, $\varepsilon\int_0^1 v^{-1+\varepsilon}H(v)\,\mathrm{d}v \to H(0)$. Indeed the measures have mass one, and their mass on $[\delta,1]$ is $1-\delta^\varepsilon \to 0$; continuity controls $[0,\delta]$. Thus $(1-a)b_1 \to H(0)$. The formula for a_1 in the preceding proof gives

$$a_1 \longrightarrow \frac{c}{(1-\alpha)^2(2-\alpha)(3-\alpha)}.$$

Combine these limits with $A_1 = 2a_1 + b_1$. This proves No-go 04. □

For each fixed $a < 1$, a finite constant $C = C(\alpha, a)$ remains possible; the argument only forces it to diverge as $a \uparrow 1$. It also says nothing against comparisons beginning at large order or large time with suitable prefactors. Reopening requires explicitly allowing that parameter dependence or removing the low orders. Historical static-endpoint tests likewise constrain an endpoint or a uniform family, not a separately chosen constant at an arbitrary positive a.

12.2.5 NG-05: chronological merging breaks wave support

A single chain has the monotone ordering needed by the first-moment representation. Sorting two chains by time looks like a direct way to recover it. Finite propagation prevents the resulting pointwise comparison.

No-go 05 (Support obstruction to pointwise concatenation)**.** In $d = 1$, no finite constant can bound every product of two root-forward chain kernels by the single-chain kernel obtained by chronological merging. The failure occurs in the $(2,2)$ split on a set of positive measure for Riesz covariance and, with domestic pairs, for white covariance.

Proof. We choose two admissible chains whose chronological merge violates a strict propagation constraint. We then keep this defect on sets of positive measure for each of the two covariance cases.

Step 1. We exhibit the positive original product and zero merged product. Work at horizon one with root $(0,0)$. The first chain has times $(1/4, 3/4)$ and positions (x, x), $x = 1/5$; the second has times $(1/2, 7/8)$ and positions (y, y), $y = -2/5$. The four original displacements and elapsed times are

$$(1/5, 1/4), \quad (0, 1/2), \quad (2/5, 1/2), \quad (0, 3/8).$$

Each displacement is strictly smaller than its elapsed time, so their Green product is 2^{-4}. The merged chain instead includes the jump from $(1/4, 1/5)$ to $(1/2, -2/5)$. Its displacement is $3/5 > 1/4$, so that Green factor vanishes. All these inequalities are strict.

Step 2. We retain the support defect under the stated covariance integrations. For white noise choose domestic pairs within each original chain. The delta contractions leave precisely the two free spatial variables x, y. Open neighborhoods of the displayed four times and these two variables preserve both conclusions and have positive contracted measure. Gaussian regularization justifies this contraction as in No-go 02. For Riesz covariance perturb all four spatial positions independently in small neighborhoods. Avoiding the domestic diagonals gives a set of positive ordinary measure on which the covariance factors are finite and strictly positive, while the same support defect persists. No multiplier can turn the zero merged product into a positive upper bound. This proves No-go 05. □

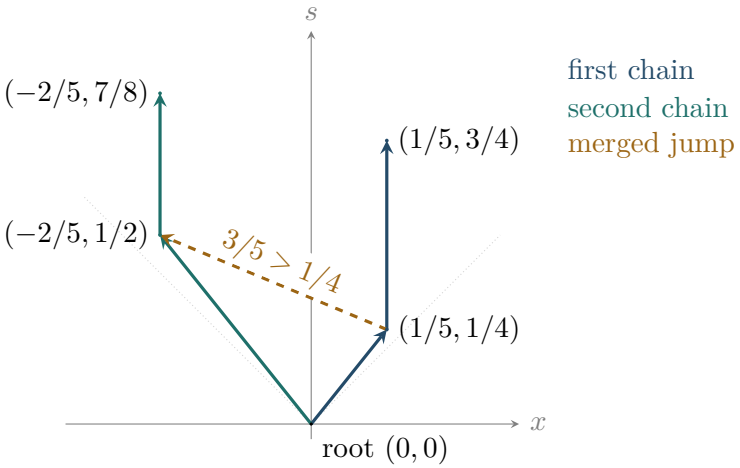

Figure 12.2: Root-forward coordinates (x, s) for No-go 05. Each solid edge lies strictly inside its propagation cone. Chronological merging inserts the dashed jump, whose distance $3/5$ exceeds its elapsed time $1/4$. The picture refutes pointwise concatenation, not an integrated comparison. For domestic white pairs the two free positions are x and y.

The time coordinates here are root-forward chain coordinates; applying a terminal-to-point convention again would change the object being tested. The result concerns pointwise concatenation. Integrated comparisons and comparisons of grouped Wick sums remain possible. Reopening requires averaging, extra displacement variables, or another

mechanism that preserves the two original propagation constraints instead of imposing the false merged one.

12.2.6 NG-06: erasing geometry before summation loses the scale

After white contractions, the temporal pairing sum is symmetric. One can exploit that symmetry immediately by forgetting the spatial indicators. The resulting bound is easy to sum but too weak for the desired exponent.

No-go 06 (The geometry-free majorant)**.** For $d = 1$, $\Gamma = \delta_0$, $0 < a < 1$, replacing every wave indicator by one while retaining only the spatial box $[-t, t]$ gives the coefficient majorant

$$A_k t^{(3-a)k} \le \frac{1}{k!}\left[\frac{2t^{3-a}}{(1-a)(2-a)}\right]^k.$$

Its sum is $\exp(2t^{3-a}/((1-a)(2-a)))$, whose time exponent $3-a$ exceeds the target $(3-a)/2$.

Proof. The spatial replacement gives $(2t)^k/2^{2k} = t^k/2^k$ for each pairing. After this replacement the sum over all pairings is symmetric in the $2k$ times. Its integral over a split (m, n) simplex equals the cube integral divided by $m!n!$. The identities

$$\sum_{m+n=2k} \frac{1}{m!n!} = \frac{2^{2k}}{(2k)!}, \qquad P_k = \frac{(2k)!}{2^k k!}, \qquad \int_0^t \int_0^t |s-r|^{-a}\, \mathrm{d}s\, \mathrm{d}r = \frac{2t^{2-a}}{(1-a)(2-a)}$$

give the stated product and its exponential sum. This proves No-go 06. □

This is a valid upper bound and a failure of its scale, not a moment lower bound. Symmetry itself remains useful. The reopening condition is a spatial estimate with enough order dependence retained before temporal symmetrization; Proposition B.1.2 retains this order dependence and sums the temporal pairings afterwards (see Remark B.1.8).

12.2.7 NG-07: block labels are not chronological ranks

Temporal singularities favor close paired times. A proposed penalty for long pairs must therefore measure time separation or actual chronological rank. Labeling all vertices of one chain before those of the other creates an artificial distance unrelated to either.

No-go 07 (Large label span does not imply a cubic denominator)**.** In white space with $0 < a < 1$, consider two length-k chains and the matching $j \leftrightarrow k + j$. Although every pair has label distance k, its unit-time diagram satisfies

$$J_k(1) \ge \left(\frac{3\,4^a}{128}\right)^k k^{-(3-a)k}.$$

Thus no estimate assigning $C^k/(k!)^3$ to these diagrams solely on account of their

block-label span can hold uniformly in k.

Proof. Let the chain times be s_j, r_j, with increments h_j, g_j from the common root. White contractions identify their paired positions, and integration of the successive spatial increments gives $2^{-k}\prod_{j=1}^{k}\min(h_j, g_j)$. Restrict both s_j, r_j to $((j-1/4)/k, j/k)$. The domain has volume $(4k)^{-2k}$, each increment is at least $3/(4k)$, and each paired difference is at most $1/(4k)$. Multiplication gives the lower bound. The contraction can again be obtained at fixed k by Gaussian smoothing; the spatial box bound and integrable disjoint temporal factors justify the limit. Stirling's formula implies $\log((k!)^3 J_k(1)) \geq ak\log k + O(k)$, contradicting any fixed C. This proves No-go 07. □

Within each window the paired vertices are adjacent in the actual chronological ordering. This example only refutes the label substitution; it supplies no new shuffle estimate or Skorohod theorem. Reopening would require a statement conditioned on actual order and an independent proof of its summed cost. The shared pure-cross direction is recorded for later work and is not developed here.

12.2.8 NG-10: an unweighted merge does not remove a crossing covariance

A two-wave convolution estimate can remove an interior chain vertex when no other factor depends on it. In a crossing pairing that vertex still interacts with a remote partner. The following order-four calculation identifies the missing weight before any all-order iteration is attempted.

No-go 10 (No finite spatial-supremum pullout in the merge lens)**.** In $d = 2$, take $\Gamma(z) = c|z|^{-\alpha}$, $c > 0$, $0 < \alpha_0 < 1/2$ and $3/2 \leq \alpha < 2 - \alpha_0$. For the root-forward $(0, 4)$ diagram with pairs $(1, 3), (2, 4)$, merging vertex two requires the weighted integral

$$W = c\int_a^b (T-v)^{-\alpha_0}\int_{\mathbb{R}^2} G_{v-a}(y-x)G_{b-v}(z-y)|w-y|^{-\alpha}\,\mathrm{d}y\,\mathrm{d}v, \qquad 0 < a < b < T.$$

Here the letters a, b, T are vertex times, so the temporal exponent is written α_0. The spatial weight has no finite uniform essential supremum on admissible merge lenses. Hence, pulling it out by a uniform supremum cannot reduce W to an unweighted two-wave convolution.

Proof. Set $t = 5$, $a = 1$, $b = 3$, $T = 4$, $x = (0, 0)$, $z = (1/2, 0)$ and $w = (1/4, 0)$. For v near 2, the point $y = w$ is strictly inside both disks $|y - x| < v - a$ and $|z - y| < b - v$. It also satisfies the outer constraint $|w - z| < T - b$, and $|x| < a$. There is therefore an interior ball about w in the merge lens. For every $M > 0$ a smaller ball has positive Lebesgue measure and $|w - y|^{-\alpha} > M$ there. This proves infinite essential supremum; the strict inequalities persist under small changes of the fixed data. The other pair contributes $(b-a)^{-\alpha_0}c|z-x|^{-\alpha}$ outside the merge, whereas the two factors for pair $(2, 4)$ depend on v, y and must remain in W. The temporal weight alone admits the bound $(T-v)^{-\alpha_0} \leq (T-b)^{-\alpha_0}$. This proves No-go 10. □

The unweighted powered-kernel convolution estimate in [8, Lemma 4.3, p. 20] assumes $1/2 < q < 1$ and $1 \le \delta \le 1/q$. It contains no covariance factor linking the integration variable to a remote vertex and does not directly estimate W above. Infinite essential supremum does not imply divergence of W or of the diagram: the Riesz singularity is locally integrable for $\alpha < 2$. A reopening condition is a covariance-weighted convolution inequality, or an explicit envelope integrable against the remaining diagram factors, with the remote-gap cost retained. No such inequality is asserted here.

12.2.9 NG-17: direct copying of the first-moment clock undercounts

The source's first-moment clock representation suggests attaching one Brownian clock to each ordered chain. A degree-two cross pair already tests whether this copying preserves the interaction. It does not, even when the two clocks are shared.

No-go 17 (Constant-correlation clock copying misses a positive factor)**.** Under the nonzero covariance hypotheses of Proposition D.2.2, let $K_\Gamma(\theta)$ be the true cross-pair transform and $J_{\Gamma,\rho}(\theta)$ the direct unweighted candidate (D.2.4), $-1 \le \rho \le 1$. Then for every $\theta > 0$,

$$0 < J_{\Gamma,\rho}(\theta) \le J_{\Gamma,1}(\theta) < K_\Gamma(\theta).$$

If $\alpha = 1$, then $J_{\Gamma,1} = (2 - 2^a)K_\Gamma$.

Proof. Recall $\mathcal{R}_\Gamma(q) = \int (q^2 + |\xi|^2)^{-1} \mu(\mathrm{d}\xi)$. The exact transform identities proved in Proposition D.2.2 give

$$w_\theta(\lambda) = \frac{\lambda^{a-2}}{2\theta\Gamma_{\mathrm{E}}(a)}[\mathcal{R}_\Gamma(\theta) - \mathcal{R}_\Gamma(\theta+\lambda)], \qquad K_\Gamma = \int_0^\infty w_\theta(\lambda)\,\mathrm{d}\lambda,$$

$$J_{\Gamma,1} = \int_0^\infty \frac{2\theta}{2\theta+\lambda} w_\theta(\lambda)\,\mathrm{d}\lambda.$$

The density is strictly positive because $\mu \neq 0$ and the resolvent strictly decreases. It is integrable: homogeneity bounds it by multiples of λ^{a-1} near zero and λ^{a-2} at infinity. The multiplier is strictly between zero and one. For smaller correlations, $u+v-2\rho\min(u,v) \ge |u-v|$, and the positive Laplace integral $\Psi_a(r,v)$ in (D.2.3) decreases with v. This proves the chain of inequalities. When $\alpha = 1$, insert $\mathcal{R}_\Gamma(q) = \mathcal{R}_\Gamma(1)/q$ and use $\int_0^\infty x^{a-1}/(x+c)\,\mathrm{d}x = c^{a-1}\Gamma_{\mathrm{E}}(a)\Gamma_{\mathrm{E}}(1-a)$ to obtain the ratio. This proves No-go 17. □

This is the already proved book obstruction, not a new clock impossibility theorem. At the static endpoint the discrepancy disappears, so homogeneity and static checks alone cannot detect it. At degree two the missing shared-clock multiplier is exactly $1 + \lambda/(2\theta)$; no higher-order correction rule follows. Reopening requires relative-order weights or a different coupling or representation that reproduces the actual cross-pair transform. Remark D.2.3 gives the full boundary of this statement, including the distinction between gap transforms and physical unequal-time moments.

12.2.10 NG-18: erasing the middle-cross shift makes an envelope too large

A later white-space comparison retains four vertices and a middle cross pair. Removing the clock-overlap penalty gives a positive upper bound. One further simplification, erasing the shift of its root kernel, also increases the bound, but increases it beyond the comparator at an explicit parameter point. This is an obstruction to closing that envelope, not a counterexample to the original comparison.

No-go 18 (The shift-erased envelope is not below the wave transform)**.** Consider the white $(1,3)$ diagram with middle-cross partition $02 \cdot 13$, common gap damping one, cross rate $\lambda \geq 0$ and self rate $\nu \geq 0$. Put $b = 1+\nu$, $c = 1+\lambda$, $A = \lambda + \lambda^2/2$. Its actual wave transform I and the shift-erased clock upper envelope $M_b(0;A)$ satisfy at $b = 1, c = 11/10$

$$I = \frac{545}{11616}, \qquad M_b(0;A) = \frac{1025}{21483}, \qquad I - M_b(0;A) = -\frac{6005}{7562016} < 0.$$

Consequently the proposed pointwise closure $M_b(0;A) \leq I$ is false.

Proof. We identify the actual wave transform and the particular shift-erased envelope separately. We then evaluate both expressions at the stated rational parameters to disprove this envelope closure, without replacing the original clock candidate by the envelope.

Step 1. We compute the actual middle-cross wave transform. We give the integral identifications so that the rational test specifies which bound fails. With singleton gap u and long-chain gaps v, w, z, the spatial factor is $\int G_u(X)G_v(Y)G_w(X-Y)G_z(Y-X)\,\mathrm{d}X\,\mathrm{d}Y$. Set $R = u+v$, $q = u-v$. Integration in R, including its Jacobian, gives the exact wave expression

$$I = \frac{1}{16}\int_{w,z>0}\int_{\mathbb{R}} e^{-b(w+z)-\lambda|q-w|}\int_0^{\min(w,z)} e^{-\max(|q|,t)}\,\mathrm{d}t\,\mathrm{d}q\,\mathrm{d}w\,\mathrm{d}z.$$

To check the spatial reduction, the derivative of the area $\{|X|<u, |Y|<v, |X-Y|<C\}$ with respect to C is $2(R-\max(C,|q|))_+$; the area vanishes at $C=0$. Integrate this against $e^{-R}/32$ for $R > |q|$. Next integrate $z \geq t$ and put $w = t+x$. Splitting the remaining q integral into $q<0$, $0 \leq q \leq t$, and $q \geq t$ gives respectively

$$\frac{1/c + 1/(2b+\lambda+1)}{16b(b+\lambda)(2b+2\lambda+1)}, \qquad \frac{1}{16b(b+\lambda)(2b+1)(2b+1+\lambda)},$$

$$\frac{1/(b+\lambda)+1/c}{16b(2b+1)(b+1)}.$$

Adding gives

$$I = \frac{2b^2+4bc+2c^2-c+1}{8bc(b+1)(2b+1)(b+c-1)(2b+2c-1)}.$$

Step 2. We identify the root kernel and the shift factor that is discarded. For the clock envelope write $h(r) = (2\pi r)^{-1/2}$ and $m(s) = 1/(\pi\sqrt{2}\sqrt{s-1/2})$, $s > 1/2$. The two spatial pair differences have covariance matrix $\left(\begin{smallmatrix} u+v+w & -w \\ -w & w+z \end{smallmatrix}\right)$. Writing $r = w + z$, its determinant is $rR + wz$, so their joint white density factors as $h(r)h(R + wz/r)$. After deleting the nonnegative clock-overlap penalty, the root kernel is

$$H_\gamma(q) = \int_{|q|}^\infty e^{-R/2} h(R+\gamma)\, \mathrm{d}R = \int_{1/2}^\infty \frac{m(s)}{s} e^{-(s-1/2)\gamma} e^{-s|q|}\, \mathrm{d}s, \qquad \gamma = \frac{wz}{r}.$$

The equality follows from the positive Gamma integral for h. The convolution of the mixture component $q \mapsto e^{-s|q|}$ with $q \mapsto e^{-A|q|}$, evaluated at w, equals $2S_{A,s}(w)/(s + A)$, where

$$S_{A,s}(w) = e^{-Aw} + \int_0^w A e^{-At} e^{-s(w-t)}\, \mathrm{d}t \le 1.$$

The inequality follows by bounding $e^{-s(w-t)}$ by one; the remaining integral is $1 - e^{-Aw}$. Replacing S by one is precisely the shift erasure. More generally, for $\eta \ge 0$, replacing it by $e^{-\eta w}$ defines

$$M_b(\eta; A) = \frac{1}{16} \int_{1/2}^\infty \frac{m(s)}{s(s+A)} \int_0^\infty h(r) e^{-b^2 r/2} \int_0^r e^{-(s-1/2)w(r-w)/r - \eta w}\, \mathrm{d}w\, \mathrm{d}r\, \mathrm{d}s.$$

Step 3. We evaluate the shift-erased envelope and compare the rational values. All integrals here are positive. Set $w = rt$ and $\tau = s - 1/2$. For $\eta, \tau \ge 0$, put $p = \sqrt{b^2 + 2\eta}$. The elementary bridge integral is

$$\int_0^1 [b^2 + 2\eta t + 2\tau t(1-t)]^{-3/2}\, \mathrm{d}t = \frac{2(p+b)}{bp((p+b)^2 + 2\tau)}.$$

It follows by integrating a quadratic power; at $\eta = \tau = 0$ both sides are b^{-3}. Substitution $z = \sqrt{2s-1}$ and partial fractions give

$$\begin{aligned} M_b(\eta; A) &= \frac{p+b}{2\pi bp} \int_0^\infty \frac{\mathrm{d}z}{(z^2+1)(z^2+c^2)(z^2+(p+b)^2)} \\ &= \frac{1 + c + p + b}{4bpc(c+1)(c+p+b)(1+p+b)}. \end{aligned}$$

The usual identity $\int_0^\infty (z^2 + q^2)^{-1}\, \mathrm{d}z = \pi/(2q)$ proves the partial fraction evaluation; coincident rates follow by continuity. At $\eta = 0$, $p = b$. Substituting the asserted rational parameters in these two expressions gives the displayed strict gap. This proves No-go 18. □

The boundary value $\nu = 0$ is a legitimate fixed-parameter transform; continuity of both rational expressions also gives an overshoot for some $\nu > 0$ nearby. The no-go does not refute $J \le I$, where J is the original shared-clock candidate, nor does it decide an integrated comparison using this envelope. The surviving middle-cross comparison retains $S_{A,1/2}(w)$, instead of replacing it by one, and obtains a smaller envelope. Reopening this particular closure requires keeping a shift cost or proving a different integrated estimate. The historical standalone record was not separately adjudicated; the subsequent middle-cross analysis and this reconstructed proof do not change that historical review status.

12.3 Covariance transformations and their limits

Covariance comparisons offer a way to use a simpler model without estimating all the pairings again. Three different requirements enter such an argument: positive definiteness, local finiteness, and uniformity of the comparison. None follows from homogeneity alone. The examples below separate these requirements. The final example also distinguishes positive semidefinite order from pointwise order, which matters for the wave mean.

12.3.1 NG-08: the translated spatial maximum

The conditional higher-dimensional argument replaces a translated wave convolution by a uniform spatial maximum. This would remove the dependence on the other vertices of a pairing. The price is an additional hypothesis, not a consequence of the covariance assumptions.

No-go 08 (A spatial maximum need not be finite)**.** Hypothesis B.2.1 fails for two-dimensional Riesz covariance of degree $-\alpha$ when $3/2 \le \alpha < 2$. For each $1 < \alpha < 2$, it also fails for some nonnegative, positive definite, locally integrable homogeneous product covariance in dimensions two and three. These examples can satisfy the model condition $\alpha + \alpha_0 < 2$.

Proof. We exhibit the boundary divergence for planar Riesz covariance and then the anisotropic product example in both dimensions. The smoothing limit shows why neither example admits the proposed uniform spatial maximum.

Step 1. We test the translated planar Riesz convolution. We restate the witnesses from Proposition B.2.5. For Riesz covariance translate the singularity to e_1, on the boundary of the unit wave disk. Write $y = e_1 + \rho(\cos\phi, \sin\phi)$ and restrict to $0 < \rho < 1/2$, $2\pi/3 \le \phi \le 4\pi/3$. Then $0 < 1 - |y|^2 \le 2\rho$, so the wave density and polar Jacobian give

$$\int G_1^{(2)}(\,\mathrm{d}y) c|y - e_1|^{-\alpha} \ge \frac{c}{3\sqrt{2}} \int_0^{1/2} \rho^{1/2-\alpha}\,\mathrm{d}\rho = \infty.$$

At $\alpha = 3/2$ the divergence is logarithmic.

Step 2. We test the product covariance and its smoothed limits. For the product example choose

$$a_1 = \frac{1 + \max\{2 - \alpha, \alpha - 1\}}{2}, \qquad a_2 = \alpha - a_1.$$

Then $0 < a_1, a_2 < 1$ and $a_1 + a_2/2 > 1$. The function $\gamma(x) = c|x_1|^{-a_1}|x_2|^{-a_2}$, constant in x_3 when $d = 3$, is locally integrable and homogeneous. Each factor is a positive Gaussian mixture, hence the product is positive definite. With $u = 1 - y_1$ and $y_2 = \sqrt{2u - u^2}\, w$, direct integration yields

$$\int G_1^{(2)}(\,\mathrm{d}y)\gamma(y - e_1) = \frac{cB((1-a_2)/2, 1/2)}{2\pi} \int_0^2 u^{-a_1}(2u - u^2)^{-a_2/2}\,\mathrm{d}u = \infty.$$

The projection of the three-dimensional wave measure onto its first two coordinates is $G_1^{(2)}$, which proves the three-dimensional claim. Gaussian smoothing converges off the singular sets, which have zero translated wave measure. Fatou's lemma therefore gives divergence in lower limit as the smoothing widths decrease to zero. Thus, smoothing cannot restore the required uniform constant. Taking $0 < \alpha_0 < 2-\alpha$ ensures admissibility. This proves No-go 08. □

This result excludes the spatial-supremum input, not moment finiteness or the required time scale. The conditional theorem remains useful where its hypothesis holds. Reopening this route for the full class would require an integrated estimate retaining the geometry lost by the supremum; Section 3.3 supplies a different full-class argument.

12.3.2 NG-09: radial lowering in three dimensions

Multiplication by $|x|^{\alpha-1}$ gives the desired endpoint degree -1. The following example shows why this degree calculation does not construct a covariance. The original endpoint review returned MEDIUM confidence and was not accepted at the HIGH threshold. The argument below is a complete reconstruction; it does not change that historical disposition.

No-go 09 (Radial lowering can destroy positive definiteness)**.** In dimension three let

$$\Gamma(x) = |x_1|^{-9/10}|x_2|^{-3/5}, \qquad F(x) = |x|^{1/2}\Gamma(x).$$

The covariance Γ satisfies the homogeneous model assumptions with $\alpha = 3/2$ and $\alpha_0 = 1/4$. The locally integrable tempered function F is not positive definite as a distribution.

Proof. We verify the original covariance, then show that the radially modified function has a heat convolution growing along the third coordinate. This contradicts the boundedness that positive definiteness would require.

Step 1. We check the original covariance and the modified function. The exponents of both coordinate factors lie in $(0, 1)$. Local integrability, temperedness, and positive definiteness of Γ follow from the one-dimensional Gaussian mixture formula, applied in each coordinate. The third factor is the constant covariance one. Multiplication by $|x|^{1/2}$ preserves local integrability and temperedness.

Step 2. We obtain the contradiction after Gaussian convolution. Fix a centered Gaussian heat density p_σ. Its convolution with F is finite at zero: the coordinate singularities are integrable and the remaining growth is polynomial. On the other hand, restrict the convolution at Le_3 to

$$1 \le y_1 \le 2, \qquad 1 \le y_2 \le 2, \qquad |y_3 - L| \le 1.$$

For $L \ge 2$, the Gaussian factor $p_\sigma(Le_3 - y)$ is bounded below there by a fixed positive constant, the coordinate powers are bounded below, and $|y|^{1/2} \ge (L-1)^{1/2}$. Hence,

$$(p_\sigma * F)(Le_3) \ge c_\sigma \sqrt{L}.$$

If F were positive definite, its quadratic form on Schwartz tests would satisfy Cauchy–Schwarz. Take a Gaussian test whose autocorrelation is p_σ, and its translate by x. The two diagonal quadratic forms are both $(p_\sigma * F)(0)$, while the cross form is $(p_\sigma * F)(x)$. Consequently,

$$|(p_\sigma * F)(x)| \le (p_\sigma * F)(0), \qquad x \in \mathbb{R}^3.$$

The lower bound along Le_3 contradicts this inequality. This proves No-go 09. □

The obstruction concerns this Euclidean radial multiplication. It leaves coordinatewise constructions and the planar endpoint argument intact; see Remark C.2.8. A successor must verify positive definiteness of its endpoint, rather than infer it from degree and sign.

12.3.3 NG-11: additive variance interpolation

A covariance mixture would be easy to handle if its second moment were log-convex in the additive variance. The following scalar calculation refutes that unrestricted principle. It is outside the strict homogeneous model and is not a counterexample to a model-specific comparison.

No-go 11 (A scalar wave moment is not log-convex in variance)**.** Let $y'' = Zy$, $y(0) = 1$, $y'(0) = 0$, where Z is centered Gaussian of variance A. For $F(A) = \mathbb{E}[y(1)^2]$,

$$F(100)^2 > F(99)F(101).$$

Thus, $\log F$ is not convex on $(0, \infty)$.

Proof. We express the scalar moment as a positive series and bound its tail. The resulting finite rational enclosures disprove the stated log-convexity inequality.

Step 1. We obtain the series and a controlled tail. Interpreting $\cosh\sqrt{z}$ by its entire power series gives

$$F(A) = 1 + \sum_{k\ge1} t_k(A), \qquad t_k(A) = \frac{2^{3k-1}(2k)!}{k!(4k)!}A^k.$$

Absolute termwise Gaussian integration follows from $\mathbb{E}\exp(2\sqrt{|Z|}) < \infty$. All displayed terms are positive. Their ratio satisfies

$$\frac{t_{k+1}(A)}{t_k(A)} = \frac{16A(2k+1)}{(4k+1)(4k+2)(4k+3)(4k+4)} \le \frac{16A}{(4k+1)^3}.$$

Write $S_{20} = 1 + \sum_{k=1}^{20} t_k(A)$ and $q_A = 16A/81^3 < 1$ for the three values in question. Then

$$S_{20} \le F(A) \le S_{20} + \frac{t_{21}(A)}{1 - q_A}.$$

Step 2. We compare the rigorous rational enclosures. Substitution in these finite rational expressions gives the following outward enclosures, with common denominator 10^6:

A	10^6 times lower bound	10^6 times upper bound
99	207442589	207442590
100	212332413	212332414
101	217304018	217304019

In particular,

$$F(100)^2 - F(99)F(101) \geq \frac{6945091633359}{10^{12}} > 0.$$

This proves No-go 11. □

Positive power-series coefficients do imply convexity of $t \mapsto \log F(e^t)$, by Hölder's inequality. Thus, geometric interpolation of amplitudes survives. An additive-covariance argument would need additional hypotheses and a separate proof; the scalar test prevents using log-convexity as a general Gaussian-wave fact.

12.3.4 NG-12: a heat–Mellin square need not be locally finite

Squaring a heat-smoothed covariance preserves positive definiteness, and a Mellin weight can prescribe homogeneity. This suggests an endpoint recipe with no angular decomposition. Its missing requirement is local finiteness of the infinite positive mixture.

No-go 12 (Failure of a heat–Mellin endpoint recipe)**.** Let $d = 3$, $\alpha = 11/10$, $\alpha_0 = 1/4$, and

$$\Gamma(x) = |x_1|^{-9/10}|x_2|^{-1/5}, \qquad F_s = p_s * \Gamma.$$

Although Γ is an admissible covariance, the putative endpoint density of degree $-\beta$, with $\beta = 9/5$,

$$H(x) = \int_0^\infty s^{(2\alpha-\beta)/2-1} F_s(x)^2 \, \mathrm{d}s = \int_0^\infty s^{-4/5} F_s(x)^2 \, \mathrm{d}s$$

does not define a locally finite measure.

Proof. The coordinate exponents show admissibility as in No-go 09. Heat convolution factorizes in the first two coordinates. For $0 < s < 1/16$ and $|x_1| \leq \sqrt{s}$, integrating the first Gaussian convolution over $\sqrt{s} \leq y_1 \leq 2\sqrt{s}$ gives

$$(p_s^{(1)} * |\cdot|^{-9/10})(x_1) \geq c s^{-9/20}.$$

For $1/2 \leq x_2 \leq 1$, integrate the second convolution over $x_2 \leq y_2 \leq x_2 + \sqrt{s}$; its value is bounded below by a positive constant. The third coordinate contributes one. On the fixed box $B = [-1, 1] \times [1/2, 1] \times [-1, 1]$, the strip $|x_1| \leq \sqrt{s}$ therefore gives

$$\int_B F_s(x)^2 \, \mathrm{d}x \geq c s^{1/2-9/10} = c s^{-2/5}.$$

Tonelli's theorem implies

$$\int_B H(x)\,\mathrm{d}x \geq c\int_0^{1/16} s^{-6/5}\,\mathrm{d}s = \infty.$$

This proves No-go 12. □

The positive-definiteness calculation for finite mixtures is not the problem. The infinite mixture has infinite mass on a compact set. This excludes the displayed recipe, not endpoint interpolation itself. A replacement must prove local finiteness, for example by controlling the coordinate singularities before integrating the smoothing scale.

12.3.5 NG-13: angular smoothing and isotropic envelopes

Smooth angular densities admit finite angular suprema. It is tempting to approximate a singular covariance by such densities and apply the Riesz estimate with that supremum as amplitude. The limit below shows why the amplitudes cannot remain bounded.

No-go 13 (No uniform isotropic envelope for a plane covariance)**.** In $\mathbb{R}^3 = \mathbb{R}^2 \times \mathbb{R}$ set

$$\Gamma(\mathrm{d}y, \mathrm{d}z) = \frac{1}{2\pi}|y|^{-1/2}\,\mathrm{d}y\,\delta_0(\mathrm{d}z).$$

This is an admissible covariance with $\alpha = 3/2$ and $\alpha_0 = 1/4$. If nonnegative measures Γ_n converge vaguely to Γ and satisfy

$$\Gamma_n(\mathrm{d}x) \leq C_n|x|^{-3/2}\,\mathrm{d}x,$$

then $C_n \to \infty$.

Proof. We verify that the plane-supported covariance is admissible. A bounded subsequence of isotropic envelope constants would force its vague limit to have a Lebesgue density, contradicting its planar mass.

Step 1. We verify the singular covariance example. The planar Riesz factor is locally integrable and positive definite by its Gaussian mixture representation. The normal Dirac covariance is positive definite: in its quadratic form the two normal coordinates coincide, leaving an integral of nonnegative tangential quadratic forms. Thus, the product is positive definite. For every $r > 0$ and Borel set A, the substitution $y = ry'$ in its defining integral gives $\Gamma(rA) = r^{2-1/2}\Gamma(A) = r^{3/2}\Gamma(A)$. Its finite mass on a radius R ball is proportional to $R^{3/2}$; polynomial mass growth also gives temperedness.

Step 2. We contradict bounded envelope constants by singular support. Suppose a subsequence of C_n were bounded by $C < \infty$. For every nonnegative compactly supported continuous f, vague convergence gives

$$\int f\,\mathrm{d}\Gamma = \lim_n \int f\,\mathrm{d}\Gamma_n \leq C\int f(x)|x|^{-3/2}\,\mathrm{d}x.$$

This is measure domination, so Γ would be absolutely continuous with respect to three-dimensional Lebesgue measure. But the compact planar annulus $\{(y,0) : 1 \le |y| \le 2\}$ has positive Γ mass and zero Lebesgue measure. This contradiction excludes every bounded subsequence, proving the asserted limit. This proves No-go 13. □

This argument applies in particular to angular smoothing whenever the smoothed covariances converge to the plane measure. It requires no ellipsoid representation. It rules out a uniform scalar isotropic density envelope, not other covariance majorants or density of any proposed cone. The reopening condition is an estimate that remains uniform without taking an angular supremum, or a comparison adapted to the singular support.

12.3.6 NG-19: discarding an independent Gaussian residual

An orthogonal Gaussian projection produces an independent residual with positive semidefinite covariance. This makes projection a useful change-of-law tool. It does not give pointwise nonnegative residual covariance, and the wave mean need not increase when that residual is restored.

No-go 19 (A positive semidefinite residual can lower the wave mean)**.** There is an admissible one-dimensional parent covariance C and an actual rank-one Gaussian projection with covariance P such that $C - P$ is positive semidefinite but

$$\mathbb{E}u_C(h;1,0) < \mathbb{E}u_P(h;1,0)$$

for all sufficiently small positive noise couplings h. The projection P is not asserted to be stationary or homogeneous.

Proof. We construct an actual Gaussian projection of the parent field and compare the two degree-two mean coefficients. Bounds on the higher-order tails then turn that coefficient gap into a strict small-coupling failure of residual monotonicity.

Step 1. We construct the parent field and its rank-one projection. Put $a = 99/100$ and

$$C((s,x),(t,y)) = (1-a)|s-t|^{-a}|x-y|^{-1/2}.$$

Its spatial degree is $\alpha = 1/2$, and $\alpha + a < 2$. Gaussian mixtures of the two power kernels verify positive definiteness and local integrability. Let $\psi(s,x) = \mathbf{1}_{[0,1]}(s)\mathbf{1}_{[-1,1]}(x)$, and $V = \mathbb{E}W(\psi)^2$. The indicator is a legal Hilbert-space test by bounded smooth approximation and dominated convergence. Local integrability and positivity of C give $0 < V < \infty$. Put $Z = W(\psi)/\sqrt{V}$ and define the covariance profile by the locally integrable kernel formula

$$m(s,x) = \frac{1}{\sqrt{V}} \int_0^1 \int_{-1}^1 C((s,x),(r,y))\,\mathrm{d}y\,\mathrm{d}r.$$

For every smooth compactly supported spacetime test f, Fubini's theorem identifies $\langle m, f\rangle = \mathbb{E}[W(f)Z]$. Thus, m is the covariance of the generalized field with Z; no

pointwise random variable $W(s,x)$ is used. Gaussian projection gives $W = Zm + W^{\perp}$ with $W^{\perp}$ independent of Z and covariance $C - P$, where $P = m \otimes m$. Cauchy–Schwarz gives its positive semidefiniteness.

Step 2. We bound the projected profile and compare the mean coefficients. Direct integration gives, on $0 \le s \le 1$,

$$E_\phi = \frac{16\sqrt{2}}{3}, \quad V = \frac{2E_\phi}{2-a}, \quad m(s,x) = \frac{B_a(s)F(x)}{\sqrt{V}},$$

where $B_a(s) = s^{1-a} + (1-s)^{1-a} \ge 1$ and $F(x) = \int_{-1}^{1} |x-y|^{-1/2}\,\mathrm{d}y$. We have $F \le 4$ everywhere and $F(x) \ge 2\sqrt{2}$ for $|x| \le 1$. Thus, m is bounded and nonnegative, and $m(s,x)m(t,y) \ge 8/V$ on the backward cone of $(1,0)$.

For a covariance D the degree-two ordinary mean coefficient is

$$A_D = \int_{0<s<t<1} \int_{\mathbb{R}^2} G_{1-t}(-y) G_{t-s}(y-z) D((s,z),(t,y))\,\mathrm{d}z\,\mathrm{d}y\,\mathrm{d}s\,\mathrm{d}t.$$

This is the single self-pair term of Proposition 2.1.1; there is no additional factorial. With $G_r(x) = \mathbf{1}_{\{|x|<r\}}/2$, integration of the parent covariance yields

$$A_C = \frac{1-a}{1-\alpha} \frac{1}{(2-\alpha-a)(3-\alpha-a)(4-\alpha-a)} = \frac{20000}{1932951} < \frac{1}{96}.$$

For covariance one the same integral is $\int_{0<s<t<1} (1-t)(t-s)\,\mathrm{d}s\,\mathrm{d}t = 1/24$. Therefore,

$$A_P \ge \frac{8}{24V} = \frac{101}{3200\sqrt{2}} > \frac{1}{48}.$$

Step 3. We pass the strict coefficient gap to the full means. We justify passage from coefficients to full means. Write the parent solution as $u_C(h) = \sum_{n\ge 0} h^n X_n$. For any fixed $r > 1$, finiteness of the second moment at amplified covariance $r^2 C$ and nonnegativity of the mixed moments in Proposition 2.1.1 give

$$\|X_n\|_2 \le \sqrt{B_r}\, r^{-n}, \qquad B_r = \mathbb{E}|u_C(r;1,0)|^2 < \infty.$$

Hence, the L^2 norm of the tail starting at $n = 4$ is at most $\sqrt{B_r}(|h|/r)^4/(1-|h|/r)$. Odd means vanish by Gaussian sign symmetry, giving $\mathbb{E}u_C(h) = 1 + h^2 A_C + O(h^4)$.

For P, the potential is the bounded profile Zm. If $M = \sup|m|$, the deterministic Picard coefficients at time one are bounded by $M^n/(2n)!$. The absolute mean series for $|h| \le 1$ is bounded by $\mathbb{E}\cosh\sqrt{M|Z|} < \infty$. Factoring h^4 from its tail and using symmetry therefore gives $\mathbb{E}u_P(h) = 1 + h^2 A_P + O(h^4)$. The strict coefficient gap proves the claimed inequality. This proves No-go 19. □

The same distinction persists under a variance tilt of the projected coordinate. For $1 < q < 2$, its density relative to the parent law is

$$L_q(Z) = q^{-1/2} \exp\Big((1-q^{-1})Z^2/2\Big), \qquad \mathbb{E}L_q^2 = [q(2-q)]^{-1/2}.$$

The equivalent Gaussian law has covariance $Q = C + (q-1)P$. The same original measurable solution has an $O(h^4)$ mean remainder under this law by Cauchy–Schwarz and the preceding L^2 tail estimate. Its degree-two coefficient is $A_Q = A_C + (q-1)A_P < qA_P - 1/96$. This is an equivalent-law statement, not a new stationary-model existence theorem for Q. To identify its degree-two coefficient, one can use the same regularization as the parent construction. If K_δ denotes the truncated temporal covariance and p_ϵ the spatial heat kernel, its cross-covariance with Z is

$$m_{\epsilon,\delta}(s,x) = \frac{(1-a)\int_0^1 K_\delta(s-r)\,\mathrm{d}r}{\sqrt{V}}(p_\epsilon * F)(x).$$

The bounds $0 \le K_\delta \le |\cdot|^{-a}$ and $F \le 4$ give $0 \le m_{\epsilon,\delta} \le 8/\sqrt{V}$. These profiles converge to m at interior times. Dominated convergence on the finite-mass terminal wave kernel identifies the added P contribution. The parent degree-two term converges in L^2, and $L_q \in L^2$ transfers its expectation to the equivalent law. Thus, the fixed-order Gaussian covariance identity indeed gives the stated A_Q, without invoking a homogeneous representation for Q. Consequently, discarding the residual also fails in this tilted comparison. A large-time bridge for specially chosen projections could still hold, but it must be proved at the required scale. Positive semidefinite order alone cannot supply it.

12.4 Phase propagation and Gaussian controls

A wave equation transports displacement and velocity together. Its scalar solution value is not a state variable for composition. Likewise, a Gaussian change of law transports an entire random solution, not merely the solution evaluated at the mean of the new noise. These distinctions explain the failures in this section. The scalar examples are diagnostics for generic proof principles; their scope is stated separately from the homogeneous stochastic wave model.

12.4.1 NG-14: scalar moments do not compose across blocks

Independent static time blocks look favorable for multiplying second moments. Independence does remove correlations between their potentials, but it does not reset the velocity to zero at a block boundary. The original record computed formal coefficients only. We include the integrable-series argument needed to turn that diagnostic into a small-variance counterexample.

No-go 14 (Two independent wave blocks do not multiply scalar moments)**.** Let Z_1, Z_2 be independent centered Gaussians of variance A. Solve $y'' = Z_1 y$ on $[0,1]$ and $y'' = Z_2 y$ on $[1,2]$, with continuous phase at time one and initial phase $(y(0), y'(0)) = (1,0)$. Then, as $A \downarrow 0$,

$$\mathbb{E}y(1)^2 = 1 + \frac{A}{3} + O(A^2), \qquad \mathbb{E}y(2)^2 = 1 + 3A + O(A^2).$$

In particular, $\mathbb{E}y(2)^2 > (\mathbb{E}y(1)^2)^2$ for all sufficiently small positive A.

Proof. We compute the full two-block phase product rather than resetting the velocity. We then control the Gaussian series remainders to show that the mismatch of scalar moments persists at small positive variance.

Step 1. We compute the first variance coefficients of the one-block and two-block moments. Define the entire functions

$$c(z) = \sum_{n\geq 0} \frac{z^n}{(2n)!}, \qquad s(z) = \sum_{n\geq 0} \frac{z^n}{(2n+1)!}.$$

The unit-time phase propagator and the terminal displacement are

$$M(z) = \begin{pmatrix} c(z) & s(z) \\ zs(z) & c(z) \end{pmatrix}, \qquad y(2) = c(Z_2)c(Z_1) + s(Z_2)Z_1 s(Z_1).$$

Expanding through total degree two in (z, w) gives

$$c(w)c(z)+s(w)zs(z) = 1+\frac{3}{2}z+\frac{1}{2}w+\frac{5}{24}z^2+\frac{5}{12}zw+\frac{1}{24}w^2+\text{terms of degree at least three.}$$

After squaring, the coefficients of z^2 and w^2 are respectively $8/3$ and $1/3$. Independence and centering eliminate the zw term. Similarly, the coefficient of z^2 in $c(z)^2$ is $1/3$.

Step 2. We justify the moment expansions and their strict difference. For completeness, these expansions admit the stated remainders after Gaussian expectation. The series of c and s have nonnegative coefficients, and

$$|c(z)| + |s(z)| \leq 2e^{\sqrt{|z|}}.$$

Consequently, the absolute series for the square of the displayed two-block displacement is bounded by $C(1+|z|)^2 e^{2\sqrt{|z|}+2\sqrt{|w|}}$. This is integrable at any fixed Gaussian variance $A_1 > 0$. Absolute integration allows termwise expectation. Odd powers in either variable vanish; every remaining term has even total degree and a nonnegative coefficient. Thus, the expectation is a convergent series $\sum_{j\geq 0} b_j A^j$ with $b_j \geq 0$ at A_1. For $0 \leq A \leq A_1$,

$$\sum_{j\geq 2} b_j A^j \leq (A/A_1)^2 \sum_{j\geq 2} b_j A_1^j = O(A^2).$$

The same argument applies to the one-block moment. Its square equals $1+2A/3+O(A^2)$, whereas the two-block moment equals $1+3A+O(A^2)$. Their difference is $7A/3+O(A^2)$. This proves No-go 14. □

This scalar model has spatially constant noise and independent static blocks, outside Hypothesis 1.2.1. It excludes the unrestricted scalar multiplication rule, not a phase-space operator estimate. Corollary 3.2.5 gives a valid replacement for independent successive blocks: it controls both phase coordinates and includes explicit block losses whose dyadic sum is finite. Its stated scope does not identify products across overlapping levels with the original evolution.

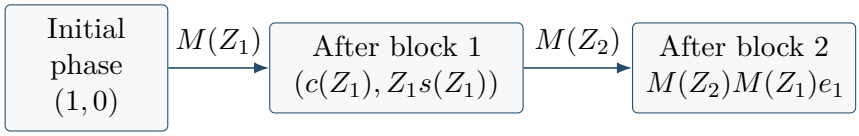

Retained displacement: $c(Z_2)c(Z_1) + s(Z_2)Z_1 s(Z_1)$.
Resetting the velocity would retain only $c(Z_2)c(Z_1)$.

True second moment: $1 + 3A + O(A^2)$.
Product of reset-block moments: $1 + \frac{2}{3}A + O(A^2)$.

Figure 12.3: Two independent scalar static Gaussian blocks, each of variance A. The second block acts on both components of the first block's phase. This is a scalar diagnostic outside the target homogeneous-noise model; see No-go 14.

12.4.2 NG-15: the missing second-order mean term

Keeping the first random Duhamel term gives a nonnegative squared norm. It is not the complete coefficient of the variance in the expected phase energy. The mean of the second Duhamel term contributes at the same order.

No-go 15 (The first variance coefficient need not be nonnegative)**.** For the scalar phase propagator M in No-go 14 and a standard Gaussian Z, write

$$\mathbb{E}\|M(\sigma Z)x\|^2 = \|M(0)x\|^2 + \sigma^2 x^{\mathsf{T}} K x + O(\sigma^4).$$

Then

$$K = \begin{pmatrix} 4/3 & 4/5 \\ 4/5 & 17/45 \end{pmatrix}, \qquad (1,-2)K(1,-2)^{\mathsf{T}} = -\frac{16}{45}.$$

The matrix K is the full first coefficient in the variance parameter, not a covariance matrix. Omitting the second-order mean term also underestimates this coefficient for $x = (1,0)^{\mathsf{T}}$.

Proof. We compute the complete first variance matrix, including the second-order mean terms. We then use the integrable series remainder to obtain an actual phase whose expected energy decreases at small coupling.

Step 1. We retain all terms of the first variance matrix. The coefficients of $M(z) = M_0 + zM_1 + z^2 M_2 + \cdots$ are

$$M_0 = \begin{pmatrix} 1 & 1 \\ 0 & 1 \end{pmatrix}, \quad M_1 = \begin{pmatrix} 1/2 & 1/6 \\ 1 & 1/2 \end{pmatrix}, \quad M_2 = \begin{pmatrix} 1/24 & 1/120 \\ 1/6 & 1/24 \end{pmatrix}.$$

Gaussian expectation of the squared phase norm gives

$$K = M_1^{\mathsf{T}} M_1 + M_0^{\mathsf{T}} M_2 + M_2^{\mathsf{T}} M_0.$$

Matrix multiplication gives the stated entries and negative value. For $e_1 = (1, 0)^\mathsf{T}$, the first random contribution is $\|M_1 e_1\|^2 = 5/4$, whereas $e_1^\mathsf{T} K e_1 = 4/3$. Thus, it is not valid even as an upper bound for the full coefficient.

Step 2. We justify the negative small-coupling energy correction. The entire series are absolutely Gaussian integrable, including their squares, by the bound in No-go 14 with the additional polynomial factor from $zs(z)$. Absolute summation of the even-degree terms at a fixed nonzero σ_1 bounds the tail of degree at least four by $C\sigma^4$ for $|\sigma| \le |\sigma_1|$. Therefore, for $x = (1, -2)^\mathsf{T}$ the actual expected energy satisfies

$$\mathbb{E}\|M(\sigma Z)x\|^2 = 5 - \frac{16}{45}\sigma^2 + O(\sigma^4).$$

This proves No-go 15. □

The example refutes arbitrary-phase covariance monotonicity for this scalar flow. It says nothing against monotonicity of the original solution-value moment with initial data $(1, 0)$ in the homogeneous model. Section 3.1 retains both contributions to the coefficient. The all-order estimate of Proposition 3.2.4 and the interaction bound of Corollary 3.2.5 retain these terms. Positivity of the first random variance does not control the cross term with the mean.

12.4.3 NG-16: replacing a tilted mean by a deterministic value

The Gaussian density cost is exact. A loss may instead enter when the random solution under the tilted law is replaced by a deterministic surrogate. The following two calculations identify the loss without asserting an obstruction to Gaussian shifts themselves.

No-go 16 (A deterministic surrogate can lose the annealed factor)**.** Let $A > 0$, $c > 0$ and $0 < r < 2$, and define

$$J_c = \sup_{H \ge 0}\{cAH^r - H^2/2\}.$$

Then $J_c = c^{2/(2-r)} J_1$, whereas

$$\sup_{H \ge 0}\{2AH^r - H^2\} = 2J_1 < J_2.$$

Moreover, for $Y = e^{\sigma Z}$, Z standard Gaussian and $\sigma > 0$, the full tilted-mean Cauchy–Schwarz bound recovers $\mathbb{E}Y^2$ exactly, while substituting $Y(h) = e^{\sigma h}$ loses a factor in its logarithm.

Proof. Substitute $H = c^{1/(2-r)} K$ in the definition of J_c. Both terms acquire the factor $c^{2/(2-r)}$. The supremum J_1 is finite, since $r < 2$, and positive, since for small positive H the positive term dominates. Factoring two from the surrogate score proves the strict comparison because $2/(2 - r) > 1$.

Let Q_h be the Gaussian shift with density $L_h = e^{hZ-h^2/2}$ relative to the standard Gaussian law. Then $\mathbb{E}L_h^2 = e^{h^2}$, so Cauchy–Schwarz gives

$$\mathbb{E}Y^2 \geq (\mathbb{E}_{Q_h} Y)^2 e^{-h^2}.$$

The exact tilted mean is $\mathbb{E}_{Q_h} Y = e^{\sigma^2/2+\sigma h}$. Maximizing its resulting exponent $\sigma^2+2\sigma h-h^2$ at $h = \sigma$ gives $e^{2\sigma^2} = \mathbb{E}Y^2$. Substitution of the deterministic value $Y(h)$ instead gives the maximum e^{σ^2}. This proves No-go 16. □

These are generic scalar score calculations, not an SPDE no-go. They identify which term is lost and show that retaining the full tilted mean can avoid the loss. A deterministic surrogate remains useful if one proves that its error is negligible on the intended exponential scale; without such an estimate it cannot identify the annealed constant.

12.4.4 NG-20: covariance profiles need not separate

A fixed spatial profile times a scalar temporal factor is easier to propagate than a general spacetime control. Such a product family is legitimate as a restriction, but it does not represent every positive control even in the white spatial model.

No-go 20 (A positive control need not have proportional covariance profiles)**.** Fix $0 < a < 1$ and one-dimensional spatial covariance $\Gamma = c_\Gamma \delta_0$, $c_\Gamma > 0$. There is a nonnegative smooth compactly supported spacetime test ψ for which

$$h_\sigma(x) = c_\Gamma \int_0^1 |\sigma - u|^{-a} \psi(u, x)\, \mathrm{d}u, \qquad 0 \leq \sigma \leq 1,$$

cannot be represented as $b(\sigma)U(x)$ with one fixed spatial U.

Proof. Choose a nonzero nonnegative smooth f_1 supported in $(1/8, 1/4)$, let $f_2(u) = f_1(1-u)$, and choose nonzero nonnegative smooth bumps q_1, q_2 supported respectively in $(-2, -1)$ and $(1, 2)$. Set $\psi(u, x) = f_1(u)q_1(x) + f_2(u)q_2(x)$. Put

$$A = \int_0^1 u^{-a} f_1(u)\, \mathrm{d}u, \qquad B = \int_0^1 (1-u)^{-a} f_1(u)\, \mathrm{d}u.$$

Since $u < 1 - u$ on the support of f_1, we have $A > B > 0$. Reflection in time gives

$$h_0 = c_\Gamma(Aq_1 + Bq_2), \qquad h_1 = c_\Gamma(Bq_1 + Aq_2).$$

Choose x_i with $q_i(x_i) > 0$. Disjoint supports imply

$$h_0(x_1)h_1(x_2) - h_1(x_1)h_0(x_2) = c_\Gamma^2(A^2 - B^2)q_1(x_1)q_2(x_2) > 0.$$

A representation by one U would make this determinant zero. The white covariance has $\alpha = 1$, so $1 + a < 2$ verifies the model parameter condition. This proves No-go 20. □

This is an exact representation obstruction. It does not prove that separable controls fail to attain a variational supremum; a theorem reducing optimizers to a smaller family would be a different statement. A useful weaker fact survives: because $|\sigma - u|^{-a} \geq 1$ on the unit time square, every nonnegative test has $h_\sigma \geq \Gamma * \int_0^1 \psi(u, \cdot)\,\mathrm{d}u$. This common lower profile does not by itself prove a phase-propagation comparison. Reopening an exact product reduction requires extra structure on the control, while an optimizer reduction requires a variational proof.

12.4.5 NG-31: initial phase and the backward cone

Two seemingly small generalizations remove essential hypotheses: replacing the specified initial phase by an arbitrary one, and checking agreement of spatial cutoffs only on the terminal observation set. Simple deterministic waves already distinguish these statements.

No-go 31 (Growth does not give every-phase lower bounds or local cutoff consistency)**.** The growth rate of a wave phase propagator need not be a lower growth rate for every nonzero initial phase. Also, two smooth initial-data masks that agree on an observation interval can give different free-wave displacements throughout that interval at a later time, even when their initial displacements agree everywhere.

Proof. For the first assertion, let $B = \left(\begin{smallmatrix} 0 & 1 \\ 1 & 0 \end{smallmatrix}\right)$. Its eigenvectors $(1,1)^{\mathsf{T}}$ and $(1,-1)^{\mathsf{T}}$ have eigenvalues 1 and -1. Hence, $\|e^{tB}\| = e^t$ for $t \geq 0$, but $e^{tB}(1,-1)^{\mathsf{T}} = e^{-t}(1,-1)^{\mathsf{T}}$.

For the second assertion take the one-dimensional free wave with zero initial displacement and nonnegative smooth velocity v supported in $(5,6)$, normalized by $\int v = 1$. Choose smooth masks χ_s, χ_l between zero and one, with $\chi_s = 1$ on $[-2,2]$ and support in $[-4,4]$, and $\chi_l = 1$ on $[-14,14]$. Both masks agree on the observation interval $[-2,2]$. The masked velocities are nevertheless $\chi_s v = 0$ and $\chi_l v = v$. D'Alembert's formula at time nine gives

$$u_s(9,x) = 0, \qquad u_l(9,x) = \frac{1}{2}\int_{x-9}^{x+9} v(y)\,\mathrm{d}y = \frac{1}{2}, \qquad -2 \leq x \leq 2.$$

Indeed, every interval $[x-9, x+9]$ in question contains $(5,6)$. This proves No-go 31. □

The first example does not refute a terminal lower bound for the original phase $(1,0)$. The second requires agreement of both displacement and velocity on the full backward cone, not only on the observer. Finite propagation with that guard survives. Thus, a successor must retain the specified phase, or prove a suitable nonvanishing unstable component, and must impose cutoff agreement on the relevant cone for both coordinates.

12.5 Topology, localization and limits of variational arguments

A useful approximation must be small in the topology in which the next argument uses it. The obstructions below distinguish a local operator from a Hilbert–Schmidt operator,

a fixed spatial cutoff from a growing one, and pointwise convergence from convergence of variational suprema. Throughout, $a = \alpha_0 \in (0,1)$ and $\Lambda = (1-\Delta)^{1/2}$, except that the positive number L denotes the temporal feature cutoff in No-go 32.

12.5.1 The first driver cannot always be Hilbert–Schmidt

The one-dimensional operator construction suggests trying the same Hilbert–Schmidt space in higher dimensions. A compact spatial observation removes infinite volume, but it does not remove the following high-frequency obstruction. The relevant compatibility is with the given noise, through its bilinear first-driver tests.

No-go 21 (A same-noise Hilbert–Schmidt obstruction)**.** Suppose that $d \in \{2,3\}$, $s \in \mathbb{R}$, and $0 < T \le 1$. Put $E_s = H^s(\mathbb{R}^d) \times H^{s-1}(\mathbb{R}^d)$ and let $S(t)$ be the massless wave phase group. For every nonzero covariance satisfying Hypothesis 1.2.1, there are a nonnegative compact smooth physical coefficient mask ζ and a compact smooth observation cutoff χ, equal to one on a sufficiently large ball, for which the localized Gaussian first-driver form has no compatible realization in $L^2(\Omega; \mathrm{HS}(E_s, E_s))$. Here compatibility means equality with the given W for each fixed smooth phase pair, as specified in the proof.

Proof. We first construct a deterministic coefficient response that is not Hilbert–Schmidt, even after the stated observation cutoff. We then realize that coefficient as an actual covariance mean. Compatibility with a mean-square Hilbert–Schmidt driver would make this response Hilbert–Schmidt, giving a contradiction.

Step 1. We identify the deterministic response and its weighted Fourier kernel. First consider a deterministic coefficient $h(u,x) = k(u)H(x)$, where $H \in C_c^\infty(\mathbb{R}^d)$ is nonzero, even and nonnegative, and $k \in W^{1,\infty}[0,T]$ satisfies $k \ge k_0 > 0$. Write $B(b)(v,w) = (0, bv)$ and

$$A_h = \int_0^T S(-u)B(h(u))S(u)\,\mathrm{d}u, \qquad S(u,\xi) = \begin{pmatrix} \cos(u|\xi|) & \sin(u|\xi|)/|\xi| \\ -|\xi|\sin(u|\xi|) & \cos(u|\xi|) \end{pmatrix}.$$

The sine quotient has its continuous value at zero. The integral is a strong operator integral on E_s: $S(u)$ is strongly continuous and uniformly bounded on compact time intervals, and multiplication by H is bounded on H^s. For the latter assertion, the weighted Fourier kernel is bounded in absolute value by a constant times $\langle \xi-\eta\rangle^{|s|}|\widehat{H}(\xi-\eta)|$, an integrable convolution kernel. This proves boundedness for every fixed real s.

Normalize the Fourier coordinates by $\mathrm{diag}(\langle\xi\rangle^s, \langle\xi\rangle^{s-1})$. Using the unitary Fourier transform, the lower-left block of A_h then has kernel

$$K_s(\xi,\eta) = (2\pi)^{-d/2}\langle\xi\rangle^{s-1}\langle\eta\rangle^{-s}\widehat{H}(\xi-\eta)\int_0^T k(u)\cos(u|\xi|)\cos(u|\eta|)\,\mathrm{d}u.$$

This formula follows from both phase coordinates: before applying the weights, the full

product, with $r = |\xi|$, $\rho = |\eta|$, is

$$\widehat{H}(\xi - \eta) \begin{pmatrix} -\dfrac{\sin(ru)}{r}\cos(\rho u) & -\dfrac{\sin(ru)}{r}\dfrac{\sin(\rho u)}{\rho} \\ \cos(ru)\cos(\rho u) & \cos(ru)\dfrac{\sin(\rho u)}{\rho} \end{pmatrix}.$$

All Fourier and time exchanges are justified on Schwartz pairs by the rapid decay of $\widehat{H}$ and then by density.

Step 2. We prove the high-frequency Hilbert–Schmidt divergence. Let $J_0 = \int_0^T k > 0$ and $B_0 = \|k\|_\infty + T\|k'\|_\infty$. Choose $\epsilon > 0$ so that $\epsilon \le 1$, $\epsilon T \le 1$ and $\widehat{H}(z) \ge \widehat{H}(0)/2 > 0$ when $|z| \le \epsilon$. If $|\xi - \eta| \le \epsilon$, then

$$\int_0^T k(u)\cos((r-\rho)u)\,\mathrm{d}u \ge J_0/2, \qquad \left|\int_0^T k(u)\cos((r+\rho)u)\,\mathrm{d}u\right| \le B_0/(r+\rho).$$

The second bound is integration by parts in the absolutely continuous function k. Product-to-sum therefore bounds the time integral in K_s from below by $J_0/8$ when $r \ge R_0 := \max(1, 2\epsilon, 4B_0/J_0)$. On the same region,

$$\langle\xi\rangle^{s-1}\langle\eta\rangle^{-s} = \langle\xi\rangle^{-1}(\langle\xi\rangle/\langle\eta\rangle)^s \ge 2^{-|s|}/(\sqrt{2}r).$$

Consequently, $|K_s(\xi,\eta)| \ge c_s/|\xi|$ there, for $c_s > 0$. If P_N cuts off Fourier frequencies to B_N, its truncated kernel is square integrable and Parseval followed by Tonelli gives

$$\|P_N K_s P_N\|_{\mathrm{HS}}^2 \ge c_s^2 |B_\epsilon||\mathbb{S}^{d-1}| \int_{R_0}^{N-\epsilon} r^{d-3}\,\mathrm{d}r \longrightarrow \infty.$$

Indeed Parseval in the second kernel variable identifies its square integral with the sum of squared images of an orthonormal basis. If A_h were Hilbert–Schmidt, every block compression would have bounded Hilbert–Schmidt norm. The displayed divergence proves otherwise. Real Hilbert–Schmidt operators and their complexifications have the same norm, so Fourier complexification has not changed the conclusion.

Step 3. We retain the obstruction after compact observation. Suppose that $\operatorname{supp} H \subset B_A$, and let $\chi = 1$ on B_{A+T+1}. With D_χ denoting multiplication of both phase coordinates, finite propagation gives

$$D_\chi A_h = A_h = A_h D_\chi.$$

For completeness, the local wave energy on a shrinking ball has boundary flux $v_t\partial_n v - (v_t^2 + |\nabla v|^2)/2 \le 0$. Zero initial data therefore remain zero in the interior cone; time reversal gives the same support assertion for $S(-u)$. Apply this first to smooth data and then use Sobolev continuity and distributional testing to pass to E_s. The coefficient acts only in B_A, and the resulting output lies in B_{A+T}. Thus the failure persists after this compact observation.

Step 4. We realize the coefficient as a covariance mean of the given noise. We next produce h as an actual covariance mean. Choose $L_0 \ge 1$ with $0 < \Gamma(B_{L_0}) < \infty$, and an

even nonnegative $q \in C_c^\infty$ equal to at least one on B_{2L_0+1}. Set $U = \Gamma * q$. Local finiteness of Γ permits differentiation on every compact set, so U is smooth, even and nonnegative, with $U(0) > 0$. Moreover,

$$Q = \int q(x)U(x)\,\mathrm{d}x \geq |B_{L_0+1}|\Gamma(B_{L_0}) > 0.$$

Choose an even nonnegative compact smooth ζ, equal to one near zero, and put $H = \zeta U$. Choose $f \in C_c^\infty(0,1)$ nonnegative and nonzero, and set

$$Z = W(f \otimes q), \qquad k(u) = \int_0^1 |u-v|^{-a} f(v)\,\mathrm{d}v.$$

For $u \in [0,1]$, $k(u) \geq \int f > 0$. Moving the derivative to the smooth zero extension of f shows $k \in C^1[0,1]$, since $|\cdot|^{-a}$ is locally integrable. Also $\mathbb{E}Z^2 = Q\int_0^1 f(u)k(u)\,\mathrm{d}u \in (0,\infty)$. The mask is applied after the covariance convolution: $H = \zeta(\Gamma * q)$.

Step 5. We state the compatible rows and derive the Hilbert–Schmidt contradiction. It remains to specify the compatible first-driver form with the correct Sobolev adjoint. For real Schwartz phases z, w put

$$v_u = [S(u)z]_1, \qquad G_w(u) = -\frac{\sin(u|D|)}{|D|}(\chi\Lambda^{2s}w_1) + \cos(u|D|)(\chi\Lambda^{2s-2}w_2),$$

and define $F_{z,w}(u,x) = \mathbf{1}_{(0,T)}(u)\zeta(x)v_u(x)G_w(u,x)$. This test lies in the raw noise completion. In fact, on a fixed compact spatial support K, its covariance norm is bounded by a constant times $\|u \mapsto \|F(u)\|_\infty\|_{L^2(0,T)}$, by local Radon mass $\Gamma(K-K)$ and the time Schur bound for $|u-v|^{-a}$. Smooth interior time approximation gives membership. Define $\ell_\chi(z,w) = W(F_{z,w})$ on the given noise space. Direct transposition, with the Sobolev weights retained, gives

$$G_w(u) = \Lambda^{2s-2}\Big((D_\chi S(-u))^{*_{E_s}} w\Big)_2.$$

In particular, multiplication by χ has not been treated as self-adjoint in E_s. Absolute Fubini in the covariance pairing now gives

$$\mathbb{E}[Z\ell_\chi(z,w)] = \int_0^T \int k(u)H(x)v_u(x)G_w(u,x)\,\mathrm{d}x\,\mathrm{d}u = \langle D_\chi A_h z, w\rangle_{E_s} = \langle A_h z, w\rangle_{E_s}.$$

All spatial factors in the raw tests have compact support and the temporal singularity is integrable, which supplies the absolute Fubini bound.

If $X \in L^2(\Omega; \mathrm{HS}(E_s, E_s))$ satisfied $\langle Xz, w\rangle_{E_s} = \ell_\chi(z,w)$ almost surely for every fixed Schwartz pair, then Cauchy–Schwarz would make $Y = \mathbb{E}[ZX]$ a Hilbert–Schmidt Bochner integral. Continuous matrix evaluation would give $\langle Yz, w\rangle = \langle A_h z, w\rangle$ for all such pairs. Density implies $Y = A_h$, a contradiction. This proves No-go 21. □

This result concerns the same-index phase spaces E_s and a compatible L^2 Hilbert–Schmidt realization. It does not concern every cutoff: the zero cutoff, for example, has no such obstruction. It is not a nonexistence result for the Stratonovich solution or its moments. A route using loss of regularity between input and output, operator norms, or a different Schatten class must supply its own estimates; changing the fixed index s alone cannot reopen this particular route.

12.5.2 A physical mask may not act on the noise quotient

A smooth physical mask is harmless on ordinary test functions. It need not preserve the zero classes of a covariance seminorm. The following is the obstruction already proved in Proposition 4.1.5; we include its witness to explain why the auxiliary completion is needed.

No-go 22 (A mask that separates noise-null representatives)**.** For $d = 2$, $\alpha = 1$, $0 < a < 1$ and $\Gamma = \delta_0(\,\mathrm{d}x_1)\,\mathrm{d}x_2$, there exist real compact smooth F and a nonnegative smooth square mask ζ for which $\mathbb{E}W(F)^2 = 0$ but $\mathbb{E}W(\zeta F)^2 > 0$. Thus multiplication by this mask does not descend to the original noise quotient, and no finite uniform covariance-norm multiplier bound holds.

Proof. Choose a nonnegative nonconstant compact smooth plateau function ψ and put $\chi = \psi^2$. The spatial covariance seminorm is

$$V(g) = \int_{\mathbb{R}} \left(\int_{\mathbb{R}} g(x_1, x_2)\,\mathrm{d}x_2 \right)^2 \mathrm{d}x_1.$$

This also shows positive definiteness of the nonnegative even tempered measure Γ; its scaling is $\Gamma(cA) = c\Gamma(A)$, as required for $d = 2$, $\alpha = 1$. Put $g(x) = \chi(x_1)\chi''(x_2)$ and $\zeta(x) = \chi(x_1)\chi(x_2) = (\psi(x_1)\psi(x_2))^2$. Then $\int \chi'' = 0$, whereas integration by parts gives

$$\int \zeta(x)g(x)\,\mathrm{d}x_2 = -\chi(x_1)^2 \int (\chi')^2.$$

Consequently, $V(g) = 0$ and $V(\zeta g) = \int \chi^4 \left(\int (\chi')^2 \right)^2 > 0$. Tensor with a nonzero nonnegative $\tau \in C_c^\infty(0,T)$. Its temporal variance is finite and strictly positive, so $F = \tau \otimes g$ has the asserted full-noise variances. This proves No-go 22. □

This covariance is not two-dimensional spatial white noise. One can still mask individual tests before taking an auxiliary completion. To reopen a multiplier argument on the original quotient, one must first prove that the chosen mask preserves its null space and then prove the required norm bound.

12.5.3 Frequency decay does not give whole-space compactness

The compact-cutoff estimates use spatial confinement as well as frequency smoothing. Removing the former loses compactness even for a deterministic Bessel multiplier; see Proposition 4.3.11.

No-go 24 (Translations defeat whole-space compactness)**.** For every $d \geq 1$ and $\gamma > 0$, the operator $\Lambda^{-\gamma}$ on $L^2(\mathbb{R}^d)$ is not compact.

Proof. Take a nonzero Schwartz function f with Gaussian Fourier transform and put $g = \Lambda^{-\gamma} f$. Then g is nonzero and Schwartz. For translations $T_h g(x) = g(x - h)$, Plancherel gives

$$\langle T_h g, g \rangle = \int e^{-i\xi\cdot h} |\widehat{g}(\xi)|^2\,\mathrm{d}\xi \longrightarrow 0 \quad (|h| \longrightarrow \infty).$$

The limit follows, for example, by integration by parts in the Fourier transform of the Schwartz function $|\widehat{g}|^2$. Choose a sufficiently large spacing b and $h_n = nbe_1$ so that distinct images $T_{h_n} g$ have squared distance at least $\|g\|_2^2$. The inputs $T_{h_n} f$ have constant norm and $\Lambda^{-\gamma} T_{h_n} f = T_{h_n} g$. Their images have no Cauchy subsequence. This proves No-go 24. □

Compact spatial cutoffs and the conditional Schatten estimates in the main text survive. No necessity at a Schatten endpoint is asserted here. A whole-space successor needs a tightness condition that prevents translation of mass, or an explicitly different topology.

12.5.4 Fixed projections do not control growing spatial masks

At each fixed radius the Cameron mean map can be compact. Its finite-rank approximations need not be uniform in that radius. The following witness uses actual unit controls for one-dimensional spatial white noise. The fixed-radius map and its compact approximation are those of Proposition 8.3.5.

No-go 25 (Escape from every fixed smooth projection)**.** Let $\Gamma = \delta_0$ in $d = 1$, and let H_I be the closed raw-noise space generated by tests supported in $I \times \mathbb{R}$, $I = (0, 1)$. Let P_J be any fixed finite-rank orthogonal projection in H_I whose range is spanned by smooth compact tests supported in $I \times \mathbb{R}$. For the physical masked mean multiplier T_R on $F = (H^{1/2} \times H^{-1/2}) \oplus \mathbb{R}^2$, with the last coordinates representing constant displacement and velocity, one has, for every $2 < r < 2/a$,

$$\sup_R \|T_R(I - P_J)\|_{H_I \to L^r((0,1);\mathcal{K}(F))} \geq c_a > 0,$$

where c_a can be chosen independently of J. Here the smooth masks m_R equal one on $[-R, R]$. For a smooth control Ψ with covariance mean h_Ψ, the operator sends (v, w, c, d) to $(0, m_R h_\Psi(s)(v + c), 0, 0)$.

Proof. We translate unit controls beyond the supports of a fixed projection while enlarging the physical mask to contain them. A unit constant-displacement input then gives a nonvanishing operator lower bound, showing why fixed-radius compactness is not uniform in radius.

Step 1. We construct unit controls killed by the fixed projection. Use the temporal equilibrium density f_a of Lemma 8.1.2, so that $\int_0^1 |s - t|^{-a} f_a(t)\, \mathrm{d}t = 1$ and $\|f_a\|_{H_a}^2 = M_a > 0$. Choose nonnegative $q \in C_c^\infty(\mathbb{R})$ with $\|q\|_2 = 1$, and put $q_n(x) = q(x - x_n)$, where $x_n \to \infty$. The controls

$$\Psi_n = \frac{f_a \otimes q_n}{\sqrt{M_a}}$$

have unit raw norm and time-independent covariance mean $q_n/\sqrt{M_a}$. Membership follows by L^2 approximation of f_a and the Schur bound for the temporal kernel. The finitely many tests spanning P_J have common compact spatial support. For all sufficiently large

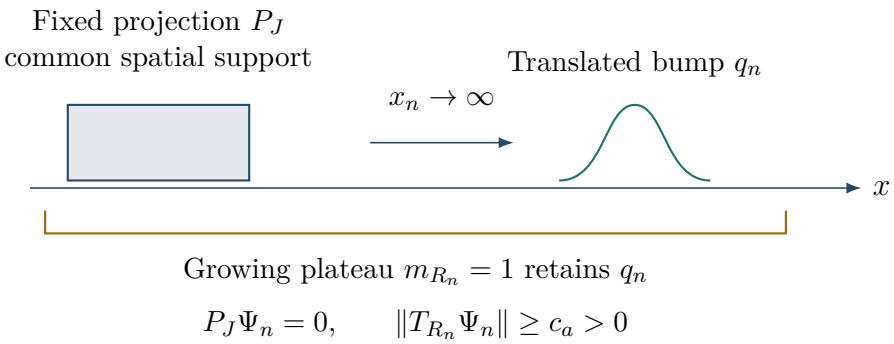

Figure 12.4: Schematic for No-go 25. For one-dimensional spatial white noise, a translated unit control is exactly orthogonal to the finitely many compact tests of P_J, while a growing mask retains its nonzero phase functional. At any fixed radius sufficiently distant bumps miss the mask.

n, spatial whiteness gives $P_J\Psi_n = 0$ exactly. Choose R_n to contain $\operatorname{supp} q_n$ in the plateau of m_{R_n}.

Step 2. We retain a positive response inside the growing mask. The constant-displacement input $e = (0, 0, 1, 0)$ has norm one. The phase dual

$$w_n = (0, \Lambda q_n / \|q\|_{H^{1/2}}, 0, 0)$$

also has norm one. Indeed its velocity norm is $H^{-1/2}$, and translation preserves $\|q\|_{H^{1/2}}$. The mean multiplier sends e to the velocity $q_n/\sqrt{M_a}$, so the $H^{-1/2}$ inner product gives, for every s,

$$\langle T_{R_n}\Psi_n(s)e, w_n\rangle_F = \frac{\|q_n\|_2^2}{\sqrt{M_a}\|q\|_{H^{1/2}}} =: c_a > 0.$$

Integrating over the unit time interval proves the bound for all r stated. This proves No-go 25. □

For a fixed R, sufficiently distant translates miss its mask, so there is no contradiction with fixed-radius compactness. A replacement must use projections depending on the radius with quantitative control, or a different localization argument. The witness does not exclude every such strategy.

12.5.5 Two distinct limitations of block costs

A nonlinear block argument must handle both small perturbations and rare large blocks. A power larger than one misses the first effect; an averaged budget alone does not bound the largest block.

No-go 26 (A pure Young power and a maximum from an average)**.** On $[0, 1]$, with $\theta = 2/3$ and $\nu = 1/\theta = 3/2$, no finite constant $C > 0$ gives $\log U(1) \leq C\|D\|_{C^\theta}^\nu$ for all scalar paths starting at zero and solving $\mathrm{d}U = U\,\mathrm{d}D$, $U(0) = 1$, when

$\|D\|_{C^\theta} = \|D\|_\infty + [D]_{C^\theta}$. Moreover, a bound on $N^{-1}\sum_{j=1}^N b_j^r$, $r > 0$, does not give a bound independent of N on $\max_j b_j$.

Proof. For $D(t) = xt$, $x > 0$, the solution is $U(t) = e^{xt}$ and $\|D\|_{C^{2/3}} = 2x$. Taking $x = 1/(16C^2)$ gives $C(2x)^{3/2} = x/\sqrt{2} < x = \log U(1)$. For the second assertion, take $b_1 = N^{1/r}$ and $b_j = 0$ for $j > 1$. Their averaged rth power is one while their maximum tends to infinity. This proves No-go 26. □

A linear-plus-power cost is not refuted. For any $\tau > 0$ and $\nu > 1$, $x \le \tau + \tau^{1-\nu}x^\nu$ gives an explicit alternative with slack. Also, if $0 < \nu < r$ and $N^{-1}\sum b_j^r \le M$, then Hölder gives $N^{-1}\sum b_j^\nu \le M^{\nu/r}$, and

$$\frac{1}{N}\sum_{b_j > K} b_j^\nu \le K^{\nu-r}M.$$

Thus an averaged tail argument survives. Reopening the block route requires an actual evolution estimate with its linear term or slack, followed by an averaged bad-block estimate. These scalar tests alone do not construct a Cameron potential or prove a wave evolution bound.

12.5.6 Concentrating temporal controls restrict integrability

Compactness of a temporal mean map has a natural upper endpoint. A concentrating control detects both excessive integrability and failure of compactness at that endpoint.

No-go 27 (The temporal concentration threshold)**.** Let $I = (0,1)$, $0 < a < 1$, and let H_a be the completion of smooth tests for $\|f\|_{H_a}^2 = \int_I\int_I f(t)f(s)|t-s|^{-a}\,\mathrm{d}t\,\mathrm{d}s$. On smooth tests set $C_a f(t) = \int_I |t-s|^{-a}f(s)\,\mathrm{d}s$. The map C_a is not bounded from H_a to $L^r(I)$ when $r > 2/a$, including $r = \infty$, and it is not compact into $L^{2/a}(I)$.

Proof. We normalize a concentrating temporal test in the covariance norm. Its local lower bound disproves boundedness above the threshold; pointwise decay away from its center separately disproves compactness at the endpoint.

Step 1. We compute the normalized concentration and its local norm lower bound. Choose $t_0 \in I$ and a nonzero nonnegative $\phi \in C_c^\infty(-1,1)$. Put

$$v_\phi = \iint \phi(u)\phi(v)|u-v|^{-a}\,\mathrm{d}u\,\mathrm{d}v \in (0,\infty), \qquad f_\epsilon(t) = \frac{\epsilon^{a/2-1}}{\sqrt{v_\phi}}\phi((t-t_0)/\epsilon).$$

For sufficiently small ϵ, its support lies in I. Changing both variables shows $\|f_\epsilon\|_{H_a} = 1$, and

$$(C_a f_\epsilon)(t_0+\epsilon y) = \frac{\epsilon^{-a/2}}{\sqrt{v_\phi}}\int |y-v|^{-a}\phi(v)\,\mathrm{d}v.$$

For $|y| \le 1$, the last integral is at least $2^{-a} \int \phi > 0$. Thus for finite r, $\|C_a f_\epsilon\|_{L^r} \ge c_r \epsilon^{1/r - a/2}$, and the analogous supremum lower bound is $c\epsilon^{-a/2}$. This proves unboundedness above $2/a$.

Step 2. We rule out a strongly convergent endpoint subsequence. For every fixed $t \ne t_0$, on the other hand, $C_a f_\epsilon(t) = O_t(\epsilon^{a/2}) \to 0$. At $r = 2/a$ the norm lower bound stays strictly positive. If a subsequence converged strongly in this L^r space, a further subsequence would converge almost everywhere to its strong limit. The limit would have to be zero, contradicting the norm lower bound. This proves No-go 27. □

The endpoint argument refutes compactness, not boundedness. Tensoring the controls with one fixed nonzero spatial profile transfers this input obstruction to a corresponding separated mean map. The corrected compact range $2 < r < 2/a$ is consistent with the witness. A larger range requires additional temporal regularity or restrictions that exclude concentration.

12.5.7 Pointwise convergence does not pass through a supremum

The Gaussian action cost must remain in a variational comparison. Even with that cost, bounded near-maximizers can escape in infinitely many directions.

No-go 30 (Escaping variational scores)**.** There are continuous functions J_n on the Hilbert space ℓ^2 tending to zero at every point such that

$$\sup_h \{J_n(h) - \tfrac{1}{2}\|h\|^2\} \ge \tfrac{1}{2}, \qquad \sup_h \{0 - \tfrac{1}{2}\|h\|^2\} = 0.$$

The witnesses for the first inequality have norm one.

Proof. Let (e_n) be the standard orthonormal sequence and set $J_n(h) = (1 - 2\|h - e_n\|)_+$. For each fixed $h \in \ell^2$, its nth coordinate tends to zero, and hence $\|h - e_n\|^2 = \|h\|^2 + 1 - 2\langle h, e_n\rangle \to \|h\|^2 + 1 \ge 1$. Thus $J_n(h) = 0$ eventually. But $J_n(e_n) = 1$, so its score at e_n is $1/2$. The limiting score is nonpositive and equals zero at $h = 0$. This proves No-go 30. □

A bounded action budget alone supplies no strong compactness in ℓ^2. To pass to an exact constant one needs a variational upper-limit argument, for example compactness of near-maximizers in a topology with the needed upper semicontinuity. Pointwise convergence, or compactness proved only with an additional fixed spatial cutoff, does not supply that argument by itself.

12.5.8 A cutoff point feature can lie outside the raw-noise image

Lemma 5.2.4 embeds the original noise into one fixed larger Gaussian space. Its closed image retains all original raw tests. It does not contain every positive-cutoff point feature. The following explicit orthogonal vector explains the role of the auxiliary noise.

No-go 32 (The point feature is outside the closed noise image)**.** Suppose that $\Gamma \neq 0$ satisfies Hypothesis 1.2.1, $t_0 > 0$, $L \in (0, \infty)$ and $\epsilon > 0$. In the feature space

$$\mathcal{G} = L^2((0,\infty)_\lambda \times \mathbb{R}_r, \nu_a(\,\mathrm{d}\lambda)\,\mathrm{d}r; H_\Gamma), \qquad \nu_a(\,\mathrm{d}\lambda) = \lambda^{a-1}\,\mathrm{d}\lambda/\Gamma_E(a),$$

let $K = \Phi H_W$ be the closed image of Lemma 5.2.4. Set $g = p_\epsilon(x - \cdot)$ and

$$v(\lambda, r) = \mathbf{1}_{\{\lambda \le L\}}\sqrt{2\lambda}e^{-\lambda(t_0 - r)}\mathbf{1}_{\{r \le t_0\}}g.$$

Then $v \notin K$. On the fixed extension $\mathcal{I}(v) = W(\Phi^{-1}Pv) + J((I - P)v)$, where P projects onto K and J is independent of W, one has $\mathrm{Var}(\mathcal{I}(v) \mid \sigma(W)) > 0$.

Proof. We construct a feature-space vector orthogonal to every raw-noise test but not to the cutoff point feature. This separates the point feature from the closed noise image and gives a positive conditional variance on the fixed extension.

Step 1. We construct the finite-norm witness. The heat profile has finite strictly positive norm:

$$\|g\|_{H_\Gamma}^2 = \int p_{2\epsilon}(y)\Gamma(\,\mathrm{d}y) > 0.$$

Finiteness follows from temperedness and Gaussian decay, and positivity from nonzero nonnegative Γ. Integrating in r also gives $\|v\|_{\mathcal{G}}^2 = \|g\|^2\nu_a((0, L]) < \infty$. Choose nonnegative nonzero smooth bumps u_A, u_B supported in compact intervals $A \subset (0, L)$ and $B \subset (L, \infty)$, respectively, and put

$$p(\lambda) = \frac{u_A(\lambda)}{\int u_A\,\mathrm{d}\nu_a} - \frac{u_B(\lambda)}{\int u_B\,\mathrm{d}\nu_a}.$$

Then $\int p\,\mathrm{d}\nu_a = 0$ and $\int_{(0,L]} p\,\mathrm{d}\nu_a = 1$. Choose $\varphi \in C_c^\infty(0, \infty)$ with $\varphi(t_0) = 1$, and define

$$q(\lambda, r) = \frac{p(\lambda)}{\sqrt{2\lambda}}(\varphi'(r) + \lambda\varphi(r))g.$$

Its support in λ stays away from zero and infinity. In particular,

$$\|q\|_{\mathcal{G}}^2 = \frac{\|g\|^2}{2}\left(\|\varphi'\|_2^2\int \frac{p^2}{\lambda}\,\mathrm{d}\nu_a + \|\varphi\|_2^2\int \lambda p^2\,\mathrm{d}\nu_a\right) < \infty,$$

where the cross term vanishes because $\int \varphi'\varphi = 0$.

Step 2. We prove orthogonality to the raw-noise image. For a smooth compact raw tensor F the isometry is

$$\Phi F(\lambda, r) = \sqrt{2\lambda}\int_{t>0,\ t\ge r} e^{-\lambda(t-r)}F_t\,\mathrm{d}t.$$

The identity

$$\int_{-\infty}^{t} e^{-\lambda(t-r)}(\varphi'(r) + \lambda\varphi(r))\,\mathrm{d}r = \varphi(t)$$

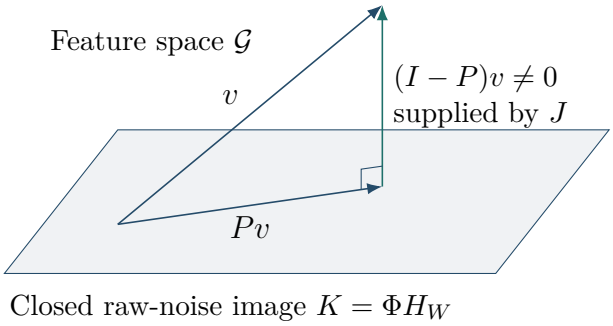

Figure 12.5: Hilbert-space schematic for No-go 32, drawn in three coordinates only. The explicit vector $q \perp K$ has $\langle v, q\rangle > 0$, so a positive finite cutoff point feature at $t_0 > 0$ has a nonzero component supplied by J. This says nothing by itself about measurability of a nonlinear limit with respect to W.

follows by differentiating $e^{-\lambda(t-r)}\varphi(r)$ in r. All integrals paired with q are absolutely integrable because its two supports are compact and its λ support stays away from zero. Consequently,

$$\langle \Phi F, q\rangle_{\mathcal{G}} = \left(\int_{t>0} \langle F_t, g\rangle_{H_\Gamma} \varphi(t)\,\mathrm{d}t\right) \int p\,\mathrm{d}\nu_a = 0.$$

Step 3. We separate the point feature and obtain the conditional variance obstruction. Density and continuity give $q \perp K$. The same calculation for the point feature instead gives

$$\langle v, q\rangle_{\mathcal{G}} = \varphi(t_0)\|g\|^2 \int_{(0,L]} p\,\mathrm{d}\nu_a = \|g\|^2 > 0.$$

Thus $(I-P)v \neq 0$. Independence of J and W yields

$$\mathrm{Var}(\mathcal{I}(v) \mid \sigma(W)) = \|(I-P)v\|^2 \geq \frac{|\langle v, q\rangle|^2}{\|q\|^2} > 0.$$

This proves No-go 32. □

The conclusion concerns positive finite cutoffs and $t_0 > 0$ in this fixed extension. It neither treats time zero nor proves that a nonlinear canonical limit retains an auxiliary component. Raw-test convergence can remove such components in a limit. The fixed-extension source construction remains valid. For a concrete surviving limit, Proposition 6.2.7 proves that the tested fixed-mask limit $Z_m(t, \phi)$ is W-measurable. That conclusion uses the operator-path and Young-flow convergence; it is not supplied or contradicted by this finite-feature obstruction.

12.6 Finite optimization and checks on review arguments

The last group concerns finite calculations. These examples are small enough that every number can be checked directly, but the distinctions they expose matter in the

infinite-dimensional proof: the two variance directions, the normalization of an energy, the active set of an optimization, and the exact inequality used in a review.

12.6.1 NG-23: both Gaussian variance directions

A rectangular Gaussian matrix has an input variance and an output variance. Keeping only one would simplify the moment estimate, but the dimensions of the two spaces cannot be ignored. This is the counterexample behind Remark 4.3.4.

No-go 23 (A one-sided variance bound fails)**.** Let $g_1, \dots, g_n$ be independent standard real Gaussians, $A_i = e_i^{\mathsf{T}}$ the coordinate row matrices, and $X = \sum_i g_i A_i$. Put $V_{\mathrm{in}} = \sum_i A_i^* A_i$ and $V_{\mathrm{out}} = \sum_i A_i A_i^*$. For $n = 16$,

$$\mathbb{E}\|X\|_{S_4}^4 = 288 > 144 = 9 \operatorname{Tr} V_{\mathrm{in}}^2.$$

The transposed family gives the analogous failure of an output-only bound. More generally, no constant independent of n bounds the left side by $\operatorname{Tr} V_{\mathrm{in}}^2$ alone for all these row matrices.

Proof. The only nonzero singular value of X is $(\sum_i g_i^2)^{1/2}$. Since $\mathbb{E}g_i^4 = 3$ and $\mathbb{E}g_i^2 g_j^2 = 1$ for $i \neq j$,

$$\mathbb{E}\|X\|_{S_4}^4 = \mathbb{E}\left(\sum_i g_i^2\right)^2 = 3n + n(n-1) = n(n+2).$$

Here $V_{\mathrm{in}} = I_n$, whereas $V_{\mathrm{out}} = n$ acts on a one-dimensional space. The proposed bound gives $9n$, which is smaller than $n(n+2)$ at $n = 16$. The ratio to $\operatorname{Tr} V_{\mathrm{in}}^2 = n$ is $n + 2$, so no fixed constant works for all n. Transposition exchanges the variance directions and preserves the singular values. This proves No-go 23. □

Scope and what survives. This is a finite-matrix counterexample, not a counterexample to a wave estimate. Proposition 4.3.3 retains both variances. At $n = 16$, its average and maximum bounds have fourth powers 1224 and 2304, respectively, and neither is contradicted by 288.

What would permit a different estimate? A one-sided estimate would need additional structure relating the two variance operators, with its dimension dependence stated. It cannot follow from the Gaussian matrix form alone.

12.6.2 NG-28: the normalization matters when bounds are compared

The occupation argument gives the upper ceiling U_2 for C_2. It is tempting to compare it with an energy expression by changing the coefficient of the gradient penalty. The comparison must be calculated: a value with penalty one is not interchangeable with a

value with penalty one-half. In particular, not every comparison value below is itself a proved upper bound for the moment constant.

Retain $q = 4-\alpha$, $k = 3-\alpha$ and $m = q/k$, and the occupation energies $\mathcal{E}_\zeta^{\mathcal{O}}$ of (11.3.1). For $z > 0$, the scalar maps are

$$F_b(z) = k\left[\frac{(q-2b)^{(q-2b)/2}}{8(q-b)^{q-b}}\left(\frac{2z}{2-\alpha}\right)^{(2-\alpha)/2}\right]^{1/k}, \qquad 0 \le b < q/2.$$

These are the maps in (11.3.7); here b is only a display parameter and $a = \alpha_0$ is the temporal exponent.

No-go 28 (An occupation ceiling need not improve a comparison value)**.** For $d = 2$, $\alpha = 5/4$, $a = 1/2$ and every nonzero admissible covariance,

$$2^m F_a(\mathcal{E}_1^{\mathcal{O}}) < U_2.$$

Thus, the reverse comparison is not valid throughout the admissible class.

Proof. We compute the ratio of the two comparison formulas with the kinetic penalty retained. At the stated parameters, its logarithm is negative, disproving the proposed ordering of these formulas.

Step 1. We express the comparison through its exact logarithmic ratio. The energies are finite and positive by Proposition 11.3.2. Put

$$\Delta = \frac{1}{2}\{q\log q + (q-2a)\log(q-2a)\} - (q-a)\log(q-a).$$

Subtracting the logarithms of F_a and F_0 gives $\log(F_a(z)/F_0(z)) = \Delta/k$. The identity in Theorem 11.3.4 gives $U_2 = 2^m(2\zeta)^{\alpha/(2k)}F_0(\mathcal{E}_\zeta^{\mathcal{O}})$. Therefore,

$$\frac{2^m F_a(\mathcal{E}_\zeta^{\mathcal{O}})}{U_2} = \exp\left\{\frac{\Delta - (\alpha/2)\log(2\zeta)}{k}\right\}.$$

Step 2. We evaluate the sign at the admissible parameter point. At the stated parameters, $q = 11/4$, $k = 7/4$, and

$$8\{\Delta - (\alpha/2)\log 2\} = \log\frac{11^{11}7^7}{2^5 9^{18}} < 0,$$

because

$$234966429149994773 < 4803028329503971872.$$

This proves No-go 28. □

Scope and what survives. This refutes an ordering of two computed quantities, not an inequality for the actual moment. It does not decide whether C_2 is below the smaller comparison value. At $\zeta = 1/2$, the logarithmic difference is instead $\Delta/k > 0$, by strict convexity of $x\log x$; that is the valid strict comparison in Corollary 11.3.5.

What would permit a different comparison? Match the covariance amplitude, admissible profiles and kinetic penalty, then prove the sign of the resulting ratio in the parameter range claimed. Comparing the names of the energies is insufficient.

12.6.3 NG-29: three safeguards in the Gram optimization

The finite optimization of Section 11.1 uses

$$F(\Phi) = 2\sum_i \ell_i \sqrt{(\langle \Phi, k_i\rangle - b_i)_+} - \frac{1}{2}\|\Phi\|^2, \qquad \ell_i > 0, \quad b_i \geq 0.$$

The Gram entries $C_{ij} = \langle k_i, k_j\rangle$ are nonnegative. Three possible simplifications fail: omitting the empty active set, invoking global concavity, and treating entrywise order as positive semidefinite order.

No-go 29 (Empty sets, concavity and matrix order)**.** Each of the following failures occurs within the finite setting above.

1. With one unit vector, $\ell = 1/10$ and $b = 4$, the nonempty-set dual infimum is negative, while the primal supremum is nonnegative.
2. With $H = \mathbb{R}$ and $k = \ell = b = 1$, the primal objective is not concave.
3. There are positive semidefinite Grams C, D with $0 \leq C_{ij} \leq D_{ij}$ for every entry but $D - C$ not positive semidefinite.

Proof. In the first example the nonempty dual is

$$D(w) = \frac{1}{100w} - 4w + \frac{w^2}{2}, \qquad w > 0.$$

Its infimum is at most $D(4) = -3199/400 < 0$, whereas $F(0) = 0$. Dropping the empty value from the maximum of dual infima therefore cannot give the primal supremum.

In the second example $F(x) = 2\sqrt{(x-1)_+} - x^2/2$. Directly, $F(0) = F(2) = 0$ but $F(1) = -1/2$, violating midpoint concavity.

For the third example take

$$C = \begin{pmatrix} 1 & 0 \\ 0 & 1 \end{pmatrix}, \qquad D = \begin{pmatrix} 1 & 1/2 \\ 1/2 & 1 \end{pmatrix}.$$

The eigenvalues of D are $3/2$ and $1/2$, while those of $D - C$ are $1/2$ and $-1/2$. All entries are ordered as claimed. This proves No-go 29. □

Scope and what survives. These are the checks in Remark 11.1.6. They explain the empty-set convention and active-set proof of Proposition 11.1.3. Entrywise comparison still works in Proposition 11.1.5: for nonnegative weights w_i, the form $\sum_{i,j} w_i(D_{ij} - C_{ij})w_j$ is nonnegative. No order on all vectors, and no covariance monotonicity for nonlinear waves, is asserted by that calculation.

What would permit a shortcut? A restricted concavity argument must first justify its active region. A matrix comparison must specify the vectors on which its quadratic form is nonnegative. Neither step follows from a convenient change of terminology.

12.6.4 NG-33: check the mathematics returned by a reviewer

A review report is also a mathematical argument and can contain an incorrect step. This historical record groups three such checks. The manuscript had the correct expressions; the examples below explain why the proposed review steps could not replace them. These are not three new counterexamples to the stochastic model.

No-go 33 (Three invalid proof steps)**.** The following assertions fail.

1. The free phase matrix $S_0(t) = \left(\begin{smallmatrix} 1 & t \\ 0 & 1 \end{smallmatrix}\right)$ is a contraction in the Euclidean norm for every $t \geq 0$.
2. For $x > 0$, an integer $n \geq 1$ and $0 < \vartheta < 1$, the series term $x^n/(n!)^\vartheta$ equals $A_n B_n$, where
$$A_n = \frac{(2x^{1/\vartheta})^n}{n!}, \qquad B_n = 2^{-\vartheta n/(1-\vartheta)}.$$
3. The denominator $k!\, k^{(2-\alpha)k}$ may always be replaced by the larger denominator $(k!)^3$ in the coefficient bound of Proposition B.1.5.

Proof. We test the three discarded review steps separately: free-phase contractivity, the unweighted series-factor identity, and the stronger factorial denominator. Each calculation concerns the stated inference rather than a new moment counterexample.

Step 1. We disprove free-phase contractivity in the stated norm. The vector $(0, 1)$ has norm one, but its image under $S_0(t)$ has norm $\sqrt{1+t^2} > 1$ for $t > 0$. To transfer this to the whole-space phase, use exactly the inhomogeneous Sobolev norm of Section 4.2: $E = H^{1/2} \times H^{-1/2}$ and $J_0 = \operatorname{diag}(\Lambda^{1/2}, \Lambda^{-1/2})$, where $\Lambda = (1 - \Delta)^{1/2}$. With $r = |\xi|$ and $\langle\xi\rangle = \sqrt{1+r^2}$, the Fourier symbol of $J_0 S(t) J_0^{-1}$ is

$$\begin{pmatrix} \cos(tr) & \langle\xi\rangle \sin(tr)/r \\ -r \sin(tr)/\langle\xi\rangle & \cos(tr) \end{pmatrix} \longrightarrow S_0(t) \qquad (r \downarrow 0).$$

Choose normalized Fourier bumps supported in balls shrinking to zero and place them in the second coordinate of $J_0 z$. Continuity of this matrix at zero shows that their image norms tend to $\sqrt{1+t^2}$. Thus $S(t)$ is not a contraction on this E. The distinction between $\langle\xi\rangle$ and $|\xi|$ matters: this is not a claim about the homogeneous energy norm. The valid estimate keeps a free-growth factor.

Step 2. We test the proposed unweighted series product. The correct identity in the second assertion is $x^n/(n!)^\vartheta = A_n^\vartheta B_n^{1-\vartheta}$. At $\vartheta = 3/4$, $n = 1$ and $x = 1$, its left side is one, whereas $A_1 B_1 = 2 \cdot (1/8) = 1/4$. Hölder applies to the weighted product, as in the proof of Proposition 3.2.4.

Step 3. We test the proposed replacement of the factorial denominator. For the third assertion choose the permitted spatial-white value $\alpha = 1$ and $k = 3$. Then $k!k^{(2-\alpha)k} = 162 < 216 = (k!)^3$. For $M > 0$, an upper bound $M/162$ does not imply the smaller upper bound $M/216$. The valid factorial weakening is instead

$$k!k^{(2-\alpha)k} \geq (k!)^{3-\alpha},$$

since $k! \leq k^k$ and $2-\alpha > 0$; at this example its right side is 36. This proves No-go 33. □

Scope and what survives. The last arithmetic check refutes an inference between numerical bounds; it does not prove that the actual coefficient exceeds $M/216$. All three corrected arguments remain in the main text. Their lesson is to check an asserted derivation against its domains, factors and quantifiers, even when the report containing it has a favorable overall verdict.

What would permit the discarded steps? Contractivity needs a suitable invariant norm or a restricted state class. The Hölder factors need their conjugate powers. A stronger factorial bound needs an additional estimate; it cannot be obtained by changing the exponent in the denominator.

Appendix A

Finite-order calculations

Before trusting an asymptotic argument, compute something by hand. What do the first terms of the second moment look like? This appendix works them out in one space dimension with initial data $(1, 0)$. Figure A.1 is the picture to keep in mind.

Already at small order the Stratonovich expansion shows its three features: pairings inside one chain, pairings between the two chains, and products of different orders. Starting from Proposition 2.1.1, Proposition A.1.1 computes every term of total order four for spatial white noise, and Proposition A.1.3 gives the order-two coefficient and an integral formula for every order-four Riesz term. Here the total order is the sum of the two Stratonovich orders; it is not a Wiener-chaos order.

These formulas test the scaling, the pairing counts and the static limit. Finitely many coefficients cannot determine the exponent or the constant, and the main argument does not rely on this appendix. A reader who wants examples first can start here after the chain notation of Chapter 2. Episode ▶ 9 of the video series covers this appendix.

A.1 Finite-order checks in one space dimension

We now compute the total-order-two and total-order-four coefficients in Proposition 2.1.1, first for spatial white noise and then for $\gamma(x) = c_\alpha |x|^{-\alpha}$ with $0 < \alpha < 1$ and $c_\alpha > 0$. Here $d = 1$ throughout. A total order is the sum of the two Stratonovich orders; it is not an orthogonal Wiener-chaos order. Write

$$A = \{(1,2),(3,4)\}, \quad B = \{(1,3),(2,4)\}, \quad C = \{(1,4),(2,3)\}.$$

These are the three pairings of four vertices. All finite integrals below retain the normalization $G(s,y) = \frac{1}{2}\mathbf{1}_{\{|y|<s\}}$ and covariance $|s-r|^{-\alpha_0}\gamma(y-z)$.

A.1.1 Spatial white noise: all order-four diagrams

For $a, b, c \geq 0$, define

$$F(a,b,c) = 4ab - (a+b-c)_+^2 + (|a-b|-c)_+^2. \tag{A.1.1}$$

This is the area of $\{(x,y) : |x| < a,\ |y| < b,\ |x-y| < c\}$. In particular, F is nonnegative and symmetric in its three arguments. To verify the formula, subtract from the rectangle the two regions where $|x-y| \geq c$; when $c \geq |a-b|$ these are two right triangles, and when $c < |a-b|$ the retained strip has area $4\min(a,b)c$. The three formulas, including $c \geq a+b$, give (A.1.1). Symmetry also follows from swapping x, y and the determinant-one change $(x,y) \mapsto (x, x-y)$.

In the following table, V is a spatial factor and q_1, q_2 are nonnegative time gaps. The contribution of a row is the integral of $V(q_1 q_2)^{-\alpha_0}$ over its domain, with ordinary Lebesgue measure in its four listed variables. The domains are

$$\begin{aligned}(0,4):&\quad a,b,c,d>0,\quad a+b+c+d<t,\\(1,3):&\quad 0<r<t,\quad a,b,c>0,\quad a+b+c<t,\\(2,2):&\quad a,b,c,d>0,\quad a+b<t,\quad c+d<t.\end{aligned}$$

The letters a, b, c, d denote increments within the nonempty chains; for $(1,3)$, r is the time of the single vertex. Values on zero-gap sets do not affect these nonnegative integrals.

Lean full

Proposition A.1.1 (White-space order four)**.** *Suppose that $d = \alpha = 1$ and $\gamma = \delta_0$. Each $J_{m,n,D}(t)$ with $m+n=4$ is given by the following table or by exchanging the two chains:*

(m,n)	D	V	q_1	q_2
$(0,4)$	A	$ac/4$	b	d
$(0,4)$	B	$a\min(b,c,d)/4$	$b+c$	$c+d$
$(0,4)$	C	$a\min(b,d)/4$	$b+c+d$	c
$(1,3)$	A	$\min(r,a)b/4$	$\lvert r-a\rvert$	c
$(1,3)$	B	$F(r,a,\min(b,c))/16$	$\lvert r-a-b\rvert$	$b+c$
$(1,3)$	C	$F(r,a,c)/16$	$\lvert r-a-b-c\rvert$	b
$(2,2)$	A	$ac/4$	b	d
$(2,2)$	B	$\min(a,c)\min(b,d)/4$	$\lvert a-c\rvert$	$\lvert a+b-c-d\rvert$
$(2,2)$	C	$F(a,c,\min(b,d))/16$	$\lvert a-c-d\rvert$	$\lvert a+b-c\rvert$

(A.1.2)

The total-order-four contribution is

$$2\sum_{D\in\{A,B,C\}} J_{0,4,D}(t) + 2\sum_{D\in\{A,B,C\}} J_{1,3,D}(t) + \sum_{D\in\{A,B,C\}} J_{2,2,D}(t). \tag{A.1.3}$$

Each entry scales as $t^{6-2\alpha_0}$ times its unit-time value.

Proof. We identify the two free spatial positions for each pairing and compute the allowed area. We then exchange the chains and collect the time and space scaling factors.

Step 1. We compute the spatial factors for each chain split. In each pairing identify its first pair's spatial positions with x and the other pair's positions with y. The two delta covariances have unit mass, so spatial integration leaves $1/16$ times the area allowed by the four Green indicators. For a single chain the position lists for A, B, C are, respectively, (x,x,y,y), (x,y,x,y) and (x,y,y,x). Their areas are $4ac$, $4a\min(b,c,d)$ and $4a\min(b,d)$.

For $(1,3)$ take the single position to be x. The long chain has positions (x,y,y), (y,x,y) or (y,y,x) for A, B, C. The first area is $4\min(r,a)b$; the other two areas are $F(r,a,\min(b,c))$ and $F(r,a,c)$. For $(2,2)$ the position lists of the two chains are $(x,x),(y,y)$ for A, $(x,y),(x,y)$ for B, and $(x,y),(y,x)$ for C. The areas are $4ac$, $4\min(a,c)\min(b,d)$ and $F(a,c,\min(b,d))$. In every case reading the paired times gives the two gaps in (A.1.2). This proves each row, with no unlisted pairing or multiplicity. The distributional delta integrations can equivalently be obtained by convolution with

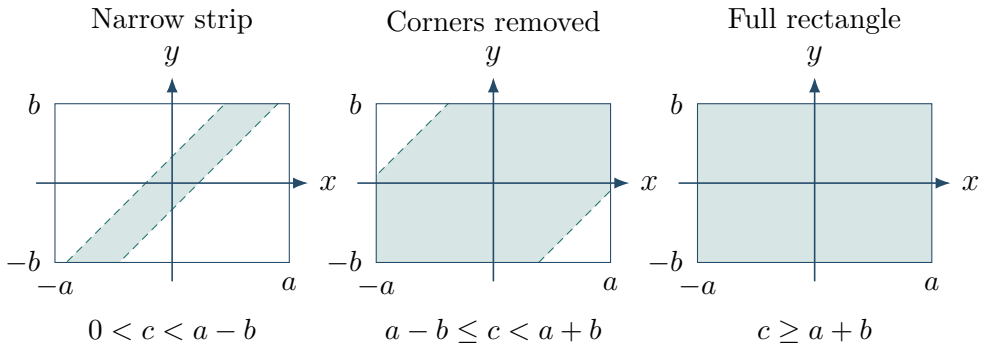

Figure A.1: The area $F(a,b,c)$ in the spatial-white order-four calculation: the shaded part is $[-a,a]\times[-b,b]\cap\{|x-y|<c\}$, and the dashed lines are the edges $|x-y|=c$ of the strip. The drawing uses $a>b>0$; here a,b,c are time-increment parameters, not covariance exponents. The three geometric cases explain the positive-part formula, without replacing the separate pairing and time-order calculations. See Proposition A.1.1.

the source's spatial approximate identity: for positive increments the remaining bounded interval indicators have only boundary discontinuities, and those boundaries have two-dimensional measure zero. The resulting areas converge to the displayed areas. They are uniformly bounded at unit time: each smoothed delta has mass one, so its integral over its paired coordinates in $[-1,1]^2$ is at most two. The four Green factors give a spatial bound $2^2/16=1/4$. Integrability of the time weights follows from the disjoint-pair bound used in Lemma A.1.2 below.

Step 2. We collect the multiplicities and the scaling. Exchanging chains gives the $(4,0)$ and $(3,1)$ sums without changing the covariance factors. This proves (A.1.3). Finally, scaling all four time variables by t gives t^4 from their measure, t^2 from the area and $t^{-2\alpha_0}$ from the covariance factors. This proves Proposition A.1.1. □

Lemma A.1.2 (Static finite-order calibration)**.** *As $\alpha_0\downarrow 0$, each unit-time coefficient in Proposition A.1.1 converges to the entry below:*

(m,n)	A	B	C	*sum*
$(0,4)$	$1/2880$	$1/8640$	$1/5760$	$11/17280$
$(1,3)$	$1/576$	$29/34560$	$1/640$	$143/34560$
$(2,2)$	$1/144$	$1/480$	$31/17280$	$187/17280$

(A.1.4)

Thus, the static total-order-four contribution is $11t^6/540$. The static total-order-two contribution is $t^3/3$. These are coefficients, not large-time asymptotic constants.

Proof. We first justify the static limit by an integrable time-cube bound. We then integrate time slacks at fixed spatial positions and evaluate the remaining polynomial sector integrals.

Step 1. We pass to the static coefficient by dominated convergence. On the unit-time domain all original time coordinates belong to $[0,1]$. The spatial factor is bounded by

$1/4$, since all positions lie in $[-1,1]$ and the two free positions have area at most four. Fix $0<\bar a<1$. For $0\le\alpha_0\le\bar a$, the temporal factors are bounded by the product with exponent $\bar a$. On the full time cube its integral is

$$\Big(\int_0^1\int_0^1 |s-r|^{-\bar a}\,\mathrm{d}s\,\mathrm{d}r\Big)^2=\Big(\frac{2}{(1-\bar a)(2-\bar a)}\Big)^2<\infty,$$

because the two pairs use disjoint labels. Dominated convergence permits setting $\alpha_0=0$ in every row.

Step 2. We reduce the coefficients to spatial sectors. We evaluate the resulting integrals by an independent spatial calculation. For fixed free positions x,y, let L_1,L_2 be the sums of absolute spatial increments along the two chains, starting at zero. Integrating their time increments first gives

$$J_{m,n,D}(1)\big|_{\alpha_0=0}=\frac{1}{16m!n!}\int_{\mathbb{R}^2}(1-L_1(x,y))_+^m(1-L_2(x,y))_+^n\,\mathrm{d}x\,\mathrm{d}y. \tag{A.1.5}$$

An empty-chain factor in this formula is defined to be one. Indeed, writing each time increment as its required absolute spatial increment plus a nonnegative slack leaves a simplex of volume $(1-L_\rho)_+^{n_\rho}/n_\rho!$. Put $w=|x-y|$. The length pairs are

(m,n)	A	B	C
$(0,4)$	$(0,\lvert x\rvert+w)$	$(0,\lvert x\rvert+3w)$	$(0,\lvert x\rvert+2w)$
$(1,3)$	$(\lvert x\rvert,\lvert x\rvert+w)$	$(\lvert x\rvert,\lvert y\rvert+2w)$	$(\lvert x\rvert,\lvert y\rvert+w)$
$(2,2)$	$(\lvert x\rvert,\lvert y\rvert)$	$(\lvert x\rvert+w,\lvert x\rvert+w)$	$(\lvert x\rvert+w,\lvert y\rvert+w)$

Step 3. We evaluate and sum the sector contributions. Divide the plane into $0\le x\le y$, $0\le y\le x$, $x\ge 0\ge y$ and their reflected sectors. Use $(x,y)=(u,u+v),(u+v,u),(u,-v)$, respectively, where $u,v\ge 0$. Each map has determinant of absolute value one. In these three sectors the integrals of $(1-L_1)_+^m(1-L_2)_+^n$, before multiplication by $2/(16m!n!)$, are

(m,n)	D	$0\le x\le y$	$0\le y\le x$	$x\ge 0\ge y$
$(0,4)$	A	$1/30$	$1/60$	$1/60$
$(0,4)$	B	$1/90$	$1/120$	$1/360$
$(0,4)$	C	$1/60$	$1/90$	$1/180$
$(1,3)$	A	$1/24$	$3/160$	$11/480$
$(1,3)$	B	$1/72$	$3/160$	$11/1440$
$(1,3)$	C	$1/48$	$1/30$	$1/48$
$(2,2)$	A	$1/18$	$1/18$	$1/9$
$(2,2)$	B	$1/30$	$1/60$	$1/60$
$(2,2)$	C	$31/1440$	$31/1440$	$31/2160$

(A.1.6)

All entries follow by integrating polynomials over the two linear constraints $L_1\le 1$, $L_2\le 1$. For example, $\int_{u,v\ge0}(1-pu-qv)_+^4\,\mathrm{d}u\,\mathrm{d}v=1/(30pq)$. The last row's first entry

and last entry are, explicitly,

$$\int_0^{1/2} \mathrm{d}v \int_0^{1-2v} (1-u-v)^2(1-u-2v)^2 \,\mathrm{d}u = \frac{31}{1440},$$
$$\int_0^{1/3} \mathrm{d}u \int_0^{(1-u)/2} (1-2u-v)^2(1-u-2v)^2 \,\mathrm{d}v$$
$$+ \int_{1/3}^{1/2} \mathrm{d}u \int_0^{1-2u} (1-2u-v)^2(1-u-2v)^2 \,\mathrm{d}v = \frac{31}{2160}.$$

The stated lengths and linear bounds similarly specify every entry of (A.1.6). Summing and multiplying by $2/(16m!n!)$ proves (A.1.4). Applying the multiplicities in (A.1.3) gives $11/540$. Lemma 2.2.1 at $\alpha_0 = 0$ gives the order-two value. This proves Lemma A.1.2. □

A.1.2 Riesz covariance: order two and an order-four integral

Lean partial

Proposition A.1.3 (Riesz finite coefficients)**.** *Suppose $d = 1$, $0 < \alpha < 1$, $0 < \alpha_0 < 1$, and $\gamma(y) = c_\alpha |y|^{-\alpha}$ with $c_\alpha > 0$. With $\beta = 4 - \alpha - \alpha_0$, the two order-two terms are*

$$\begin{aligned} \mathbb{E}X_2(t,x) &= \frac{c_\alpha t^\beta}{(1-\alpha)(2-\alpha-\alpha_0)(3-\alpha-\alpha_0)(4-\alpha-\alpha_0)}, \\ \mathbb{E}X_1(t,x)^2 &= \frac{c_\alpha}{(1-\alpha)(2-\alpha)} \int_0^t v^{-\alpha_0} \left[\frac{(2t-v)^{3-\alpha} - v^{3-\alpha}}{2(3-\alpha)} - (t-v)v^{2-\alpha} \right] \mathrm{d}v. \end{aligned} \tag{A.1.7}$$

Their total is $\mathbb{E}X_1^2 + 2\mathbb{E}X_2$.

The following explicit unit-domain integral gives every order-four term. For $m+n = 4$, let

$$H_m = \{h \in (0,\infty)^4 : \sum_{l=1}^{m} h_l < 1, \ \sum_{l=m+1}^{4} h_l < 1\},$$

with an empty sum equal to zero. For each index l, let $b(l)$ be the first index in its own nonempty chain, and define

$$S_l(h) = \sum_{i=b(l)}^{l} h_i, \qquad Y_l(h,U) = \sum_{i=b(l)}^{l} h_i U_i,$$

where $U_1, \dots, U_4$ are independent uniform variables on $[-1,1]$. Then, for $D = A, B, C$,

$$\begin{aligned} J_{m,n,D}(t) = c_\alpha^2 t^{2\beta} \int_{H_m} \left(\prod_{l=1}^{4} h_l \right) \prod_{(j,q)\in D} |S_j(h) - S_q(h)|^{-\alpha_0} \\ \times \mathbb{E}_U \left[\prod_{(j,q)\in D} |Y_j(h,U) - Y_q(h,U)|^{-\alpha} \right] \mathrm{d}h. \end{aligned} \tag{A.1.8}$$

This is a finite nonnegative integral. It specifies all five splits and all three pairings without an unspecified kernel. The total coefficient uses the multiplicities in (A.1.3).

Proof. We compute the two order-two coefficients directly. For order four, we express Green increments through uniform variables and check finiteness before using the resulting unit-domain formula.

Step 1. We evaluate the order-two terms. Direct integration on the two intervals gives

$$\int_{\mathbb{R}^2} G(s,y)G(r,z)c_\alpha|y-z|^{-\alpha}\,\mathrm{d}y\,\mathrm{d}z = \frac{c_\alpha\big((s+r)^{2-\alpha}-|s-r|^{2-\alpha}\big)}{2(1-\alpha)(2-\alpha)}.$$

Integrate on $s>r$ and double, set $v=s-r$, and integrate r over $(0,t-v)$. This proves the second formula in (A.1.7). In the single-chain term with increments r,v, the spatial integral is $c_\alpha r v^{1-\alpha}/(1-\alpha)$. Thus, the remaining integral is $c_\alpha(1-\alpha)^{-1}\int_{r+v<t} r v^{1-\alpha-\alpha_0}\,\mathrm{d}r\,\mathrm{d}v$, which gives its first formula by two elementary integrations.

Step 2. We identify the four-increment formula and its scaling. For order four set each spatial increment equal to $h_l U_l$. The Green factor $\frac{1}{2}\mathbf{1}_{[-h_l,h_l]}$ is h_l times the law of $h_l U_l$. The map from increments to vertex positions is triangular within each chain with determinant one. Consequently, the four spatial integrals give exactly the product $\prod_l h_l$ and the expectation in (A.1.8); the factors $1/16$ are already incorporated in the four uniform probability laws. The time increments give the domain H_m and the differences S_j-S_q. Scaling time and space by t contributes t^8 from the eight integrations and $t^{-2\alpha-2\alpha_0}$ from the two covariance factors, giving $t^{2\beta}$.

Step 3. We check integrability on the enlarged time and space cubes. Finiteness can be checked without a numerical argument. On the unit-time domain all vertex positions lie in $[-1,1]$. Enlarge the time domain to $[0,1]^4$ and the spatial domain to $[-1,1]^4$, and bound the Green indicators by one. The two time covariance factors involve disjoint pairs and are integrable since $\alpha_0<1$. The same is true of the two spatial factors since $\alpha<1$. Tonelli's theorem now gives a finite bound. This proves Proposition A.1.3. □

Remark A.1.4 (Normalization and static Riesz check)**.** The same integrable bound with any fixed exponent $\bar{a}\in(\alpha_0,1)$ permits $\alpha_0\downarrow 0$ at these fixed orders. From (A.1.7), the static total-order-two coefficient is

$$\frac{c_\alpha 2^{3-\alpha}}{(1-\alpha)(2-\alpha)(3-\alpha)(4-\alpha)}.$$

For example, the double integral of $(s+r)^{2-\alpha}-|s-r|^{2-\alpha}$ on $[0,1]^2$ is $(2^{4-\alpha}-4)/((3-\alpha)(4-\alpha))$, which verifies this value after adding twice the single-chain coefficient. If one chooses the normalization $c_\alpha=(1-\alpha)/2$, this coefficient tends to $1/3$ as $\alpha\uparrow 1$, in agreement with the white-space value. More generally, at each fixed $\alpha_0\in(0,1)$ the two normalized coefficients in (A.1.7) tend to $c_0/2$ and c_0, respectively. For the second coefficient, the bracket at $t=1$ tends to $(1-v)^2$, the prefactor tends to $1/2$, and dominated convergence gives $\frac{1}{2}\int_0^1 v^{-\alpha_0}(1-v)^2\,\mathrm{d}v=c_0$. The brackets are uniformly bounded for α near one, so $Cv^{-\alpha_0}$ is an integrable dominator. This is a finite-coefficient normalization check; unnormalized $|y|^{-\alpha}$ must not be identified with δ_0.

A.1.3 Calibration table and limits of the finite-order test

Let M_2 and M_4 denote only the total-order-two and total-order-four contributions. The results above give

covariance and time regime	$M_2(t)$	$M_4(t)$
$\delta_0, \quad 0 < \alpha_0 < 1$	$2c_0 t^{3-\alpha_0}$	$t^{6-2\alpha_0}\, M_4(1)$
$\delta_0, \quad \alpha_0 = 0$	$t^3/3$	$11t^6/540$
$c_\alpha \lvert y\rvert^{-\alpha}, \quad 0 < \alpha_0 < 1$	$t^\beta M_2(1)$	$t^{2\beta} M_4(1)$
$c_\alpha \lvert y\rvert^{-\alpha}, \quad \alpha_0 = 0$	$\dfrac{c_\alpha 2^{3-\alpha} t^{4-\alpha}}{(1-\alpha)(2-\alpha)(3-\alpha)(4-\alpha)}$	$t^{8-2\alpha} M_4(1)$

Here c_0 is defined in Lemma 2.2.1; the fractional-time white coefficient $M_4(1)$ is the explicit four-dimensional time integral in (A.1.2), and the Riesz coefficients are specified by (A.1.7)–(A.1.8). No closed form for those remaining integrals is asserted.

Remark A.1.5 (Purpose of these calculations)**.** The static exponent from the published Chen–Hu theorem is $(4-\alpha)/(3-\alpha)$; see [20, Theorem 1.2, (1.9), p. 2147]. Both κ and the G0 exponent ρ have this boundary limit. The finite coefficient limits above are justified separately by dominated convergence; they do not exchange $t \to \infty$ and $\alpha_0 \downarrow 0$ and do not verify an asymptotic constant. In particular, the disputed printed white-space constant in the separate Chen–Hu source audit is not used here. The single-chain rows agree with the first-moment expansion, and all mixed rows are nonnegative, consistent with the Jensen comparison. Relative to the Skorohod expansion, the rows with self-pairings are present here and cannot be dropped: already $M_2 = \mathbb{E}X_1^2 + 2\mathbb{E}X_2$. This is a structural comparison only, not a Skorohod result. Finally, any fixed truncation is a polynomial in t^β with nonnegative coefficients, so its logarithm divided by t^κ tends to zero. Orders two and four can falsify a normalization or an incorrect pairing rule, but cannot determine an all-order factorial power or prove either principal goal.

No-gos 03 and 04 use these finite coefficients to disprove a squared-mean comparison with unit prefactor for every time and a coefficient constant uniform near $\alpha_0 = 1$, respectively. Neither test determines the large-time constant.

Appendix B

Direct upper bounds and static interpolation

Theorem 3.3.8 covers all of Hypothesis 1.2.1, and its proof is long. Is there a shorter way in simpler cases? Yes: estimate the pairing integrals of Proposition 2.1.1 directly. The price is extra assumptions; the reward, explicit constants. This appendix has no figure.

Section B.1 bounds the spatial factors first and then sums the temporal pairings. It reaches the correct scale when $\alpha \le 1$ (Proposition B.1.5), with separate constants for one-dimensional Riesz and white noise (Proposition B.1.2). Section B.2 goes beyond $\alpha = 1$, but only under an extra bound on translated convolutions (Proposition B.2.2); Proposition B.2.5 shows where that bound fails. Section B.3 gives a third route for isotropic Riesz covariance, by interpolation with static noise.

Each restriction is part of its statement. These bounds neither replace the proof of Chapter 3 nor give the sharp constant, and the main argument does not rely on them. On a first reading, Section B.1 is enough. Episode ▶ 9 of the video series covers this appendix.

B.1 Upper bounds for spatial exponents at most one

The upper bound at scale t^{κ} is proved for $0 < \alpha \le 1$ in dimensions one, two and three under the standing assumptions. The separate one-dimensional Riesz estimates retain their sharper constants and white endpoint. Degree-one covariance in dimensions two and three does not mean full spatial white noise. Section 3.3 treats the higher exponents by a separate argument. The intrinsic constant is identified in Theorem 11.2.6.

We retain the two-chain expansion of Proposition 2.1.1, but estimate its spatial and temporal factors in a different order. The spatial estimate keeps a power of the number of pairs. After taking a common spatial maximum, we sum all temporal pairings before using the ordered time domains.

Throughout this section $0 < \alpha_0 < 1$. We first work in dimension one with either of the spatial covariances

$$\begin{cases} \gamma(y) = c_\alpha |y|^{-\alpha}, & 0 < \alpha < 1, \quad c_\alpha > 0, \\ \gamma = c_\delta \delta_0, & \alpha = 1, \quad c_\delta > 0. \end{cases} \tag{B.1.1}$$

Put $b = 2 - \alpha$, $q = 3 - \alpha$, $\beta = 4 - \alpha - \alpha_0$, and

$$Z = \frac{2}{(1-\alpha_0)(2-\alpha_0)}, \qquad K_{\mathrm{sp}} = \begin{cases} \dfrac{c_\alpha 2^{2-\alpha}(1-\alpha)^{-\alpha}}{(2-\alpha)^{2-\alpha}}, & 0 < \alpha < 1, \\ c_\delta, & \alpha = 1. \end{cases} \tag{B.1.2}$$

These parameters satisfy Hypothesis 1.2.1, so the fixed-order integrability and mixed expansion already established apply.

B.1.1 A spatial bound retaining the ordered increments

For $m+n=2k$, label the two chains in block order as in (2.1.1). For each vertex l write $h_l = s_l - s_{p(l)} > 0$ and $y_l = x_l - x_{p(l)}$, with a separate root zero in each chain. Thus, x_l is the sum of increments in its own chain up to label l. The spatial change of variables has determinant one. In this section x_l denotes a spatial position and y_l its increment; this local notation differs from the position variables y_l in (2.1.1). The terminal evaluation point of $u(t,x)$ remains denoted by x. Let p_ϵ be the centered Brownian Gaussian density of variance ϵ and mass one, and set $\gamma_\epsilon = p_\epsilon * \gamma$. Allow a separate positive ϵ_e for every pair $e \in D$ and define

$$S_{D,\boldsymbol{\epsilon}}(h) = \int_{\mathbb{R}^{2k}} \prod_{l=1}^{2k} G(h_l, y_l) \prod_{(i,j)\in D} \gamma_{\epsilon_{i,j}}(x_j - x_i)\,\mathrm{d}y, \qquad G(h,y) = \tfrac{1}{2}\mathbf{1}_{\{|y|<h\}}.$$

This is an ordinary nonnegative integral; no pointwise delta value is used.

Lean full

Lemma B.1.1 (Spatial estimate)**.** *Suppose (B.1.1) holds, $k \geq 1$, and D is any pairing of the two chains. Orient every pair (i,j) by $i<j$ and let O_D and C_D be its opening and closing label sets. Then, uniformly in $\boldsymbol{\epsilon}$,*

$$S_{D,\boldsymbol{\epsilon}}(h) \leq \begin{cases} \left(\dfrac{c_\alpha}{1-\alpha}\right)^k \displaystyle\prod_{i\in O_D} h_i \prod_{j\in C_D} h_j^{1-\alpha}, & 0<\alpha<1, \\ \left(\dfrac{c_\delta}{2}\right)^k \displaystyle\prod_{i\in O_D} h_i, & \alpha = 1. \end{cases} \tag{B.1.3}$$

In particular, if $\sum_{l=1}^{2k} h_l \leq 2t$, then

$$S_{D,\boldsymbol{\epsilon}}(h) \leq K_{\mathrm{sp}}^k \frac{t^{bk}}{k^{bk}}. \tag{B.1.4}$$

Proof. We first obtain uniform convolution bounds. Descending label integration then removes each closing covariance and opening mass in order, and an increment maximum gives the final spatial bound.

Step 1. We bound the Riesz and white convolutions. We first record the convolution bounds. For $0<\alpha<1$, the integral of the even decreasing function $|y|^{-\alpha}$ over an interval of fixed length is maximal when the interval is centered at zero. Therefore,

$$\sup_z \int_{\mathbb{R}} G(h,y) c_\alpha |y+z|^{-\alpha}\,\mathrm{d}y = \frac{c_\alpha h^{1-\alpha}}{1-\alpha}.$$

By Tonelli's theorem, the integral with γ_ϵ equals the $p_\epsilon(w)\,\mathrm{d}w$ average of the unsmoothed integrals with shifts $z-w$. Its nonnegative mass-one average is therefore bounded by the same supremum. In the white case, $\gamma_\epsilon = c_\delta p_\epsilon$, so

$$\sup_z \int_{\mathbb{R}} G(h,y)\gamma_\epsilon(y+z)\,\mathrm{d}y \leq \frac{c_\delta}{2}.$$

Both estimates are uniform in $\epsilon > 0$.

Step 2. We integrate all increments in descending label order. Now integrate *all* spatial increments in descending label order $2k, 2k-1, \dots, 1$. Before processing label l, the remaining covariance factors are exactly those pairs whose closing labels are at most l; the bounds from the removed pairs depend only on h. If $l \in C_D$, its pair is (i, l) with $i < l$ and $x_l - x_i = y_l + z$, where z is independent of y_l. Every other remaining pair has both endpoints smaller than l, so its two positions are independent of y_l: positions involve only earlier increments in their own block chain. Thus, the only covariance involving y_l is its own pair, and the convolution bound removes it. If $l \in O_D$, its partner has a larger label and its covariance factor has already been removed. All remaining covariances have endpoints smaller than l, so integration of y_l gives only $\int G(h_l, y_l)\,\mathrm{d}y_l = h_l$. This also preserves the stated invariant for the next label. Tonelli's theorem and the nonnegativity of all factors justify each step. There are k labels of each type, proving (B.1.3) for every split and pairing.

Step 3. We maximize the remaining increment product. For Riesz covariance, weighted arithmetic–geometric mean gives

$$\prod_{i \in O_D} h_i \prod_{j \in C_D} h_j^{1-\alpha} \le \left(\frac{2t}{bk}\right)^{bk} (1-\alpha)^{(1-\alpha)k}.$$

Indeed, the weights are one at the k openings and $1-\alpha$ at the k closings, with total bk, and the sum of the increments is at most $2t$. Multiplication by $(c_\alpha/(1-\alpha))^k$ gives (B.1.4) with the stated K_{sp}. In the white case, $\prod_{i \in O_D} h_i \le (2t/k)^k$; multiplying by $(c_\delta/2)^k$ gives the same conclusion with $b = 1$ and $K_{\mathrm{sp}} = c_\delta$. This proves Lemma B.1.1. □

B.1.2 Summing temporal pairings before using time ordering

Define the total-order coefficients

$$A_k(t) = \sum_{m=0}^{2k} \mathbb{E}[X_m(t,x) X_{2k-m}(t,x)], \qquad A_0(t) = 1.$$

They do not depend on x, by spatial stationarity. By Proposition 2.1.1, $\mathbb{E}u^2(t,x) = \sum_{k \ge 0} A_k(t)$.

Lean partial

Proposition B.1.2 (One-dimensional upper bound)**.** *Under* (B.1.1)*, for every $k \ge 1$ and $t > 0$,*

$$A_k(t) \le \frac{(2ZK_{\mathrm{sp}})^k t^{\beta k}}{k!\, k^{bk}} \le \frac{(2ZK_{\mathrm{sp}})^k t^{\beta k}}{(k!)^q}. \tag{B.1.5}$$

Consequently,

$$\mathbb{E}u^2(t,x) \le \exp(C_{\mathrm{dir}} t^\kappa), \qquad C_{\mathrm{dir}} = q(2ZK_{\mathrm{sp}})^{1/q}, \quad \kappa = \frac{\beta}{q}. \tag{B.1.6}$$

Proof. We extract one spatial bound common to all pairings, then use symmetry of their temporal sum. We count all chain splits, pass the fixed-order limits and sum the factorial bound.

Step 1. We separate the common spatial bound from the temporal pairing sum. We first work with the Gaussian spatial smoothing and temporal truncation in [17, (2.9), (2.11), (2.23)–(2.24)]. Let $X_n^{\epsilon,\delta}$ be the smoothed Stratonovich term, using common parameters in every factor. Wick's formula expresses each mixed expectation of total order $2k$ as a sum over $D \in \Pi_k$. After the chain reversal in Proposition 2.1.1, its spatial factor is the one in Lemma B.1.1; its temporal factors are nonnegative and bounded by $|s_i - s_j|^{-\alpha_0}$. For times in $[0,t]^m_< \times [0,t]^{2k-m}_<$, the increments sum to the two terminal times and therefore to at most $2t$. Extract (B.1.4), which is independent of the time vector, the split, the pairing, and the smoothing parameters. The remaining temporal sum is

$$F_k(s_1, \dots, s_{2k}) = \sum_{D \in \Pi_k} \prod_{(i,j) \in D} |s_i - s_j|^{-\alpha_0}.$$

Every permutation of the $2k$ labels bijects Π_k, so F_k is fully symmetric. Moreover,

$$\int_{[0,t]^2} |s - r|^{-\alpha_0} \, \mathrm{d}s \, \mathrm{d}r = Zt^{2-\alpha_0}, \qquad \int_{[0,t]^{2k}} F_k(s) \, \mathrm{d}s = P_k (Zt^{2-\alpha_0})^k < \infty.$$

The second equality uses the disjoint endpoints of every pairing. Partitioning the time cube according to the order within each block now gives

$$\int_{[0,t]^m_< \times [0,t]^{2k-m}_<} F_k(s) \, \mathrm{d}s = \frac{P_k (Zt^{2-\alpha_0})^k}{m!(2k-m)!}. \tag{B.1.7}$$

Ties have measure zero. Crucially, this symmetry is applied to the *sum* of pairings after taking the common spatial bound, not to an individual temporally weighted diagram.

Step 2. We count pairings and splits. The number of pairings obeys $P_0 = 1$ and $P_k = (2k-1)P_{k-1}$, by choosing the partner of the smallest label. Hence, $P_k = (2k)!/(2^k k!)$. The binomial identity gives

$$\sum_{m=0}^{2k} \frac{1}{m!(2k-m)!} = \frac{2^{2k}}{(2k)!}.$$

Multiplying (B.1.7) by the spatial bound and summing over m yields

$$\sum_{m=0}^{2k} \mathbb{E}[X_m^{\epsilon,\delta} X_{2k-m}^{\epsilon,\delta}] \le K_{\mathrm{sp}}^k \frac{t^{bk}}{k^{bk}} \frac{2^{2k}}{(2k)!} \frac{(2k)!}{2^k k!} (Zt^{2-\alpha_0})^k = \frac{(2ZK_{\mathrm{sp}})^k t^{\beta k}}{k! \, k^{bk}}.$$

The same proof covers empty chains, with $X_0^{\epsilon,\delta} = 1$.

Step 3. We remove regularization and sum the full series. By Lemma 2.5.2, each smoothed factor converges in L^2. Products converge in L^1 by Cauchy–Schwarz; for fixed k the sum over splits is finite. The bound is uniform in ϵ, δ, so it passes to $A_k(t)$. Since $k! \le k^k$ and $b > 0$, we have $k! \, k^{bk} \ge (k!)^{b+1} = (k!)^q$, proving both inequalities in (B.1.5).

Finally, for $z \geq 0$ and $q \geq 1$,

$$\sum_{k\geq 0} \frac{z^k}{(k!)^q} = \sum_{k\geq 0} \left(\frac{z^{k/q}}{k!}\right)^q \leq \left(\sum_{k\geq 0} \frac{z^{k/q}}{k!}\right)^q = \exp(qz^{1/q}).$$

Apply this inequality with $z = 2ZK_{\mathrm{sp}}t^\beta$, adding the separately defined term $A_0 = 1$. Proposition 2.1.1 then gives (B.1.6). This proves Proposition B.1.2. □

B.1.3 Spectral bounds for $0 < \alpha \leq 1$ in all three dimensions

We now retain Hypothesis 1.2.1 with $d \in \{1, 2, 3\}$ and $0 < \alpha \leq 1$. The covariance is nonnegative and nonnegative definite as in Section 1.2; when it is a distribution, both these properties and its homogeneity are understood distributionally. Let μ be its positive Radon spectral measure in the convention $\gamma(x) = \int e^{i\xi\cdot x}\mu(\,\mathrm{d}\xi)$, and put $V = \mu(\{\xi : |\xi| \leq 1\})$. No isotropy or spectral density is assumed. Write G_h for the positive wave-kernel measure of mass h, and $G_{h,\eta} = p_\eta * G_h$ for $\eta > 0$; set $G_{h,0} = G_h$. The measure notation includes the sphere kernel in dimension three. The mixed-moment definition of $A_k(t)$ is now applied to the present d-dimensional solution.

Lean full

Lemma B.1.3 (Low-α convolution bound)**.** *Under the preceding assumptions with $0 < \alpha < 1$, for every $R, h > 0$,*

$$\mu(\{\xi : |\xi| \leq R\}) = VR^\alpha, \qquad \int_{\mathbb{R}^d} \min\{h, |\xi|^{-1}\}\mu(\,\mathrm{d}\xi) = \frac{V}{1-\alpha}h^{1-\alpha}. \tag{B.1.8}$$

For $\epsilon > 0$ and $\eta \geq 0$,

$$0 \leq \int_{\mathbb{R}^d} G_{h,\eta}(\,\mathrm{d}y)\gamma_\epsilon(y+z) \leq \frac{V}{1-\alpha}h^{1-\alpha}, \qquad z \in \mathbb{R}^d. \tag{B.1.9}$$

The estimate is uniform in both smoothing parameters and in z.

Proof. We compute the absolute Fourier envelope from spectral ball masses. We then use the finite Gaussian-weighted measure to justify Fourier integration and bound the translated convolution.

Step 1. We compute the homogeneous spectral envelope. The spectral measure of $\gamma(c\,\cdot)$ is the pushforward of μ under $\xi \mapsto c\xi$. Homogeneity and uniqueness of the Fourier transform on tempered distributions therefore give $\mu(A/c) = c^{-\alpha}\mu(A)$ for every Borel set A. Equivalently, $\mu(cA) = c^\alpha\mu(A)$. This proves the ball-mass formula. Since μ is Radon, $V < \infty$, and continuity from above gives $\mu(\{0\}) = \lim_{R\downarrow 0} VR^\alpha = 0$. By the layer-cake identity and Tonelli's theorem,

$$\int_{\mathbb{R}^d} \min\{h, |\xi|^{-1}\}\mu(\,\mathrm{d}\xi) = \int_0^h \mu(\{\xi : |\xi| \leq u^{-1}\})\,\mathrm{d}u = V\int_0^h u^{-\alpha}\,\mathrm{d}u.$$

The endpoint of each indicator has no effect on its u integral. Since $\alpha < 1$, the last expression is the finite quantity in (B.1.8). This computation uses ball masses, not a radial density for μ.

Step 2. We obtain the smoothed convolution bound. Gaussian weighting gives a finite measure, by the polynomial ball growth of μ. Thus, Fourier Fubini is justified for γ_ϵ and the finite measure $G_{h,\eta}$. From the source's wave-kernel formulas [17, (2.3)–(2.5), p. 7],

$$\widehat{G}_h(\xi) = \frac{\sin(h|\xi|)}{|\xi|}, \qquad G_h(\mathbb{R}^d) = h,$$

with value h in the Fourier formula at zero. The Fourier multipliers of p_ϵ and p_η have absolute value at most one, with the latter multiplier equal to one when $\eta = 0$. Consequently,

$$\left|\int G_{h,\eta}(\,\mathrm{d}y)\gamma_\epsilon(y+z)\right| \le \int_{\mathbb{R}^d} \frac{|\sin(h|\xi|)|}{|\xi|}\mu(\,\mathrm{d}\xi) \le \int_{\mathbb{R}^d} \min\{h, |\xi|^{-1}\}\mu(\,\mathrm{d}\xi).$$

Nonnegativity of γ as a distribution implies $\gamma_\epsilon \ge 0$, since Gaussian translates are nonnegative test functions; $G_{h,\eta}$ is also nonnegative. This proves the lower bound in (B.1.9). Combining the preceding displays proves its upper bound. No positivity of the oscillatory Fourier integrand is asserted. This proves Lemma B.1.3. □

Lean full

Lemma B.1.4 (Degree-one convolution bound)**.** *Under the preceding covariance assumptions with $\alpha = 1$, for every $h > 0$, $\epsilon > 0$, $\eta \ge 0$, and $z \in \mathbb{R}^d$,*

$$0 \le \int_{\mathbb{R}^d} G_{h,\eta}(\,\mathrm{d}y)\gamma_\epsilon(y+z) \le \frac{\pi V}{2}. \tag{B.1.10}$$

No isotropy or angular density is required.

Proof. We resolve the degree-one spectral measure into radial and angular parts. We retain the radial oscillation and evaluate it as a one-dimensional heat convolution, whose bound is uniform in direction.

Step 1. We obtain the polar spectral decomposition. Fourier uniqueness, applied to the distributional homogeneity as above, gives $\mu(cA) = c\mu(A)$ and $\mu(\{0\}) = 0$. Define a finite measure on the unit sphere by

$$\sigma(E) = \mu\{\xi : 0 < |\xi| \le 1,\ \xi/|\xi| \in E\}.$$

Its total mass is V. Homogeneity implies that the corresponding sector of radius R has mass $R\sigma(E)$. Subtracting two such sectors shows that a polar rectangle $(r_1, r_2] \times E$ has mass $(r_2 - r_1)\sigma(E)$. Uniqueness of measures on these generating rectangles therefore gives the polar decomposition $\mu(\,\mathrm{d}\xi) = \,\mathrm{d}r\,\sigma(\,\mathrm{d}\theta)$, $r > 0$, $\theta \in \mathbb{S}^{d-1}$. The real stationary covariance is even; Fourier uniqueness makes μ, and hence σ, even.

Step 2. We express the convolution through its radial oscillatory integral. Use the Brownian Gaussian convention, so the combined covariance and Green smoothing multiplier is e^{-ar^2} with $a = (\epsilon + \eta)/2 > 0$. Gaussian weighting makes the spectral measure finite. Fourier Fubini and evenness give

$$\begin{aligned} \int G_{h,\eta}(\,\mathrm{d}y)\gamma_\epsilon(y+z) &= \int_{\mathbb{S}^{d-1}} I_a(h, \theta\cdot z)\sigma(\,\mathrm{d}\theta), \\ I_a(h,v) &= \int_0^\infty e^{-ar^2}\frac{\sin(hr)}{r}\cos(rv)\,\mathrm{d}r. \end{aligned} \tag{B.1.11}$$

The radial integral is absolutely convergent: its integrand is bounded near zero and Gaussian-decaying at infinity. Passing from the complex exponential to cosine introduces no factor two, since both antipodal directions are already included in σ.

Step 3. We identify that integral with a bounded one-dimensional convolution. Let $g_h(v) = \frac{1}{2}\mathbf{1}_{\{|v|<h\}}$ and let $p^{(1)}_{2a}(v) = (4\pi a)^{-1/2}e^{-v^2/(4a)}$ be the one-dimensional Gaussian density. Their Fourier transforms are $\sin(hr)/r$ and e^{-ar^2}. The one-dimensional inversion factor is $1/(2\pi)$ in the source convention, so

$$(g_h * p^{(1)}_{2a})(v) = \frac{1}{2\pi}\int_{\mathbb{R}} e^{irv}e^{-ar^2}\frac{\sin(hr)}{r}\,\mathrm{d}r = \frac{1}{\pi}I_a(h,v).$$

The sign in the inversion exponential is immaterial because the integrand pairs evenly under $r \mapsto -r$. Since $p^{(1)}_{2a}$ has mass one and $0 \le g_h \le 1/2$, we obtain $0 \le I_a(h,v) \le \pi/2$. Integrating against σ, whose mass is V, proves (B.1.10). This retains the oscillation until the one-dimensional integral is evaluated; the divergent absolute Fourier envelope at $\alpha = 1$ is not used. This proves Lemma B.1.4. □

Lean partial

Proposition B.1.5 (Upper bound for $\alpha \le 1$)**.** *Suppose that Hypothesis 1.2.1 and the standing covariance positivity assumptions hold, $d \in \{1,2,3\}$, $0 < \alpha \le 1$, and $V > 0$. Define*

$$K^{\mathrm{gen}}_{\mathrm{sp}} = \begin{cases} \dfrac{V2^{2-\alpha}(1-\alpha)^{-\alpha}}{(2-\alpha)^{2-\alpha}}, & 0 < \alpha < 1, \\ \pi V, & \alpha = 1, \end{cases} \qquad C^{\mathrm{gen}}_{\mathrm{dir}} = q(2ZK^{\mathrm{gen}}_{\mathrm{sp}})^{1/q}. \tag{B.1.12}$$

With the same A_k, b, q, β, and Z as above, for $k \ge 1$ and $t > 0$,

$$A_k(t) \le \frac{(2ZK^{\mathrm{gen}}_{\mathrm{sp}})^k t^{\beta k}}{k!\,k^{bk}} \le \frac{(2ZK^{\mathrm{gen}}_{\mathrm{sp}})^k t^{\beta k}}{(k!)^q}, \qquad \mathbb{E}u^2(t,x) \le \exp(C^{\mathrm{gen}}_{\mathrm{dir}}t^{\kappa}). \tag{B.1.13}$$

Proof. We apply the descending-label spatial argument in every dimension using the appropriate closing bound. We then sum temporal pairings and pass the Green and noise limits in their prescribed order.

Step 1. We obtain a common spatial bound in each dimension. First smooth the noise as in [17, (2.9), (2.11), (2.23)–(2.24)]. In dimension three also use $G_{h,\eta}$ with $\eta > 0$, as in the source's pp. 13–14. The increment change of variables is now a triangular map on vectors in $\mathbb{R}^d$, still of determinant one. The descending-label proof of Lemma B.1.1 depends only on which increments enter each position, not on their dimension. Its invariant therefore remains valid: at a closing label there is exactly one covariance depending on that vector increment, and at an opening label its pair has already been removed. If $0 < \alpha < 1$, Lemma B.1.3 gives the closing bound $Mh_l^{1-\alpha}$ with $M = V/(1-\alpha)$. At $\alpha = 1$, Lemma B.1.4 gives the constant closing bound $M = \pi V/2$. Every opening gives mass

h_l, uniformly in η and all noise-smoothing parameters. For $\alpha < 1$, the same weighted arithmetic–geometric mean calculation gives

$$M^k \prod_{i \in O_D} h_i \prod_{j \in C_D} h_j^{1-\alpha} \le (K_{\mathrm{sp}}^{\mathrm{gen}})^k \frac{t^{bk}}{k^{bk}}.$$

At $\alpha = 1$, ordinary arithmetic–geometric mean on the k opening increments gives $M^k \prod_{i \in O_D} h_i \le (2M)^k t^k / k^k$, which is the same bound with $b = 1$ and $K_{\mathrm{sp}}^{\mathrm{gen}} = \pi V$. Both cases use $\sum_l h_l \le 2t$. For $d = 1, 2$ one may use the Green densities directly; their opening mass and closing convolution obey these same bounds.

Step 2. We sum the temporal factors. Replace the nonnegative truncated temporal factors by $|s_i - s_j|^{-\alpha_0}$ before taking their pairing sum. The temporal symmetry, cube integral and split count in (B.1.7) do not involve the spatial dimension. Thus, exactly the multiplication of counts in the proof of Proposition B.1.2 gives the first bound in (B.1.13) for the regularized moments.

Step 3. We remove regularizations and sum the coefficient bounds. We spell out the limit in dimension three. Fix every noise-smoothing parameter and first let $\eta \downarrow 0$. At each time vector, the Gaussian moment formula is a finite sum of bounded continuous products of the smoothed covariance functions, integrated against products of the finite Green measures. These products of measures converge weakly as $\eta \downarrow 0$, with the same masses $\prod_l h_l$. At fixed noise smoothing the Gaussian covariance factors are uniformly bounded, so a constant times $\prod_l h_l$ dominates on each bounded time simplex. Dominated convergence applies also to the covariance between two approximations with different η values. The resulting common joint covariance limit proves the L^2 Cauchy property of each fixed-order random integral. This is the inner limit used in the source's definition on pp. 13–14. Products of two factors converge in L^1 by Cauchy–Schwarz, so the moment inequality survives this limit. Next send the noise-smoothing parameters to zero using the fixed-order L^2 convergence of Lemma 2.5.2, and again pass products in L^1. In dimensions one and two only the latter limit is required. The bounds at both stages are uniform.

We have proved the first coefficient bound for $A_k(t)$. The factorial inequality and nonnegative-series argument in Proposition B.1.2 apply unchanged, with $K_{\mathrm{sp}}^{\mathrm{gen}}$ in place of K_{sp} and $A_0 = 1$. This proves Proposition B.1.5. □

Remark B.1.6 (Scope of the spectral estimates)**.** If $V = 0$, spectral homogeneity gives $\mu(B_R) = 0$ for every R, hence $\mu = 0$ and $u = 1$; the noise-free conclusion is immediate. Otherwise, all angular and dimensional dependence is allowed in V. For $0 < \alpha < 1$, the example $\gamma(x) = c|x_1|^{-\alpha}$ in dimensions two or three has its spectral measure supported on an axis; a full-dimensional density is not required. The absolute Fourier envelope diverges at $\alpha = 1$, where the separate oscillatory calculation in Lemma B.1.4 is essential. The endpoint is not obtained by taking a limit in $K_{\mathrm{sp}}^{\mathrm{gen}}$ for $\alpha < 1$. For $d = 1$ and $\gamma = c_\delta \delta_0$, the source convention gives $\mu(\mathrm{d}\xi) = c_\delta \, \mathrm{d}\xi/(2\pi)$ and $V = c_\delta/\pi$. Hence, the endpoint constant $K_{\mathrm{sp}}^{\mathrm{gen}} = \pi V = c_\delta$ agrees exactly with Proposition B.1.2, with no extra antipodal factor. In dimensions two and three the endpoint covers degree-one homogeneous covariance, not full spatial white noise. No result for $\alpha > 1$ follows from these estimates.

B.1.4 Checks on the scale, constants and scope

Lean partial

Corollary B.1.7 (First-moment calibration)**.** *Let K_* be K_{sp} under (B.1.1), or $K_{\mathrm{sp}}^{\mathrm{gen}}$ under the hypotheses of Proposition B.1.5. Put $C_{2,*} = q(2ZK_*)^{1/q}$. Then*

$$\mathbb{E}u(t,x) \le \exp(C_{1,*}t^{\kappa}), \qquad C_{1,*} = q\left(\frac{ZK_*}{2^{3-\alpha}}\right)^{1/q} = \frac{C_{2,*}}{2^{(4-\alpha)/(3-\alpha)}}. \tag{B.1.14}$$

In either nonzero case $2C_{1,*} < C_{2,*}$. Conditionally on a first-moment lower rate at least L_*, $2L_* \le 2C_{1,*} < C_{2,*}$, consistently with Proposition 1.4.4.

Proof. For one chain of length $2k$, the increments sum to at most t. The spatial estimate in Lemma B.1.1, or in the proof of Proposition B.1.5, therefore applies with $t/2$ in place of t. The temporal pairing sum on one ordered simplex is $P_k(Zt^{2-\alpha_0})^k/(2k)!$. Using the same regularization and limit order as in the respective upper-bound proof gives

$$\mathbb{E}X_{2k}(t,x) \le \frac{(ZK_*/2^{b+1})^k t^{\beta k}}{k!\,k^{bk}} \le \frac{(ZK_*/2^{3-\alpha})^k t^{\beta k}}{(k!)^q}.$$

Every odd term has zero expectation. The L^2 expansion permits taking expectations of partial sums, and the resulting nonnegative even series is summed by the scalar inequality in the proof of Proposition B.1.2. This gives (B.1.14). If the first-moment lower rate is at least L_*, (B.1.14) implies $L_* \le C_{1,*}$. In the stated nonzero cases $K_* > 0$, hence $C_{1,*} > 0$; and $(4-\alpha)/(3-\alpha) > 1$ gives $2C_{1,*} < C_{2,*}$. This proves Corollary B.1.7. □

Remark B.1.8 (Checks and comparison with the uniform pairing bound)**.** The argument preserves the factor $k^{-(2-\alpha)k}$ from the spatial increment maximum. Replacing the spatial volume merely by a constant times $t^{(2-\alpha)k}$ would lose the factorial power needed in (B.1.5). This proof does not use the common-Laplace-parameter norm majorant of Proposition 2.7.1, and it does not assert a stronger factorial estimate for every individual diagram. Instead, the temporal ordering is exploited after summing pairings in (B.1.7). Thus, the scoped G0 obstruction remains valid. For unit white covariance, the bound on the total-order-two coefficient is $2Z$, whereas the exact value from Lemma 2.2.1 is $2c_0$; their ratio is $2(3-\alpha_0) > 4$. At the static endpoint the exact order-four coefficient is $11/540$, while the first bound in (B.1.5) gives $1/2$. These are checks of normalization, not evidence of sharp constants.

No-go 06 quantifies the loss avoided here: discarding the spatial constraints before summation gives the wrong time exponent.

Remark B.1.9 (Boundary and literature comparisons)**.** As $\alpha_0 \downarrow 0$, the time exponent tends to $(4-\alpha)/(3-\alpha)$, the Chen–Hu static exponent cited in Remark A.1.5. This is an exponent calibration, not an interchange of the static and large-time limits. With the Riesz normalization $c_\alpha = (1-\alpha)/2$, the displayed K_{sp} tends to one as $\alpha \uparrow 1$, matching unit white covariance. For comparison only, the Skorohod upper bound of Balan–Conus [4, Theorem 2.1(b), (8), (10), p. 1492] has time exponent $(2H+2-a)/(3-a)$. Setting $H = 1-\alpha_0/2$ and $a = \alpha$ yields the same κ. Their covariance normalization

contains $H(2H-1)$ and they use a Skorohod mild solution. No constants or solutions are identified, and their theorem is not an input to the present proof. The current coverage of this section is $0 < \alpha \leq 1$ in $d = 1, 2, 3$, including the one-dimensional white case. It does not address $1 < \alpha < 2 - \alpha_0$ in dimensions two and three.

B.2 Higher spatial exponents under a convolution bound

The convolution assumption below is additional to homogeneity, and the concrete applications cover only the stated Riesz ranges. Section 3.3 establishes the full general upper scale by a separate argument. This alternative route is not an input to Theorem 11.2.6.

We retain the standing covariance assumptions and take $d \in \{2, 3\}$ and $1 < \alpha < 2-\alpha_0$. Put $\delta = \alpha - 1$, $q = 3 - \alpha$, and $\beta = 4 - \alpha - \alpha_0$. Here δ is an exponent, not a smoothing parameter. Write p_ϵ for the centered Gaussian density with covariance ϵI, $\gamma_\epsilon = p_\epsilon * \gamma$, and $G_{h,\eta} = p_\eta * G_h$, with $G_{h,0} = G_h$.

Hypothesis B.2.1 (Spatial maximum)**.** There is $M > 0$ such that, for every $h > 0$, $z \in \mathbb{R}^d$, $\epsilon > 0$, and $\eta \geq 0$,

$$0 \leq \int_{\mathbb{R}^d} G_{h,\eta}(\,\mathrm{d}y)\gamma_\epsilon(y + z) \leq Mh^{-\delta}. \tag{B.2.1}$$

The same M works for all translations and both Gaussian widths. In particular, each pairing edge may have its own positive covariance width and each Green factor its own nonnegative smoothing width.

This uniform maximum is an additional assumption, not a consequence of homogeneity. No-go 08 gives admissible covariances for which the translated wave convolution diverges.

Proposition B.2.2 (Conditional upper bound)**.** *Suppose that Hypotheses 1.2.1 and B.2.1 hold in the range specified above. Choose and fix*

$$\frac{1}{1-\alpha_0} < r < \frac{1}{\delta}, \qquad r' = \frac{r}{r-1}, \qquad \theta = \alpha_0 r', \qquad a = 1 - \frac{\delta r}{2}.$$

Define the explicit, nonsharp constants

$$Z_\theta = \frac{2}{(1-\theta)(2-\theta)}, \qquad D_a = e^2(e/a)^{2a}, \qquad K = 12M[\Gamma(1-\delta r)D_a]^{1/r} Z_\theta^{1/r'}. \tag{B.2.2}$$

For the total-order coefficients $A_k(t)$ of Section B.1,

$$A_k(t) \leq \frac{K^k t^{\beta k}}{(k!)^q} \quad (k \geq 1), \qquad \mathbb{E}u^2(t,x) \leq \exp\{qK^{1/q}t^\kappa\}. \tag{B.2.3}$$

These estimates hold for every $t > 0$ and $x \in \mathbb{R}^d$.

Proof. We retain the singular closing increments instead of replacing them by a spatial maximum. Hölder on the common pairing-time measure separates those increments from the temporal factors. Dirichlet and symmetry estimates then recover the required factorial power before the regularization limits.

Step 1. We verify parameters and perform the spatial elimination. The interval for r is nonempty because $\delta + \alpha_0 < 1$. Thus, $\delta r < 1$, $\theta < 1$, and $1/2 < a < 1$. We use the source's noise regularization from Chen [17, (2.9), (2.11), (2.23)–(2.24)], as in Section B.1. Its nonnegative temporal covariance is bounded by $|s_i - s_j|^{-\alpha_0}$, and its spatial covariance on an edge e is $\gamma_{\epsilon_e+\epsilon'_e}$, where $\epsilon_e, \epsilon'_e > 0$ are the two endpoint noise widths. Indeed, $p_{\epsilon_e} * p_{\epsilon'_e} = p_{\epsilon_e+\epsilon'_e}$; equal widths give the source's $\gamma_{2\epsilon}$. Every such positive covariance width is covered by Hypothesis B.2.1. In dimension three first smooth the Green measures as prescribed on pp. 13–14 of that source.

Fix $m + n = 2k$, $k \geq 1$, and put $\Omega_{m,n} = [0,t]^m_< \times [0,t]^n_<$. Use the two separate roots and increments $h_l = s_l - s_{p(l)}$ of Section B.1. For $D \in \Pi_k$, orient its pairs by increasing block label and denote their opening and closing sets by O_D, C_D. Descending integration of the vector increments gives

$$S_D(h) \leq M^k \prod_{i \in O_D} h_i \prod_{j \in C_D} h_j^{-\delta} \leq M^k (2t/k)^k H_D(h), \qquad H_D(h) = \prod_{j \in C_D} h_j^{-\delta}.$$

Indeed, before label l is integrated, the remaining covariances have closing labels at most l. At a closing label exactly its own pair depends on that increment, as $\gamma_\epsilon(y_l + z)$; all other endpoints have smaller labels. Hypothesis B.2.1 removes this factor. At an opening its pair is already removed and the integral is the Green mass h_l. This proves the invariant in every dimension and for empty chains. Tonelli applies by positivity. Finally, the k opening increments sum to at most $2t$, so ordinary arithmetic–geometric mean gives the second inequality. We have not applied the low-α conclusion of Lemma B.1.1.

Step 2. We separate the spatial gap powers and temporal pairing factors. Set $T_D(s) = \prod_{(i,j)\in D} |s_i - s_j|^{-\alpha_0}$. Hölder's inequality on counting measure on Π_k times Lebesgue measure on $\Omega_{m,n}$ gives

$$\sum_D \int_{\Omega_{m,n}} H_D T_D \, \mathrm{d}s \leq \left(\sum_D \int_{\Omega_{m,n}} H_D^r \, \mathrm{d}s \right)^{1/r} \left(\sum_D \int_{\Omega_{m,n}} T_D^{r'} \, \mathrm{d}s \right)^{1/r'}. \tag{B.2.4}$$

Both integrals are finite by the following computations. If the two chains contain k_1, k_2 closing labels, then $k_1 + k_2 = k$ and the simplex change to increments has determinant one. The Dirichlet integral, including the unused terminal gap with exponent zero, gives

$$\int_{\Omega_{m,n}} H_D^r \, \mathrm{d}s = \frac{\Gamma(1-\delta r)^k t^{(2-\delta r)k}}{\Gamma(1+m-\delta r k_1)\Gamma(1+n-\delta r k_2)}.$$

To see the normalization, in a chain of length m the k_1 closing increments have Dirichlet parameter $1 - \delta r$, the other increments have parameter one, and the terminal gap has parameter one. Scaling gives $t^{m-\delta r k_1}$. Iterating the beta integral gives the displayed Gamma quotient. Empty chains contribute $\Gamma(1) = 1$. The two denominator arguments

are positive and have average $1 + ak$. Log convexity of Γ therefore bounds their product below by $\Gamma(1 + ak)^2$. An elementary lower bound makes the constant explicit:

$$\Gamma(1 + ak) \geq \int_{ak}^{ak+1} x^{ak} e^{-x} \, \mathrm{d}x \geq e^{-1}(a/e)^{ak} k^{ak} \geq e^{-1}(a/e)^{ak}(k!)^a.$$

Since $k \geq 1$, its square is at least $D_a^{-k}(k!)^{2-\delta r}$. Writing $P_k = |\Pi_k|$, we obtain

$$\sum_D \int_{\Omega_{m,n}} H_D^r \, \mathrm{d}s \leq \frac{P_k[\Gamma(1 - \delta r) D_a]^k t^{(2-\delta r)k}}{(k!)^{2-\delta r}}.$$

The sum $\sum_D T_D^{r'}$ is symmetric in all $2k$ time labels, because a permutation bijects the pairings. On the full cube each pairing has integral $(Z_\theta t^{2-\theta})^k$. Therefore,

$$\sum_D \int_{\Omega_{m,n}} T_D^{r'} \, \mathrm{d}s = \frac{P_k (Z_\theta t^{2-\theta})^k}{m!n!} \leq \frac{P_k (Z_\theta t^{2-\theta})^k}{(k!)^2}.$$

Here $m!n! \geq (k!)^2$ since $m + n = 2k$. Symmetry is used only for the pairing sum, not for an individual diagram. Also, $P_k = \prod_{j=1}^k (2j - 1) \leq 2^k k!$ and $k^k \geq k!$. Combining these bounds with (B.2.4) and the opening estimate proves, uniformly in all regularization parameters,

$$\sum_D \int_{\Omega_{m,n}} S_D T_D \, \mathrm{d}s \leq \frac{\{4M[\Gamma(1 - \delta r) D_a]^{1/r} Z_\theta^{1/r'}\}^k t^{\beta k}}{(k!)^q}.$$

Indeed, the time power is $1 + (2 - \delta r)/r + (2 - \theta)/r' = 3 - \delta - \alpha_0 = \beta$; the factorial power is $1 + (2 - \delta r)/r + 2/r' - 1 = 2 - \delta = q$. There are $2k + 1 \leq 3^k$ splits, giving the asserted K.

Step 3. We pass the fixed-order limits. We now pass to the solution using the independent fixed-order construction in Lemma 2.5.2, which applies under Hypothesis 1.2.1. In dimension three, fix the noise smoothing first and send the Green smoothing to zero. Smoothed spatial covariances are bounded and continuous. Products of the finite Green measures converge weakly, with masses $\prod_l h_l$. At fixed noise smoothing all covariance factors are bounded, so a constant times $\prod_l h_l$ dominates the time integrals on bounded simplexes. The same argument for mixed Green approximations gives a common joint covariance limit, and hence the fixed-order L^2 Cauchy property. This is the inner limit of the source's pp. 13–14, detailed in Proposition B.1.5. Next remove the noise smoothing using Lemma 2.5.2's fixed-order L^2 convergence. In dimension two only this latter limit is needed. At each stage products converge in L^1, since

$$\|YZ - Y'Z'\|_1 \leq \|Y - Y'\|_2 \|Z\|_2 + \|Y'\|_2 \|Z - Z'\|_2.$$

Each split sum is finite and the bound is uniform. Thus, it passes to $A_k(t)$; zero chains remain the constant one. These convergence inputs use the standing assumptions, not $\alpha \leq 1$.

Step 4. We sum the full coefficient series. Finally, Proposition 2.1.1 supplies the nonnegative full series under these same hypotheses. Since $q > 1$, for $z \geq 0$,

$$\sum_{k\geq 0} \frac{z^k}{(k!)^q} = \sum_{k\geq 0} \left(\frac{z^{k/q}}{k!}\right)^q \leq \left(\sum_{k\geq 0} \frac{z^{k/q}}{k!}\right)^q = e^{qz^{1/q}}.$$

Take $z = Kt^\beta$ and use $A_0 = 1$ and $\beta/q = \kappa$. This proves Proposition B.2.2. □

Lean full

Lemma B.2.3 (Riesz spatial maxima)**.** *Let $\gamma(x) = c|x|^{-\alpha}$, $c > 0$. In dimension three, for $1 < \alpha < 2$, Hypothesis B.2.1 holds with the optimal uniform constant $M_3 = c2^{1-\alpha}/(2-\alpha)$. In dimension two, for $1 < \alpha < 3/2$, it holds with*

$$M_2 = c\left\{4^\alpha + \frac{2\alpha}{3/2-\alpha} 4^{\alpha-3/2}\right\}.$$

Proof. We compute the spherical maximum in dimension three and bound small translated ball masses in dimension two. Gaussian averaging preserves those bounds, and an approximate-identity limit proves the stated optimality in dimension three.

Step 1. We evaluate the three-dimensional spherical convolution. From Chen [17, (2.5), p. 7], the wave measures are

$$G_h^{(2)}(\,\mathrm{d}y) = \frac{\mathbf{1}_{\{|y|<h\}}\,\mathrm{d}y}{2\pi\sqrt{h^2-|y|^2}}, \qquad G_h^{(3)}(\,\mathrm{d}y) = \frac{\sigma_h(\,\mathrm{d}y)}{4\pi h},$$

where σ_h is surface measure on the sphere of radius h. Both have mass h and satisfy $G_h(hA) = hG_1(A)$. Thus, the unsmoothed convolution is $ch^{1-\alpha}F_d(z/h)$, where $F_d(w) = \int G_1^{(d)}(\,\mathrm{d}y)|y+w|^{-\alpha}$. In dimension three spherical coordinates give, for $\rho = |w| > 0$,

$$F_3(w) = \frac{(1+\rho)^v - |1-\rho|^v}{2v\rho}, \qquad v = 2-\alpha \in (0,1).$$

For $0 < \rho < 1$ this is the average of the convex function $f(s) = (1+s)^{v-1}$ on $[-\rho,\rho]$. Its derivative has numerator $\rho[f(\rho)+f(-\rho)] - \int_{-\rho}^{\rho} f(s)\,\mathrm{d}s \geq 0$, by the endpoint chord bound for a convex function. For $\rho > 1$, every distance $\sqrt{1+\rho^2+2\rho u}$, $-1 \leq u \leq 1$, increases with ρ, so its negative power decreases. The formula is continuous at $\rho = 1$ and at zero. Its maximum is therefore $F_3(e_1) = 2^{1-\alpha}/(2-\alpha)$.

Step 2. We bound the planar convolution by local ball masses. In dimension two we claim $G_1(B(w,R)) \leq 2R^{3/2}$ for $0 < R \leq 1/4$. Rotate $w = (A,0)$, $A \geq 0$. If $A < 1/2$, the ball lies in $|y| < 3/4$, where the density is at most $2/(\pi\sqrt{7})$; its mass is at most $2R^2/\sqrt{7}$. If $A \geq 1/2$, write $y = (x,v)$. On the ball $|v| \leq R$ and $x \geq 1/4$. Put $L = \sqrt{1-v^2}$. Inside the disk, $1-|y|^2 = (L-x)(L+x)$ with $L+x > 1$. Each horizontal slice has length at most $2R$, so integrating $(L-x)^{-1/2}$ gives at most $2\sqrt{2R}$. The v range has length at most $2R$, giving mass at most $(2\sqrt{2}/\pi)R^{3/2} \leq 2R^{3/2}$, as claimed. Layer cake now gives

$$F_2(w) \leq 4^\alpha + \alpha\int_0^{1/4} R^{-\alpha-1}G_1(B(-w,R))\,\mathrm{d}R \leq M_2/c.$$

This includes centers outside the disk and is uniform in w.

Step 3. We retain smoothing uniformity and prove the optimality claim. Finally, Tonelli and the Gaussian convolution rule give

$$\int G_{h,\eta}(\,\mathrm{d}y)\gamma_\epsilon(y+z) = \int p_{\epsilon+\eta}(w)(G_h * \gamma)(z-w)\,\mathrm{d}w.$$

Mass-one averaging preserves both supremum bounds, for all widths in Hypothesis B.2.1. We justify the approximate identity used for optimality. For $f(x) = |x|^{-\lambda}$ in $\mathbb{R}^j$, $0 < \lambda < j$, fix $x \neq 0$. In the convolution $\int p_\epsilon(x-y)f(y)\,\mathrm{d}y$, a small neighborhood of x gives convergence by continuity. On $|y| < |x|/2$ the integral is bounded by a constant times $\epsilon^{-j/2}e^{-|x|^2/(8\epsilon)}$, since f is integrable on that ball. On the remaining region outside the neighborhood of x, f is bounded and the Gaussian tail tends to zero. Thus, $p_\epsilon * f(x) \to f(x)$ for every $x \neq 0$. In dimension three Fatou's lemma at a maximizing shift as $\epsilon \downarrow 0$, $\eta = 0$, now recovers the unsmoothed value; the single singular point has zero sphere measure. Hence, no smaller uniform constant is possible. This proves Lemma B.2.3. □

Corollary B.2.4 (Riesz moment bounds)**.** *For isotropic Riesz covariance $c|x|^{-\alpha}$, the bounds in* (B.2.3) *hold in dimension three for $1 < \alpha < 2 - \alpha_0$, and in dimension two for $1 < \alpha < \min\{3/2, 2-\alpha_0\}$, with $M = M_d$ in* (B.2.2)*.*

Proof. These Riesz functions are nonnegative, homogeneous of degree $-\alpha$, locally integrable since $\alpha < d$, and nonnegative definite. For the last property, the identity

$$|x|^{-\alpha} = \frac{1}{\Gamma(\alpha/2)} \int_0^\infty s^{\alpha/2-1} e^{-s|x|^2}\,\mathrm{d}s$$

represents the covariance as a positive mixture of positive definite Gaussians. To justify this distributionally, take a complex Schwartz function φ, put $\widetilde{\varphi}(x) = \overline{\varphi(-x)}$, and set $\psi = \varphi * \widetilde{\varphi}$. This is Schwartz and $\int |x|^{-\alpha}|\psi(x)|\,\mathrm{d}x < \infty$: local integrability controls the origin and rapid decay controls infinity. Tonelli applied with $|\psi|$ therefore proves absolute integrability of the mixture against ψ, so Fubini applies. Each Gaussian has nonnegative integral against ψ, as follows from its positive Fourier transform and the factor $|\widehat{\varphi}|^2$. The mixture consequently has nonnegative integral against ψ. This proves nonnegative definiteness as a tempered distribution. The stated ranges satisfy $\alpha + \alpha_0 < 2$, and Lemma B.2.3 supplies the additional spatial hypothesis with all Gaussian uniformities. Proposition B.2.2 applies. This proves Corollary B.2.4. □

Another possible reduction would merge two neighboring wave kernels. No-go 10 explains why an unweighted convolution estimate cannot simply discard the covariance linking a merged vertex to its remote partner in a crossing diagram.

Proposition B.2.5 (Obstructions to the spatial hypothesis)**.** *In dimension two, Riesz covariance with $3/2 \le \alpha < 2$ fails Hypothesis B.2.1. For every $1 < \alpha < 2$ there are nonnegative, nonnegative definite homogeneous locally integrable covariance functions in both dimensions two and three that fail it.*

Proof. We exhibit a divergent planar Riesz convolution at the boundary, then construct an anisotropic product covariance with the same obstruction in both dimensions. Approximate-identity limits transfer these divergences to the smoothed uniform-bound question.

Step 1. We identify the divergent boundary configurations. For the first claim set $h = 1$, $z = -e_1$, and $y = e_1 + \rho(\cos\phi, \sin\phi)$. On the wedge $0 < \rho < 1/2$, $2\pi/3 \le \phi \le 4\pi/3$, we have $0 < 1 - |y|^2 \le 2\rho$. Therefore,

$$\int G_1^{(2)}(\,\mathrm{d}y)c|y - e_1|^{-\alpha} \ge \frac{c}{3\sqrt{2}} \int_0^{1/2} \rho^{1/2-\alpha}\,\mathrm{d}\rho = \infty.$$

This includes logarithmic divergence at $\alpha = 3/2$. For the second claim choose $a_1 = (1 + \max\{2 - \alpha, \alpha - 1\})/2$ and $a_2 = \alpha - a_1$. Then $0 < a_1, a_2 < 1$ and $a_1 + a_2/2 > 1$. The function $\gamma(x) = c|x_1|^{-a_1}|x_2|^{-a_2}$, independent of x_3 in dimension three, is locally integrable, tempered, and homogeneous of degree $-\alpha$. The Gaussian mixture identity in the preceding proof applied separately to each coordinate shows nonnegative definiteness; products of these Gaussians and the constant function in the third coordinate are positive definite. More explicitly, for the Schwartz autocorrelation ψ used in the preceding proof, choose $N > 1$ and bound $|\psi(x)| \le C_N \prod_{j=1}^d (1 + |x_j|)^{-N}$. Then $\int \gamma(x)|\psi(x)|\,\mathrm{d}x < \infty$, by the product of one-dimensional integrals and $a_1, a_2 < 1$. Tonelli with $|\psi|$ and then Fubini justify the two Gaussian-mixture integrals against ψ. Their integrands are nonnegative quadratic forms, proving the assertion also for the covariance independent of x_3. With $u = 1 - y_1$ and then $y_2 = \sqrt{2u - u^2}\,w$, Tonelli gives

$$\int G_1^{(2)}(\,\mathrm{d}y)\gamma(y - e_1) = \frac{cB((1 - a_2)/2, 1/2)}{2\pi} \int_0^2 u^{-a_1}(2u - u^2)^{-a_2/2}\,\mathrm{d}u = \infty.$$

Step 2. We transfer the product example to dimension three and remove smoothing. The beta factor is finite and the integral diverges at zero. The projection of $G_1^{(3)}$ onto its first two coordinates is $G_1^{(2)}$: the two sphere graphs each have surface Jacobian $(1 - |y|^2)^{-1/2}$, divided by 4π. Hence, the same divergence holds in dimension three. For radial Riesz covariance, the approximate-identity argument in Lemma B.2.3 applies. For the product covariance, Gaussian factorization and Tonelli give

$$(p_\epsilon * \gamma)(x) = c \prod_{j=1}^2 (p_\epsilon^{(1)} * |\cdot|^{-a_j})(x_j).$$

In dimension three the third coordinate integrates to one. Each factor converges when $x_j \neq 0$ by the same argument with dimension one and exponent $a_j < 1$. This does not require the product kernel to be bounded at infinity; it is unbounded along its singular axes. The singular sets have zero shifted Green measure in both dimensions. Fatou with $\eta = 0$ implies that the smoothed convolution tends to infinity in lower limit as $\epsilon \downarrow 0$. Even if both widths must be positive, take $\eta = \epsilon$ and use their sum in the Gaussian identity above. Thus, no uniform M exists. This proves Proposition B.2.5. □

Remark B.2.6 (Calibrations and scope)**.** The printed first-moment statement and unconditional comparison are Theorem 1.4.1 and Proposition 1.4.4. Under the additional spatial hypothesis, Cauchy–Schwarz and Proposition B.2.2 give $\mathbb{E}u(t,x) \le \exp\{qK^{1/q}t^{\kappa}/2\}$, and hence $2L_* \le qK^{1/q}$ if the intended first-moment lower bound holds. No sharp first- or second-moment constant is identified. As $\alpha_0 \downarrow 0$, the exponent tends to $(4-\alpha)/(3-\alpha)$, consistently with the Chen–Hu static calibration in Remark B.1.9; no interchange of limits is claimed. For the Riesz cases here, the Skorohod comparison of Balan–Conus [4, Theorem 2.1(b), p. 1492; p. 1490] applies with $a = \alpha < d$, $\alpha < 2$, and $H = 1 - \alpha_0/2 > 1/2$. Its exponent $(2H+2-a)/(3-a)$ is κ. This comparison is restricted to those Riesz cases, with a different solution concept and covariance normalization; it is not an input here, and no equality with the Balan–Chen–Wang second-moment asymptotics is inferred. The obstructions above concern only the spatial supremum, not existence, moment finiteness, or failure of the target time scale. In particular, arbitrary homogeneous covariances remain outside this conditional argument, even when $\alpha + \alpha_0 < 2$.

B.3 Riesz bounds by interpolation with static noise

This alternative argument concerns isotropic Riesz covariance in dimensions two and three. It does not use the preceding conditional proposition, settle general anisotropic covariance, or identify the sharp constant. The full upper and intrinsic formula use separate arguments.

We use the static Stratonovich model of Chen–Hu as one input and the space-degree-one estimate of Section B.1 as the other. The static source allows nonnegative generalized covariances, not only Riesz functions: see its standing assumptions (1.2)–(1.3), p. 2145, and its explicit generalized-covariance convention (2.18), p. 2152, in [20]. In the latter convention every covariance factor is heat regularized before its defining limit. A nonnegative, even, positive-definite tempered Radon measure is such a generalized covariance. In each application below we separately verify its homogeneity range and static Dalang condition before using the source's quantitative coefficient estimates (5.1) and (5.15). Positive definiteness of a weighted endpoint is proved in Lemma C.1.1, or is an explicit assumption in Hypothesis C.2.2; weighting a measure alone is not being used to assert that property. Chen's variational finiteness theorem supplies only finiteness of the static constant, not a coefficient-rate theorem.

For $d \in \{2,3\}$, $c > 0$, and $0 < \lambda < \min\{2,d\}$, write

$$\gamma_\lambda(x) = c|x|^{-\lambda}, \qquad \gamma_{\lambda,\epsilon} = p_\epsilon * \gamma_\lambda.$$

All these covariances use the same amplitude c and Gaussian convention. They are nonnegative, locally integrable, and homogeneous. Their nonnegative definiteness follows from

$$\gamma_\lambda(x) = \frac{c}{\Gamma(\lambda/2)} \int_0^\infty s^{\lambda/2-1} e^{-s|x|^2}\, \mathrm{d}s.$$

Indeed, each Gaussian is positive definite. For a Schwartz autocorrelation ψ, the integral $\int |x|^{-\lambda}|\psi(x)|\,\mathrm{d}x$ is finite by $\lambda < d$ and rapid decay. Tonelli with $|\psi|$, followed by Fubini,

therefore justifies the positive Gaussian mixture as a tempered distribution. The source hypotheses for the Riesz covariances below are thus satisfied.

Lemma B.3.1 (Static coefficient input)**.** *Let $U_n(t,x)$ be the ordered Stratonovich integrals for static Gaussian noise with covariance γ_χ, where $d \in \{2,3\}$ and $1 < \chi < 2$. Put $U_0 = 1$ and*

$$B_k(t) = \sum_{m=0}^{2k} \mathbb{E}[U_m(t,x)U_{2k-m}(t,x)].$$

Then $B_0 = 1$, and there is a finite constant $C_{\mathrm{st}} = C_{\mathrm{st}}(\chi, c, d) > 0$ such that

$$0 \le B_k(t) \le \frac{C_{\mathrm{st}}^k t^{(4-\chi)k}}{(k!)^{3-\chi}}, \qquad k \ge 1, \quad t > 0. \tag{B.3.1}$$

Proof. We identify the full static coefficient sum using the imported fixed-order inputs. The imported upper coefficient rate controls all sufficiently large orders; the finitely many remaining orders are absorbed into one constant.

Step 1. We verify the static input and pairing interpretation. The static solution has data $(1,0)$ and wave operator Δ, as here. The degree satisfies $\chi < \min\{2,d\}$, so the Riesz covariance meets the source's Dalang condition. From Chen–Hu [20, Theorem 3.8(i), p. 2165], the fixed-order integrals exist in L^2. Their product rule and Wick expectation formula in that source's (2.17) and (2.19), pp. 2151–2152, identify B_k with the complete nonnegative sum over the $2k+1$ splits and every pairing of the $2k$ vertices. In particular, it includes within-chain pairs; no orthogonality of different orders is asserted. Empty chains contribute the factor one.

Step 2. We convert the upper coefficient rate into an all-order bound. From [20, (5.1), p. 2173, and (5.15), p. 2180], specialized to $p = 2$, we have

$$B_k(t) = t^{(4-\chi)k} B_k(1), \qquad \limsup_{k\to\infty} \frac{1}{k} \log\left((k!)^{3-\chi} B_k(1)\right) < \infty.$$

Only the finite upper coefficient rate from the latter formula is used. Choose $R > 0$ larger than this upper limit. For some $k_0 \ge 1$, $(k!)^{3-\chi} B_k(1) \le e^{Rk}$ for all $k \ge k_0$. Each of the remaining coefficients is finite by the fixed-order L^2 property. Increase e^R, if necessary, to a finite positive C_{st} that also dominates $((k!)^{3-\chi} B_k(1))^{1/k}$ for $1 \le k < k_0$. Homogeneity gives (B.3.1). The source results are imported inputs; this finite-order enlargement is the only deduction about their constant needed here. This proves Lemma B.3.1. □

Proposition B.3.2 (Interpolation bound for Riesz covariance)**.** *Suppose that $d \in \{2,3\}$, $c > 0$, $0 < \alpha_0 < 1$, and $1 < \alpha < 2 - \alpha_0$. Let the spatial covariance be $\gamma_\alpha(x) = c|x|^{-\alpha}$, and let $A_k(t)$ denote the full total-order-$2k$ coefficient of the second moment, as in Proposition 2.1.1. Choose and fix*

$$\alpha_0 < \vartheta < 2 - \alpha, \qquad b_0 = \frac{\alpha_0}{\vartheta}, \qquad \chi = \frac{\alpha - \vartheta}{1 - \vartheta}. \tag{B.3.2}$$

Let V_1 be the spectral mass of the unit ball for γ_1, in the convention of Lemma B.1.4, and define

$$Z_{b_0} = \frac{2}{(1-b_0)(2-b_0)}, \qquad C_{\mathrm{low}} = 2Z_{b_0}\pi V_1, \qquad C = C_{\mathrm{low}}^{\vartheta} C_{\mathrm{st}}^{1-\vartheta}, \qquad q = 3-\alpha,$$

where C_{st} is supplied by Lemma B.3.1 for the displayed χ. Then, for every $k \geq 1$, $t > 0$, and $x \in \mathbb{R}^d$,

$$A_k(t) \leq \frac{C^k t^{(4-\alpha-\alpha_0)k}}{(k!)^{3-\alpha}}, \qquad \mathbb{E}u^2(t,x) \leq \exp\left(qC^{1/q}t^{\kappa}\right). \tag{B.3.3}$$

The finite constants may depend on α, α_0, c, d and the fixed choice of ϑ, but not on k, t, x.

Proof. We interpolate the regularized covariance factors on one common positive measure containing all pairings and splits. We bound the low endpoint directly, pass fixed-order limits for the target and static endpoint, and only then use the static coefficient estimate.

Step 1. We verify the endpoint parameters. The interval for ϑ is nonempty by $\alpha + \alpha_0 < 2$. Since $\alpha > 1$, we have $0 < \vartheta < 1$, $0 < b_0 < 1$, and

$$\chi - 1 = \frac{\alpha - 1}{1-\vartheta} > 0, \qquad 2 - \chi = \frac{2-\alpha-\vartheta}{1-\vartheta} > 0.$$

Thus, both endpoint covariances are admissible in dimensions two and three. Moreover,

$$\alpha = \vartheta + (1-\vartheta)\chi, \qquad \alpha_0 = \vartheta b_0. \tag{B.3.4}$$

Step 2. We place all three covariance profiles on the same measure. Fix $k \geq 1$ and $t > 0$. Use a common spatial noise width $\epsilon > 0$ and the target's temporal cutoff width $\delta > 0$. The covariance on each pairing edge has spatial width 2ϵ. In dimension three first use $G_{h,\eta} = p_\eta * G_h$ with $\eta > 0$; in dimension two take $\eta = 0$. For each split $m + n = 2k$ and pairing $D \in \Pi_k$, use the two separate roots, increments $h_l = s_l - s_{p(l)}$, and positions x_l of Section B.1. Define a common positive measure $\nu_{k,t,\eta}$ by

$$\int \Phi \, \mathrm{d}\nu_{k,t,\eta} := \sum_{m=0}^{2k} \sum_{D \in \Pi_k} \int_{[0,t]^m_< \times [0,t]^{2k-m}_<} \mathrm{d}s \int \Phi(m, D, s, y) \prod_{l=1}^{2k} G_{h_l,\eta}(\,\mathrm{d}y_l).$$

Here y_l are vector increments and each x_l is their cumulative sum within its own chain. Empty blocks have empty products and their own root conventions. This measure is finite: the spatial mass at fixed times is $\prod_l h_l$, the time domains are bounded, and both discrete sums are finite. It is the same measure for all three covariance profiles.

For $\lambda \in \{1, \alpha, \chi\}$ and $b > 0$, put

$$H_\lambda = \prod_{(i,j)\in D} \gamma_{\lambda,2\epsilon}(x_i - x_j), \qquad T_b = \prod_{(i,j)\in D} |s_i - s_j|^{-b}.$$

The pointwise identity $\gamma_\alpha = \gamma_1^{\vartheta}\gamma_\chi^{1-\vartheta}$ retains the amplitude c, since $c^{\vartheta}c^{1-\vartheta} = c$. Hölder's inequality on the Gaussian probability measure gives

$$\gamma_{\alpha,2\epsilon}(z) \leq \gamma_{1,2\epsilon}(z)^{\vartheta}\gamma_{\chi,2\epsilon}(z)^{1-\vartheta}, \qquad z \in \mathbb{R}^d.$$

These convolutions are finite because the degrees are below d. Let Q_δ denote the product of the target's truncated temporal covariances. From the regularization in Chen [17, (2.9), (2.11)],

$$0 \le Q_\delta \le T_{\alpha_0} = T_{b_0}^{\vartheta}.$$

This uses only domination by the original temporal power; no interpolation property of distinct temporal cutoffs is required.

Let $A_k^{\epsilon,\delta,\eta}(t) = \int Q_\delta H_\alpha \, \mathrm{d}\nu_{k,t,\eta}$ be the target regularized coefficient. The Gaussian moment formula and the separate chain reversals in Proposition 2.1.1 identify it with the finite sum of regularized mixed moments. Also set

$$L_k^{\epsilon,\eta}(t) = \int T_{b_0} H_1 \, \mathrm{d}\nu_{k,t,\eta}, \qquad B_k^{\epsilon,\eta}(t) = \int H_\chi \, \mathrm{d}\nu_{k,t,\eta}.$$

The second expression is the regularized static coefficient, by the Gaussian moment formula with all pairings and splits. The first is a deterministic integral with original temporal covariance. We do not identify it with a stochastic integral having mixed regularizations. Hölder's inequality on the full measure, including its two discrete variables, yields

$$A_k^{\epsilon,\delta,\eta}(t) \le \left(L_k^{\epsilon,\eta}(t)\right)^{\vartheta} \left(B_k^{\epsilon,\eta}(t)\right)^{1-\vartheta}. \tag{B.3.5}$$

Step 3. We bound the low endpoint before passing limits. The deterministic estimates in the proof of Proposition B.1.5, at spatial degree one and temporal degree b_0, apply to $L_k^{\epsilon,\eta}$. In detail, Lemma B.1.4 gives the closing bound $\pi V_1/2$, uniformly in both smoothing widths. Descending integration and the opening arithmetic–geometric mean give the common spatial bound $(\pi V_1)^k t^k / k^k$. The temporal pairing sum is symmetric on the full time cube. Its integral, after summing every split as in (B.1.7), is $2^k (Z_{b_0} t^{2-b_0})^k / k!$. Hence,

$$L_k^{\epsilon,\eta}(t) \le \frac{C_{\mathrm{low}}^k t^{(3-b_0)k}}{k!\, k^k} \le \frac{C_{\mathrm{low}}^k t^{(3-b_0)k}}{(k!)^2}. \tag{B.3.6}$$

The original temporal integral is finite since $b_0 < 1$. The static regularized coefficient is finite because its covariance is bounded at fixed ϵ. Thus, the Hölder step has finite right side.

Step 4. We remove Green and noise regularization in order. We pass to fixed-order limits before using the static coefficient bound. In dimension three fix ϵ, δ and let $\eta \downarrow 0$. The target and static smoothed covariance factors are bounded continuous functions of the spatial positions. Products of the finite Green measures converge weakly with masses $\prod_l h_l$. A constant times this product dominates each time integrand at fixed noise smoothing, so dominated convergence applies on the bounded time simplexes. The same argument with two Green widths gives a common mixed covariance limit, and hence fixed-order L^2 convergence. This identifies the static limit with the measure convention of Chen–Hu [20, (2.22), pp. 2152–2153]. The target uses the corresponding inner limit in Chen [17, pp. 13–14]. We need no limit identification for $L_k^{\epsilon,\eta}$: its uniform upper bound in (B.3.6) suffices.

Next let the noise-smoothing parameters tend to zero. From Chen–Hu [20, Theorem 3.8(i), p. 2165], each fixed static order converges in L^2 to U_n. For the target, the fixed-order L^2 convergence follows from Lemma 2.5.2. If Y, Y', Z, Z' are the corresponding approximations and limits, then

$$\|YZ - Y'Z'\|_1 \le \|Y - Y'\|_2 \|Z\|_2 + \|Y'\|_2 \|Z - Z'\|_2.$$

Therefore, every fixed split product converges in L^1. The finite sums over the $2k+1$ splits converge as well; a zero-order factor stays equal to one. This argument applies directly in dimension two, where no Green smoothing is needed. Passing to these limits in (B.3.5), using (B.3.6), gives

$$A_k(t) \le \left(\frac{C_{\mathrm{low}}^k t^{(3-b_0)k}}{(k!)^2} \right)^{\vartheta} B_k(t)^{1-\vartheta}.$$

Only now apply Lemma B.3.1. No monotonicity in ϵ and no uniform static large-time bound in that parameter have been assumed.

Step 5. We combine the endpoint powers and sum. The powers combine without a counting loss. Indeed, by (B.3.4),

$$\begin{aligned} 2\vartheta + (1-\vartheta)(3-\chi) &= 3 - \alpha, \\ \vartheta(3-b_0) + (1-\vartheta)(4-\chi) &= 4 - \alpha - \alpha_0. \end{aligned}$$

This proves the coefficient bound in (B.3.3). The constant term is $A_0 = 1$. Since $q = 3 - \alpha > 1$, the scalar inequality $\sum_{k \ge 0} z^k/(k!)^q \le e^{qz^{1/q}}$ proved in Proposition B.1.2 applies with $z = Ct^{4-\alpha-\alpha_0}$. Proposition 2.1.1 identifies the nonnegative full coefficient series with $\mathbb{E}u^2(t,x)$. Here $(4-\alpha-\alpha_0)/q = \kappa$. This proves Proposition B.3.2. □

Remark B.3.3 (Calibrations and remaining scope)**.** The time exponent in (B.3.3) tends to $(4-\alpha)/(3-\alpha)$ as $\alpha_0 \downarrow 0$, in agreement with the Chen–Hu static exponent. This does not interchange the static and large-time limits or assert uniformity of the constants. Cauchy–Schwarz gives $\mathbb{E}u(t,x) \le \exp(qC^{1/q}t^{\kappa}/2)$. If the first-moment lower rate is at least L_*, this upper bound implies $2L_* \le qC^{1/q}$. Thus, the first-moment and Jensen calibrations are retained, without identifying a sharp constant. The Skorohod comparison remains only the comparison recorded in Remark B.2.6; its exponent agrees, but its solution concept and covariance normalization differ. No Skorohod estimate is used in this proof. The argument covers isotropic Riesz covariance throughout the stated higher-degree range in dimensions two and three, including the previously uncovered two-dimensional interval $3/2 \le \alpha < 2 - \alpha_0$. This argument does not cover arbitrary homogeneous covariances: anisotropic profiles need not factor into the admissible endpoints. The intrinsic second-moment formula is given separately in Theorem 11.2.6. No novelty is asserted here.

Appendix C

Covariance comparisons in higher dimensions

Suppose a bound is known for simple covariances, such as products of one-dimensional ones. Can it be carried over to a general homogeneous covariance in dimension two or three? Sometimes. A pointwise factorization is not enough: each factor must itself be a covariance, and the comparison must keep the amplitudes and the scaling. This matters most for measure-valued and anisotropic covariances. This appendix has no figure.

We keep Hypothesis 1.2.1 and the mixed pairing formula of Chapter 2. Section C.1 builds planar endpoints and proves the transfer (Proposition C.1.3). Section C.2 gives product constructions in dimension three and a conditional transfer (Proposition C.2.5). It does not claim a factorization for every three-dimensional covariance. Section C.3 identifies the physical and spectral forms of the spatial energy for measure covariances; this identity does not remove the assumptions of the transfers.

The upper bound of Chapter 3 and the constant of Chapter 11 do not rely on these comparisons. On a first reading, the two transfer statements are enough. Episode ▶ 9 of the video series covers this appendix.

C.1 General homogeneous covariance in dimension two

This section gives planar endpoint constructions and a transfer under its stated hypotheses. It does not use the preceding Riesz interpolation argument as an input. The full upper and intrinsic formula use separate methods.

Throughout this section $d = 2$. Write Γ for the spatial covariance as a nonnegative, even, positive-definite tempered Radon measure. For a locally integrable covariance function, this means $\Gamma(\mathrm{d}x) = \gamma(x)\,\mathrm{d}x$. The measure interpretation uses the Gaussian approximation framework of Chen [17, pp. 2–3, 13] and Chen–Hu [20, pp. 2145–2147, 2151–2153]. All products of covariance factors below are taken after Gaussian smoothing; no product or fractional power of distributions is used. Homogeneity means

$$\Gamma(rA) = r^{2-\alpha}\Gamma(A), \qquad r > 0, \tag{C.1.1}$$

for Borel sets A. This is equivalent to the covariance homogeneity in Hypothesis 1.2.1. If $\Gamma = 0$, the noise vanishes and $u = 1$. We first treat $\Gamma \neq 0$ and $1 < \alpha < 2$.

Lemma C.1.1 (Planar endpoint covariances)**.** *Suppose that Γ satisfies the preceding assumptions, and let $\alpha < \chi < 2$. Define the finite angular measure*

$$\sigma(E) = (2-\alpha)\Gamma\{x : 0 < |x| \le 1,\ x/|x| \in E\}, \qquad S = \sigma(\mathbb{S}^1).$$

On $\mathbb{R}^2 \setminus \{0\}$ define the weighted measures

$$\Gamma_{\mathrm{low}}(\,\mathrm{d}x) = |x|^{\alpha-1}\Gamma(\,\mathrm{d}x), \qquad \Gamma_{\mathrm{st}}(\,\mathrm{d}x) = |x|^{\alpha-\chi}\Gamma(\,\mathrm{d}x), \tag{C.1.2}$$

with zero mass at the origin. Both are nonnegative, even, positive-definite tempered Radon measures. Their measure scaling exponents are 1 and $2-\chi$, respectively. For every $h > 0$, $\epsilon > 0$, $\eta \geq 0$, and $z \in \mathbb{R}^2$,

$$\int G_{h,\eta}(\,\mathrm{d}y)(p_\epsilon * \Gamma_{\mathrm{low}})(y+z) \leq \frac{S}{4}. \tag{C.1.3}$$

If $\vartheta = (\chi-\alpha)/(\chi-1)$, then $0 < \vartheta < 1$ and

$$(p_\epsilon * \Gamma)(z) \leq (p_\epsilon * \Gamma_{\mathrm{low}})(z)^{\vartheta}(p_\epsilon * \Gamma_{\mathrm{st}})(z)^{1-\vartheta}. \tag{C.1.4}$$

No angular density or isotropy is assumed.

Proof. We identify the physical polar measure and its two weighted endpoints. We prove their positive definiteness separately, estimate the low endpoint through line integrals, and apply Hölder on the original heat-weighted measure.

Step 1. We obtain the polar measure and endpoint integrability. Since $2-\alpha > 0$, scaling and local finiteness force $\Gamma(\{0\}) = 0$. The unit-ball mass is finite, so $S < \infty$. It is positive: otherwise scaling would make every ball have zero mass, contradicting $\Gamma \neq 0$. Evenness of Γ implies evenness of σ. For $0 < a < b$ and Borel $E \subset \mathbb{S}^1$,

$$\Gamma\{x : a < |x| \leq b,\ x/|x| \in E\} = \frac{b^{2-\alpha} - a^{2-\alpha}}{2-\alpha}\sigma(E) = \int_a^b r^{1-\alpha}\,\mathrm{d}r\,\sigma(E).$$

These polar rectangles form a generating family. Uniqueness of measures, first on finite annuli and then on their increasing union, identifies the polar pushforward with $r^{1-\alpha}\,\mathrm{d}r\,\sigma(\,\mathrm{d}\omega)$. Hence, for every nonnegative Borel function f, Tonelli gives

$$\int f(x)\Gamma(\,\mathrm{d}x) = \int_{\mathbb{S}^1}\int_0^\infty f(r\omega)r^{1-\alpha}\,\mathrm{d}r\,\sigma(\,\mathrm{d}\omega). \tag{C.1.5}$$

Extended values are permitted. In particular, the formula applies to the nonnegative wave density used below.

The endpoint polar measures are therefore $\mathrm{d}r\,\sigma(\,\mathrm{d}\omega)$ and $r^{1-\chi}\,\mathrm{d}r\,\sigma(\,\mathrm{d}\omega)$. Their radial integrals are finite near zero because $\chi < 2$. Rapid decay of a Schwartz function controls their integrals at infinity, uniformly in direction. They are thus locally finite and tempered, and their stated scaling and evenness follow directly. If Γ has a density, the two weighted measures also have locally integrable densities.

Step 2. We prove positive definiteness of the low endpoint. To prove positive definiteness of the low endpoint, evenness gives the full-sphere line representation

$$\int f(x)\Gamma_{\mathrm{low}}(\,\mathrm{d}x) = \frac{1}{2}\int_{\mathbb{S}^1}\int_{\mathbb{R}} f(r\omega)\,\mathrm{d}r\,\sigma(\,\mathrm{d}\omega). \tag{C.1.6}$$

It holds for nonnegative Borel f, and for Schwartz f by absolute integrability. For a complex Schwartz function φ, put $\widetilde{\varphi}(x) = \overline{\varphi(-x)}$ and $\psi = \varphi * \widetilde{\varphi}$. Fubini in line and perpendicular coordinates gives

$$\int_{\mathbb{R}} \psi(r\omega)\,\mathrm{d}r = \int_{\omega^\perp} \left| \int_{\mathbb{R}} \varphi(s\omega + v)\,\mathrm{d}s \right|^2 \mathrm{d}v \geq 0.$$

Schwartz decay justifies all these integrals, uniformly for unit ω. Integrating against the finite measure σ in (C.1.6) proves $\Gamma_{\mathrm{low}}(\psi) \geq 0$. The factor $1/2$ is essential because both orientations of each line occur on the full sphere.

Step 3. We prove positive definiteness of the static endpoint. For the static endpoint put $\lambda = \chi - \alpha > 0$. For $x \neq 0$,

$$|x|^{-\lambda} = \frac{1}{\Gamma(\lambda/2)} \int_0^\infty s^{\lambda/2-1} e^{-s|x|^2}\,\mathrm{d}s.$$

For each $s > 0$, the measure $e^{-s|x|^2}\Gamma(\,\mathrm{d}x)$ is positive definite. Indeed, the Fourier transform of $e^{-s|x|^2}\psi(x)$ is a positive Gaussian convolution of $|\widehat{\varphi}|^2$. Its pairing with the original positive spectral measure is nonnegative; Schwartz decay makes the pairing finite. Moreover,

$$\int |\psi(x)||x|^{-\lambda}\Gamma(\,\mathrm{d}x) = \int |\psi(x)|\Gamma_{\mathrm{st}}(\,\mathrm{d}x) < \infty$$

by the endpoint polar integrability just proved. Tonelli with $|\psi|$, followed by Fubini, justifies the Gaussian mixture against ψ. Thus, $\Gamma_{\mathrm{st}}(\psi) \geq 0$. This uses smooth Gaussian multiplication of the original covariance and a convergent mixture, not a fractional power of that covariance.

Step 4. We bound the planar wave convolution. We next prove the convolution estimate directly. Use the planar wave density

$$G_h(y) = \frac{\mathbf{1}_{\{|y|<h\}}}{2\pi\sqrt{h^2 - |y|^2}},$$

with value zero on the circle. Write $z = a\omega + b\omega^\perp$ for a unit perpendicular vector. If $|b| < h$, put $A = \sqrt{h^2 - b^2}$. Translation along the line gives

$$\int_{\mathbb{R}} G_h(z - r\omega)\,\mathrm{d}r = \frac{1}{2\pi} \int_{-A}^{A} \frac{\mathrm{d}s}{\sqrt{A^2 - s^2}} = \frac{1}{2}.$$

If $|b| \geq h$, the open support is empty or tangent and the line integral is zero. The tangency point has zero line Lebesgue measure. Formula (C.1.6) and nonnegative Tonelli yield

$$(G_h * \Gamma_{\mathrm{low}})(z) = \frac{1}{4} \int_{\mathbb{S}^1} \mathbf{1}_{\{|z\cdot\omega^\perp|<h\}} \sigma(\,\mathrm{d}\omega) \leq \frac{S}{4}.$$

Evenness, Gaussian convolution, and Tonelli now give

$$\int G_{h,\eta}(\,\mathrm{d}y)(p_\epsilon * \Gamma_{\mathrm{low}})(y + z) = \left[p_{\epsilon+\eta} * (G_h * \Gamma_{\mathrm{low}})\right](z) \leq \frac{S}{4}.$$

For $\eta = 0$, use the unsmoothed Green measure. The Gaussian average has mass one, so the same constant works for all widths.

Step 5. We compare the regularized endpoints by Hölder. Finally, the measure $p_\epsilon(z - x)\Gamma(\,\mathrm{d}x)$ is finite. Gaussian decay and polynomial radial growth prove this directly; the endpoint convolutions are finite for the same reason. The identity

$$\vartheta(\alpha - 1) + (1 - \vartheta)(\alpha - \chi) = 0$$

and absence of an origin atom permit Hölder's inequality on this unnormalized positive measure:

$$\begin{aligned}(p_\epsilon * \Gamma)(z) &= \int |x|^{\vartheta(\alpha-1)}|x|^{(1-\vartheta)(\alpha-\chi)}p_\epsilon(z - x)\Gamma(\,\mathrm{d}x) \\ &\le (p_\epsilon * \Gamma_{\mathrm{low}})(z)^{\vartheta}(p_\epsilon * \Gamma_{\mathrm{st}})(z)^{1-\vartheta}.\end{aligned}$$

This proves Lemma C.1.1. □

Lemma C.1.2 (General planar static coefficient input)**.** *Let Ξ be a nonnegative, even, positive-definite tempered Radon measure on $\mathbb{R}^2$ with $\Xi(rA) = r^{2-\chi}\Xi(A)$, where $1 < \chi < 2$. For static Stratonovich noise with covariance Ξ, data $(1, 0)$, and wave operator Δ, let $U_n(t, x)$ be its ordered integrals, with $U_0 = 1$. There is a finite $C_{\mathrm{st}} = C_{\mathrm{st}}(\Xi) > 0$ such that, for $k \ge 1$ and $t > 0$,*

$$0 \le B_k(t) := \sum_{m=0}^{2k} \mathbb{E}[U_m(t, x)U_{2k-m}(t, x)] \le \frac{C_{\mathrm{st}}^k t^{(4-\chi)k}}{(k!)^{3-\chi}}. \tag{C.1.7}$$

Also $B_0 = 1$.

Proof. We treat zero covariance directly. For nonzero covariance, homogeneity verifies the static spectral condition, and the cited finite coefficient rate is converted to a bound valid at every order.

Step 1. We verify the static covariance hypotheses. If $\Xi = 0$, then $U_n = 0$ for $n \ge 1$, and hence $B_k = 0$ for $k \ge 1$. The choices $C_{\mathrm{st}} = 1$ and $B_0 = 1$ give the conclusion. We may therefore assume $\Xi \ne 0$.

Fourier uniqueness transfers covariance homogeneity to its positive spectral measure μ_Ξ: $\mu_\Xi(rA) = r^\chi \mu_\Xi(A)$. Its unit-ball mass is finite because the spectral measure is Radon. On dyadic annuli this gives

$$\int_{\mathbb{R}^2} (1 + |\xi|^2)^{-1}\mu_\Xi(\,\mathrm{d}\xi) \le \mu_\Xi(B_1) + 2^\chi \mu_\Xi(B_1) \sum_{j \ge 0} 2^{j(\chi-2)} < \infty.$$

This verifies the static Dalang condition without an angular density. The present Ξ also satisfies the source's covariance assumptions: it is a nonnegative positive-definite tempered distribution, and $1 < \chi < 2 = d$. The source expressly includes generalized covariances and uses their heat-regularized interpretation [20, p. 2152, (2.18)]. Thus, the coefficient estimate invoked below is a direct application within the source's stated class,

not an extension from density kernels. From Chen–Hu [20, Theorem 3.8(i), p. 2165], every fixed order exists in L^2. The product and Wick formulas (2.17) and (2.19), pp. 2151–2152, identify B_k with all pairings and all splits of the total order, including self-pairs and empty chains. Thus, every coefficient is finite and nonnegative.

Step 2. We state the imported finiteness input used by the coefficient rate. We make explicit the finiteness input in the source's coefficient upper rate. The variational constant $\mathcal{M}$ in Chen–Hu [20, p. 2147] is finite under the displayed Dalang condition. The source's invocation on p. 2175 identifies $2^{\chi/(4-\chi)}\mathcal{M}$ with the square-root variational quantity covered by Chen [15, Theorem 1.1, p. 2]. That theorem explicitly states finiteness under Dalang's condition and permits generalized nonnegative positive-definite covariances. We import that finiteness, not a sharp value or its proof.

Step 3. We turn the rate into an all-order constant. From Chen–Hu [20, (5.1), p. 2173, and (5.15), p. 2180], with $p = 2$, it follows that

$$B_k(t) = t^{(4-\chi)k} B_k(1), \qquad \limsup_{k\to\infty} \frac{1}{k} \log\left((k!)^{3-\chi} B_k(1)\right) < \infty.$$

Choose a finite $R > 0$ larger than this upper limit. For all sufficiently large k, $(k!)^{3-\chi} B_k(1) \le e^{Rk}$. Increase e^R to a finite positive constant dominating the kth roots of the finitely many remaining quantities. The resulting C_{st} proves (C.1.7) by homogeneity. These are the source's general homogeneous-covariance statements, not a Riesz specialization. This proves Lemma C.1.2. □

Proposition C.1.3 (Planar homogeneous-covariance upper bound)**.** *Let $d = 2$, $0 < \alpha_0 < 1$, and $1 < \alpha < 2 - \alpha_0$. Suppose that the nonzero spatial covariance Γ is nonnegative, even, positive definite and tempered, with (C.1.1). Choose and fix*

$$\alpha_0 < \vartheta < 2 - \alpha, \qquad b_0 = \alpha_0/\vartheta, \qquad \chi = (\alpha - \vartheta)/(1 - \vartheta).$$

Use the endpoint measures and physical angular mass S of Lemma C.1.1. Put

$$Z_{b_0} = \frac{2}{(1-b_0)(2-b_0)}, \qquad C_{\mathrm{low}} = Z_{b_0} S, \qquad C = C_{\mathrm{low}}^{\vartheta} C_{\mathrm{st}}^{1-\vartheta}, \qquad q = 3 - \alpha,$$

where C_{st} is from Lemma C.1.2 for $\Xi = \Gamma_{\mathrm{st}}$. For the Stratonovich solution with data $(1, 0)$, every $k \ge 1$, $t > 0$, and $x \in \mathbb{R}^2$ satisfy

$$A_k(t) \le \frac{C^k t^{(4-\alpha-\alpha_0)k}}{(k!)^{3-\alpha}}, \qquad \mathbb{E}u^2(t,x) \le \exp\left(qC^{1/q} t^{\kappa}\right). \tag{C.1.8}$$

Constants may depend on the covariance, α_0, and the fixed choice of ϑ, but not on k, t, x.

Proof. We verify the planar endpoint parameters and use a common positive measure for all diagrams. We interpolate the regularized coefficients, bound the low endpoint by its line-convolution estimate, and then pass to the fixed-order limits before summing.

Step 1. We verify the original and endpoint spectral conditions. The parameter interval is nonempty. We have $0 < \vartheta < 1$, $0 < b_0 < 1$, and

$$\chi - \alpha = \frac{\vartheta(\alpha - 1)}{1 - \vartheta} > 0, \qquad 2 - \chi = \frac{2 - \alpha - \vartheta}{1 - \vartheta} > 0.$$

Thus, Lemma C.1.1 applies, with its interpolation weight equal to ϑ. The original spectral measure has ball growth of exponent α, by the same Fourier homogeneity argument used in Lemma C.1.2. A dyadic sum gives the time-dependent spectral condition (1.5) of Chen [17, p. 3], since $\alpha < 2 - \alpha_0$. The low endpoint has spectral ball exponent one and $b_0 < 1$; the static endpoint has exponent $\chi < 2$. Thus, Lemma 2.5.2 applies to the target, and the imported static fixed-order theorem is used within its stated range.

Step 2. We form the common measure and apply Hölder. Fix $k \geq 1$, $t > 0$, and common noise widths $\epsilon, \delta > 0$. The spatial covariance on each edge has width 2ϵ. No Green smoothing is needed in dimension two. On the disjoint union over $m = 0, \ldots, 2k$ and $D \in \Pi_k$, define the finite positive measure $\nu_{k,t}$ by

$$\int \Phi \, \mathrm{d}\nu_{k,t} := \sum_{m=0}^{2k} \sum_{D \in \Pi_k} \int_{[0,t]^m_< \times [0,t]^{2k-m}_<} \mathrm{d}s \int \Phi(m, D, s, y) \prod_{l=1}^{2k} G_{h_l}(\, \mathrm{d}y_l).$$

Here each chain has its own root, $h_l = s_l - s_{p(l)}$, the y_l are its increments, and x_l is its cumulative position. A zero-length chain has empty products. At fixed times the spatial mass is $\prod_l h_l$; bounded time simplexes and finite discrete sums therefore make $\nu_{k,t}$ finite.

For $J \in \{\Gamma, \Gamma_{\mathrm{low}}, \Gamma_{\mathrm{st}}\}$ write

$$H_J = \prod_{(i,j) \in D} (p_{2\epsilon} * J)(x_i - x_j), \qquad T_b = \prod_{(i,j) \in D} |s_i - s_j|^{-b}.$$

The Gaussian covariance functions are bounded and continuous at each fixed width: their positive spectral measures are tempered, so Gaussian weighting makes them finite. Let Q_δ be the product of the target's truncated temporal covariances. The source regularization gives $0 \leq Q_\delta \leq T_{\alpha_0} = T_{b_0}^{\vartheta}$. Lemma C.1.1, at the common edge width, gives $H_\Gamma \leq H_{\Gamma_{\mathrm{low}}}^{\vartheta} H_{\Gamma_{\mathrm{st}}}^{1-\vartheta}$.

The Gaussian moment formula and the two separate chain reversals in Proposition 2.1.1 identify the target regularized coefficient with $\int Q_\delta H_\Gamma \, \mathrm{d}\nu_{k,t}$. Define

$$L_k^\epsilon(t) = \int T_{b_0} H_{\Gamma_{\mathrm{low}}} \, \mathrm{d}\nu_{k,t}, \qquad B_k^\epsilon(t) = \int H_{\Gamma_{\mathrm{st}}} \, \mathrm{d}\nu_{k,t}.$$

The latter is the regularized static coefficient, including every split and pairing. The former is only a deterministic integral with original temporal power. Hölder's inequality on the full common measure, including its discrete variables, yields

$$A_k^{\epsilon,\delta}(t) \leq \left(L_k^\epsilon(t)\right)^{\vartheta} \left(B_k^\epsilon(t)\right)^{1-\vartheta}. \tag{C.1.9}$$

No interpolation of different temporal cutoff kernels is asserted.

Step 3. We estimate the low endpoint with the full temporal pairing sum. We bound L_k^ϵ directly. Orient each pair by increasing block label. Descending integration of increments, as in Lemma B.1.1, removes at a closing label its only remaining covariance factor. Lemma C.1.1 bounds that integral by $S/4$. At an opening label its paired covariance has already been removed, so the Green integral is its mass h_l. The k opening increments sum to at most $2t$. Thus, the common spatial bound is

$$(S/4)^k \prod_{i \in O_D} h_i \le (S/2)^k \frac{t^k}{k^k}.$$

The temporal pairing sum is invariant under every permutation of its $2k$ labels. Each pairing integrates on the full time cube to $(Z_{b_0} t^{2-b_0})^k$. Partitioning by the two within-block orders, and then summing all splits, gives

$$\begin{aligned}\sum_{m=0}^{2k} \sum_{D \in \Pi_k} \int_{[0,t]^m_< \times [0,t]^{2k-m}_<} T_{b_0} \, \mathrm{d}s &= \frac{(2k)!}{2^k k!} (Z_{b_0} t^{2-b_0})^k \sum_{m=0}^{2k} \frac{1}{m!(2k-m)!} \\ &= \frac{2^k}{k!} (Z_{b_0} t^{2-b_0})^k.\end{aligned}$$

Symmetry is used for the sum, not for an individual pairing. The integral is finite because $b_0 < 1$. Multiplication gives

$$L_k^\epsilon(t) \le \frac{(Z_{b_0} S)^k t^{(3-b_0)k}}{k!\, k^k} \le \frac{C_{\mathrm{low}}^k t^{(3-b_0)k}}{(k!)^2}. \tag{C.1.10}$$

At fixed ϵ, bounded covariance and the finite common measure make B_k^ϵ finite as well. These observations also justify finiteness in the Hölder estimate.

Step 4. We remove noise smoothing at fixed order. We next take fixed-order limits. The target orders converge in L^2 by Lemma 2.5.2. For the static orders the corresponding input is Chen–Hu [20, Theorem 3.8(i), p. 2165]. For products of two fixed orders, the inequality

$$\|YZ - Y'Z'\|_1 \le \|Y - Y'\|_2 \|Z\|_2 + \|Y'\|_2 \|Z - Z'\|_2$$

gives L^1 convergence. There are only $2k+1$ split products, and a zero-order factor stays equal to one. Hence, $A_k^{\epsilon,\delta}(t) \to A_k(t)$ and $B_k^\epsilon(t) \to B_k(t)$ as the noise widths vanish. The uniform deterministic estimate (C.1.10) needs no stochastic limit interpretation. Passing to limits in (C.1.9) gives

$$A_k(t) \le \left(\frac{C_{\mathrm{low}}^k t^{(3-b_0)k}}{(k!)^2} \right)^\vartheta B_k(t)^{1-\vartheta}.$$

Only now apply Lemma C.1.2. No monotonicity in the spatial width or uniform static smoothed asymptotic was used.

Step 5. We combine powers and sum the full moment series. The parameter identities $\alpha = \vartheta + (1-\vartheta)\chi$ and $\alpha_0 = \vartheta b_0$ imply

$$2\vartheta + (1-\vartheta)(3-\chi) = 3 - \alpha, \qquad \vartheta(3-b_0) + (1-\vartheta)(4-\chi) = 4 - \alpha - \alpha_0.$$

This yields the coefficient bound in (C.1.8) with $C = C_{\mathrm{low}}^{\vartheta} C_{\mathrm{st}}^{1-\vartheta}$. The constant coefficient is $A_0 = 1$. For $q = 3 - \alpha > 1$ and $z \geq 0$,

$$\sum_{k\geq 0} \frac{z^k}{(k!)^q} = \sum_{k\geq 0} \left(\frac{z^{k/q}}{k!}\right)^q \leq \left(\sum_{k\geq 0} \frac{z^{k/q}}{k!}\right)^q = e^{qz^{1/q}}.$$

Proposition 2.1.1 supplies the nonnegative full series for the target solution. Take $z = Ct^{4-\alpha-\alpha_0}$ and use $(4 - \alpha - \alpha_0)/q = \kappa$. This proves Proposition C.1.3. □

Corollary C.1.4 (Full planar parameter range)**.** *In dimension two, under Hypothesis 1.2.1 and the standing covariance positivity assumptions, the upper bound* $\mathbb{E}u^2(t,x) \leq \exp(C_{\mathrm{dir}} t^{\kappa})$ *holds throughout* $0 < \alpha < 2 - \alpha_0$*, with a finite constant* C_{dir} *depending on* α_0 *and the spatial covariance. A nonnegative generalized covariance is interpreted as the homogeneous measure and its Gaussian approximations described above.*

Proof. For $0 < \alpha \leq 1$, apply Proposition B.1.5. For $1 < \alpha < 2 - \alpha_0$, apply Proposition C.1.3. If the covariance vanishes, $u = 1$ and $C_{\mathrm{dir}} = 0$ suffices. This proves Corollary C.1.4. □

Remark C.1.5 (Planar calibrations and remaining goals)**.** The exponent tends to $(4 - \alpha)/(3 - \alpha)$ as $\alpha_0 \downarrow 0$, consistently with the static source, without an interchange of limits or uniformity claim for the constants. For the nonzero higher-exponent case, Cauchy–Schwarz gives $\mathbb{E}u(t,x) \leq \exp(qC^{1/q}t^{\kappa}/2)$. If the first-moment lower rate is at least L_*, this implies $2L_* \leq qC^{1/q}$. No sharp constant is identified. The existing comparisons with Skorohod exponents, in their stated Riesz subclasses, concern different solution concepts and are not inputs here. The planar endpoint construction is dimension-specific; no general higher-exponent result in dimension three follows from it. Section 3.3 treats the full homogeneous-covariance class by a separate argument. The intrinsic constant is identified separately in Theorem 11.2.6.

C.2 Three-dimensional bounds from covariance endpoints

The endpoint constructions and conditional moment transfer are retained as an alternative route. No general three-dimensional factorization is asserted. The full upper and intrinsic formula do not use these factorizations.

We first construct the product endpoints. Zero coordinate exponents below mean constant factors, not one-dimensional white noise.

Lean full

Lemma C.2.1 (Strict product endpoints)**.** *Let* $0 \leq a_j < 1$ *for* $j = 1, 2, 3$*, let* $\alpha = a_1 + a_2 + a_3 \in (1, 2)$*, and choose* $0 < \vartheta < 2 - \alpha$*. Put* $\chi = (\alpha - \vartheta)/(1 - \vartheta)$ *and define*

$$\begin{aligned} &L_j = \max\{0, (a_j - 1 + \vartheta)/\vartheta\}, \qquad U_j = \min\{1, a_j/\vartheta\}, \\ &\Lambda = \frac{1 - \sum_j L_j}{\sum_j U_j - \sum_j L_j}, \qquad b_j = L_j + \Lambda(U_j - L_j), \qquad v_j = \frac{a_j - \vartheta b_j}{1 - \vartheta}. \end{aligned} \tag{C.2.1}$$

Then $0 < \Lambda < 1$, $\sum_j b_j = 1$, $\sum_j v_j = \chi$, *and*

$$a_j = \vartheta b_j + (1-\vartheta)v_j, \qquad a_j > 0 \Longrightarrow 0 < b_j, v_j < 1, \qquad a_j = 0 \Longrightarrow b_j = v_j = 0.$$

For any $c > 0$, *the ordinary covariance densities*

$$\gamma_a(x) = c\prod_{j=1}^{3} |x_j|^{-a_j}, \qquad \gamma_b(x) = c\prod_{j=1}^{3} |x_j|^{-b_j}, \qquad \gamma_v(x) = c\prod_{j=1}^{3} |x_j|^{-v_j}$$

are nonnegative, even, positive definite, locally integrable and tempered. Their covariance homogeneity exponents are $\alpha, 1, \chi$, *respectively, with* $\alpha < \chi < 2$. *For every* $\epsilon > 0$ *and* $z \in \mathbb{R}^3$,

$$(p_\epsilon * \gamma_a)(z) \le (p_\epsilon * \gamma_b)(z)^{\vartheta}(p_\epsilon * \gamma_v)(z)^{1-\vartheta}. \tag{C.2.2}$$

A factor with exponent zero is defined to be one everywhere.

Proof. We first show that the coordinate endpoint intervals admit a strict interior choice with the required sums. We then verify the covariance properties of the resulting product densities and apply Gaussian Hölder.

Step 1. We choose strict coordinate endpoints and verify their sums. We have $\vartheta < 1$. There are at least two positive coordinates, since every $a_j < 1$ and $\sum_j a_j > 1$. At a zero coordinate, $L_j = U_j = 0$. At a positive coordinate, $L_j < U_j$: if $a_j \ge \vartheta$, then $U_j = 1$ and $L_j < 1$; if $a_j < \vartheta$, then $U_j = a_j/\vartheta > 0$, and either $L_j = 0$ or $U_j - L_j = (1-\vartheta)/\vartheta > 0$.

Let $I = \{j : L_j > 0\}$ and $r = |I|$. For $r = 0$ the sum of the lower endpoints is zero; for $r = 1$ it is less than one. For $r \ge 2$,

$$\sum_{j\in I} a_j \le \alpha < 2 - \vartheta \le r - (r-1)\vartheta,$$

because the last inequality is equivalent to $(r-2)(1-\vartheta) \ge 0$. Therefore,

$$\sum_j L_j = \frac{\sum_{j\in I} a_j - r + r\vartheta}{\vartheta} < 1.$$

If some $a_j \ge \vartheta$, its upper endpoint equals one and a different positive coordinate has positive upper endpoint. Otherwise, $\sum_j U_j = \alpha/\vartheta > 1$. Hence, $\sum_j L_j < 1 < \sum_j U_j$, which proves $0 < \Lambda < 1$ and $\sum_j b_j = 1$. At every positive coordinate, $L_j < b_j < U_j$, so $0 < b_j < 1$. The inequalities $b_j < U_j \le a_j/\vartheta$ and $b_j > L_j \ge (a_j - 1 + \vartheta)/\vartheta$ give $0 < v_j < 1$. At a zero coordinate $b_j = v_j = 0$. The reconstruction identity is immediate, and summing it gives $\sum_j v_j = \chi$. Finally,

$$\chi - \alpha = \frac{\vartheta(\alpha-1)}{1-\vartheta} > 0, \qquad 2 - \chi = \frac{2-\alpha-\vartheta}{1-\vartheta} > 0.$$

Step 2. We verify local integrability and positive definiteness. For any of the three exponent vectors e, local integrability is a product of one-dimensional integrals with exponents

below one. For a Schwartz function ψ, choose $N > 1$ and use $|\psi(x)| \le C_N \prod_j (1+|x_j|)^{-N}$. This proves absolute integrability against γ_e and also temperedness. For each active coordinate, $0 < e_j < 1$, use

$$|u|^{-e_j} = \frac{1}{\Gamma(e_j/2)} \int_0^\infty s^{e_j/2-1} e^{-su^2} \, \mathrm{d}s.$$

The product over the active coordinates is a positive mixture of Gaussian functions in those coordinates, constant in all other coordinates. Each such Gaussian is positive definite. For a complex Schwartz φ, set $\psi = \varphi * \widetilde{\varphi}$, where $\widetilde{\varphi}(x) = \overline{\varphi(-x)}$. The absolute integrability just proved permits Tonelli with $|\psi|$ and then Fubini for the mixture against ψ. Its quadratic form is nonnegative. No Euler Gamma factor at exponent zero is introduced. Evenness and homogeneity follow from the displayed densities.

Step 3. We compare the smoothed densities at common amplitude. The reconstruction of each exponent and the common amplitude imply $\gamma_a = \gamma_b^{\vartheta} \gamma_v^{1-\vartheta}$ almost everywhere; values on singular coordinate planes do not change these locally integrable covariances. Hölder's inequality on the Gaussian probability measure gives (C.2.2). Its endpoint convolutions are finite by the product integrability and Gaussian decay. The amplitude remains $c^{\vartheta} c^{1-\vartheta} = c$. This proves Lemma C.2.1. □

We now take $d = 3$, $0 < \alpha_0 < 1$, and $1 < \alpha < 2 - \alpha_0$. Let Γ be a nonnegative, even, positive-definite tempered spatial covariance, with homogeneity exponent α. As a positive distribution it is a Radon measure satisfying $\Gamma(rA) = r^{3-\alpha}\Gamma(A)$; a covariance function is identified with its density measure. Gaussian convolution is used for all covariance products. Choose and fix

$$\alpha_0 < \vartheta < 2 - \alpha, \qquad b_0 = \alpha_0/\vartheta, \qquad \chi = (\alpha - \vartheta)/(1 - \vartheta). \tag{C.2.3}$$

Then $0 < b_0 < 1$ and $\alpha < \chi < 2$, by the identities in the preceding proof. The zero target covariance is trivial, since then $u = 1$.

Hypothesis C.2.2 (Gaussian covariance comparison)**.** There are nonnegative, even, positive-definite tempered endpoint covariances Γ_{low} and Γ_{st} on $\mathbb{R}^3$ with measure scaling

$$\Gamma_{\mathrm{low}}(rA) = r^2 \Gamma_{\mathrm{low}}(A), \qquad \Gamma_{\mathrm{st}}(rA) = r^{3-\chi} \Gamma_{\mathrm{st}}(A),$$

such that, for every $\epsilon > 0$ and $z \in \mathbb{R}^3$,

$$(p_\epsilon * \Gamma)(z) \le (p_\epsilon * \Gamma_{\mathrm{low}})(z)^{\vartheta} (p_\epsilon * \Gamma_{\mathrm{st}})(z)^{1-\vartheta}. \tag{C.2.4}$$

This is a condition on deterministic covariance measures and their Gaussian convolutions. It assumes no moment estimate. We do not assert that every homogeneous covariance in dimension three admits these endpoints.

Lean full

Lemma C.2.3 (Plane-supported endpoints)**.** *Retain* (C.2.3)*, let $c > 0$, and let $a_1, a_2 \ge 0$ satisfy $s = a_1 + a_2 = \alpha - 1$. In coordinates $(y, z) \in \mathbb{R}^2 \times \mathbb{R}$, put*

$$m(\mathrm{d}y, \mathrm{d}z) = \mathrm{d}y \, \delta_0(\mathrm{d}z), \qquad v_j = \frac{a_j}{1 - \vartheta}, \qquad \Gamma_{\mathrm{pl}} = c \prod_{j=1}^{2} |y_j|^{-a_j} m.$$

Zero coordinate powers mean one. Then

$$\Gamma_{\mathrm{low}} = cm, \qquad \Gamma_{\mathrm{st}} = c\prod_{j=1}^{2} |y_j|^{-v_j} m$$

satisfy Hypothesis C.2.2 for Γ_{pl}. *In the spectral convention of Lemma B.1.4, this low endpoint has* $V_{\mathrm{low}} = c/\pi$.

Proof. We verify the exponents and covariance properties of the plane-supported measures. We then apply Hölder to their ordinary densities on the same plane measure and compute the low endpoint spectral mass.

Step 1. We verify the endpoint parameters and measure scaling. Since $0 < s < 1 - \alpha_0$ and $\vartheta < 2 - \alpha = 1 - s$,

$$0 \le a_j < 1, \qquad 0 \le v_j < 1, \qquad v_1 + v_2 = \frac{s}{1-\vartheta} = \chi - 1 < 1.$$

A measure $f_e(y)\,\mathrm{d}y\,\delta_0(\,\mathrm{d}z)$, with $f_e(y) = \prod_j |y_j|^{-e_j}$ and $0 \le e_j < 1$, is locally finite. For a Schwartz test function, product-weighted rapid decay proves absolute integrability and temperedness. Its scaling exponent as a measure is $2 - e_1 - e_2$. Thus, the three measures in the statement have exponents $3 - \alpha$, 2, and $3 - \chi$. They are even and nonnegative.

Step 2. We include the normal Dirac measure in the positivity argument. We verify positive definiteness, including the normal Dirac measure. Each positive coordinate power has the Gaussian mixture

$$|u|^{-e} = \frac{1}{\Gamma(e/2)} \int_0^\infty r^{e/2-1} e^{-ru^2}\,\mathrm{d}r, \qquad 0 < e < 1;$$

a zero coordinate contributes the positive-definite constant one. Consequently, f_e is a positive mixture of positive-definite tangential Gaussian functions. For $\varphi \in \mathcal{S}(\mathbb{R}^3)$, its quadratic form against the plane measure is

$$\int_{\mathbb{R}} \mathrm{d}z \int_{\mathbb{R}^2}\int_{\mathbb{R}^2} f_e(y - y')\varphi(y,z)\overline{\varphi(y',z)}\,\mathrm{d}y\,\mathrm{d}y'.$$

Absolute Fubini follows by setting

$$A(u) = \int_{\mathbb{R}}\int_{\mathbb{R}^2} |\varphi(y+u,z)\varphi(y,z)|\,\mathrm{d}y\,\mathrm{d}z.$$

Rapid decay gives $A(u) \le C_N \prod_j (1 + |u_j|)^{-N}$. Hence, $\int f_e(u)A(u)\,\mathrm{d}u < \infty$ for $N > 1$, by one-dimensional integrability. Integrating the nonnegative Gaussian quadratic forms proves positive definiteness. This argument includes the low endpoint, where both coordinate powers are zero.

Step 3. We compare the Gaussian convolutions on the plane. For $\epsilon > 0$ and $w \in \mathbb{R}^3$, apply Hölder on the finite positive measure $p_\epsilon(w - (y,z))m(\,\mathrm{d}y,\,\mathrm{d}z)$. Its mass is $p_\epsilon^{(1)}(w_3)$. If $f(y) = \prod_j |y_j|^{-a_j}$, the identity between ordinary densities

$$cf = c^\vartheta \left(cf^{1/(1-\vartheta)}\right)^{1-\vartheta}$$

holds m-almost everywhere. Both endpoint convolutions are finite, since $v_j < 1$ and the Gaussian decays at infinity. Hölder gives exactly (C.2.4); no power of a distribution is taken.

Step 4. We compute the spectral normalization of the low endpoint. Finally, the low spectral measure is

$$\mu_{\mathrm{low}}(\,\mathrm{d}\xi) = \frac{c}{2\pi}\delta_0(\,\mathrm{d}\xi_1)\delta_0(\,\mathrm{d}\xi_2)\,\mathrm{d}\xi_3.$$

This follows from the unit spectral atom of a constant and the one-dimensional Fourier identity for δ_0 in the stated convention. Its unit-ball mass is c/π, so the uniform closing bound of Lemma B.1.4 is $c/2$. This proves Lemma C.2.3. □

Lean full

Lemma C.2.4 (Linear images and finite positive sums)**.** *Fix the parameters in* (C.2.3)*. The covariance comparison of Hypothesis C.2.2 is preserved by simultaneously pushing the target and its two endpoints forward under any invertible linear map $T : \mathbb{R}^3 \to \mathbb{R}^3$. It is also preserved by finite sums with nonnegative weights, when all component comparisons use the same α, ϑ, χ.*

Proof. We first extend the comparison from isotropic to general nondegenerate Gaussian kernels. We then track the common determinant factor under linear maps and use discrete Hölder for finite positive sums.

Step 1. We extend the Gaussian convolution comparison. First the comparison extends to every centered nondegenerate Gaussian probability density q_Σ with covariance matrix Σ. Choose $a > 0$ below the smallest eigenvalue of Σ. The Gaussian convolution identity gives $q_\Sigma = p_a * q_{\Sigma - aI}$. Put $F_J = p_a * J$ for each $J \in \{\Gamma, \Gamma_{\mathrm{low}}, \Gamma_{\mathrm{st}}\}$. These functions are nonnegative, bounded, and continuous: Gaussian weighting makes their positive tempered spectral measures finite, and the covariance bound is $|F_J(x)| \le F_J(0) < \infty$. Tonelli and Hölder on the Gaussian probability measure yield

$$q_\Sigma * \Gamma \le q_{\Sigma - aI} * \left(F_{\Gamma_{\mathrm{low}}}^{\vartheta} F_{\Gamma_{\mathrm{st}}}^{1-\vartheta}\right) \le (q_\Sigma * \Gamma_{\mathrm{low}})^{\vartheta}(q_\Sigma * \Gamma_{\mathrm{st}})^{1-\vartheta}.$$

Every convolution here is finite.

Step 2. We push all three measures through the same linear map. Write $J_T = T_{\#}J$ and $d_T = |\det T|$. Pushforward preserves nonnegativity, evenness, local finiteness, temperedness, and homogeneous scaling, since T is invertible and commutes with scalar dilation. For positive definiteness, take a complex Schwartz function φ and put $\psi(y) = \varphi(Ty)$. Then

$$(\varphi * \widetilde{\varphi})(Ty) = d_T(\psi * \widetilde{\psi})(y).$$

The quadratic form of $T_{\#}J$ is therefore d_T times a nonnegative quadratic form of J. With $\Sigma = \epsilon T^{-1}(T^{-1})^{\top}$, direct Gaussian change of variables gives, for every $\epsilon > 0$ and x,

$$(p_\epsilon * J_T)(x) = d_T^{-1}(q_\Sigma * J)(T^{-1}x).$$

Apply the preceding comparison. The two endpoint factors contribute $d_T^{-\vartheta} d_T^{-(1-\vartheta)} = d_T^{-1}$, which is the target factor. This proves the comparison for the three pushed-forward measures.

Step 3. We take finite weighted sums of endpoint triples. For the finite-sum assertion, let Γ_i, L_i, S_i, $1 \le i \le N$, be component triples, and let $w_i \ge 0$. At a fixed width and translation put $l_i = (p_\epsilon * L_i)(x)$ and $s_i = (p_\epsilon * S_i)(x)$. Finite sums preserve all required covariance properties and scalings. Discrete Hölder gives

$$\begin{aligned} p_\epsilon * \left(\sum_i w_i \Gamma_i \right) &\le \sum_i (w_i l_i)^\vartheta (w_i s_i)^{1-\vartheta} \\ &\le \left(p_\epsilon * \sum_i w_i L_i \right)^\vartheta \left(p_\epsilon * \sum_i w_i S_i \right)^{1-\vartheta}. \end{aligned}$$

Zero weights cause no ambiguity, since both powers are positive. The all-zero target also satisfies the comparison. This proves Lemma C.2.4. □

The linear maps in Lemma C.2.4 act on the noise covariances. All moment estimates below still use the original isotropic wave kernel. Endpoint spectral masses and variational quantities are computed for the transformed covariances; their values need not be unchanged by a nonorthogonal map.

For the low endpoint let $V_{\mathrm{low}} = \mu_{\mathrm{low}}(B_1)$ in the spectral convention of Lemma B.1.4, and put

$$Z_{b_0} = \frac{2}{(1-b_0)(2-b_0)}, \qquad C_{\mathrm{low}} = 2 Z_{b_0} \pi V_{\mathrm{low}}.$$

For the static endpoint, write

$$\mathcal{Q}_{\mathrm{st}}(g) = \int_{\mathbb{R}^3} \int_{\mathbb{R}^3} g(y+z)^2 g(y)^2 \, \mathrm{d}y \, \Gamma_{\mathrm{st}}(\mathrm{d}z), \qquad \mathcal{F}_3 = \{ g \in W^{1,2}(\mathbb{R}^3) : \|g\|_2 = 1 \},$$

using real Sobolev functions, and define

$$\begin{aligned} \mathcal{M}_{\mathrm{st}} &= \sup_{g \in \mathcal{F}_3} \left\{ \mathcal{Q}_{\mathrm{st}}(g)^{1/2} - \|\nabla g\|_2^2 \right\}, \\ Q &= 3 - \chi, \qquad \nu_{\mathrm{st}} = 4 - \chi, \qquad \Lambda_{\mathrm{st}} = 2 \left(\frac{2\sqrt{\mathcal{M}_{\mathrm{st}}}}{4-\chi} \right)^{4-\chi}. \end{aligned} \tag{C.2.5}$$

The functional is precisely Chen–Hu's (1.11), p. 2147, for the endpoint covariance, with unit gradient penalty. The positive-measure energy above agrees with the spectral form on every real Sobolev profile by Lemma C.3.1; thus no density is assigned to a singular covariance. The lemma also supplies finiteness, since $\chi < 2$ gives Dalang's condition as checked below. Nonnegativity follows by dilating a unit-L^2 Schwartz function: its energy term is nonnegative and its gradient penalty tends to zero.

Proposition C.2.5 (Conditional three-dimensional transfer)**.** *Under the preceding assumptions and Hypothesis C.2.2, with $\Gamma \neq 0$, there is a finite constant $C > 0$ such that*

$$A_k(t) \le \frac{C^k t^{(4-\alpha-\alpha_0)k}}{(k!)^{3-\alpha}} \quad (k \ge 1), \qquad \mathbb{E}u^2(t,x) \le \exp\left(q C^{1/q} t^\kappa \right), \quad q = 3 - \alpha. \tag{C.2.6}$$

The estimates hold for all $t > 0$ and $x \in \mathbb{R}^3$, with data $(1, 0)$. The constant may depend on the fixed covariances, α_0, and ϑ, but not on k, t, x. In addition, the explicit variational upper constant satisfies

$$\limsup_{t\to\infty} t^{-\kappa} \log \mathbb{E}u^2(t,x) \le q \left(C_{\mathrm{low}}^{\vartheta} \Lambda_{\mathrm{st}}^{1-\vartheta} \right)^{1/q}. \tag{C.2.7}$$

This constant is not asserted sharp and is not substituted into the pure all-time exponential bound in (C.2.6).

Proof. We verify the static input and establish a regularized coefficient comparison on one common measure. We identify the static and target Green limits separately before removing noise widths. We then sum the all-time coefficient bound and retain the finite low orders when deriving the sharper asymptotic constant.

Step 1. We state and verify the imported static coefficient input. We first record the general static input needed here. For a static endpoint covariance Ξ of exponent χ, Fourier uniqueness gives $\mu_\Xi(rA) = r^\chi \mu_\Xi(A)$ for its positive spectral measure. Its unit-ball mass is finite, and

$$\int_{\mathbb{R}^3} (1 + |\xi|^2)^{-1} \mu_\Xi(\,\mathrm{d}\xi) \le \mu_\Xi(B_1) + 2^\chi \mu_\Xi(B_1) \sum_{j\ge 0} 2^{j(\chi-2)} < \infty.$$

Thus, the static Dalang condition holds. Let U_n be the source's ordered integrals for this covariance. Its nonnegative positive-definite tempered-distribution class is explicitly included by the generalized covariance convention in [20, p. 2152, (2.18)]; its homogeneity degree satisfies $0 < \chi < 2 < 3$. No density or angular regularity is added here. Let $U_0 = 1$, and set $B_k(t) = \sum_{m=0}^{2k} \mathbb{E}[U_m(t,x) U_{2k-m}(t,x)]$. If $\Xi = 0$, then $B_k = 0$ for $k \ge 1$, and $C_{\mathrm{st}} = 1$ suffices in the bound below. For the remaining static calculation, assume $\Xi \ne 0$. From Chen–Hu [20, Theorem 3.8(i), p. 2165, and (2.17), (2.19)–(2.22), pp. 2151–2153], the expectation and product rules give finite nonnegative coefficients with every split and pairing included; the latter formulas also specify the two-chain and measure conventions. Finiteness of the variational input follows from Chen [15, Theorem 1.1, p. 2], which gives a finite square-root variational supremum under Dalang's condition. Chen–Hu identify that supremum with $2^{\chi/(4-\chi)}\mathcal{M}$ on p. 2175. Hence, their coefficient-rate constant involving $\mathcal{M}$ is finite. For $\Xi = \Gamma_{\mathrm{st}}$ this functional is $\mathcal{M}_{\mathrm{st}}$ defined above. Only finiteness, not a sharp value, is needed for the all-time coefficient bound.

From Chen–Hu [20, (5.1), p. 2173, and (5.15), p. 2180], at $p = 2$,

$$B_k(t) = t^{(4-\chi)k} B_k(1), \qquad \limsup_{k\to\infty} \frac{1}{k} \log \left((k!)^{3-\chi} B_k(1) \right) < \infty.$$

For $\Xi \ne 0$, choose $R > 0$ above this upper limit, then enlarge e^R to cover the kth roots of the finitely many remaining quantities $(k!)^{3-\chi} B_k(1)$. We obtain a finite $C_{\mathrm{st}} = C_{\mathrm{st}}(\Xi) > 0$ such that

$$B_k(t) \le \frac{C_{\mathrm{st}}^k t^{(4-\chi)k}}{(k!)^{3-\chi}}, \qquad k \ge 1, \quad t > 0. \tag{C.2.8}$$

Also $B_0 = 1$. We apply this source bound only after taking the fixed-order noise limits, with $\Xi = \Gamma_{\mathrm{st}}$.

Step 2. We verify the target hypotheses and form the common regularized measure. For the target, the same spectral scaling calculation has exponent α. Its dyadic sum for the weight $(1 + |\xi|^2)^{-(2-\alpha_0)/2}$ is finite because $\alpha < 2 - \alpha_0$. The target fixed-order limit is supplied by Lemma 2.5.2. The endpoint Γ_{low} has covariance exponent one, with $V_{\mathrm{low}}, C_{\mathrm{low}}$ defined above. Finiteness of V_{low} follows from the Radon spectral measure. It is positive: otherwise homogeneity gives $\mu_{\mathrm{low}} = 0$, contradicting (C.2.4) and $\Gamma \neq 0$.

Fix $k \geq 1$, $t > 0$, and positive widths ϵ, δ, η. Noise width ϵ means edge covariance width 2ϵ; δ is the target temporal cutoff and η is Green smoothing. Write $X_n^{\epsilon,\delta,\eta}(t,x)$ for the source's ordered integral against its smoothed field $W_{\epsilon,\delta}$, with every Green kernel replaced by $G_{h,\eta}$, and set $X_0^{\epsilon,\delta,\eta} = 1$. Explicitly, the target coefficient is

$$A_k^{\epsilon,\delta,\eta}(t) = \sum_{m=0}^{2k} \mathbb{E}\left[X_m^{\epsilon,\delta,\eta}(t,x) X_{2k-m}^{\epsilon,\delta,\eta}(t,x)\right].$$

On the full disjoint union over all splits $m + n = 2k$ and all $D \in \Pi_k$, define a common finite positive measure by

$$\int \Phi \,\mathrm{d}\nu_{k,t,\eta} := \sum_{m=0}^{2k} \sum_{D\in\Pi_k} \int_{[0,t]^m_< \times [0,t]^{2k-m}_<} \mathrm{d}s \int \Phi(m, D, s, y) \prod_{l=1}^{2k} G_{h_l,\eta}(\,\mathrm{d}y_l).$$

Each chain has its own root; $h_l = s_l - s_{p(l)}$, y_l is an increment, and x_l is the cumulative position in its chain. Empty chains use empty products. The spatial mass is $\prod_l h_l$, so bounded time simplexes and finite discrete sums prove finiteness. This measure does not depend on which covariance is inserted.

For $J \in \{\Gamma, \Gamma_{\mathrm{low}}, \Gamma_{\mathrm{st}}\}$ set

$$H_J = \prod_{(i,j)\in D} (p_{2\epsilon} * J)(x_i - x_j), \qquad T_b = \prod_{(i,j)\in D} |s_i - s_j|^{-b}.$$

If Q_δ is the product of the target temporal covariances, the source cutoff gives $0 \leq Q_\delta \leq T_{\alpha_0} = T_{b_0}^{\vartheta}$. The covariance hypothesis gives $H_\Gamma \leq H_{\Gamma_{\mathrm{low}}}^{\vartheta} H_{\Gamma_{\mathrm{st}}}^{1-\vartheta}$ at the same edge width. Define the deterministic low endpoint and the regularized static coefficient by

$$L_k^{\epsilon,\eta}(t) = \int T_{b_0} H_{\Gamma_{\mathrm{low}}} \,\mathrm{d}\nu_{k,t,\eta}, \qquad B_k^{\epsilon,\eta}(t) = \int H_{\Gamma_{\mathrm{st}}} \,\mathrm{d}\nu_{k,t,\eta}.$$

Gaussian moments and separate chain reversal identify the target regularized coefficient with $\int Q_\delta H_\Gamma \,\mathrm{d}\nu_{k,t,\eta}$. The static identity has temporal covariance one and includes self-pairings. Hölder on the entire common measure yields

$$A_k^{\epsilon,\delta,\eta}(t) \leq \left(L_k^{\epsilon,\eta}(t)\right)^{\vartheta} \left(B_k^{\epsilon,\eta}(t)\right)^{1-\vartheta}. \tag{C.2.9}$$

No stochastic identity is assumed for $L_k^{\epsilon,\eta}$ with its original temporal power, and no relation between different temporal cutoff kernels is used.

Step 3. We estimate the deterministic low endpoint. Lemma B.1.4 applies to the low endpoint with no angular-density assumption. Its uniform closing bound is $\pi V_{\mathrm{low}}/2$. Descending increment integration removes the only remaining covariance at each closing label; at each opening the paired covariance is already removed and the Green mass is h_l. The k opening increments sum to at most $2t$. Consequently, the common spatial bound is $(\pi V_{\mathrm{low}})^k t^k/k^k$, uniformly in ϵ, η. After summing pairings, the temporal integrand is symmetric in all $2k$ labels. Its full cube integral is $P_k(Z_{b_0} t^{2-b_0})^k$, where $P_k = (2k)!/(2^k k!)$. The block-order factors and the binomial split sum give

$$P_k \sum_{m=0}^{2k} \frac{1}{m!(2k-m)!} = \frac{2^k}{k!}.$$

Therefore,

$$L_k^{\epsilon,\eta}(t) \le \frac{C_{\mathrm{low}}^k t^{(3-b_0)k}}{k!\, k^k} \le \frac{C_{\mathrm{low}}^k t^{(3-b_0)k}}{(k!)^2}. \tag{C.2.10}$$

Here $b_0 < 1$ makes the original temporal cube integral finite. At fixed spatial width, the static covariance is bounded, so its regularized coefficient is finite too. This justifies the finite right side in (C.2.9).

Step 4. We identify the static source and its zero-Green-width integral. We now identify the static inner Green limit with the source's prescribed zero-Green-width approximant. Take the source's static isonormal noise W^{st} with covariance Γ_{st} and set $W_\epsilon(x) = W^{\mathrm{st}}(p_\epsilon(x-\cdot))$. All widths are therefore on the source's Gaussian space, and the covariance is $p_{2\epsilon} * \Gamma_{\mathrm{st}}$. This covariance is bounded and continuous, since Gaussian weighting makes its positive tempered spectral measure finite. It has a continuous modification. Indeed, with μ_{st} the spectral measure,

$$\mathbb{E}|W_\epsilon(x+h) - W_\epsilon(x)|^2 \le |h|^2 \int_{\mathbb{R}^3} |\xi|^2 e^{-\epsilon|\xi|^2} \mu_{\mathrm{st}}(\,\mathrm{d}\xi).$$

The integral is finite by temperedness. Gaussian eighth moments are therefore bounded by a constant times $|h|^8$. Kolmogorov's continuity criterion in dimension three, applied on compact sets and then on a countable exhaustion, gives the claimed modification. We choose this version. For $n \ge 1$ define $\Phi_n(\mathbf{x}) = \prod_{j=1}^n W_\epsilon(x_j)$ as an L^2 random variable. Gaussian moments show that Φ_n is continuous as a map from $(\mathbb{R}^3)^n$ to L^2 and uniformly bounded there: if $v_\epsilon = (p_{2\epsilon} * \Gamma_{\mathrm{st}})(0)$, then

$$\|\Phi_n(\mathbf{x})\|_2^2 \le P_n v_\epsilon^n.$$

The continuity follows by applying the same finite Gaussian moment formula to $\mathbb{E}|\Phi_n(\mathbf{x}) - \Phi_n(\mathbf{x}')|^2$. Its separable continuous image is strongly measurable.

Let $\mathfrak{g}_{n,t,x}^\eta$ be the finite positive ordered Green-chain measure, including its time variables, from the source's kernel (2.13), with each Green factor smoothed by p_η. For $\eta = 0$, its spatial marginal is exactly the measure $\mu_n^{t,x}$ specified immediately before (2.22), pp. 2152–2153. Its mass is finite because each spatial factor has mass its time gap. Thus,

$$U_n^{\epsilon,0}(t,x) := \int \Phi_n(\mathbf{x}) \mathfrak{g}_{n,t,x}^0(\,\mathrm{d}\mathbf{s},\, \mathrm{d}\mathbf{x})$$

exists as a Bochner integral in L^2. We verify its agreement with the source's pathwise integral, rather than identifying it only by notation. Put $\rho = \mathfrak{g}^0_{n,t,x}$ and $M_n = P_n^{1/2} v_\epsilon^{n/2}$, and denote the pathwise integral by $J_n = \int \Phi_n \, \mathrm{d}\rho$. The continuous field version makes the integrand jointly measurable. Since

$$\int \mathbb{E}|\Phi_n| \, \mathrm{d}\rho \le M_n \rho(1) < \infty, \qquad \|J_n\|_2 \le \int \|\Phi_n\|_2 \, \mathrm{d}\rho \le M_n \rho(1),$$

the pathwise integral exists almost surely and belongs to L^2. For every $Y \in L^2$, Cauchy–Schwarz and Fubini give

$$\mathbb{E}[Y J_n] = \int \mathbb{E}[Y \Phi_n] \, \mathrm{d}\rho.$$

Bochner duality gives the same identity for the L^2 integral. Taking $Y = J_n - U_n^{\epsilon,0}$ identifies the two random variables almost surely. Changing to another jointly measurable field modification leaves the integral unchanged by Fubini. Since the static integrand is independent of the time variables, this is the integral against $\mu_n^{t,x}$ in the source's convention and hence its smoothed approximant $S_{n,\epsilon}$ with common width, from Chen–Hu [20, (3.1), p. 2153, and the convention preceding (2.22)]. Define $U_n^{\epsilon,\eta}$ by the same formula with $\mathfrak{g}^\eta_{n,t,x}$, and retain $U_0^{\epsilon,\eta} = 1$.

Step 5. We identify both inner Green limits in mean square. In the second and mixed moments of these integrals, the Gaussian moment factors are bounded continuous functions of all spatial positions. For each pair of time vectors, weak convergence of the products of Green measures, including mixed products with one width already zero, applies to these functions. The masses are unchanged. A constant depending only on n, ϵ times the product of all time gaps dominates the resulting time integrals. This is integrable on the two bounded time simplexes. Hence, as $\eta \downarrow 0$,

$$\mathbb{E}\left[(U_n^{\epsilon,\eta})^2\right] \longrightarrow \mathbb{E}\left[(U_n^{\epsilon,0})^2\right], \qquad \mathbb{E}\left[U_n^{\epsilon,\eta} U_n^{\epsilon,0}\right] \longrightarrow \mathbb{E}\left[(U_n^{\epsilon,0})^2\right].$$

Subtracting twice the second limit from the two square terms proves $U_n^{\epsilon,\eta} \to U_n^{\epsilon,0}$ in L^2. This identifies the limit with the source approximant, rather than only showing that positive-width approximants are Cauchy. For the target we specify the zero-Green-width object as well. At fixed ϵ, δ, its field covariance is $\gamma_\delta^0(s-r)(p_{2\epsilon} * \Gamma)(y-z)$, where

$$\gamma_\delta^0(u) = \Gamma(\alpha_0)^{-1} \int_0^{1/\delta} e^{-\lambda|u|} \lambda^{\alpha_0 - 1} \, \mathrm{d}\lambda, \qquad \gamma_\delta^0(0) = \frac{\delta^{-\alpha_0}}{\alpha_0 \Gamma(\alpha_0)}.$$

Here $\Gamma(\alpha_0)$ is Euler's gamma function. The variance $v_{\epsilon,\delta} = \gamma_\delta^0(0)(p_{2\epsilon} * \Gamma)(0)$ is finite. This field has a jointly continuous modification. The temporal covariance satisfies $\gamma_\delta^0(0) - \gamma_\delta^0(h) \le C_\delta |h|$, by $1 - e^{-\lambda|h|} \le \lambda|h|$. The spatial increment bound just proved applies to $p_{2\epsilon} * \Gamma$. The joint increment variance is therefore bounded by $C_{\epsilon,\delta}(|h_0| + |h'|^2)$. Gaussian twelfth moments are bounded by $C_{\epsilon,\delta}|h|^6$ for $|h| \le 1$. Kolmogorov's criterion in dimension four supplies the version.

Let $\mathfrak{f}^{\eta}_{n,t,x}$ be the ordered Green measure of the target's kernel (2.16), with $s_{n+1} = t$, $x_{n+1} = x$: its factors are $G_{s_{j+1}-s_j,\eta}$. Define

$$\Psi_n(\mathbf{s}, \mathbf{x}) = \prod_{j=1}^{n} W_{\epsilon,\delta}(s_j, x_j),$$
$$X_n^{\epsilon,\delta,0}(t, x) = \int \Psi_n(\mathbf{s}, \mathbf{x}) \mathfrak{f}^{0}_{n,t,x}(\,\mathrm{d}\mathbf{s},\, \mathrm{d}\mathbf{x}).$$

The Gaussian moment bound is $\|\Psi_n\|_2^2 \le P_n v_{\epsilon,\delta}^n$. Joint measurability, finite measure mass, and the preceding Fubini argument show that this Bochner integral equals the pathwise integral in the target's prescribed convention [17, pp. 13–14]. The same definition at positive η gives $X_n^{\epsilon,\delta,\eta}$ above. Its second and mixed $\eta/0$ moments converge by weak Green convergence against the bounded continuous Gaussian moment functions, with dominating bound a constant times the product of the time gaps. Thus,

$$\|X_n^{\epsilon,\delta,\eta} - X_n^{\epsilon,\delta,0}\|_2 \longrightarrow 0.$$

This proves the inner-limit identification with the target approximant. Both order-zero objects remain one.

Step 6. We remove noise widths and sum the all-time coefficient bound. First take this Green limit in (C.2.9), using the uniform bound (C.2.10). Next send the noise widths to zero. The static fixed-order L^2 limit is from Chen–Hu [20, Theorem 3.8(i), p. 2165]; the target fixed-order limit is from Lemma 2.5.2. Products of two fixed orders converge in L^1, since

$$\|YZ - Y'Z'\|_1 \le \|Y - Y'\|_2 \|Z\|_2 + \|Y'\|_2 \|Z - Z'\|_2.$$

The split sums are finite, and zero-order factors remain one. We obtain

$$A_k(t) \le \left(\frac{C_{\mathrm{low}}^k t^{(3-b_0)k}}{(k!)^2} \right)^{\vartheta} B_k(t)^{1-\vartheta}.$$

Only now use (C.2.8). Neither monotonicity of spatial smoothing nor a uniform smoothed static asymptotic was needed. The identities

$$2\vartheta + (1-\vartheta)(3-\chi) = 3 - \alpha,$$
$$\vartheta(3-b_0) + (1-\vartheta)(4-\chi) = 4 - \alpha - \alpha_0$$

give the coefficient estimate with $C = C_{\mathrm{low}}^{\vartheta} C_{\mathrm{st}}^{1-\vartheta}$. Finally, $A_0 = 1$, $q = 3 - \alpha > 1$, and

$$\sum_{k\ge 0} \frac{z^k}{(k!)^q} \le \left(\sum_{k\ge 0} \frac{z^{k/q}}{k!} \right)^q = e^{q z^{1/q}}, \qquad z \ge 0.$$

The nonnegative full series of Proposition 2.1.1, with $z = C t^{4-\alpha-\alpha_0}$ and $(4-\alpha-\alpha_0)/q = \kappa$, yields the moment estimate. It remains to prove (C.2.7). The precise upper coefficient rate in Chen–Hu's (5.15), p. 2180, at $p = 2$ is

$$\limsup_{k\to\infty} \left((k!)^Q B_k(1) \right)^{1/k} \le 2^{-Q} 2^{\nu_{\mathrm{st}}} \left(\frac{2\sqrt{\mathcal{M}_{\mathrm{st}}}}{\nu_{\mathrm{st}}} \right)^{\nu_{\mathrm{st}}}$$
$$= \Lambda_{\mathrm{st}}.$$

Step 7. We retain the precise asymptotic coefficient rate and its low-order remainder. The factor two follows from $\nu_{\mathrm{st}} - Q = 1$; the logarithm in the source applies to the entire coefficient-rate product. Fix $r > 0$. There is $N_r \geq 1$, depending on the fixed endpoint and r but not on t, such that

$$B_k(1) \leq \frac{(\Lambda_{\mathrm{st}} + r)^k}{(k!)^Q}, \qquad k \geq N_r.$$

Static coefficient homogeneity and the already established coefficient Hölder inequality therefore give, simultaneously for every $t > 0$ and $k \geq N_r$,

$$A_k(t) \leq \frac{D_r^k t^{\beta k}}{(k!)^q}, \qquad D_r = C_{\mathrm{low}}^{\vartheta}(\Lambda_{\mathrm{st}} + r)^{1-\vartheta}, \qquad \beta = 4 - \alpha - \alpha_0.$$

For each $1 \leq k < N_r$ the same inequality with the exact static coefficient gives $A_k(t) \leq d_k t^{\beta k}$, where

$$d_k = \frac{C_{\mathrm{low}}^{\vartheta k} B_k(1)^{1-\vartheta}}{(k!)^{2\vartheta}} < \infty.$$

Adding $A_0 = 1$ and the nonnegative series yields

$$\mathbb{E}u^2(t,x) \leq P_r(t) + e^{qD_r^{1/q} t^{\kappa}}, \qquad P_r(t) = 1 + \sum_{k=1}^{N_r - 1} d_k t^{\beta k}.$$

This finite power sum has $\log P_r(t)/t^{\kappa} \to 0$; its exponents need not be integers. The logarithm of a sum of two positive terms is at most the larger logarithm plus $\log 2$. Consequently, the required limsup is at most $qD_r^{1/q}$. Let $r \downarrow 0$ to obtain (C.2.7). This also covers a zero static rate, without division by that rate. The exact static homogeneity makes N_r independent of t; no target coefficient homogeneity or smoothed static asymptotic was invoked. The finitely many low orders were kept, so this argument does not replace the all-time constant by the asymptotic one. This proves Proposition C.2.5. □

Lean partial

Corollary C.2.6 (Ordinary product and Riesz covariances in dimension three)**.** *Let $d = 3$, $0 < \alpha_0 < 1$, and $1 < \alpha < 2 - \alpha_0$. The coefficient and all-time moment estimates in (C.2.6), and the asymptotic estimate in (C.2.7), hold for either of the following spatial covariances, with $c > 0$:*

1. $\gamma(x) = c \prod_{j=1}^{3} |x_j|^{-a_j}$, *where* $0 \leq a_j < 1$ *and* $\sum_j a_j = \alpha$;
2. $\gamma(x) = c|x|^{-\alpha}$.

In the first case the constant depends only on $a_1, a_2, a_3, c, \alpha_0$; in the second it depends only on α, c, α_0. A zero coordinate exponent denotes a constant factor; the case $a_j = 1$ and any interpretation of it as coordinate white noise are excluded.

Proof. In both cases choose the fixed midpoint $\vartheta = (\alpha_0 + 2 - \alpha)/2$ and define b_0, χ by (C.2.3). Then $\alpha_0 < \vartheta < 2 - \alpha$, and all subsequent choices depend only on the data in the statement. For the product covariance, Lemma C.2.1 supplies b, v by its explicit

interval formula. Its same-amplitude endpoint densities γ_b, γ_v are admissible covariance measures of exponents one and χ. Their common-width Gaussian inequality is exactly Hypothesis C.2.2.

For the Riesz covariance take $\gamma_1(x) = c|x|^{-1}$ and $\gamma_\chi(x) = c|x|^{-\chi}$. Each degree $e \in \{1, \alpha, \chi\}$ is less than three, so the corresponding density is locally integrable and tempered. Positive definiteness follows from the Gaussian mixture

$$c|x|^{-e} = \frac{c}{\Gamma(e/2)} \int_0^\infty s^{e/2-1} e^{-s|x|^2} \, \mathrm{d}s.$$

For a Schwartz autocorrelation, absolute integrability follows from $e < 3$ near zero and rapid decay at infinity. Tonelli and Fubini therefore justify integrating the positive Gaussian quadratic forms. The affine identity $\alpha = \vartheta + (1-\vartheta)\chi$ gives $\gamma_\alpha = \gamma_1^\vartheta \gamma_\chi^{1-\vartheta}$ almost everywhere, with the same amplitude c. Hölder on the Gaussian probability measure proves the required common-width comparison for every ϵ, z. Thus, in both cases all endpoint hypotheses are discharged. Proposition C.2.5 applies. This proves Corollary C.2.6. □

Lean partial

Corollary C.2.7 (Finite sums of linear images)**.** *Let $d = 3$, $0 < \alpha_0 < 1$, and $1 < \alpha < 2 - \alpha_0$. Let Γ_i, $1 \le i \le N$, belong to one of the following classes, always with homogeneity exponent α:*

1. *the ordinary products in Corollary C.2.6;*
2. *the isotropic Riesz covariances in that corollary;*
3. *the plane-supported measures of Lemma C.2.3, with $a_1 + a_2 = \alpha - 1$.*

Let $T_i : \mathbb{R}^3 \to \mathbb{R}^3$ be invertible linear maps, and let $w_i \ge 0$ with $\sum_i w_i > 0$. Then the coefficient, all-time moment, and nonsharp variational estimates (C.2.6)–(C.2.7) hold for

$$\Gamma = \sum_{i=1}^N w_i (T_i)_\# \Gamma_i.$$

The constants may depend on all fixed component data, maps and weights. The endpoints and their variational quantities are those constructed in the proof.

Proof. Choose the common midpoint $\vartheta = (\alpha_0 + 2 - \alpha)/2$, and let b_0, χ be given by (C.2.3). Lemma C.2.1 supplies the ordinary-product endpoints. For a Riesz component use $c_i|x|^{-1}$ and $c_i|x|^{-\chi}$: the Gaussian-mixture calculation in the preceding proof verifies their covariance properties, and $\alpha = \vartheta + (1-\vartheta)\chi$ gives their Gaussian comparison by Hölder. Lemma C.2.3 supplies the plane-supported endpoints. Thus, every component has an endpoint triple with these same fixed parameters.

Apply Lemma C.2.4 first to T_i on each triple, then to the finite weighted sums. The resulting endpoints are

$$\Gamma_{\mathrm{low}} = \sum_i w_i (T_i)_\# \Gamma_{\mathrm{low},i}, \qquad \Gamma_{\mathrm{st}} = \sum_i w_i (T_i)_\# \Gamma_{\mathrm{st},i}.$$

They satisfy Hypothesis C.2.2. The target is nonzero because all components are positive nonzero measures and some weight is positive. Proposition C.2.5 now applies to these actual target and endpoint measures. No addition or coupling identity for random solutions is used. This proves Corollary C.2.7. □

Remark C.2.8 (Scope and calibrations)**.** As $\alpha_0 \downarrow 0$, the time exponent tends to $(4-\alpha)/(3-\alpha)$, agreeing with the static source without interchanging limits or asserting uniform constants. Cauchy–Schwarz gives $\mathbb{E}u(t,x) \le \exp(qC^{1/q}t^{\kappa}/2)$. Conditionally on a first-moment lower bound with the intended constant L_*, both upper constants above are at least $2L_*$, by the same inequality and the argument of Proposition 1.4.4. The author version's printed variational definitions (1.11)–(1.13), with gradient penalties one and one-half, require normalization clarification. Their intended correction remains unspecified. This qualification concerns the source-dependent calibration; neither the first-moment upper constant nor that calibration is an input to the upper-bound proof here. Neither upper constant is asserted sharp. Comparisons with Skorohod exponents are restricted to the published Riesz and strictly positive product-exponent cases satisfying their stated hypotheses; see Balan–Conus [4, Theorem 2.1(b), p. 1492]. Their different solution concept and covariance normalization are not inputs here. The zero-exponent product cases, plane-supported measures, linear images and finite sums above do not enlarge that published comparison. The product construction changes coordinate powers; it is not Euclidean radial lowering of the original covariance. For a general three-dimensional covariance, Hypothesis C.2.2 remains an additional condition, verified here for the stated families and their finite positive sums of invertible linear images. No representation or density theorem for arbitrary covariances is asserted, and no uniform estimate for a limiting infinite mixture is proved. Section 3.3 treats the full covariance class by a different argument. These endpoint comparisons are not inputs to the intrinsic constant theorem 11.2.6.

Euclidean radial lowering can destroy positive definiteness, even for an admissible coordinate-product covariance; see No-go 09. Two other substitutes fail for different reasons: a heat–Mellin square can have infinite local mass, while angular smoothing of a singular covariance cannot retain a uniform isotropic density envelope; see No-gos 12 and 13.

C.3 Physical and spectral energy for measure covariances

This section justifies the positive-measure energy used in (C.2.5). It does not assume Hypothesis C.2.2 or the conditional moment bound. The imported analytic input is the finiteness of the variation on the right of (1.5), stated in the closing sentence of Chen [15, Theorem 1.1, p. 2].

This identification of variational functionals does not remove the additional hypotheses of the separate moment argument. It does not resolve general covariance factorization.

Lemma C.3.1 (Sobolev energy identification)**.** *Let Ξ be a nonnegative, even, positive-definite tempered Radon covariance on $\mathbb{R}^3$, with $\Xi(rA) = r^{3-\chi}\Xi(A)$ for $0 < \chi < 2$. Let μ_Ξ be its positive even spectral measure in the convention $\Xi = \int e^{i\xi\cdot x}\mu_\Xi(\,\mathrm{d}\xi)$, understood distributionally, and use the Fourier transform $\widehat{h}(\xi) = \int e^{-i\xi\cdot x}h(x)\,\mathrm{d}x$. For every real $g \in W^{1,2}(\mathbb{R}^3)$,*

$$\mathcal{Q}_\Xi(g) := \int_{\mathbb{R}^3}\int_{\mathbb{R}^3} g(y+z)^2 g(y)^2\,\mathrm{d}y\,\Xi(\,\mathrm{d}z) = \int_{\mathbb{R}^3} |\widehat{g^2}(\xi)|^2\mu_\Xi(\,\mathrm{d}\xi) < \infty. \tag{C.3.1}$$

The physical expression is independent of the Borel representative of g. There is a finite $C_0 \geq 0$, depending on Ξ, such that

$$\mathcal{Q}_\Xi(g) \leq \frac{1}{2}\|g\|_2^2\|\nabla g\|_2^2 + C_0\|g\|_2^4. \tag{C.3.2}$$

Proof. We use the imported finiteness only on smooth profiles. Two distinct Cauchy–Schwarz bounds control the physical and spectral approximation errors. We then identify both strong limits and pass the quartic bound to the full Sobolev class.

Step 1. We obtain the smooth-profile energy bound. Fourier uniqueness gives $\mu_\Xi(rA) = r^\chi\mu_\Xi(A)$. Since its unit-ball mass is finite, the dyadic estimate with $\sum_{j\geq 0} 2^{j(\chi-2)}$ verifies Dalang's condition. For a real Schwartz function h put

$$\mathscr{E}(h) = \int |\widehat{h}(\xi)|^2\mu_\Xi(\,\mathrm{d}\xi), \qquad Q(f) = \mathscr{E}(f^2).$$

Schwartz Fourier pairing identifies $Q(f)$ with its ordinary positive-measure integral. From the finiteness assertion in Chen [15, Theorem 1.1, closing sentence for the variation in (1.5), p. 2], restricted to real unit-L^2 Schwartz profiles, there is $C_0 \geq 0$ such that $Q(g) \leq \frac{1}{2}\|\nabla g\|_2^2 + C_0$ for $\|g\|_2 = 1$. For $f \neq 0$, quartic homogeneity gives

$$Q(f) = \|f\|_2^4 Q(f/\|f\|_2) \leq \frac{1}{2}\|f\|_2^2\|\nabla f\|_2^2 + C_0\|f\|_2^4.$$

The same inequality is immediate for $f = 0$. Only Schwartz pairings have been used at this point, so this import presupposes no energy identification for nonsmooth profiles. If $N(f)^2 = \|f\|_2^2 + \|\nabla f\|_2^2$, it follows that $Q(f)^{1/2} \leq DN(f)^2$ for some finite D.

Step 2. We estimate the two types of bilinear pairing. We need two different Cauchy–Schwarz inequalities. For real Schwartz f, h, spectral Cauchy–Schwarz gives

$$\begin{aligned} 0 \leq P(f,h) &:= \int \Xi(\,\mathrm{d}z)\int f(y+z)^2 h(y)^2\,\mathrm{d}y \\ &= \int \widehat{f^2}(\xi)\overline{\widehat{h^2}(\xi)}\mu_\Xi(\,\mathrm{d}\xi) \leq Q(f)^{1/2}Q(h)^{1/2}. \end{aligned}$$

Evenness makes the Fourier sign convention in this real pairing immaterial. On the other hand, Cauchy–Schwarz on the positive measure $\mathrm{d}y\,\Xi(\,\mathrm{d}z)$ gives

$$\mathscr{E}(fh) = \int \Xi(\,\mathrm{d}z)\int f(y+z)f(y)h(y+z)h(y)\,\mathrm{d}y \leq Q(f)^{1/2}Q(h)^{1/2}.$$

All these are absolutely convergent Schwartz pairings. In particular, $\mathscr{E}(fh)$ is the quadratic energy of fh, not the quartic expression $Q(fh)$.

Step 3. We compare the physical and spectral approximation maps. Let $\mathfrak{m}(\,\mathrm{d}y,\,\mathrm{d}z) = \mathrm{d}y\,\Xi(\,\mathrm{d}z)$ and define

$$A_f(y,z) = f(y+z)f(y), \qquad B_f(\xi) = \widehat{f^2}(\xi).$$

The measure $\mathfrak{m}$ is positive and sigma-finite. The decomposition

$$A_f - A_h = (f-h)(y+z)f(y) + h(y+z)(f-h)(y)$$

and the bound for P imply

$$\|A_f - A_h\|_{L^2(\mathfrak{m})} \le D\Big(N(f) + N(h)\Big)N(f-h).$$

Since $f^2 - h^2 = (f-h)(f+h)$, the bound for $\mathscr{E}$ gives

$$\|B_f - B_h\|_{L^2(\mu_\Xi)} \le DN(f-h)N(f+h) \le D\Big(N(f) + N(h)\Big)N(f-h).$$

Step 4. We identify their strong limits for a Sobolev profile. Choose real Schwartz $f_n \to g$ in $W^{1,2}$. These estimates make both A_{f_n} and B_{f_n} Cauchy in their respective L^2 spaces. Pass to a subsequence with $f_n \to g$ Lebesgue-almost everywhere. Translation invariance of Lebesgue measure and sigma-finite Fubini give

$$f_n(y+z)f_n(y) \longrightarrow g(y+z)g(y) \quad \text{for } \mathfrak{m}\text{-almost every } (y,z).$$

Thus, the strong $L^2(\mathfrak{m})$ limit is A_g. The same Fubini argument shows that changing the Borel representative of g does not change this limit.

Also

$$\|f_n^2 - g^2\|_1 \le \|f_n - g\|_2(\|f_n\|_2 + \|g\|_2) \longrightarrow 0.$$

Hence, $\widehat{f_n^2} \to \widehat{g^2}$ uniformly on all frequencies. A subsequence of its strong $L^2(\mu_\Xi)$ limit converges μ_Ξ-almost everywhere, and must agree with this uniform limit. Consequently, that strong limit is B_g. For every n, $\|A_{f_n}\|^2_{L^2(\mathfrak{m})} = Q(f_n) = \|B_{f_n}\|^2_{L^2(\mu_\Xi)}$. Passing to the strong limits proves (C.3.1), including finiteness. Passing the Schwartz quartic bound to the same limit proves (C.3.2). This proves Lemma C.3.1. □

In particular, for $\|g\|_2 = 1$ the energy is at most $\|\nabla g\|_2^2/2 + C_0$. Therefore, the supremum of $\mathcal{Q}_\Xi(g)^{1/2} - \|\nabla g\|_2^2$ is finite. Applied to $\Xi = \Gamma_{\mathrm{st}}$, the profile-by-profile identity justifies the measure-form functional in (C.2.5) without assigning a density to the covariance or borrowing a disputed special-case constant.

Appendix D

Static comparisons and the clock obstruction

Two comparisons are natural here, and both stop short of the constant. As the temporal correlation approaches the static case, how do the moments compare with the static ones? And the first moment has a Brownian clock representation: can it be copied for the second moment? The first question gives useful inequalities. The second gets a negative answer at low order, for the construction tried here. This appendix has no figure.

The appendix recalls Proposition 2.1.1, the upper bound of Chapter 3 and the source-version qualifications in Section 1.4. Section D.1 compares the solution with its static counterpart (Proposition D.1.3) and shows, by temporal interpolation, that the upper growth rates are log-convex under the stated assumptions (Proposition D.1.7). Section D.2 tests direct clock copying at small order (Proposition D.2.2). The obstruction concerns that one representation, not every two-clock construction.

Neither comparison identifies the constant of Theorem 11.2.6, and the main argument does not rely on this appendix. Episode ▶ 9 of the video series covers it.

D.1 A static lower comparison and a near-static mean gap

The comparison in this section does not identify the intrinsic constant of Theorem 11.2.6; no novelty or numerical normalization is claimed.

Fix a nonzero spatial covariance in Hypothesis 1.2.1, and put

$$\nu = 3 - \alpha > 1, \qquad a_{\max} = \min(1, 2 - \alpha), \qquad \beta(a) = 4 - \alpha - a,$$
$$\kappa(a) = \frac{\beta(a)}{\nu}, \qquad \kappa_{\mathrm{st}} = \frac{4 - \alpha}{\nu}.$$

Here the temporal exponent varies: $u^{(a)}$ denotes our canonical solution with covariance $|s - r|^{-a}\Gamma$, for $0 < a < a_{\max}$. At $a = 0$ define $u^{(0)} = U$ to be the static canonical solution with the same spatial covariance and initial data $(1, 0)$. This endpoint means the temporal covariance one, not a substitution into $\Gamma_{\mathrm{E}}(a)$. The notation $\gamma^0_{\delta,a}$ records the temporal exponent a in the same Laplace-prefix regularization previously denoted by γ^0_δ.

Imported static input. From Chen–Hu [20, Theorem 1.2, (1.9), p. 2147], the static first-mean rate L_0 exists and

$$0 < L_0 := \lim_{t\to\infty} t^{-\kappa_{\mathrm{st}}} \log \mathbb{E}U(t, x) < \infty, \qquad \lim_{t\to\infty} t^{-\kappa_{\mathrm{st}}} \log \mathbb{E}U(t, x)^2 = 2^{\kappa_{\mathrm{st}}} L_0. \tag{D.1.1}$$

We use only the common $p^{\kappa_{\mathrm{st}}}$ factor for $p = 1, 2$; no numerical value of the static variational constant or its white-noise specialization is adopted. Strict positivity in that formula follows by using a nonzero Gaussian competitor: its interaction and gradient terms scale as $Ac^{\alpha/2}$ and Bc^2, with $A, B > 0$, so their difference is positive for small c. Finiteness and the moment law are the imported source result. The static kernel and integral conventions are its (2.10)–(2.14), p. 2150; the fixed-order limits agree with its Theorem 3.8(i), p. 2165. We supply the static series convergence needed below from our regularized fractional-time upper bound, without using the source's quantitative (4.3). The generalized-covariance convention is explicit in its (2.18), p. 2152. Our spectral ball law gives

$$\int \frac{\mu(\,\mathrm{d}\xi)}{1+|\xi|^2} \le \mu(B_1) + C_\alpha \mu(B_1) \sum_{j\ge 0} 2^{j(\alpha-2)} < \infty.$$

Thus, the static Dalang condition holds in every admissible dimension. Measure homogeneity of degree $d - \alpha$ is equivalent to distributional homogeneity of degree $-\alpha$, so the source's (1.8) applies in its explicit generalized-covariance convention. The static object is identified by its canonical heat-limit expansion; no uniqueness assertion for other mild solutions is used.

For $a > 0$ write $X_n^{(a)}$ for our fixed-order terms; at zero use the corresponding static terms. Set

$$m_k(a) = \mathbb{E}X_{2k}^{(a)}(1,0), \qquad m_0(a) = 1.$$

Lemma D.1.1 (Mean coefficients for the power covariance)**.** *For every $0 \le a < a_{\max}$, the coefficients $m_k(a)$ are nonnegative, and*

$$\mathbb{E}u^{(a)}(t,x) = \sum_{k\ge 0} m_k(a) t^{\beta(a)k}. \tag{D.1.2}$$

The series $F_a(z) = \sum_{k\ge 0} m_k(a) z^k$ is finite for every $z \ge 0$. If $0 < a < b < a_{\max}$, then

$$m_k(a) \le m_k(0)^{1-a/b} m_k(b)^{a/b}, \qquad k \ge 1. \tag{D.1.3}$$

Proof. We construct the static endpoint series using a regularized positive comparison. We then interpolate single-chain coefficients on one common spatial measure, remove the spatial width, and recover the mean series by homogeneity.

Step 1. We construct the static fixed-order limits and summable series. We first justify the static endpoint and its norm series. At positive spatial widths its ordered terms are the bounded-variance Gaussian Bochner integrals of Lemma 3.3.6, with a time-constant field. Lemma 2.5.1, applied with temporal multiplier one to the diagonal and mixed-width second moments, gives a common finite diagram limit. The same Hilbert Cauchy argument as in Lemma 2.5.2 therefore gives the static fixed-order limits $X_n^{(0)}$, with the source's heat-limit convention. This uses no infinite solution series.

Fix any $b_0 \in (0, a_{\max})$ and $\delta_0 > 0$, and put $c = \gamma^0_{\delta_0,b_0}(1) > 0$. Let $U_N^\epsilon(r;1,x)$ be the static partial series at horizon one and noise amplitude $r > 1$. Compare its finite Wick sum with that of the fractional-time partial series at widths ϵ, δ_0, exponent b_0 and

amplitude $r/\sqrt{c}$. Since $\gamma^0_{\delta_0,b_0}(s-r') \geq c$ for $s, r' \in [0,1]$, every pair factor on the second side dominates the static pair factor. Positivity, then the full regularized bound (3.3.31), gives

$$\mathbb{E}|U^\epsilon_N(r;1,x)|^2 \leq \mathbb{E}|u^{\epsilon,\delta_0}_{b_0}(r/\sqrt{c};1,x)|^2 \leq B_{b_0}(1;r/\sqrt{c}) < \infty,$$

uniformly in N, ϵ. The notation B_{b_0} means the bound in (3.3.31) at temporal exponent b_0. Both positive-width full series exist by Lemma 3.3.6. Letting $N \to \infty$ at fixed ϵ preserves this bound. Lemma 3.3.7 now applies to the static family (with only the spatial width varying). It proves absolute L^2 convergence of its limiting series at horizon one, with geometric coefficient bounds for every $r > 1$. Static fixed-order homogeneity gives

$$\|X^{(0)}_n(t,x)\|_2 = t^{(4-\alpha)n/2}\|X^{(0)}_n(1,0)\|_2.$$

Choosing $r > \max\{1, t^{(4-\alpha)/2}\}$ in those bounds proves norm summability at every fixed $t > 0$. The resulting series has precisely the source's canonical static kernels and fixed-order limits.

Step 2. We interpolate the temporal powers at fixed spatial smoothing. For a single chain of length $2k$, use the initial-chain variables of Proposition 2.1.1. At common positive spatial width ϵ, let $\omega_{\epsilon,D}$ be its finite positive spatial Green–Wick measure on the unit time simplex, with covariance $\gamma_{2\epsilon}$ on every pair. It is finite because that covariance is bounded and the Green masses are the time gaps. Define

$$m^\epsilon_k(a) = \sum_{D\in\Pi_k} \int \prod_{\{j,h\}\in D} |s_j - s_h|^{-a}\, \mathrm{d}\omega_{\epsilon,D}, \qquad 0 \leq a < a_{\max}.$$

These time integrals for the power covariance are finite. At fixed ϵ the spatial factors and Green masses are bounded on the finite horizon; the disjoint pair endpoints give integrable powers on the full time cube since $a < 1$. Diagonals are null there. On the disjoint union of the pairing measures, the time multiplier at a is exactly the a/b power of its multiplier at b. Hölder's inequality therefore gives

$$m^\epsilon_k(a) \leq m^\epsilon_k(0)^{1-a/b} m^\epsilon_k(b)^{a/b}.$$

This is an identity for the power covariance; no exponent-dependent Laplace cutoff or Euler Gamma normalization is being interpolated.

Step 3. We remove the common spatial width. We justify removal of the common spatial width. For each positive exponent, the proof of Lemma 2.5.2 gives this limit with the power covariance as well. Indeed, writing $F_{\epsilon,\eta,D}$ for the diagram with common temporal cutoff η, (2.5.5) gives

$$F_{\epsilon,\eta,D} \leq F_{\epsilon,0,D} \leq F_{\epsilon,\eta,D} + r_a(\eta), \qquad r_a(\eta) \longrightarrow 0,$$

uniformly in ϵ. First pass to the spatial limit at fixed η, then send η to zero. The resulting limit is exactly the joint diagram value from that lemma. At zero exponent the multiplier is one, so Lemma 2.5.1 gives the spatial limit directly; the positive-width Wick

calculation and the imported static fixed-order convergence identify it with the static expectation. Thus, $m_k^\epsilon(a) \to m_k(a)$ at all three fixed exponents $0, a, b$, proving (D.1.3) and nonnegativity. No convergence uniform in a is claimed.

Step 4. We identify the homogeneous positive mean series. Scaling all times and spatial displacements by t in a regularized one-chain diagram gives the factor $t^{2(2k)-\alpha k-ak} = t^{\beta(a)k}$ and changes the spatial width to ϵ/t^2. Passing to the just established limits proves $\mathbb{E}X_{2k}^{(a)}(t,x) = t^{\beta(a)k} m_k(a)$. Odd expectations vanish by Wick's formula. For positive a the independently proved norm summability in Lemma 2.6.1 justifies the mean-series interchange. At zero the static norm series just proved does so, with nonnegative even means. This proves (D.1.2). Since $\beta(a) > 0$, every $z \geq 0$ equals $t^{\beta(a)}$ for some $t \geq 0$, and the series is finite. This proves Lemma D.1.1. □

Lean full

Lemma D.1.2 (Type of a positive coefficient series)**.** *Let $\nu \geq 1$, $c_k \geq 0$, $c_0 = 1$, and suppose $F(z) = \sum_{k\geq 0} c_k z^k < \infty$ for every $z \geq 0$. If*

$$\tau = \limsup_{z\to\infty} z^{-1/\nu} \log F(z) < \infty,$$

then

$$K := \limsup_{k\to\infty} \left((k!)^\nu c_k\right)^{1/k} < \infty, \qquad \tau = \nu K^{1/\nu}. \tag{D.1.4}$$

Conversely, finite K implies the same finite τ and equality.

Proof. We first bound each coefficient by evaluating the positive series at an order-dependent argument. Conversely, a finite coefficient type gives an exponential series bound after keeping finitely many low orders separately.

Step 1. We pass from growth type to coefficient type. If $\tau < \infty$, choose $L > \tau$. Since $c_0 = 1$, $\tau \geq 0$, and continuity of the power series on compact positive intervals gives $F(z) \leq C_L e^{Lz^{1/\nu}}$ for all $z \geq 0$. For $k \geq 1$, the inequality $c_k z^k \leq F(z)$ at $z = (\nu k/L)^\nu$ yields

$$c_k \leq C_L e^{\nu k} \left(\frac{L}{\nu k}\right)^{\nu k}.$$

Monotonicity of $\log x$ and integration on $[1, k]$ give

$$k\log k - k + 1 \leq \log(k!) \leq k\log k - k + 1 + \log k.$$

Consequently, $K \leq (L/\nu)^\nu$. Letting $L \downarrow \tau$ proves $K \leq (\tau/\nu)^\nu$, including $K = 0$ when $\tau = 0$.

Step 2. We recover growth type from the coefficient bound. Conversely, for any $A > K$ all sufficiently large coefficients obey $c_k \leq A^k/(k!)^\nu$. Hence, for a polynomial P with nonnegative coefficients,

$$F(z) \leq P(z) + \sum_{k\geq 0} \frac{(Az)^k}{(k!)^\nu} \leq P(z) + \exp\{\nu(Az)^{1/\nu}\}.$$

The last inequality is the elementary ℓ^ν bound $\sum a_k^\nu \le (\sum a_k)^\nu$, applied to $a_k = (Az)^{k/\nu}/k!$. The polynomial contributes zero to the normalized logarithmic growth. Therefore, $\tau \le \nu A^{1/\nu}$; let $A \downarrow K$. Combining both inequalities proves the equality when either quantity is finite. This proves Lemma D.1.2. □

Proposition D.1.3 (Static temporal-minimum comparison)**.** *For every* $0 < a < a_{\max}$*,* $T > 0$ *and* $p \in \{1, 2\}$*,*

$$\mathbb{E}[u^{(a)}(T, x)^p] \ge \mathbb{E}\left[U\left(T^{1-a/(4-\alpha)}, x\right)^p\right]. \tag{D.1.5}$$

In particular,

$$\liminf_{T\to\infty} T^{-\kappa(a)} \log \mathbb{E}[u^{(a)}(T, x)^p] \ge p^{\kappa_{\mathrm{st}}} L_0, \qquad p = 1, 2. \tag{D.1.6}$$

Proof. We compare finite regularized moments with a static model using the minimum temporal covariance on the horizon. We remove regularizations at fixed order, sum, and then identify the static effective time.

Step 1. We compare the finite expected powers at positive widths. Fix positive common spatial and temporal noise widths ϵ, δ. On $[0, T]$, the source's Laplace-prefix temporal covariance satisfies

$$\gamma^0_{\delta,a}(s - r) \ge c_{\delta,T} := \gamma^0_{\delta,a}(T) > 0, \qquad c_{\delta,T} \longrightarrow T^{-a} \quad (\delta \downarrow 0).$$

Compare the order-N partial series of $u^{(a)}$ with the same partial series of a static model having covariance $c_{\delta,T}\gamma_{2\epsilon}$. At positive widths, the mean or squared moment is a finite Wick sum of the same terminal Green kernels and pairings. Every spatial factor is the same nonnegative $\gamma_{2\epsilon}$; every time factor on the first side is at least $c_{\delta,T}$. Thus, the finite expected powers are ordered for $p = 1, 2$. For $d = 3$, remove Green smoothing first at these fixed positive noise widths using the bounded covariance calculation preceding Lemma 2.5.1.

Step 2. We pass fixed-order limits and the convergent series. Now send (ϵ, δ) jointly to zero at fixed N. Lemma 2.5.2 gives the fractional-time L^2 limits. Static fixed-order L^2 convergence gives all static split products in L^1, by Cauchy–Schwarz. Dependence on $c_{\delta,T}$ is a finite polynomial at fixed order, so its limit is the static model with noise amplitude $\sigma = T^{-a/2}$. This requires no uniform approximation in T or in a varying infinite-order series. At every fixed $\sigma, T > 0$, static norm homogeneity gives

$$\sigma^n \|X^{(0)}_n(T, x)\|_2 = \|X^{(0)}_n(\sigma^{2/(4-\alpha)}T, x)\|_2.$$

Thus, the amplitude-scaled static norm series is summable at the effective time already covered by Lemma D.1.1. Finally, let $N \to \infty$ using the two L^2 expansions, with the static one supplied in Lemma D.1.1. Means and squared moments converge, preserving the finite-order inequality. No covariance-order coupling of the two Gaussian fields is asserted.

Step 3. We identify the static amplitude clock and its rate. Write U_σ for the static solution with noise amplitude σ. In its pth moment, a total order $2k$ has amplitude factor σ^{2k} and, by static diagram homogeneity, time factor $T^{(4-\alpha)k}$. For $p = 1, 2$, the finite sums and then the convergent nonnegative moment series therefore give the exact identity

$$\mathbb{E}[U_\sigma(T,x)^p] = \mathbb{E}[U(\sigma^{2/(4-\alpha)}T,x)^p].$$

Only moments are identified; no spatially indexed random fields are coupled. At $\sigma = T^{-a/2}$ this proves (D.1.5). The effective static time tends to infinity and

$$\left(T^{1-a/(4-\alpha)}\right)^{\kappa_{\mathrm{st}}} = T^{\kappa(a)}.$$

The imported static rates (D.1.1) now prove (D.1.6). This proves Proposition D.1.3. □

Proposition D.1.4 (Near-static strict gap from the mean rate)**.** *Define*

$$M(a) = \limsup_{T\to\infty} T^{-\kappa(a)} \log \mathbb{E}u^{(a)}(T,x), \qquad K(a) = \limsup_{k\to\infty} \left((k!)^\nu m_k(a)\right)^{1/k}.$$

Then $K(0) = (L_0/\nu)^\nu > 0$, and $K(b) < \infty$ for every $0 < b < a_{\max}$. Fix such a b and choose any finite $B_b \geq \max\{2K(0), K(b)\}$. For $0 < a < b$,

$$M(a) \leq L_0 \left(\frac{B_b}{K(0)}\right)^{a/(b\nu)}. \tag{D.1.7}$$

In particular, with

$$a_* := \frac{b\log 2}{\log(B_b/K(0))} \in (0,b], \tag{D.1.8}$$

every $0 < a < a_*$ satisfies

$$\liminf_{T\to\infty} T^{-\kappa(a)} \log \mathbb{E}[u^{(a)}(T,x)^2] > 2M(a). \tag{D.1.9}$$

Proof. We convert mean growth rates into coefficient types. Coefficient interpolation then bounds the positive-exponent mean rate, and the static lower comparison gives the strict gap on the stated window.

Step 1. We identify finite endpoint coefficient types. By Lemma D.1.1, the substitution $z = T^{\beta(a)}$ identifies the normalized logarithmic type of $F_a(z)$ with the mean limsup $M(a)$; at zero it equals L_0. The imported static law and Lemma D.1.2 give $K(0) = (L_0/\nu)^\nu$. For positive b, Cauchy–Schwarz and Theorem 3.3.8, applied at temporal exponent b, give $M(b) < \infty$. The same type lemma therefore gives $K(b) < \infty$. There is no use of a printed first-moment rate constant.

Step 2. We interpolate the coefficient types and apply the static lower rate. Multiplying (D.1.3) by $(k!)^\nu$, taking kth roots and then limsups yields

$$K(a) \leq K(0)^{1-a/b} B_b^{a/b}.$$

To justify this even if coefficients vanish, for any $\eta > 0$ both endpoint root sequences are eventually bounded by $K(0) + \eta$ and $B_b + \eta$; take their weighted product and then let $\eta \downarrow 0$. Lemma D.1.2 now gives

$$M(a) = \nu K(a)^{1/\nu} \le L_0 \left(\frac{B_b}{K(0)} \right)^{a/(b\nu)},$$

proving (D.1.7). Since $B_b/K(0) \ge 2$, the window in (D.1.8) is positive and at most b. For $0 < a < a_*$,

$$2M(a) < 2L_0 \cdot 2^{1/\nu} = 2^{\kappa_{\mathrm{st}}} L_0,$$

because $\kappa_{\mathrm{st}} = 1 + 1/\nu$. Combine this with Proposition D.1.3 at $p = 2$. This proves Proposition D.1.4. □

Remark D.1.5 (Scope and calibrations)**.** The static lower comparison holds at every admissible positive temporal exponent; the strict gap from twice the first-moment limsup is asserted only in the nonempty window (D.1.8). Its endpoint depends on the fixed covariance and the chosen reference exponent b; no uniformity over covariance shapes is claimed. As $a \downarrow 0$, the comparison clock has exponent tending to one, the growth exponent tends to κ_{st}, and the mean upper bound tends to L_0. The static second-moment constant is exactly $2^{\kappa_{\mathrm{st}}} L_0$.

The gap concerns $\mathbb{E}u$, which is positive by its pairing series; no theorem for $\mathbb{E}|u|$ or all moment orders is asserted. If an intended source first-mean lower rate $L_*(a)$ is valid, then $L_*(a) \le M(a)$, so (D.1.9) also improves the corresponding Jensen rate $2L_*(a)$ in this window. This does not establish the original lower target $2^{\kappa_{\mathrm{st}}} L_*(a)$, or either sharp bound for arbitrary a. The intrinsic formula in Theorem 11.2.6 does not identify either printed source endpoint. The proof here uses the ordinary Stratonovich pairing expansion, including self-contractions; no Skorohod result or sibling-project development is made.

D.1.1 Temporal interpolation of the full moment

The constant at a fixed positive temporal exponent is identified in Theorem 11.2.6.

Retain the fixed nonzero covariance and the notation of this section. For $p = 1, 2$, set $c_{p,0}(a) = 1$ and, for $k \ge 1$,

$$c_{1,k}(a) = m_k(a), \qquad c_{2,k}(a) = \sum_{m=0}^{2k} \mathbb{E}[X_m^{(a)}(1,0) X_{2k-m}^{(a)}(1,0)]. \tag{D.1.10}$$

The zero-exponent terms are the static limits constructed in Lemma D.1.1.

Lemma D.1.6 (Interpolation of the full moment coefficients)**.** *For $0 \le a < a_{\max}$ and $p = 1, 2$, the coefficients are nonnegative and*

$$\mathbb{E}[u^{(a)}(t,x)^p] = \sum_{k \ge 0} c_{p,k}(a) t^{\beta(a)k} < \infty, \qquad t > 0. \tag{D.1.11}$$

If $0 \le a_1 < a < a_2 < a_{\max}$ and $\theta = (a - a_1)/(a_2 - a_1)$, then

$$c_{p,k}(a) \le c_{p,k}(a_1)^{1-\theta} c_{p,k}(a_2)^{\theta}, \qquad k \ge 0. \tag{D.1.12}$$

Proof. We interpolate the full coefficient sum at common spatial smoothing, retaining all splits. We then identify each endpoint limit and use diagram homogeneity to obtain the full positive moment series.

Step 1. We place the mean and second-moment diagrams on their common measures. Work first at a common positive spatial noise width ϵ and at unit horizon. For each split $m+n=2k$ and pairing D, let $\omega_{\epsilon,m,n,D}$ be the finite positive spatial Green–Wick measure in the initial-chain convention of Proposition 2.1.1, with covariance $\gamma_{2\epsilon}$. For $p=1$ take the disjoint union over the single specified split $(m,n)=(0,2k)$ and all pairings. For $p=2$, take the disjoint union over every $m=0,\dots,2k$ and all pairings. In particular, the two empty-chain orientations are distinct terms for $p=2$, whereas $p=1$ has just one. Wick's formula has coefficient one for each pairing on each ordered domain.

Step 2. We interpolate the temporal power factors. With $\omega_{\epsilon,p,k}$ denoting this disjoint-union measure, define its time integral for the power covariance by

$$c^{\epsilon}_{p,k}(a)=\int \prod_{\{j,h\}\in D}|s_j-s_h|^{-a}\,\mathrm{d}\omega_{\epsilon,p,k}.$$

The pairing label in the multiplier is that of its component. These integrals are finite: the spatial covariances and Green masses are bounded on the unit horizons, and the disjoint pair endpoints give integrable factors on the full time cube since $a<1$. The multiplier at a is exactly the product of the endpoint multipliers to powers $1-\theta,\theta$, off null diagonals. Hölder's inequality on the disjoint union gives

$$c^{\epsilon}_{p,k}(a)\le c^{\epsilon}_{p,k}(a_1)^{1-\theta}c^{\epsilon}_{p,k}(a_2)^{\theta}.$$

Step 3. We identify all fixed-order limits. For each fixed positive endpoint, the all-chain bound (2.5.5) and the common temporal-cutoff sandwich used in Lemma D.1.1 identify the time-domain spatial limit with the joint diagram value. This applies to every unequal or empty split, not only to a mean diagram. At exponent zero, the multiplier is one and Lemma 2.5.1 gives the same limit. The static diagonal and mixed-width Gaussian limits identify those diagram values with the split expectations of the constructed static terms: products converge in L^1 by Cauchy–Schwarz, and the terminal-to-initial chain reversal is the one in Proposition 2.1.1, applied before removing widths. For positive exponents this identification is Proposition 2.1.1. The union is finite at fixed k; passing to the spatial limit proves (D.1.12) and nonnegativity. No interpolation of exponent-dependent Laplace prefixes is used.

Step 4. We use homogeneity and the convergent moment series. Every diagram has $2k$ time Jacobians, $2k$ Green scaling factors, k spatial covariance factors and k temporal factors. Thus, its homogeneous time degree is $4k-\alpha k-ak=\beta(a)k$, including both empty-chain cases. For positive a, the full second-moment series follows from Proposition 2.1.1; the mean series is (D.1.2). At zero, the static norm series gives convergence of the finite partial means and squared moments. Each finite moment expansion has nonnegative mixed terms, so its increasing limit may be regrouped by total order $2k$. The homogeneity just proved then gives (D.1.11). This proves Lemma D.1.6. □

For $p = 1, 2$ define the normalized time growth rates

$$\begin{aligned} \overline{\Lambda}_p(a) &= \limsup_{T\to\infty} T^{-\kappa(a)} \log \mathbb{E}[u^{(a)}(T,x)^p], \\ \underline{\Lambda}_p(a) &= \liminf_{T\to\infty} T^{-\kappa(a)} \log \mathbb{E}[u^{(a)}(T,x)^p]. \end{aligned} \tag{D.1.13}$$

Here $p = 1$ concerns $\mathbb{E}u$, not $\mathbb{E}|u|$.

Lean partial

Proposition D.1.7 (Log-convexity of the upper growth type)**.** *The functions $\overline{\Lambda}_p(a)$, $p = 1, 2$, are positive and finite on $0 \le a < a_{\max}$. For the endpoints and θ in Lemma D.1.6,*

$$\overline{\Lambda}_p(a) \le \overline{\Lambda}_p(a_1)^{1-\theta} \overline{\Lambda}_p(a_2)^{\theta}. \tag{D.1.14}$$

In particular, $\log \overline{\Lambda}_p$ is convex and $\overline{\Lambda}_p$ is continuous on $(0, a_{\max})$.

Proof. We establish that all rates are positive and finite, convert coefficient interpolation into growth-type interpolation, and then use convex secant slopes to obtain interior continuity.

Step 1. We verify positivity and finiteness of the rates. Put $C_p = p^{\kappa_{\mathrm{st}}} L_0 > 0$. The imported static law gives $\overline{\Lambda}_p(0) = \underline{\Lambda}_p(0) = C_p$. Proposition D.1.3 gives $\underline{\Lambda}_p(a) \ge C_p$ for positive a. The full upper bound gives finiteness for $p = 2$. Cauchy–Schwarz gives finiteness for $p = 1$, whose mean is at least one by its positive series. Hence, all logarithms and rates used here are well defined, positive and finite.

Step 2. We transfer coefficient interpolation to the logarithmic type. Let $F_{p,a}(z) = \sum_{k\ge 0} c_{p,k}(a) z^k$. It is finite for every $z \ge 0$, by Lemma D.1.6. Its normalized logarithmic type equals $\overline{\Lambda}_p(a)$: spatial stationarity makes the moment independent of x, while $z = T^{\beta(a)}$ and $z^{1/\nu} = T^{\kappa(a)}$. Lemma D.1.2 therefore gives

$$K_p(a) := \limsup_{k\to\infty} \left((k!)^{\nu} c_{p,k}(a)\right)^{1/k} = \left(\frac{\overline{\Lambda}_p(a)}{\nu}\right)^{\nu}.$$

Multiplying the coefficient interpolation by $(k!)^{\nu}$, taking kth roots and then limsups gives

$$K_p(a) \le K_p(a_1)^{1-\theta} K_p(a_2)^{\theta}.$$

More explicitly, the two endpoint root sequences are eventually bounded by $K_p(a_i) + \eta$; let $\eta \downarrow 0$ after taking their weighted product. This argument permits zero or oscillating coefficient subsequences. Taking the $1/\nu$ power and multiplying by ν proves (D.1.14).

Step 3. We obtain continuity from the convex slope bounds. For completeness, continuity follows directly from secant slopes. Write $f = \log \overline{\Lambda}_p$. If $L < l \le x < y \le r < R$ are in $(0, a_{\max})$, convexity gives

$$\frac{f(l) - f(L)}{l - L} \le \frac{f(y) - f(x)}{y - x} \le \frac{f(R) - f(r)}{R - r}.$$

Both outer slopes are finite. They bound the absolute difference quotient on each compact interior interval, proving continuity of f, and hence of its exponential. This proves Proposition D.1.7. □

Lean partial

Corollary D.1.8 (Recovery of the static moment constant)**.** *Put* $C_p = p^{\kappa_{\mathrm{st}}} L_0$, $p = 1, 2$. *For every fixed* $0 < b < a_{\max}$ *and* $0 < a < b$,

$$C_p \le \underline{\Lambda}_p(a) \le \overline{\Lambda}_p(a) \le C_p \left(\frac{\overline{\Lambda}_p(b)}{C_p} \right)^{a/b}. \tag{D.1.15}$$

Consequently,

$$\lim_{a \downarrow 0} \underline{\Lambda}_p(a) = \lim_{a \downarrow 0} \overline{\Lambda}_p(a) = C_p, \qquad p = 1, 2, \tag{D.1.16}$$

and

$$\lim_{a \downarrow 0} \frac{\underline{\Lambda}_2(a)}{\overline{\Lambda}_1(a)} = 2^{\kappa_{\mathrm{st}}}. \tag{D.1.17}$$

Proof. The lower estimate is Proposition D.1.3. For the upper estimate, apply Proposition D.1.7 with endpoints $0, b$, using $\overline{\Lambda}_p(0) = C_p$. This proves (D.1.15). The finite ratio $\overline{\Lambda}_p(b)/C_p$ is at least one. With b and the covariance fixed, its a/b power tends to one. Squeezing both rates proves (D.1.16). The numerator and denominator in (D.1.17) tend to $2^{\kappa_{\mathrm{st}}} L_0$ and $L_0 > 0$, respectively. Division gives the asserted ratio. This proves Corollary D.1.8. □

Remark D.1.9 (Order of limits and comparison with the intrinsic constant)**.** The static calibration now concerns the constant, not only the time exponent. It is an iterated statement: first take a time liminf or limsup at each fixed a, with its own normalization $T^{-\kappa(a)}$, and then send $a \downarrow 0$. No uniformity over covariances or T, no simultaneous limit, and no existence of the time limit at a fixed positive a follows. Only the upper rate is asserted to be log-convex on the interior.

Neither $L_*(a)$ nor $L^*(a)$ enters this argument. The constant L_0 is the static first-mean rate. Parameter continuity alone does not identify the conjectured curve. The separate intrinsic second-moment value is proved in Theorem 11.2.6. No all-p, absolute-first-moment, Skorohod, novelty or circulation result is claimed.

D.2 A small-order test for direct Brownian clock copying

The result concerns a specified gap-transform substitution. It does not rule out ordering corrections, a diagonal-only representation, one-sided/asymptotic use, or the original sharp conjecture.

Theorem 6.1 of [17, pp. 37–42] represents the time Laplace transform of a *fixed-order* mean by a spatial Brownian path and an independent scalar Brownian clock. The proof uses nonnegative cut sums c_l, obtained from one-chain time order on p. 38, before the wave-to-heat substitution on p. 39. Remark 6.3, p. 42, singles out that order as the obstruction for more copies. We test the direct replacement by two spatial Brownian paths and two scalar Brownian clocks, without an additional ordering weight.

All transforms below are at fixed total order. We begin with the original admissible case $d = \alpha = 1$, $\Gamma = \delta_0$, $0 < a < 1$, and $G_s(y) = \frac{1}{2}\mathbf{1}_{\{|y|<s\}}$. This is a falsification case for an intended general representation, not a restriction of Theorem 1.5.2.

Lean full

Lemma D.2.1 (White-space low-order Laplace transforms)**.** *The* $(1,1)$ *cross-pair gap transform is*

$$\begin{aligned} K_\times(\theta_1,\theta_2) &:= \int_0^\infty \int_0^\infty e^{-\theta_1 s-\theta_2 t}|s-t|^{-a}\frac{\min(s,t)}{2}\,\mathrm{d}s\,\mathrm{d}t \\ &= \frac{\Gamma_{\mathrm{E}}(1-a)}{2(\theta_1+\theta_2)^2}\big(\theta_1^{a-1}+\theta_2^{a-1}\big), \qquad \theta_1,\theta_2>0. \end{aligned} \tag{D.2.1}$$

In particular, $K_\times(\theta,\theta) = \Gamma_{\mathrm{E}}(1-a)/(4\theta^{3-a})$*. For the empty-plus-length-two self-pair, independent gap damping gives*

$$K_{\mathrm{self}}(\eta_1,\eta_2) := \int_0^\infty \int_0^\infty e^{-\eta_1 r_1-\eta_2 r_2} r_2^{-a}\frac{r_1}{2}\,\mathrm{d}r_1\,\mathrm{d}r_2 = \frac{\Gamma_{\mathrm{E}}(1-a)}{2\eta_1^2\eta_2^{1-a}}. \tag{D.2.2}$$

Proof. We compute the cross-pair transform by splitting its time domain into two cones, then evaluate the independent gap integrals for the self-pair.

Step 1. We compute the cross-pair Laplace transform. The spatial cross factor is

$$\int G_s(y)G_t(z)\delta_0(y-z)\,\mathrm{d}y\,\mathrm{d}z = \frac{1}{4}\int \mathbf{1}_{\{|y|<s\wedge t\}}\,\mathrm{d}y = \frac{\min(s,t)}{2}.$$

Split its time integral into $s = t+v$ and $t = s+v$, with $v>0$. Each part is one half the product of

$$\int_0^\infty te^{-(\theta_1+\theta_2)t}\,\mathrm{d}t = (\theta_1+\theta_2)^{-2}$$

and $\int_0^\infty e^{-\theta_i v}v^{-a}\,\mathrm{d}v = \Gamma_{\mathrm{E}}(1-a)\theta_i^{a-1}$. All integrands are nonnegative and finite since $a<1$, so Tonelli justifies the separation. This proves (D.2.1).

Step 2. We compute the self-pair gap transform. For one length-two chain, its delta covariance forces the two positions equal. The second Green factor is $G_{r_2}(0) = 1/2$, and integration of the first gives mass r_1. The time difference is r_2. The two elementary Laplace integrals therefore give (D.2.2). This proves Lemma D.2.1. □

The source's analytic time covariance is

$$\gamma_a^{\mathrm{an}}(z) = \big(z\,\operatorname{sgn}\Re z\big)^{-a}, \qquad \Re z \neq 0,$$

with the power taken on the right half-plane. For $r>0, v\geq 0$, put

$$\Psi_a(r,v) = \frac{1}{\Gamma_{\mathrm{E}}(a)}\int_0^\infty \lambda^{a-1}e^{-r\lambda-v\lambda^2/2}\,\mathrm{d}\lambda. \tag{D.2.3}$$

From the source's complex Laplace identity [17, (6.3), p. 41], and the Gaussian characteristic function, $\Psi_a(r,v) = \mathbb{E}(r+iZ)^{-a}$ when Z is centered normal with variance v. Fubini

at fixed $r > 0$ is justified by $\int_0^\infty \lambda^{a-1} e^{-r\lambda}\,\mathrm{d}\lambda < \infty$. In particular, Ψ_a is nonnegative, decreases with v, and $\Psi_a(r,v) \le r^{-a}$.

Return to an arbitrary nonzero covariance in Hypothesis 1.2.1, with temporal exponent a, so $0 < a < 1$, $0 < \alpha < 2$ and $a + \alpha < 2$. Define

$$h_\Gamma(w) = \int e^{-w|\xi|^2/2} \mu(\,\mathrm{d}\xi) = (p_w * \Gamma)(0), \qquad \mathcal{R}_\Gamma(q) = \int \frac{\mu(\,\mathrm{d}\xi)}{q^2 + |\xi|^2}.$$

Both are positive and finite for $w, q > 0$. Spectral homogeneity gives $h_\Gamma(w) = w^{-\alpha/2} h_\Gamma(1)$ and $\mathcal{R}_\Gamma(q) = q^{\alpha-2}\mathcal{R}_\Gamma(1)$. The cross-pair gap transform at common damping is

$$K_\Gamma(\theta) = N_2(\theta)^2$$

with temporal exponent a in (2.3.1). This is the spatial-regularization limit of the $(1,1)$ diagram.

Let B_1, B_2 be independent spatial standard Brownian motions. For auxiliary standard Brownian clocks with $\mathbb{E}[\beta_1(u)\beta_2(v)] = \rho \min(u,v)$, $-1 \le \rho \le 1$, independent of the spatial paths, the clock difference has variance

$$v_\rho(u,v) = u + v - 2\rho \min(u,v).$$

At common damping $\theta > 0$, the direct unweighted, unrestricted two-clock covariance substitution yields the averaged candidate

$$J_{\Gamma,\rho}(\theta) := \frac{1}{4}\int_0^\infty \int_0^\infty e^{-\theta^2(u+v)/2} h_\Gamma(u+v) \Psi_a(\theta|u-v|, v_\rho(u,v))\,\mathrm{d}u\,\mathrm{d}v. \tag{D.2.4}$$

Values on $u = v$ do not affect the integral. The factor $1/4$ is one factor $1/2$ for each wave-to-heat gap transform; $h_\Gamma(u+v)$ is the spatial average of $\Gamma(B_1(u) - B_2(v))$. This average is interpreted by spatial heat regularization. For the white covariance it is $(2\pi(u+v))^{-1/2}$. The analytic covariance, not its absolute-value bound, is being copied.

Lean full

Proposition D.2.2 (Obstruction to unweighted constant-correlation clock copying)**.** *For every covariance and parameters just specified, put*

$$w_\theta(\lambda) = \frac{\lambda^{a-2}}{2\theta\Gamma_{\mathrm{E}}(a)}\Big(\mathcal{R}_\Gamma(\theta) - \mathcal{R}_\Gamma(\theta+\lambda)\Big), \qquad \lambda > 0. \tag{D.2.5}$$

This is a positive integrable density, and

$$\begin{aligned} K_\Gamma(\theta) &= \int_0^\infty w_\theta(\lambda)\,\mathrm{d}\lambda, \\ 0 < J_{\Gamma,\rho}(\theta) \le J_{\Gamma,1}(\theta) &= \int_0^\infty \frac{2\theta}{2\theta+\lambda} w_\theta(\lambda)\,\mathrm{d}\lambda < K_\Gamma(\theta). \end{aligned} \tag{D.2.6}$$

When $\alpha = 1$,

$$J_{\Gamma,1}(\theta) = (2 - 2^a) K_\Gamma(\theta). \tag{D.2.7}$$

Thus, this direct analytic clock-copying family, including independent clocks and a single shared clock, fails to reproduce the cross-pair transform throughout the original nonzero covariance class.

Proof. We first compute the exact original cross transform. We bound the clock candidates and evaluate the largest one, corresponding to a shared clock. Comparing the two positive densities gives strict loss, and degree-one homogeneity then gives its exact factor.

Step 1. We compute the density of the original cross transform. First evaluate the cross transform. Temporarily smooth the spatial covariance, so Fourier and time Fubini are absolute. For $r = |\xi|$, direct integration over $s = t + v$ and $t = s + v$ gives

$$\int_0^\infty \int_0^\infty e^{-\theta(s+t)-\lambda|s-t|} \widehat{G}_s(\xi)\overline{\widehat{G}_t(\xi)}\,\mathrm{d}s\,\mathrm{d}t = \frac{2\theta+\lambda}{2\theta(\theta^2+r^2)((\theta+\lambda)^2+r^2)}.$$

For example, on the first cone the v-integral uses

$$\int_0^\infty e^{-(\theta+\lambda)v}\sin(r(t+v))\,\mathrm{d}v = \frac{(\theta+\lambda)\sin(rt)+r\cos(rt)}{(\theta+\lambda)^2+r^2}.$$

Integrating the remaining sine-square and sine-cosine terms against $e^{-2\theta t}$, and adding the second cone, gives the displayed identity. The value at $r = 0$ is its continuous limit.

Step 2. We remove spatial smoothing in the nonnegative spectral expression. The resulting spectral integrand is nonnegative. Removing the spatial Gaussian multiplier and using the Laplace formula for the power covariance therefore gives

$$\begin{aligned} K_\Gamma(\theta) &= \frac{1}{\Gamma_{\mathrm{E}}(a)}\int_0^\infty \lambda^{a-1}\frac{2\theta+\lambda}{2\theta}\int \frac{\mu(\,\mathrm{d}\xi)}{(\theta^2+|\xi|^2)((\theta+\lambda)^2+|\xi|^2)}\,\mathrm{d}\lambda \\ &= \int_0^\infty w_\theta(\lambda)\,\mathrm{d}\lambda. \end{aligned}$$

The second equality is partial fractions, with $(\theta+\lambda)^2-\theta^2 = \lambda(2\theta+\lambda)$. The smoothing passage is justified by monotone convergence in this nonnegative spectral expression and the finite quadratic form in Lemma 2.3.1. Alternatively, homogeneity directly bounds the density near zero by a constant times λ^{a-1}, and at infinity by a constant times λ^{a-2}. Its strict positivity follows from $\mathcal{R}_\Gamma(\theta) - \mathcal{R}_\Gamma(\theta+\lambda) > 0$, since $\mu \neq 0$.

Step 3. We prove integrability and compare the clock correlations. The candidate integrals are well defined and positive. The bound $\Psi_a(\theta|u-v|, v_\rho) \le (\theta|u-v|)^{-a}$, together with $h_\Gamma(w) = h_\Gamma(1)w^{-\alpha/2}$, supplies an absolute majorant. With $w = u+v$, $q = u-v$, the Jacobian is $1/2$ and $-w < q < w$. It is a constant times

$$\int_0^\infty e^{-\theta^2 w/2} w^{-\alpha/2}\int_{-w}^{w}|q|^{-a}\,\mathrm{d}q\,\mathrm{d}w = \frac{2}{1-a}\int_0^\infty e^{-\theta^2 w/2}w^{1-\alpha/2-a}\,\mathrm{d}w < \infty.$$

Here $a < 1$ and $a + \alpha/2 < 2$. The same bound dominates the spatial heat-regularized averages, whose spatial factor is $h_\Gamma(w+2\epsilon) \le h_\Gamma(w)$. This is an averaged spectral bound, not pointwise covariance monotonicity. Since $v_\rho(u,v) \ge |u-v| = v_1(u,v)$, monotonicity of Ψ_a gives $J_{\Gamma,\rho} \le J_{\Gamma,1}$.

Step 4. We evaluate the shared-clock candidate and compare its density. We compute the latter by nonnegative Tonelli. Write $A = \theta\lambda + \lambda^2/2$. Integration in q gives $2(1-e^{-Aw})/A$. Also

$$\mathcal{R}_\Gamma(q) = \frac{1}{2}\int_0^\infty e^{-q^2 w/2}h_\Gamma(w)\,\mathrm{d}w,$$

by the elementary resolvent integral and spectral Tonelli. Consequently,

$$\begin{aligned} J_{\Gamma,1}(\theta) &= \frac{1}{4\Gamma_{\mathrm{E}}(a)} \int_0^\infty \frac{\lambda^{a-1}}{A} \int_0^\infty h_\Gamma(w) \left(e^{-\theta^2 w/2} - e^{-(\theta+\lambda)^2 w/2} \right) \mathrm{d}w \, \mathrm{d}\lambda \\ &= \frac{1}{\Gamma_{\mathrm{E}}(a)} \int_0^\infty \frac{\lambda^{a-2}(\mathcal{R}_\Gamma(\theta) - \mathcal{R}_\Gamma(\theta+\lambda))}{2\theta+\lambda} \, \mathrm{d}\lambda \\ &= \int_0^\infty \frac{2\theta}{2\theta+\lambda} w_\theta(\lambda) \, \mathrm{d}\lambda. \end{aligned}$$

The q-integral's factor two cancels its coordinate Jacobian $1/2$; the resolvent identity supplies the other factor two. Since $w_\theta > 0$ and $2\theta/(2\theta+\lambda) < 1$ for every $\lambda > 0$, the strict inequality follows.

Step 5. We compute the exact loss at spatial degree one. Finally, if $\alpha = 1$, homogeneity gives $\mathcal{R}_\Gamma(q) = \mathcal{R}_\Gamma(1)/q$. Substitution in the two densities gives

$$\begin{aligned} K_\Gamma(\theta) &= \frac{\mathcal{R}_\Gamma(1)}{2\theta^2 \Gamma_{\mathrm{E}}(a)} \int_0^\infty \frac{\lambda^{a-1}}{\theta+\lambda} \, \mathrm{d}\lambda, \\ J_{\Gamma,1}(\theta) &= \frac{\mathcal{R}_\Gamma(1)}{\theta^2 \Gamma_{\mathrm{E}}(a)} \int_0^\infty \lambda^{a-1} \left(\frac{1}{\theta+\lambda} - \frac{1}{2\theta+\lambda} \right) \mathrm{d}\lambda. \end{aligned}$$

The real Beta identity

$$\int_0^\infty \frac{x^{a-1}}{x+c} \, \mathrm{d}x = c^{a-1} \Gamma_{\mathrm{E}}(a) \Gamma_{\mathrm{E}}(1-a), \qquad c > 0,$$

follows by scaling and $(r, s) \mapsto (r+s, r/s)$ in the positive product of the two Gamma integrals. Their finiteness uses $0 < a < 1$. Evaluation of these two integrals gives $J_{\Gamma,1}/K_\Gamma = 2(1 - 2^{a-1}) = 2 - 2^a$, proving (D.2.7). This proves Proposition D.2.2. □

Remark D.2.3 (Normalization and scope of the obstruction)**.** At the static endpoint define the time covariance directly as one. The candidate with $\Psi_0 = 1$ gives

$$J_{\Gamma,\rho}(\theta) = \int \frac{\mu(\mathrm{d}\xi)}{(\theta^2 + |\xi|^2)^2} = K_\Gamma(\theta).$$

This follows by integrating $we^{-\theta^2 w/2} h_\Gamma(w)/4$ spectrally. In the white case it equals $1/(4\theta^3)$. Thus, static and homogeneous-degree checks alone miss the positive-a loss. Relative to the shared-clock value $\rho = 1$, the omitted cross-pair multiplier is exactly $1 + \lambda/(2\theta)$. For smaller correlations the deficit can be larger. This does not assert a correction rule at higher orders.

The transforms $K_\times$ use gap damping. For the auxiliary cutoff function

$$F(T_1, T_2) = \int_0^{T_1} \int_0^{T_2} |s-t|^{-a} \frac{\min(s,t)}{2} \, \mathrm{d}s \, \mathrm{d}t,$$

nonnegative Fubini adds $1/(\theta_1\theta_2)$ to its double external-horizon transform. This function is not an unequal-time solution correlation. Reversing chains ending at different physical

times instead shifts the cross covariance to $|T_1 - T_2 - s + t|^{-a}$. Setting the two damping parameters equal is also not the single Laplace transform of a diagonal-horizon moment. For a self-pair at common gap damping, one external horizon instead adds $1/\theta$, recovering the known first-mean coefficient.

The proposition rules out exactly the analytic covariance substitution in (D.2.4), with product heat-chain measure, unrestricted operational-time rectangle and constant Brownian correlation. Additional relative-order weights,other derived clock couplings,matrix representations,modulus inequalities and their possible asymptotics are not covered. In particular, the inequality at this first cross pair leaves open a shared-clock lower comparison or asymptotic equivalence at higher orders. This finite clock calculation does not identify the intrinsic value proved in Theorem 11.2.6 with the source's all-moment conjecture. This is not a Skorohod result or a no-go for every two-clock method.

No-go 17 summarizes the missing degree-two multiplier. No-go 18 records a different degree-four obstruction: erasing an additional shift makes one upper envelope too large to close its comparison, without refuting the comparison itself.

Appendix E

The AI work in numbers

This appendix records how much of the work was done, by which kind of model, and how often the checks failed. It counts what the project's own records show. Every number is produced by a short script from files kept in the repository, and the scripts are kept with it, so a reader can rebuild each figure and each table. The record covers 21 days, from October 27 to November 16, 2026 (dates in UTC), with 2,387 recorded changes (commits). The retained reviews-folder census ends on November 12. For November 12 to November 15 the figure also shows a separate count of recovered review attempts, and the last section lists the reviews of the publication closeout.

Who did the work

The mathematics, the LaTeX source and the bookkeeping were drafted by a GPT-family model working through Codex. Its work was checked by reviewers from other model families: Claude (Opus 5.5) at first, and from November 1 DeepSeek V4 Pro as the main reviewer, with Kimi K3. A GPT model also reviewed the Lean statements. Appendix F lists what the Lean companion checks. A review counts only when the reviewer comes from a different family from the author of the work it checks.

	Sessions or records	Input tokens	Output tokens
Worker: GPT (Codex)	88 sessions	22.62 billion	50.7 million
Claude Code logs	32,229 usage records	11.28 billion (cache)	39.5 million
DeepSeek V4 Pro	237 sessions	75.9 + 188.8 million	2.08 million

Most of the worker's input, 98.9%, was text it had already read and that was served again from a cache; 29.7 million of its output tokens were internal reasoning. Counting cached input on both sides, the worker read about 85 times as much as the DeepSeek reviews. The Claude Code figures include Opus 5.5, Fable 5.2 and synthetic usage records, covering editing and coordination as well as reviews. They count logged assistant usage records, not verified API calls. Only the DeepSeek figures carry a cost figure, a cost counter of 72.56 computed by OpenCode, which is not an invoice and whose currency was not verified; the other models were used on subscriptions, whose costs are not recorded in these logs. The worker machine's logs hold no token counts for Kimi, so these totals leave Kimi out; the closeout records at the end of this appendix carry Kimi's own reported counts. These totals are a snapshot taken at 2026-11-16 16:48Z from those logs. The DeepSeek line includes the recorded usage of the re-read calls of November 16, 2026, described at the end of this appendix, which ran on the same machine; the token figure given there is part of these totals and must not be added to

them. The totals cover the sessions and usage records that one machine retained, not all activity. Only recorded usage fields are summed; usage with no record, including the abandoned attempt described in the closeout section, is not included.

Reviews

At that historical census, the repository held 731 review folders. Of these, 434 contain at least one review run; the others hold preparation, decisions or diagnostics. A *run* is one review task sent to one reviewer model, with or without a usable report. There were 627 runs, and 43 further follow-up requests within the same reviewer sessions.

Reviewer	Runs	Completed	Not completed	Met bar	FAIL	MEDIUM	Hours
Claude (Opus 5.5)	244	228	16	147	6	77	21.2
DeepSeek V4 Pro	152	147	5	56	0	35	11.7
Kimi K3	107	91	16	81	0	4	8.0
GPT (Codex)	124	124	0	41	70	19	14.5
Total	627	590	37	325	76	135	

Hours are summed over the runs whose time was recorded: Claude (Opus 5.5) 244 of 244; DeepSeek V4 Pro 89 of 152; Kimi K3 22 of 107; GPT (Codex) 124 of 124.

Met the bar means a completed run graded PASS or PASS WITH NOTES at HIGH confidence, which is what the project required before a result could be accepted. Meeting the bar is not the same as acceptance: the final decision was recorded separately, and only the Claude and GPT reports record it in a form that can be counted. Of the 76 FAIL grades, 70 came from the GPT reviews of the Lean companion; they reported defects in the Lean statements or in their match with this book, which then had to be repaired. Runs that did not complete stopped on usage limits, timeouts or reports in the wrong format. Figure E.1 shows the work day by day and marks 15 milestones, from setting up the project to closing the Lean correspondence gates; their commits are listed in `scripts/ai-statistics/milestones.json`.

The figure covers only this book, which began on October 26, 2026. The system that wrote it is older. The bibliography and the paper library have been kept since December 2021. The collection of LaTeX sources began in January 2026, the wiki in its present form in April 2026, and the library of skills in the same month. The book took a month because that work was already done. The dates and the commits behind them are in `scripts/ai-statistics/infrastructure.json`.

Approaches that did not work

As of November 16, 2026, the record holds 44 failed approaches and corrections: 33 mathematical (18 approaches that cannot work and 15 counterexamples or corrected claims), 4 defects in the source paper, 6 failures of a method of checking, and 1 process

record. Chapter 12 has 33 numbered mathematical entries with written arguments at their printed scopes. NG-33 is a broader historical group of refuted reviewer objections; its printed counterpart proves three representative cases. The remaining items in that group are not claimed proved there. In the first snapshot of the record, on November 10, there were 42 entries, and 8 of the mathematical ones were marked as proved in the book, 14 as reviewed and adjudicated, and 11 as recorded only. In the current snapshot, *proved in book* denotes a written proof at the record's stated scope, not scientific acceptance. NG-33 remains *reviewed and adjudicated* because only part of its historical group is printed. The earlier review of NG-09 did not meet its acceptance threshold. None of these records refutes the main theorems.

What the numbers do not show

Counts of runs and tokens measure effort, not correctness: a thousand commits do not prove a theorem, and a passed review is a check, not a proof. Some figures are incomplete. The worker machine's logs hold no Kimi tokens, and only 22 of the 107 Kimi runs have a recorded time; some DeepSeek runs recorded only their last request, so DeepSeek hours are too low; and the dates of 114 runs are taken from folder names. The token totals come from the logs of one machine. The 2,387 commits are counted in the working repository; the public history has fewer, because commits that changed only private files are left out of it. A short list of review folders could not be classified and is kept with the scripts.

The grey bars count 118 review attempts recovered from retained records for November 12 to November 15. They are attempts, not completed reviews: some were blocked or returned an unusable report. Their UTC days use recorded launch, client-session and panel-dispatch evidence; some are bounded or decoded rather than exact invocation clocks. Actual model identity is not verified for every attempt, so this series is not split by reviewer. We show them separately from the 627-run census; together they still do not establish a complete project-wide inventory. These are counts of review tasks, not provider requests, and activity with no retained record is missing. Of these attempts, 25 are represented in the closeout ledger below.

The publication closeout reviews of November 2026

This section covers only the closeout reviews before publication, in November 2026: 35 records in the experiment's run ledger, whose snapshot is dated November 15, 2026. The figures come from the dated correction of that ledger recorded on November 15, 2026 (`experiment/ledger-updates/2026-11-15-cold-closeout/run-ledger-v4.json`, commit `c2359a4f`, blob `eab20562`). Earlier corrections added verified model identities and accounting fields and separated one raw report's hash from that of its parsed copy (C003). The current snapshot preserves all 29 older rows unchanged and adds 6 later cold-review records, including the author's bounded decision on the uniform-product

review. Reported grades and token objects remain unchanged. The experiment itself is the way of doing mathematics described in the Preface, and its primary record is the whole repository: its history, proofs, failed approaches, human and AI work, sources, reviews and the Lean companion. The run ledger instruments only this closing round, and only partly; its own coverage note says what it includes. Its records are not added to the totals above, and its token counts, reported for some records only, are not totals for the project. The table counts the outcome recorded for each record, by the model that actually ran; historical running records retain their snapshot status (one record, whose provisional outcome is not accepted). No record accepts the whole book: each acceptance is limited to the scope its review stated. The preserved older rows retain their historical status: a row marked as running describes its snapshot date, not a live process now.

Six later calls add scoped observations in this November 15 update. A whole-source call returned inconclusive at medium confidence; a focused call returned pass with notes at high confidence but did not complete the required core reconstruction. Four local calls returned three passes and one pass with notes, all at high confidence. Two were accepted as scoped mathematical evidence with notes and two were partial. For the uniform-product check, the author accepted a bounded exception for one automatic native retry, with the incident disclosed. The original JSON-format failure in one report remains recorded; a copy in which only the JSON punctuation was corrected is not another review. These calls do not replace a complete independent review of the book. The combined critical review of Chapter 12 was not obtained: one attempt exhausted its context and the next stopped at a safeguard with invalid partial output. It was never marked passed. A separate high-confidence review of whether Chapter 12 faithfully states its evidence and limitations does not replace that missing assessment. Author-side source comparisons and delivery checks are not additional independent scientific votes.

The 35-record ledger remains a dated snapshot. A separate evidence addendum links later observations to its original identifiers, including its missing launch clocks and C011's terminal report. The recovered inventory contains 118 documented review attempts: 25 already represented in this ledger and 93 additional records, with 4 same-session follow-ups listed separately. It is a timeline inventory, not a new completion, pass-rate or acceptance table; it does not add tokens or costs to the snapshots above. Its public metadata are in `experiment/ledger-updates/2026-11-15-evidence-update/review-attempts.json`.

Outcome	DeepSeek `deepseek-v4-pro`	Kimi `k3`	Model not recorded	No model call	All
Accepted at the stated scope	3	2	0	0	5
Not accepted	9	0	1	0	10
Invalid report	2	6	0	0	8
Recovery refused	0	0	0	1	1
Recovered	0	0	0	4	4
Preflight (no call)	0	0	0	3	3
Continuation (no new vote)	0	2	0	0	2
Timed out	0	1	0	0	1
Running at snapshot	0	0	1	0	1
Records	14	11	2	8	35

Token counts are given for the 25 original review records, per model, reporting format and accounting scope, in the form in which the review tool reported them. Only the 24 records with reported usage are summed; a record without figures is shown as having no reported value, and nothing is estimated. Records separately marked as derived recoveries, parser refusals, preflights or audit addenda do not represent new provider calls in this ledger. Format continuations count toward usage only when nonoverlap is verified. For the 5 records with scopes S2 and S4 the reported counts cover only the final step, not the whole session. The formats, as recorded in the ledger:

A: `{cache:{read:number,write:number},input:number,output:number,reasoning:number,total:number}`

B: `list[{inputCacheCreation:number,inputCacheRead:number,inputOther:number,output:number};{inputCacheCreation:number,inputOther:number,output:number}]`

C: `list[{inputCacheCreation:number,inputCacheRead:number,inputOther:number,output:number}]`

D: `{input:number,output:number,reasoning:number}`

Accounting scopes are kept separate:

S1: The usage object as the tool reported it; no wider total is implied.

S2: The final step of a panel run only, not the whole session.

S3: One response of the model; no session total is implied.

S4: The final step only; the usage of an earlier abandoned attempt is unknown.

These are sums of known reported components, not actual all-activity totals. A review record counts a review task, not a provider-stream total. An automatic retry within one later review record opened two streams of generated output; it is separate from the recorded repairs to report formats. Usage and cost for the earlier abandoned stream are unavailable. The reported final-step total is not the whole invocation. Actual whole-run usage and cost remain unknown, as does whether the whole run stayed within its approved token limit.

Model (form)	Reported totals	Reported on
`deepseek-v4-pro` (DeepSeek), format A, scope S1	`cache.read` 0, `cache.write` 0, `input` 1,986,239, `output` 33,007, `reasoning` 121,948, `total` 2,141,194	5 of 14
`deepseek-v4-pro` (DeepSeek), format A, scope S3	`cache.read` 0, `cache.write` 0, `input` 1,154,041, `output` 61,540, `reasoning` 193,545, `total` 1,409,126	5 of 14
`deepseek-v4-pro` (DeepSeek), format A, scope S4 (header/final-step only)	`cache.read` 15,488, `cache.write` 0, `input` 34, `output` 12,327, `reasoning` 60,815, `total` 88,664	1 of 14
`deepseek-v4-pro` (DeepSeek), format D, scope S2 (header/final-step only)	`input` 19,811, `output` 10,253, `reasoning` 34,463	3 of 14
`k3` (Kimi), format B, scope S1	`inputCacheCreation` 0, `inputCacheRead` 5,405,065, `inputOther` 264,438, `output` 100,424	1 of 9
`k3` (Kimi), format C, scope S1	`inputCacheCreation` 0, `inputCacheRead` 75,707,586, `inputOther` 2,503,780, `output` 493,885	8 of 9
Model not recorded, format D, scope S2 (header/final-step only)	`input` 26,040, `output` 2,515, `reasoning` 3,621	1 of 2
Model not recorded, scope S1	no reported value	1 of 2

Known reported cost components of the closeout records (not actual all-activity cost): `deepseek-v4-pro` (DeepSeek), format A, scope S1: 1.52 (currency not recorded; 4 records; known reported components only); `deepseek-v4-pro` (DeepSeek), format D, scope S2: 0.12 (currency not recorded; 3 records; known reported components only); `deepseek-v4-pro` (DeepSeek), format A, scope S3: 0.87 (currency not recorded; 4 records; known reported components only); Model not recorded, format D, scope S2: 0.04 (currency not recorded; 1 record; known reported components only).

Later evidence and the author's decision

Missing cells in the original ledger mean that a value was not verified in that snapshot, not that no record could ever be recovered. Original launch records or CLI receipts now supply 6 of its previously missing start clocks:

Record	Recorded clock (UTC)	Kind
C001	2026-11-13 20:47:11.227388	Runner launch
C006	2026-11-14 00:00:37.645321	Runner launch
C007	2026-11-14 00:22:13.811729	Runner launch
C009	2026-11-14 00:32:32.408329	Runner launch
C010	2026-11-14 00:52:24.214003	Runner launch
C011	2026-11-14 01:19:53.631078	CLI receipt start

These are client-runner or CLI receipt clocks, not independently measured provider API boundaries. They were read from retained records, not calculated by subtracting a duration from a later clock. The original ledger's nulls remain unchanged.

For 3 other panel records, the retained clocks record an OpenCode client session's creation and last update. These do not establish the review invocation's exact start or finish. For the remaining panel record, only its UTC day is bounded by the recorded panel creation and the next role's receipt under the documented sequential workflow. Its exact start, finish and actual model remain unknown. The evidence addendum keeps recorded clocks, client clocks, decoded clocks and bounds distinct.

C011 was still running at the original snapshot. Its later receipt records an invalid report; a punctuation-only recovery returned pass with notes at medium confidence. The review is terminal and remains unaccepted under the high-confidence standard. This is later evidence about the same invocation, not another review or an upgraded grade.

On November 15, 2026, the author chose the policy of an *honest-standing release with the grades stated plainly*. This decision changes no grade, supplies no missing review and does not turn scoped evidence into whole-book scientific acceptance. It selects how the record is disclosed; it is not a public-release act or the final release accept file. The dated observation and decision metadata are in `experiment/ledger-updates/2026-11-15-evidence-update/observations.json`.

The re-reads after the readability pass

After the reviews counted above, the proofs were rewritten so that their steps are easier to follow. Statements and existing displayed formulas were kept, apart from the separately approved corrections described below. Inside the proofs, sentences were added, removed or reordered. Of the 249 proofs in the 33 technical files, 208 changed and 41 stayed identical byte for byte. In 3 statements the wording was corrected under separate approval. The 4 proofs of the reader edition are not counted here. The earlier reviews stay bound to the text they received, and they do not cover the sentences added later.

Every one of the 249 proofs, changed or not, was then sent again, the old text beside the new, to DeepSeek V4 Pro. The editor was a GPT model, so the reader came from a different family. Each call was asked to read both texts in full, to rebuild the deductions, and to say whether a step or a qualification had been lost. All calls were made on November 16, 2026. Table E.1 gives the counts. This series is separate from the 627 review runs and the 118 recovered attempts above, and its numbers must not be added

to theirs. It changes no earlier grade, and it is not an acceptance of the book. These scoped re-reads do not upgrade the inconclusive whole-book cold read or replace the missing skeptic synthesis of Chapter 12.

Table E.1: Re-reads of the proofs after the readability pass. The last three rows are our own check of what the reports wrote, not grades given by the reader.

Calls made	59
with a report	58
without a report (the output limit was reached)	1
Reports graded PASS	44
Reports graded PASS WITH NOTES	14
Proofs sent, counting every repeat	364
Scopes prepared but never sent	16
Reports that cover the final text	38
graded PASS	28
graded PASS WITH NOTES	10
Earlier calls, on text that changed later or was sent again	21
Proofs of the final text covered, each by one report	249
old and new text both reported as read in full	249
Report's reasoning checked for the proof	226
Checked, but resting on a parent result with a stated limit	9
Report's reasoning partial for the proof	14

A grade belongs to a call, not to a proof. All 58 reports stated high confidence for their call, and none gave a confidence for a single proof. The 364 proofs sent include repeats: some files were sent at more than one frozen source revision, and some proofs appeared in more than one assigned scope, so this is not a number of distinct proofs. The call without a report has no grade; it is not counted as a pass or as an inconclusive review, and its proofs were read in later calls.

The last three rows of the table are the authors' side of the work. The number 14 there counts proofs and the number 14 above counts reports; that they are equal is a coincidence. For each proof we checked the reasoning that the report wrote down. *Checked* means that the deductions in the report hold as written for that proof. It is a local check; it does not prove that everything the proof depends on is sound. For 9 proofs the check rests on a parent result whose own check has a stated limit. These fall into 8 groups and repeat their parents' limits; they are not further gaps. *Partial* means that a deduction the report was asked to give is missing or does not hold as written in the report. It does not by itself show an error in the book. Our checks of the book's text found no new mathematical defect in these proofs. Before the final calls, four added sentences that stated more than the proof gives or misdescribed a calculation were corrected (the rank-one witness, "canceling half", the strictly positive profile, and the complex-vector components), and sentence boundaries were repaired. For one of the partial proofs the

central argument was checked and only further derivations that the call had been asked for are missing. In one report the requested word-for-word comparison of a corrected statement was wrong, although its mathematics was checked; that comparison was not obtained. This is a separate limit and is not one of the partial proofs.

Some usage is unknown. In 4 calls the client program restarted an interrupted answer by itself, and the logs kept the usage of the final answer only. Of these, 3 happened before the author prospectively allowed automatic transport recovery under the later policy; they keep the status *held*, and none of them covers the final text. The other one was allowed in advance, and its report covers 10 proofs of the final text. The available finish records report 5,042,639 tokens, of which 207,872 were cached input. The client's own cost counter for these records sums to 5.84 in the client's units; it is not an invoice, and its currency was not verified. The usage of the interrupted answers, the whole cost and the number of requests that reached the provider are unknown, and no estimate is given. No whole-invocation token-limit compliance is claimed.

Three kinds of help in this pass were not reviews and are counted nowhere above. The editor, a GPT model, rewrote the proofs under written rules, and each file had to pass mechanical checks that existing statements, displayed formulas, labels and references were kept, with separately approved original-text changes recorded as exceptions. The 3 statement corrections, the other repairs of the original text and the removal of unused setup in the proof of Proposition 10.1.5 were separate edits of the original text, made at the author's decision and not by the editor. In 11 read-only runs, Claude Fable 5.2 listed the places where a reader has to stop and the passages that repeat; 53 such places were listed and given to the editor to fill. These runs were editorial aids and were not counted as scientific reviews. GPT helpers assisted in checking the reports' reasoning, which is an author-side check and not an independent vote.

The data are in `reviews/2026-11-16-readable-final-source/`. They are bound to the text of the proofs at development commit `cdef8c83` of the private development repository. The editorial record is `scripts/ai-statistics/reviews/readability-pass-2026-11-16.json`.

The review of the Lean companion's references

Before release v0.10.0 of the Lean companion, its references to lines of this book were moved to the book's final text, and that work was reviewed in 3 calls to GPT-6.1-Sol at high effort, read-only, on November 16, 2026. The companion's text was written by a Claude model, so the reviewer came from a different family. The first call returned FAIL at high confidence, with 7 major and 2 minor findings about the companion's descriptions and quotation ranges. After the corrections, a narrower confirmation returned FAIL at high confidence again, with 2 major findings, because two corrections had not reached every description. A second confirmation returned PASS WITH NOTES at high confidence, with no fatal or major finding and 1 minor note, and that report was accepted. The two earlier reports are kept. The first call checked a sample of the references with broad mechanical checks; the two confirmations checked only the

corrections. Together the calls took about 25 minutes. They used 11,775,176 input tokens, of which 11,261,952 were cached, and 59,443 output tokens, of which 20,596 were reasoning; these counts include each other as stated and must not be added again. No cost was recorded, which is not the same as zero. This series is separate from every count above. It checked the references and the repairs, not the mathematics of this book or the analytic inputs outside Lean, and it is not a human check. The author accepted release v0.10.0 on November 16, 2026. The record is `scripts/ai-statistics/reviews/lean-reanchor-review-2026-11-16.json`.

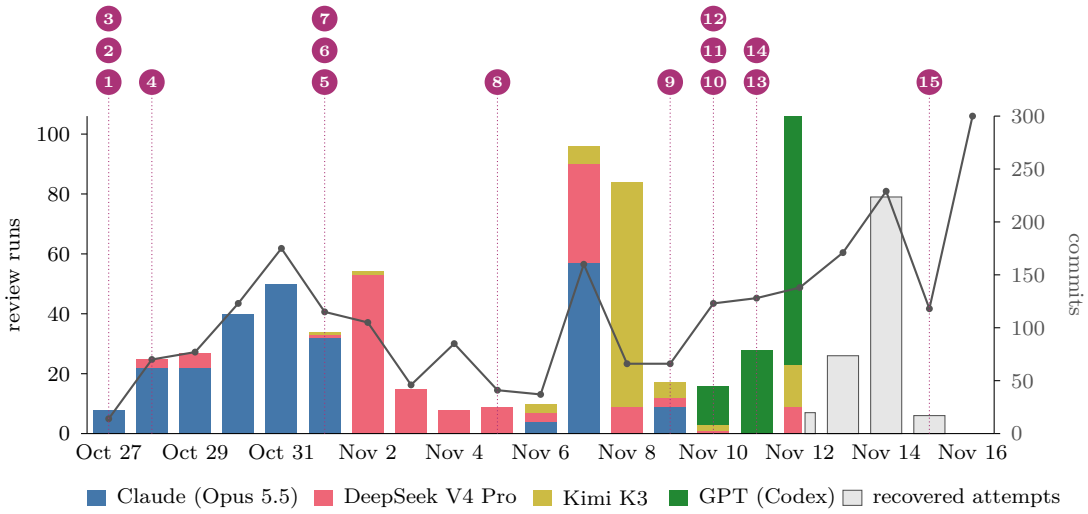

1 Oct 26: Project set up: notes scaffold and source manifest
2 Oct 27: Gate G0: one bound for every pairing cannot reach the target scale
3 Oct 27: Gate G1: all fifteen order-four white-noise terms computed
4 Oct 28: Upper bound at the correct time scale established after review
5 Oct 31: Goal revised: derive the actual constant, not match a predicted value
6 Nov 1: Variational formula for the second-moment constant integrated
7 Nov 1: DeepSeek and Kimi become the reviewers
8 Nov 5: Reading edition of about twenty pages written
9 Nov 9: Lean checks reach the actual Gaussian objects
10 Nov 9: Fifth whole review: PASS WITH NOTES at MEDIUM, not accepted
11 Nov 9: Lean companion recorded
12 Nov 10: Technical text organized as a book
13 Nov 11: Appendix E added: the AI work in numbers
14 Nov 11: Lean correspondence gates closed through wave L4
15 Nov 15: Final publication-facing PDF on master

Figure E.1: Review runs per day by reviewer (bars, left scale) and commits per day (line, right scale), with the project's 15 milestones (numbered circles). Days are in UTC, and each circle sits on the UTC day of the milestone's commit; the key gives the date as recorded. Claude returned after November 1 for checks of rendered pages. The coloured bars stop on November 12, where the census of review runs ends; the grey bars count recovered review attempts, which are not part of the census. The figure starts with this book; the system behind it was built earlier, as the text says.

Appendix F

What Lean checks

Some steps of this book were also checked in Lean, a proof assistant. They live in a separate Lean package, the Lean companion. This appendix describes its release v0.10.0 (DOI 10.5281/zenodo.24295453), which contains the formalization waves through L14 and refers to the lines of this book's final text. The waves were checked at commit `8f51004` of the private development repository; the release is cut from that commit, its receipts are those of the release commit `c8d8e07`, and the companion's `provenance/DEVELOPMENT.md` lists every change between the two.

For each listed result, the entry identifies what Lean proves and what remains outside that proof. Read the result reference and its title as one entry. Where the conclusion is narrower, the entry states which part is proved and which part is not yet formalized. Where a checked statement assumes an analytic fact, the entry names it as a supplied input. Where the checked steps take no additional analytic input, the entry states their assumptions and describes work left outside Lean. A supplied input is a hypothesis of the Lean proof, not an additional conclusion it establishes.

F.1 How to read the entries

Every result with a row here, except those listed as not formalized, carries a small link in the left margin of the text, beside its heading or its displayed equation: the word Lean and, under it, the class that this appendix prints for the result. The link leads to the result's row. *Full* means that every conclusion is formalized under the book's hypotheses. *Narrower* means that Lean works under the book's hypotheses but proves only the conclusion specified in the entry; the remaining part is not yet formalized. *Supplied* means that every conclusion is proved with analytic inputs supplied as hypotheses. *Partial* means that Lean checks only the stated steps, parts or narrower form, using the listed supplied inputs, if any; it does not prove the whole result as stated in the book. The entry states which hypotheses the checked steps take and which analytic work is left outside Lean. Lean checks the formal statements. Their match with the statements of this book was reviewed by AI models and has not been verified by a person. A result without a link carries no Lean claim; this does not mean that the result is in doubt.

Some entries name a registered modelling choice by a code. Lean proves the statements for the model; the identification named in each line is not proved in Lean.

M1 In dimension three the wave Green measure is defined through Mathlib's sphere measure; that it equals the surface measure used in the text is not proved in Lean.

M2 The Gaussian space over finitely many coordinates is represented by normalized Hermite coefficient vectors; that Bochner integrals in it agree with the coordinatewise

integrals is not proved in Lean.

M3 The smoothed covariance $p_\varepsilon * \Gamma$ is taken as the measure with density γ_ε; that it equals Mathlib's convolution of measures is not proved in Lean.

M4 The two-chain diagram integrals are the deterministic integrals of a diagram model; their identification with the joint limit in the text at arbitrary vertexwise widths is not proved in Lean (the positions form is proved in dimension one).

M5 The completion spaces $H_t \otimes G$, H_t, H_I and H_Γ are realized as L^2 completions under the kernel and covariance forms; no tensor-product identification and no isometry between H_{sp} and H_Γ is proved in Lean.

M6 H^1 is the graph of the weak gradient in $L^2 \times L^2$, with the topology of Mathlib's H^1; that every real element of Mathlib's H^1 arises from it is not proved in Lean.

Three points apply to every entry. Lean checks the statements as written in Lean. Their correspondence with this book was reviewed by AI models from a different family from the author of the formal statements; it has not been verified by a person. A supplied input is a named mathematical hypothesis: its proof and its application to the book's objects are not certified merely by using it in Lean. The entries distinguish these inputs from the conclusions Lean proves. They do not certify the book's main stochastic moment theorems end to end.

F.2 How the match with the book was reviewed

The statements added in wave L9, and the changes that wave made to existing entries of the coverage record, were checked against the book in eight independent correspondence reviews, done by AI models from a different family than the one that wrote the formal statements. The reviews found documentation corrections only, and no error in a Lean proof. The corrections were made and re-checked over ten confirmation rounds. During them the author fixed three conventions for the record: a result counts as formalized in full only if every conclusion is a Lean conclusion under the book's hypotheses, and otherwise the missing part is named; a result about an object the companion models by a registered standard choice counts in full, while a result that needs an object the companion does not construct counts as narrower; and the record's index lists, for each label, only the sections where it is treated. A final confirmation passed with high confidence, and the author accepted wave L9 on November 12, 2026, with a correction of the count of public definitions recorded as a documentation-only successor.

The statements added in waves L10 to L14, and the changes those waves made to existing entries of the coverage record, were checked against the manuscript in correspondence reviews. The reviews were done by AI models from a different family than the one that wrote the formal statements, under the conventions the author fixed in wave L9. Each wave's reviews found documentation corrections only, and no error in a Lean proof. The corrections were made, and a confirmation review passed with high confidence.

The author accepted waves L10 and L11 on November 13, 2026:

- In wave L10, one assembly step of Proposition 3.3.5 assumed a bound on the pairings of the cut-off coefficients that the manuscript does not state as a hypothesis. Wave L11 proves that bound from a supplied expansion of the coefficients.
- In wave L11, the Gaussian space is represented by Hermite coefficient vectors. Lemmas 3.2.2 and 3.3.1 hold with the manuscript's hypotheses but narrower conclusions, on a Fourier-side model not identified with the physical-space operators.

The author accepted wave L12 the same day, recording that the smoothed covariance of Lemma 2.3.1 is modelled by its density; with that choice the lemma is formalized in full.

Waves L13 and L14 were accepted together, with three further modelling choices recorded:

- the second moment's two-chain pairing integrals are represented by a deterministic diagram model, with the mixed-moment expansion of Proposition 2.1.1 supplied as an input;
- the occupation spaces are modelled by their L^2 completions;
- H^1 is modelled as the graph of the weak gradient.

On these models:

- Propositions 8.2.5, 8.2.8, 11.3.2 and 4.1.2, and Lemma 7.3.2, are formalized in full.
- Theorem 11.3.4 is formalized in both forms with the exact constant C_{occ} over the occupation class itself, without its moment sentence $C_2 \le U_2$.
- Propositions B.1.2 and B.1.5 have their diagram values and coefficient bounds proved on the model, and their statements about the solution follow from the supplied Proposition 2.1.1.

Open items in the record:

- Theorems 3.3.8 and 11.2.6 are outside Lean.
- Theorem 11.4.3 is formalized for the variational value S_2^{pos} rather than for C_2, with the white spatial energy supplied.
- Several results rest on named inputs, each listed with the result that supplies it. These include Propositions 2.1.1 and C.2.5, the first-moment series, and the signed multiplier form.
- No theorem of the manuscript is verified end to end.

These reviews are not a human verification, and they do not check the analytic inputs that stay outside Lean.

For release v0.10.0, the companion's references to lines of this book were moved to its final text. That work was reviewed by a model from a different family; the first review and one confirmation failed on the companion's descriptions and quotation ranges, the corrections were made, and a further confirmation passed (Appendix E). The author accepted release v0.10.0 on November 16, 2026.

F.3 How the Lean package was checked



lean-pkg: registers Lean packages and records their checks.

The companion was built and checked with lean-pkg [11], a tool for registering and checking Lean packages that the author developed (version 0.29.0). For commit c8d8e07, lean-pkg records that the package builds from scratch with no unproved steps, and that every public declaration, and each of the 4502 listed claims, uses only Lean's three standard axioms (`propext`, `Classical.choice` and `Quot.sound`). A second, separate check confirms that the proofs of all 3653 theorems prove their statements as restated in a separate file. The list of claims has 2261 verified and 0 open. These checks concern the Lean statements themselves; whether those statements say what the book says is the AI-reviewed match described above. The private development verification record for commit `8f51004` reports a separate kernel replay on a computing cluster: all 141 library modules and the umbrella module passed `leanchecker -fresh`, and all 142 targets also passed its default mode. The three libraries used only for the separate statement check were not included in this replay. That replay is of the gate commit. The release commit `c8d8e07` drops two claims that name Lean-generated declarations and the one compared theorem that named one of them; the receipts above are those of the release.

F.4 The results

In short: With the manuscript's hypotheses, 48 labelled results are formalized in full and 16 with a narrower conclusion; Proposition 10.2.3 in full with two inputs supplied; steps, parts or narrower forms of 34 further labelled results; the entries distinguish supplied hypotheses, where present, from analytic work left outside Lean; Theorem 3.3.8 and Theorem 11.2.6 are outside Lean. The 101 labelled results fall into five groups.

F.4.1 Formalized with the paper's own hypotheses; nothing supplied (48)

Equation (1.2.4)	The growth exponent kappa
Lemma 2.3.1	Homogeneous damped norms and temporal tails
Lemma 3.1.1	Two static contraction bounds

Lemma 3.2.3	Exact cutoffs for finite Gaussian words
Lemma 3.3.3	A coefficient bound for a product with nonnegative coefficients
Lemma 3.3.6	The finite terminal-chain Wick formula
Lemma 3.3.7	Uniform series tails from scaled moments
Proposition 4.1.1	Translated spectral mass
Proposition 4.1.2	Auxiliary mask norm
Lemma 4.1.3	Temporal covariance completion
Lemma 4.1.6	Modulated amplitudes
Equation (4.1.7)	Schur bound for the temporal form
Lemma 4.1.7	Correlated trigonometric products
Lemma 4.1.8	Continuous sine factors
Proposition 4.2.1	Uniform scalar row
Corollary 4.2.2	A time exponent above one half
Lemma 4.2.4	Hilbert-valued finite Bessel inequality
Lemma 4.3.1	Scalar power estimates
Lemma 4.3.2	Two Hermitian trace bounds
Proposition 4.3.3	Finite Gaussian matrix moment
Remark 4.3.4	Both variance directions are necessary
Equation (5.1.1)	driver parameters
Lemma 5.2.1	Finite Gaussian linear images
Lemma 5.2.3	Original spatial space and heat
Lemma 7.3.1	Gaussian envelope for the original covariance
Lemma 7.3.2	Global regularity of the original mean
Lemma 8.1.1	Gamma and Beta identities
Lemma 8.1.2	Exact potential and mass
Lemma 8.2.1	The physical two-point integral
Lemma 8.2.3	Deterministic Fourier bound for the spatial energy
Proposition 8.2.5	The physical four-linear extension
Lemma 8.2.7	Exact row maximum
Proposition 8.2.8	The full physical occupation class
Lemma 10.2.8	Supremum with the Gaussian quadratic cost
Lemma 11.1.1	Scalar and Hilbert identities
Proposition 11.3.2	Original occupation energy and dilation
Corollary 11.4.4	Uniform relative width of the bound formulas
Proposition A.1.1	White-space order four
Lemma B.1.1	Spatial estimate
Lemma B.1.3	Low-alpha convolution bound
Lemma B.1.4	Degree-one convolution bound
Lemma B.2.3	Riesz spatial maxima
Lemma C.2.1	Strict product endpoints
Lemma C.2.3	Plane-supported endpoints
Lemma C.2.4	Linear images and finite positive sums
Lemma D.1.2	Type of a positive coefficient series
Lemma D.2.1	White-space low-order Laplace transforms
Proposition D.2.2	Obstruction to unweighted constant-correlation clock copying

F.4.2 With the paper's hypotheses; Lean proves a narrower conclusion (16)

Lemma 3.2.2. *Gaussian cutoff form bound.*

Lean proves: With the lemma's hypotheses and nothing supplied, Equation (3.2.5), in coefficient form and as an operator-norm bound with $A_0 \geq 0$ and B bounded self-adjoint on the cutoff Hilbert space, uniformly in ϵ, m and the band, for finitely many real modes, Hermite degree at most N in the m multiplied coordinates, on a Fourier-side model.

Not yet formalized: The Fourier-side model is not identified with the physical-space operators.

Lemma 3.3.1. *Dimension-independent Gaussian contractions.*

Lean proves: With the lemma's hypotheses and nothing supplied, Equation (3.3.1), its band-compressed form, the phase-insertion bound $\sqrt{R_\alpha}\,\rho^{(\alpha-2)/2}$, the sandwich bound $R_\alpha \rho^{\alpha-4}$ with self-adjointness and Equation (3.3.2), for finitely many real modes, on a Fourier-side model, without tensoring by another Hilbert factor.

Not yet formalized: The Fourier-side model is not identified with the physical-space operators.

Proposition 4.1.5. *A physical mask need not preserve noise-null tests.*

Lean proves: The proposition, with its hypotheses, for the covariance functional: $\mathbb{E}W(F)^2$ is read as the covariance functional of the test F.

Not yet formalized: The noise W is not constructed, and the identification of $\mathbb{E}W(F)^2$ with the variance of the noise is not formalized.

Proposition 7.3.3. *The unmasked Rayleigh rate.*

Lean proves: With the section's hypotheses and nothing supplied, the statements about the Rayleigh supremum Equation (7.3.4): for λ defined as its square root, a uniform positive floor, the Lipschitz bounds and I_Ψ positive and finite.

Not yet formalized: The operator statements (H_s self-adjoint, form domain H^1, spectral bottom E_s, $\lambda = \sqrt{-E_s}$) are not formalized.

Lemma 7.3.5. *Radon and Rayleigh dilation.*

Lean proves: The bijection and the four identities with the section's hypotheses (Hypothesis 1.2.1, $\Gamma \neq 0$, $a = \alpha_0$) and nothing supplied, for the variance in its integral form and the rate defined as the square root of the real Rayleigh supremum Equation (7.3.4).

Not yet formalized: The identification of the variance and the rate with $\mathbb{E}W(\Psi)^2$ (Lemma 6.3.6) and $\sqrt{-E_s}$ (Proposition 7.3.3) is not formalized.

Proposition 7.3.6. *Intrinsic variational lower bounds.*

Lean proves: The proposition with the section's hypotheses and nothing supplied, including the boundedness of the value sets and the supremum statements (S_c^{pos} finite, positive, equal to $c^{(4-\alpha)/(3-\alpha)} S_1^{\mathrm{pos}}$), with λ the square root of the real Rayleigh supremum and v_Ψ the cost in its integral form.

Not yet formalized: $Q_2 \geq S_2^{\mathrm{pos}}$ is not formalized.

Lemma 8.2.2. *Smooth temporal controls.*

Lean proves: λ is the square root of the supremum of the real Rayleigh quotient, and I_Ψ, v_Ψ are given by their integral formulas; Equation (8.2.2) is proved both in the form that every number below the bound is exceeded by some admissible score and in its supremum form, with nothing supplied.

Not yet formalized: The identifications of λ with $\sqrt{-E_s}$ and of v_Ψ with $\mathbb{E}W(\Psi)^2$ are not formalized.

Proposition 8.2.4. *The finite smooth spatial ratio.*
Lean proves: Equation (8.2.4), with nothing supplied, both in the form that every y below the bound is exceeded by some $I_\Psi - v_\Psi/2$ and as a bound on the supremum, with λ the square root of the real Rayleigh supremum and v_Ψ given by its integral formula. $R_0 < \infty$ is proved by Lemma 8.2.3.
Not yet formalized: The identification of λ and v_Ψ with $\sqrt{-E_s}$ and $\mathbb{E}W(\Psi)^2$ is not formalized.

Proposition 8.2.6. *The spatial energy and static lower variational expression.*
Lean proves: Equation (8.2.10), with nothing supplied, both in an existential form (every y below $M_a^{-1/k} F_0(\mathcal{E}_{\mathrm{sp}})$ is exceeded by some $I_\Psi - v_\Psi/2$) and in its supremum form, with λ the square root of the Rayleigh supremum Equation (7.3.4) and v_Ψ by its integral formula.
Not yet formalized: The identification of λ and v_Ψ with $\sqrt{-E_s}$ and $\mathbb{E}W(\Psi)^2$ is not formalized.

Lemma 10.2.7. *Exact Rayleigh tail bound.*
Lean proves: The bound with integrability and the finite head integral.
Not yet formalized: The "In particular" application to the coarse-envelope bound of another proposition is not formalized.

Lemma 11.2.1. *Inclusion into the covariance space and the smooth mean.*
Lean proves: Equation (11.2.1) for every real Hilbert G ($H_t \otimes G$ the kernel completion of $L^2(I;G)$, M5), the inclusion of $\mathcal{C}_{\mathrm{pos}}$ in H_I with $\|\Psi\|^2 = v_\Psi$, the variance identity in integral form and the row and Schur bounds.
Not yet formalized: The mean identity of Equation (11.2.2) and the canonical versions are not formalized.

Lemma 11.2.2. *Finite covariance vectors and entrywise order.*
Lean proves: With the section's hypotheses and nothing supplied, that k_i^R and k_i^∞ lie in H_I (M5), that both Grams factor into the temporal pairing and B_Γ, and that both are positive semidefinite.
Not yet formalized: The label row Equation (11.2.4) ($\mathcal{T}_R$, v_L not constructed) and the entrywise order are not formalized.

Lemma 11.3.1. *Full-profile squares in the original space.*
Lean proves: With the section's hypotheses and nothing supplied, $Q : H^1 \to H_{\mathrm{sp}}$ with $\langle Q(f), Q(h)\rangle = B_\Gamma(f^2, h^2)$, continuous on H^1 (M6), and for fields of $\mathcal{O}$ modelled by joint representatives $\rho_g \in H_I$ (M5) both identities of Equation (11.3.2) and $\langle \Psi, \rho_g\rangle \le \sqrt{v_\Psi A(g)}$.
Not yet formalized: These identities and this bound are not restated on the class $\mathcal{O}$ itself.

Lemma 11.3.3. *Countable Rayleigh near-occupations.*
Lean proves: Equation (11.3.6) with the section's hypotheses and nothing supplied, with g_ε in the class $\mathcal{O}$ itself (strongly H^1-measurable fields, read as a.e.-strongly measurable); λ is the square root of the real Rayleigh supremum and v_Ψ the integral-form cost.
Not yet formalized: The identification of λ and v_Ψ with $\sqrt{-E_s}$ and $\mathbb{E}W(\Psi)^2$ is not formalized.

Theorem 11.3.4. *The computed occupation ceiling.*

Lean proves: With the section's hypotheses and nothing supplied, for $\mathfrak{c} > 0$: $\mathfrak{c} I_\Psi - v_\Psi/2 \le U_\mathfrak{c}$ for nonnegative smooth controls, $S^{\mathrm{pos}}_\mathfrak{c} \le U_\mathfrak{c}$ with the exact C_{occ}, and, for every $\zeta > 0$, $U_\mathfrak{c} = \mathfrak{c}^m (2\zeta)^{\alpha/(2k)} F_0(\mathcal{E}^{\mathcal{O}}_\zeta)$, over the class $\mathcal{O}$ itself; λ and v_Ψ in Rayleigh and integral form.

Not yet formalized: $C_2(\Gamma, a) \le U_2$ is not formalized.

Corollary 11.3.5. *A common spatial-energy bracket.*

Lean proves: With the section's hypotheses and nothing supplied, Equation (11.3.9) and the comparison $S^{\mathrm{pos}}_2 \le 2^m F_0(\mathcal{E}^{\mathcal{O}}_{1/2}) < 2^m F_a(\mathcal{E}^{\mathcal{O}}_{1/2})$ for the variational value S^{pos}_2 in place of $C_2(\Gamma, a)$ (identified by Theorem 11.2.6), with $\mathcal{E}^{\mathcal{O}}_{1/2}$ over the class $\mathcal{O}$ itself; λ is the square root of the real Rayleigh supremum.

F.4.3 Every conclusion proved; named analytic inputs supplied as hypotheses (1)

Proposition 10.2.3. *Comparison with the Rayleigh integral, including jumps and zero law.*

Inputs supplied:

(1) `TubeAttained`: every tube $\mathcal{T}_r$ is closed and $\{d_\delta \le r\} = \mathcal{T}_r$ (first part of Equation (10.2.4) of Lemma 10.2.2, proved there from the compactness of $\mathcal{M}_\delta$; nonzero law only)

(2) `TubeTail`: $\mathbb{P}(d_\delta(X) > r) \le e^{-r^2/(2\delta)}$ for $r \ge 0$ (second part of Equation (10.2.4), proved there from the imported Gaussian isoperimetric theorem of Borell and Sudakov–Tsirelson; nonzero law only)

F.4.4 Steps checked, not the result itself; analytic inputs either supplied as hypotheses or left outside Lean (34)

Lemma 2.2.1. *White-space test.*

Lean proves: With nothing supplied, every value of Equation (2.2.1) and $A_1(t) = 2c_0 t^{3-\alpha_0}$ for the diagram integrals of the model M4 (white noise, $d = 1$, $\alpha_0 < 1$); the statements about $\mathbb{E}X_1^2$, $\mathbb{E}X_2$ and the contribution to Equation (2.1.3) follow from the supplied mixed-moment expansion of Proposition 2.1.1 for random variables standing for the chaos terms of the solution.

Not yet formalized: The solution is not constructed.

Input supplied:

(1) `MixedMoment`: the statement of Proposition 2.1.1 (Equation (2.1.2) and Equation (2.1.3)): the diagram limits exist and are finite, $\mathbb{E}[X_m X_n] = \sum_D J_{m,n,D}(t)$ with the products integrable, u^2 integrable and $\mathbb{E}u^2 = \sum_k A_k(t)$; true for the solution under Hypothesis 1.2.1, not proved

Proposition 2.6.2. *Mild construction from the fixed-order limits.*

Lean proves: Only the multiplication bound Equation (2.6.4) of the proof, for F a real polynomial of total degree at most n in finitely many independent standard Gaussians and H a real combination of them.

Not yet formalized: The extension of this bound to the closed space of degree at most n, the almost-sure identification and the mild-solution statement Equation (2.6.3) are not formalized.

Inputs supplied:

(1) the closure step of Equation (2.6.4) (approximation in $\mathscr{P}_{\le n}$, the L^2 Cauchy property of the products and the almost-sure identification of the limit with HF); not formalized

(2) the fixed-order limits X_n in $\mathscr{P}_{\le n}$ (in the proof of Proposition 2.6.2) and the proof of Equation (2.6.3); not formalized

Lemma 3.2.1. *A complex phase bound.*

Lean proves: With the lemma's hypotheses, the numerical-range and scalar steps on $W(L)$ with nothing supplied, and, with the inputs below, the bounds 3, $6(1+\lambda h)$, 6 (times $e^{\lambda h}$) for $C_h(L)$, $F_h(L)$, $H_h(L)$, the root comparisons 7/6, 6/5 and the bound $100e^{2\lambda h}$ for the weighted block map.

Not yet formalized: The identification of the weighted block map with $\mathcal{M}_z(h)$ is not formalized.

Inputs supplied:

(1) Equation (3.2.1) (Crouzeix–Palencia, imported in the manuscript) for C_h, F_h, H_h at $L = A_0 - zB$ with its holomorphy precondition: operators of norm at most $(1+\sqrt{2})M$ whenever the scalar function is bounded by M on $W(L)$

(2) the inverse-root integral representation in the proof of Lemma 3.2.1 for $L^* = A_0 - \overline{z}B$ (bounded holomorphic calculus): $Q' - 1 = \pi^{-1}\int_0^\infty J(t)\,\mathrm{d}t$ with J strongly measurable and $\|J(t)\| \le (|z|d/(1-\delta_a))t^{-1/2}\kappa^{a-3}$

Proposition 3.2.4. *All regularized static phase orders.*

Lean proves: The Cauchy coefficient estimate, the arithmetic at $\lambda = n/h$ and the series bound of the proof, and from them both displays for abstract Banach-space quantities, with the circle bound (or the inputs of Lemma 3.2.1 and Equation (3.2.5)), entireness, the coefficient identification, the norm comparisons, the cutoff removals and the free bound supplied.

Not yet formalized: Phases are not constructed.

Inputs supplied:

(1) the bound $100e^{2\lambda h}$ for the phase propagator on the coupling disc of radius $\delta_{\alpha/2}\lambda^{2-\alpha/2}/d'$, for every $d' \ge d_n$, $d' > 0$ (in the proof of Proposition 3.2.4), supplied in `StaticPhaseCauchy`

(2) in `static_phase_all_orders_cp` the circle bound is derived from Lemma 3.2.1 and three named inputs: `FockSandwich` (Equation (3.2.5) in operator form), `CPInputs` (Equation (3.2.1), inverse-root integral) and `PropagatorBlock`, with positive A_0 and self-adjoint B at every cutoff (supplied, with the named inputs)

(3) in `FockSandwichModel.static_phase_all_orders_model` (wave L12) `FockSandwich`, $A_0 \ge 0$ and $B = B^*$ are proved on the Fourier-side model, not identified with physical space

(4) the added restriction of `static_phase_all_orders_model`: an orthonormal real family ψ_m of size m in $L^2(\mu_\epsilon)$ for every Gaussian cutoff m (so $\mu \ne 0$; the case $\mu = 0$, where every positive-order term vanishes, is not covered by that wrapper)

(5) the phase entries are entire in the coupling (in the proof of Proposition 3.2.4)

(6) the identification of the n-th coefficient, applied to $S_b(f,g)$ times the vacuum, with the cutoff n-th Duhamel phase via Lemma 3.2.3, with $\|z\|_{1/h} \le n\|z\|_{n/h}$; Lemma 3.2.3 is

proved with several coordinates per color (`FiniteWordCutoff`), but the identification of the phase coefficients is not formalized

(7) $\|S_b(f,g)\|_{n/h} \le \|(f,g)\|_{1/h}$ (in the proof of Proposition 3.2.4)

(8) the removal of the band and Gaussian cutoffs, as convergence of the norms (in the proof of Proposition 3.2.4)

(9) the free bound $\|Z_0(h)\|_{1/h} \le \sqrt{e}\,\|(f,g)\|_{1/h}$ (in the proof of Proposition 3.2.4)

Corollary 3.2.5. *Summable static interaction bounds.*

Lean proves: Equation (3.2.10) in full; Equation (3.2.9), with the identification of the interaction map with $\sum_n \sigma^n Y_n$ and the order bounds derived from the primitive inputs below; and Equation (3.2.11) from the per-block bound on adapted phases; the Gaussian parity, the first-variance bounds and that per-block bound are supplied.

Inputs supplied:

(1) for the order bounds (Equation (3.2.7), $n \ge 1$; circle bound from Lemma 3.2.1): `FockSandwich` (Equation (3.2.5) in operator form), `CPInputs` (Equation (3.2.1) with the inverse-root integral) and `PropagatorBlock` (the weighted block map as $\mathcal{M}_z(h)$), with positive A_0 and self-adjoint B at every cutoff (supplied, with the named inputs, in `StaticInteractionCompleted`)

(2) `FockSandwich`, $A_0 \ge 0$ and $B = B^*$ are proved in wave L12 on the Fourier-side model (`FockSandwichModel.static_interaction_model_paper`), with the added restriction of an orthonormal real family ψ_m of size m in $L^2(\mu_\epsilon)$ for every Gaussian cutoff m (so $\mu \ne 0$; the case $\mu = 0$, where every positive-order term vanishes, is not covered by that wrapper)

(3) the remaining inputs of Proposition 3.2.4 for the order bounds: entireness in the coupling, the coefficient identification, the band and the cutoff removals (see that row)

(4) the free estimate $\|\mathcal{S}_0(\mp h)\|_\lambda \le \sqrt{e}$, the group law $\mathcal{S}_0(-h)\mathcal{S}_0(h) = 1$, $Z_0 = \mathcal{S}_0(h)(f,g)$ and the norm comparisons $\|Z_n\|_\lambda \le (\lambda h)^{-1}\|Z_n\|_{1/h}$, $\|(f,g)\|_{1/h} \le \|(f,g)\|_\lambda$ (in the proof of Corollary 3.2.5); an abstract complete real inner product space stands for $L^2(\Omega; X_\lambda)$

(5) Gaussian symmetry, $\mathbb{E}\langle Y_r, Y_s\rangle_\lambda = 0$ for $r+s$ odd (in the proof of Corollary 3.2.5)

(6) the first-variance bounds of Proposition 3.1.2, $\mathbb{E}\|Y_1\|^2 \le e$ times Equation (3.1.6) and $|\mathbb{E}\langle Y_0, Y_2\rangle| \le N\sqrt{e}$ times Equation (3.1.7) (in the proof of Corollary 3.2.5)

(7) for Equation (3.2.11), the per-block bound $\|\mathcal{I}_j y\|^2 \le (1 + \mathcal{E}(h_j, \sigma_j, \lambda))\|y\|^2$ on phases adapted to the past (Equation (3.2.9) with density and tensoring with the independent past, in the proof of Corollary 3.2.5), adaptation being an abstract predicate preserved by each block, and $\|\mathcal{S}_0(h_j)\|^2 \le e^{\lambda h_j}$

Lemma 3.3.2. *Complex sums and changing phase weights.*

Lean proves: With the lemma's hypotheses, the adjoint sandwich bound and the numerical-range and scalar steps on $W(A_0 - V)$ with nothing supplied; with the inputs below, the bound $100e^{2\Lambda h}$ for the weighted block map; and Equation (3.3.3) for given finite jump data and, for the scalar conversion factors, along any monotone time partition.

Not yet formalized: The weighted block map is not identified with the propagator in X_Λ.

Inputs supplied:

(1) Equation (3.2.1) (Crouzeix–Palencia) for C_h, F_h, H_h at $L = A_0 - V$ with weight Λ: operators of norm at most $(1+\sqrt{2})M$ whenever the scalar function is bounded by M on $W(L)$

(2) the inverse-root integral representation in the proof of Lemma 3.3.2 for $L^* = A_0 - V^*$: $Q' - 1 = \pi^{-1} \int_0^\infty J(t)\,\mathrm{d}t$ with J strongly measurable and $\|J(t)\| \le (D/(1-\delta_a))t^{-1/2}\kappa^{a-3}$

Lemma 3.3.4. *A fixed degree-split estimate.*

Lean proves: Equation (3.3.6) with $C_{\mathrm{split}} = 100^8 e^8 \max\{1, 12\delta^{-2}\}$ for any $\delta > 0$, on a finite Fock model of the cutoff Gaussian space with abstract spatial operators, for coefficients of an evolution; the segment bound, the Dyson cube identity, the invariance of the cross subspaces, entire coefficients and Equation (3.3.1) are supplied.

Not yet formalized: The evolution is not constructed.

Inputs supplied:

(1) Equation (3.3.1) for the modes of each color at every $\rho > 0$, as the named input `FockColumn` of `FockForm`

(2) the segment bound of Lemma 3.3.2 for the background propagators, $\|P_z(t,s)\| \le 100e^{2\Lambda(t-s)}$ on every interval free of background endpoints, as applied in Equation (3.3.9) (`SegmentBound`); its operator theory is not formalized

(3) Equation (3.3.13) on the torus of the background radii, with the integrability of the word on each simplex (`DysonCrossCube`); variation of constants is not formalized

(4) the invariance of every cross subspace $\mathscr{Z}_S$ under the background propagator (in the proof of Lemma 3.3.4; `BackgroundPreserves`) and the absolute convergence of the ordinary coefficients on every polydisc (in the proof of Lemma 3.3.4; `EntireCoefficients`); the cutoff evolution, its propagators and the coefficients $U_{\boldsymbol{r}}v$ are not constructed

Proposition 3.3.5. *Uniform interval coefficients.*

Lean proves: Equation (3.3.19) (length substitution, split count, product-coefficient identity), assembled from Equation (3.3.22), with Lemma 3.3.3 proved, Lemma 3.3.4 assembled on its supplied inputs, $Q_{r,q}$ identified with the cutoff inner product (real part used) from the supplied Duhamel word expansion, for $R_\alpha, \sigma_i > 0$, and the sum to Equation (3.3.20).

Inputs supplied:

(1) Equation (3.3.22) combined with the reflection parity (in the proof of Proposition 3.3.5), the coefficient as the sum over degree vectors $\boldsymbol{k}$ ($\sum_i k_i = k$) and splits $r_i + q_i = 2k_i$ of $Q_{\boldsymbol{r},\boldsymbol{q}}$

(2) the inputs of Lemma 3.3.4 for every split (Equation (3.3.1), the segment bound of Lemma 3.3.2, Equation (3.3.13), the invariance of the cross subspaces and entire coefficients; see the row of Lemma 3.3.4), with the interval endpoints (a_i, b_i) in $[0,T]$, $b_i - a_i \le h_i$, and any $\delta > 0$ in $C_{\mathrm{split}} = 100^8 e^8 \max\{1, 12\delta^{-2}\}$

(3) for Equation (3.3.20), the power-series identity at $s = 1$, the vanishing of odd coefficients and the zero-order bound $e\|v\|^2$ (all in the proof of Proposition 3.3.5)

(4) the Duhamel word expansion of the ordinary coefficients (in the proof of Proposition 3.3.5; `DuhamelWords`): $U_{\boldsymbol{r}}v$ and the cutoff coefficient $c_{\boldsymbol{r}}$ are the same finite sum of integrals of words with r_i insertions of color i, uncut and cut; the evolutions are not constructed

(5) from `DuhamelWords` Lean proves $|Q_{\boldsymbol{r},\boldsymbol{q}}| \le |\langle c_{\boldsymbol{r}}, c_{\boldsymbol{q}}\rangle|$, which the earlier step row assumed as the added hypothesis `hQ` (accepted by Le for now on 2026-11-12); $Q_{\boldsymbol{r},\boldsymbol{q}}$ is the real part of $\langle U_{\boldsymbol{r}}v, U_{\boldsymbol{q}}v\rangle_{1/T}$

(6) the reduction to $\sigma_i > 0$ (zero noise and sign change, in the proof of Proposition 3.3.5); not formalized

Proposition 4.1.4. *Completion on the same noise.*

Lean proves: Only the finite Gaussian comparison: for A and $B - A$ positive semidefinite, every seminorm N and $p \geq 1$, $\int N^p \, \mathrm{d}\mathcal{N}(0, A) \leq \int N^p \, \mathrm{d}\mathcal{N}(0, B)$ with both moments finite.

Not yet formalized: The identification of A and B with the masked covariance and auxiliary Gram matrices, Equation (4.1.8), the contraction extension and joint Gaussianity are not formalized.

Inputs supplied:

(1) the covariance matrix A of the masked evaluations $W(\zeta_R F_1), \ldots, W(\zeta_R F_m)$ and the auxiliary Gram matrix B of N_R (in the statement and the proof of Proposition 4.1.4), which need the noise W and the completion of the test space

(2) $A \leq B$ in positive semidefinite order, from $\mathbb{E}W(\zeta_R F)^2 \leq N_R(F)^2$ (Proposition 4.1.2 with $H = H_a^{\mathbb{C}}$ and Equation (4.1.8), in the proof of Proposition 4.1.4)

(3) the joint centered Gaussian law of the masked evaluations, so that their law is $\mathcal{N}(0, A)$ (in the statement and the proof of Proposition 4.1.4)

Proposition 4.2.3. *Form and phase kernel.*

Lean proves: Only the finite, algebraic or scalar steps of this result listed in the companion's statement ledger.

Not yet formalized: The result itself.

Assumptions and limits: The checked steps take no analytic input beyond the paper's hypotheses: the Lean statements are definitions and a matrix identity for arbitrary real parameters. The reading of the parameters as cosines and sines of a phase and as a covariance coefficient, the continuous extension at zero frequency, and the Bessel-weighted change of coordinates and the weight $1/\sqrt{\langle\xi\rangle\langle\eta\rangle}$ that lead to Equation (4.2.17) are not hypotheses of these statements; they are outside Lean (see the statement-ledger entry `DimensionalMatrix`).

Proposition 4.2.5. *Both variance directions.*

Lean proves: A bound on an abstract variance tied to $\mathbb{E}|\ell_R|^2$ only through the named input Equation (4.2.18). The spectral core (the sums of the ν_R-integrals of Equation (4.2.18), both directions, the $h^{2\beta}$ form) in full with no input.

Not yet formalized: ℓ_R, the spaces E_r and J are not constructed.

Inputs supplied:

(1) Equation (4.2.18) (last claim of Proposition 4.2.3, needs the construction of the noise), supplied as `hlink`, `ofReal(var R t0 h z w)` $\leq$ the ν_R lower integral of $\|\texttt{coef}(Jz, Jw)\|^2$, the manuscript's display with $U = Jz$, $V = Jw$

(2) J maps the phases into $L^2(\mathbb{R}^d; \mathbb{C}^2)$ preserving inner products (`hJL2`, `hJ`; at the manuscript's definition of J), weaker than the manuscript's unitary J

(3) the identity $\|z\|^2_{E_{s-\gamma}} = \|\langle\xi\rangle^{-\gamma} Jz\|_2^2$ (`hnormSG`; in the proof of Proposition 4.2.5)

Lemma 5.1.8. *Fixed-interval operator construction.*

Lean proves: Only the finite, algebraic or scalar steps of this result listed in the companion's statement ledger.

Not yet formalized: The result itself.

Assumptions and limits: The checked step takes no analytic input beyond the paper's hypotheses: the Lean statement assumes only $C \geq 0$, $h > 0$ and $L \geq 0$. The variance budget Equation (5.1.12) and the Schatten estimate it feeds are not hypotheses of this statement; they are outside Lean (see the statement-ledger entry `InteractionDriver`).

Lemma 5.1.9. *Hölder path limit.*

Lean proves: Only the finite, algebraic or scalar steps of this result listed in the companion's statement ledger.

Not yet formalized: The result itself.

Assumptions and limits: The checked steps take no analytic input beyond the paper's hypotheses: the Lean statements assume only order conditions on the real exponents. The Gaussian moment bounds for increments, the dyadic chaining argument and the Hölder interpolation are not hypotheses of these statements; they are outside Lean (see the statement-ledger entry `InteractionDriver`).

Lemma 7.1.1. *Canonical law scaling.*

Lean proves: Only the finite, algebraic or scalar steps of this result listed in the companion's statement ledger.

Not yet formalized: The result itself.

Assumptions and limits: The checked steps take no analytic input beyond the paper's hypotheses: the Lean statements assume only $T > 0$ and $\alpha < 3$. The scaling of the Gaussian noise and its covariance, the equality in law of the rescaled solution, the scaling of the Green measure and the extension to the full series and its second moment are not hypotheses of these statements; they are outside Lean (see the statement-ledger entry `DirectEvent`).

Lemma 7.2.1. *Coupled Gaussian block inputs.*

Lean proves: Only the finite, algebraic or scalar steps of this result listed in the companion's statement ledger.

Not yet formalized: The result itself.

Assumptions and limits: The checked step takes no analytic input beyond the paper's hypotheses: the Lean statement assumes only $\delta > 0$. The rescaled noise and its mean shift are not hypotheses of this statement; they are outside Lean (see the statement-ledger entry `JointTilt`).

Lemma 7.2.4. *Indexed cone and terminal displacement.*

Lean proves: Every conclusion, for an abstract ground family (flows, vectors, duals, rates and observable, with the properties of the compact mean family supplied as inputs).

Not yet formalized: The identification of the abstract ground family with the physical wave family of the compact mean family is not formalized.

Inputs supplied:

(1) `GroundFamily` data fields `P`, `e`, `ell`, `lam` (Equation (6.3.11), Equation (6.3.13), Proposition 6.3.1): flows $P_\sigma(t)$, vectors e_σ, bounded linear duals ℓ_σ, rates λ_σ, for $\sigma \in I = [0,1]$, $t \geq 0$ ($\Pi_\sigma = e_\sigma \ell_\sigma$ and $Q_\sigma = I - \Pi_\sigma$ are derived definitions `GroundFamily.Pi`, `GroundFamily.Q`, not fields)

(2) `GroundFamily` data fields `e0`, `obs` (Section 7.2): the data $e_0 \in F$ and the bounded linear observable $O_\phi : F \to \mathbb{R}$

(3) `GroundFamily` fields `d0`, `lam_pos`, `d0_pos` (Proposition 6.3.1, Equation (6.3.4)): a gap $d_0 > 0$ and $\lambda_\sigma > 0$ on I (weakening of $\sqrt{\varepsilon} \leq \lambda_\sigma$)

(4) `GroundFamily` fields `ell_e`, `P_Pi`, `Pi_P` (Proposition 6.3.4, Equation (6.3.14)): $\ell_\sigma(e_\sigma) = 1$ and $P_\sigma(t)\Pi_\sigma = \Pi_\sigma P_\sigma(t) = e^{\lambda_\sigma t}\Pi_\sigma$ on I for $t \geq 0$

(5) `GroundFamily` field `normalized_complement` (Proposition 6.3.5, Equation (6.3.17)): for every $0 < \eta < d_0$ a C_η with $\|e^{-\lambda_\sigma t} P_\sigma(t) Q_\sigma\| \leq C_\eta e^{-\eta t}$ uniformly over $\sigma \in I$, $t \geq 0$

(6) `GroundFamily` fields `e_cont`, `ell_cont` (Proposition 6.3.4): norm continuity of $\sigma \mapsto e_\sigma$ and $\sigma \mapsto \ell_\sigma$ on I
(7) `GroundFamily` fields `margin_ell`, `margin_obs` (Equation (6.3.15)): $\inf_I \ell_\sigma(e_0) > 0$ and $\inf_I O_\phi(e_\sigma) > 0$

Lemma 7.2.5. *Composition over time blocks and regularized products.*
Lean proves: Only the finite, algebraic or scalar steps of this result listed in the companion's statement ledger.
Not yet formalized: The result itself.
Input supplied:
(1) The Lean statement takes as hypotheses: (1) the recurrence $d(n+1) \le Cd(n) + C^n e_{\mathrm{src}}$ for every n, for the difference $d(n)$ of the first n ordered products (`hstep`); in the proof of Lemma 7.2.5 it comes from operator-norm submultiplicativity for the product factors, after the finite factor lists are extended by identities; (2) $d(0) \le 0$ (`hzero`). The conditions $C \ge 1$ and $e_{\mathrm{src}} \ge 0$ are parameter conditions. The moments of C and of the error are outside Lean (see the statement-ledger entry `ActualEvent`).

Proposition 7.2.7. *Original point lower rate at the Gaussian quadratic cost.*
Lean proves: Only the finite, algebraic or scalar steps of this result listed in the companion's statement ledger.
Not yet formalized: The result itself.
Assumptions and limits: The checked step takes no analytic input beyond the paper's hypotheses: the Lean statement assumes only $\delta > 0$. The Gaussian change of law, the event on which the penalty bound holds and the limit $\delta \to 0$ are not hypotheses of this statement; they are outside Lean (see the statement-ledger entry `ActualEvent`).

Proposition 7.3.4. *Monotone rates and the original point moment.*
Lean proves: The mask family and every rate statement with the section's hypotheses and nothing supplied, for $\lambda_{R,s}$ defined as the square root of the real Rayleigh supremum of $m_R h_s$; Equation (7.3.5), derived from Equation (7.2.14) as a supplied input, for a real function in place of the point moment.
Not yet formalized: Compact ground rates are not formalized.
Input supplied:
(1) Equation (7.2.14) of Proposition 7.2.7 for the masks m_R, all large R and one fixed x, with the compact ground rate of $m_R h_s$ read as its Rayleigh rate and v_Ψ as its integral form; used only by the point-moment display

Proposition 9.2.5. *Averaged block mean tends to zero.*
Lean proves: Every conclusion, for abstract random paths with the supplied moment bound.
Not yet formalized: The operator paths $M_R(Y_m)$ and the residual noises are not constructed, so the identification of these paths with the manuscript's block paths is not formalized.
Inputs supplied:
(1) the moment bound of Corollary 9.2.4 (from Proposition 9.2.3) on the unstopped block paths: almost surely C^θ, p-th norm power integrable, $(\mathbb{E}\|M_R(Y_m)\|^p)^{1/p} \le C\sqrt{p}\, R^{d/Q}$
(2) measurability of the C^θ norm of the stopped block paths (implicit in the manuscript)

Proposition 9.3.2. *Closed form and quarter-power phase.*

Lean proves: For an abstract bounded Hermitian pairing on Mathlib's H^1 with Equation (9.3.1) supplied, Equation (9.3.3), the form version of $A \geq 1$, the step $\|u\|^2_{H^{1/2}} \leq bz$ and the bounded resolvent of the form (self-adjoint, positive, injective, norm at most 1, unique weak solution).

Not yet formalized: H_V, $D(A^{1/2}) = H^1$, Equation (9.3.4) and $H^{-1/2}$ are not formalized.

Inputs supplied:

(1) `SignedMultiplierForm P k`: Equation (9.3.1), the conclusion of Lemma 9.3.1 (not formalized), for an abstract bounded operator P on H^1 standing for the pairing v_V; the multiplier V is not constructed

(2) the self-adjointness of P: the Hermitian pairing of the proof of Lemma 9.3.1

Lemma 10.1.1. *Free wave form and compact Young baseline.*

Lean proves: Both compact-baseline displays on an abstract nonzero Hilbert space with a supplied free group, isometric velocity reversal and weakly vanishing translations, for a Young evolution given only by convergence of its left Young sums; and $W_t^{\mathsf{T}} J_{\mathrm{symp}} W_t = J_{\mathrm{symp}}$ per frequency and the force skewness for the L^2 pairing.

Not yet formalized: J_E and the preservation of ω on E are not formalized.

Inputs supplied:

(1) the free wave group on $E = H^{1/2} \times H^{-1/2}$ with its group law, the isometric velocity reversal with $S_E(-h) = \mathcal{R} S_E(h) \mathcal{R}$, and the spatial translations, isometric, commuting with $S_E(h)$ and weakly null as $|y| \to \infty$ (in the proof of Lemma 10.1.1); E is an abstract nonzero real Hilbert space

(2) Proposition 6.2.4 on $\mathcal{L}(E)$ (in the proof of Lemma 10.1.1): the left Young sums of X over partitions of $[s,t]$ converge in operator norm to $U_X(t,s) - I$; supplied in the weaker form of convergence along some nontrivial filter of finite node lists in $[s,t]$ (no ordering, endpoint or mesh condition)

Proposition 11.1.3. *Positive conic maximizer.*

Lean proves: Only the finite, algebraic or scalar steps of this result listed in the companion's statement ledger.

Not yet formalized: The result itself.

Assumptions and limits: The checked step takes no analytic input beyond the paper's hypotheses: the Lean statement assumes only positive weights and active labels, $\langle \Phi, k_i \rangle - b_i \geq 0$. Dual coercivity, the existence and uniqueness of the dual minimizer, attainment and the maximum over active sets are outside Lean (see the statement-ledger entry `PositiveGram`).

Proposition 11.1.5. *Entrywise Gram comparison.*

Lean proves: Only the finite, algebraic or scalar steps of this result listed in the companion's statement ledger.

Not yet formalized: The result itself.

Assumptions and limits: The checked step takes no analytic input beyond the paper's hypotheses: the Lean statement assumes only nonnegative weights and the entrywise order $C_{ij} \leq D_{ij}$, a hypothesis of Proposition 11.1.5. The Gram realization (Lemma 11.1.4) and the optimization over weights are outside Lean (see the statement-ledger entry `PositiveGram`).

Proposition 11.4.2. *Exact white spatial energy.*

Lean proves: Only the finite, algebraic or scalar steps of this result listed in the companion's statement ledger.

Not yet formalized: The result itself.

Input supplied:

(1) The Lean statements take as hypothesis: (1) the inequality Equation (11.4.1) of Lemma 11.4.1, $0 \le b - 2zA + z^2/3$ for every real z, with $A = \int_{\mathbb{R}} f^4$ and $b = \int_{\mathbb{R}} (f')^2$ for a real unit $f \in H^1(\mathbb{R})$ (hypothesis `h` of `WhiteCDF.cdf_square_bound`). The bound $3A^2 \le b$ that `WhiteCDF.energy_upper` assumes is the conclusion of `cdf_square_bound`. The white-model statements assume only $c \ge 0$, and $0 < a < 1$ for Hypothesis 1.2.1. The variational energy, its domain and its attainment are outside Lean (see the statement-ledger entries `WhiteCDF` and `WhiteModel`).

Theorem 11.4.3. *Explicit white moment bounds.*

Lean proves: Equation (11.4.2) for the variational value S_2^{pos} in place of $C_2(c,a)$ (identified by Theorem 11.2.6), for $c > 0$ and $0 < a < 1$, with the value $\mathcal{E}_{\mathrm{sp}} = c^2/6$ of Proposition 11.4.2 supplied (each bound uses one inequality of it), and that M_a, $K_0(a)$ and both bound formulas are positive.

Not yet formalized: The time exponent sentence and the case $c = 0$ are not formalized.

Input supplied:

(1) Proposition 11.4.2: the spatial energy of $c\delta_0$ is $c^2/6$ for $c > 0$; the lower bound uses only $c^2/6 \le \mathcal{E}_{\mathrm{sp}}$ (the sech profile), the upper bound only $\mathcal{E}_{\mathrm{sp}} \le c^2/6$ (the CDF square, Equation (11.4.1)); not proved

Proposition A.1.3. *Riesz finite coefficients.*

Lean proves: With nothing supplied, Equation (A.1.7) and $A_1 = J_{1,1} + 2J_{2,0}$ for the diagram integrals of M4, and Equation (A.1.8) with finiteness for all splits and pairings; the order-two statements about $\mathbb{E}X_2$, $\mathbb{E}X_1^2$ follow from the supplied mixed-moment expansion of Proposition 2.1.1.

Not yet formalized: The solution is not constructed. That the total coefficient uses the multiplicities of Equation (A.1.3) is not formalized.

Input supplied:

(1) `MixedMoment`: the statement of Proposition 2.1.1: the diagram limits exist and are finite, $\mathbb{E}[X_m X_n] = \sum_D J_{m,n,D}(t)$ with the products integrable, u^2 integrable and $\mathbb{E}u^2 = \sum_k A_k(t)$; true for the solution under Hypothesis 1.2.1, not proved (order-two wrapper `riesz_small_paper'` only)

Proposition B.1.2. *One-dimensional upper bound.*

Lean proves: Equation (B.1.5) on the model M4 at every noise width, uniformly, with nothing supplied, and for the limit coefficients (Riesz case: the supplied convergence of every diagram as the noise width tends to zero (Lemma 2.5.2)); the form $\sum_m \mathbb{E}[X_m X_{2k-m}]$ and Equation (B.1.6) hold for random variables with the supplied mixed-moment expansion of Proposition 2.1.1.

Not yet formalized: The solution is not constructed.

Inputs supplied:

(1) `MixedMoment`: the statement of Proposition 2.1.1 (with its proof): every diagram limit exists and is finite, $\mathbb{E}[X_m X_n] = \sum_D J_{m,n,D}(t)$, u^2 integrable and $\mathbb{E}u^2 = \sum_k A_k(t)$;

TRUE for the solution under Hypothesis 1.2.1; about random variables standing for the unconstructed solution and chaos terms

(2) `DiagramLimits` (Riesz case only): every model diagram converges to `diagramLim` as $\epsilon \to 0+$; part of Lemma 2.5.2, invoked in the proof of Proposition B.1.2; TRUE under Hypothesis 1.2.1; proved for white noise (`D1Upper.diagramLimits_white`) and implied by `MixedMoment`

Proposition B.1.5. *Upper bound for alpha <= 1.*

Lean proves: Under Hypothesis 1.2.1 with $d \in \{1, 2, 3\}$, $\alpha \leq 1$ and $V > 0$, both inequalities of Equation (B.1.13) on the diagram model at every noise width $\epsilon > 0$ with nothing supplied; the first inequality for $A_k(t) = \sum_m \mathbb{E}[X_m X_{2k-m}]$ and $\mathbb{E}u^2 \leq \exp(C_{\mathrm{dir}}^{\mathrm{gen}} t^{\kappa})$ for random variables with the supplied mixed-moment expansion of Proposition 2.1.1.

Not yet formalized: The solution is not constructed.

Input supplied:

(1) `MixedMoment`: the statement of Proposition 2.1.1: the diagram limits exist and are finite (the manuscript proves them by Lemma 2.5.2 and the η-limit paragraph in the proof of Proposition B.1.5), $\mathbb{E}[X_m X_n]$ is the sum of the diagram limits, $\mathbb{E}u^2 = \sum_k A_k(t)$; TRUE for the solution under Hypothesis 1.2.1

Corollary B.1.7. *First-moment calibration.*

Lean proves: $C_{1,*} = C_{2,*}/2^{(4-\alpha)/(3-\alpha)}$ and $2C_{1,*} < C_{2,*}$ with nothing supplied, Equation (B.1.14) for random variables with the supplied mixed-moment expansion of Proposition 2.1.1 and the supplied first-moment series of the chaos expansion, and the conditional rate clause for an abstract first moment.

Not yet formalized: The solution is not constructed. The Proposition 1.4.4 comparison is commentary.

Inputs supplied:

(1) `MixedMoment`: the statement of Proposition 2.1.1; here it gives $\mathbb{E}X_n = \sum_D J_{n,0,D}(t)$ (with $X_0 = 1$), the odd terms zero and the diagram limits; TRUE for the solution under Hypothesis 1.2.1

(2) `FirstMomentSeries`: $X_0 = 1$, u integrable and $\mathbb{E}u = \sum_n \mathbb{E}X_n$ (the definition of X_n at the start of Section 2 and the proof of Corollary B.1.7, "the L^2 expansion permits taking expectations of partial sums"); TRUE for the solution and its chaos terms

Corollary C.2.6. *Ordinary product and Riesz covariances in dimension three.*

Lean proves: With the corollary's hypotheses, that the product and Riesz targets are nonzero covariances with scaling $3 - \alpha$ whose endpoints satisfy Hypothesis C.2.2, and, from the supplied Proposition C.2.5, the coefficient, moment and asymptotic bounds for an abstract model of $A_k(t)$, $\mathbb{E}u^2$ and $\mathcal{M}_{\mathrm{st}}$; the asymptotic bound is for every spectral measure of the low endpoint.

Input supplied:

(1) `ThreeTransfer`: the exact statement of Proposition C.2.5 (proved in the manuscript) for an abstract `ThreeMomentModel` at the midpoint ϑ; true for the manuscript's $A_k(t)$, $\mathbb{E}u^2(t, x)$ and $\mathcal{M}_{\mathrm{st}}$, which the package does not construct

Corollary C.2.7. *Finite sums of linear images.*

Lean proves: With the corollary's hypotheses, that $\sum_i w_i (T_i)_{\#}\Gamma_i$ is a nonzero covariance with scaling $3-\alpha$ whose endpoints satisfy Hypothesis C.2.2, and, from the supplied Proposition C.2.5, the coefficient, moment and asymptotic bounds for an abstract model of $A_k(t)$, $\mathbb{E}u^2$ and $\mathcal{M}_{\mathrm{st}}$; the asymptotic bound is for every spectral measure of the low endpoint.

Input supplied:

(1) `ThreeTransfer`: the exact statement of Proposition C.2.5 (proved in the manuscript) for an abstract `ThreeMomentModel` at the midpoint ϑ; true for the manuscript's $A_k(t)$, $\mathbb{E}u^2(t,x)$ and $\mathcal{M}_{\mathrm{st}}$, which the package does not construct

Proposition D.1.7. *Log-convexity of the upper growth type.*

Lean proves: Every conclusion, for an abstract moment function with the supplied coefficient, interpolation, static-law, minorant and upper-bound facts.

Not yet formalized: The moments $\mathbb{E}u^{(a)}(T,x)^p$ of the solution are not constructed, so their identification with that function is not formalized.

Inputs supplied:

(1) Equation (D.1.1) (Chen–Hu static law): $0 < L_0$ and $T^{-\kappa_{\mathrm{st}}} \log \mathbb{E}U(T,x)^p \to p^{\kappa_{\mathrm{st}}} L_0$ for $p = 1, 2$ (fields `L0_pos`, `static_law`)

(2) Equation (D.1.11) of Lemma D.1.6 with $c_{p,0}(a) = 1$ (Equation (D.1.10)), nonnegative coefficients, summable for $t > 0$, $0 \le a < a_{\max}$ (field `series`)

(3) Equation (D.1.12) of Lemma D.1.6 (field `holder`)

(4) Equation (D.1.6) of Proposition D.1.3, as: every $y < p^{\kappa_{\mathrm{st}}} L_0$ is eventually below $T^{-\kappa(a)} \log \mathbb{E}u^{(a)}(T,x)^p$, $0 < a < a_{\max}$ (field `minorant`)

(5) Equation (3.3.28) of Theorem 3.3.8 at temporal exponent a: $\mathbb{E}u^{(a)}(T,x)^2 \le e(T+2)^d \exp(CT^{\kappa(a)})$ for $T \ge 1$, one finite C (field `full_upper`)

(6) Cauchy–Schwarz $(\mathbb{E}u^{(a)}(T,x))^2 \le \mathbb{E}u^{(a)}(T,x)^2$ (field `cauchy_schwarz`; in the proof of Proposition D.1.7)

Corollary D.1.8. *Recovery of the static moment constant.*

Lean proves: Every conclusion, for an abstract moment function with the supplied facts of the logconvexity proposition and the static minorant and law.

Not yet formalized: The moments of the solution are not constructed, so their identification with that function is not formalized.

Inputs supplied:

(1) Equation (D.1.6) of Proposition D.1.3 (field `minorant`) and $\overline{\Lambda}_p(0) = C_p$ from Equation (D.1.1) (fields `L0_pos`, `static_law`)

(2) the inputs of Proposition D.1.7: Equation (D.1.11) and Equation (D.1.12) of Lemma D.1.6 (fields `series`, `holder`), Equation (3.3.28) of Theorem 3.3.8 (field `full_upper`), Cauchy–Schwarz (field `cauchy_schwarz`)

F.4.5 Not formalized (2)

Theorem 3.3.8	Full upper scale
Theorem 11.2.6	Intrinsic original second-moment constant

Besides these rows, the companion checks 2239 further computations that do not correspond to a single numbered result of the book.

F.5 Counts and growth

Which numbered results the table counts. The table covers 220 numbered theorems, propositions, lemmas and corollaries. Besides the two main theorems recorded as outside Lean, 123 further results (56% of the total) are not formalized. The separately numbered no-gos in Chapter 12 are not added to this count; Appendix G counts them with the other results. Some restate results listed here; the listed coverage retains its own scope.

Status	Results	Share
Formalized with the paper's own hypotheses	44	20%
With the paper's hypotheses; narrower conclusion	16	7%
Every conclusion proved; inputs supplied	1	0%
Steps checked; inputs supplied	34	15%
Main theorems outside Lean	2	1%
Not formalized	123	56%
Total	220	100%

The groups above also contain 4 rows for displayed equations or remarks, which are not numbered results. This is why the first group above has 48 rows and the first line of this table 44.

How the companion grew. Each stage is a tagged commit of the companion, from its creation on November 9 to the version described in this appendix. Claims counts the Lean declarations the companion lists for checking, and Theorems counts those among them that are theorems (the others are definitions); Results covered counts the rows of the lists above.

Stage	Date	Claims	Theorems	Results covered
`L0-companion-created`	November 9	88	82	25
`ledger-gate`	November 10	88	82	28
`L1-gate`	November 10	117	104	28
`L2-gate`	November 10	223	188	29
`L3-gate`	November 10	557	470	33
`L4-gate`	November 11	724	611	40
`reanchor-975feb3`	November 11	724	611	40
`L5-gate`	November 11	972	810	46
`L6-gate`	November 11	1463	1210	59
`L7-gate`	November 12	1731	1430	67
`L8-gate`	November 12	2108	1747	71
`L9-gate`	November 12	2468	2050	80
`L10-gate`	November 13	2757	2268	82
`L11-gate`	November 13	2955	2423	82
`L12-gate`	November 13	3107	2541	85
`L13-gate`	November 13	4504	3654	101
`L14-gate`	November 13	4504	3654	101

Appendix G

How far each result has been checked

This appendix records how far the numbered results of this book have been checked, in the three ways used in this project: by AI review, by Lean and by people. It is generated from the verification ledger, a table in the book's repository with one row for each of the 253 numbered theorems, propositions, lemmas, corollaries and no-go results. The counts below are those of the ledger on November 16, 2026. The ledger in the repository is the current record, and it changes as results are checked. The ledger released with this version of the book is at

`github.com/chenle02/stratonovich-ham-second-moment/blob/v1.0.0/VERIFICATION.md`

For credit, the ledger divides the results into five groups by chapter: group I is Chapters 1–3 (the setting and the upper bound), group II is Chapters 4–7 (Gaussian approximation and the lower bound), group III is Chapters 8–11 (the matching upper bound and the constant), group IV is Appendices A–D, and group V is the no-go results of Chapter 12. Table G.1 gives the counts.

Table G.1: How far the numbered results have been checked, by group (ledger of November 16, 2026).

	I	II	III	IV	V	All
Numbered results	31	72	82	35	33	253
Lean						
Formalized in full	6	16	11	11	0	44
Formalized, narrower conclusion	2	4	10	0	0	16
Every conclusion, inputs supplied	0	0	1	0	0	1
Steps checked; inputs supplied or left outside Lean	8	11	7	8	0	34
Outside Lean	1	0	1	0	0	2
No Lean claim	14	41	52	16	33	156
Checked by a person						
Checked	0	0	0	0	0	0
Disputed	0	0	0	0	0	0
Not yet checked	31	72	82	35	33	253

AI review. The repository keeps the AI reviews of this project in dated folders, with the responses to their findings. A folder may hold several review runs, or only preparation, decisions or diagnostics, and not every run produced a usable report. Appendix E

summarizes these records. No review grade is assigned to an individual result, so the table has no row for them. An AI review shows where to look; it is not a proof.

Lean. The Lean rows come from the coverage file of the Lean companion from which Appendix F is generated; the script that generates this appendix checks the ledger's Lean entries and numbers of claims against that file. Of the 253 results, 95 have some Lean claim, and two more, all main theorems, are recorded as outside Lean. Appendix F says, result by result, what Lean checks and which inputs it takes as given. A Lean entry never covers the analytic inputs, and whether the Lean statements say what the book says was reviewed by AI, not by a person.

People. To record a check, a mathematician opens a pull request that changes exactly one row of the ledger and says what was checked (the statement, the proof, the cited inputs and their hypotheses) and what was not. A result restated from a cited source is checked against that source, not reproved. To report a gap or an error, a reader opens an issue naming the result's label and the step in question; the row is then marked as disputed, and it returns to checked only through a new pull request that links the closed issue. On the date above, no result had yet been checked in this way. This is the column where readers can help most.

G.1 What the main theorems rest on

The four main theorems of this book are Theorems 3.3.8, 11.2.6, 11.3.4 and 11.4.3. This section lists recorded citation links for these theorems in Chapters 2–11, as a reading aid.

A result *rests directly on* another result when its statement or its proof cites that result, cites an equation assigned to it, or uses a preceding-result phrase recognized by the script, subject to the recorded link corrections. A theorem *rests on* every result reached by following these links. The list is made by a script from the source of the book (`scripts/critical-path/make_critical_path.py`). It shows which results a proof cites. It does not say that a proof is correct, and it is not a review. It can err in both directions: a result cited only for comparison is counted, and a result used without being cited by its label is missed. The second happens often: a result is cited in the sentence that introduces a statement, or it is used by name. For 52 results, AI-assisted author-side reading of the statements and proofs was recorded: the results that most others depend on, and the results that the script did not reach. This added 28 links and removed 2; each is recorded with the words that justify it in `scripts/critical-path/link-corrections.json`. The other results were not read in this way, and the third column of the list below may miss links for them. In that column a number in parentheses is a result cited only in the sentences that introduce the statement; it is shown for the reader and is not counted as a link.

The recorded graph reaches 168 of the 180 results with printed proofs in Chapters 2–11, including the four main theorems themselves. The second-moment theorem reaches 153 other results in this graph. Table G.3 gives the count by chapter. Of the 168 results, Lean formalizes 29 in full and 15 with a narrower conclusion, proves one with supplied

Table G.2: What each main theorem rests on: the number of other results reached in the recorded graph, excluding the theorem named in the row, and their Lean classes as in Appendix F (the last column counts the results with no Lean claim or outside Lean).

Theorem	Title	Results	Full	Narrower	Supplied	Partial	None
Theorem 3.3.8	Full upper scale	20	6	2	0	5	7
Theorem 11.2.6	Intrinsic original second-moment constant	153	25	8	1	21	98
Theorem 11.3.4	The computed occupation ceiling	157	26	10	1	21	99
Theorem 11.4.3	Explicit white moment bounds	167	29	15	1	22	100

inputs and checks steps of 23; the other 100 have no Lean claim or are outside Lean. No result has been checked by a person.

Table G.3: The results the four main theorems rest on, by chapter, with their Lean classes. Counts include the four main theorems.

Chapter	Proved results	Rested on	Full	Narrower	Supplied	Partial	None
2	11	9	1	0	0	1	7
3	15	12	5	2	0	4	1
4	24	22	12	0	0	3	7
5	16	16	2	0	0	2	12
6	18	18	0	0	0	0	18
7	14	14	2	3	0	6	3
8	19	17	5	3	0	0	9
9	14	14	0	0	0	2	12
10	29	27	0	1	1	1	24
11	20	19	2	6	0	4	7
All	180	168	29	15	1	23	100

The list below gives all results reached by the recorded graph in Chapters 2–11, in book order. The third column gives recorded direct links. The fourth counts other listed results that reach the row through these links; a large count indicates many recorded citation paths, not mathematical indispensability. The last column is its Lean class; a dash means no Lean claim.

Result	**Title**	**Rests directly on**	**Used by**	**Lean**
Proposition 2.1.1	Mixed terms	2.4.1, 2.5.1, 2.5.2, 2.5.3, 2.6.1, 2.6.2	40	—
Lemma 2.3.1	Homogeneous damped norms and temporal tails	(2.3.2)	50	full

Lemma 2.3.2	Translated covariance Cauchy–Schwarz	—	50	—
Lemma 2.4.1	Pairing product envelope	2.3.2	49	—
Lemma 2.5.1	Positive spatial Wick-measure limit	—	49	—
Lemma 2.5.2	Joint diagram limits and fixed-order construction	2.3.1, 2.4.1, 2.5.1	48	—
Lemma 2.5.3	Corrected crude estimate	2.3.1, 2.4.1, 2.5.2	47	—
Lemma 2.6.1	Uniform vertexwise regularization bound	2.3.1, 2.4.1, 2.5.2, 2.5.3 (2.6.2)	46	—
Proposition 2.6.2	Mild construction from the fixed-order limits	2.5.2, 2.6.1	41	partial
Lemma 3.1.1	Two static contraction bounds	—	12	full
Lemma 3.2.1	A complex phase bound	—	11	partial
Lemma 3.2.2	Gaussian cutoff form bound	3.1.1	11	narrower
Lemma 3.2.3	Exact cutoffs for finite Gaussian words	(3.2.2)	10	full
Lemma 3.3.1	Dimension-independent Gaussian contractions	3.1.1, 3.2.2	10	narrower
Lemma 3.3.2	Complex sums and changing phase weights	3.2.1	10	partial
Lemma 3.3.3	A coefficient bound for a product with nonnegative coefficients	(3.3.5)	9	full
Lemma 3.3.4	A fixed degree-split estimate	3.2.1, 3.2.3, 3.3.1, 3.3.2	9	partial
Proposition 3.3.5	Uniform interval coefficients	3.2.3, 3.3.3, 3.3.4	8	partial
Lemma 3.3.6	The finite terminal-chain Wick formula	—	9	full
Lemma 3.3.7	Uniform series tails from scaled moments	3.3.6 (3.3.5)	8	full
Theorem 3.3.8	Full upper scale	2.1.1, 2.5.2, 2.5.3, 2.6.2, 3.3.4, 3.3.5, 3.3.6, 3.3.7	7	outside
Proposition 4.1.1	Translated spectral mass	—	77	full
Proposition 4.1.2	Auxiliary mask norm	4.1.1	76	full
Lemma 4.1.3	Temporal covariance completion	—	81	full
Proposition 4.1.4	Completion on the same noise	4.1.2, 4.1.3	75	partial
Lemma 4.1.6	Modulated amplitudes	4.1.3	76	full
Lemma 4.1.7	Correlated trigonometric products	4.1.6	75	full
Lemma 4.1.8	Continuous sine factors	4.1.3, 4.1.7	74	full
Proposition 4.2.1	Uniform scalar row	(4.1.7)	69	full
Corollary 4.2.2	A time exponent above one half	4.2.1	68	full
Proposition 4.2.3	Form and phase kernel	4.1.2, 4.1.3, 4.1.4, 4.1.8	73	partial
Lemma 4.2.4	Hilbert-valued finite Bessel inequality	(4.2.3, 4.2.5)	68	full

Proposition 4.2.5	Both variance directions	4.1.2, 4.1.3, 4.1.8, 4.2.1, 4.2.2, 4.2.3, 4.2.4	67	partial
Proposition 4.2.6	Column and adjoint-column maps	4.2.5	66	—
Lemma 4.3.1	Scalar power estimates	—	69	full
Lemma 4.3.2	Two Hermitian trace bounds	4.3.1	68	full
Proposition 4.3.3	Finite Gaussian matrix moment	4.3.1, 4.3.2	67	full
Lemma 4.3.5	Cutoff factorization	—	77	—
Proposition 4.3.6	Whole-space cutoff singular values	4.3.5	72	—
Proposition 4.3.7	Both compact envelopes	4.3.5, 4.3.6	70	—
Lemma 4.3.8	Compact positive order and trace	—	69	—
Proposition 4.3.9	Localized finite variance bounds	4.3.7, 4.3.8	67	—
Corollary 4.3.10	Finite Gaussian operators	4.3.3, 4.3.8, 4.3.9	66	—
Proposition 5.1.1	Compact operator path on the original noise space	5.1.2, 5.1.8, 5.1.9	8	—
Lemma 5.1.2	Basis in the prescribed quotient	4.1.3	72	—
Lemma 5.1.3	Covariance coefficients	4.2.3, 5.1.2	70	—
Lemma 5.1.4	Deterministic coefficient operators	4.2.3, 5.1.3	69	—
Lemma 5.1.5	Both variances and their tails	4.2.5, 4.2.6, 4.3.7, 5.1.2, 5.1.4	65	—
Lemma 5.1.6	Compact domination of positive tails	4.3.8 (5.1.5)	65	—
Lemma 5.1.7	Retained finite Gaussian variance powers	4.3.3, 4.3.8, 4.3.10	65	—
Lemma 5.1.8	Fixed-interval operator construction	4.3.9, 4.3.10, 5.1.2, 5.1.5, 5.1.6, 5.1.7	64	partial
Lemma 5.1.9	Hölder path limit	4.2.2, 4.2.5, 4.3.10, 5.1.4, 5.1.5, 5.1.8 (5.1.1)	63	partial
Lemma 5.2.1	Finite Gaussian linear images	—	61	full
Proposition 5.2.2	Gaussian transfer and stability	5.1.8, 5.1.9, 5.2.1	60	—
Lemma 5.2.3	Original spatial space and heat	4.1.4 (5.2.2)	60	full
Lemma 5.2.4	Feature isometry preserving the given noise	5.1.2	60	—
Proposition 5.2.5	Canonical sources on the extended space containing the given noise	5.2.2, 5.2.3, 5.2.4	59	—
Lemma 5.2.6	Regularity for each fixed cutoff	5.2.5	42	—
Proposition 5.2.7	Ordinary source response	4.2.3, 5.1.4, 5.2.5	47	—
Lemma 6.1.1	Chains and mixed-order comparison	2.5.2, 2.6.1, 5.2.6 (5.2.5)	41	—

Proposition 6.1.2	Ordinary solutions and tested moments	2.6.1, 6.1.1	40	—
Proposition 6.1.3	Canonical point-moment limit and conditional transfer	2.1.1, 2.5.2, 6.1.2	38	—
Lemma 6.2.1	Constants and finite propagation	5.1.4	47	—
Proposition 6.2.2	Extended operator path	5.1.4, 5.2.2, 5.2.5	48	—
Lemma 6.2.3	Ordinary response on all of F	5.2.7, 6.2.1	44	—
Proposition 6.2.4	Linear Young evolution	—	46	—
Proposition 6.2.5	Gaussian Young and physical flows	6.2.2, 6.2.4	38	—
Lemma 6.2.6	Identification with the ordinary source equation	6.1.2, 6.2.3	38	—
Proposition 6.2.7	Original average and original point moment	6.1.2, 6.1.3, 6.2.5, 6.2.6	35	—
Proposition 6.2.8	Compact deterministic base	6.2.3, 6.2.7	34	—
Proposition 6.3.1	Ground states and a uniform rate gap	—	32	—
Lemma 6.3.2	Uniform fractional phase norms	(6.3.1)	29	—
Proposition 6.3.3	The complementary wave on E	6.3.1, 6.3.2	28	—
Proposition 6.3.4	The growing projection on the wave phase space	6.2.7, 6.2.8, 6.3.3	27	—
Proposition 6.3.5	Complementary wave evolution and parameter dependence	6.3.3, 6.3.4 (7.2.4)	15	—
Lemma 6.3.6	The original mean and variance	—	45	—
Proposition 6.3.7	Binding with the original control and cost fixed	6.3.1, 6.3.6	13	—
Lemma 7.1.1	Canonical law scaling	2.5.2, 2.6.1 (7.2.6)	15	partial
Lemma 7.2.1	Coupled Gaussian block inputs	5.1.4, 6.2.2	39	partial
Proposition 7.2.2	Change of law on the whole norm-Borel space	7.2.1	15	—
Lemma 7.2.3	Uniform block error	6.2.4, 6.2.8, 6.3.4, 7.2.1	14	—
Lemma 7.2.4	Indexed cone and terminal displacement	6.2.7, 6.3.4, 6.3.5 (7.2.3)	14	partial
Lemma 7.2.5	Composition over time blocks and regularized products	5.2.2, 5.2.4, 5.2.5, 6.2.3, 6.2.5, 6.2.8, 7.2.1 (7.2.6)	22	partial
Proposition 7.2.6	The square observable and canonical comparison	6.1.2, 6.1.3, 6.2.5, 6.2.6, 6.2.7, 7.1.1, 7.2.2, 7.2.5	14	—
Proposition 7.2.7	Original point lower rate at the Gaussian quadratic cost	6.2.4, 7.2.1, 7.2.3, 7.2.4, 7.2.6	13	partial
Lemma 7.3.1	Gaussian envelope for the original covariance	(7.3.2)	14	full

Lemma 7.3.2	Global regularity of the original mean	7.3.1	13	full
Proposition 7.3.3	The unmasked Rayleigh rate	6.3.7, 7.3.2	12	narrower
Proposition 7.3.4	Monotone rates and the original point moment	6.3.1, 6.3.7, 7.2.7, 7.3.3	10	partial
Lemma 7.3.5	Radon and Rayleigh dilation	(7.3.4, 7.3.6)	7	narrower
Proposition 7.3.6	Intrinsic variational lower bounds	3.3.8, 6.3.6, 7.3.4, 7.3.5	6	narrower
Lemma 8.1.1	Gamma and Beta identities	(8.1.2)	6	full
Lemma 8.1.2	Exact potential and mass	8.1.1	5	full
Lemma 8.2.1	The physical two-point integral	(7.3.6)	39	full
Lemma 8.2.2	Smooth temporal controls	7.3.3, 7.3.4, 8.1.2	4	narrower
Lemma 8.2.3	Deterministic Fourier bound for the spatial energy	2.3.1	4	full
Proposition 8.2.4	The finite smooth spatial ratio	8.2.2, 8.2.3	3	narrower
Proposition 8.2.5	The physical four-linear extension	6.3.6, 8.2.1 (8.2.8)	38	full
Proposition 8.2.6	The spatial energy and static lower variational expression	8.2.4, 8.2.5	2	narrower
Lemma 8.3.1	Fractional covariance products	8.2.1, 8.2.5	32	—
Proposition 8.3.2	Compact spatial mean map	4.3.6, 8.3.1	26	—
Lemma 8.3.3	Supported original tensor space	(8.3.2)	30	—
Proposition 8.3.4	The compact temporal mean, without trace class	(8.3.5)	29	—
Proposition 8.3.5	The compact time-space mean	6.2.3, 8.3.2, 8.3.3, 8.3.4	25	—
Lemma 8.3.6	Supported residual paths	5.2.2, 6.2.2, 7.2.1	25	—
Proposition 8.3.7	Cameron covariance and averaged bound	5.2.2, 7.2.1, 8.3.2, 8.3.5, 8.3.6	24	—
Lemma 8.4.1	Refined growth and uniform inverse control	6.2.4	17	—
Proposition 8.4.2	Multiplicative upper perturbation	8.4.1	10	—
Lemma 9.1.1	Uniform cutoff and physical mean	8.3.1	24	—
Lemma 9.1.2	Uniform heat and frequency tails	9.1.1 (9.1.4)	23	—
Lemma 9.1.3	Dimension-free Hilbert tensor extension	(9.1.4)	27	—
Proposition 9.1.4	Uniform approximation of the completed mean	8.3.4, 9.1.1, 9.1.2, 9.1.3	22	—
Proposition 9.1.5	Uniform-radius Cameron bound	5.2.2, 8.3.6, 8.3.7, 9.1.4 (7.2.1)	12	—

Lemma 9.2.1	Uniform rescaled outer maps	4.3.5	13	—
Proposition 9.2.2	Radius-explicit compact envelopes	4.3.6, 4.3.7, 9.2.1	12	—
Proposition 9.2.3	Radius-explicit path moments	4.2.5, 4.3.10, 5.1.2, 5.1.4, 5.1.5, 5.1.9, 9.2.2 (5.1.1)	11	—
Corollary 9.2.4	Deterministic covariance residuals	5.2.2, 7.2.1, 9.2.3 (9.2.5)	10	—
Proposition 9.2.5	Averaged block mean tends to zero	9.2.4	9	partial
Lemma 9.3.1	The limiting multiplier	4.3.5	19	—
Proposition 9.3.2	Closed form and quarter-power phase	9.3.1, 9.3.3	18	partial
Lemma 9.3.3	The bottom and spectral wave	6.2.1, 9.3.2	18	—
Proposition 9.3.4	Identification with the physical wave	6.3.4, 8.3.7, 9.3.2, 9.3.3	16	—
Lemma 10.1.1	Free wave form and compact Young baseline	6.2.4 (5.2.2, 5.2.4, 5.2.6, 5.2.7, 6.2.2)	22	partial
Lemma 10.1.2	Covariance means and source primitives	5.2.2, 5.2.5, 5.2.7	9	—
Proposition 10.1.3	Source conservation	10.1.1, 10.1.2	8	—
Proposition 10.1.5	The exact completed block mean	6.2.2, 8.3.5, 8.3.7, 10.1.1	9	—
Proposition 10.2.1	First Wiener chaos realization on the support	—	15	—
Lemma 10.2.2	Compact images and attained tube radii	10.2.1	13	—
Proposition 10.2.3	Comparison with the Rayleigh integral, including jumps and zero law	10.2.2	12	supplied
Proposition 10.2.4	Eligibility of the E law	8.3.3, 8.3.5, 8.3.6, 8.3.7, 9.1.4, 9.2.4, 9.2.5, 10.1.5, 10.2.1	8	—
Lemma 10.2.5	The endpoint functional	7.2.5, 10.1.1	12	—
Proposition 10.2.6	Coarse tube envelope and operator moment	6.2.4, 8.4.1, 9.1.5, 10.2.3, 10.2.5	11	—
Lemma 10.2.7	Exact Rayleigh tail bound	10.2.6	9	narrower
Lemma 10.3.1	Unique potential and fixed-radius lift	—	17	—
Proposition 10.3.2	Spectral rate in E	6.2.4, 9.3.4, 10.3.1	15	—
Proposition 10.3.3	Uniform completed-field averaging	8.3.4, 9.1.3, 10.3.2	13	—
Lemma 10.3.4	Explicit physical primitive and growth bounds	8.4.1, 9.1.4, 10.1.1	11	—
Proposition 10.3.5	Finite-mesh physical mean-product bound	8.4.2, 10.3.2, 10.3.4	9	—
Corollary 10.3.6	Every polynomial control radius	10.3.3, 10.3.5	8	—
Proposition 10.3.7	Residual comparison and the integrated rate	8.4.2, 10.3.4, 10.3.6	7	—

Lemma 10.4.1	Restriction and fixed-parameter finiteness	6.2.2, 10.1.1, 10.2.4, 10.2.5, 10.2.6, 10.2.7	7	—
Lemma 10.4.2	The same regularized fast noises preserving the given noise	5.1.1, 5.2.2, 5.2.7, 6.1.3, 6.2.5, 6.2.6, 10.1.3	7	—
Lemma 10.4.3	Compact-data source identification	—	7	—
Proposition 10.4.4	Cone identity and an average of squares	6.1.2, 6.2.1, 10.4.2, 10.4.3	6	—
Proposition 10.4.5	Exact original point transfer and polynomial cost	6.1.3, 7.1.1, 7.2.6, 7.2.7, 10.1.1, 10.4.1, 10.4.2, 10.4.4	5	—
Lemma 10.5.1	Signed variational expression and quantitative radial envelope	10.2.6, 10.3.3, 10.3.4 (10.2.4, 10.2.5)	7	—
Proposition 10.5.2	Finite-delta bulk and exact tail	10.2.7, 10.3.7, 10.5.1 (10.2.6)	6	—
Proposition 10.5.3	Two limits on the same moment	10.4.1, 10.5.1, 10.5.2	5	—
Proposition 10.5.4	Pointwise upper bound from the signed variational expression	7.2.7, 10.4.5, 10.5.3	4	—
Lemma 11.1.1	Scalar and Hilbert identities	—	11	full
Lemma 11.1.2	Interior dual minimum	—	11	—
Proposition 11.1.3	Positive conic maximizer	11.1.1, 11.1.2	10	partial
Lemma 11.1.4	Real Gram realization	11.1.3	9	—
Proposition 11.1.5	Entrywise Gram comparison	11.1.3, 11.1.4	8	partial
Lemma 11.2.1	Inclusion into the covariance space and the smooth mean	8.3.3, 9.1.3 (10.3.1)	10	narrower
Lemma 11.2.2	Finite covariance vectors and entrywise order	9.1.4, 10.3.1, 11.1.5, 11.2.1 (7.3.6, 10.5.4, 11.2.6)	7	narrower
Lemma 11.2.3	Uniform optimizer norm and positive smoothing	10.3.3, 11.1.3, 11.2.1, 11.2.2	6	—
Proposition 11.2.4	Signed variational values bounded by the variational value over nonnegative controls	7.3.6, 10.3.2, 10.3.3, 11.2.1, 11.2.2, 11.2.3	5	—
Proposition 11.2.5	Cutoff removal for the optimized variational expression	7.3.3, 11.2.1, 11.2.4	4	—
Theorem 11.2.6	Intrinsic original second-moment constant	7.2.7, 7.3.3, 7.3.6, 10.5.4, 11.2.5	3	outside
Lemma 11.3.1	Full-profile squares in the original space	8.2.5, 11.2.1 (8.2.8)	4	narrower
Proposition 11.3.2	Original occupation energy and dilation	8.2.5	3	full
Lemma 11.3.3	Countable Rayleigh near-occupations	7.3.3, 11.3.1	3	narrower

Theorem 11.3.4	The computed occupation ceiling	11.2.6, 11.3.2, 11.3.3 (8.2.6)	2	narrower
Corollary 11.3.5	A common spatial-energy bracket	8.1.2, 8.2.6, 11.2.6, 11.3.4	1	narrower
Lemma 11.4.1	A square identity for the distribution function	—	2	—
Proposition 11.4.2	Exact white spatial energy	8.2.5, 11.4.1 (8.2.6)	1	partial
Theorem 11.4.3	Explicit white moment bounds	8.2.6, 11.2.6, 11.3.5, 11.4.2	0	partial

The recorded graph does not reach 12 results with printed proofs in these chapters: Lemma 2.2.1, Proposition 2.7.1, Proposition 3.1.2, Proposition 3.2.4, Corollary 3.2.5, Proposition 4.1.5, Proposition 4.3.11, Lemma 8.2.7, Proposition 8.2.8, Proposition 10.1.4, Lemma 10.2.8, Corollary 11.4.4. This does not mean that they have no mathematical use. Of Proposition 3.1.2, the proof of Proposition 3.3.5 uses one calculation, the free-phase energy bound at the end of its proof, and none of its conclusions.

Bibliography

[1] Raluca Balan, Le Chen, and Yiping Ma, *Parabolic Anderson model with rough noise in space and rough initial conditions*, Electron. Commun. Probab. **27** (2022), Paper No. 65, 12; MR4529633

[2] Raluca M. Balan, *Stratonovich solution for the wave equation*, J. Theoret. Probab. **35** (2022), 2643–2689. Available at 2105.08802; MR4509081

[3] Raluca M. Balan, Le Chen, and Xia Chen, *Exact asymptotics of the stochastic wave equation with time-independent noise*, Ann. Inst. Henri Poincaré Probab. Stat. **58** (2022), 1590–1620; MR4452644

[4] Raluca M. Balan and Daniel Conus, *Intermittency for the wave and heat equations with fractional noise in time*, Ann. Probab. **44** (2016), 1488–1534; MR3474476

[5] Raluca M. Balan, Maria Jolis, and Lluís Quer-Sardanyons, *Intermittency for the hyperbolic Anderson model with rough noise in space*, Stochastic Process. Appl. **127** (2017), 2316–2338; MR3652415

[6] Raluca M. Balan and Jian Song, *Hyperbolic Anderson model with space-time homogeneous Gaussian noise*, ALEA Lat. Am. J. Probab. Math. Stat. **14** (2017), 799–849; MR3731795

[7] ———, *Second order Lyapunov exponents for parabolic and hyperbolic Anderson models*, Bernoulli **25** (2019), 3069–3089; MR4003574

[8] Raul Bolaños Guerrero, David Nualart, and Guangqu Zheng, *Averaging 2d stochastic wave equation*, Electron. J. Probab. **26** (2021), Paper No. 102, 32; MR4290504

[9] Christer Borell, *The Brunn-Minkowski inequality in Gauss space*, Invent. Math. **30** (1975), 207–216; MR399402

[10] Matthew T. Calef and Douglas P. Hardin, *Riesz s-equilibrium measures on d-rectifiable sets as s approaches d*, 2008. Preprint; the interval-density statement is on p. 1.

[11] Le Chen, *lean-pkg: a registry and trust gate for Lean 4 formalization packages*, 2026. Software, version 0.29.0, November 9, 2026, https://github.com/lean-pkg/lean-pkg; DOI 10.5281/zenodo.24095258 (this version), 10.5281/zenodo.23272098 (all versions).

[12] Le Chen and Robert C. Dalang, *Moment bounds and asymptotics for the stochastic wave equation*, Stochastic Process. Appl. **125** (2015), 1605–1628; MR3310358

[13] Le Chen and Nicholas Eisenberg, *Interpolating the stochastic heat and wave equations with time-independent noise: solvability and exact asymptotics*, Stoch. Partial Differ. Equ. Anal. Comput. **11** (2023), 1203–1253. Available at 2108.11473; MR4624137. Published version of arXiv:2108.11473v1

[14] Le Chen, Yuhui Guo, and Jian Song, *Moments and asymptotics for a class of SPDEs with space-time white noise*, Trans. Amer. Math. Soc. **377** (2024), 4255–4301; MR4748620

[15] Xia Chen, *Exponential asymptotics for Brownian self-intersection local times under Dalang's condition*, Electron. J. Probab. **28** (2023), Paper No. 119, 17; MR4660700

[16] ———, *Time-dependency in hyperbolic Anderson model: Stratonovich regime*, Preprint arXiv:2510.01412 (2025)

[17] ———, *Time-dependency in hyperbolic Anderson models: Stratonovich regime*, 2026. Author manuscript, available at https://web.math.utk.edu/~xchen3/aap-chen-2025.pdf (retrieved October 26, 2026). Theorem 1.2 supersedes that of arXiv:2510.01412v1.

[18] Xia Chen, Aurélien Deya, Jian Song, and Samy Tindel, *Hyperbolic Anderson model 2: Strichartz estimates and Stratonovich setting*, Int. Math. Res. Not. IMRN **21** (2023), 18575–18628; MR4665631

[19] Xia Chen, Aurélien Deya, Jian Song, and Samy Tindel, *Solving the hyperbolic Anderson model 1: Skorohod setting*, Ann. Inst. Henri Poincaré Probab. Stat. **61** (2025), 1794–1814; MR4947171

[20] Xia Chen and Yaozhong Hu, *Hyperbolic anderson equations with general time-independent gaussian noise: Stratonovich regime*, Ann. Probab. **53** (2025), 2144–2195. Available at 2403.08603; MR4988274. Published version of arXiv:2403.08603

[21] Daniel Conus and Robert C. Dalang, *The non-linear stochastic wave equation in high dimensions*, Electron. J. Probab. **13** (2008), no. 22, 629–670; MR2399293

[22] Ivan Corwin and Promit Ghosal, *KPZ equation tails for general initial data*, Electron. J. Probab. **25** (2020), Paper No. 66, 38; MR4115735

[23] Michel Crouzeix and César Palencia, *The numerical range as a spectral set*, 2017. Author preprint, arXiv:1702.00668v1; numbering used here refers to this version.

[24] Robert C. Dalang, *Extending the martingale measure stochastic integral with applications to spatially homogeneous s.p.d.e.'s*, Electron. J. Probab. **4** (1999), no. 6, 29; MR1684157

[25] Robert C. Dalang and Carl Mueller, *Intermittency properties in a hyperbolic Anderson problem*, Ann. Inst. Henri Poincaré Probab. Stat. **45** (2009), 1150–1164; MR2572169

[26] Robert C. Dalang, Carl Mueller, and Roger Tribe, *A Feynman-Kac-type formula for the deterministic and stochastic wave equations and other P.D.E.'s*, Trans. Amer. Math. Soc. **360** (2008), 4681–4703; MR2403701

[27] Francisco J. Delgado-Vences and Marta Sanz-Solé, *Approximation of a stochastic wave equation in dimension three, with application to a support theorem in Hölder norm*, Bernoulli **20** (2014), 2169–2216; MR3263102

[28] Amir Dembo and Ofer Zeitouni, *Large deviations techniques and applications*, Second, Applications of Mathematics (New York), vol. 38, Springer-Verlag, New York, 1998. MR1619036

[29] Eleonora Di Nezza, Giampiero Palatucci, and Enrico Valdinoci, *Hitchhiker's guide to the fractional Sobolev spaces*, Bull. Sci. Math. **136** (2012), 521–573; MR2944369

[30] Peter K. Friz and Martin Hairer, *A course on rough paths*, Universitext, Springer, Cham, [2020] ©2020. With an introduction to regularity structures, Second edition of [3289027]. MR4174393

[31] Galileo Galilei, *Sidereus nuncius, or The sidereal messenger*, University of Chicago Press, Chicago, 1989. Translated with introduction, conclusion, and notes by Albert Van Helden.

[32] M. Gubinelli, B. Ugurcan, and I. Zachhuber, *Semilinear evolution equations for the Anderson Hamiltonian in two and three dimensions*, Stoch. Partial Differ. Equ. Anal. Comput. **8** (2020), 82–149; MR4058957

[33] Yaozhong Hu and Xiong Wang, *Matching upper and lower moment bounds for a large class of stochastic PDEs driven by general space-time Gaussian noises*, Stoch. Partial Differ. Equ. Anal. Comput. **12** (2024), 1–52; MR4709538

[34] Svante Janson, *Gaussian Hilbert spaces*, Cambridge Tracts in Mathematics, vol. 129, Cambridge University Press, Cambridge, 1997. MR1474726

[35] Andrej Karpathy, *LLM Wiki*, 2026. GitHub gist, April 4, 2026, https://gist.github.com/karpathy/442a6bf555914893e9891c11519de94f.

[36] Andrei K. Lerner, *A simple proof of the A_2 conjecture*, Int. Math. Res. Not. IMRN **14** (2013), 3159–3170

[37] Shuhui Liu, Yaozhong Hu, and Xiong Wang, *Nonlinear stochastic wave equation driven by rough noise*, J. Differential Equations **331** (2022), 99–161. Available at 2110.13800; MR4435914

[38] Jian Song, Xiaoming Song, and Fangjun Xu, *Fractional stochastic wave equation driven by a Gaussian noise rough in space*, Bernoulli **26** (2020), 2699–2726; MR4140526

[39] V. N. Sudakov and B. S. Cirel′son, *Extremal properties of half-spaces for spherically invariant measures*, Zap. Naučn. Sem. Leningrad. Otdel. Mat. Inst. Steklov. (LOMI) **41** (1974), 14–24, 165; MR0365680. Problems in the theory of probability distributions, II

[40] Yongjin Sung, Wonshik Choi, Christopher Fang-Yen, Kamran Badizadegan, Ramachandra R. Dasari, and Michael S. Feld, *Optical diffraction tomography for high resolution live cell imaging*, Optics Express **17** (2009), 266–277

[41] Béla Sz.-Nagy, *Über Integralungleichungen zwischen einer Funktion und ihrer Ableitung*, Acta Sci. Math. (Szeged) **10** (1941), 64–74

[42] Terence Tao, *Math 2.0*, 2026. Lecture slides, Caltech, 2026, slide "The era of proof abundance", https://teorth.github.io/tao-web/slides/math-2-0-caltech-2026.pdf.

[43] ———, *Post on Mathstodon about the reporting bias against negative results*, 2026. January 17, 2026, https://mathstodon.xyz/@tao/115911902186528812.

[44] Gerald Teschl, *Mathematical methods in quantum mechanics*, Second, Graduate Studies in Mathematics, vol. 157, American Mathematical Society, Providence, RI, 2014. With applications to Schrödinger operators. MR3243083

[45] Joel A. Tropp, *Second-order matrix concentration inequalities*, Appl. Comput. Harmon. Anal. **44** (2018), 700–736. Proof pinpoints refer to arXiv:1504.05919v2

[46] Albert Van Helden, *Saturn*, 1995. The Galileo Project, Rice University, https://galileo.library.rice.edu/sci/observations/saturn.html.

[47] John B. Walsh, *An introduction to stochastic partial differential equations*, École d'été de probabilités de Saint-Flour, XIV—1984, 1986, pp. 265–439. MR876085

[48] Xuan Wu, *The KPZ equation and the directed landscape*, Ann. Probab. **54** (2026), 1212–1257. Available at 2301.00547; MR5061894. Published version of arXiv:2301.00547

[49] L. C. Young, *An inequality of the Hölder type, connected with Stieltjes integration*, Acta Math. **67** (1936), 251–282; MR1555421

Working words and common misreadings

The proof uses a few everyday words in a fixed sense. This list collects them, and then names the misreadings that are easiest to make. It adds no assumption and no statement. For symbols see the List of notation, and for page numbers the Index.

Working words

Chain. The ordered n-vertex wave kernel g_n: wave Green factors at n times in increasing order. The n-th term of the solution integrates n noise factors against one chain (Section 1.4).

Order. The number of noise factors in a term. Terms of different orders need not be orthogonal here, and the total order $m + n$ of a product is not a Wiener-chaos order.

Pairing. A matching of noise factors two by two, made when an expectation is taken. The second moment sums over all pairings of the vertices of two chains (Proposition 2.1.1). A self-pairing matches two vertices of the same chain.

Canonical solution. The sum of the fixed-order limits, obtained from the regularized classical equations (Proposition 2.6.2).

Phase. Displacement and velocity together. Localized perturbations lie in $E = H^{1/2} \times H^{-1/2}$; constant data are carried in $F = E \oplus \mathbb{R}^2$ (Section 6.2). A restarted wave needs both components (No-go 14).

Mask. A smooth compactly supported spatial function that multiplies the physical potential. The lower bound takes a numerical supremum after fixed-mask bounds; the upper point comparison uses growing supports (Propositions 7.3.4 and 10.4.5).

Radius. The size of the region where the mask equals one. The upper point comparison chooses a radius growing with its fast time horizon; lower-bound masks remain fixed before time asymptotics (Chapters 7 and 9).

Block. One interval of a subdivision of the time axis. The noise in one block is correlated with the noise in the others, so bounds do not simply multiply across blocks.

Control. A vector in the covariance Hilbert space that specifies a Gaussian mean shift. The lower bound uses nonzero nonnegative smooth compact tests $\Psi \in \mathcal{C}_{\mathrm{pos}}$; the upper bound also uses signed completed controls $\Phi \in H_I$. The shift is toward the induced mean.

Gaussian cost. The price of that shift: $v_\Psi/2$, half the variance of $W(\Psi)$. It is paid once for the whole time interval, not once per block.

Variational value. The nonnegative-control value $S_c^{\mathrm{pos}} = \sup_{\Psi \in \mathcal{C}_{\mathrm{pos}}} (cI_\Psi - v_\Psi/2)$ (Proposition 7.3.6). The constant of Theorem 11.2.6 is S_2^{pos}.

Ceiling. An upper bound for the constant, computed from occupation and energy estimates (Theorem 11.3.4).

Clock. An auxiliary scalar Brownian motion used with a spatial Brownian path to represent the time Laplace transform of the expectation of one expansion term (Section D.2). Copying it with two clocks, constant correlation and no extra weight fails for the first cross pairing (Proposition D.2.2).

Common misreadings

"This is the Skorohod model." It is not. Stratonovich second moments retain self-pairings and mixed terms with $m \neq n$. In the Skorohod chaos expansion, unequal orders are orthogonal and there are no self-contractions. The exponent comparisons here require the cited covariance and data hypotheses; they identify neither solutions nor leading constants.

"Theorem 3.3.8 gives the constant." It gives an upper bound at scale T^κ, with a constant not claimed sharp. The exact asymptotic constant is identified in Theorem 11.2.6, by a separate argument.

"The white-noise formulas evaluate the constant." They give two-sided bounds (Theorem 11.4.3). The spatial energy is evaluated in Proposition 11.4.2; its relation to the moment constant gives bounds, not an evaluation of the full intrinsic supremum.

"The ceiling is the constant." The ceiling is not asserted to be attained or to equal the constant.

"S_1^{pos} is the first-moment constant." It is an auxiliary variational value. No identification with a first-moment constant is asserted.

"The arXiv version of the source is the one cited." Statements from Xia Chen's paper are cited from his public author version, posted on his homepage at the University of Tennessee and retrieved on October 26, 2026 [17]. Its Theorem 1.2 differs from the statement in arXiv:2510.01412v1 [16].

List of notation

The tables collect recurring notation and point to its definition or principal use. Symbols introduced for one calculation are defined there. Several letters are reused in different sections; the scope column records the main distinctions. These tables do not add assumptions to the model.

Model, noise and scaling parameters

Symbol	Meaning and scope	Definition or use
d	Spatial dimension, $d \in \{1, 2, 3\}$.	Hypothesis 1.2.1
α	Exponent in the spatial covariance homogeneity relation.	Hypothesis 1.2.1
α_0, a	Temporal covariance exponent; $a = \alpha_0$ in the integrated arguments.	(1.2.2)
Γ, γ	Spatial covariance measure; γ denotes its density when one exists and otherwise the corresponding distribution.	Hypothesis 1.2.1
μ	Spectral measure, in the Fourier convention fixed by the hypothesis.	Hypothesis 1.2.1
$\dot{W}$, $W(f)$	Gaussian forcing and its isonormal realization on covariance test classes, respectively.	(1.2.2); Section 5.1
$\mathbb{E}$	Expectation under the underlying probability measure.	(1.5.7)
κ	Normalization exponent $(4 - \alpha - \alpha_0)/(3 - \alpha)$ in the moment bounds and limit.	(1.2.4)
β, ν	In the interval-field estimates, $\beta = 4 - \alpha - \alpha_0$ and $\nu = 3 - \alpha$. These letters have different local uses in path estimates.	Section 3.3
R_α	Spectral-mass constant in the independent upper bound.	(1.5.1)
Γ_E, Beta	Euler Gamma and Beta functions; Γ_E is distinct from the covariance measure Γ.	Lemma 8.1.1
χ	Degree of an auxiliary static covariance in the comparison arguments; it need not equal α.	Section C.2

Solutions, kernels and pairing expansions

Symbol	Meaning and scope	Definition or use
$u(t,x)$	Canonical Stratonovich solution with displacement 1 and velocity 0 at time zero.	(1.2.1); Proposition 2.6.2
G_t	Wave Green measure, with mass t and support in the closed radius-t ball.	(1.4.1); Lemma 6.2.1
g_n, $S_n(g_n)$	Ordered chain kernel and its multiple Stratonovich integral.	(1.4.1)
$X_n(t,x)$	The nth Stratonovich term $S_n(g_n)$; its iteration order is not an orthogonal chaos order.	Proposition 2.1.1
I_1, I_2, Π_k	The two ordered chains and the pair partitions of their $2k$ vertices.	(2.1.1)
P_k	Number of pair partitions, $(2k)!/(2^k k!)$.	(2.7.2)
$J_{m,n,D}$	Pairing integral for chain lengths m,n and pair partition D.	(2.1.1)
N_0, N_1, N_2	Laplace-damped wave norms used in the construction estimates.	(2.3.1)
$B_K(t)$	Numerical majorant obtained by estimating each pairing separately; it is not the actual second moment.	(2.7.2)

Covariance spaces and wave evolution

Symbol	Meaning and scope	Definition or use
H_W	Completion of smooth positive-time tests modulo covariance-null tests for the original noise.	Section 5.1
I	The unit time interval; control tests have support in $(0,1)$, while compact parameter families also use $[0,1]$.	(7.3.1); Section 6.3
H_t, H_{sp}	Temporal and spatial covariance Hilbert spaces.	Section 8.3
H_I	Covariance space of tests supported in $I\times\mathbb{R}^d$, embedded in H_W.	Lemma 8.3.3
Λ	Bessel multiplier $(1-\Delta)^{1/2}$.	Section 4.2
E_r, E	Wave phase $E_r = H^r \times H^{r-1}$; the balanced phase is $E = H^{1/2}\times H^{-1/2}$.	Section 5.1
F, e_0	Extended phase $F = E\oplus\mathbb{R}^2$ and the vector encoding constant initial displacement.	(6.2.1)

Continued on the next page

Symbol	Meaning and scope	Definition or use
$S_E(t)$, $S_F(t)$	Free wave groups on the respective phase spaces.	Lemma 6.2.1
$M_R(W)$	Integrated Gaussian interaction operator path with spatial localization radius R.	Proposition 5.1.1
U_D	Young evolution driven by an operator path D in the interaction representation.	(6.2.8)
$P_D(t,s)$	Physical wave evolution obtained by conjugating the interaction flow by the free wave group.	(6.2.14); Section 10.1
$B_E(V)$	Potential insertion $(u,v) \mapsto (0,Vu)$ on E.	Lemma 10.3.1
ω, J_E	Symplectic form and its representing skew-adjoint operator on E.	Lemma 10.1.1

Regularization, spatial masks and time blocks

Symbol	Meaning and scope	Definition or use
p_ϵ	Gaussian heat kernel used for spatial smoothing; its covariance normalization is specified locally.	Lemma 7.3.1
ρ, Y_ρ	A pair of noise-smoothing widths and the corresponding regularized source. In damped phase estimates, ρ instead denotes a positive damping parameter.	Proposition 5.2.5; Section 6.1
R, η_R, m_R	Spatial radius, cutoff profile and physical mask. In the uniform-radius arguments, $\eta_R = \eta(\cdot/R)$ and $m_R = \eta_R^2$.	Section 9.1
δ, r_T	Long-time normalization $\delta = T^{-\kappa}$ and shrinking spatial scale $r_T = T\delta$. Smoothing parameters denoted by δ elsewhere are local.	Lemma 7.1.1
g_δ	Fast-noise amplitude $\delta^{(1-a)/2}$.	(7.2.1)
B, N, s_m, τ	Fast block length, number of full blocks, slow block starts and final block length. Here $\tau \in [0,B)$.	(7.2.1)
$T_{\delta,m}$	Isometry used to pull each fast-time test back to the original Gaussian noise.	(7.2.2)
X_m, H_m	Random block operator input and its deterministic mean shift; these local symbols differ from the Stratonovich terms $X_n(t,x)$.	(7.2.3)
R_δ	Growing spatial radius $\delta^{-1}+2$ in the point upper bound; it differs from the shrinking scale r_T.	Section 10.4

Continued on the next page

Symbol	Meaning and scope	Definition or use
γ, θ, β	Auxiliary spatial and temporal regularity exponents. Here γ is not the covariance distribution and β is not the coefficient-growth exponent.	(5.1.1)

Controls, means and variational constants

Symbol	Meaning and scope	Definition or use
$\mathcal{C}_{\mathrm{pos}}$	Nonzero nonnegative smooth compact spacetime controls; separation into time and space factors is not required.	(1.5.3)
$h_{\Psi,s}$	Deterministic covariance mean induced by the control Ψ.	(1.5.4)
v_Ψ	Original Gaussian variance, equal to the squared covariance-space norm of the control.	(1.5.5); (6.3.21)
$\lambda_{\Psi,s}$, I_Ψ	Positive Rayleigh growth rate and its integral over the unit interval, for nonzero covariance.	(7.3.4)
$\mathcal{R}_\Psi(s)$	Squared Rayleigh rate used in the introductory constant formula.	(1.5.6)
S_c^{pos}	Supremum of $cI_\Psi - v_\Psi/2$. The coefficient-one value is auxiliary; the coefficient-two value identifies C_2.	Proposition 7.3.6; Theorem 11.2.6
$C_2(\Gamma, a)$	Intrinsic second-moment constant, including its zero-covariance value.	(11.2.8)
k, q, m	In the spatial-energy and constant calculations, $k = 3 - \alpha$, $q = 4 - \alpha$ and $m = q/k$. These are local conventions.	Section 8.2; (7.3.8)
f_a, M_a	Temporal equilibrium density and its total mass. M_a is distinct from the mean-growth rate $M(a)$.	(8.1.1); (8.1.3)
$K(s,t)$, $K_0(a)$	Original temporal kernel $\lvert s-t\rvert^{-a}$ and its maximal row integral $2^a/(1-a)$.	(11.2.1); (11.4.2)
$B_\Gamma(f,h)$	Physical two-point covariance pairing.	(8.2.1)
$A_{\mathrm{sp}}(f)$, $b(f)$	Spatial covariance energy of f^2 and gradient energy $\lVert\nabla f\rVert_2^2$.	Section 8.2
R_{sp}	Best homogeneous spatial energy ratio, extended to real unit H^1 profiles.	Proposition 8.2.5; Proposition 8.2.6
$\mathcal{E}_{\mathrm{sp}}$	Supremum of $A_{\mathrm{sp}}(f) - b(f)/2$ over unit spatial profiles.	(8.2.9)

Continued on the next page

Symbol	Meaning and scope	Definition or use
$F_0(z)$	Scalar map from spatial energy to a variational bound; it is distinct from the wave phase F.	(8.2.10)
$\mathcal{O}$, $T(g)$	Admissible time-dependent unit spatial profiles and their integrated gradient energy.	Proposition 8.2.8
$A(g)$, C_{occ}	Original temporal occupation energy and its homogeneous ratio supremum.	(11.3.1)
$\mathcal{E}_\zeta^{\mathcal{O}}$	Occupation energy with gradient penalty $\zeta T(g)$, using the original temporal kernel.	(11.3.1)
$K_\star$, $\mathcal{E}_\star^{\mathcal{O}}$	Auxiliary damped temporal kernel and its occupation energy; these differ from the original-kernel quantities.	(8.2.11); (8.2.14)
C_t, T_R, $\mathcal{T}_R$	Temporal, spatial and combined covariance-mean maps. Their domains and radius dependence are specified at each construction.	Propositions 8.3.4 and 8.3.5; Section 9.1
$\mathcal{S}_R$, V_{up}	Signed-control variational value at radius R and its limsup along the growing radii.	(10.5.1)

Gaussian geometry and finite optimization

Symbol	Meaning and scope	Definition or use
$\mathcal{K}(E)$	Compact operators on the Hilbert phase E.	Proposition 5.1.1
$\mathscr{B}_\delta$	Banach space of block paths with its weighted temporal norm.	Proposition 10.2.4
C, $\mathcal{M}_\delta$	In Gaussian enlargement, $Ch = \mathbb{E}[XW(h)] = \sqrt{\delta}\,\mathcal{M}_\delta h$. The letter C elsewhere often denotes an estimate constant.	(10.2.1)
H_{seen}, H_{CM}	Visible isonormal subspace and Cameron–Martin image of the covariance map.	(10.2.1); (10.2.2)
E_0	Closed support space of the Gaussian input; this is distinct from the wave phase E.	(10.2.1)
M_δ	Expected squared operator norm of the physical endpoint in the upper argument.	Section 10.5
C_{ij}	Finite Gram matrix entries $\langle k_i, k_j\rangle$, assumed nonnegative in the positive-cone optimization.	(11.1.1)
$\mathfrak{F}_C$, $\mathscr{S}(C)$	Finite-control objective and its supremum.	(11.1.1)
D_A^C, d_A^C	Dual objective and its infimum for a selected subset A. The empty subset has value zero.	(11.1.2)
w^A, Φ_A	Positive dual minimizer and the corresponding positive combination of Gram vectors.	(11.1.5); Proposition 11.1.3

Static comparisons and local outlook notation

Symbol	Meaning and scope	Definition or use
L_0, κ_{st}	Static first-mean rate and static time exponent; the comparison retains the source normalization stated there.	(D.1.1)
$M(a)$	Normalized first-mean limsup in the near-static comparison; it is not the equilibrium mass M_a.	Proposition D.1.4
ρ	In the clock comparison only, correlation of the two auxiliary Brownian clocks; neither a source width nor a damping parameter.	(D.2.4)
p	In future-work moment statements, a fixed moment order. Elsewhere it may be an auxiliary integrability or Schatten index.	Conjecture 1.9.1; Section 4.3
p, ν	Locally, $p = 2 - \alpha_0$ in the interval-field argument, while $\nu = 1/\theta$ in Young growth estimates.	Section 3.3; Lemma 8.4.1
A, z_*	In the conditional upper-tail discussion, $A = 2^{-m}C_2$ and $z_* = mA$. This A is not the occupation energy $A(g)$.	Section 1.9.2
$\mathcal{I}(z)$	Conditional upper-tail rate on the stated range of thresholds.	(1.9.3)
H_a	Covariance Hilbert space for the spatial-white optimizer conjecture.	Section 1.9.3
J_a, τ_y	Control objective and spatial translation in the optimizer conjecture.	Conjecture 1.9.2
h, $b(t)$, φ	In the smooth logarithmic-wave outlook, $h = \log\lvert u\rvert$ and $h = b(t) + \varphi$. This $b(t)$ is distinct from the spatial energy $b(f)$.	(1.9.4); (1.9.5)

Subject index

active subsets, 272, 273
adjacent dyadic grids, 88
admissibility threshold, 3
amplitude of noise, *see* covariance, amplitude
Anderson model, *see* hyperbolic Anderson model
anisotropic covariances, 359, 378
averaging
  completed mean fields, 254
  squares versus square of an average, 263, 264

backward light cone, *see* finite propagation
Bessel inequality, 108
Beta function, 196
Borell–Sudakov–Tsirelson theorem, *see* Gaussian isoperimetric theorem
Brownian clocks
  copying obstruction, 393
  low-order transforms, 392

Cameron map
  block embedding, 213
  uniform radius bound, 222
Cameron–Martin formula, 177
Cameron–Martin shift, 177
Cameron–Martin space, 242
Cauchy–Schwarz inequality
  translated covariance, 36
chaos expansion, *see* Wiener chaos
chapter roadmap, 5
coefficient estimates
  degree allocation, 73, 74
  interval products, 82
coercivity
  finite dual problem, 271
compact operators
  cutoff factorization, 115
  positive-order domination, 121
  whole-space obstruction, 124
compactness
  images of Hilbert balls, 244
constant initial data, 153
convolution bounds
  degree-one case, 344
  obstructions, 352
  translated spatial maximum, 348
covariance
  amplitude, 3, 281
  dyadic temporal majorant, 88
  homogeneous, 3
  positive definiteness, 3, 359
  spatial measure, 3, 198
  spectral measure, 3, 93
  temporal, 3, 96
  zero case, 15, 281
covariance coefficients, 128
covariance comparison
  linear images and sums, 370, 378
  planar endpoints, 359, 363
  plane-supported endpoints, 368
  product endpoints, 366
  three-dimensional hypothesis, 368
covariance space
  null tests and completion, 96, 97
  supported tensor product, 209
Crouzeix–Palencia theorem, 61
cutoff, *see* spatial cutoff
cutoff removal
  optimized variational value, 280

direct upper bounds
  conditional higher exponents, 348
  one dimension, 341
  spatial exponent at most one, 345
distributional phase space, 153
dual optimization
  finite-subset identity, 272
  positive minimizer, 271

Duhamel expansion, 65
dyadic intervals, 88, 92

exponential tilting
  available moment orders, 22

factorial bounds, 55, 82
feature isometry, 141
Feynman–Kac representations
  comparison of stochastic products, 7
finite propagation, 153, 263
finite-order checks
  Riesz covariance, 336
  spatial white noise, 333
  static calibration, 334, 337
first moment
  Jensen comparison, 14
  near-static comparison, 387
  source bounds, 13
Fock space
  degree cutoffs, 64, 65
Fourier transform
  normalization, 93
fractional Sobolev norms, 166, 207
fractional temporal noise, *see* covariance, temporal
free wave
  norm lower bound, 235
frequency estimates, 102, 104
functional calculus
  bounded operators, 61
  signed static wave, 232

Gagliardo–Nirenberg inequality
  sharp one-dimensional constant, 287
Gamma function
  recurrence and duplication, 196
Gaussian action, *see* Gaussian cost
Gaussian change of measure, 177
Gaussian comparison
  finite linear images, 139
  source transfer, 139
Gaussian contractions, 57, 71
Gaussian cost
  original covariance norm, 184, 250
  variance-half normalization, 186, 281
Gaussian creation and annihilation operators, 64
Gaussian enlargement, 245
Gaussian isoperimetric theorem, 244
Gaussian matrices
  Hermitian dilation, 114
  moment bounds, 113
Gaussian mean
  compact spatial map, 208
  compact temporal map, 209
  completed space-time map, 210
  original control and variance, 171
Gaussian operator paths
  construction, 126
  fixed-interval limit, 134
  Hölder regularity, 136
  radius dependence, 227
Gaussian operators
  finite variance estimates, 121, 122
Gaussian support
  first-chaos realization, 242
Gaussian tails
  bulk-tail decomposition, 267
Gram matrices
  entrywise comparison, 274
  nonnegative entries, 270
  realization, 272
  singular and zero cases, 272, 273
Green function, *see* Green measure
Green measure, 12, 153
ground state, *see* ground states
ground states, 164
  common trial function, 164, 172
  compact potential family, 164

heat smoothing, 141, 189
Hermite degree, 65, 66
higher moments
  even-order conjecture, 20
  real-order extension, 22
homogeneity
  measure scaling, 3, 193
  moment scaling, 174
homogeneous covariance, *see* covariance, homogeneous

hyperbolic Anderson model, 3, 281
hyperbolic secant profile, 288

initial data
  constant displacement, 3, 153
  velocity, 153, 182
intermittency
  near-static mean gap, 387
interval fields, 72, 82
isonormal Gaussian process, 126, 242

Jensen's inequality, 14

Khintchine inequality
  Gaussian matrices, 113
KPZ fixed point
  comparison and limitations, 24

Laplace transforms
  clock comparison, 392
  cross-pair discrepancy, 393
  damped wave norms, 33, 34
large deviations
  conditional upper-tail rate, 22
log-convexity
  moment growth type, 390
logarithmic wavefields, 24
lower bound
  fixed Gaussian control, 186
  nonnegative controls, 193

masked solutions
  mixed-order comparison, 149
  tested moments, 151
measure-valued covariance
  energy identification, 380
mild solution
  construction, 52
  regularized identification, 160
mixed orders, 31, 149
moment growth, 88, 281

no-go results, 291
  a deterministic surrogate can lose the annealed factor, 314
  a mask that separates noise-null representatives, 320
  a one-sided variance bound fails, 327
  a positive control need not have proportional covariance profiles, 315
  a positive semidefinite residual can lower the wave mean, 309
  a pure Young power and a maximum from an average, 322
  a same-noise Hilbert–Schmidt obstruction, 317
  a scalar wave moment is not log-convex in variance, 306
  a spatial maximum need not be finite, 304
  an occupation ceiling need not improve a comparison value, 328
  constant-correlation clock copying misses a positive factor, 301
  divergence of the first coefficient ratio, 296
  empty sets, concavity and matrix order, 329
  escape from every fixed smooth projection, 321
  escaping variational scores, 324
  failure of a heat–Mellin endpoint recipe, 307
  failure of the all-time comparison with unit prefactor, 295
  growth does not give every-phase lower bounds or local cutoff consistency, 316
  large label span does not imply a cubic denominator, 299
  no finite spatial-supremum pullout in the merge lens, 300
  no uniform cubic factorial denominator per diagram, 294
  no uniform isotropic envelope for a plane covariance, 308
  radial lowering can destroy positive definiteness, 305
  support obstruction to pointwise concatenation, 297
  the common-parameter majorant has the wrong scale, 293
  the first variance coefficient need not be nonnegative, 313

the geometry-free majorant, 299
the point feature is outside the closed noise image, 325
the shift-erased envelope is not below the wave transform, 302
the temporal concentration threshold, 323
three invalid proof steps, 330
translations defeat whole-space compactness, 320
two independent wave blocks do not multiply scalar moments, 311
noise
auxiliary independent extension, 141
preservation of the original process, 141, 143
noise-null quotient, *see* covariance space, null tests and completion
noncommutative Khintchine inequality, *see* Khintchine inequality, Gaussian matrices
nonseparable controls, *see* positive controls, nonseparable tests
numerical range, 61

occupation profiles
admissible class, 205
near-Rayleigh selection, 284
original covariance energy, 283
one-third trick, *see* adjacent dyadic grids
operator products
arbitrary residual paths, 258
finite-mesh means, 256
uniform growth bounds, 255
operator tails
compact domination, 133
optimizer
compactness conjecture, 23
uniform norm bound and smoothing, 277
order of limits
same endpoint and block length, 268

pairings
counting, 55, 73
cross-pairings, 31, 333
empty chains, 31, 85
finite product bound, 40
ordered chain kernels, 12, 31
self-pairings, 31, 333
uniform-estimate obstruction, 55, 56
Peetre's inequality, 116
periodic extension
auxiliary cutoff factorization, 115
phase norms
changes at interval endpoints, 72, 78
physical masks, 95, 218
physical wave
identification, 160, 233
point moments
finite-propagation transfer, 264
higher-order obstruction, 21
positive coefficient series
type, 385
positive cone
Gram maximizer, 272
positive controls
admissible class, 188
coefficient homogeneity, 193
dilation, 193
nonseparable tests, 188

quadratic forms
closed-form representation, 230

Rayleigh integral
Gaussian comparison, 245
tail estimate, 250
Rayleigh quotient
mask removal, 191
unmasked rate, 190
regularization
joint source widths, 46
order of limits, 49, 260
uniform vertex bound, 50
regularized sources, *see* source convergence
resolvent estimates, 33, 61
Riesz covariance
finite coefficients, 336
spatial maxima, 351
static interpolation, 355
Riesz equilibrium density, *see* temporal equilibrium density

rough noise
  proposed spectral extensions, 25
Rytov transformation, 24

scaling
  exact law of the canonical solution, 174
scaling exponent, 4, 88
Schatten norms, 113, 118
Schur's test, 115, 209
second moment
  complete mixed expansion, 31
  explicit spatial-white bounds, 289
  independent upper bound, 15, 88
  intrinsic limiting constant, 15, 281
self-contractions, *see* pairings, self-pairings
series tails
  uniform summability, 87
signed controls
  comparison with positive controls, 278
  upper variational expression, 266, 269
signed potentials
  closed quadratic form, 230
  limiting multiplier, 230
  spectral wave, 232
sine propagator, 33, 101
  zero frequency, 101, 105
singular values
  whole-space cutoffs, 118
Skorohod interpretation
  comparison with Stratonovich, 7
small-noise normalization, 174
Sobolev embeddings
  higher-moment ranges, 21
source convergence
  operator paths, 139
  ordinary response, 146
  point moments, 152, 260
  regularized random fields, 143, 145
source normalization
  first-moment comparison, 13, 379
spatial cutoff
  covariance quotient obstruction, 99
  explicit radius dependence, 226, 227
  growing-radius mean, 229
  heat and frequency tails, 218
  uniform mean bounds, 218, 221
spatial energy
  deterministic Fourier bound, 200
  physical and spectral forms, 380
  variational definition, 204
  white-noise evaluation, 288
spatial pairings
  four-linear extension, 202
  measure covariance, 198
spatial ratio, 201
spatial white noise
  energy maximizer, 288
  explicit moment bounds, 289
  relative bound width, 289
spectral gap, 164, 180
spectral measure
  translated mass bounds, 94
spectral projections
  complementary evolution, 166, 169
  growing mode, 168
static limit
  first-correction conjecture, 24
  moment constants, 391
  temporal-minimum comparison, 386
static noise
  all-order phase bounds, 65
  first variance estimate, 59
  temporal interpolation, 355, 390
Stratonovich correction, *see* Stratonovich interpretation
Stratonovich integrals
  ordered expansion, 12
  self-pairings, 31
Stratonovich interpretation, 7, 52
  comparison with Skorohod, 7
symplectic conservation
  limiting wave, 239
  regularized sources, 238
symplectic form, 235
Sz.-Nagy inequality, *see* Gagliardo–Nirenberg inequality

temporal equilibrium density, 197
  mass, 197
temporal modulation, 99
tensor products
  covariance spaces, 209
  Hilbert-valued extension, 220

time blocks
composition and restart, 182
correlated inputs, 176, 184
positive cone, 180
terminal interval, 184, 256
uniform error, 178
trace inequalities, 112, 121
trigonometric covariance products, 100

universality
open scaling question, 24

variance bounds
column and adjoint-column maps, 110
input and output directions, 108, 115
variational constant
intrinsic second moment, 281
occupation ceiling, 285
spatial-energy bracket, 286
variational methods
possible extensions, 28

Walsh's guitar example, 1
wave kernel, *see* Green measure
wave phase
complex norm bound, 61
displacement and velocity, 59, 105
extended constant-data space, 153
white noise, *see* spatial white noise
Wick contractions, *see* pairings
Wick formula
terminal chains, 85
Wick measures
spatial limit, 44
Wiener chaos
iteration order versus chaos order, 7, 65

Young integration
Gaussian flow moments, 158
inverse evolution, 215
linear evolution, 157
perturbation bounds, 215, 216
Young's inequality
convolution, 209
scalar powers, 112